Radiocarbon dating Late Pleistocene megafauna in southern Europe



Eileen Jacob

Merton College

University of Oxford

A thesis submitted for the degree of

Doctor of Philosophy

Trinity 2019

For my family

Acknowledgements

To summarise: 'An expert is one who knows more and more about less and less' —Nicholas Murray Butler.

This was a long journey and at many points I was carried. It takes a village to raise a PhD, and long after the specifics of LADs have faded from my memory I will remember the people this PhD allowed me to work with.

Thanks to many:

First and foremost to my supervisors, Thomas Higham and Thibaut Devièse, for guiding me right and sticking by me when life got complicated.

To the Clarendon fund for making this all possible. To Merton college and Irene Lemos for financial and logistical support; to the Meyerstein/Schools fund and the NERC Radiocarbon grant for supporting my research and travels.

To an amazing list of expert collaborators, from generous advisors to museum curators to in-the-trench excavators: Juan Arenas, Paolo Boscato, Elisabetta Cioppi, Rob Dinnis, Katerina Douka, Maurizio Gatta, Jean-Luc Guadelli, Aleta Guadelli, Angharad Jones, Adrian Lister, Víctor Sauque, Tony Stuart, Elizabeth Walker, and many more. To Luke Spindler, Sam Brown, and Mike Buckley for the ZooMS collaboration.

To the ORAU lab. To Dan for teaching me the lab and introducing me to the climbing wall. To Dave and Pete for suffering my cursed attempts to use the mass specs and my weird experiments stewing on the benches. To Jane, Kathryn, Barbara, and Luke for humouring my crowding of the centrifuges and answering my dumb questions. To Liz, Emma, and Diane for all the P-numbers and paperwork help.

To John Pouncett, Rick Schulting, Mike Dee, and others for teaching me the ropes on OxCal and GIS. To Nyree and Chris for generously giving your time to teach me how to use the SEM and make sense of its data.

To Greger Larson, Nick Barton, and Christopher Bronk-Ramsey for your feedback at the transfer and confirmation stages. You gave valuable guidance and the fresh perspectives needed to keep me from getting lost in the woods.

To Lorena, fellow radiocarboner and office-commiserater. To Rachel Hopkins, C14 guru. To Hannah, Nyree, Alyssa, Becca, Becca 2 (which is which?), Jaime, Maciej, Steve, Danielle, and all the fellow research fodder. To friends Theresa, Tyra, Sofia, Lauren, John, and Paul. It would have been unbearable without you all.

To the open-source heroes that freely gave the many statistical, graphical, and publishing tools used in this thesis. Most of these are referenced accordingly, but I want express thanks for their teaching. I'm indebted to Yihui Xie, Chester Ismay, and Ulrik Lyngs for developing the R Markdown template on which this thesis is built.

Finally, to my family and Jimmy for providing solace and strength with arguable sanity. Here's to future healthy adventures.

To you: I hope I mentioned you, since you're probably here looking for your name. If you feel wrongly forgotten, then I thank you now, for whatever good deed you did! If you're just reading this to pass the time in the Bodleian: may I recommend Douglas Adams' work? It features aliens and dolphins, neither of which I managed to work into this thesis.

For my next trick, I will say goodbye to Oxford. It's been a weird seven years. Keep the kebabs hot and the Latin fresh.

Eileen Jacob
Merton College, Oxford
Summer 2019

Abstract

In the last 100,000 years, mainland Europe lost over a dozen large mammal species. These were part of a global extinction event that occurred during heightened climatic variability and the expansion of modern humans. The role of these two factors in driving the extinctions has been debated for decades. To move the debate forward, precise and accurate chronological estimates of fossils are needed to link species to climatic events and human activities. Unfortunately many fossil chronology datasets are small, contain unreliable dates, and are not spatially representative.

This poor temporal constraint is in part due to the challenges of radiocarbon dating Pleistocene bone. Radiocarbon dating requires sufficient collagen to be extracted from a bone sample. Heat and aridity both degrade collagen, so faunal specimens from southern European sites in particular often fail to produce sufficient collagen. This has resulted in a dearth of reliable dates from the Mediterranean and an incomplete picture of when and where fauna disappeared in Europe. Resolving southern European faunal histories is particularly important as southern Europe has been posited as both the region species retracted to prior to extinction and where the earliest modern humans arrived in Europe.

This thesis tested approaches to improving sampling and pretreatment for radiocarbon dating poorly-preserved bone. It then produced new radiocarbon dates from three carnivore species in southern Europe: cave lions, cave hyenas, and leopards. These dates were combined with critically evaluated radiocarbon dates to model extinctions and interactions between fauna, climate, and modern humans using both established and novel modelling tools.

Key methodological results found sample preservation could vary dramatically within sites and even individual bones. Proposed alternatives to the standard ABA pretreatment produced lower-quality collagen but sometimes produced yields where ABA did not, presenting an opportunity for further purification. Critical evaluation of radiocarbon datasets was important, as inclusion of less-robust dates altered some model results.

Models were inconclusive on the still-small leopard dataset but suggested both cave lions and hyenas went extinct in southern Europe earlier than northern Europe. Time series analysis of OxCal kernel density estimate models suggested observational densities of hyenas lagged human densities and cave lions lagged climate changes, while Bayesian spatial extinction models estimated that both species went extinct in mid-latitude Europe at the last glacial maximum and terminal Pleistocene, respectively. A ‘pincer effect’ is suggested to interpret these results, where modern humans limited species’ ability to shift ranges during glacial expansions. These results are compared to other Pleistocene extinctions and discussed in relation to ecological theories.

Contents

List of Figures xvii

List of Tables xxi

Date conventions and abbreviations xxv

1 Introduction 1

1.1 Research questions . . . 3
1.2 Thesis structure . . . 4

I Background 7

2 Carnivores in Late Pleistocene Europe 9

2.1 The Late Pleistocene setting . . . 9
2.2 LP fauna events . . . 11
2.2.1 Extinction . . . 11
2.2.2 Range shift . . . 13
2.2.3 Survival . . . 15
2.2.4 Extinct European carnivores . . . 16
2.3 Explaining LP fauna events . . . 19
2.3.1 Climate change . . . 20
2.3.2 Humans . . . 23
2.3.3 Combined models . . . 24
2.3.4 Limitations of LQE studies . . . 26
2.4 Significance . . . 29
2.4.1 Ecological consequences . . . 29
2.4.2 Archaeological importance . . . 30
2.4.3 Modern significance . . . 31
2.5 Chronology and modelling faunal histories . . . 32
2.5.1 Need for improved chronology . . . 33
2.5.2 Improving chronological data . . . 34
2.5.3 Modelling spatio-temporal data . . . 35
2.6 Conclusions . . . 38

3 Radiocarbon dating poorly-preserved bone **39**
3.1 Diagenesis of bone . . . 39
3.2 Screening developments . . . 41
3.2.1 %N screening . . . 41
3.2.2 Other methods of bone quality analysis . . . 42
3.3 Pretreatment developments . . . 43
3.3.1 ABA . . . 44
3.3.2 Ultrafiltration . . . 45
3.3.3 Chromatography . . . 46
3.4 Improving collagen yields . . . 48
3.4.1 EDTA . . . 49
3.4.2 Dialysis . . . 50
3.5 Conclusions . . . 51

II Materials and methods **53**

4 Radiocarbon experiments **55**
4.1 %N screening . . . 55
4.1.1 Materials . . . 56
4.1.2 Methods . . . 56
4.2 Caldey hyenas . . . 57
4.2.1 Materials . . . 61
4.2.2 Methods . . . 61
4.3 Salt containing samples . . . 63
4.3.1 Materials . . . 64
4.3.2 Methods . . . 64
4.4 Dialysis . . . 66
4.4.1 Materials . . . 66
4.4.2 Methods . . . 66
4.5 EDTA . . . 67
4.5.1 Materials . . . 67
4.5.2 Methods . . . 68

5 Zoological samples **73**
5.1 Evaluation criteria . . . 73
5.2 Previously published dates . . . 75
5.3 New samples . . . 77
5.4 ZooMS identifications . . . 79

6 Radiocarbon methods **83**
6.1 ORAU routine protocols . . . 83
6.1.1 Sample %N screening and preparation . . . 83
6.1.2 Treatment and measurement . . . 84
6.1.3 Modified AG pretreatment . . . 86
6.2 HPLC protocol . . . 86
6.2.1 Hydrolysis and sample preparation . . . 86
6.2.2 HPLC . . . 87
6.2.3 HPLC background correction . . . 88

7 Modelling data and methods **89**
7.1 Data . . . 89
7.1.1 Radiocarbon dates: evaluation and calibration . . . 89
7.1.2 Climatic and archaeological records . . . 90
7.2 Bayes' Theorem . . . 91
7.3 Extinction date estimates . . . 92
7.4 Spatial patterns . . . 93
7.4.1 Data . . . 94
7.4.2 Species distribution models . . . 94
7.4.3 Spatial extinction models . . . 95
7.5 Kernel density estimates and time series . . . 96
7.5.1 Climate time series . . . 97
7.5.2 KDE models as time series . . . 98
7.5.3 Time series analysis . . . 99
7.6 Conclusions . . . 102

III Experimental results **103**

8 %N tests **105**
8.1 %N at Zafarraya . . . 105
8.2 %N versus collagen yields . . . 105
8.3 Intra-bone variation in %N . . . 106
8.4 Discussion . . . 107
8.5 Conclusions . . . 110

9 Caldey hyena tests **111**
9.1 Micro photography . . . 111
9.2 FTIR . . . 113
9.3 Pyrolysis GC-MS . . . 116
9.4 AMS data . . . 117
9.5 Discussion . . . 119
9.5.1 Sample reliability . . . 119
9.5.2 Hyena extirpation in the UK . . . 120
9.6 Conclusions . . . 121

10 Characterizing failed bone samples **123**
10.1 Collagen yields and graphitisation . . . 123
10.2 FTIR . . . 124
10.3 SEM . . . 131
10.4 Discussion . . . 134
10.5 Conclusions . . . 136

11 Dialysis collagen extraction **137**
11.1 Collagen yields . . . 137
11.2 Collagen quality . . . 138
11.2.1 Carbon and nitrogen content . . . 138
11.2.2 FTIR . . . 140
11.3 Discussion . . . 146
11.4 Conclusions . . . 147

12 EDTA decalcification **149**
12.1 Comparison with HCl decalcification . . . 149
12.2 Decalcification over days . . . 151
12.3 EDTA and temperature . . . 152
12.4 EDTA in the microwave . . . 153
12.4.1 Time and EDTA replacements . . . 154
12.4.2 Sample size and grain size . . . 156
12.4.3 Bone preservation . . . 157
12.4.4 Microwave temperature . . . 160
12.5 Analysis of EDTA-extracted collagen . . . 160
12.5.1 FTIR . . . 160
12.5.2 %N and CN ratios . . . 164
12.5.3 Radiocarbon ages . . . 165
12.6 Discussion . . . 166
12.7 Conclusions . . . 170

13 Summary of experimental results **173**

IV Radiocarbon results and models **177**

14 New samples **179**
14.1 ZooMS results . . . 179
14.2 %N and pretreatment . . . 181
14.3 Radiocarbon dates . . . 184
14.3.1 Other species . . . 190

15 Species chronologies **191**
15.1 Evaluation scores . . . 191
15.2 Cave lions . . . 193
15.2.1 Extinction estimates . . . 195
15.2.2 Non-radiocarbon evidence . . . 205
15.3 Cave hyenas . . . 206
15.3.1 Extinction estimates . . . 207
15.3.2 Non-radiocarbon evidence . . . 218
15.4 Leopards . . . 219
15.4.1 Extinction estimates . . . 220
15.4.2 Non-radiocarbon evidence . . . 221

16 Spatio-temporal modelling **223**
16.1 Spatial extinction models . . . 223
16.1.1 Lions . . . 224
16.1.2 Hyenas . . . 227
16.1.3 Leopards . . . 230
16.2 KDE models . . . 232
16.3 Time series . . . 233
16.3.1 Results . . . 237

V Discussion and conclusions **241**

17 Carnivore extinctions in Pleistocene Europe **243**
17.1 Summary of extinctions . . . 243
17.1.1 When do they go extinct? . . . 243
17.1.2 Where do they go extinct? . . . 244
17.1.3 Comparison with literature . . . 249
17.2 Extinctions in context . . . 249
17.2.1 Other Eurasian extinctions . . . 249
17.2.2 Modern humans and climate . . . 250
17.2.3 Species-specific responses . . . 253
17.2.4 Refugia . . . 254
17.2.5 Inter-specific interactions . . . 254
17.2.6 The global LQE . . . 255
17.3 Practical lessons . . . 257
17.3.1 Size and quality of radiocarbon datasets . . . 257
17.3.2 LQE research . . . 258
17.3.3 Conservation and ecology . . . 259

18 Conclusions **261**
18.1 Summary findings . . . 261
18.2 Limitations . . . 263
18.2.1 Experiments . . . 263
18.2.2 Megafauna . . . 264
18.3 Future work . . . 265
18.3.1 Experimental . . . 265
18.3.2 Megafauna . . . 266
18.4 Final reflections . . . 268

Appendices **273**

A Extinctions and extirpations <100 ka **273**

B Sites sampled for this project **287**
B.1 Successfully dated . . . 287
B.2 Failed to be dated . . . 290

C Experimental results data **293**
C.1 %N Zafarraya . . . 293
C.2 Dialysis . . . 301
C.3 EDTA . . . 302
C.3.1 Agitation and bone grain size . . . 302
C.3.2 Carbon and %N content . . . 304
C.3.3 Microwave yields . . . 305

D ZooMS results **311**

E Samples collected for radiocarbon dating **315**
E.1 Collected samples and %N values . . . 316
E.2 Pretreatment results of new samples . . . 325
E.3 Combustion and AMS results of new samples . . . 330

F Species radiocarbon dates **333**
F.1 Leopards . . . 334
F.2 Lions . . . 335
F.3 Hyenas . . . 343

G Radiocarbon date evaluation scores **355**
G.1 Leopards . . . 356
G.2 Lions . . . 357
G.3 Hyenas . . . 362

H Modern human dates **371**

I HPLC background correction notes **381**
I.1 R code for HPLC correction 382

J Models and code **385**
J.1 OxCal extinction estimates 385
J.2 KDE models 386
J.3 MaxEnt features 386
J.3.1 Leopards 386
J.3.2 Lions 387
J.3.3 Hyenas 388
J.3.4 AMH 391

Works Cited **393**

List of Figures

2.1 GRIP and NGRIP δ^{18}O ice core records 11
2.2 Binomial test of the temporal proximity of leopard LAD and AMH arrival in southern Europe using the methods and data in Araujo et al. (2017), repeated 500 times 28

4.1 Example of a bone sub-sampled in six locations for %N values . . . 57
4.2 *Bos* and hyena specimens sampled for this study and photographed under natural light 63

5.1 Southern European sites with large carnivores, either previously dated or sampled for this project 77

8.1 Histogram showing %N values for 259 samples from Zafarraya: 229 new to this study and 30 previously measured in Wood et al. (2013a) 106
8.2 Graph showing the relationship between %N and ultrafiltered collagen yields from 50 bones 107
8.3 Results of sub-sampling eight bones with %N results as box plots . 108

9.1 Microscopic views of the *Bos* bone surface and Caldey samples at the locations where they were previously sampled for radiocarbon dating 112
9.2 FTIR spectra of the three hyena tooth samples and the two bones used as comparison samples 114
9.3 Pyrolysis products from Caldey hyena tooth Z/1983/076.287 117
9.4 Percent carbon (%C) and CN ratios of dated Latton bone and Caldey samples 118

10.1 FTIR spectra of Ghar Dalam AG fraction results compared to standards: hydroxyapatite, raw Latton bone powder, and AG-extracted Latton collagen 128
10.2 FTIR spectra of AG fraction results from southern European sites compared to raw Latton bone powder and AG-extracted Latton collagen 129
10.3 Second derivative of FTIR diagnostic region of Ghar Dalam P44211 AG fraction, raw Latton bone powder, and AG-extracted Latton gelatin 131

10.4 Representative SEM images of P44208 through P44211 samples, AG-extracted fractions . . . 132
10.5 Grains from P44211 raw bone powder . . . 133
10.6 Locations analysed for composition from P44208 AG yield . . . 133

11.1 Comparison of %yield of the acid-soluble (dialysis) fraction and ABA (HCl) yield of the acid-insoluble fraction on a series of bone samples 139
11.2 Comparing mean %yields of dialysis and routine AG products of two bone standards . . . 139
11.3 CN vs %C values of dialysis fractions compared to Latton bone standards extracted with routine AG and AF protocols (from the ORAU database) . . . 140
11.4 FTIR spectra of dialysis fraction samples compared to standards: hydroxyapatite, raw Latton bone powder, and AF-extracted Latton collagen . . . 143

12.1 Gelatin yields of bone samples that were crushed or powdered . . . 151
12.2 Collagen yield (mg) of samples (500 mg bone powder) decalcified in EDTA that was replaced every 24 hr for 5 days and 10 days . . . 152
12.3 Mean %yield collagen of Latton bone decalcified in EDTA, then heated at different temperatures for 90 min . . . 153
12.4 %yield collagen of powdered Latton bone microwaved 30° C in EDTA for increasing durations, compared to %yields of acid protocols used on the same batch of Latton powder . . . 155
12.5 Modelled %yield collagen of Latton bone decalcified in the microwave over time . . . 156
12.6 Mean %yield collagen of Latton bone decalcified in EDTA in the microwave for 90–360 min . . . 157
12.7 Mean %yield collagen of bone standards decalcified in EDTA compared to yields from the ORAU database . . . 159
12.8 AG and EDTA %yields of archaeological samples . . . 160
12.9 Mean %yield collagen of Latton bone decalcified in EDTA in the microwave at lower temperatures with chilled solvent and glassware 161
12.10FTIR spectra of Latton bone product after soaking in 0.5 M EDTA for increasing lengths of time and gelatinised . . . 162
12.11Close up of diagnostic region in Fig . . . 163
12.12CN *vs* %C values of EDTA-extracted Latton collagen, as well as acid-only and AG-extracted collagen from the same drill batch of bone powder . . . 165

14.1 %N results for samples collected for this thesis, coloured by country of origin . . . 181
14.2 Graph showing the relationship between %N and collagen yields from 110 bones, coloured by chemistry pretreatment . . . 183

15.1 Radiocarbon dates included in the analyses below 192
15.2 Scores received by non-HPLC pretreated radiocarbon dates (n = 300), by species 192
15.3 Proportion of fails, by evaluation metric 193
15.4 Radiocarbon dates of cave lions, shading by mean calibrated age BP 194
15.5 Radiocarbon dates of cave hyenas, shading by mean calibrated age BP 206
15.6 Radiocarbon dates of leopard, shading by mean calibrated age BP . 219

16.1 Spatio-temporal estimation of lion extinction across Eurasia 225
16.2 Lion ecological niche and weighted extinction models 226
16.3 Spatio-temporal estimation of hyena extinction across Eurasia . . . 228
16.4 Hyena ecological niche and weighted extinction models 229
16.5 Spatio-temporal estimation of leopard extinction in Europe 231
16.6 Leopard ecological niche and weighted extinction models 232
16.7 KDE model of cave lion radiocarbon dates 234
16.8 KDE model of cave hyena radiocarbon dates 235
16.9 AMH radiocarbon dates used for modelling in this thesis 236
16.10AMH KDE distribution in Eurasia after 50 ka cal BP 237
16.11Time series tested for causality 238

17.1 Extinction estimates for three species 245
17.2 Extinction estimates for lions and hyenas by region using the GRIWM estimator, OxCal boundary models, and LADs 248
17.3 Extinction estimates from Appendix A compared to this project's estimates for leopards, hyenas, and lions 251

List of Tables

2.1 Mainland European and Siberian Pleistocene megafauna extinctions in the past 100 ky . . . 13
2.2 Counts of genera extinct, >40 kg . . . 14
2.3 Popular explanations of the LQE . . . 21

4.1 Radiocarbon dates obtained on bones from Zafarraya using the ultrafiltration protocol (Wood et al. 2013a). . . . 56
4.2 Radiocarbon dates from Caldey Island hyenas (Stuart and Lister 2014) 60
4.3 Samples used in the Caldey hyena study . . . 62
4.4 Samples analysed when they produced an uncharacterised yield . . 64
4.5 Samples used for dialysis experiments . . . 66
4.6 Bone samples used in the EDTA experiments . . . 68
4.7 Conditions of EDTA and HCl solutions with bone (crushed or powdered) for decalcification comparisons . . . 69

5.1 Criteria used to evaluate radiocarbon dates . . . 75
5.2 Cave lion dates from southern Europe . . . 76
5.3 Published leopard dates from southern Europe . . . 76
5.4 Cave hyena dates from southern sites . . . 76
5.5 By species, samples collected for this project . . . 79
5.6 By site, samples collected for this project . . . 80

6.1 The HPLC method used to collect eight amino acids, including Hyp, from Devièse et al. (2018). Pumps run continuously at 18 ml/min with a proportion of water and 0.3% phosphoric acid. . . . 88

9.1 FTIR bands observed across all the hyena bone/tooth samples . . . 115
9.2 Additional FTIR bands observed in the *Bos* bone . . . 116
9.3 GRIWM estimates for hyena extinction in Europe, comparing different datasets . . . 121

10.1 Samples that produced an unidentified white material that failed to graphitize . . . 124
10.2 Samples that produced an unidentified white material but were not graphitized due to low quality metrics . . . 124
10.3 FTIR peaks from P44211 AG sample yield . . . 130

10.4 Spectra quantification for P44208: two raw bone grains (Fig. 10.5) and AG product (Fig. 10.4). Composition data are expressed as percentage of elements in the the sample. Note that Na is at the detection limit and is not likely to be accurate. 134
10.5 Spectra quantification for P44208 across multiple grains from the AG product (Fig. 10.6). Composition data are expressed as percentage by atomic weight of the sample. Note that Na is at the detection limit and are not likely to be accurate. 134

11.1 FTIR bands reflecting collagen-related peaks, observed in Latton AF standard and most dialysis samples 144
11.2 FTIR bands reflecting apatite-related peaks, observed in Latton bone powder and some dialysis samples 145

12.1 Mean yields of collagen from ~500 mg bone starting weight 150
12.2 Comparison of EDTA and AF yields of bone standards from ORAU database 159
12.3 FTIR peaks from pure EDTA powder 164
12.4 Radiocarbon dating results of three bones decalcified with EDTA . 166

14.1 Summary of ZooMS results obtained from Zafarraya 180
14.2 Samples collected for this project by site and their %N results . . . 182
14.3 Pretreatments and resulting success in %yield and dating for this project 183
14.4 By site, samples that produced ⩾1 %yield collagen and subsequently produced a radiocarbon date 184
14.5 New dates obtained for this thesis. 186
14.6 Further information on dated sample identification and context. . . 188

15.1 Calibrations of all lion dates that were not rejected and were not greater-than ages. 196
15.2 GRIWM results estimating extinction date for cave lions 201
15.3 Subregion GRIWM estimates for cave lions 202
15.4 Comparison of the means of cave lion GRIWM estimates of subregions 202
15.5 Comparison of the means of cave lion GRIWM estimates of subregions 202
15.6 OxCal boundary results estimating extinction date for lions in Europe 203
15.7 Subregion OxCal boundary estimates for cave lions 204
15.8 Comparison of the means of cave lion OxCal estimates of subregions 204
15.9 Comparison of the means of cave lion OxCal estimates of subregions 204
15.10 Comparison of OxCal and GRIWM subregion extirpation estimates for lions 205
15.11 Count of scores from hyena radiocarbon date evaluation 207
15.12 Calibrations of all hyena (or hyena-chewed bone) dates that were not rejected and were not greater-than ages. 208

15.13GRIWM results estimating extinction date for hyenas in Europe . . 214
15.14Subregion GRIWM estimates for hyenas 215
15.15Comparison of the means of cave hyena GRIWM estimates of subregions 215
15.16Comparison of the means of cave hyena GRIWM estimates of subregions 215
15.17OxCal results estimating extinction date for hyenas in Europe . . . 216
15.18Subregion OxCal boundary estimates for hyenas 217
15.19Comparison of the means of hyena OxCal estimates of subregions . 217
15.20Comparison of the means of hyena OxCal estimates of subregions . 217
15.21Comparison of the OxCal and GRIWM subregion extirpation estimates 218
15.22Calibrations of leopard dates 220
15.23GRIWM results estimating extinction date for leopards in Europe, depending on whether the low-scoring radiocarbon date was included 221
15.24OxCal results estimating extinction date for pardus in Europe . . . 221

16.1 Results of the modified Wald chi-square statistics used to test non-causality on the 'reverse' relationships as a check for spurious relationships 239
16.2 Results of the modified Wald chi-square statistics used to test non-causality 239

A.1 GRIWM estimates for steppe bison and CladeX bison 274
A.2 GRIWM estimate for extirpation of *Elasmotherium sibiricum* . . . 275
A.3 Subregion GRIWM estimates for giant deer and a global estimate using all dates 278
A.4 GRIWM estimates for extinction of musk ox, depending on whether Siberian mid/late Holocene dates are included or excluded 279
A.5 Radiocarbon dates of musk ox used in GRIWM estimates. Only includes dates with finite estimates after calibration. 279
A.6 GRIWM estimate for extirpation of saiga antelope from Europe, not including Urals or Siberian dates 283
A.7 Direct dates of *S. hemitoechus* from El Castillo, Spain 284
A.8 Subregion GRIWM estimates for cave bear and a global estimate using all dates 285

C.1 %N and %yield of bone samples from Zafarraya. 293
C.2 Dialysis extractions of bone samples. 301
C.3 Comparison of EDTA- and HCl-extracted collagen from Latton bone. 302
C.4 %N, %C, and CN ratios of EDTA-extracted collagen. 304
C.5 EDTA Latton collagen yields in the microwave, different durations. 305
C.6 Yields of non-Latton bones decalcified in 0.5 M EDTA in the microwave 308
C.7 EDTA Latton collagen yields in the microwave, modified conditions. 309

D.1 ZooMS results from Zafarraya. 311

E.1 All samples collected for this thesis. 316
E.2 All pretreatment extractions attempted for this thesis. 325
E.3 All combustions attempted for this thesis and radiocarbon results. . 330

F.1 Direct radiocarbon dates of leopards in Europe. 334
F.2 Direct radiocarbon dates of cave lions in Europe and Asia. 335
F.3 Direct radiocarbon dates of cave hyenas and bones chewed/digested by hyenas in Europe and Asia. 343

G.1 Matrix of date scores for leopards. 356
G.2 Matrix of date scores for lions. 357
G.3 Matrix of date scores for hyenas. 362

H.1 Random sample of 242 radiocarbon dates of AMH from Carotenuto et al. (2018) used in KDE, environmental niche, and OxCal boundary models. 371

I.1 HPLC dates obtained for this thesis and their corrected results . . . 382
I.2 Standards (Ash Bend) used for the HPLC background corrections of dates obtained for this thesis 382
I.3 Description of input variables required for the HPLC background correction. The function requires two data frames: uncorrected samples (`hplc.samples`) and background measurements (`stds`). . . 382

J.1 Bio-climatic variables used in niche models 386
J.2 Features of MaxEnt model with LGM climate predictors for leopards 387
J.3 Feature metrics of the above MaxEnt model for leopards 387
J.4 Features of MaxEnt model with LGM climate predictors for lions . 388
J.5 Feature metrics of the above MaxEnt model for lions 388
J.6 Features of MaxEnt model with LGM climate predictors for hyenas 389
J.7 Feature metrics of the above MaxEnt model for hyenas 390
J.8 Features of MaxEnt model with LGM climate predictors for modern humans. 391
J.9 Feature metrics of the above MaxEnt model for modern humans . . 392

Date conventions and abbreviations

Dating conventions

BP . . . . . Literally 'before present', but used to report radiocarbon years before 1950 AD (100 BP = 1850 AD). Assumed to be uncalibrated unless specified otherwise with 'cal'.

cal . . . . . 'Calibrated', used to clarify whether the radiocarbon date being reported has been calibrated (e.g. 2000 cal BP).

ka . . . . . 'Kiloannum', or unit of one thousand years. 2 ka = 2000 years.

ma . . . . . 'Megaannum', or unit of one million years. 2 ma = 2×10^6 years.

ya . . . . . Years ago.

Abbreviations

$\sim$ . . . . . Approximately. $\sim$ 2 ka BP = about 2000 years before present.

ABA . . . . . Acid-base-acid.

AMH . . . . . Anatomically modern humans.

AMS . . . . . Accelerator mass spectrometry.

C14 dating . Radiocarbon dating.

EDTA . . . . Ethylenediaminetetraacetic acid.

EDX . . . . . Energy-dispersive X-ray spectroscopy.

ENM . . . . . Ecological niche model.

FTIR . . . . . Fourier transform infrared spectroscopy.

GI . . . . . Greenland interstadial.

GIC . . . . . General information criterion.

GISP2 . . . . Greenland Ice Sheet Project 2.

GRIWM . . . Gaussian-resampled, inverse-weighted McInerney et al. method.

GS . . . . . Greenland stadial.

HE . . . . . Heinrich event.

HPLC . . . . High performance liquid chromatrography.

HYP . . . . . HPLC-extracted hydroxyproline radiocarbon date protocol. Hyp (not capitalized) refers to hydroxyproline.

KDE . . . . . Kernal density estimate.
LGM . . . . . Last Glacial Maximum.
LP . . . . . Late Pleistocene
LQE . . . . . Late Quaternary Extinction Event.
MP . . . . . Middle Palaeolithic.
NGRIP . . . North Greenland Icecore Project.
OIS . . . . . Oxygen isotope stage.
ORAU . . . . Oxford Radiocarbon Accelerator Unit.
OSL . . . . . Optically-stimulated luminescence.
SEM . . . . . Scanning electron microscopy.
U-series . . . Uranium-series dating.
UP . . . . . Upper Palaeolithic.
VAR model . Vector autoregressive model.

1 Introduction

> '... an understanding of what drove the extinctions of large animals over the past 100,000 years requires detailed analysis on a species-by-species basis. This means trying to find new fossils and verifying the estimated age of specimens previously found...' (Price et al. 2018, pg. 25)

Over the last 100,000 years, many large mammal species went extinct across the globe. This Late Quaternary Extinction (LQE) profoundly altered ecological systems while modern humans expanded out of Africa and faced heightened climatic instability. The coincidence of human expansion and climatic instability has led to a decades-long debate over which (or both) are to blame for the extinctions.

This debate is not resolved. Papers continue to come to different conclusions about what drove the extinctions (discussed in Monjeau et al. 2017). There are several reasons for this stalemate, but two key themes emerge. First, the underlying data for species is often limited, flawed, and unrepresentative. As Price et al. recently commented of multi-species LQE analyses, 'the reliability of results is largely governed by the "GIGO" principle: garbage in, garbage out' (2018, pg. 24). For megafauna, the key data form is chronometric dates of fossils. Without clarity on when a specimen lived, it cannot be connected to climate or archaeological records. Radiocarbon dating is the most direct and precise method of determining the age of fossils within the past ~50 ky (Bronk Ramsey 2008; Wood 2015), but many

radiocarbon datasets are neither accurate nor spatially representative for species. The lack of robust, precise chronologies is a serious limitation in studying the LQE.

Second, different species cannot be assumed to have responded in the same way to modern humans and climate changes. Models that do not consider the ecological requirements of individual species risk confounding signals and miss opportunities to build subtler extinction stories. Extinction presents a straightforward data point to model, but it is also, by definition, an anomaly. Species responded to climatic events throughout their histories, and many coexisted with humans for millennia. Understanding not just the singular event of extinction, but responses to climate and humans through species histories, helps gauge whether LQE extinction theories can be generalised across species and continents.

This project aimed to improve faunal chronologies and test approaches for modelling interactions between fauna, climate change, and modern humans. To improve chronologies, methodological issues of radiocarbon dating poorly-preserved bones were explored. New radiocarbon dates were obtained from under-represented regions and existing dates were critically evaluated. With these, different statistical models were built to explore species' spatial and temporal patterns. By applying multiple tools, different hypotheses were tested and the robustness of results cross-checked. Species were analysed individually, evaluating their specific responses to climatic events and modern humans, and the influence of less-robust radiocarbon dates explicitly investigated.

This project focused on the three European large carnivores that were lost in the LQE: cave lions, cave hyenas, and leopards. (Leopards are not extinct, but they were extirpated from Europe.) Carnivores have specific ecological roles and face specific pressures from modern humans which are often not considered in LQE analyses. European leopards have very few radiocarbon dates, and while hyenas and cave lions have relatively large datasets, they do not cover their full spatial ranges.

In particular, southern Europe's hot climate degrades collagen in bone, which is the component isolated for radiocarbon dating. This has resulted in few dates from southern Europe. This limits understanding of fauna responses to human arrival in

Europe, which likely occurred 50–40 ka cal BP via southern or central Europe. It also limits understanding of responses to climate change, such as whether species retracted into southern Europe during periods of glacial expansion. Obtaining radiocarbon dates from southern Europe makes datasets for the three species more representative and enables testing of hypotheses that involve range shifts.

1.1 Research questions

This project aimed to improve radiocarbon dating of poorly preserved bone, as southern Europe has difficult preservation conditions. Dated samples were then added to models of Late Pleistocene carnivores in Europe to explore the role of modern humans and climate on carnivore histories.

The following questions informed sampling approaches and pretreatment protocols of samples with poor preservation:

1. How variable is collagen preservation within a site and a single bone?
2. How useful is %N screening and other tests for predicting collagen yields and assessing sample quality?
3. Can alternative pretreatment protocols produce high-quality collagen yields in poorly-preserved samples?

Questions related to carnivore extinctions fall under four themes:

1. *North vs south*: Did carnivores disappear from southern Europe earlier or later than northern Europe? Was this pattern species-specific or general?
2. *Climate vs humans*: Were carnivore spatio-temporal patterns related to climatic and/or modern human patterns?
3. *Carnivores vs herbivores*: Did carnivores respond in similar ways, and did they respond differently from herbivores?

4. *Model robustness*: Does including less-reliable radiocarbon dates significantly change model results? How do models compare to each other and reported stratigraphic associations of species?

Questions of north *vs* south connect to modern human arrival, as humans appear to settle in northern Europe later than in southern Europe. An earlier disappearance of carnivores in the south around the time of modern human arrival implicates modern humans, while a northern-first disappearance supports an environmental explanation. Comparing climate and human signals, particularly through time, informs species' responses to abrupt climate change and humans. Comparing carnivores and herbivores informs mechanisms of extinction, such as ecological cascades and competitive exclusion. Finally, testing the influence of less-robust radiocarbon dates helps establish best practices for building datasets.

1.2 Thesis structure

This thesis is organised into five main parts. The background chapters (2–3) introduce current extinction theories, limitations of existing chronologies and modelling approaches, and challenges of radiocarbon dating poorly-preserved bone. The methods and materials chapters (4–7) describe radiocarbon methodological experiments and routine protocols, newly-obtained faunal samples, and modelling tools. The next section (chapters 8–13) presents the results of the methodological experiments, including experiment-specific discussions and conclusions. Faunal dates and modelling results are presented next (chapters 14–16). Newly-obtained samples, date evaluation results, extinction estimates, and spatio-temporal models are presented. For each model, the influence of low-reliability dates are considered, and extinction estimates are compared to reported stratigraphic associations. In the discussion (chapter 17) the results of these models are compared and a narrative suggested to explain them. Carnivore spatial patterns and extinctions are contextualised in existing theories around the LQE, and the usefulness of the project's tools and approaches are considered. Finally, the conclusion (chapter 18)

summarises key findings from the methodological experiments and carnivore models, discusses the project's limitations, and makes suggestions for future work.

Part I

Background

2

Carnivores in Late Pleistocene Europe

In the mid-Late Pleistocene (~50–40 ka), Europe was home to seven large (>44 kg) predators: cave hyenas, leopards, cave lions, brown bears, wolves, cave bears[1], Neanderthals, and newly-arrived modern humans. Today, only wolves, brown bears, and modern humans remain. Many large herbivores also disappeared from Europe in the Late Pleistocene (LP) as part of a global extinction event. The context for this dramatic ecological change and the questions surrounding its cause are introduced here.

2.1 The Late Pleistocene setting

The LP began ~100 ka and contained the final glacial cycle. While the Pleistocene epoch witnessed multiple glaciations after 2.6 ma, the final glacial was particularly characterised by high-eccentricity and high-frequency climate changes (Fig. 2.1). These 25 stadial-interstadial cycles were superimposed over a downward trend towards the last glacial maximum (LGM) at about 22 ka (Dansgaard et al. 1993; Rasmussen et al. 2014). Each cycle was marked by rapid warming of 5°–16° C in <50 years (Guillevic et al. 2013; Steffensen et al. 2008), followed by gradual cooling. There were also abrupt downturns, called Heinrich events (HEs), caused

[1] Cave bears were mostly herbivorous with some possible examples of omnivory (Baca et al. 2016; Bocherens 2015; Krajcarz et al. 2016).

by Laurentide ice drifting into the Atlantic and cooling sea surface temperatures (Bond et al. 1992; Heinrich 1988; Sánchez Goñi and Harrison 2010).

Europe in the LP was a place of climatic instability. Northern latitudes were dominated by shifting ice fronts and southern latitudes by aridity patterns (Müller et al. 2011; Sánchez Goñi and Harrison 2010). Europe was broadly divided into these Palaearctic and Mediterranean biotic zones with a latitudinal front that shifted with climate cycling (Huntley et al. 2003; Huntley et al. 2013; Van Meerbeeck et al. 2011; Webb and Bartlein 1992). The distinct Palaearctic zoogeographical region dominated northern Eurasia from the Pleistocene to the Holocene.

The Pleistocene faunal suite is distinct for its megafauna, including megaherbivores that were generally broad-spectrum and opportunistic foragers (Brugal and Croitor 2007). While some typical associations of species existed, Pleistocene species appeared in variable combinations, and nonanalogue communities—assemblages of species with no modern equivalents—were also prevalent (Graham and Grimm 1990; Lundelius 1989; Stewart 2009; Stewart et al. 2003).

The LP also saw turnover of hominin species. Neanderthals, after evolving from *H. heidelbergensis* ~300–600 ka ago (Hublin 2009), likely went extinct between 41–39 ka cal BP (Higham et al. 2014). Anatomically modern humans (AMH) moved into Europe earlier. They interbred with Neanderthals (Fu et al. 2015; Green et al. 2010) and temporally overlapped for 2,600–5,400 years (Higham et al. 2014). AMH appeared in Russia and Italy by 45 ka cal BP (Anikovich et al. 2007; Douka et al. 2014), and the diagnostic Aurignacian tool industry was widespread across Europe by 43–40 ka cal BP (Douka et al. 2012; Higham et al. 2011; Nigst et al. 2014; Zilhao 2006). Whether these early AMH had greater ecological impacts than Neanderthals, such as through intensity of resource use or population increase, is debated (Barnosky et al. 2004; Dogandžić and McPherron 2013; Mellars and French 2011), as are the mechanisms by which humans may have affected carnivore populations. The possible impacts of AMH are discussed more in chapter 2.3.

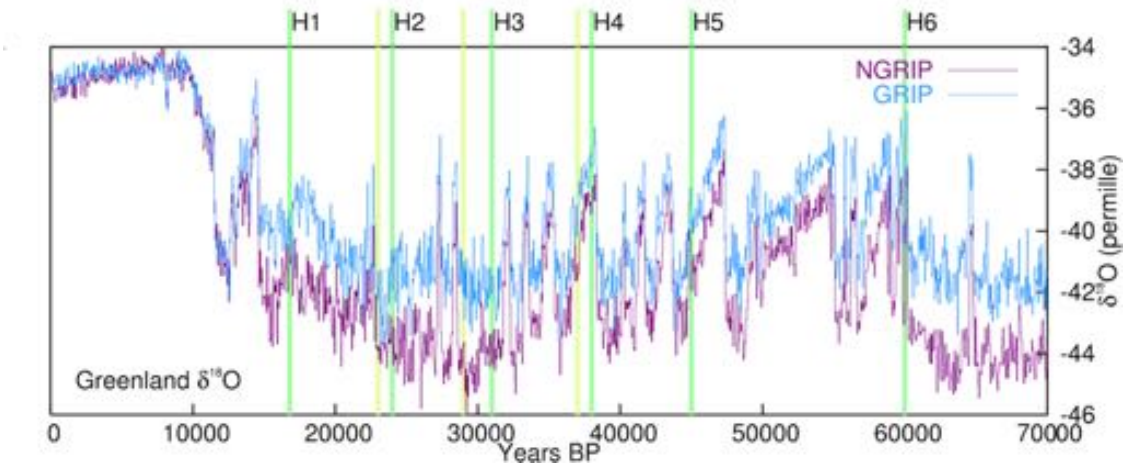


Figure 2.1: GRIP and NGRIP δ^{18}O ice core records. Records from GRIP GRIP members (1993) and NGRIP NGRIP members (2004); figure modified from McInnes (2006). Age estimates of Heinrich events (H) are from Hemming (2004) (green) and alternatives from Bond et al. (1992) (yellow).

2.2 LP fauna events

Species respond to environmental change in four ways: they evolve; they go extinct; they shift distribution; or they persist in the same range, perhaps through reduced numbers or niche adaptations. There are examples of all four responses in the LP, though extinction has captured the most attention.

2.2.1 Extinction

Something over 40 Eurasian large (>44 kg) genera went extinct in the Pleistocene (Anderson 1984; Smith et al. 2003)[2]. In the last 100 ky, between 10–20 large species went extinct in mainland Europe and Holarctic Asia, though technically some of these were extirpations (Table 2.1). Genetic studies have also revealed exterminations of distinct clades within species (Hofreiter and Stewart 2009). These 'ghost turnovers' and population events may be obscured in the fossil record but mark important events in a species' history (Barnett et al. 2009; Cooper et al. 2015; Rohland et al. 2005).

[2]The size cut-off of 44 kg is an arbitrary tradition (Brook and Bowman 2004); many smaller species, including several Mediterranean island dwarf species, also went extinct.

The prior glacial saw extinctions, including an event at the onset of the Eemian (Stuart 1999), but there were far more in the LP. Europe's losses were part of the global Late Quaternary Extinction (LQE) that exterminated 65% of megafauna genera (Koch and Barnosky 2006). All continents lost species, with megafauna being particularly hard-hit (Grayson 2001; Martin 1984). The extinctions spanned the final glacial into the Holocene as species experienced 'extinction lags' into the early-middle Holocene (Brooks et al. 1999; Lister and Stuart 2008). Historical extinctions are usually counted in the current, ongoing mass extinction (Barnosky et al. 2011; May et al. 1995).

Compared to other continents, Europe's losses were moderate (Table 2.2). Africa lost only 14% of genera >44 kg, but Australia lost 86% (Elias and Schreve 2007). By this measure, Europe lost 15 genera (57%) (Martin 1984), but these apparent imbalances can change with the species' mass cut-off (Wroe et al. 2013). Survivals can also be considered: only one megafauna genus survives in Australia, but nine do in Europe (Martin 1984).

The LQE was the most selective extinction event since the Late Cretaceous event 65 ma (Alroy 1999). The LQE was top-heavy, with all fauna >1000 kg going extinct in Europe, the Americas, and Australia (Wroe et al. 2004). Body mass and extinction risk were correlated (Brook and Bowman 2004; Polishchuk 2010), though some have argued that life-history factors such as reproductive rate were stronger predictors of extinction (Zuo et al. 2013). Today, body size remains a significant variable throughout the 'pathway' to extinction both in absolute terms and relative to other species with similar traits (Davidson et al. 2009). However, geographic range, population density, group size, mass-specific production, and home range are all more powerful predictors of extinction risk (Cardillo et al. 2005). Body size was a more significant extinction risk factor during the LP than today.

Sometimes extinction comes with a caveat: surviving 'hangers-on' that are usually ignored when quoting a species' extinction point. The Siberian mammoths of the Taimyr Peninsula and Wrangel Island (MacPhee et al. 2002; Stuart 2005; Vartanyan et al. 2008a) are the most obvious examples of members of a 'functionally

Table 2.1: Mainland European and Siberian Pleistocene megafauna extinctions in the past 100 ky. Carnivores and omnivores are in bold. Counts are not identical to Table 2.2 due to discriminating between species and counting some extirpations as Asian survivals. List updated from Barnosky et al. (2004) and Pushkina and Raia (2008). Species chronologies, including species excluded from this list due to poor chronological constraint, are summarised in Appendix A.

Extinctions <100 ka		Survivals	
Bison priscus	Steppe bison	*Alces alces*	Moose
Bos baikalensis	Baikal yak	*Camelus bactrianus*	Bactrian camel
Bos primigenius	Aurochs	*Canis lupus*	**Wolf**
Coelodonta antiquitatis	Woolly rhino	*Cervus elaphus*	Red deer
Crocuta crocuta spelaea	**Cave hyena**	*Dama dama*	Fallow deer
Elasmotherium sibiricum	Unicorn rhino	*Equus ferus*	Wild horse
Equus hydruntinus	Pleistocene ass	*Equus hemionus*	Onager
Hippopotamus antiquus	European hippo	*Panthera pardus*	**Leopard**
Homo neanderthalensis	**Neanderthals**	*Rangifer tarandus*	Reindeer
Homo sp. Altai	**Denisovans**	*Saiga tartarica*	Saiga antelope
Mammuthus primigenius	Mammoth	*Sus scrofa*	Wild boar
Megaloceros giganteus	Giant deer	*Ursus arctos*	**Brown bear**
Ovibos moschatus	Musk ox		
Palaeoloxodon antiquus	Straight-tusked elephant		
Panthera spelaea	**Cave lion**		
Spirocerus kiakhtensis	Screw-horn antelope		
Stephanorhinus hemitoechus	Narrow-nosed rhino		
Stephanorhinus kirchbergensis	Merck's rhino		
Ursus spelaeus	**Cave bear**		

extinct' (Stewart and Cooper 2008, p. 2446) species. Also, extirpations from Europe are treated as a type of extinction in this project, but depending on context these might better be treated as range shifts or retractions.

2.2.2 Range shift

Shifts in ranges were necessitated by rapid climate changes. If the geographic range of a species' suitable ecological niche shifts, either through changes in the species' tolerances or through changes to the environment, then the species must follow (Martínez-Meyer et al. 2004). The ability to (re)colonise a suitable habitat depends on both a species' dispersal power and the difficulty in reaching the habitable patch (Bowler and Benton 2005). Suitable niches would have fragmented

Table 2.2: Counts of genera extinct, >40 kg. From Martin (1984) and Elias and Schreve (2007).

Continent	Extinct	Survivals	Total	Extinct (%)
Africa	7	42	49	14.30%
Asia	24	22	46	52.20%
Australia	19	3	22	86.40%
Europe	15	9	24	62.50%
North America	33	12	45	73.30%
South America	46	12	58	79.30%

or shifted to new locations over the course of the LP at all scales, from major environmental types to micro-climates.

The largest environmental shift occurred at the Holocene transition, which witnessed rapid forest expansion and reduction of the 'mammoth steppe': the cold, productive herbaceous landscape favoured by megaherbivores (Huntley et al. 2013). However, this postdates the extinction of several species, including hyenas, and leopards never inhabited such northern latitudes (chapter 2.2.4).

More relevant to carnivores were the frequent stadial-interstadial cycles throughout the LP. These may have driven species through repeated range contractions and expansions. The typical example is of a species expanding its range during interstadials, particularly to higher latitudes, then retracting to lower latitudes in step with glacier expansions (Stewart and Cooper 2008). Contractions were into refugia, spaces that populations persist in when more marginal populations are periodically exterminated. This refuge hosts a reservoir population that supplies individuals to recolonize spaces when they once again become tolerable, so long as habitable spaces are sufficiently connected to enable dispersal (Mann et al. 2015). Retractions are typically thought to be subpopulation extinctions rather than migrations. This is borne out by palaeogenetic studies, though genetic bottlenecks (decreased population) and refugial contractions (decreased range) need not always occur together (Bennett and Provan 2008; Stewart and Cooper 2008).

What qualifies as a refuge depends on the species' tolerances: tundra species will see interstadials as retractions to northern refugia and Mediterranean species

vice versa. Northern Iberia, for example, was periodically home to cold-type fauna including mammoths, reindeer, and woolly rhinos between MIS 6 (~190 ka) and the LGM; this is seen as an expanded southern front during stadials (Álvarez-Lao and García 2010).

Refugial populations can be difficult to distinguish from genetic bottlenecks and increased endemism (Bennett and Provan 2008; Stewart et al. 2003). The refuge concept originated in plant studies (Bennett and Provan 2008), which did not have to distinguish between subpopulation migrations and extirpations. These issues have muddled the refuge concept, and it has not been picked up in modern ecology as readily as in palaeontology.

2.2.3 Survival

Some 43% of European genera survived the LP-Holocene transition (Martin 1984), not including species reduced to relict populations as Holocene 'extinction debts' (Fiedel 2009; Stuart et al. 2004). The carnivores to survive in Europe were wolves, brown bears, and modern humans.

Survival was not random. On continents, small species were more likely to survive the transition than large ones. Generalist species also tended to fare better, especially compared to more specialised but taxonomically close species (Purvis et al. 2000). The success of generalist and smaller species has persisted into the current extinction event (Davies et al. 2004; Devictor et al. 2008). Wolves and brown bears fit this pattern: unlike cats, they are not obligate carnivores and sometimes eat vegetation (McLellan et al. 2017; Stahler et al. 2006).

Survival implies resilience and stability, but species may have experienced high rates of subpopulation exterminations. A species occupied suitable habitat patches, but the connectivity between patches affected population dynamics. In highly patchy landscapes, 'movement' often takes the form of a metapopulation experiencing exterminations and recolonizations from neighbouring subpopulations (Bowler and Benton 2005; Brown and Kodric-Brown 1977), while highly connected patches will behave as a single large population (Hanski 1998). Patchy landscapes need not

produce species extinction; as long as the intrinsic rate of recolonisation is greater than extinction across patches, the metapopulation equilibrates (Hanski 1994).

This dynamism is evinced by genetic signals that show multiple extinct and overwritten clades within a species (Hofreiter and Stewart 2009). A bottleneck in cave lions after 48 ka BP exterminated multiple haplotypes which was followed by re-expansion of one haplotype (Barnett et al. 2009), and cave hyenas experienced inputs from African hyenas after their initial divergence ~3 ma (Rohland et al. 2005). Multiple genetic clades have similarly been identified in cave bears (Hofreiter et al. 2007) and Pleistocene brown bears (Valdiosera et al. 2007).

Recolonization in patchy landscapes is similar to the refugia model. Refugia are implied to operate on a larger spatial and demographic scale, but in practice attempting to distinguish the two may be impossible, particularly at the low spatio-temporal resolution of the Pleistocene.

There have also been attempts to identify cryptic refugia: small, suitable habitats that exist outside the expected area (de Lafontaine et al. 2014; Schmitt and Varga 2012; Stewart and Lister 2001). Isolated populations persisted in suitable microclimates but were likely vulnerable in their isolation and low abundance. They are being increasingly recognised in the high-velocity climate oscillations of the LP, though their significance to a species' genetic history was probably low.

2.2.4 Extinct European carnivores

This project focuses on extinct cave hyena, cave lion, and the extirpated leopard. Brown bear and grey wolf did not go extinct, though both survive in reduced ranges in Europe (Jdeidi et al. 2010; McLellan et al. 2017). Carnivores were chosen because they play crucial ecological roles but are far less studied than the classic steppe megaherbivores (chapter 2.4).

2.2.4.1 Cave hyena (*Crocuta crocuta spelaea*)

Cave hyenas were larger than modern African hyenas and used caves as shelters. Modern spotted hyenas survive in diverse habitats and have diverse diets (Salnicki

et al. 2001). Based on chewed and digested bones recovered from Pleistocene sites, cave hyenas seem to have been similar. It is impossible to distinguish hunting and scavenging, but they ate medium-sized prey like horse, reindeer, and deer, as well as more challenging prey like woolly rhino, cave bear, cave lions, and other cave hyenas (Diedrich and Zák 2006; Fourvel et al. 2014; Stuart and Lister 2014). They probably lived in clans like modern hyenas.

As top-level, cave-dwelling carnivores, cave hyenas shared many similarities with hominids. The relationship between the two is debated. Modern hyenas often live in close proximity to humans (Bohm and Höner 2015), but they are smaller and live in more open landscapes (Stuart and Lister 2014). Some caves show both human and hyena occupation in the same layers and scavenging of both human-killed and human remains (Guadelli et al. 2013). It may have been a close, antagonistic relationship, in which both species followed prey herds but competed for caves. A more distant relationship has also been proposed based on alternating hyena-human occupation layers in caves and hyenas avoiding larger caves (Diedrich 2011; Diedrich and Zák 2006).

Hyenas appear to have gone extinct before the LGM (Stuart and Lister 2014). Hyena last appearance dates (LADs) for northern countries such as the UK and Belgium are 34–31 ka BP (Dinnis et al. 2016), whereas overall LADs comes from Italy and Bulgaria at 26 ka BP (Stuart and Lister, 2014). However, there are few radiocarbon dates of hyenas in southern Europe. There are four from Italy, one from Spain, and one from Greece (Stuart and Lister 2014) (chapter 5). There are also dates <34 ka BP from northern sites whose reliability are contended, such as from Caldey Island, UK (Dinnis et al. 2016).

Humans may have competed with hyenas for prey or shelter, or the extinction of herbivores could have deprived hyenas of their prey. The latter is unlikely since many prey species survive past the LGM. An apparent southern retraction of hyenas also undermines the idea that humans had a role to play, as Italy contains the first European appearance of AMH. Alternatively, the climatic downturn towards the LGM could have made Europe inhospitable to hyenas. While a

climate simulation suggests that most of southern Europe would have still been tolerable to hyenas during the LGM (Varela et al. 2010), the model time-bins radiocarbon dates. This artificially increases sightings of hyenas around the LGM and, consequently, their apparent tolerance of LGM climate conditions. (Such modelling issues are discussed more below, and the specific simulation is critiqued in Stuart and Lister (2014).) This leaves the southern half of the extinction story unclear, and AMH may yet feature in it.

2.2.4.2 Leopard (*Panthera pardus*) and cave lion (*Panthera spelaea*[3])

Leopards favoured southern and central Europe in the LP (Sauqué and Cuenca-Bescós 2013), though they have been found as far north as northern Germany and the UK (Currant 2004; Diedrich 2013). Cave lions had a broad range from the UK and Mediterranean through Siberia and Beringia (Kahlke 2014; Stuart and Lister 2011). Like modern leopards, LP leopards were solitary, but cave lions lived in small groups (Stuart and Lister 2011). Leopards sometimes dragged prey back to caves (Sauqué et al. 2016b), and both cats used caves for shelter and having kittens (Ghezzo and Rook 2015). There may have been competition for caves between cats, hyenas, and humans. Prey may also have been fought over; modern hyenas and lions steal kills from each other (Höner et al. 2002) and African leopards, lions, and hyenas have significant dietary overlap (Hayward and Kerley 2008).

Fewer dates are available of the large cats in Europe than of hyenas (chapters 5 and 15). The current reliable LAD for lion comes from Germany with a tooth dated to 12,375 ± 50 BP (OxA-17268), about a millennium younger than the most recent Mediterranean date (Stuart and Lister 2011). Interestingly, African lions expanded into southeastern Europe in the Holocene and were mentioned by Classical writers, though they retreated in the Iron Age (Sommer and Benecke 2006).

The picture for leopards is even less clear. The only direct dates from southern-latitude leopards come from pre-LGM contexts (Ghezzo et al. 2014; Ghezzo and Rook 2015). In Iberia, there are claimed terminal Pleistocene/Holocene leopard

[3]Sometimes *P. leo spelaea;* here the phylogeny of Barnett et al. (2016) is used.

remains at Las Pajucas (11.4 ka) (Altuna 1972) and El Juyo (13.29 ka) (Castaños 1983), but these are based on stratigraphic association. Though Holocene survival has not been demonstrated with direct radiocarbon dates, most leopards after 50 ka come from Iberia, where they seem to retract (Sanchis et al. 2015; Sauqué and Cuenca-Bescós 2013; Sommer and Benecke 2006).

Leopards continue to survive as a threatened species in Africa and Asia across diverse habitats (Stein et al. 2016). Modern leopards can live near human communities and snatch livestock and pets (Athreya et al. 2013), but Pleistocene humans did not bring commensal prey and could have easily chased off individual leopards. However, leopards had limited tolerance for the higher latitudes of LP Europe and their contraction into the Iberian peninsula may have been a consequence of habitat fragmentation during stadials.

In contrast, cave lions went extinct in the terminal Pleistocene. Their broader range across Siberia suggests they may have been better adapted to the Pleistocene steppe than the Mediterranean. The marginalisation of prey due to changing and retracting ranges may have cut cave lions populations off from key food sources. The rapid woodland expansion in the terminal Pleistocene/Holocene in southern Europe may have also been intolerable to cave lions, though exactly why is unclear: modern lions tolerated it when they moved into southeast Europe during the middle Holocene. Modern humans tend to kill lions as retaliation for livestock hunting rather than any particular territorial conflict (Lichtenfeld et al. 2015), but unlike modern lions, cave lions used caves for shelter. The challenge of finding caves for raising young without human interference may have additionally stressed cave lion populations.

2.3 Explaining LP fauna events

The loss of carnivores in Europe was part of a global extinction event that has usually been attributed to climate change, the arrival of AMH, or some combination of the two. From these three suspects, several models have been proposed (Table 2.3). Many of them arose from studying extinctions in North America, which

occurred more abruptly than in Eurasia. Those that have most currency in Eurasia are discussed here.

2.3.1 Climate change

Modern climate change is predicted to be responsible for the extinction of 15–37% of terrestrial species (Thomas et al. 2004), attesting to the potential impact of rapid climate change on species (Maclean and Wilson 2011). The Pleistocene certainly witnessed high-oscillation climate changes and the final shift to the Holocene, but these changes may have had more-or-less direct effects.

Some studies argue for a relatively direct role for climate change. Nogués-Bravo et al. (2010) found correlation with simulated climate change 'footprint size' and extinction scale in Europe, though not all continents conformed to this pattern. Lorenzen et al. (2011) correlated the demography of six Eurasian herbivores with climate change, though they argue two went extinct through a combination of humans and climate change. Their study has the additional time-depth of genetic data and population capacity estimates, but carnivores do not feature. Cooper et al. (2015) compared genetic events and extinctions/invasions to the Greenland ice core climate record. Unusually, they claim that turnovers rarely occurred during stadials but instead during the beginning of interstadials and the terminal Pleistocene. Earlier interstadials (>40 ka) did not seem to have the same impacts; the authors suggest humans in Europe after ~40 ka disrupted 'subpopulation connectivity' (Cooper et al. 2015, p. 605) and compounded the stress of climate variability.

While these studies find correlation between extinction and climate change, they have limitations. Lorenzen et al. (2011) and Cooper et al. (2015) omit several species due to lack of confidence in species' estimated extinction dates, and Nogués-Bravo et al. (2010) use a climate metric that overwrites stadial-interstadial variability. None of the studies discuss underlying ecological mechanisms and they assume species independence. Modern cases suggest that species interactions, particularly reduction in available food/prey, tends to be the proximate cause of extinction rather than intolerance of abiotic climate factors (Cahill et al. 2013),

Table 2.3: Popular explanations of the LQE. Based on Burney and Flannery (2005) and Koch and Barnosky (2006) with updated citations.

Theory	Description	Example	Comment
Climatic			
Habitat loss, fragmentation	Loss of suitable habitats due to climate change	Guthrie (1984)	Key theory for Eurasian steppe
Variability	Rapid loss-and-gain of habitat exceeds ability to disperse	d'Errico and Sánchez Goñi (2003)	More popular for Neanderthals but linked to refugia model
Self-organised instability	System collapse from systemic dynamics	Forster (2003)	Eurasia's extinctions too protracted
Co-evolutionary disequilibrium	Disruption of co-evolved animal-plant interactions	Graham and Lundelius (1984)	European species tended to be generalists, not specialists
Natural disasters	Megadroughts, single cooling event, bolide impact	Firestone et al. (2007)	Little attention in Europe–extinctions too protracted
Combined			
Coupe de grâce	Combined habitat loss and hunting doomed populations	Elias and Schreve (2007)	Popular for explaining Eurasian extinctions over time
Fire synergy	Herbivore decline (hunted) leads to landscape change through increased fires	Burney (1999)	Little evidence for landscape burning in Europe
Human			
Blitzkrieg	Rapid hunting of prey and carnivores to extinction	Martin (1984)	Extinctions in Eurasia protracted
Protracted overkill	As above but over a longer period of time	Stuart (1999)	More popular in Eurasia than blitzkrieg
Secondary predation	Extermination of predators leads to boom-bust of herbivore populations	Whitney-Smith (2001)	Difficult to identify in record–needs high temporal resolution
Keystone herbivores	Loss of megaherbivores leads to wider ecosystem collapse	Gill et al. (2009)	Causality reversed from habitat loss
Habitat alteration	Modification of habitats by humans, mostly through fire	Bowman (1998)	Discussed for Australia and islands; little evidence in Europe
Introduced species	Human-brought dogs, rats, livestock, etc.	Grayson (2001)	Discussed for Holocene island colonisations

though climate change is implicated as the disturber of ecosystems. Both Lorenzen et al. (2011) and Cooper et al. (2015) also invoke humans in their final explanations as additional stressors to climate change.

Others have focused specifically on habitat fragmentation, which increases extinction risk (Reed 2004). Modern case studies attest to the combined effects of climate change and habitat fragmentation (Lawton et al. 2010; Ramesh et al. 2016; Warren et al. 2001). To recolonize a habitat, a species' range had to be geographically interconnected; too much fragmentation could disrupt the pattern of megafaunal dispersal. Loss of species richness through increasing patchiness increases community fragility and can induce multi-species extinctions (Hanski 2015; Villard and Metzger 2014). Even if a dominant species appears abundant shortly after habitats become patchy, it will go eventually go extinct due to loss of other interdependent species and compound the number of extinctions (Tilman et al. 1994). The widespread presence of nonanalogue or disharmonious communities in the Pleistocene has been seen as evidence for greater habitat diversity than at present, since the required cross-section of environmental factors to maintain the communities no longer exists (Lundelius 1989). The loss of several of these environments coincided with the Holocene, but whether this fragmentation led to extinction would have been species-specific (Stewart 2008; 2009).

Today, humans contribute to habitat fragmentation and block re-colonisation from distant refugia. They separate suitable patches by modifying landscapes, and they stymy would-be colonisations by hunting individuals that encroach on human communities. The Pleistocene steppe in particular has been seen as prone to cycles of extinction and re-colonisation from distant refugia (Mann et al. 2015) that the arrival of humans may have disrupted (Lister and Stuart 2008).

While fragmentation is an important feature of modern ecology, it may not have been so relevant in the Pleistocene. Climate change tends to produce an overall range shift with fragmentation limiting a species' ability to follow that shift. Simulations of species' ranges and the impacts of temperature and AMH on these ranges have found not all species were fragmented by LP climate change. In Varela Sara et al.'s (2014)

range simulations, tundra species were negatively affected by LGM temperatures but temperate species were positively affected. Carotenuto et al. (2018) similarly found variation in temperature-dependent range changes between species. Basic climatic factors, though not necessarily more dynamic ones (*e.g.* seasonality or decadal-scale variability), do not explain all extinctions. Furthermore, Palaeolithic humans did not engage in significant landscape modification; modern human communities have a far more dramatic impact on population connectivity than Palaeolithic ones did.

2.3.2 Humans

In historical times humans have been ecologically calamitous. Humans hunt species to rarity or extinction; they modify habitats; they introduce exotic species, sometimes with disastrous results; and they exterminate pests. Archaeologically, these behaviours and their ecological impacts are clearest in island colonisations by agriculturalists; they are not so visible on Pleistocene continents (Wroe et al. 2004). The question is whether Palaeolithic hunter-gatherers were destructive enough to instigate continent-wide extinctions.

The classic model is overkill or 'blitzkrieg', where humans rapidly overhunted species to extinction. Martin (1984) laid out eight points of evidence in favour of global overhunting of which two are particularly key here: the LQE was too abrupt and acute to be due to stepped climate changes, and extinctions followed the footsteps of humans as they colonised each continent.

Despite plenty of detailed critiques of overkill (Barnosky et al. 2004; Elias and Schreve 2007; Koch and Barnosky 2006; Wroe et al. 2004), humans remain popular culprits in LQE papers (see review in Monjeau et al. 2017). However, Europe is often cast as an exception where AMH, if an agent of extinction, had a subtler role (Araujo et al. 2017; Koch and Barnosky 2006; Sandom et al. 2014). Neanderthals, once characterised as having limited tool making and hunting skills, made technological suites comparable to early AMH (Villa and Roebroeks 2014). This weakens the idea that humans were remarkably more efficient hunters than Neanderthals. Furthermore, species LADs are staggered over the past 50 ka;

some species coexisted with humans for tens of millennia and relict populations sometimes persisted into the Holocene (Lister and Stuart 2019; Vartanyan et al. 2008a). Some suggest this staggering reflects AMH's delayed colonisation of the high-latitude arctic, which required special technologies and knowledge of herd movements (Araujo et al. 2017; Barnosky et al. 2004). It is not clear whether this south/north split existed; as discussed below, obtaining absolute dates on Europe's southern species is particularly challenging and their absence from data sets could produce false patterns. There was no abrupt, single wave of extinction in Europe that would preclude climate change as a variable.

That said, humans could have prompted knock-on effects. Overhunting of prey and competitive exclusion for shelters may explain carnivore extinctions (Grayson and Delpech 2003). Humans overhunting keystone megaherbivores in particular could have instigated cascade effects that led to further extinctions (Owen-Smith 1987), though this requires that megaherbivores went extinct before carnivores, which is not clear. Conversely, second-order predation models a 'boom-bust' cycle in which humans primarily reduced predator populations through competitive exclusion and extermination. This resulted in a brief rise in herbivores before the overexploitation of flora caused niche collapses and herbivore extinctions (Whitney-Smith 2001). This 'boom' is difficult to identify from the fossil record as it would occur over a brief period; there is no clear signal in Europe. There is also little evidence that predator extinctions shortly predated herbivore extinctions.

2.3.3 Combined models

Given that both climate change and human expansion occurred concurrently, it is sensible to consider whether both had roles to play in the LP. Combined, climate and humans may have driven fauna from shrinking habitats and extirpated species. Prescott et al. (2012) find this to be the case across five landmasses, including their combined 'Palaearctic Eurasia'. Barnosky et al. (2004) also take a middling stance for Europe, arguing for two waves of extinction that saw warm-adapted species disappear in the lead-up to the LGM (~45–20 ka) and cold-adapted species at the

terminal Pleistocene (12–9 ka). They argue a significant demographic increase in AMH over Neanderthals stressed animal populations but allowed some to persist in high-latitude refugia away from humans. Elias and Schreve (2007) suggest humans were the 'coup de grâce' for stressed populations globally, including Europe. Bartlett et al. (2016) attempted to quantify the explanatory power of climate change and human arrival on extinctions, coming to a global estimate of 60% human, 25% climate, and 15% combined. Araujo et al. (2017) argue humans had even stronger explanatory power on the global scale; climate was an 'additive rather than synergistic' (p. 216) factor. However, neither climate variance nor human arrival dates were statistically correlated with most Eurasian species in their study.

Invoking both climate and humans sidesteps the polarity of the debate and enables discussions of how the two interacted to affect fauna. However, Prescott et al. (2012) and Barnosky et al. (2004) employ a 'long view' for climate over the past 700 ky that smooths over the heightened variability of the last 100 ky. This suppresses climate's significance on shorter timescales. Bartlett et al. (2016) look at the past 80 ky with a climate simulation binned to 4 ky averages which, while higher-resolution than the previous two studies, still elides abrupt climate events like Heinrich events. Araujo et al. (2017) manage millennial-scale resolution but cannot reject their null model (neither climate nor human arrival are connected to an extinction) for most Eurasian species. Barnosky et al.'s (2004) suggestion that warm-tolerant species disappear first in Europe relies on limited chronological data; Elias and Schreve's (2007) model would be supported with evidence of populations declining before AMH arrived, which again requires substantial chronological data for both AMH and fauna.

Attempting to disentangle the relative influence of two concurrent events on extinctions is challenging given the low temporal resolution of the climate and fossil data used in these studies. Europe often fails to follow the global narrative the authors favour. Extenuating explanations are given (high latitude refugia, coexistence with Neanderthals, *etc.*) but are not themselves being tested. While investigating the 'explanatory weights' (Monjeau et al. 2017, p. 201) of variables

is an important way of avoiding the stalled climate *vs.* humans debate, attempts have so far failed to clarify the Eurasian case.

2.3.4 Limitations of LQE studies

The cause of the disappearance of Pleistocene fauna has been debated since their fossils were discovered, yet studies continue to come to contradictory conclusions. There are many reasons for this (see Monjeau et al. 2017) but some are particularly relevant to Europe.

Global studies are looking for a broad pattern that Europe often fails to fit. Pleistocene Europe contained the two distinct Mediterranean and Palaearctic biogeographic zones. Lumping the two together conflates differences between their faunal histories and perhaps explains why studies sometimes find only weak causal signals in their European results. However, other continents contain multiple ecological zones too and do produce correlations, and dividing Europe into Mediterranean and Arctic regions does not always improve explanatory power (Araujo et al. 2017). Variations in data size and quality between continents also means Europe, which has comparatively large radiocarbon datasets and high-resolution climate records, might have its data coarsened for the sake of continental comparisons.

Even studies that look closely or exclusively at Europe struggle with small datasets (chapter 2.5.1). In general there is a bias towards considering Palaearctic species such as mammoth, woolly rhino, and bison, in part because they have larger chronological datasets than southern species (Lorenzen et al. 2011). Carnivores as well are underrepresented; Araujo et al. (2017) and Cooper et al. (2015) both included only cave bears and cave lions, for example, and did not consider carnivores as a separate group from herbivores. When Pleistocene carnivores are specifically considered, such as in niche tolerance models, their patterns sometimes differ from herbivores (Carotenuto et al. 2018; Varela et al. 2014), so conclusions reached about herbivores are not necessarily relevant to carnivores.

Differences in data and methods make studies incomparable and their conclusions contradictory. Approaches to climate data alone vary widely. Climate data may

come directly from ice core records (Cooper et al. 2015) or a simulation (Bartlett et al. 2016; Sandom et al. 2014). Data is time binned to different resolutions, from millennial-scale (Araujo et al. 2017) to simple pre- and post-LGM (Sandom et al. 2014). Time depth ranges from the last 50 ka (Cooper et al. 2015) to 700 ka (Prescott et al. 2012). Climate records may be temporally linked to fauna and archaeological dates in different ways, from essentially ignoring offsets (Araujo et al. 2017) to tying ice-core records to the radiocarbon calibration curve (Cooper et al. 2015). Different climate factors may be considered as well: annual temperature, annual rainfall, variance of rainfall or temperature, summer/winter versions of these, estimates of climate change 'velocity', and others (*e.g.* Araujo et al. 2017; Bartlett et al. 2016; Sandom et al. 2014). Ideally a model is robust to some parameter variations like time bin sizes (Araujo et al. 2017; Bartlett et al. 2016), but here entirely different parameters are being tested.

The statistical approaches also vary and are sometimes not robust. Araujo et al. (2017), for example, used binomial tests to assess whether climate variance and/or human arrivals are correlated with species' LADs. The human test compared the proportion of values from 1000 randomly-chosen time windows that were equal to or greater than the temporal distance between the species' LAD and AMH arrival. Results per species are not stable when repeated (Fig. 2.2) and results depend on the chosen time window (122,500 years in the paper). Cooper et al. (2015) used a chronological framework that increases the durations of several interstadials (Rasmussen and Svensson 2016), and Prescott et al.'s (2012) models are sensitive to the chosen human arrival date, which is debated in some of their tested regions (Lima-Ribeiro et al. 2012). More generally, results may not be replicable: though most papers include datasets in their supplementary material, none discussed here published model code or the complete results of climate simulations. Lack of model transparency is a larger issue in multi-parameter LP extinction simulations (Yule et al. 2014), but even in these comparatively simple tests data is manipulated enough that clearer methods and codes would be helpful.

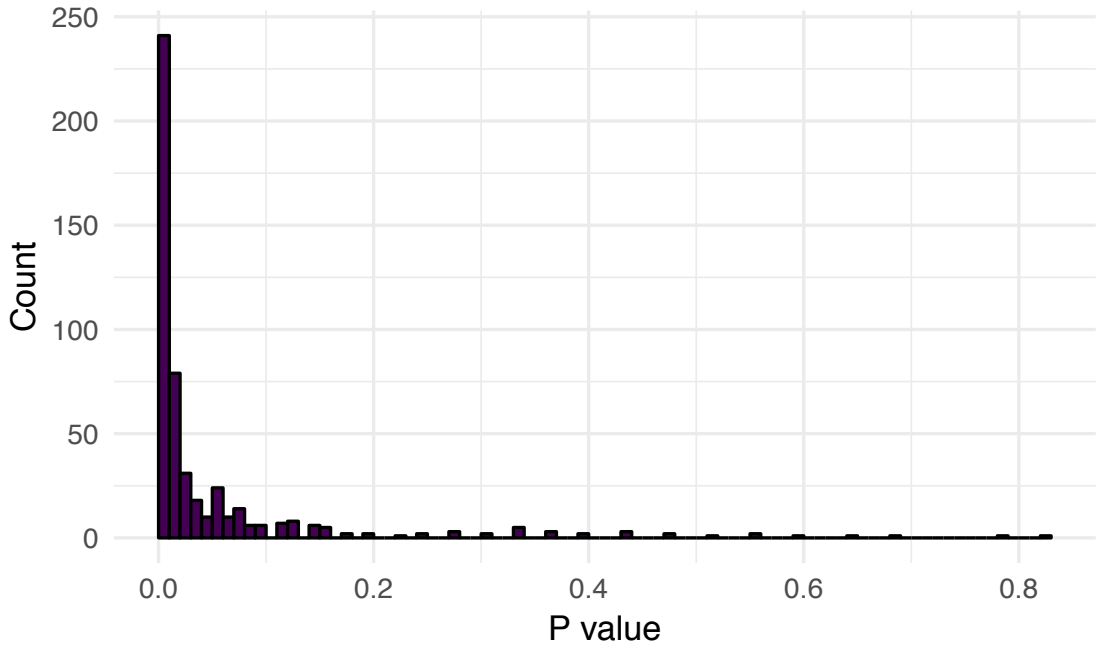


Figure 2.2: Binomial test of the temporal proximity of leopard LAD and AMH arrival in southern Europe using the methods and data in Araujo et al. (2017), repeated 500 times. P values vary between simulations, suggesting results (the authors reported p = 0.256) are not robust.

Other studies do not use statistical tests but consider spatio-temporal patterns of species individually (Sauqué and Cuenca-Bescós 2013; Stuart et al. 2004; Stuart and Lister 2011; Stuart and Lister 2012; Stuart and Lister 2014). This is a perfectly valid approach, especially when datasets are small and do not satisfy test assumptions (*e.g.* normality and random sampling). However, this approach cannot truly incorporate high-resolution climate data and relies on similarly non-quantified interpretations of archaeological events. It is also difficult to scale up to multi-species and multi-continent perspectives.

LQE papers are overwhelmingly focussed on extinctions rather than patterns of range shifts, local extirpations, and fauna assemblage dynamics. This is partly because LADs make simple, single statistical points to consider on a continental scale. There are papers considering range changes of individual species (Sauqué and Cuenca-Bescós 2013; Stuart and Lister 2011; Stuart and Lister 2012) and ecological niche modelling (Carotenuto et al. 2018; Martínez-Meyer et al. 2004; Varela et al. 2014), but few attempt to incorporate this high-resolution data into

climatic/archaeological models. Such resolution is unobtainable in global studies and for some European species, but there is scope to attempt a finer-grained study for Europe. This would allow inclusion of extirpations and not just complete extinctions in Europe (leopards), comparison of Mediterranean *vs* arctic patterns, and perhaps spatial trends in population responses to human colonisation of sub-regions (the Iberian peninsula, Italian peninsula, the Danube corridor, *etc.*).

Variation in methods and datasets make studies incomparable, and the tendency to take a global perspective overwrites subtleties of Europe's biogeographic history. Several European species remain little-studied and there is room to explore spatio-temporal patterns of species presence/absence in sub-regions of Europe.

2.4 Significance

Faunal events in the LP had profound consequences for ecological systems and prehistoric humans. The LQE is also the closest past case study for modern conservationists trying to mitigate the current anthropogenic extinction event.

2.4.1 Ecological consequences

Ecologically, Europe by the mid-Holocene was dramatically different from the LP. While climate change was the main driver, the loss of species and fragmentation of classic faunal suites had ramifications as well. The loss of large herbivores altered vegetation dynamics, contributing to canopy closure and loss of steppe tundra. Loss of carnivores prompted trophic cascades that reduced food web complexity and resilience.

Today, large herbivores are key players in maintaining an ecological system (Malhi et al. 2016). Browsing, grazing, and trampling limit canopy closure and encourage landscape heterogeneity (Bakker et al. 2016); digestion accelerates nutrient cycling, lateral distribution, and seed dispersal (Hobbs 1996); competition suppresses small herbivore abundances (Daskin and Pringle 2016); and juveniles and elderly members are prey sources for carnivores.

These dynamics also occurred in the LP (Doughty et al. 2010; Gill 2014; Whitney-Smith 2001). The closure of woodlands in Europe's Holocene could be due to reduced numbers of large herbivores that had maintained heterogeneous landscapes through browsing (Mitchell 2005; Owen-Smith 1987; Vera 2000). Modern livestock grazing in European floodplains can produce a mosaic of grassland and forest (Bakker et al. 2016) similar to what Pleistocene landscapes are thought to have been like, and large herbivores are implicated in maintaining modern savannah (Asner and Levick 2012) and tundra (Zimov et al. 2012).

Further north, Europe lost its 'mammoth steppe' to waterlogged tundra. Heavy grazing accelerated nutrient cycling and deep-rooted grasses, which encouraged transpiration and drier steppe; the loss of megaherbivores may have accelerated the transition to waterlogged tundra with low faunal biomass (Zimov et al. 2012). However, it is also possible that herbivore extinctions followed climate-driven vegetation changes, not *vice versa* (Graham and Lundelius 1984; Lister and Stuart 2008).

Carnivores maintain trophic structures. Their removal instigates trophic cascades as top carnivores regulate both abundances and behaviours of mesopredators and herbivores (Ripple et al. 2014; Ritchie and Johnson 2009; Terborgh et al. 2001). Removal of large species elevates abundances of smaller species; this signal is clearest in ecosystems with low primary productivity (Daskin and Pringle 2016). This 'can lead to simpler ecosystems with fewer interspecific interactions, shorter food chains, and less resilience' (Malhi et al. 2016, p. 842). However, while the role of modern carnivores is well documented, Pleistocene carnivores are less studied than the classic megaherbivores. Whitney-Smith's (2001) boom-bust model is one of the few to explicitly give carnivores a role in the LQE. That said, there are extant relatives to cave lions and cave hyenas, and the leopard survives outside Europe; these species all manage biodiversity and herbivore numbers (Ritchie and Johnson 2009).

2.4.2 Archaeological importance

The LP reorganised ecological webs and prey resources on an unprecedented scale for AMH. Humans succeeded in a global dispersal and became the sole hominid

when Denisovans and Neanderthals went extinct. In Europe, humans became the apex predator, but they also lost high-risk, high-yield megaherbivore prey. While the importance of the largest megaherbivores to AMH diets is debated (Stewart 2004), the Upper Palaeolithic saw increasing dietary breadth and investment in hunting small prey (Stiner and Kuhn 2006). Mobility of human groups remained high, but there was increasing evidence for seasonal stopovers in the form of housing, perhaps based around ungulate herds (Hoffecker 2005). The Holocene witnessed further decreased mobility amidst woodland closure (Holt and Formicola 2008; Lovis et al. 2006). These changes were not straightforward responses to megafauna extinctions—climate change and socio-cultural factors were also at play—but they were implicated.

Carnivore extinctions probably had little direct impact on human communities. Modern large carnivores do attack humans but not at high frequency (Löe and Röskaft 2004), and trophy and retaliation hunting of carnivores by humans is a far larger phenomenon (Karanth and Chellam 2009). There is little research on the ecological relationship between hunter-gatherers and carnivores. The Hadza of Tanzania scavenge predators' kills and find night hunting to be dangerous due to the likelihood of encountering lions and leopards (Marlowe 2004). The loss of large cats and hyenas in Europe may have reduced hunting risk for humans, though the survival of other carnivores would not have eliminated risk entirely. The loss of carnivores reduced competition for caves and the cascade effects mentioned above would have increased small prey numbers. The observed broadening of hunting strategies in the Palaeolithic may in part be a response to increased smaller prey.

2.4.3 Modern significance

Current rates of species loss are two to three orders of magnitude above background levels (May et al. 1995; Pimm et al. 2014). This extinction is anthropogenic, both directly and through human-driven climate change (Barnosky et al. 2011; Maclean and Wilson 2011). In the midst of this crisis the LQE gains importance as the past case study.

Large carnivores capture public imagination and garner disproportionate conservation attention (Sergio et al. 2006). Conservation strategies may assume that environmental factors or human interference are more pressing priorities. Understanding the mechanisms of past carnivore extinctions and their knock-on effects can inform such policies. Understanding resilience, refugia, and behavioural adaptability are useful for the same reasons.

If carnivore extinctions were human-driven, human destructive abilities were great even without a population of seven billion and the full might of industry and landscape reshaping. Extinct species were unable to coexist with humans; current survivors are evidently more resilient (Balmford 1996) but perhaps due to marginal ranges. If species are so fragile in human hands, then it will take more invasive conservation work, including reintroductions and maintenance of nature reserves, to ensure sustainable ecosystems (Donlan 2005; Malhi et al. 2016).

If climate variability emerges as the more destructive force, then habitat construction and preservation of biodiversity reservoirs become key to minimising future extinctions. More hands-off conservation strategies may be employed in exchange for focus on limiting climate change. Slowly-changing environmental variables are more fundamental than acute events in precipitating rapid ecosystem shifts (Dakos and Hastings 2013; Scheffer et al. 2001), which calls for strategies that retain overall resilience through factors 'such as land use, nutrient stocks, soil properties and biomass of long-lived organisms' (Scheffer et al. 2001, p. 596).

The LP's ecological changes affected all surviving species, including humans. Understanding the role of carnivores in this tumultuous past is the broad context of this research project.

2.5 Chronology and modelling faunal histories

Better understanding LP fauna histories requires both good data and appropriate analysis of that data. Both of these aspects are introduced here with further details in materials and methods (chapters 5 and 6) and modelling (chapter 7).

2.5.1 Need for improved chronology

To explore the relationship between fauna, climate, and humans, events must be placed on a common timeline. Climate records for the last glacial cycle can reach annual resolution (Rasmussen et al. 2014), and the arrival of AMH in Europe has long garnered research attention so that large-scale spatio-temporal models can be produced (Higham et al. 2014). The weak link is faunal chronologies.

The presence of a species in a region during climatic and/or archaeological events can only be established if the remains of specimens can be identifed, provenanced, and dated with sufficient accuracy and precision. Identification depends on visual expertise and recording of illustrations or photographs; otherwise techniques like ZooMS or genetics screening are required (Buckley et al. 2009; Lister and Stuart 2013). Provenence is largely a matter of excavation recording, but establishing chronology is a more complex undertaking. An excavation may find fauna in association with human artefacts or in a stratigraphic layer correlated to local environmental records (like pollen spectra), but these fortunate cases may only establish relative chronologies that are difficult to scale up to continental patterns.

Chronometric dating solves this problem by placing samples on an absolute timeline. Within the past ~50 ky, radiocarbon dating is the most direct and precise method of determining the age of fossils. This has made radiocarbon dating fundamental to LP chronologies (Bronk Ramsey 2008; Wood 2015).

Unfortunately, many chronological datasets for species are neither accurate nor representative. The lack of robust, precise chronologies is an enduring limitation in studying LP species. Without them, estimates of local and global disappearances will be inaccurate. Cooper et al. (2015), for example, omit some species from simulations because they lack precision in their terminal date estimates. Though the LAD can be used instead of more elaborate statistical extinction models, enlarging the dataset is necessary to mitigate the caveat that the LAD is a *terminus post quem* (Fiedel 2009).

The size of datasets varies by species. Eurasian mammoths have over a thousand vetted radiocarbon dates; straight-tusked elephants have two (Stuart

2005). Carnivores sit at the lower end: hyenas have about 100 direct dates from Eurasia (Dinnis et al. 2016; Stuart and Lister 2014), cave lions 95 (Stuart and Lister 2011), and leopards just a handful (Sauqué and Cuenca-Bescós 2013; Sommer and Benecke 2006).

There are multiple reasons why certain species have little chronological data. Some species have received more interest, particularly the classic steppe-tundra megaherbivores. There are fewer carnivores in archaeological sites and their remains are much smaller than mammoths—they are not often a researcher's first choice for destructive sampling. There has also been a lack of appreciation for the importance of directly dating the specimen of interest as opposed to dating bulk soil or other species from the same stratigraphic layer. Finally, radiocarbon dating is challenging, if not impossible, for specimens that come from sites of poor collagen preservation.

Poor preservation explains the dearth of dates from southern Europe: heat and aridity both degrade collagen (Hedges 2002). This also contributes to imbalances in dataset sizes since steppe species are more likely to be well-preserved. There are no reliable direct dates from Mediterranean-dwelling pygmy hippos, for example, and of the ~100 hyena dates, only six come from Italy, Greece, or Spain. This geographical imbalance limits the robustness of LADs and the ability to identify spatio-temporal patterns such as range contractions. If understanding of LP species is to improve, it is critical to address these chronological problems.

2.5.2 Improving chronological data

Improving the size of species radiocarbon datasets is only helpful if the dates are accurate and precise enough to answer the research question. Criteria for building robust chronologies reflect both logical and methodological considerations. The following have been summarised from Waterbolk (1971) and Wood (2011):

1. *Samples must be logically related to the event of interest.* Dating an identified bone of a leopard will reflect the time since death of that organism. Dating a deer bone from the same layer requires extra assumptions about the security of

the stratigraphic layer and the speed of its formation, which logically distances the date from the event of interest. It is best to stay as close to the event of interest as possible.

2. *The sample must be a closed system.* Samples must be chosen with post-depositional behaviour in mind. Bone collagen is generally a reliably closed system, for example, but bone apatite is known to exchange carbon with groundwater (Zazzo and Saliège 2011).
3. *The laboratory method removes exogenous contaminants without introducing contaminants.* Ideally there are ways of checking the completeness of contaminant removal. Introduced contamination can be subtracted from the result as a background so long as it is consistent; there should be quality checks in the lab protocol.
4. *Calibration and Bayesian modelling are done when possible, with transparent models and robustness checks.* Calibrating dates to calendar years enables comparison with other chronologies such as climate records. Bayesian modelling combines multiple kinds of information to build chronological models.

These criteria are discussed in more detail with sample selection and date evaluation criteria (chapter 5).

2.5.3 Modelling spatio-temporal data

Chronological data can be analysed to reveal patterns through space and time. Bayesian modelling of radiocarbon dates in software like OxCal (Bronk Ramsey 2009) is a fundamental aspect of archaeological interpretation today. It is a powerful tool in archaeology as it allows multiple kinds of information to be combined in statistical models. Radiocarbon dates are calibrated, putting them on a common calendar age, and chronological models are built that incorporate multiple kinds of evidence. Such statistical methods can identify outliers, compare the likelihood of interpretations, increase precision, and obtain estimates of chronological events such as phase durations. A full review of Bayesian modelling is beyond the reach of this thesis, but the basic principles and tools are introduced in chapter 7 and

many useful discussions exist (Bayliss 2009; Bronk Ramsey 2009; Bronk Ramsey 2017; Litton and Buck 1995; Pettitt and Zilhão 2015).

There is potential to explore paleontological data using a Bayesian approach. Studies regularly calibrate radiocarbon dates and archaeologists use phase models to estimate AMH arrivals (*e.g.* Douka et al. 2014; Higham et al. 2014; Wood et al. 2016). Few palaeontology papers go beyond calibration to build more complex chronological models. This is largely unnecessary when dealing simply with LADs, but extinction dates can also be estimated with a Bayesian approach.

LADs suffer two key analytical weaknesses: they are almost certainly not 'true' last dates for a species but a *terminus post quem*, and they reduce extinction to a single event in space and time when in reality extinction 'is usually the product of spatially-heterogenous population declines over time' (Carlson et al. 2018b, p. 3). An extinction estimate that accounts for LADs being too early could more accurately match a species' extinction to contemporaneous climate and archaeological events. Understanding spatio-temporal patterns of LP fauna would allow for more nuanced discussions of fauna resilience to AMH movements and climate effects.

There are methods for addressing both limitations. Extinction estimators have been developed for ecology and palaeontology, with a popular one in palaeontology being the Gaussian-resampled, inverse-weighted McInerney et al. method (GRIWM) (Bradshaw et al. 2012; Saltré et al. 2015). This estimator incorporates the uncertainty in radiocarbon dates and reduces bias compared to the LAD, though the resulting estimate has reduced precision. The GRIWM method also performs best when the underlying extinction distribution is not abrupt (*i.e.* not logarithmic or uniform), which is an assumption that might be challenged for LQE extinctions. Solow and Beet (2014) created an ecology Bayesian extinction date estimator based on species sightings. The estimator allows for sightings to be weighted by confidence so that amateur bird sightings, for example, can be down-weighted relative to a verified photograph. This estimator has been incorporated into the R package `spatExtinct` that interpolates extinction estimates across a map, creating a spatially-explicit extinction date surface (Carlson et al. 2018b). Georeferenced sightings can be

interpolated over a generic raster grid or a species distribution model produced by a package such as `dismo` (Hijmans et al. 2013) or `biomod2` (Thuiller et al. 2014).

`spatExtinct` was developed for modern ecological data, but in theory paleontological data can be used. 'Sightings' become georeferenced radiocarbon dates and the plausibility ranking can account for the reliability of the date. Species distribution models have been successfully produced from paleontological data (*e.g.* Carotenuto et al. 2018). This approach would add a spatial dimension to extinctions, creating a spatio-temporal model. The downside to the Solow and Beet (2014) estimator is that it does not include chronometric errors, so some average value for dates has to be used.

Another approach is to remove space as a parameter and instead divide Europe into multiple, independently-considered regions. This approach easily allows temporal uncertainty to be incorporated into Bayesian chronological models. In OxCal, phase boundaries can model AMH arrival in the region based on given archaeological radiocarbon dates, which can then be compared to the region's LAD or estimated extinction. Outside of OxCal, statistical models like linear models can be used to evaluate the relative explanatory power of climate and human activity on a species' disappearance while accounting for autocorrelation of time series (Bolker et al. 2009; McCullagh 1983). These approaches depend on sensible geographic subdivisions and requires that each region have a large enough dataset to produce meaningful results, but it does straightforwardly account for chronological uncertainty in data in a way that modern ecological extinction estimators do not.

Levels of 'activity' of a species through time may also be modelled. While simply summing radiocarbon dates (Broughton and Weitzel 2018; Crema et al. 2016) is overly influenced by the calibration curve and sampling biases (Bronk Ramsey 2017), other methods have been explored. Kernal density estimation (KDE) is one such approach which can be easily modelled in OxCal (Bronk Ramsey 2017). KDE is a frequentist statical approach which does not presuppose an underlying distribution in the observed dates; the result needn't be normal and the peaks in the distribution may reflect 'activity'. Careful interpretation is needed, with particular

account taken of sampling biases, but in general KDE models of radiocarbon dates are less influenced by the calibration curve (Bronk Ramsey 2017).

Modelling is a tool for exploring data and different approaches have pros and cons. Using multiple approaches allows the data to be explored from different angles and informally tests the robustness of the data to different analyses.

2.6 Conclusions

The Late Pleistocene saw the previous great extinction event, but it remains poorly characterised in large parts of the world. Europe's classic steppe species have relatively large chronological and genomic datasets, but southern Europe and its carnivores are not among these well-studied species. There are holes in the data, both in chronology and space. Carnivores perform important ecological roles and interact with humans in different ways from herbivores; they are worth better understanding, and they cannot be assumed to have followed herbivores' histories. Southern Europe is neglected largely because of issues of collagen preservation in warm climates, which makes radiocarbon dating specimens challenging. Therefore radiocarbon methodology is an important facet of improving datasets and testing whether carnivore distributions correlate with climatic or archaeological events.

3 Radiocarbon dating poorly-preserved bone

3.1 Diagenesis of bone

While a variety of organic materials can be radiocarbon dated, bone collagen is the key material in palaeontology. Bone is associated with the event of interest—the death of the animal—making it preferable to more tenuously connected materials (Waterbolk 1971). It is also a common material in sites. Bone is only 20% organic, but the inorganic hydroxyapatite has been shown to exchange carbonates with groundwater, making it a difficult dating material (Zazzo and Saliège 2011). Collagen (85–90% of the total organic component) is instead routinely targeted.

For radiocarbon results to be accurate, samples must be free of contaminating carbon, which can distort apparent ages. This effect is increasingly dramatic as material approaches radiocarbon's limit of ~50 ka BP: 1% modern carbon contamination will decrease a 40 ka BP sample's apparent age to 33 ka BP (Bronk Ramsey 2008). Contamination may enter a bone during deposition, post-excavation storage, or laboratory handling. In practice this means that many Pleistocene radiocarbon determinations are suspect (Higham 2011).

Samples must also have sufficient endogenous carbon for measurement. Collagen

is prone to degradation over time, particularly in hot or hydrologically active environments (Hedges 2002). Diagenesis of bone, and specifically collagen, is complex and not very well understood. Microbial action and hydrolysis appear to be common mechanisms of collagen degradation with burial conditions like soil pH, hydrological action, temperature, and physical erosion all contributing (Hedges 2002; van Doorn et al. 2012). Collagen abundance also tends to drop off abruptly after a period of comparative stability, with an inflection point around 0.5% collagen by weight of the sample bone (% wt) (Dobberstein et al. 2009; van Doorn et al. 2012; Pestle and Colvard 2012). Collagen contains acid-soluble and acid-insoluble fractions (Elster et al. 1991); the soluble fraction may preserve better in arid environments than the insoluble fraction (Goldenberg et al. 2017; Marom-Rotem et al. 2012; Olsson et al. 1974). There is some evidence that peptides and individual amino acids in collagen are affected differently, such as hydrophylic glycine being lost in wet environments, glutamine being prone to deamidation, and carbon-rich amino acids being prone to bacterial action (Cleland et al. 2015; van Doorn et al. 2012; Wilson et al. 2012). However, overall collagen composition seems to remain stable until collagen preservation is marginal (<0.5% wt) (Pestle and Colvard 2012), which is relevant to bone quality indicators for radiocarbon dating (chapter 3.2.1).

Minerals and elements in the burial environment can exchange with bone. Humics, complex large molecules found in soil, may cross-link with collagen and perhaps stabilize (and contaminate) it (Hedges 2002). Bone mineral absorbs many exogenous elements from the burial environment, including uranyl, fluoride, strontium, and mercury (Hedges 2002), but only mercury seems to affect collagen preservation (as an antibacterial agent) (Ochoa-Lugo et al. 2017). The mineral fraction may also recrystallise and precipitate secondary minerals like calcite, though how recrystallisation affects collagen loss is not clear (Collins et al. 2002; Trueman et al. 2008).

The mechanisms of bone diagenesis are incompletely characterized, but it is known that time, high temperature, and hydrological activity all degrade collagen alongside further site-specific issues like bacterial action and mineral subsitutions.

Collagen loss occurs without altering the remaining fraction's composition until only marginal amounts remain, after which its components are altered in unequal ways. Deamidation of specific nitrogen-rich amino acids, for example, would reduce nitrogen abundance faster than carbon, creating a high CN ratio (see below). The behaviour of soluble and insoluble protein fractions possibly varies. These processes affect which samples can be successfully radiocarbon dated.

3.2 Screening developments

3.2.1 %N screening

It is impossible to evaluate the collagen content of a bone from visual inspection. The ORAU currently measures nitrogen content by mass (%N) of bone samples as a screening test for collagen content. Nitrogen exists in the proteinaceous component of bone rather than the mineral, so it is thought to be a proxy for collagen content. To pass, a sample must have >0.76% N and produce >1% wt collagen (Brock et al. 2010b). In practice, however, bones as low as 0.5% N may be passed, especially if the sample is of special significance or from a site that produces no higher %N samples (Brock et al. 2012). Brock et al. (2010a; 2012) tested different potential bone quality indicators (*e.g.* colour, hardness, CN ratio) and found %N to have the strongest predictive value. When %N is over 0.76%, 84% of bone samples successfully produce >1.0% wt collagen (Brock et al. 2012). However, this success is lower for bones >25 ka BP. The authors suspect this is due to a greater proportion of collagen being degraded into short-chain fragments which are lost during ultrafiltration.

Aside from %N, the atomic CN ratio is used as a quality indicator both for whole bone and collagen (Van Klinken 1999). Modern collagen has a CN value of 3.21 (Ambrose 1990); Brock et al. (2010b; 2010a) suggest the acceptable range to be 2.9–3.5. When whole bone is measured at the ORAU, the CN ratio rises significantly in low-collagen samples as the proportion of nitrogen is reduced. Some samples with high CN ratios still produce enough collagen, but samples with CN above 6.5–7.0 become increasingly likely to fail (Brock et al. 2010a; Brock et al. 2012).

There remain uncertainties with %N measurement on bone. While a very high (>4) %N indicates contamination (4% is about the value of living bone), an acceptable %N range may be a combination of bone collagen and exogenous proteins and/or humics. Particularly in Palaeolithic bone, %N may also constitute degraded proteins that can pass through ultrafilters used in pretreatment (Brock et al. 2012). This may explain why 58% of poor-quality samples with a %N of 0.75–0.99 still failed to produce 1% weight collagen (Brock et al. 2012).

It is also unclear how %N—and, by extension, collagen content—varies across a bone. Less than 5 mg of bone powder is required for a %N measurement, drilled from a single spot on the bone, while radiocarbon pretreatment usually requires 500–700 mg of crushed bone (Brock et al. 2010b). It is possible that, in bone of variable preservation, remaining collagen could be present in different locations in the bone. Variation in %N from the same bone has been observed (Brock pers. comm.) but not studied in detail.

3.2.2 Other methods of bone quality analysis

Other methods for bone quality screening have been used, including radiography (Sołtysiak et al. 2018), scanning electron miscroscopy and dispersion energy spectroscopy (SEM-EDS) (da Cruz et al. 2007; Ochoa-Lugo et al. 2017), and infrared spectroscopy (IR) (Brock et al. 2018; Fernandes 2013; Lebon et al. 2016). Combined use of X-ray and thermal neutron radiography (TNR) was used to create a visual map of protein presence in bone, which could be valuable in identifying regions of highest preservation in valuable samples (Sołtysiak et al. 2018). The method is nondestructive but requires expensive instrumentation not present in radiocarbon labs; TNR and X-ray are also not automated to screen multiple samples.

IR, particularly attenuated total reflection Fourier transform infrared spectroscopy (ATR-FTIR), is more convenient in that sample preparation is minimally destructive and analysis is rapid. IR has been used to assess the mineral fraction of bone for health and isotope analyses (Beasley et al. 2014; Boskey and Camacho 2007; Cersoy et al. 2016; Lloret et al. 2006; Paschalis et al. 2011), but there are fewer

cases that specifically assess samples for collagen preservation or contamination. Using ATR-FTIR, the peak ratio of amide and phosphate bands in the spectra (I/PO_4) approximate the collagen content of the bone. Lebon et al. (2016) calibrated the ratio to quantify bone collagen content, and while results were in good agreement with %N values down to 0.7, the method only reliably detected samples with %N >0.5.

IR can also detect contaminants. Fernandes (2013) used ATR-FTIR to assess collagen quality of samples from different radiocarbon pretreatment protocols, and Brock et al. (2018) used FTIR to check the effectiveness of pretreatment protocols at removing known contaminants. While FTIR lacks the sensitivity to quantify collagen content in low-collagen bones or very trace amounts of contamination, it is a quick method for evaluating samples.

SEM-EDS allows visual study of bone samples and measurement of element composition, both of which can reveal diagenic alterations. SEM-EDS has been used to identify mercury substitutions and mineralisation of collagen fibrils in vertabrae from mercury-rich burials, for example (Ochoa-Lugo et al. 2017). Elemental mapping of a sample can identify collagen and/or hydroxyapatite presence (da Cruz et al. 2007). SEM-EDS is inefficient as a screening method as samples are individually prepared on stubs and usually gold or carbon coated, but in special cases it is useful to investigate contaminants and diagenic processes.

The above methods are limited either by having to evaluate individual samples manually (X-ray, TNR, SEM-EDS) or by sensitivity limits (FTIR). However, they are able to characterise samples and contaminants in a way that rapid-screening %N cannot, making them a useful complement when investigating the quality and character of samples.

3.3 Pretreatment developments

Pretreatment chemistry is designed to isolate autochthonous carbon and remove exogenous carbon from bone. Many types of contaminants may be present, including

degraded proteins from soil or bone (van Klinken and Hedges 1995), humics (humic acids, fulvic acids, and humins), salts, museum preservatives, and others (Brock et al. 2013a). Strictly speaking, most radiocarbon pretreatments do not isolate collagen, but a more complex gelatinous mix that includes collagen. These 'protein remnants' (Brown et al. 1988) make up what is usually dated.

Today pretreatment at the ORAU is based on acid-base-acid (ABA) washes and gelatinisation, followed by ultrafiltration or HPLC.

3.3.1 ABA

Bone was once considered a problematic material for radiocarbon dating (Taylor 1987) and pretreatment methods struggled to find a balance between contaminant removal and sufficient collagen retention (Evin et al. 1971). While the acid-alkali method was developed in the 1960s (Berger and Libby 1966), it failed to remove all contaminants (Arslanov and Svezhentsev 1993). Longin (1971) introduced combined acid and gelatinisation. After soaking a sample in 8% HCl for 2 hr, samples were soaked in 3 pH water at 90° C for several hours. The collagen solubilised in the water, whereas other materials, particularly sedimentary and mineralogical carbonates, remained in the acid residue and could be separated by centrifugation prior to dating. Results agreed well with other materials (charcoal, wood) of the same age. While a significant improvement, this did not remove all contaminants (Gurfinkel 1987). Later, an additional base wash before gelatinisation was introduced to remove humics (Arslanov and Svezhentsev 1993). Another acid wash followed, as CO_2 can be absorbed during the base wash. A variant of this acid-base-acid treatment is still used at the ORAU (Brock et al. 2010b).

ABA requires significant manual handling and several stages of centrifugation and pouring, which introduces risk of sample loss and lab contamination. It typically takes ~36 hr to complete gelatinisation. Attempts to quicken or automate the process (Hedges et al. 1989) have not been retained by the lab (Brock et al. 2010b). In part this is due to individual variation between samples. Large samples may need an additional acid wash to completely demineralise, for example.

Particularly in Pleistocene samples, ABA bone dates can disagree with other kinds of ages (*e.g.* thermoluminescence dates or radiocarbon dates from other materials) (Higham et al. 2009). Similarly, charcoals dated by ABA become asymptotic as they approach radiocarbon's age limit, suggesting ABA does not completely remove contamination (Chappell et al. 1996). While ABA remains the fundamental basis of modern pretreatment protocols (Wood 2015), it is rarely in itself sufficient for producing reliable dates on Pleistocene bone.

3.3.2 Ultrafiltration

The gelatin obtained from the ABA method is not strictly collagen but a mix of proteins and possible contaminants. Collagen chains are large: α peptide chains 90–120 kilo Daltons (kDa), β dimers ~200 kDa, and complete collagen molecules 285–300 kDa (Zhang et al. 2006). However, collagen may degrade into small protein components both as a process of diagenesis and during gelatinisation, and gelatin may contain small contaminants such as fragmentary proteins, salts, and small humics. Brown et al. (1988) hypothesised that removal of these smaller materials would improve purity of the final gelatin. When they passed gelatin through ultrafilters of 30 kDa, they found several radiocarbon ages of the ultrafiltered (>30 kDa) samples were older than their <30 kDa fractions. This discrepancy was most pronounced in the oldest samples (>40 ka BP).

The ORAU currently uses a modified version of the Longin (1971) ABA procedure with 30 kDa ultrafiltration (Brock et al. 2013b; Brock et al. 2010b; Brock et al. 2007; Bronk Ramsey et al. 2000; Bronk Ramsey et al. 2004b). Comparison with ABA-only pretreatment has shown improved results, usually in the form of older ages in pre-Holocene material (Bronk Ramsey et al. 2004b; Higham 2011; Higham et al. 2006b). In some cases, samples treated by ultrafiltration 'age' several millennia compared to previous results. Results obtained through ultrafiltration are also generally considered more reliable. For example, age discrepancies in ultrafiltered bone samples from the Palaeolithic Grotte du Renne sequence are attributed to stratigraphic mixing rather than sample contamination (Higham et al. 2010).

However, ultrafiltration does not remove larger (>30 kDa) contaminants such as some humics or glues (van Klinken and Hedges 1995). Brock et al. (2013a) also found that the final filtered product contains diverse compounds, including non-collagenous proteins and inorganic substances, and no particular protein was completely removed. Some identified proteins came from human skin, implying handling contamination, and some <30 kDa material remained. Sample material is also lost from filtration and increased handling. Gelatinisation can partially degrade collagen, so some desired collagen may be lost in the <30 kDa fraction. The lost material sometimes makes ultrafiltration unfeasible, such as for small, low-collagen samples. While demonstrably an improvement in accuracy, ultrafiltration does not make low-collagen bone more accessible.

3.3.3 Chromatography

ABA and ultrafiltration approximately isolate collagen, but there have been attempts to target specific bone components like CO_2 from peptide bonded amino acids (the ninhydrin method) (Nelson 1991; van Klinken and Hedges 1995), collagen-specific peptides (Hedges and Van Klinken 1992), and specific amino acids. These attempts have often come with partial success and/or impracticalities that have prevented their routine use.

The amino acid hydroxyproline (Hyp) is often revisited because it makes up 12% of collagen by mass but is otherwise rare in nature. It is formed from proline after being fixed in the collagen matrix with an enzyme absent in bacteria (Hall and Cannon 2002; Stafford et al. 1982). Dating only Hyp would represent a 'gold standard' in bone sample purity. Dating multiple amino acids (AAs) would also be advantageous over an ultrafiltered aggregate, as fragmentry protein chains <3.5 kDa are not lost during HPLC and potential contamination from bacterial proteins *etc.* are unlikely to be a significant problem (Brock et al. 2013a).

High performance liquid chromatography (HPLC) has been used to separate amino acids for decades, but early protocols were often time-intensive; required large samples; and introduced carbon from columns, resins, derivitizations, and/or

extra handling. A continuous-flow HPLC was routine at the ORAU for a time (Law and Hedges 1989), but it was stopped due to problematic column bleed, most pronounced in low-yield collagen samples (Brock et al. 2010b).

Nonetheless, experiments sometimes yielded promising results. Ho et al. (1969) used liquid chromatography to isolate bulk AAs from Pleistocene bone saturated with tar. Later, Stafford et al. (1982; 1988) targeted proline and hydroxyproline with a resin column and chemical separations, but the results were mixed. A quicker process combined five AAs for radiocarbon dating, which required smaller starting samples and successfully dated some bone with only 0.1–0.2% N (Stafford et al. 1991). Gillespie et al. (Gillespie et al. 1984; Gillespie et al. 1986) used HPLC to isolate amino acids in bulk, and injection on a second column could isolate Hyp. Unfortunately results tended not to be reliable on low-collagen samples >20 ka (Gillespie et al. 1986). Van Klinken et al. (1994) used HPLC to separate the tripeptides GlyProHyp and GlyProAla, but poorly preserved samples distorted the chromatogram to the point that peaks could not be isolated.

Van Klinken and Mook (1990) introduced a faster protocol that did not require derivitization. Five amino acids could be separated in a 145-minute run, and further AAs could be isolated by re-injecting material. Reversed-phase HPLC avoided the issue of isotopic fractionation over a peak seen in ion-exchange HPLC. O'Connell and Hedges (2001) used this system to demonstrate its usefulness for dietary isotopic analysis, but it required large starting samples and had limited precision.

HPLC was revisited more recently at the ORAU. The procedure to isolate five AAs, including Hyp, was described in McCullagh et al. (2010). Applications of dating Hyp followed (Marom et al. 2013; Marom et al. 2012; Nalawade-Chavan et al. 2014a; Nalawade-Chavan et al. 2014b). Successes included significantly older ages from early-mid Upper Palaeolithic human remains at Kostenki 14 and Sungir, Russia. A low-collagen (0.3% N) horse bone from Kostenki 14 was successfully dated, but as only Hyp was selected the starting weight was very large (140 g of bone with 30 mg hydrolysate injected) (Marom et al. 2013). A Neanderthal

treated with a collagen-based glue, however, did not produce helpful radiocarbon results (Marom et al. 2013).

More recent improvements to the protocol have demonstrated the value of dating Hyp in Palaeolithic samples (Devièse et al. 2017; Devièse et al. 2018). This approach is particularly valuable when samples have been treated with conservatives or glues. It is not always used, as it is challenging to extract sufficient Hyp from low-collagen samples and requires additional time. HPLC and ultrafiltration offer trade-offs depending on the size, age, treatment, and significance of the sample.

3.4 Improving collagen yields

There are potential benefits to increasing the collagen yields from pretreatment, especially when samples are of low preservation. Greater yields can enable dating of otherwise too-small samples and increase the proportion of samples that are suitable for HPLC. Whole sites sometimes remain undated due to poor preservation, a challenge that will only be solved with improved pretreatments.

While HCl is the usual agent for demineralising bone in radiocarbon labs, it has some limitations. There is variation in the way HCl and the compounds in bone interact. Theoretically, HCl breaks down the mineral components of bone, but it may also attack peptide bonds (Pestle 2010). Poorly preserved bones may be more susceptible to this, perhaps due to fragmented peptide chains or the accumulation of crosslinks with humics (van Klinken and Hedges 1995). A fraction of bone protein is acid-soluble and therefore discarded during the ABA protocol (Elster et al. 1991). HCl-treated samples cannot be used for DNA analysis either; this can be frustrating when trying to reconstruct population histories with a combination of genetics and radiocarbon dating as multiple samples are required.

Two alternative approaches to collagen extraction, EDTA and dialysis, were selected here for experiments based on promising results in previous research and their potential for improving yields in low-collagen samples.

3.4.1 EDTA

EDTA, a chelator, has been used in other disciplines to decalcify bone. EDTA is routinely used to produce thin-sections in histology (Castania et al. 2015) and in aDNA studies (Kemp et al. 2014), and it has garnered attention for radiocarbon dating since the 1970s (El-Daoushy et al. 1978; Masters 1987; Olsson et al. 1974; Olsson 2000).

More recently Tuross (2012) successfully used EDTA to decalcify ~500 mg whole-bone pieces. This could minimise handling losses from repeatedly pouring off HCl from crushed/powdered samples, reduce losses of acid-soluble protein (EDTA dissolves around pH 8), and might retain fragmentary proteins better than ultrafiltration. The sample can also be used for DNA analysis, as Korlević et al. (2018) demonstrated with a combined EDTA-ABA protocol for DNA and radiocarbon dating.

There are three challenges to using EDTA. First, EDTA is slow-acting: at room temperature, decalcification approaches its maximum in thin-sections after about five days (Kiviranta et al. 1980; Sanderson et al. 1995) and thicker pieces can take weeks (Callis and Sterchi 1998; Castania et al. 2015; Shah et al. 1995; Tuross 2012). Second, EDTA contains carbon, so its removal prior to graphitisation must be thorough (Olsson et al. 1974; Tuross 2012; Korlević et al. 2018). Third, studies specific to radiocarbon have not always found EDTA yields to be higher than HCl or the final dates to be more accurate (El-Daoushy et al. 1978; Hedges and Van Klinken 1992; cf. Olsson 2000).

Protocols using EDTA vary. Several add acidic buffers (Castania et al. 2015; Pérez-Heredia et al. 2008). Others vary EDTA concentration, frequency of solution replacement, total time, size of starting samples, volume of solution, and temperature. Agitation and microwaving have been used with mixed results (Callis and Sterchi 1998; Imaizumi et al. 2013; Madden and Henson 1997; Sangeetha et al. 2013). The most efficient decalcification protocol, designed for histology, placed the solutions in a microwave at 45° C for 10–15 hr (Madden and Henson 1997), but this has not been tried for crushed bone. Tuross' (2012) paper specifically uses EDTA

for radiocarbon pretreatment, but the use of whole bones soaked for weeks in EDTA is impractically slow.

Few have tried comparing EDTA to modern HCl pretreatment. El-Daoushy et al. (1978) found EDTA results to be more accurate compared to the Longin (Longin 1971) method, and when Tuross (2012) compared EDTA and HCl across six bones, only one pair fell outside one standard deviation of each other. However, neither study compared EDTA to ultrafiltered samples. Korlević et al. (2018) used the ABA-ultrafiltration protocol after a sample was soaked in EDTA for DNA extraction; the radiocarbon results agree with just ABA-ultrafiltration results, but the study does not date a fraction decalcified solely with EDTA. EDTA has not been combined with HPLC for radiocarbon dating, though HPLC has been used to separate EDTA in pharmacology (Narola et al. 2011).

EDTA is routinely used in genetics and histology to decalcify bone. If it is at least of comparable effectiveness to HCl, it could be a useful agent, as a single sample could be divided for dating and genetics analysis. There is also reason to hypothesise that EDTA may destroy less protein than HCl, so that poorly-preserved samples may have higher collagen yields through EDTA decalcification.

3.4.2 Dialysis

ABA isolates collagen that remains insoluble in acid but some collagen peptides are acid-soluble and lost during ABA treatment (Elster et al. 1991). It is possible that bones may retain some acid-soluble proteins even if there is little insoluble collagen left (van Doorn et al. 2012). Being able to isolate and radiocarbon date this soluble fraction could be a useful option for bone with little preserved collagen.

Dialysis has been used in the past on collagen (Berger et al. 1964; Hassan and Hare 1978; Marom-Rotem et al. 2012; Olsson et al. 1974) and osteocalcin (Ajie et al. 1991). Acid-soluble peptides spontaneously recombine into collagen chains when the solution pH is raised (Burjanadze and Bezhitadze 1992); dialysis in water removes salts and recombines solubilised proteins into a precipitate that can be dated. The use of 3.5 kDa dialysis tubing would remove small contaminants similarly

to ultrafilters through osmosis. However, in these earlier studies dialysis was slow and the results not better than the Longin method. Recently Goldenberg et al. (2017) used dialysis to date bones from Israel, a hot and arid region. While the dates did not always agree with the insoluble-fraction dates, they were able to date some bones with the soluble fraction even when there was insufficient insoluble collagen.

The potential of dialysis is in recovering protein that would otherwise be lost in the ABA protocol and combining the two yields to date low-collagen bones. Even if dialysis is not as effective at purifying samples as ultrafiltration, if enough material is recovered then the combined protein fractions can be put through HPLC to isolate amino acid(s). Further work is needed to characterise the dialysis preciptitate and establish whether the recoverable acid-soluble fraction is large enough for HPLC separation.

3.5 Conclusions

Radiocarbon dating low-collagen bone is a persistent challenge. It can be difficult to identify the best bones for destructive sampling and current pretreatments require trade-offs between accuracy and sample size. Ultrafiltration and HPLC both improve the accuracy of Pleistocene radiocarbon results but require larger starting samples due to increased sample losses. Demineralisation with HCl is a component of both ultrafiltration and HPLC protocols, but significant material can be lost during HCl soaking and rinsing. A method that improves collagen yields relative to HCl would increase the number of samples that could be dated reliably, either with ultrafiltration or HPLC.

Before deciding to treat a bone, the ORAU screens samples for nitrogen content, which is a fairly accurate, if not completely understood, proxy for collagen presence. However, many Pleistocene bones do not pass the %N minimum, and of those that pass, many still fail pretreatment. The potential variation in %N across an individual site and bone could be better understood, as should potential explanations for %N results that don't match resulting collagen yields.

Laboratory developments have improved accuracy of Pleistocene radiocarbon dates, but there remain challenges to dating poorly-preserved bones. These challenges have limited direct dates on fauna from southern Europe. Attempting many samples will only partially solve this issue; methods themselves also need to be improved.

Part II

Materials and methods

4
Radiocarbon experiments

The methodological experiments for this project fall under two themes: sample preservation characterisation (%N screening, Caldey hyena samples, and failed samples) and alternative sample pretreatment protocols (dialysis and EDTA). The materials and methods for these experiments are introduced here. Radiocarbon dating protocols are described in chapter 6 and the statistical tools used to model fauna extinctions are described in chapter 7.

4.1 %N screening

Measuring %N as a screening step can save labour and consumables by predicting which samples are worth pretreating. An individual site may contain bones with variation in preservation; prescreening enables chemists and archaeologists to choose the best-preserved samples, thereby saving time, money, and sample destruction.

Questions remain about the relationship between %N and protein content. The 0.76 %N cut-off sometimes produces false positives and negatives, which in some cases may be due to localised variation in collagen content within a bone. Since %N measurement requires only ~5 mg of bone powder, variation in bone could be missed. The aims of this experiment were to quantify the rate of false positives

and negatives from bones from a difficult Pleistocene context and to study whether there is significant variation in %N results across individual bones.

4.1.1 Materials

Bones for this study come from the Pleistocene cave site of Zafarraya in Malaga, Spain. The site contains a Mousterian sequence with Neanderthal remains, though the precise chronology remains contested (Wood et al. 2013a). Previous work showed significant variation in %N between bones (Wood 2011; Wood et al. 2013a). Of 30 samples screened in these studies, only three passed the 0.76% threshold and 18 had %N <0.2. For this new study, a further 229 samples were analysed. The bones come from the entire Pleistocene sequence (layers UA to UE). While samples used here were mostly unidentifiable fragments, previous analyses found several mammal species, including panther, lynx, hyena, fox, brown bear, ibex, and auroch (Barroso Ruiz and Bailon 2003; Barroso Ruiz 2010; Geraads 1995; Geraads et al. 2013). Challenges with reliable radiocarbon dating have been due, in part, to the difficulty in finding bones with sufficient collagen preservation: only three dates were produced with robust ultrafiltration treatment in Wood et al. (2013a) (Table 4.1).

Table 4.1: Radiocarbon dates obtained on bones from Zafarraya using the ultrafiltration protocol (Wood et al. 2013a).

OxA	Age BP	Error	Species	Context
21810	46300	2500	*Capra*	Mousterian
21813	>49300		*Capra ibex*	Mousterian
23198	>46700		*Capra pyrenaica*	Mousterian

4.1.2 Methods

The %N values of 229 bones were measured using the same methods as described in Brock et al. (2012). Samples were first surface cleaned by air abrasion with fine aluminium oxide powder to remove contaminants, and then a cortical bone surface was drilled using a tungsten carbide spherical burr drill bit and the powder discarded. A small amount of bone powder (3–5 mg) was then drilled from this cleaned spot



Figure 4.1: Example of a bone sub-sampled in six locations for %N values.

and collected for analysis. The bone powder was weighed into clean tin capsules and the %N and %C contents were measured using an automated carbon and nitrogen elemental analyzer (Carlo Erba EA1108). An in-house alanine standard (Merck, 05129, UK) was used for instrument calibration and quality control.

Collagen was extracted from a subset of fifty bones of sufficient size (>1 g). As much as possible, two bones were selected from each 0.1% bin of %N results to extract collagen from. Some bins had zero or one bone, in which case the one bone was selected. The routine ABA method plus ultrafiltration described in Brock et al. (2010b) was used. Collagen mass was weighed and the %yield calculated as the ratio of collagen to starting bone sample mass.

Eight bones were selected for sub-sampling to assess %N variation within bones. The samples chosen were large enough to take 4–11 %N measurements per bone. Drill spots were spaced across a bone and their locations recorded (Fig. 4.1). The bone powder was then analyzed for %N as above.

4.2 Caldey hyenas

Cave hyenas (*Crocuta crocuta spelaea*) appear to have gone extinct before the LGM, with last appearance dates (LADs) across Europe falling around 27–26

ka BP (Stuart and Lister 2014). These late dates come from several countries, including Italy, Greece, Bulgaria, France, Belgium, and the UK. The UK has more than 50 radiocarbon dates on hyenas from >20 sites, though not all of these dates are considered reliable (Stuart and Lister 2014). These dates range from background radiocarbon ages to a handful of dates around 27 ka. The most recent ultrafiltered radiocarbon dated dates on hyenas from the UK come from Caldey Island, Wales (Table 4.2). The youngest Caldey teeth date to 27100 ± 750 BP, 27200 ± 360 BP, and 27470 ± 240 BP.

In a more recent review of Pleistocene fauna in the UK, seven of 16 hyena radiocarbon dates are rejected as unreliable (Dinnis et al. 2016). Of those seven rejected dates, six come from sites on Caldey Island. The authors reject these dates over concerns that the samples may have been treated by the original excavators with Ronseal, a polyurethane wood varnish. Ronseal contains propylene glycol ($C_3H_8O_2$), colourants, and other polymers ("Ronseal Quick Drying Varnish" 2009). In a Caldey excavation report, the excavators praised Ronseal as 'it soaks into the bone, strengthens it, and gives a pleasing shiny finish from which dust is later easily removed' (Van Nédervelde and Davies 1975, p. 3). The curatorial team at the National Museum Cardiff, where the samples are stored, observed no obvious varnish on the samples, but Dinnis et al. were concerned about the possibility of trace or adsorbed preservative not visible on the surface of the samples. They suggest it was 'more likely than not that Nédervelde's Caldey collections were treated with something' (2016, p. 4). Therefore they did not include the Caldey radiocarbon dates in their discussion of hyena extinction.

If the Caldey dates were accepted, they would shift the UK extirpation of hyenas from ~32 ka BP, which Dinnis et al. (2016) supported as the best estimate, to ~28 ka BP. The later estimate is comparable to the latest dates in continental northwest Europe (Dinnis et al. 2016). Caldey would represent a brief re-colonization of the UK by hyenas or a marginal surviving population.

The dates' rejection depends on the samples being contaminated with a consolidant. The potentially problematic dates were produced at the ORAU by AMS

measurement of ultrafiltered collagen. This method (ORAU's treatment code 'AF') consists of the ABA pretreatment plus filtration of sample gelatin in 30 kDa filters (Brock et al. 2010b), which is considered best practice for Pleistocene bone dates (Stuart and Lister 2014). Prior to the ABA procedure, these samples were solvent washed (indicated by the * in the treatment code AF*), a step the ORAU lab performs on bone samples suspected of being contaminated (Brock et al. 2010b).

While AF* pretreatment is routine for bone samples, it is still possible the samples are inaccurate. Over the last few years, the ORAU has redated a range of bone samples by dating the specific amino acid hydroxyproline (HYP). In some cases, even if the original date's quality metrics such as %C and the CN ratio were acceptable, the new HYP dates turned out to be significantly older (Devièse et al. 2017; Devièse et al. 2018). There was insufficient material to re-date the Caldey samples with HYP protocol, so other means of assessing their reliability were explored. Here, microscopic inspection, FTIR, and Py-GC/MS were used to check for the presence of contaminants, including Ronseal.

Table 4.2: Radiocarbon dates from Caldey Island hyenas (Stuart and Lister 2014). CRA is the conventional radiocarbon age, expressed in years BP with ±1 standard deviation. PCode refers to pretreatment code; AF is ultrafiltered collagen and * refers to an additional solvent protocol for contaminant removal (Brock et al. 2010b). Yield represents the weight of ultrafiltered gelatin in milligrams. %yield is the percent yield of extracted collagen as a function of the starting weight of the bone analysed. CN ratio is the atomic mass ratio between the two elements at graphitization. %C is the carbon present in the combusted sample. Stable isotope ratios are expressed in per mille relative to vPDB with a mass spectrometric precision of ±0.2‰. OxA- is the code given to the date; X- refers to a health warning issued with the date.

Site	Element	Museum code	PCode	%yield	CRA	Error	CN	%C	δ^{13}C	δ^{15}N	OxA-
Nanna's Cave	Left P2 tooth	Z/1983/076.1699	AF	2.9	27100	750	3.1	4%	-17.7	7.7	9673
Ogof-yr-Ychen	Canine	Z/1983/076.286	AF	2.8	37400	700	3.3	46%	-18.2	10.8	9691
Ogof-yr-Ychen	Canine	Z/1983/076.286	AF	1.7	33000	600	3.3	44%	-19.4	9.0	X-2278-43
Ogof-yr-Ychen	P4 tooth	Z/1983/076.287	AF	1.3	27200	360	3.5	43%	-19.1	10.1	9692
Ogof-yr-Ychen	P4 tooth	Z/1983/076.287	AF	2.0	31750	600	3.2	45%	-18.8	9.0	X-2278-44
Potter's Cave	Humerus	7:NMGW 91.7H	AF	1.4	28000	310	3.4	47%	-18.8	9.7	9693
Potter's Cave	Humerus	7:NMGW 91.7H	AF	1.8	27470	240	3.2	45%	-19.2	9.2	19215
Eel Point Cave	Left M1 tooth	8:NMGW 90.SSH (116)	AF	2.4	41400	1600	3.4	46%	-18.7	11.2	9694

4.2.1 Materials

Two of the six dates rejected by Dennis et al. come from the same specimen from Potter's Cave, so there are five hyena specimens in question (Table 4.2). Three of the five hyena remains were able to be sampled for this project (Table 4.3; Fig. 4.2). All three samples were teeth and were selected because they were clearly identifiable as hyena teeth and relatively intact. They also had documentation in the sample bags about when they were previously sampled for radiocarbon dating. A few micrograms of the surface of the teeth were scraped off with a scalpel and stored in treff tubes for further analysis.

In addition, the ORAU has stored excess collagen from four of the five samples. There was insufficient material for re-dating through the HYP protocol, but there was enough (a few milligrams) to analyse with pyrolysis GC-MS. The ORAU database also has recorded information about the samples, including their CN ratios, isotope results, collagen yields, and %C. These metrics can inform the reliability of the radiocarbon dates.

Two other specimens were included in this study for reference. The first is mammoth bone from Latton, Wiltshire which is used as a lab standard at the ORAU (Brock et al. 2010b). This Pleistocene bone is not treated with any conservatives and has good collagen preservation. The second reference sample is a bone of *Bos* from Ogof Morfran (Specimen 2004.16H/22), another Welsh site excavated by Davies. This bone was clearly varnished (Fig. 4.2). As for the hyena teeth, flakes off the surface of the bones were sampled for this study. Other than the Latton bone, all the samples are stored in the National Museum Cardiff, which kindly permitted sampling.

4.2.2 Methods

All the samples were first visually inspected and photographed with a binocular microscope with digital camera attachment. Small flakes of the three teeth and two comparative samples were then analysed with FTIR as in chapter 4.3.2.2.

Table 4.3: Samples used in the Caldey hyena study. Bone powder came from sampling at the National Museum Cardiff; some samples had excess collagen stored in the ORAU lab from previous dating.

Site	Element	Lab/museum code	Material used
Nanna's Cave	P2 tooth	Z/1983/076.1699	Bone powder only
Ogof-yr-Ychen	Canine	Z/1983/076.286	Bone powder, collagen
Ogof-yr-Ychen	P4 tooth	Z/1983/076.287	Bone powder, collagen
Potter's Cave	Humerus	7:NMGW 91.7H	Collagen only
Eel Point Cave	M1 tooth	8:NMGW 90.SSH (116)	Collagen only
Ogof Morfran	*Bos* sp. metatarsal	2004.16H/22	Bone powder only
Latton Bone	Mammoth bone	P25774	Bone powder, collagen

Samples were also analysed by pyrolysis-GC/MS. This method offers higher sensitivity than FTIR and might reveal trace contaminants. The instrumentation consist of an EGA/PY-3030D Micro Furnace Pyrolyzer (Frontier Lab, Japan) connected to a 6890 gas chromatograph equipped with a split/splitless injector. About 500 µg of sample was placed in the glass capsule, which was then put under a gentle stream of nitrogen to ensure an inert atmosphere and flame-sealed and placed in the pyrolysis chamber. The sample was pyrolized for 10 minutes at 400° C. An HP 5MS column (30 m × 0.25 mm, film thickness 0.25 µm, Agilent Technologies, USA) coupled with a deactivated silica column (2 m × 0.32 mm, Agilent Technologies, USA) was used for the chromatographic separation. Analyses were performed under 1 mL/min helium flow, with a split ratio 1:20. A program temperature was chosen for the chromatographic oven: 50° C isothermal for 2 min, 15° C/min up to 300° C and 300° C isothermal for 15 min. The mass spectrometer was operated in EI positive mode (70 eV, scanning m/z 50-600). The MS transfer line temperature was 300° C. The MS ion source was kept at 230° C and the MS quadrupole at 150° C. All pyrograms obtained were evaluated with the programs MSD ChemStation D.02.00.275 (Agilent Technologies).



Figure 4.2: *Bos* and hyena specimens sampled for this study and photographed under natural light. Far left: *Bos* metatarsus (2004.16H/22). Teeth, clockwise from top left: hyena P2 (Z/1983/076.1699); hyena P4 (Z/1983/076.287); hyena canine (Z/1983/076.286). All copyright National Museum Cardiff.

4.3 Salt containing samples

Over the course of this project some samples behaved irregularly during routine collagen extraction. In particular, some yielded a white substance that did not have the texture of good collagen and did not yield graphite when combusted. These samples were investigated to try to characterise what diagenetic process produced these false yields.

Table 4.4: Samples analysed when they produced an uncharacterised yield. The sample amount is the amount of bone powder drilled for pretreatment, yield is the amount of material extracted from the AG protocol, and %N is the percentage nitrogen present in the sample.

Sample	P number	Site	Country	Species	Sample used (mg)	Yield (mg)	%N
GD/16753	P44208	Ghar Dalam	Malta	*C. elaphus*	970	4.10	0.07%
AL/C/2	P44209	Ghar Dalam	Malta	*C. elaphus*	830	2.00	0.08%
AL/B/15	P44210	Ghar Dalam	Malta	*C. elaphus*	1000	2.00	0.07%
GD-16	P44211	Ghar Dalam	Malta	*C. elaphus*	1340	2.50	0.05%
Paglicci 5	P45640	Paglicci	Italy	*C. crocuta*	1200	2.09	0.02%
Castel 2	NA	Castelcivita	Spain	*C. crocuta*	940	1.55	0.17%
T.10376	P44409	Tilos	Greece	*P. antiquus falconeri*	725	1.91	0.08%
T.10.A.2	P44413	Tilos	Greece	*P. antiquus falconeri*	942	7.16	0.16%

4.3.1 Materials

Four bone samples of *Cervus elaphus* from the Pleistocene cave site of Ghar Dalam, Malta were provided by Dr Victoria Herridge from the Natural History Museum for radiocarbon dating. Previous attempts to date bone from Ghar Dalam had failed due to poor collagen preservation. Only a few samples were tried previously, however, and larger samples could here be provided, warranting another attempt. After sampling, the rest of the material was returned to the Natural History Museum. Latton bone (P25774), a lab standard at the ORAU, was also AG treated and used for comparison. This Pleistocene bone is not treated with any conservatives and has good collagen preservation.

In addition, four bones that produced 'false yields' from this project's samples were further analysed with the methods described below (Table 4.4). More details about these samples can be found in chapter 5.3.

4.3.2 Methods

4.3.2.1 Collagen extraction

Collagen was extracted using the routine AG protocol described in Brock et al. (2010b). Bones were crushed with a steel mortar and hammer, then treated with

the ABA protocol plus gelatinisation. The gelatinised product was freeze-dried, and the resulting white material weighed and the %yield calculated as the ratio of 'gelatin' to starting bone sample mass. As a quality check, the ORAU requires this %yield to be at least 1% of starting mass.

As samples P44208, P44210, and P44211 produced sufficient gelatin material (>20 mg), a fraction of the AG yield was re-dissolved in ultrapure MilliQ water and then ultrafiltered as in the AF protocol in Brock et al. (2010b). Ultrafiltration is considered best practice for bone samples, particularly Pleistocene ones, but is known to reduce yields as fragmented collagen chains may pass through the 3.5 kD filter (Brock et al. 2013a).

4.3.2.2 FTIR and SEM analyses

To characterise the unusual yields, the AG yields were analysed with FTIR and SEM. FTIR was performed in ATR mode. Less than 1 mg of sample was pressed on the diamond crystal with the lowered high-pressure anvil (GladiATR, PIKE Technologies, Madison, USA). Infrared spectra were collected on with Cary 600 Series FTIR Spectrometer (Agilent Technologies, Santa Clara, USA) with spectral resolution of 4 cm^{-1} and accumulation of 64 scans in range 370–4000 cm^{-1}. In addition to the four sample AG yields, hydroxyapatite standard and the raw (not pre-treated) bone powder from sample P44211 were analysed.

SEM samples were loaded onto carbon adhesive tabs (Agar Scientific, Essex, UK) and carbon coated (Bio-Rad Microscience Ltd, Hemel Hempstead, UK). Samples were examined under vacuum with a JEOL JSM-5910 scanning electron microscope (JEOL (UK) Ltd, Watchmead, UK). EDS microanalysis and quantification was conducted with INCAx-sight x-ray instrument (model 7274) and INCA Energy software (version 5.05, Oxford Instruments Analytical Ltd, High Wycombe, UK). Analysis was conducted from SEM photomicrographs acquired with 15 kV at 14 mm distance. Composition data were expressed as percentage of elements in the the sample. Both individual grain analysis and element mapping were used.

Table 4.5: Samples used for dialysis experiments. Details about the non-standard samples are described in more detail in chapter 5.3.

Sample source	Sample	Aliquots used
Standard P25774	Latton	7
Standard P19651	Ash Bend	3
Italy	Santi 3	1
Italy	Cucigliana 6596	1
Bulgaria	Vasil C	1
Italy	Santi 1	1
Italy	Santi 2	1
Italy	Santi 4	1
Italy	Equi 102873	1
Italy	Equi 5438	1
Italy	CM 3	1

4.4 Dialysis

Dialysis was explored to better understand the size of yields obtainable from Pleistocene bones from different preservation qualities and to characterise the quality of the resulting yield. If the yield was sufficiently large and mostly proteinaceous, then the material might be suitable for further purification such as by HPLC.

4.4.1 Materials

A variety of bones was used in the dialysis experiments (Table 4.5). These include high-yield lab standards (Brock et al. 2010b) as well as low-yield bones collected during this project from Italy and Bulgaria.

4.4.2 Methods

The dialysis protocol is based on Goldenberg et al. (2017). Crushed bones were demineralised in 15 ml of 1M HCl for 24 hours. The sample was centrifuged and the supernatant refrigerated in sealed glass tubes. The insoluble pellet was continued on ABA protocol from the NaOH solvent onwards (chapter 6) without ultrafiltration. The gelatin yield of this fraction was measured.

The supernatant was filtered through cleaned Ezee filters. The sample was then poured into 3.5 kDa dialysis tubing (Spectra/Por® 3, Spectrum, 132720, UK) that had been soaked in MilliQ water for one hour to remove surface humectant. The bag was placed in 3 L of MilliQ water with a magnetic stirrer. The water was replaced after one hour, then the next morning (~15 hours), then after 6 hours and left overnight (total ~40 hr). The following day the sample had a visible precipitate. The contents of the bag were centrifuged and the supernatant poured away. The precipitate was frozen and freeze-dried, then the yield measured.

The samples' %N and CN ratios were measured as in Brock et al. (2012). The samples were prepared and the %N calculated as in chapter 4.1.2. The CN ratio, the atomic mass ratio of carbon and nitrogen, was calculated from the same result. The samples were also analysed on FTIR to characterise the precipitate. FTIR was performed as in chapter 4.3.2.2. In addition to the dialysis samples, hydroxyapatite standard, raw (not pre-treated) bone powder, and AG collagen from standard Latton bone were analysed with FTIR for comparison.

4.5 EDTA

EDTA as a decalcification agent was tested with different conditions and samples. Experiments aimed to compare EDTA and ABA collagen yield sizes, evaluate the quality of the EDTA-extracted collagen, and accelerate an EDTA decalcification protocol.

4.5.1 Materials

Bone samples came from a variety of sources (Table 4.6), including lab standards from Mary Rose, Latton, and Lemon Mine sites (Brock et al. 2010b). Excavated Pleistocene material came from Spain and Bulgaria, and a shaft of a medieval femur from Bordersley Abbey, UK. Like the background bone standards, Bordersley has been used in the lab before and is known to have high collagen preservation (Devièse pers. comm.).

Table 4.6: Bone samples used in the EDTA experiments.

Site	Sample	Collagen content
Bordersley Abbey	P39649	High
Cariguela	C-III 17	None
Grotta Cala	D6 II	Low
Latton	P25774	High
Lemon Mine	P18801	High
Mary Rose	P40018	High
Zafarraya	P42230	Low
Zafarraya	P43019	Low
Zafarraya	40-003	Low

Samples were either crushed by smashing with a steel pestle or drilled as bone powder and stored in 30 mL baked-out glass tubes with screw caps until used, after which glass caps were used to allow air flow. All materials are as used in routine lab protocols (Brock et al. 2010b) except for the disodium EDTA (Sigma Aldrich, 03865, UK).

4.5.2 Methods

4.5.2.1 Comparison with HCl decalcification

Decalcification by HCl and EDTA were compared under different conditions. Samples were either decalcified in 20 mL 0.5M EDTA solution (EDTA dissolved in MilliQ adjusted to pH 8 with NaOH pellets), or decalcified in 20 mL 0.5M HCl.

Conditions were modified across samples to measure their impact on collagen yields (Table 4.7). For some samples, solution was replaced every 2 hr for a total of 14 hr of submersion, similar to the total time in the routine protocol. Unlike the routine protocol, samples here were not left in HCl/EDTA overnight, but topped up with MilliQ and refrigerated at the end of a working day. Another set of samples were soaked in 20 mL of HCl/EDTA for 24 hr. Samples were also either submerged in an ultrasonic bath for this duration or left to sit on the lab bench.

After decalcification, all samples were rinsed in MilliQ water three times, gelatinised in 10 mL pH 3 water overnight at 75° C, Ezee-filtered, and freeze-dried

Table 4.7: Conditions of EDTA and HCl solutions with bone (crushed or powdered) for decalcification comparisons.

Condition	Agitated (14 hr)	On bench (14 hr)	Overnight (24 hr)
Crushed	Agitated-crushed	On bench-crushed	Overnight-crushed
Powder	Agitated-powder	On bench-powder	Overnight-powder

as in Brock et al. (2010b). After freeze-drying, samples were weighed as a measure of collagen yield (%yield). Further evaluation of the collagen is described below.

4.5.2.2 EDTA decalcification over time

Five crushed bone samples were soaked in 20 mL of 0.5M EDTA solution and left to sit at room temperature. One sample was removed every 24 hr to measure the change in yield over five days. This experiment was then repeated with ten samples over ten days. After removal, samples were centrifuged and rinsed three times, gelatinised, Ezee-filtered, and freeze-died as in Brock et al. (2010b).

4.5.2.3 EDTA and temperature

Aliquots of powdered Latton bone (200 mg each) were left in 20 mL of 0.5M EDTA solution for 72 hours at room temperature. After this, the samples were centrifuged and the EDTA replaced with 10 mL of 0.5 EDTA. The samples were then placed in a heating block for 90 minutes to evaluate the effect of EDTA and temperature. Pairs of aliquots were placed in the heating block at room temperature (26° C), 40° C, 50° C, and 60° C. After, the samples were processed as above for %yield. A pair of 200 mg aliquots were also AG treated as comparison %yield values.

4.5.2.4 EDTA in the microwave

To test the effect of heat and agitation, samples in EDTA solution were placed in a Milestone microwave digestion system (ETHOS EASY) with a MAXI-44 sample rotor. For all the experiments, bone aliquots were placed in 100 mL glass vessels with 0.5 M EDTA solution. After an aliquot was removed from the microwave run, the sample was transferred to a 30 mL glass tube and centrifuged four times, with

the supernatent poured away and replaced with MilliQ water each time. Samples were then rinsed and processed for %yield as above.

Aliquots were also extracted with the routine AG protocol (chapter 6). The %yield of these routine extractions were compared to the EDTA yields from the same bone. Three Latton bone aliquots were also decalcified in HCl without the NaOH step that is usually part of the AG protocol to more specifically compare the effect of HCl comapared to EDTA. Parameters were varied in a series of experiments, described below.

4.5.2.4.1 Time and EDTA replacements The microwave was set to ramp up to 200 W (40° C) over 10 min and maintain temperature. Samples of 200 mg were placed in 10 mL of 0.5 M EDTA and removed at different times to measure the extent of decalcification. Samples were removed at 10, 30, 45, 60, 90, 120, 180, 270, 360, and 720 minutes.

In one experimental run, the EDTA solution was replaced after 90 and 270 minutes to test if replacement increased yields. In all other cases the EDTA was not replaced.

4.5.2.4.2 Sample size and grain size Most samples were 200 mg, but samples of 400 mg were also tested. Both crushed bone and powdered (drilled) bone were tested in the microwave setup as above, with aliquots removed after different durations in the microwave. EDTA is slow-acting relative to HCl and it was possible that sample size and grain size would affect the rate at which EDTA decalcified samples.

4.5.2.4.3 Bone preservation In the majority of cases, lab standard bone from Latton or Lemon Mine were used. These Pleistocene bones are known to have good collagen preservation while being of background radiocarbon age. Bones with poorer preservation were also EDTA-extracted their EDTA and AG %yields compared. Because EDTA is a chelater and HCl and acid, it was possible that the two substances would interact with poorly-preserved collagen differently. Of particular interest was

whether EDTA might solubilise fragmentary collagen chains in poorly-preserved samples less than HCl, thereby producing relatively greater yields.

Samples of 200 mg in 10 mL 0.5 M EDTA were run in the microwave as above (40° C with a 10 min ramp), removed at 90 or 180 minutes without replacing EDTA. Samples were rinsed, gelatinised, filtered, and freeze-dried as above.

4.5.2.4.4 Microwave temperature In one experiment, the microwave was set to run at 25° C instead of 40° C. The glassware and EDTA solution were refrigerated at 5° C overnight beforehand. This was done to test whether the 40° C was causing partial solubilisation of sample collagen.

4.5.2.5 Analysis of EDTA collagen

As in the %N experiments above, EDTA decalcification results were measured as a %yield of collagen (chapter 4.1.2). Subsets of EDTA-extracted collagen were also evaluated with FTIR as in chapter 4.3.2.2, and %N and CN ratios were measured as in chapter 4.4. These tests could identify differences from AG-extracted collagen and identify incomplete removal of EDTA salts. EDTA-decalcified samples of Mary Rose and Latton bone were radiocarbon dated to compare their fraction modern carbon with the expected value for lab bone standards. The radiocarbon dating protocol is described in chapter 6.

5 Zoological samples

In addition to the methodology experiments, this project explored Pleistocene fauna chronologies through radiocarbon dating of bone collagen. Previously dated samples were evaluated for reliability and new samples were obtained to increase species' datasets.

5.1 Evaluation criteria

Many radiocarbon dates discussed in relation to fauna extinctions are problematic in their association and accuracy. The re-evaluation of Pleistocene radiocarbon dates have revealed many to be erroneously young (Chappell et al. 1996; Higham 2011), and re-evaluation of site sequences have found discrepancies between the age of dated artefacts and the events they are assumed to relate to (Higham et al. 2010; Lister and Stuart 2013). Therefore published dates must be carefully evaluated before they are accepted for Bayesian modelling or discussions of LADs.

Several papers on megafauna chronology have employed lists of criteria to score or pass/fail radiocarbon dates (Barnosky and Lindsey 2010; Cooper et al. 2015; Dinnis et al. 2016; Krasinski and Haynes 2010; Lister and Stuart 2013). Here, radiocarbon dates were scored and ranked by a combination of chemistry and fauna-association metrics. While a stricter pass/fail approach was considered along

the lines of Lister and Stuart (2013), a score-based system can be used to evaluate the impact of less-confident dates on models. This both tests the robustness of the models themselves and gauges the relative importance of restricting datasets to high-reliability radiocarbon dates.

To be considered in the first place, a date must have come from collagen from the specimen of interest. Indirect dates were not included in models, though they are discussed in relation to model results. Samples must have also been identified as the species of interest through reported morphology, genetics, or ZooMS. Unlike Lister and Stuart (2013), identification of the skeletal element was not required, though identification of the material (bone, tooth, soft tissue) gained a point in the criteria system. Chewed or partially digested bones, markers of hyena activity, were also included.

The evaluation criteria are described in Table 5.1. Non-HPLC samples are scored out of a possible 9 points, with high = 9, medium = 7–8, and low <7. HPLC dates are evaluated slightly differently, with some different thresholds. They are also scored out of 7, not 9 points, as yield and %yield are not meaningful when 25 mg or more collagen is needed to be injected on the HPLC anyway. An HPLC date is scored high = 7, medium = 6, and low <6. Samples with particular reasons to be outright rejected are 'scored' as rejected. (An example of a rejection is in chapter 15.4, where some medieval leopards are rejected as imports by humans.)

The function is simplistic and in some cases relies on the judgement of the user. For example, 'Species' is evaluated as a simple yes/no; uncertainty on species identification cannot be partially weighted (*e.g.* to genus, but not species, level). Data with empty fields, such as literature dates without reported isotopes, are given 0s for those fields. Despite these limitations, it separates well-reported, high-quality radiocarbon dates from those with little documentation or problematic metrics. Literature dates and their scores are reported in chapter 15 and evaluation results in Appendix G.

Table 5.1: Criteria used to evaluate radiocarbon dates.

Metric	Criteria	Criteria (HPLC)	Description
Species	Species is identified	Species is identified	A yes/no of whether the species field is not empty.
Material	Material dated is identified	Material dated is identified	A yes/no of whether the material column (e.g. bone, tooth) is not empty.
Pretreatment	Pretreatment codes AF, AF, or NRC (HPLC)	Pretreatment codes AF, AF, or NRC (HPLC)	A point is awarded for pretreatments AF, AF, and NRC/HPLC.
Yield	Produced >5 mg collagen	Not evaluated - sufficient yield is required to run on HPLC	A point for >5 mg collagen, ORAU's recommended minimum yield. HPLC samples are not evaluated this way, as >25 mg collagen is required to inject on the HPLC.
%yield	Collagen yield ≥1% by sample starting mass	Not evaluated - sufficient yield is required to run on HPLC	A point for ≥1% yield collagen. HPLC samples are not evaluated this way, as >25 mg collagen is required to inject on the HPLC.
%carbon	On combustion, sample mass between 30–50% carbon	On combustion, sample mass between 30–50% carbon	A point for %C by mass falling in the expected range for protein. Hyp falls within the same range.
δ^{13}C	On combustion, sample δ^{13}C between -22– -18 ‰	On combustion, sample δ^{13}C between -28– -20 ‰	A point for carbon isotopes falling within the expected range for terrestrial material; NRC is different as Hyp expected δ^{13}C is different from bulk collagen.
δ^{15}N	On combustion, sample δ^{15}N between 2–12 ‰	On combustion, sample δ^{15}N between 2–12 ‰	A point for nitrogen isotopes falling within the expected range for terrestrial material. Hyp samples tend to fall in the same range.
CN	On combustion, sample CN ratio between 2.9–3.5	On combustion, sample CN ratio between 4.8–5.4	A point for CN ratios falling in the expected range. Hyp CN is expected to be around 5.0.

5.2 Previously published dates

Survey of the literature found few direct dates of cave hyenas, cave lions, and European leopards. Many Pleistocene dates did not come directly from the specimen of interest but from associated species or 'bulk soil'. Some dates were produced from apatite or burnt bone. Others, particularly those produced pre-1980, could not be linked to a laboratory number. Context of the specimen always required consideration. Leopards with medieval radiocarbon ages, for example, were not considered LADs since they were imported for entertainment (Freedman and Evans

Table 5.2: Cave lion dates from southern Europe. The La Garma dates come from the same lion individual and are statistically identical.

Site	Country	Material	Lab code	Date BP	Error	Source
La Garma	Spain	Bone	OxA-18698	13830	55	Cueto et al. (2016)
La Garma	Spain	Bone	OxA-18699	13835	60	Cueto et al. (2016)
Jou'l Llobu	Spain	Bone	OxA-10186	46400	2100	Stuart and Lister (2011)
Urtiaga Cave	Spain	Bone	OxA-10121	13770	120	Stuart and Lister (2011)

Table 5.3: Published leopard dates from southern Europe.

Site	Country	Material	Lab code	Date BP	Error	Source
Equi	Italy	Bone	Beta 360175	33000	260	Ghezzo and Rook (2015)
Jou'l Llobu	Spain	Bone	OxA-10173	46600	2300	Pinto Llona (2007)

2015). The result is very few vetted dates for each species from southern Europe (Tables 5.2–5.4), with sites incompletely covering the Mediterranean (Fig. 5.1). All literature dates evaluated, including those outside the Mediterranean, are reported in chapter 15 and Appendix F.

Table 5.4: Cave hyena dates from southern sites. From Stuart and Lister (2014).

Site	Country	Material	Lab code	Date BP	Error
Agios Georgios Cave	Greece	Tooth	OxA-17009	29340	240
Amalda	Spain	Bone	OxA-10398	39900	700
Arene Candide	Italy	Bone	OxA-10658	27050	550
Grotta Paglicci	Italy	Tooth	OxA-10523	26120	330
Grotta Pocala	Italy	aDNA	VERA-2532	38220	920/820
Grotta Paglicci	Italy	Bone	OxA-10657	29100	1600

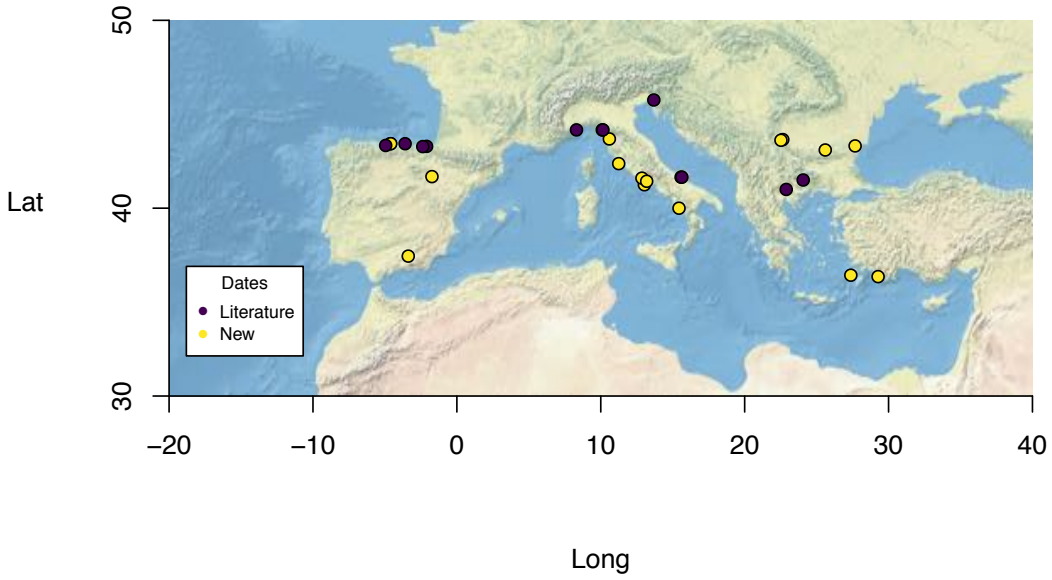


Figure 5.1: Southern European sites with large carnivores, either previously dated or sampled for this project.

5.3 New samples

236 bone and tooth samples were collected for this project from sites in southern Europe (Fig. 5.1). One sample from Zafarraya, Spain which was identified by the excavators as a leopard is included here (Tables 5.5 and 5.6). Another 72 samples from Zafarraya were analysed with ZooMS, but the results did not reach species-level identification and so are not included in these tables (chapter 5.4).

Of the 236 samples collected, only 78 produced %N $\geqslant$0.3. This cutoff is tallied here to give a first impression of preservation and was used to decide whether to attempt extracting collagen from a sample. For sites where no samples had %N $\geqslant$0.3, the highest-%N sample(s) were tried in hopes of finding false negatives.

The majority of samples collected for this project are carnivores but some other species were sampled for the following reasons:

- Some bones had evidence of hyena gnawing or digestion, and so were dated as proxies of hyena activity.

- The site has questions of interspecific interactions. These may arise from apparently coexisting carnivores or patterns of hominid-carnivore interaction. This is why some wolves, hominids, and brown bears were sampled.

- The site shows an overall shift in fauna assemblage. Kozarnika cave in Bulgaria, for example, shows periodic incursions of cold fauna despite evidence an overall temperate climate (Guadelli 2011). Dating these rare cold specimens can test if carnivores responded as well.

- Samples were taken for fauna on Mediterranean islands and mainland straight-tusked elephant, which are all poorly chronologically constrained (Masseti 2001; Poulakakis et al. 2002; Sen et al. 2014; Stathopoulou and Theodorou 2001). However the 52 samples all failed %N and collagen extractions failed on a subset that were tried.

- Constraining stratigraphy. Bayesian model precision and robustness is improved when there is a sequence of dates through site layers and sometimes when there are more dates per layer. Some were sampled to provide this extra data.

In general the highest-%N samples at each site and site were selected for extraction. Sometimes the highest-available %N samples at a site or for a species were still low-%N (*e.g.* at Tilos). The larger %N experiment conducted on Zafarraya material (chapter 8) illustrated that some low-%N samples might surprisingly produce sufficient collagen for dating, perhaps due to localised variation in preservation, and so attempting extractions was worthwhile in such cases. In the case of Equi, small samples were first measured for %N, and then a subset sampled for the larger amount of bone powder required for dating. These were selected for high %N and the shape of the bone—the museum preferred broken long bones were sampled, as they could be drilled in the inside hollow.

Table 5.5: By species, samples collected for this project. %N pass is here ⩾0.3.

Species	%N passes	Samples (n)
Boar	1	1
Bovid	1	1
Brown bear	6	9
Cave hyena	18	55
Cave lion	4	12
Deer	2	5
Giant elk	4	4
Horse	0	3
Human (H. sp.)	2	9
Leopard	11	23
Narrow-nosed rhino	0	2
Neanderthal	0	2
Pygmy elephant	16	39
Straight-tusked elephant	3	7
Tortoise	0	1
Unknown	6	56
Wolf	4	6
Woolly rhino	0	1
Total	**78**	**236**

More details about the sample chemistry results are in chapter 15 and Appendix E. Sites are summarised in Appendix B.

5.4 ZooMS identifications

Bone samples are often too fragmentary to identify as belonging to a particular species. Zafarraya, Spain was one site where the majority of faunal material was highly fragmentary, and so 72 samples were analysed with the ZooMS technique to identify their genus and possibly species. The samples were selected from the upper few stratigraphic levels, which were most relevent to determining last appearances, and had already had sufficient collagen extracted to be run. Samples were run at ZooMS laboratories at the University of Manchester and the University of York.

Unfortunately, the poor collagen quality and imprecise resolution of the technique meant that samples could not be identified to species level. In particular, while

Table 5.6: By site, samples collected for this project. %N pass is here ⩾0.3.

Site	%N passes	Samples (n)
Bulgaria		
Kozarnica	0	4
Manastira	6	19
Redaka II	0	14
Vasil Levski	0	2
Crete		
Crete (museum)	2	2
Greece		
Akrotiri Aetokremnos	0	2
Tilos	17	41
Italy		
Castelcivita Cave	6	6
Cava Muracci	0	11
Cucigliana	6	9
Grotta dei Santi	4	4
Grotta della Cala	2	4
Grotta Paglicci	1	8
Grotte di Equi	12	26
La Sassa	6	8
Other		
Lough Boora	5	5
Palaeoloxodon	0	2
Spain		
Cariguela	3	36
La Llera	0	1
La Silluca Cave	3	3
Los Rincones	5	11
Zafarraya	0	18
Total	**78**	**236**

6 carnivores were identified, neither the genus nor species could be distinguished, making the samples unusable in this project. Full details of the ZooMS results are in Appendix D.

6 Radiocarbon methods

Pretreatment for routine ultrafiltration (AF) follows from Brock et al. (2010b) but has been modified here depending on the %N value of the samples. Samples >0.76% N followed routine pretreatment including ultrafiltration. Others were not ultrafiltered to obtain an initial gelatin (AG) yield. Depending on the yield, the samples were then ultrafiltered, hydrolysed for HPLC, passed on to experimental dialysis extraction (chapter 4.4), or rejected.

6.1 ORAU routine protocols

6.1.1 Sample %N screening and preparation

6.1.1.1 %N screening

All samples were measured for %N to decide which extraction protocol to apply. The method is described in detail in chapter 4.1.2 and follows Brock et al. (2012). In short, a small amount of bone powder (3–5 mg) was drilled from a cleaned spot on the bone and collected for analysis. The bone powder was weighed into tin capsules and the %N and %C contents were measured using an automated carbon and nitrogen elemental analyzer. An in-house alanine standard was used for calibration and quality control.

6.1.1.2 Sample preparation

Bone samples were manually cleaned by sandblasting. A small piece of bone was drilled off with a tungsten carbide drill bit, then crushed with a steel pestle and mortar. At the ORAU, samples are usually 500–700 mg, though up to 1 g can be used (Brock et al. 2010b). Here larger amounts (1–2 g) were crushed when samples had low %N values.

6.1.2 Treatment and measurement

6.1.2.1 ABA treatment

Samples with %N >0.76 went through the routine protocol as in Brock et al. (2010b). Samples were loaded into glass tubes, all previously baked at 500° C for at least three hours to remove organic material. All samples were treated with 0.5M hydrochloric acid for 1–2 hr, followed by three rinses with ultrapure MilliQ™ deionised water. After each rinse, samples were separated by centrifugation and decanting. This full round of acid and three water rinses was repeated. For the third acid wash, samples were left to soak overnight (~12 hr), then rinsed as before. Samples were then soaked in 0.1M sodium hydroxide for 30 min and then rinsed three times in water, followed by 0.5M acid for 15 minutes and three water rinses.

Samples were gelatinized by leaving in pH 3 water in a 75° C oven for 20 hours. The resulting gelatin was filtered with 9 µm polyethylene Ezee-filter™ (Elkay, UK). The filters were previously cleaned by ultrasonicating in MilliQ water for 20 min and then passed though fresh MilliQ water. At this point, AG (gelatin) samples would be freeze-dried at -18° C in a VaCo 5 freeze-dryer (Zirbus, Germany) overnight (~18 hr).

Samples for ultrafiltration were transferred into a cleaned ultrafilter (Vivaspin™ 15—30 kD MWCO) and centrifuged until 0.5—1.0 mL of the >30 kD gelatin fraction remained. This gelatin was removed from the ultrafilter with ultrapure water and baked-out glass pipettes before being freeze-dried as above. The cleaning protocol for ultrafilters is described in Brock et al. (2007).

After freeze-drying, the dried collagen was weighed and stored in Treff tubes. Samples with sufficient collagen (>5 mg and >1% of starting sample weight) went on to combustion, graphitization, and measurement.

6.1.2.2 Combustion

Combustion occurred as in Brock et al. (2010b). A CF-IRMS system with an elemental analyser (Carlo-Erba NA 2000) and gas source isotope mass spectrometer (Sercon 20/20) was used. Samples were combusted (1000° C) and oxidised (1800° C), converting into NO_x (which is then reduced via a reduction column into N_2) and CO_2. Water vapour was removed with a chemical trap. Gas passed through a GC column with Carbosieve™ (Supelco G60/80 mesh; Bellefonte, Pennsylvania, USA) packing medium and a helium carrier gas stream of 100 ml/min. This separated the N_2 and CO_2. A small portion of the sample (2%) was admitted to the mass spectrometer through a 50:1 splitter in N_2 and CO_2 gas pulses. The remaining CO_2 was trapped in a 10 ml rig (Bronk Ramsey and Hedges 1997) containing a glass vial submerged in liquid nitrogen. Sample isotopic ratios are quoted relative to results of an in-house alanine standard run for quality control (Brock et al. 2010b).

6.1.2.3 Graphitisation

Samples were graphitised according to Dee and Bronk Ramsey (2000) and Brock et al. (2010b). The rig containing the trapped CO_2 also contained 2.0–2.5 mg of iron powder (<10 µm, 99.9%, Sigma Aldrich) that had been previously out-gassed in the presence of 500 mbar H_2 at 450° C for 1 hr. Hydrogen gas was added to the sample in the ratio of 2.2 H_2:CO_2 and the rig valve closed before heating at 560° C for 6 hr. The resulting graphites could be large at 1.8 mg of C, small at 0.8 mg of C, or very small at 0.2 mg of C.

6.1.2.4 AMS measurement

Samples were dated on the lab's HVEE AMS system (Bronk Ramsey et al. 2004a). All dates issued by the ORAU have a unique OxA number. Some non-routine dates

here (HPLC) are of the type OxA-X-wwww-pp, or 'samples that are research measurements using non-standard or experimental methods' (Brock et al. 2010b, p. 111).

6.1.3 Modified AG pretreatment

Many samples had %N < 0.76 and were unlikely to produce sufficient collagen after ultrafiltration. Sometimes the ORAU dates samples without ultrafiltration (AG protocol), but results are best regarded as *terminus ante quem* dates (Brock et al. 2010b). Even in the AG protocol, handling and water rinses can result in material loss, and the dialysis experiment (chapter 4.4) required retention of the acid used in demineralisation.

Therefore, some samples with low %N values were subjected to a modified AG pretreatment in preparation of dialysis. After crushing, samples were soaked in 0.5M HCl solution for ~24 hr. Samples were then centrifuged and the solution pipetted and stored in cleaned glass vials in a refrigerator until used for dialysis. The solids were soaked in 0.1M NaOH for 30 mins, rinsed once with ultrapure water, soaked in 0.5M HCl for 15 min, rinsed once with ultrapure water, then gelatinised in 3 pH water in a 75° C oven for 20 hours. The resulting gelatin was filtered with Ezee-filters and freeze-dried.

The resulting collagen was weighed. If the yield was large enough (>20 mg), samples were either hydrolysed for HPLC or dissolved in ultrapure water and ultrafiltered as routine samples. Smaller yields were stored as collagen for modified-AG dates and the acid fraction dialyzed (dialysis method in chapter 4.4).

6.2 HPLC protocol

6.2.1 Hydrolysis and sample preparation

Sample preparation and HPLC protocol follows Devièse et al. (2018). From the freeze-dried collagen, 12–16 mg was hydrolysed in 150 µl of 6M HCl (roughly at a ratio of 1 ml of 6M HCl per 10 mg collagen). The test tubes were flushed with nitrogen gas for five minutes to produce an inert atmosphere, then capped and set in

a heating block at 110° C for 24 hr. After, the samples were evaporated in a Genevac EZ-2 vacuum evaporator (Genevac Ltd, Ipswich, UK). Once dry, tubes were filled with 700 µl of MilliQ deionised water with a Gilson 1000 µl pipette with a plastic Gilson Diamond® 100–1000 µl tip, then shaken to dissolve the sample. Baked glass pipettes were used to transfer the sample into a 2 ml BP Plastipak™ syringe with a Thermo Scientific 0.2 µm syringe filter. This was then filtered into a baked out Waters® HPLC 1 ml total recovery vial (P/N 186000384C) with a 9 mm screw cap (Agilent Technologies). Another 300 µl of MilliQ water was added to the original test tube, loaded into the same syringe and filter, and filtered into the HPLC vial to recover as much sample as possible. The filled HPLC vials were then frozen until use.

6.2.2 HPLC

Chromatography was performed on a Varian ProStar HPLC system with autosampler (model 410), two isocratic pumps (models 210 and 320), column oven at 30° C with a Primsep A column (22x250 mm, particle size 5 µm), and a UV detector (model 320) at 205 nm. Samples were injected with an autosampler (model 410) and collected in a fraction collector (model 701) controlled by Star workstation PC software (version 6.0). The autosampler was modified with a 1 ml syringe and 2 ml sample loop, enabling up to 1 ml of sample to be injected at one time.

The HPLC system used two eluents at varying ratios: MilliQ deionised water and 0.3% phosphoric acid (diluted with MilliQ deionised water). The ratio was controlled by the method programme. Both 0.3% phosphoric acid and MilliQ had a flowrate of 18 ml/min throughout the method. The full method programme is listed in Table 6.1. Hyp eluted in 100% water (0–55 min), and the remainder of the run ensured the HPLC system was fully flushed between samples.

The fraction collector program was manually programmed and linked to the HPLC method selected. Eluate was collected in 37 ml fractions in baked-out test tubes. Using the chromatogram for guidance, tubes containing Hyp were selected and loaded onto a Genevac EZ-2 Plus vacuum evaporator and spun until little solution remained. This was then transferred with a glass pipette into an HPLC vial,

which was spun on the Genevac until dry. This usually required an intermediate step (before loading into an HPLC vial) of transferring incompletely evaporated fractions into two glass fraction collector tubes before further evaporation. Once the HPLC vial was completely dry, a dark yellow-brown residue remained. Vials were then frozen until graphitisation.

Table 6.1: The HPLC method used to collect eight amino acids, including Hyp, from Devièse et al. (2018). Pumps run continuously at 18 ml/min with a proportion of water and 0.3% phosphoric acid.

Time (min)	0.3% phosphoric acid eluent
0 - 55	0%
55 - 56	Linear gradient between eluents
56 - 290	100%

To prepare the Hyp reside for combustion, the residue was reconstituted in 30 µL pH 3.0 (HCl) water and loaded onto 20 mg of Chromosorb™ (W/AW, mesh size 30–60, Phase Separations Ltd.) in cleaned cylindrical tin capsules. The Chromosorb™, an inert silica material, is used as a combustion substrate. The capsule was closed and loaded onto the mass spectrometer for combustion as normal.

6.2.3 HPLC background correction

A background correction different to the routine protocol correction was applied to HPLC results (Devièse et al. 2017; Devièse et al. 2018). Both the raw radiocarbon dates and the calculated correction are reported in the results. The calculation and required data for the background correction is reported in Appendix I.

7 Modelling data and methods

Here the statistical models and tools used in this project are introduced. Multiple statistical tools in this project use Bayesian principles (chapter 2.5.3), and so a short introduction of Bayes' Theorem is included here. This is followed with more specific methods for estimating extinction dates, building spatio-temporal models, and analysing kernel density estimates (KDEs) with time series models.

Calibration, Bayesian boundary modelling, and kernel density chronological modelling were conducted in OxCal (Bronk Ramsey 2009). Other analyses were conducted in R version 3.5.0 (R Core Team 2018). Further details on models are in Appendix J.

7.1 Data

7.1.1 Radiocarbon dates: evaluation and calibration

The main data in this project are radiocarbon dates of fauna. Samples were presented in chapter 5 along with the criteria for gauging the reliability of the sample: samples were scored high, medium, low, or outright rejected. The influence of lower-confidence dates is considered in several models below, either by testing models twice (with and without the low-score dates) or down-weighting the low-score dates.

To build models, radiocarbon dates required calibration, which enabled comparison of multiple kinds of chronological information by placing dates on a shared timeline. A radiocarbon date is a measurement of duration in which radiometric decay of ^{14}C has occurred in a system. This duration, reported as 'radiocarbon years', is not directly equivalent to calendar years because the atmospheric concentration of ^{14}C has varied through time. This past variation in ^{14}C concentration can be accounted for with calibration curves, which measure the offset between ^{14}C years and calendar years using records such as tree rings and speleothems. These curves have been combined into models like IntCal13 (Reimer et al. 2013) to calibrate individual radiocarbon dates. This project used the software program OxCal 4.3 to calibrate and model results (Bronk Ramsey 2009).

7.1.2 Climatic and archaeological records

In addition to radiocarbon dates from a species of interest, climatic and archaeological data are needed to test the above hypotheses. These were used in the KDE and time series models described below and in Appendix J.2 and chapter 16.3.

There are multiple proxies for climate in the Pleistocene, but a relatively straightforward continuous variable is the GISP2 Greenland ice core oxygen isotope record ($\delta^{18}O$) (Rasmussen et al. 2014; Seierstad et al. 2014). This proxy generalises over the whole of Europe but is high-precision and widely used. A distinguishing feature of stadials in the Mediterranean was their aridity, whereas northern Europe was determined more by winter temperatures (Müller et al. 2011; Nebout et al. 2002; Sánchez Goñi et al. 2008; Sánchez Goñi et al. 2013). This different manifestation of the $\delta^{18}O$ signal in Europe should be considered when interpreting results using the $\delta^{18}O$ record.

Snapshot climate variables from the LGM were also used in the ecological niche models (more in chapter 7.4.2). Climate data was drawn from the WorldClim database, version 1.4, of the CCSM4 Last Glacial Maximum snapshot at 10 minute resolution (Hijmans et al. 2005).

Archaeological evidence in Europe is generally greater than palaeontological evidence, making it possible to produce regional estimates of AMH arrival and activity. Direct skeletal evidence is sparse, so materials like lithics, hearths, and cutmarked bones are used as evidence for AMH activity (*e.g.* Douka et al. 2014; Higham et al. 2014; Wood et al. 2016). This introduces debate over whether a lithic industry was produced by AMH or Neanderthals. There are some specific industries that remain debated:

- The Uluzzian industry in Italy and Greece. It is debated whether this industry was produced by Neanderthals or AMH, with a recent analysis of associated dental remains arguing for AMH (Benazzi et al. 2011; Benazzi et al. 2015).
- Other 'transitional' industries, including the Szeletian, Bohunician, and Châtelperronian (Higham et al. 2014).
- The proto-Aurignacian, though fewer argue against it being AMH-made (Bailey et al. 2009; Benazzi et al. 2015).

For the purposes of this thesis, a conservative late arrival scenario is used, where both the Uluzzian and transitional industries are attributed to Neanderthals and only the proto-Aurignacian and later industries attributed to AMH. The possible influence of an earlier arrival scenario is considered in chapter 17 and would be worth testing in future work. For KDE and time series models of AMH, a 10% random sample (n = 242) was taken from the radiocarbon dataset in Carotenuto et al. (2018). The sampled dates are reported in Appendix H.

7.2 Bayes' Theorem

Bayesian modelling tests the likelihood of a hypothesis given external information. A classic example from archaeology is interpreting a radiocarbon date recovered from a stratigraphic profile. The radiocarbon date is a Gaussian distribution based on observed ^{14}C content and a background correction. The context from which it was sampled has no influence on this independent measurement. However, if the sample was recovered from a stratigraphic layer below the Campanian Ignimbrite

tephra layer, then it can be inferred that the date should predate the eruption (and be >39 ka). This can be used to revise the estimate of the age of the sample.

This kind of reasoning is formalised in Bayes' Theorem, which evaluates the probability of an event given external information about the conditions related to that event:

$$P(A \mid B) = \frac{P(B \mid A)\, P(A)}{P(B)}$$

Where $P(A \mid B)$ is the conditional probability of event A given B, $P(B \mid A)$ is the conditional probability of event B given A, and $P(A)$ and $P(B)$ are the independent likelihoods of each event. The initial belief in A before accounting for B (the *prior probability* $P(A)$) is multiplied by the support B lends A (the *normalized likelihood* $P(B \mid A)/P(B)$) to produce the *posterior probability* ($P(A \mid B)$) of A accounting for B.

Continuing the above example, $P(A)$ would be the estimated age of the sample, the Campanian Ignimbrite date would be $P(B)$, and $P(A \mid B)$ is the revised probability of $P(A)$ given $P(B)$. If the radiocarbon date is 42 ka, then $P(A \mid B)$ will have high confidence, as the date should be greater than the eruption date; but if the date is 32 ka, then $P(A \mid B)$ will have lower confidence, as the radiocarbon date does not accord with the prior information about the relationship between the eruption and the sample. (This example is employed in Wood et al. (2012).)

This principle is used in OxCal chronological models, which incorporate radiocarbon dates with external information (Bayliss et al. 2007; Bronk Ramsey 2009; Litton and Buck 1995). It is also used in the OxCal implementation of kernel density estimates (Bronk Ramsey 2017) and the spatial-temporal extinction estimates (Carlson et al. 2018b).

7.3 Extinction date estimates

In this project, three different extinction estimators were used and their results compared: LADs, OxCal `Boundary` estimates (Bronk Ramsey 2009), and GRIWM

estimates (Bradshaw et al. 2012; Saltré et al. 2015). In addition to overall species' extinctions, radiocarbon dates were subsetted into regions and extinction estimates produced, enabling comparison of regional disappearances. The subregions were northern Europe (>50° N), southern Europe (<47° N), central Europe (47–50° N), and Asia/Siberia (<40° E). Welch two-sample t-tests were used to test whether different estimates and regional estimates were significantly different. Estimates were also produced with low-score dates excluded to evaluate their influence. Results are presented in chapter 15.

7.4 Spatial patterns

Extinction estimators 'flatten' the dynamics of extinctions: there is little way to evaluate populations through space and time. Direction and location in which species retract is an important aspect of their responses to climatic and AMH activity.

Two spatial models were produced. First, a `spatExtinct` map interpolated observations (radiocarbon dates) across a map to produce a spatio-temporal extinction map (chapter 2.5.3) (Bond et al. 2019; Carlson et al. 2018a; Carlson et al. 2018b). The map is shaded by date of estimated last appearance, suggesting regions of early retraction and late survival.

Second, using GRIWM extinction estimates, a single time-slice `spatExtinct` map was produced estimating the likelihood of survival in a location near the time of extinction. This was weighted with an ecological niche model—the potential range of a species based on observed appearances—built with the R package `dismo` (Hijmans et al. 2013). The resulting heat map's hot spots reflect likely locations of extinction.

These models can include some level of uncertainty: `spatExtinct` allows for a categorical confidence weighting of observations. As Carlson et al. (2018b) warn that low-confidence observations can skew models, low-score radiocarbon dates were down-weighted.

The maps produced can visualise the spatial and temporal retraction of each species, revealing whether northern or southern Europe was that species' most

suitable niche and where it went extinct. The key limitation of this approach is the loss of radiocarbon date uncertainties, as the Solow and Beet extinction estimator (Solow and Beet 2014) used in `spatExtinct` requires an average value for each date.

7.4.1 Data

Species occurrence data were mean values of finite calibrated radiocarbon dates. Dates of all scores were included in the models, but dates were given a confidence weight based on their score. To produce environmental models, absence data is also needed; these were randomly sampled from a blank map. Climate data was drawn from the WorldClim database, version 1.4, of the CCSM4 Last Glacial Maximum snapshot at 10 minute resolution (Hijmans et al. 2005). The bio-climatic variables were used: annual mean temperature, temperature seasonality, temperature annual range, annual precipitation, and precipitation seasonality (coefficient of variation). These were chosen to approximate annual-scale climate conditions and seasonality, as opposed to the (overly-precise, for these purposes) quarterly and monthly bio-climatic variables available. Additional elevation data was added from NASA (2009).

7.4.2 Species distribution models

`MaxEnt` is species distribution modelling software integrated in R through the package `dismo` (Hijmans et al. 2013; Phillips et al. 2017). `MaxEnt` models generally perform well, but they are prone to overfitting (Warren and Seifert 2011; Moreno-Amat et al. 2015). `ENMeval` tunes `MaxEnt` models and allows the user to select the best model based on number of metrics (Muscarella et al. 2014). Here `ENMeval` was used with the 'maxent.jar' algorithm. The algorithm is the Java-based implementation from `dismo`, as opposed to the more recent (2017) `ENMeval`-internal version, 'maxnet'. The two can produce subtly different results, and 'maxnet' does not provide variable importance information, so the older algorithm was used here (Phillips 2017; Phillips et al. 2017).

The recommendations of Phillips and Dudík (2008) and Merow et al. (2013) were used for model tuning. Models with a regularization parameter between 1–15

and hinge feature classes were run, and the model with the lowest delta-AICc selected. Hinge features are piecewise linear functions; they generalise thresholds and linear features. An example would be a species that has a linear relationship with temperature until a certain temperature limit, beyond which it cannot tolerate. Hinge features include the possibility of smooth linear functions, and so it is redundant to evaluate both linear and hinge features in `MaxEnt` models (Phillips and Dudík 2008; Elith et al. 2010).

Small numbers of species occurrence observations are a common problem in ecology. Using specific modelling approaches, such as jackknife validation, can mitigate this problem and produce models that perform well with <20 observations (Pearson et al. 2007). The jackknife approach has been used for the leopard dataset, since it has so few finite radiocarbon dates. The 'checkerboard2' method was used for the larger lion and hyena datasets (Hijmans et al. 2013; Carlson et al. 2017; Carlson et al. 2018b).

7.4.3 Spatial extinction models

Estimates of extinction were produced using package `SpatExtinct` (Carlson et al. 2018b) with the same radiocarbon datasets used in the species distribution models. The dates' scores were used as confidence weights in the model; the high-score dates were given more confidence, and therefore more influence over the model, than medium- and low-score dates. A model was produced that estimates timing of extinction over space, and another model was produced estimating probability of persistence at the species' GRIWM estimate of extinction. The former produces estimated dates, whereas the latter is a snapshot probability: the likelihood a species was or was not extinct at the given time, across space.

The latter was multiplied by the species' distribution map to produce a weighted distribution of persistence. This combined map models a combination of radiocarbon information plus environmental suitability. In Carlson et al. (2018b), this combined map was used to estimate where a possibly-extinct species was most likely to survive;

here, it is used to estimate where the definitely-extinct species was most likely to have last survived (Bond et al. 2019; Carlson et al. 2018a).

The main limitation of this approach is the static climatic data. Species lived through stadial and interstadial conditions, but only one can be modelled at a time, and the high-resolution bio-climatic variables available for the LGM are not available for a Pleistocene interstadial. Here LGM conditions were modelled as a 'worst-case' model, but it does not necessarily reflect conditions at the time of a species' extinction. As it is, GRIWM estimates suggest it probably is a fair snapshot for cave hyenas (chapter 15.3), but less so for lions (chapter 15.2); this is discussed as part of the results.

7.5 Kernel density estimates and time series

The relationships between megafauna, modern humans, and climate change is fundamentally one of time: does the pattern in climate explain the subsequent pattern in megafauna? (The same for humans and fauna, and for climate and humans.) There is an implied delay between the observed independent variable and the faunal response, though at the low temporal resolution of Pleistocene radiocarbon dates the two are sometimes assumed to be concurrent. Furthermore, the relationship might exist prior to the singular event of extinction; for example, if a climatic downturn explains an extinction, past downturns might explain past dips in population as well. It is also possible that humans might be subject to climatic variables while still having effects on fauna. A seeming correlation between humans and fauna might not reflect the effect of humans on fauna, but rather the effect of climate on both.

The idea that time is in itself a variable, and more specifically that past observations of a variable inform future observations, is central to time series analysis. Used widely in econometrics and signal processing, time series analysis is a set of statistical approaches for working with variables observed through time (time series) (Amiri and Ventelou 2012; Chatfield 2003; Mudelsee 2013). Particular approaches are required because time series violate the assumption that observations

are independent from each other, which is a key assumption in many statistical tests. Time series analysis instead incorporates this characteristic into its models. This approach suits the question of fauna, climate, and modern humans, as they coexisted not just at the point of extinction but through long periods of time.

Here, time series models were built from climate records and KDE models of fauna and AMH. These models were tested to evaluate the relationships between climate, fauna, and modern humans through their period of overlap.

7.5.1 Climate time series

If climate effects faunal populations, then the faunal response to a climate shift ought to lag behind it in time. In time series terms, climate is a leading variable, and faunal reponse is a lag variable. The position of humans is less simple. They might be affected by climate alongside fauna, but they might also have a compounding effect on fauna.

Climate records are time series, and indeed time series analysis is used in climate studies (Mudelsee 2013). In terms of the Pleistocene, the Greenland oxygen isotope records are time series. The main difference between them and traditional economic time series, or more recent climate records, is the uncertainty in the observation time due to counting errors in ice core rings (Rasmussen et al. 2014; Seierstad et al. 2014). While the ice core record is precise relative to many Pleistocene radiocarbon dates, the cumulative nature of counting errors means the ice core and radiocarbon timelines are not necessarily synchronous (Brauer et al. 2014; Rasmussen and Svensson 2016). Furthermore, using Greenland oxygen isotope records as a climatic proxy for continental Europe assumes that oxygen isotopes, which most closely reflect local atmospheric temperature (Rasmussen et al. 2014), reflect European climate both in scale and time. In reality lags between Greenland climate signals and continental European records have been suggested, though mostly at timescales below the uncertainty in Pleistocene radiocarbon dates. Attempts have been made to synchronise the oxygen isotope and radiocarbon record through tie points (Brauer

et al. 2014; Cooper et al. 2015), but they produce their own caveats, particularly regarding durations of glacial-interglacial cycles (Rasmussen and Svensson 2016).

The time series approach described below attempts to minimise the effects of these uncertainties by testing the relative, rather than absolute, relationship of the climate and species time series. Rather than perfectly synchronizing the two records, their overall 'shapes' are being compared. So long as absolute time offsets between the two records are significantly smaller than the uncertainties of the records themselves, they should have little effect on the results.

7.5.2 KDE models as time series

There is no high-resolution record of Pleistocene carnivore population levels through time. Even population estimates of Pleistocene modern humans, which have far more dates and been given more attention, differ by orders of magnitude (French 2015; Hawks 2008; Mellars and French 2011; Tallavaara et al. 2015). However, OxCal's kernel density estimate (KDE) models are models of observation density: where there are more observations (dates), the relative density in the model is higher (Bronk Ramsey 2017). Therefore, without making any absolute estimates of population, the KDE models estimate the relative pattern of species observations through time. If the sample is representative of the wider population and the KDE modelling approach dampens the influence of the calibration curve on the resulting distribution, then the KDE model is in a sense a time series.

Researchers have simply summed radiocarbon dates together and normalised their densities to create an equivalent model. Summed dates have been used as models of 'activity levels' at a site through time and as relative population estimates (Broughton and Weitzel 2018; Crema et al. 2016). However, summed distributions are influenced by the underlying structure of the calibration curve (Bronk Ramsey 2017). This means peaks in likelihood may be artefacts of the calibration curve rather than the dataset. Summed dates also tend to be quite 'noisy' or highly structured, which again produce spurious patterns. OxCal's KDE models try to mitigate these issues. The approach is explained in detail in Bronk Ramsey (2017), where it is

demonstrated that the combined KDE and Bayesian approach produces less noisy models and better reduces the influence of the calibration curve on the final model.

If a KDE model of a species is an approximation for its 'population' through time, then it might be treated as a time series. It is a highly biased one in terms of the sample (not random), but that bias carries through all attempts to interpret the radiocarbon dataset in terms of a species' activity, presence/absence, and extinction.

For this project, OxCal was used to produce kernel density estimates of species' activity through time, including the sampled AMH dataset (Bronk Ramsey 2017). KDEs model activity through time in a way that is difficult to discern by simply plotting radiocarbon dates in series. KDEs are also able to include radiocarbon uncertainties, which the spatial methods do not, and does so in a more robust way than simply summing dates.

7.5.3 Time series analysis

7.5.3.1 General approach

Time series are often informed by past behaviour; for example, if a value grows the previous three time steps, then it is more likely to grow in the fourth step. Previous steps that inform the current steps are called lags. Lags may also be seasonal, where an observation is not informed by the immediate previous observation but by some regular cycle of the k^{th} lag (*e.g.* the fourth lag in a quarterly time series or the twelfth lag in a monthly series). In addition to internal lags, a time series may be informed by an external time series and its lags, or other features like underlying linear or logarithmic trends.

The climate records from Greenland and a KDE model of modern humans were used as independent time series variables to model the response variable, the KDE distribution of the species. The species' time series was first modelled without the other two variables: this was the null model, where the shape of the time series (its own lags) explained its pattern. Another model was then built that included the climate and modern human record variables. Different lags became different variables in the model, so the length of the lag did not have to be pre-guessed;

finding meaningful lags was part of building the model. Finally, these two models were compared: if the second model better explained the faunal time series than the model built only with the faunal time series, then the null model was rejected. The climate/human time series lead the faunal series and the faunal series lags.

Because the model tests multiple lags and selects the most explanatory, the absolute duration (lag length) is less important than the overall pattern through time. This reduces the importance of asynchrous periods between the radiocarbon and oxygen records, as well as the potential lag between shifts in the Greenland oxygen isotope record and climatic/environmental changes on continental Europe. If the offset between the two records was consistent through time (*i.e.* the carbon record was consistently 1000 years older than the climate record), the time series model might model this as a 'lag' and produce a spuriously significant result. However, asynchronous periods in the climate and radiocarbon records are not consistent through time (Rasmussen and Svensson 2016), reducing the risk of a false offset through the whole series. As a check that the model was not identifying false lead-lags, models where climate lagged fauna/human records were tested. The idea that the human/fauna KDEs lead the climate signal is fairly illogical, and if the test found significance in this direction of lead-lag, that might reflect the influence of systematic offsets in the radiocarbon and climate records.

In time series analysis, the final test comparing two models is called a causality test. However, the test is not really claiming to test whether one time series *causes* another; it is only saying that one time series is better explained with additional information from the other time series. Interpreting that result still falls outside the scope of the test.

7.5.3.2 VAR models

A vector autoregressive model (VAR) incorporates multivariate time series in a 'neutral' model, where the relationship between time series variables is not pre-assumed; rather, they are all treated as endogenous to the model. If y_t is a vector of m time series variables, then a VAR(p) model of k lags is generalized as

$$y_t = v + A_0 y_t + A_1 y_{t-1} + ... + A_k y_{t-k} + \epsilon_t$$

where y_t and v are $m \times 1$ matrices of the variables, $A_0, A_1, ...A_k$ are $m \times m$ matrices of coefficients, and ϵ_t is an m-element vector of residuals. Additional exogenous variables and deterministic terms can also be added as

$$y_t = v + A_0 y_t + A_1 y_{t-1} + ... + A_k y_{t-k} + \boldsymbol{BD_t + GX_t} + \epsilon_t$$

where D_t and X_t are vectors of deterministic components and exogenous variables, respectively, and B and G are parameter matrices (Chatfield 2003; Lütkepohl 2007).

Here, y_t are three series: climate, AMH, and the species. No stochastic exogenous variable X_t was included, but a dummy variable for structural breaks in the isotope record was included as D_t.

7.5.3.3 Methods

The Toda and Yamamoto (1995) method was used to test for long-run causality between climate, modern humans, and fauna. The approach uses a modified Wald test of non-causality (Zapata and Rambaldi 1997), but the models tested are built so as to avoid issues of non-stationarity and possible co-integration (Amiri and Ventelou 2012; Bauer and Maynard 2012; Wolde-Rufael 2005). While both stationarity and co-integration can be tested for, the tests can suffer from low power, and incorrectly identifying the unit root and level of co-integration strongly affects causality tests (Zapata and Rambaldi 1997). The Toda and Yamamoto (1995) approach circumvents these problems by building a vector autoregressive model (VAR) in levels from the untransformed data and modifying the VAR so that the final Wald test statistic has the desired chi-square distribution (Bauer and Maynard 2012; Wolde-Rufael 2005).

To build the models, the δ^{18}O climate record was evaluated for structural time breaks using breakpoint estimation as in Zeileis et al. (2002) and Zeileis et al. (2010). Five breaks were found and implemented in the VAR model as an exogenous

variable. KDE distributions of AMH and fauna were exported from OxCal with points every five years; these were aggregated into 50-year bins by mean density to match the sampling rate of the δ^{18}O record.

All series were evaluated for non-stationarity with the augmented Dickey-Fuller test for non-stationarity (Dickey and Fuller 1979) and the Kwiatkowski-Phillips-Schidt-Shin (KPSS) test for stationarity (Kwiatkowski et al. 1992). Time series were tested at increasing difference order until both tests were satisfied. The maximum integration order among all the time series was selected as d_{max}.

A vector autoregressive model was built from the data levels (without integration). The model was built with a maximum lag order of 20, and then the generalized information criterian (GIC) selection algorithm in R package `FitAR` was used to select an appropriate lag order (McLeod and Zhang 2006; Zhang et al. 2010; McLeod et al. 2013). Approximate GIC values were calculated and the exact GIC calculated from the best six approximate-GIC candidate models. A tuning value of 0.001 was used. The chosen lag order model was evaluated for autocorrelation, and if needed, the lag order was increased to remove autocorrelation.

Finally, a VAR model was built with the correct lag order, k, plus d_{max} additional lags (from the maximum order of integration above). The modified Wald non-causality test was used to evaluate the model's k coefficients; the d_{max} additional lags were not tested. The addition of unevaluated lags forces the test statistic to have the necessary asymptotic distribution. The null (non-causality) was rejected below the 5% level.

7.6 Conclusions

This project has two components: optimising radiocarbon pre-treatment of bone samples and applying radiocarbon dating to investigate Pleistocene carnivore extinctions. Both require working with complex samples and relatively small datasets, but they have relevance to wider methodological and ecological questions. The results of the laboratory experiments are presented in the next chapter, followed by the results of radiocarbon dating and modelling.

Part III

Experimental results

8
%N tests

8.1 %N at Zafarraya

As expected from previous work (Wood et al. 2013a), the majority (87.34%) of Zafarraya bones measured for %N failed to produce values over the threshold of 0.76% (Fig. 8.1). Only 6% of bones had %N values >1% N. The distribution of results did not show multi-modality, which might have suggested two subpopulations of bones in terms of preservation. Comparison with samples' contexts did not reveal a spatial trend in %N results, either horizontally by grid square or vertically by depth. Rather, there seems to be general variability in %N across the site.

8.2 %N versus collagen yields

In total, 36 of the 50 selected bones (72%) produced collagen yields correctly predicted by their %N values (Fig. 8.2). These bones were divided evenly between correctly predicted passes (>1% collagen yield) and fails. However, 14 bones (28%) produced incorrectly predicted collagen yields. Eight bones below the 0.76% N threshold produced >1% collagen (false negatives) and six bones over 0.76% N produced <1% collagen (false positives). The more lenient 0.5% N cut-off made more incorrect predictions overall (34%) due to increased false positives.

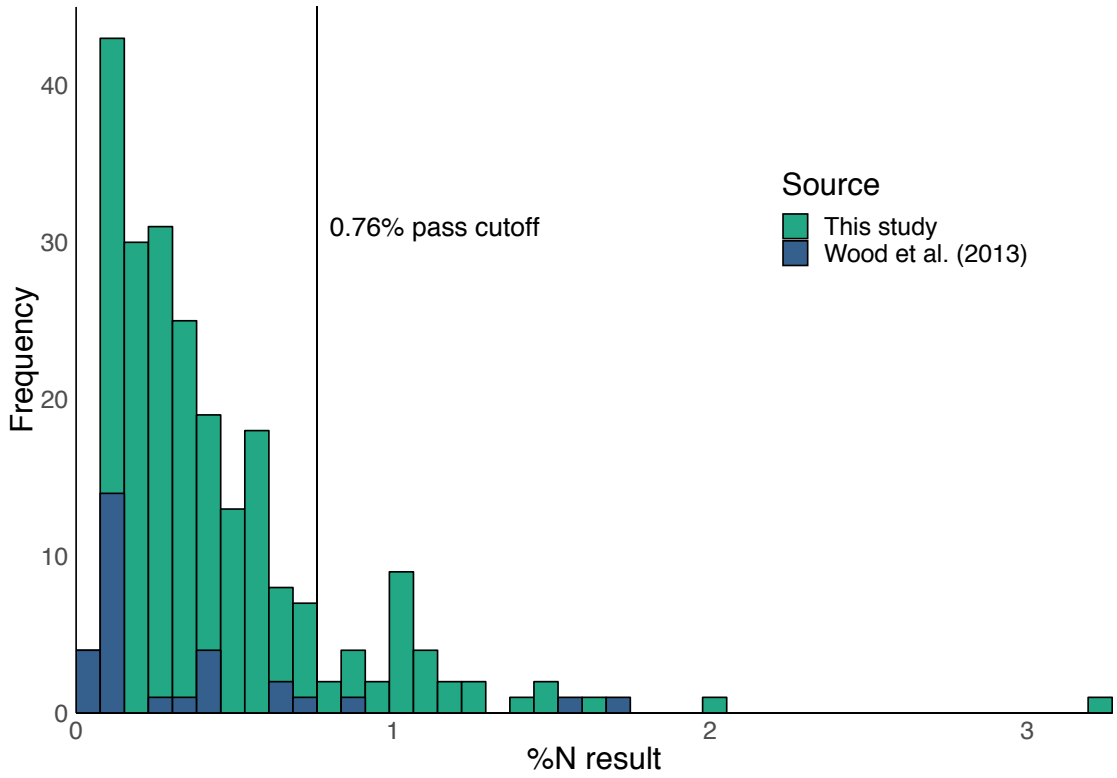


Figure 8.1: Histogram showing %N values for 259 samples from Zafarraya: 229 new to this study and 30 previously measured in Wood et al. (2013a).

8.3 Intra-bone variation in %N

Eight large bones were sub-sampled at between 4 and 11 points to characterise %N variation. As shown in Fig. 8.3, the intra-bone variation of some bones was significant. The largest range in a bone was 0.75% (Bone 2); given a modern bone is about 4% nitrogen (Stafford et al. 1988), this represents some 19% of a bone's potential nitrogen content. Measurement error on the mass spectrometer is ∼0.3‰ and so cannot explain most of this variation.

Three of the bones (Bones 1–3) had samples that spanned the 0.76 %N cut-off. If only sampled once, each bone could have failed or passed the screening depending on where it was drilled. This suggests that the preservation of some bones is being incompletely characterised by a single %N measurement, leading to false passes and failures.

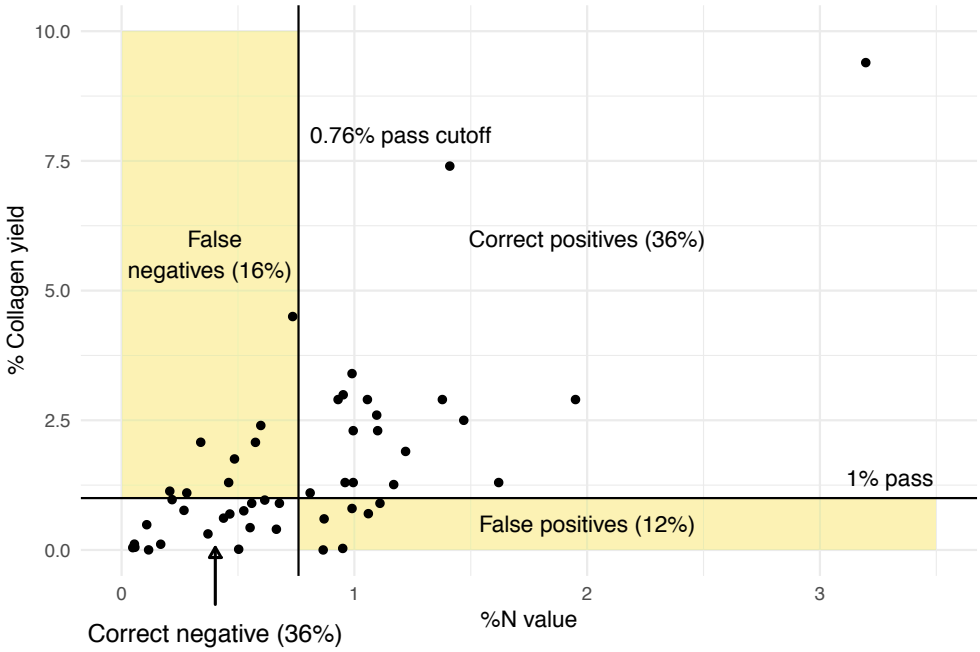


Figure 8.2: Graph showing the relationship between %N and ultrafiltered collagen yields from 50 bones. The lines on the graph represents the cut-offs used at the ORAU (%N >0.76 and collagen yield >1%).

8.4 Discussion

This study found that %N correctly predicted collagen yields 72% of the time, similar to the 73% likelihood from previous results (Brock et al. 2012). Of the 28% incorrectly identified bones, there are examples where %N failed to predict both high and low collagen yields. There are multiple and complex processes involved in bone diagenesis, which makes explaining these results challenging (Collins et al. 2002; Dobberstein et al. 2009; van Klinken and Hedges 1995). That bones with low %N may produce collagen is surprising. Brock et al. (2012) found all bones with <0.24% N failed to produce sufficient collagen, suggesting that %N screening is not missing bones with regions of collagen preservation. However, this study found samples with %N as low as 0.207 that produced collagen yields >1% weight. One explanation is that these bones contained variation in collagen preservation not revealed by a single %N measurement. The subsampling results suggest that

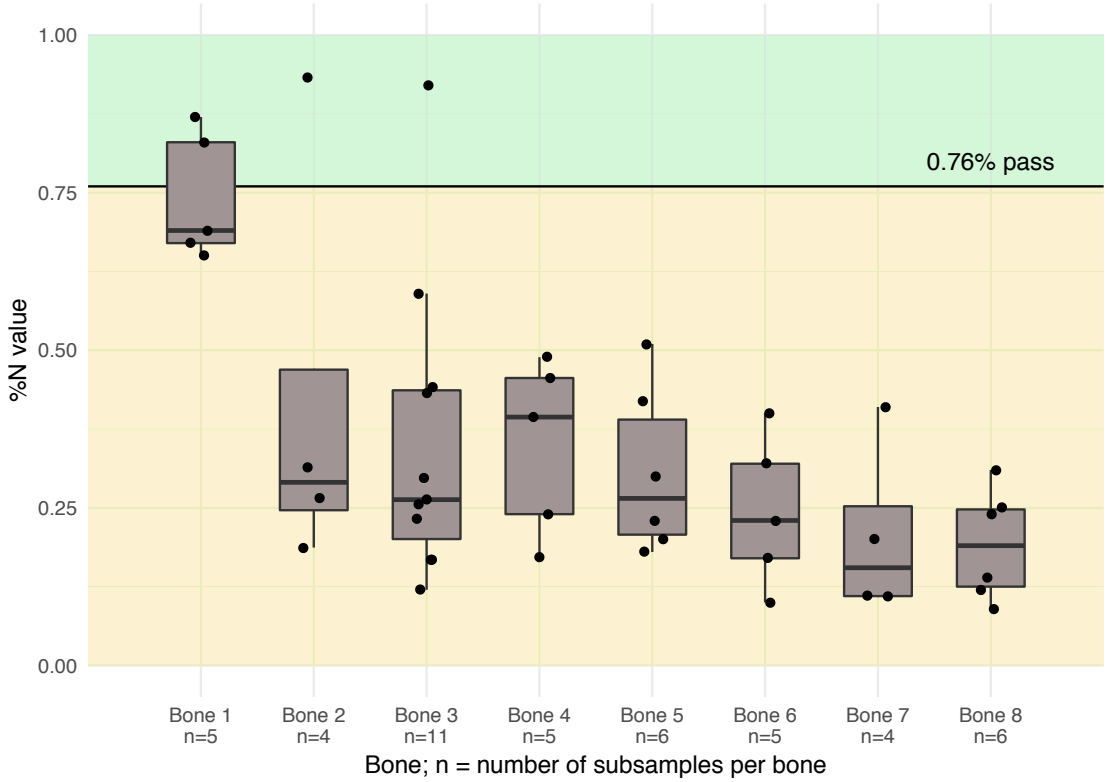


Figure 8.3: Results of sub-sampling eight bones with %N results as box plots. The number of samples taken from each bone is listed below the box plot.

significant variation in %N can exist in bones. Some bones may be rejected based on a single %N measurement, when in fact a measurement taken from a different point in the bone may have passed.

Another possibility is that deamidation of collagen has removed nitrogen while significant partially degraded protein remains. This process removes the nitrogen-containing amide group from asparagine and glutamine and has been observed in ancient bones (Cleland et al. 2015; van Doorn et al. 2012; Wilson et al. 2012). van Doorn et al. (2012) found that deamidation was accelerated in particular burial conditions, such as hydrological activity and low soil pH. In these accelerated cases deamidation could reduce nitrogen content before other protein-destroying processes are complete.

Six bones in this study produced high %N values but little collagen. There are three hypotheses that might explain these false positives. First, some of the high %N results may be due to contaminated regions, perhaps from humics, nitrates,

bacteria, or fungi. Humics are complex large molecules that can contain nitrogen and carbon. They are soluble in basic solutions and the base wash in ABA is meant to remove them (Head et al. 1987; van Klinken and Hedges 1995), but they may be a source of nitrogen in the initial %N screening. Presence of nitrates has been used to explain misleadingly high nitrogen values in bones from the Neolithic settlement of Çatalhöyük (Brock et al. 2012). Microbes and fungi that produce collagenase have also been isolated from archaeological bone (Child 1995). If still present in the bone matrix, they may contribute to the %N value before pretreatment. Second, the samples that go on to pretreatment may contain collagen-free areas, despite a seemingly good %N screen. A larger bone sample (∼1 g) was used for collagen extraction than %N measurement (∼5 mg) and so there may be less protein in the extraction fraction than the %N fraction. Third, the quality of the collagen itself may be problematic. In Pleistocene bones, large chains of collagen may degrade into smaller fragments. These will still contain nitrogen but may be lost during ABA-gelatinization and ultrafiltration. Ultrafiltration in particular could allow small-chain collagen fragments to pass through the 30 kDa filter (Brock et al. 2013a). Material from Zafarraya is Pleistocene in age, and so the quality of the collagen, not just its abundance, may be part of the variation in results. Any of these explanations may be relevant to a given site, depending on the post-depositional context of the bones.

Nitrogen variability exists within individual bones as well. While the above diagenetic processes may be occurring at locales within a bone, little is currently known about intra-bone nitrogen variation. Further exploration of the correlation between sub-sampled %N and collagen yields would be useful, as the size of these higher nitrogen regions and their link to collagen yields is unclear. This could include mapping bones to understand which bone or part of the bone is more likely to have collagen preserved, similar to the way DNA is optimally preserved in the petrous bone (Pinhasi et al. 2015). One potential method is to use non-destructive FTIR to characterise sources of nitrogen in a sample (Lebon et al. 2016), but this has not yet been widely applied to difficult archaeological samples such as low-collagen bones or bones treated with organic conservation materials.

8.5 Conclusions

This study reveals that using %N as a simple pre-screening metric can be problematic, and there are likely unexplained processes that can undermine the predictive value of %N. Particularly in difficult Pleistocene sites where bones are producing marginal (>0.2% N) or variable values, it may be worth attempting pretreatment in hopes of finding some false negatives. Some of the Zafarraya material discarded by Wood et al. (2013a) based on %N values, for example, may be worth revisiting.

This study also reveals significant variation in %N values when a bone is drilled in multiple locations. Again, in sites where preservation is likely to be problematic and for particularly important samples, it can be worth taking multiple %N measurements in the hope of finding a location to drill for dating where the collagen might be differentially better preserved than in other areas.

While %N continues to be a useful screening tool for radiocarbon dating and isotope analysis—it is cheap, rapid, and requires little sample destruction—there are situations where it can be worth relaxing the use of the 0.76% cut-off. Indeed, this is already done at the ORAU when site conditions and overall preservation warrants trying lower-%N bones (Brock et al. 2010b). This requires sample destruction and may not always be worth the risk, but for archaeologists working with difficult samples it is useful to be aware of these frequent exceptions and the scale of variability that can exist in a single site and even a single bone.

9 Caldey hyena tests

Hyena teeth from Caldey Island, Wales were analysed to identify potential treatment with conservative. Namely, the excavators had written about using Ronseal, a wood varnish, to strengthen bones. The teeth were already radiocarbon dated; this investigation aimed to assess the reliability of those dates.

9.1 Micro photography

From visual inspection alone, the hyena samples look clean of conservation material, whereas the *Bos* metatarsus is strikingly red varnished with dirt and small stones adhered to it (Fig. 4.2). The *Bos* bone is coated in a glossy red substance that has adhered material to the bone. When inspected and photographed under a microscope, the hyena teeth show no such colourant or glossy texture, including at the locations where they were previously sampled for dating (Fig. 9.1).

It is possible that the teeth were cleaned in the past, leaving residual varnish in the tooth matrix not visible to the eye. It is also possible the teeth were treated with a different consolidant not recorded by the excavators (Van Nédervelde and Davies 1975). As a first observation, however, the hyena samples do not appear to have been varnished.



Figure 9.1: Microscopic views of the *Bos* bone surface and Caldey samples at the locations where they were previously sampled for radiocarbon dating. Row-wise from top left: Ogof Morfran *Bos* bone surface (2004.16H/22, x10 magnification); Eel Point cave (8:NMGW 90.SSH (116), x10); Nanna's Cave (Z/1983/076.1699, x4); Ogof-yr-Ychen (Z/1983/076.286, x10); Ogof-yr-Ychen (Z/1983/076.287, x4); Potter's Cave (7:NMGW 91.7H, x4).

9.2 FTIR

A few micrograms of Caldey teeth, untreated Latton bone, and a surface flake from the *Bos* metatarsus were evaluated with FTIR (Fig. 9.2).

The three Caldey samples share similar spectra with bands characteristic of amides, phosphates, and carbonates (Fig. 9.2 and Table 9.1). These components are found in bone/tooth mineral and protein. Bands corresponding to amides I, II, and III are present in the samples, though the bands of amides II and III are very weak in both Ogof Ychen 286 and Nanna's Cave 1699. The double peaks at 1454 and 1413 cm^{-1} and the small peak at 873 cm^{-1} correspond to carbonates. The strong peak at 1023 cm^{-1} and the shoulder at 961 cm^{-1} correspond to phosphates. Both are components of apatite. The broad band between 2600–3600 cm^{-1} corresponds to water and overwrites the N-H stretching of collagen. A small peak at 2920 cm^{-1} reflects C-H stretching observed in collagen. The double peaks at 2359 and 2341 cm^{-1} reflect atmospheric CO_2.

The hyena spectra are similar to the Latton bone spectrum. Like the hyena samples, the amide II and III peaks are weak in the Latton bone, despite it having relatively good collagen preservation. In general agreement between the spectra supports the Caldey teeth being clean enamel-collagen.

Like the Caldey and Latton samples, the *Bos* surface flake has peaks corresponding to phosphates, carbonates, CH stretching, and amides I and II. It also has additional bands (Fig. 9.2; Table 9.2). Bands at 2850–2900, 1600–1800, and 1000–1220 cm^{-1} in particular are not present in the other samples and are not identifying components in bone/tooth. These distinct peaks have been observed from polyurethane varnishes (Coleman et al. 1988; Hu et al. 2009; Queiroz et al. 2003; Trovati et al. 2009; Yang et al. 2001), which Ronseal is. The double peaks at 2852 and 2921 cm^{-1} are attributed to C-H_2 stretching with carbonyl. The large peak at 1714 cm^{-1} likely reflects stretching of a carbonyl group. The double peak at 1217 and 1224 cm^{-1} corresponds to C-O stretching. Amides, while present, are in slightly different positions and have different strengths than in the bone samples; Amide III

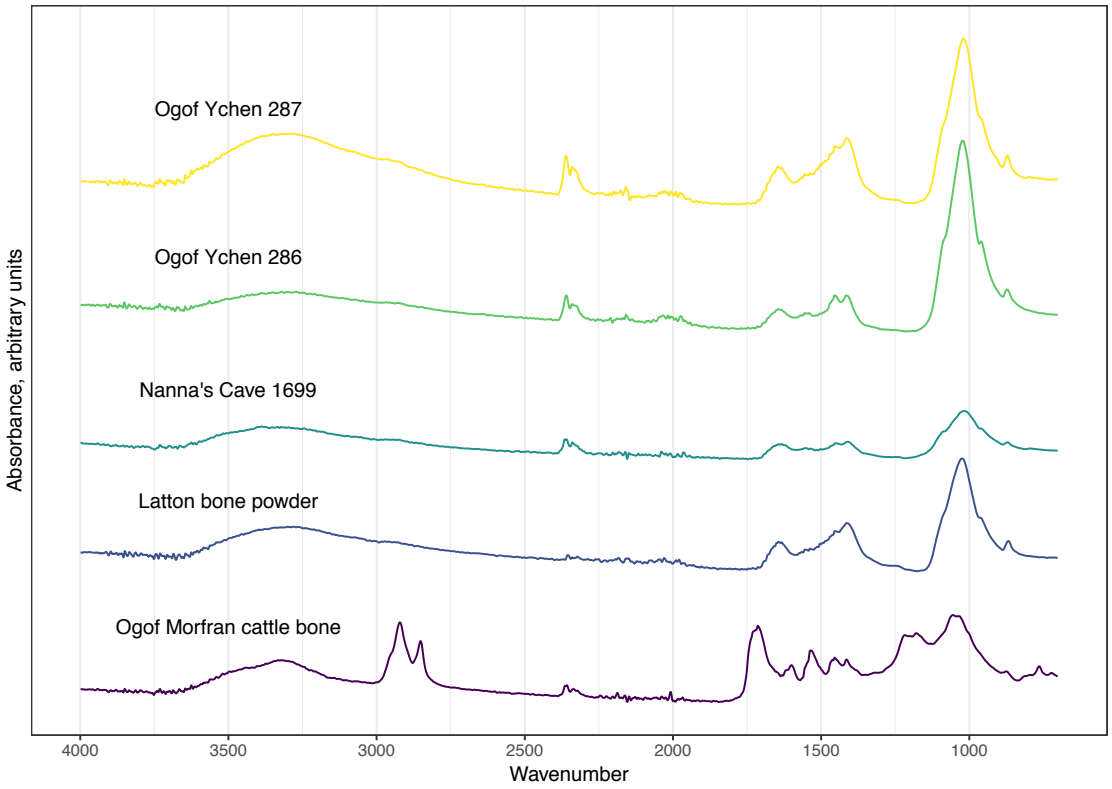


Figure 9.2: FTIR spectra of the three hyena tooth samples and the two bones used as comparison samples.

is probably hidden as a shoulder in the 1217 cm^{-1} C-O band (Perrin et al. 2000). Amides are components of varnishes in some characterization studies, suggesting the amides may not only reflect bone powder but the conservative material too. Overall the *Bos* profile is consistent with bone and a polyurethane substance, though some differences in the profile may be attributable to the *Bos* bone coming from another site and undergoing different diagenetic processes.

Spectroscopy has been used to evaluate bone before (Beasley et al. 2014; Brock et al. 2018; Lebon et al. 2016), but different kinds of IR (ATR, DRIFT, IR-SF) data are not always directly comparable. The sensitivity of FTIR might not reveal trace quantities of material. However, the apatite-collagen signal of the Caldey samples matches the Latton bone and lacks the distinct peaks seen in the contaminated *Bos* bone. This suggests the hyena samples have not been treated with the same substance.

Table 9.1: FTIR bands observed across all the hyena bone/tooth samples. (Additional bands unique to the *Bos* bone are listed in Table 9.2). v and v_1 = symmetric stretching, v_2 = asymmetric stretching (nonlinear) / bending (linear), v_3 = bending vibrations (nonlinear).

Value cm^{-1}	Assignment	References
∼3320	vH_2O, $vN-H$	Bereuter et al. (1997); Devièse (2009); Kamińska and Sionkowska (1996); Raif and Harmand (1993); Reiche et al. (2002); Walters et al. (1990)
∼2920	$vC-H$ with carbonyl	Bereuter et al. (1997); Devièse (2009); Raif and Harmand (1993); Reiche et al. (2002)
1642	Amide I	Bereuter et al. (1997); Chang and Tanaka (2002); Devièse (2009); Kaminská et al. (2011); Raif and Harmand (1993); Reiche et al. (2002)
1556	Amide II	Bereuter et al. (1997); Chang and Tanaka (2002); Devièse (2009); Kaminská et al. (2011); Raif and Harmand (1993); Reiche et al. (2002)
1454	$v_3CO_3^{2-}$	Chang and Tanaka (2002); Devièse (2009); Ooi et al. (2007); Raif and Harmand (1993); Reiche et al. (2002)
1413	$v_3CO_3^{2-}$	Chang and Tanaka (2002); Devièse (2009); Ooi et al. (2007); Raif and Harmand (1993); Reiche et al. (2002)
1249	Amide III	Chang and Tanaka (2002); Raif and Harmand (1993)
1023	$v_3PO_4^{3-}$	Chang and Tanaka (2002); Ooi et al. (2007); Paschalis et al. (2011); Reiche et al. (2002); Walters et al. (1990)
961	$v_1PO_4^{3-}$	Chang and Tanaka (2002); Devièse (2009); Ooi et al. (2007); Paschalis et al. (2011); Walters et al. (1990)
873	$v_2CO_3^{2-}$	Chang and Tanaka (2002); Devièse (2009); Ooi et al. (2007); Paschalis et al. (2011); Reiche et al. (2002); Walters et al. (1990)

Table 9.2: Additional FTIR bands observed in the *Bos* bone. v and v_1 = symmetric stretching, v_2 = asymmetric stretching (nonlinear) / bending (linear), v_3 = bending vibrations (nonlinear).

Value cm^{-1}	Assignment	References
2920	vC – H_2 with carbonyl	Hu et al. (2009); Pardini and Amalvy (2008); Perrin et al. (2000); Trovati et al. (2009); Yang et al. (2001)
2852	vC – H_2 with carbonyl	Hu et al. (2009); Pardini and Amalvy (2008); Perrin et al. (2000); Trovati et al. (2009); Yang et al. (2001)
2009	PO_4^{3-}	Joschek et al. (2000); Ooi et al. (2007)
1730	vC=O carbonyl	Hu et al. (2009); Perrin et al. (2000); Trovati et al. (2009); Yang et al. (2001)
1714	vC=O carbonyl	Coleman et al. (1988); Hu et al. (2009); Pardini and Amalvy (2008); Queiroz et al. (2003); Trovati et al. (2009); Yang et al. (2001)
1600	Amide I vC=O	Coleman et al. (1988); Perrin et al. (2000); Queiroz et al. (2003); Trovati et al. (2009)
1537	Amide II vC-N, v_2N–H	Pardini and Amalvy (2008); Perrin et al. (2000); Trovati et al. (2009)
1217	vC–O	Hu et al. (2009); Trovati et al. (2009); Yang et al. (2001)
1178	C–H bending	Coleman et al. (1988); Queiroz et al. (2003)
1057	$v_3PO_4^{3-}$	Lebon et al. (2008); Lloret et al. (2006)
764	C–H bending	Coleman et al. (1988); Queiroz et al. (2003)

9.3 Pyrolysis GC-MS

T. Devieèse kindly offered to analyse bone powder from sample Z/1983/076.287 by pyrolysis GC-MS at the University of Pisa (Fig. 9.3).

Ronseal contains propylene glycol ($C_3H_8O_2$), colourants, and other polymers ("Ronseal Quick Drying Varnish" 2009). However, the spectrum here is typical of collagen, with the main pyrolysis products being cyclic nitrogen-containing compounds. Pyrrole and alkyl-pyrroles are also typical collagen products in these conditions. The results do not contain peaks that would suggest other products are present. While we did not have the opportunity to analyse all three Caldey samples, this one at least lacks identifiable contaminants.

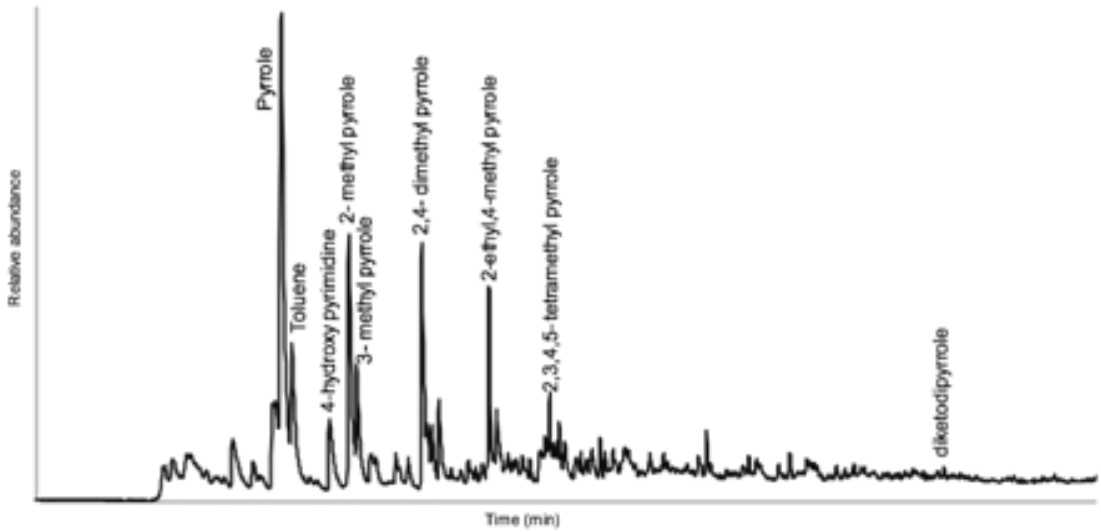


Figure 9.3: Pyrolysis products from Caldey hyena tooth Z/1983/076.287.

9.4 AMS data

Quality criteria for radiocarbon dates suggest the samples had little collagen, but there is little evidence for contamination (Table 4.2). However, three of the teeth were re-dated more recently, and not all of the results agree with each other.

The CN ratios of all the dates fall within the tolerated range of 2.9—3.5, though OxA-9692 is at the 3.5 limit. The later re-date of this tooth has an improved CN of 3.2. OxA-9673 from Nanna's Cave has a low %C (4%) and was collected into an ampoule rather than graphitised, though its CN ratio is an acceptable 3.1. The others all have typical bone %C values. The isotopic values of the samples are internally consistent and fit terrestrial mammals, though they are of limited use without site-level comparative values. The %yield for all the samples were low but above the lab's required 1% minimum.

When %C and CN ratios are plotted, the Caldey samples mostly fall within the general range of Latton bone results (Fig. 9.4). The exception is OxA-9673 from Nanna's Cave with low %C that was collected by ampoule.

Three of the samples were later redated. When compared with a student t-test, the paired dates from both the Ogof-yr-Ychen teeth are significantly different (p

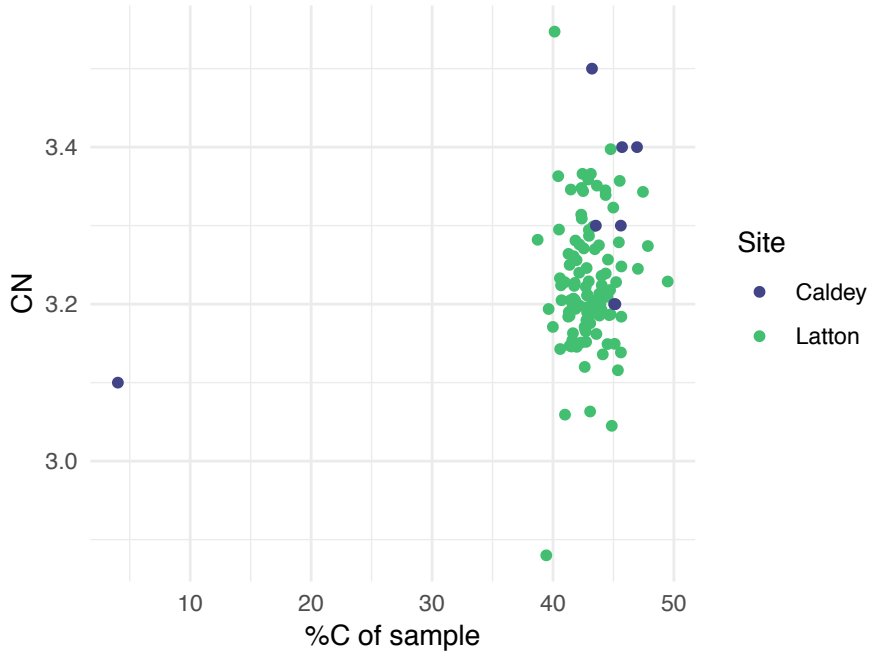


Figure 9.4: Percent carbon (%C) and CN ratios of dated Latton bone and Caldey samples.

<0.05), but the Potter's Cave results are not significantly different. One of the Ogof samples produced a younger second date and the other an older second date. These two re-dates were given OxA-X codes, nominally as health warnings, but notes in the database report that the concern was over the low collagen yields and small starting sample size. The sample yields were low, but still higher than the 1% minimum, and the original dates had similarly low yields.

All of the Ogof-yr-Ychen dates were produced from samples that had the same pretreatment, so it is difficult to say which dates are more reliable. The conservative choice seems to be to accept the OxA-X dates with the improved CN ratios, but these dates were never published or included in the papers discussed here.

The Nanna's Cave date falls outside the expected %C values, and so ought to be treated cautiously. The two dates from the Potter's Cave sample are statistically similar and have acceptable date quality metrics, and so seem fair to accept.

9.5 Discussion

9.5.1 Sample reliability

Negative evidence is never absolutely conclusive and there remains the possibility that the Caldey samples are in some way contaminated. The samples underwent the optional solvent wash during pretreatment and were ultrafiltered, but there are examples in the literature of samples contaminated with substances resistant to even these lab purification protocols (Brock et al. 2018; Devièse et al. 2017; Marom et al. 2013). Some glues or varnishes may not be visible to the eye and/or be invisibly embedded in the sample matrix. There is also the possibility that the Caldey samples were contaminated with collagen-based glue, which would not be distinguishable from sample protein in FTIR spectra and would not be removed with lab pretreatment. There is no visual evidence for glued breaks on the samples, however, nor any written comments from the excavators that materials other than Ronseal were used.

In this case, the Caldey samples look to be clean bone collagen/apatite through visual inspection, through FTIR, and through pyrolysis GC-MS. In addition, the samples were radiocarbon dated with ultrafiltration, the recommended protocol for Pleistocene collagen (Higham 2011; Lister and Stuart 2013). While the collagen yields were not high, there were no significant problems with the sample isotopes or CN ratios that would suggest contamination when they were dated. The samples accepted in Dinnis et al. (2016) were also ultrafiltered. From these results, there is no particular reason to reject the Caldey samples. Simply because they are younger than expected does not make them erroneous.

Ideally, the samples would be dated with a more robust protocol, such as dating just the amino acid hydroxyproline through HPLC (Devièse et al. 2018). However, this method requires >30 mg of collagen, and given previous yields of these teeth, it was calculated too much sample would be destroyed (>500 mg each). In the future, if protocols are improved so that smaller sample sizes are required, then these samples could be dated. Until then, these analyses make for a more thorough

quality check than most radiocarbon samples receive and suggest the Caldey dates can be considered in discussions of hyena chronology.

9.5.2 Hyena extirpation in the UK

While hyena extinction is modelled in subsequent chapters alongside other carnivores, here UK extirpation of hyenas are considered and compared with published dates.

The Caldey hyena dates represent some of the youngest hyena dates in Europe, but the youngest raw radiocarbon date does not reflect the true extinction date. In addition to measurement uncertainties and the need for calibration, the youngest observation is only a *terminus post quem* for true extinction. Here exinction has been estimated with the GRIWM method (chapter 2.5.3). The GRIWM estimator incorporates the uncertainty in radiocarbon dates and reduces bias compared to the LAD, though the resulting estimate has lower precision.

Compared to the GRIWM estimate using dates accepted by Dinnis et al., the UK GRIWM estimate that includes the Caldey dates is significantly younger, with a median difference of ∼4400 years (Table 9.3). When the larger dataset from Stuart and Lister (2014) is used, there is little change in Caldey-included and Caldey-excluded estimates due to the inclusion of the similarly late date from Paviland Cave, which Dinnis et al. reject. However, including the Caldey dates significantly narrows the confidence interval from ∼3600 years to ∼1000 years.

With the inclusion of the Caldey dates, the UK extinction estimate overlaps with the overall European extinction estimate (that excludes Caldey). There are dates of <30 ka cal BP from Italy, Greece, Bulgaria, France, and Belgium. The Caldey dates suggest a similar, relatively abrupt disappearance of hyenas across the whole continent around ∼30 ka cal BP, shortly before the LGM. This is explored more in chapter 15.3.

The wider uncertainty in the GRIWM estimate makes it difficult to say whether Caldey represents continuity or a recolonisation event, though other late dates from the UK and northwest Europe suggests continuity was likely.

Table 9.3: GRIWM estimates for hyena extinction in Europe, comparing different datasets. From/To: 95.4% confidence interval range.

Data	Caldey dates	Median cal BP	From	To
Europe: Stuart and Lister (2014)	Including Caldey	29552	30557	28346
Europe: Stuart and Lister (2014)	Excluding Caldey	29404	30526	28265
UK: Stuartand Lister (2014)	Including Caldey	30148	31179	30148
UK: Stuartand Lister (2014)	Excluding Caldey	29984	31823	28262
UK: Dinnis et al. (2016)	Including Caldey	30088	31211	27187
UK: Dinnis et al. (2016)	Excluding Caldey	34500	35947	32241

9.6 Conclusions

The Caldey hyena teeth samples were ultrafiltered before their measurement on the AMS, and while ideally they would be re-dated with the HYP protocol (Devièse et al. 2018), the limited material available made this approach impossible. Visual inspection, FTIR analysis, and pyrolysis GC-MS were employed to characterise the Caldey hyena teeth specimens. These analyses revealed neither the presence of conservation materials such as Ronseal nor other contaminants. Based on the data generated during radiocarbon measurements and the additional analyses reported here, there is no reason to reject the Caldey dates. Caldey Island remains the site of the LAD of hyenas in the UK at around 27 ka BP / 30 ka cal BP. Furthermore, the Caldey hyena dates are included in subsequent modelling chapters, though evaluated on the same criteria as all other dates.

10 Characterizing failed bone samples

Over the course of this project several samples produced a white material after chemistry pretreatment that failed upon graphitisation, either due to insufficient carbon or poor quality metrics during graphitization. The material does not appear to be collagen, and some of these samples were tested to better understand what the material is.

Samples came from a variety of sites. The investigation aimed to characterise these non-collagen yields and, if they were a similar material across samples, consider how the pretreatment protocol was interacting with the samples to produce this material.

10.1 Collagen yields and graphitisation

Collagen for all samples were extracted using the routine AG protocol described in Brock et al. (2010b) and chapter 6. The gelatinised product was freeze-dried, and the resulting white material weighed and the %yield calculated. When samples produced sufficient material (>20 mg and >1% yield), a fraction of the AG yield was re-dissolved and then ultrafiltered as in the AF protocol in Brock et al. (2010b) (Table 10.1). In addition, sample P44413 produced enough material to attempt hydrolysis for HPLC dating (chapter 6) (Table 10.2). The ultrafiltered and HPLC

Table 10.1: Samples that produced an unidentified white material that failed to graphitize. The sample size is the amount of bone powder drilled for pretreatment. AG %yield is the percent yield of extracted collagen as a function of the starting weight of the bone analysed after AG extraction. AF used (mg) is the amount of AG collagen used for AF extraction; AF %yield is relative to bone sample amount. %C and %N are the percentage carbon and nitrogen present in the combusted sample, respectively. Stable isotope ratios (δ^{13}C) are expressed in permille (‰) relative to vPDB with a mass spectrometric precision of ±0.2‰ (Coplen 1994).

Sample ref	ORAU code	Sample size (mg)	AG %yield	AF used (mg)	AF %yield	%C	δ^{13}C	%N
GD/16753	P44208	970	4.10	30.30	0	0.46%	-20.2	0.07%
AL/C/2	P44209	830	2.00	NA	NA	0.33%	-19.5	0.08%
AL/B/15	P44210	1000	2.00	11.30	0	0.31%	-24.0	0.07%
GD-16	P44211	1340	2.50	22.90	0	0.23%	-23.2	0.05%
Paglicci 5	P45640	1200	2.09	14.76	0	6.42%	-19.2	0.02%

Table 10.2: Samples that produced an unidentified white material but were not graphitized due to low quality metrics. Headers are as for Table 10.1, except AF/NRC used means the sample was either ultrafiltered (AF) or hydrolysed for HPLC (NRC).

Sample Ref	ORAU code	Sample size (mg)	AG %yield	AF/NRC used (mg)	AF/NRC %yield	%N
Castel 2	NA	940	1.55	8.67 (AF)	0.13	0.17%
T.10376	P44409	725	1.91	NA	NA	0.08%
T.10.A.2	P44413	942	7.16	50.42 (NRC)	0.00	0.16%

samples failed to produce enough material to graphitise. About 5 mg of the AG gelatin material that had been obtained following the AG procedure for five samples was then graphitised. The samples failed to produce sufficient carbon for measurement on the AMS. The data collected during graphitisation revealed that these samples contained little carbon and nitrogen compared to a normal collagen sample (Table 10.1). This suggests that, despite their visible similarity to collagen, the samples were not proteinaceous.

10.2 FTIR

FTIR spectra are similar across all the failed samples and are distinct from hydroxyapatite and Latton collagen (Fig. 10.1). Some samples that failed to produce carbon during combustion showed similar sprectra to the Ghar Dalam samples

(Fig. 10.2). Tilos samples come from another Mediterranean island, while Silluca is Spanish and Paglicci and Castelcivita are Italian. Despite these different locations and presumably different burial conditions, the final product looks to be similar.

These samples lack most amide peaks associated with bone collagen but show peaks related to phosphates and carbonates. The peak at 1630 cm^{-1} (Table 10.3) is likely due to C=O bending from carbonate and/or water, rather than amide I, though the two overlap and a similar peak is present in the Latton gelatin sample (Kannan et al. 2006; Lebon et al. 2010; Lopes et al. 2018; Quarta et al. 2014; Wang et al. 2010).

There is a peak at ~1430 cm^{-1} in the treated samples, though it is relatively small compared to Latton raw bone. This peak is attributed to v_3 CO_3, with slight variation in peak location reflecting different carbonate substitutions (Antonakos et al. 2007; Lebon et al. 2010; Lopes et al. 2018; Quarta et al. 2014; Wopenka and Pasteris 2005).

The failed samples also share four peaks (plus a shoulder) between 1300–900 cm^{-1}, which match neither Latton standard AG gelatin nor the hydroxyapatite standard (Fig. 10.2). While analysing IR spectra of poorly-preserved bones, Gianfrate et al. (2007) similarly observed 'a band group at 1215–1120–950–901 cm^{-1}, with the four peaks often sharp and intense, which is not yet identified' (p. 318; see also their Fig. 3). The peak at 1215 cm^{-1} has been identified as related to P=O stretching, though the exact position of the band can shift in the presence of other materials (Antonakos et al. 2007; Han et al. 2018; Larkin 2011). The peak at 1095 cm^{-1} has been observed in archaeological bone and attributed to phosphate in presence of fluorine (Khwaileh et al. 2018; Leung et al. 1990; Wright and Schwarcz 1996). In general a peak centered 900–1200 cm^{-1} reflects 'poorly' crystalline bone and can be decomposed into multiple peaks related to phosphate and carbonate (Antonakos et al. 2007; Gadaleta et al. 1996; Lebon et al. 2008; Lebon et al. 2010; Leung et al. 1990; Paschalis et al. 1997; Paschalis et al. 2011). The second derivative of this region (Fig. 10.3) reveals several sub-peaks related to $v_3PO_4^{3-}$ from stoichiometric hydroxyapatite and carbonate-enriched hydroxyapatite. Both

kinds of hydroxyapatite are found in elevated amounts in diagenetically altered bone (Gadaleta et al. 1996; Lebon et al. 2010; Leung et al. 1990; Lopes et al. 2018).

A literature search did not find any characterisation of this particular set of peaks between 900–1215 cm^{-1}. The spectra do not match known substitutions and recrystallised apatites that have been observed in diagenetically altered bone, including fluorapatite, chlorapatite, dahllite, calcite, barite, trona, and crandallite (Dal Sasso et al. 2016; Farre et al. 2014; Khwaileh et al. 2018; Leung et al. 1990; Ren et al. 2014; Trueman et al. 2004; Yi et al. 2013). In particular, the diagnostic calcite peak at 872 cm^{-1} is absent, and geological variants of calcite, like brushite and gypsum, do not match the spectra (Khwaileh et al. 2018; Mason et al. 2009). The typical phosphate-carbonate doublet at 605 and 565 cm^{-1} is altered so that the peak at 605 cm^{-1} is very small, though the supression of this peak into a 'shelf' has been observed in NaOH-treated hydroxyapatite (Barakat et al. 2009). The spectra do not match salts produced during pretreatment either (Ambrose 1990). None of the bones studied here were believed to have been treated with a conservative material, and they come from multiple excavations and museums, making it less likely they were all treated or contaminated with the same unknown substance. Nonetheless, the spectra do not appear to match commonly-used conservatives on bone (Brock et al. 2018; D'Elia et al. 2007; Lebon et al. 2016).

It is likely these peaks reflect partial, but incomplete, removal of carbonates in the presence of exogenous phosphates, carbonate-enriched apatite, and possibly substitutions with fluorine and/or chlorine. The peaks in 900–1215 reflect the partial removal of carbonate groups during pretreatment but the persistence of phosphates and likely francolite, which leaves a subset of peaks identified when the typical phosphate peak is decomposed in other studies. This agrees with studies of apatite materials and altered bone. While phosphate and carbonate are components of fresh bone, authigenic growth and recrystallization can introduce exogenous phophate and carbonate in bone (Trueman et al. 2008). Carbonate substitutes for both -OH and PO_4^{3-} positions, and both carbonate and P=O bands shift in the presence of other substituents (Antonakos et al. 2007; Larkin 2011; Mason et al. 2009; Ren

et al. 2014; Wopenka and Pasteris 2005). Fluorine and chlorine substitute for -OH ions in bone through exchange with the burial environment (Kannan et al. 2006; Tripp et al. 2018; Wopenka and Pasteris 2005; Wright and Schwarcz 1996), and both elements have both been identified in collagen even after ultrafiltration (Brock et al. 2013a). SEM analysis of these samples identified Cl, Ca, P, and limited Na in gelatin of these samples, supporting this interpretation (chapter 10.3).

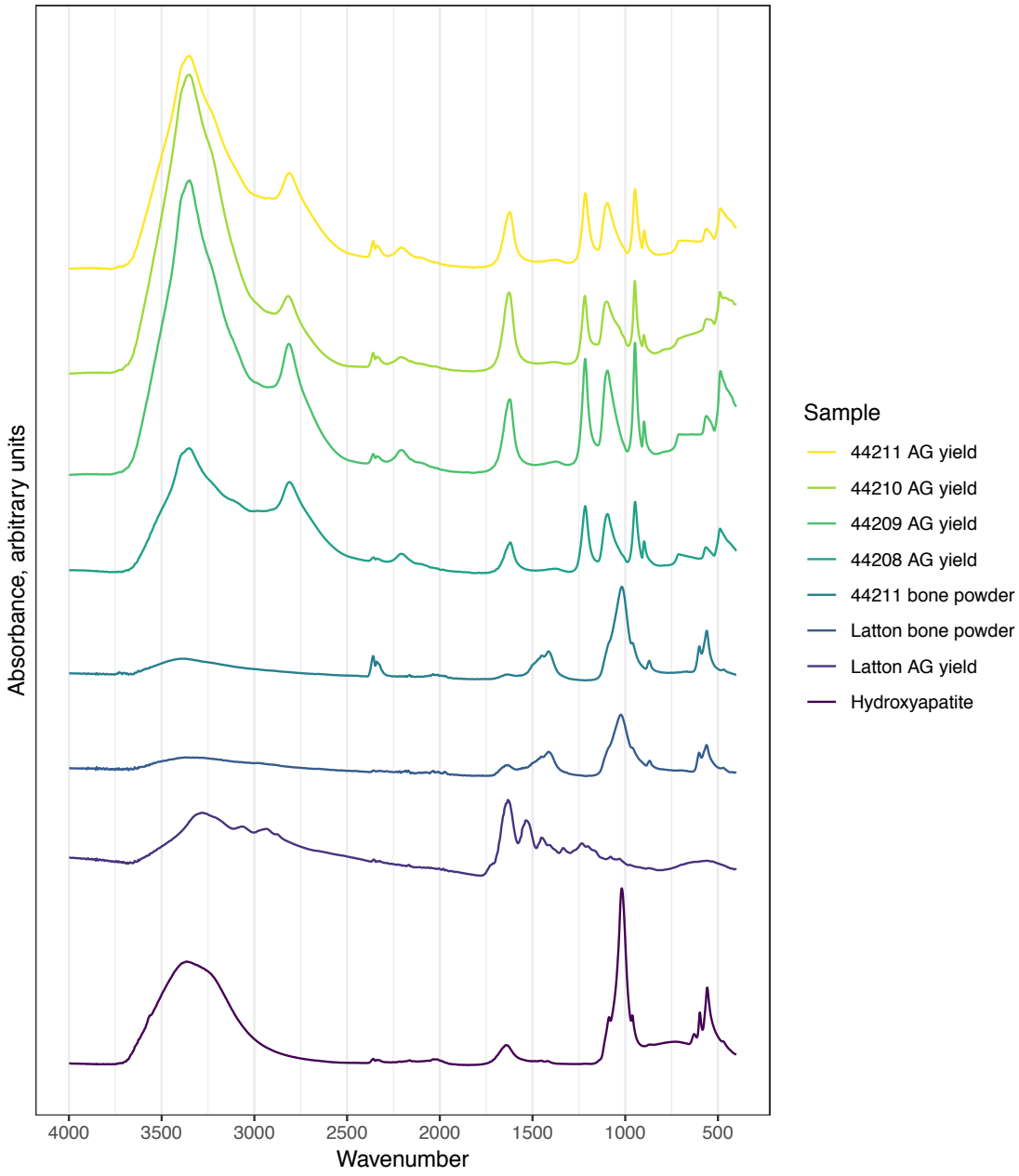


Figure 10.1: FTIR spectra of Ghar Dalam AG fraction results compared to standards: hydroxyapatite, raw Latton bone powder, and AG-extracted Latton collagen.

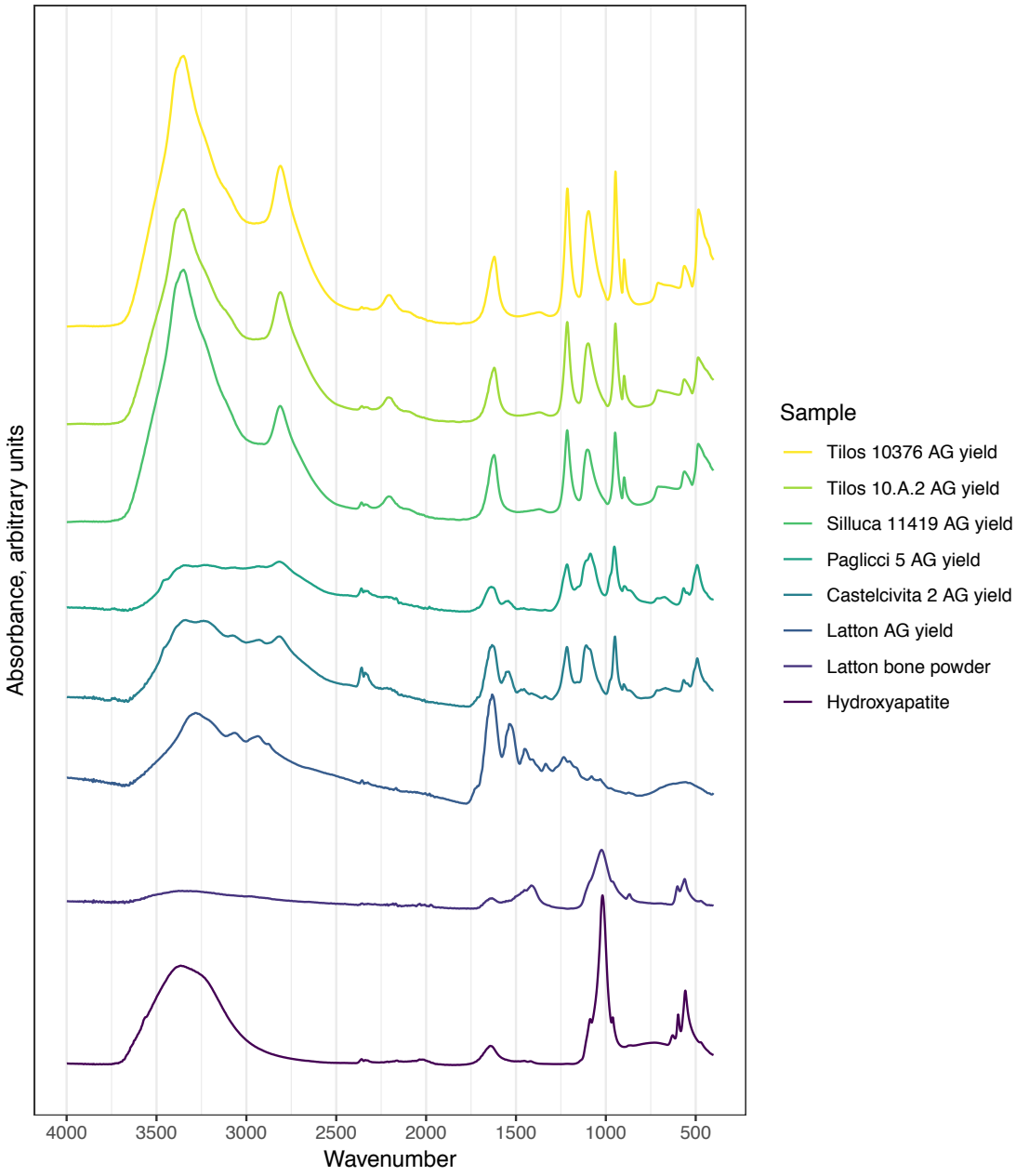


Figure 10.2: FTIR spectra of AG fraction results from southern European sites compared to raw Latton bone powder and AG-extracted Latton collagen.

Table 10.3: FTIR peaks from P44211 AG sample yield. v and v_1 = symmetric stretching, v_2 = asymmetric stretching (nonlinear) / bending (linear), v_3 = bending vibrations (nonlinear), v_4 = bending vibrations (antisymmetric).

Value cm^{-1}	Assignment	References
495	v_4PO_4	Lopes et al. (2018)
563	v_4PO_4	Lopes et al. (2018); Uysal et al. (2013)
602	v_4PO_4	Leung et al. (1990); Lopes et al. (2018); Uysal et al. (2013)
667	v_4CO_3	Antonakos et al. (2007)
898	CH out-of-plane; v_2CO_3	Chang and Tanaka (2002); Ooi et al. (2007); Pretsch et al. (2000)
945	CH out-of-plane	Bereuter et al. (1997); Chang and Tanaka (2002); Devièse (2009); Kaminská et al. (2011); Raif and Harmand (1993); Reiche et al. (2002)
1095	v_3PO_4; v_1CO_3; PO_2^-	Antonakos et al. (2007); Leung et al. (1990); Paschalis et al. (2011); Trueman et al. (2004); Uysal et al. (2013)
1215	P=O stretching	Antonakos et al. (2007); Han et al. (2018); Larkin (2011)
$\sim$ 1420	v_3CO_3; -OH bending	Antonakos et al. (2007)
1629	C=O stretch; CO_3 with H_2O	Chang and Tanaka (2002); Lebon et al. (2010); Lopes et al. (2018); Quarta et al. (2014); Raif and Harmand (1993); Reiche et al. (2002); Wang et al. (2010)
2205	Alkyne C(—)C (medial / disubstituted)	Pretsch et al. (2000)
2810	CH elongation	Bereuter et al. (1997); Devièse (2009); Raif and Harmand (1993); Reiche et al. (2002)
3350	vH_2O; -OH	Antonakos et al. (2007); Kamińska and Sionkowska (1996); Labs-Hochstein and MacFadden (2006); Raif and Harmand (1993); Wang et al. (2010)

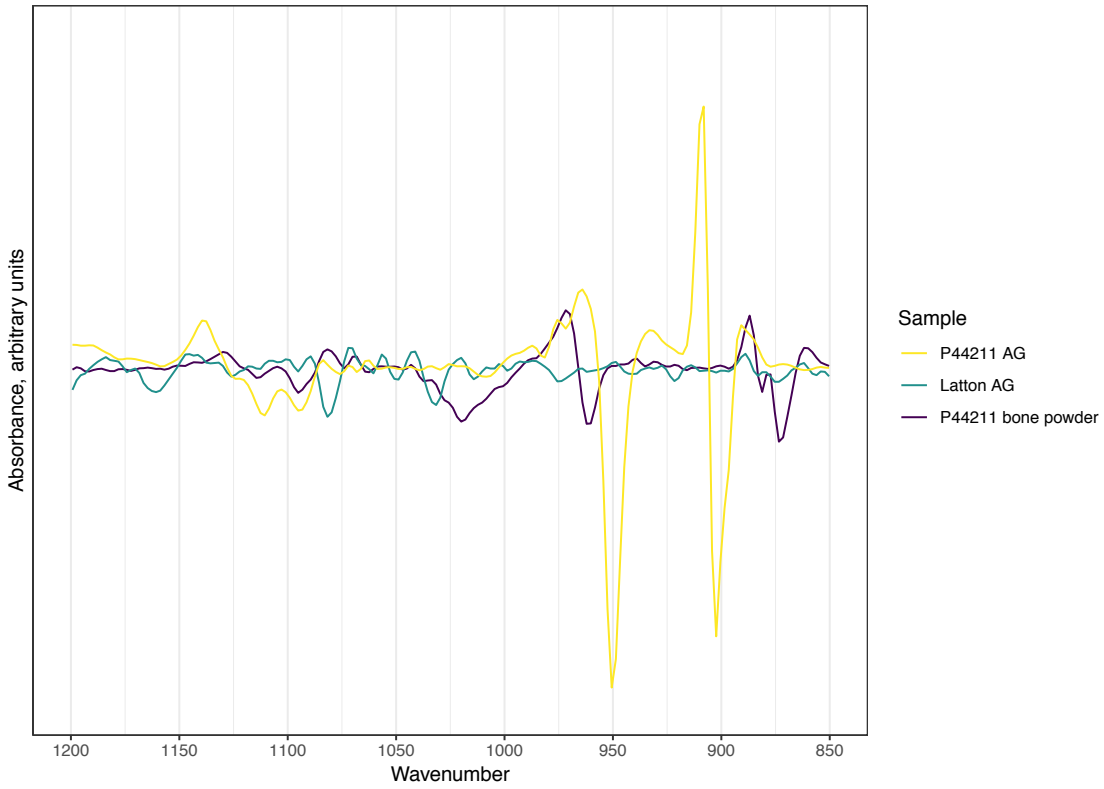


Figure 10.3: Second derivative of FTIR diagnostic region of Ghar Dalam P44211 AG fraction, raw Latton bone powder, and AG-extracted Latton gelatin.

10.3 SEM

SEM samples showed different morphologies, from crystalline to hydrated sheets (Fig. 10.4), suggesting mineral components of bone were surviving pretreatment. The 'sticky' substance is not typical of collagen, which tends to be fibrous and dry after pretreatment (Brock et al. 2010b). The crystal-like rods are more expected of raw bone and and their presence in some samples, such as P44208, suggests incomplete demineralization of the sample (Barakat et al. 2009).

Two raw bone grains of P44208 contained calcium and phosphorus (Table 10.4), and one grain contained chlorine (Fig. 10.4). The AG product from this same sample showed increases in relative chlorine and phosphorus, with trace amounts of sodium (Fig. 10.5 and Table 10.4). (Lighter elements, including Na and N, are at the limit of detection and quantitative measurements are not accurate (Welton 1984).) Sub-sampling the AG yield (Fig. 10.6) shows relative homogeneity in

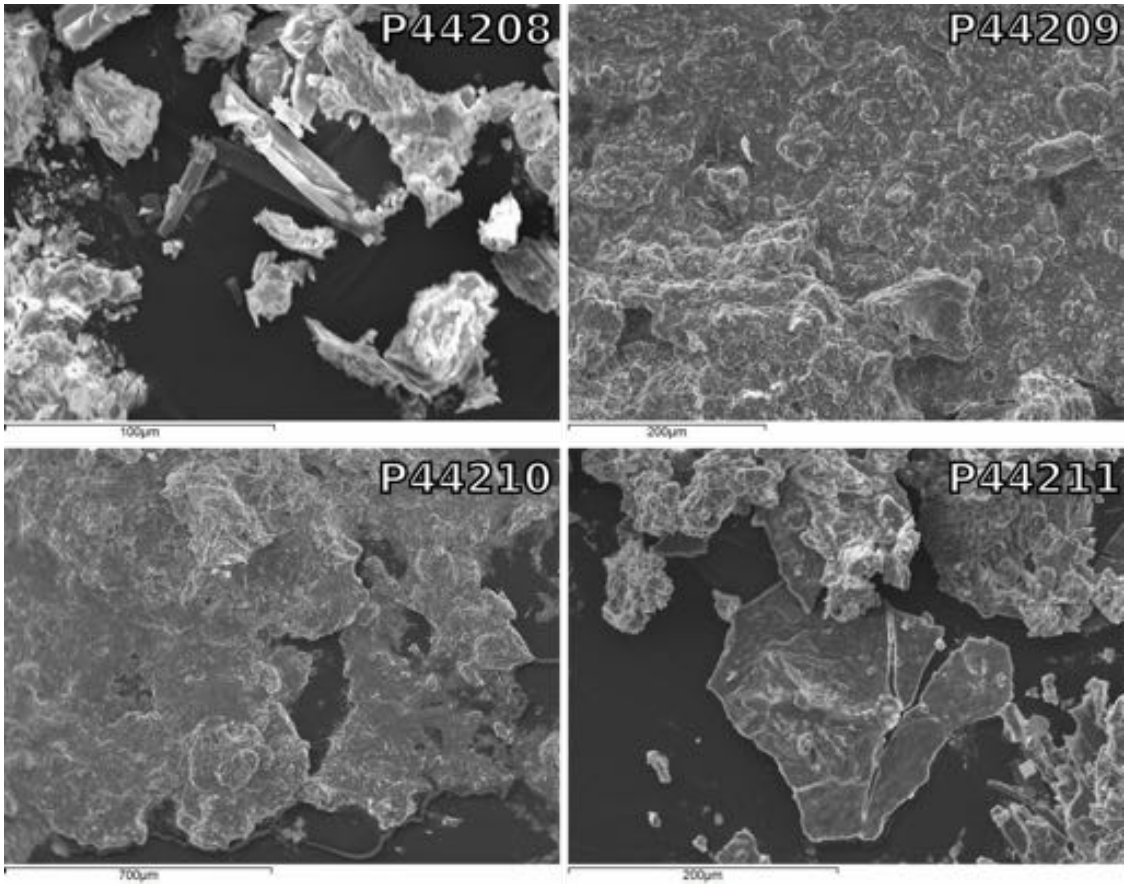


Figure 10.4: Representative SEM images of P44208 through P44211 samples, AG-extracted fractions.

elemental composition, despite variation in morphology/crystallinity. All locations contained Cl, P, and Ca; Na was only detected in some locations, though again this could be due to limited detectability.

While Cl could theoretically be introduced to the samples during pretreatment (through HCl), SEM analysis suggests at least some Cl was already present in bone samples, perhaps through substitution in the apatite matrix as chlorapatite. Though Na levels are not reliable, their low levels across all sub-samples suggests the material is not mostly NaCl salt, though its presence has been documented in some pretreatment yields (through taste!) (Ambrose 1990).

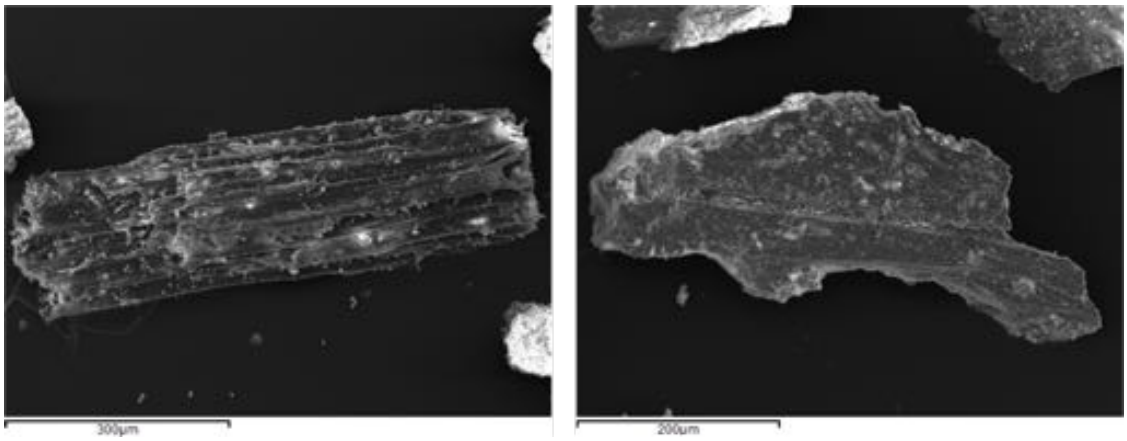


Figure 10.5: Grains from P44211 raw bone powder.

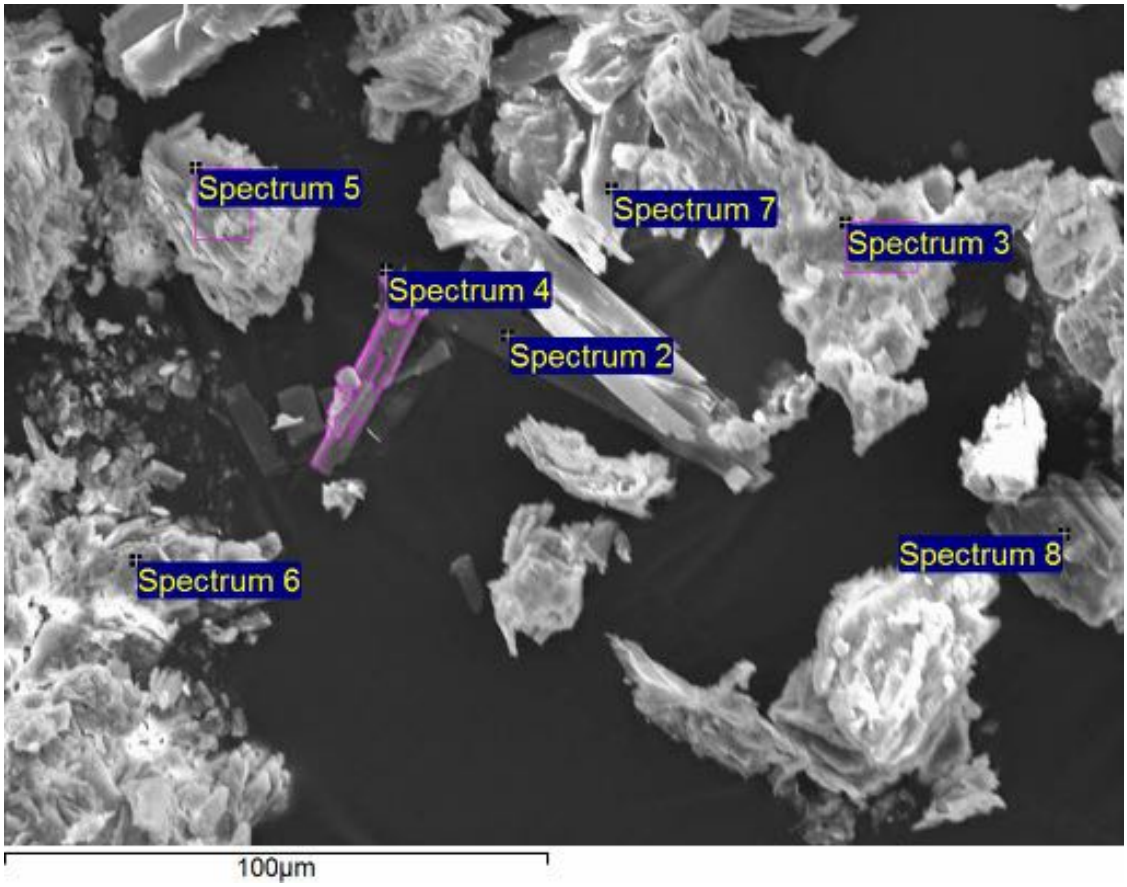


Figure 10.6: Locations analysed for composition from P44208 AG yield. Spectrum 1 is the overall composition.

Table 10.4: Spectra quantification for P44208: two raw bone grains (Fig. 10.5) and AG product (Fig. 10.4). Composition data are expressed as percentage of elements in the the sample. Note that Na is at the detection limit and is not likely to be accurate.

	Bone grain 1		Bone grain 2		AG yield	
Element	Weight%	Atomic%	Weight%	Atomic%	Weight%	Atomic%
C	50.06	56.5	24.37	41.27	0	0
N	15.95	15.43	0	0	0	0
O	32.51	27.55	23.61	30.02	24.59	42.08
Na	0	0	0.37	0.33	0	0
P	0.23	0.1	13.75	9.03	18.53	16.38
Cl	0	0	1.82	1.05	30.05	23.21
Ca	1.24	0.42	36.08	18.31	26.83	18.33

Table 10.5: Spectra quantification for P44208 across multiple grains from the AG product (Fig. 10.6). Composition data are expressed as percentage by atomic weight of the sample. Note that Na is at the detection limit and are not likely to be accurate.

Location	1	2	3	4	5	6	7	8
O	59.33	42.08	49.07	40.21	63.49	40.57	54.28	13.77
Al	0	0	0.88	0	0	1.52	0	0
Na	1.22	0	0	11.44	0	0	0	0
Si	0.89	0	1.44	0.59	0.47	2.39	0.34	0
P	10.54	16.38	14.26	10.53	11.5	11.57	13.97	22.56
S	0.56	0	0	0	0	0	0	0
Cl	15.11	23.21	18.34	25.53	13.45	26.82	17.99	33.53
Ca	12.07	18.33	16	11.7	11.09	17.13	13.42	30.14
Br	0.28	0	0	0	0	0	0	0

10.4 Discussion

The AG protocol failed to remove some carbonates and phosphates from the samples, and both FTIR and EDX elemental analysis suggests introduction of chlorine and/or other substitutes in the samples both before and during pretreatment. Element substitutions in bone and hydroxyapatite have been documented (da Cruz et al. 2007; Demnati et al. 2014; Ochoa-Lugo et al. 2017; Wright and Schwarcz 1996). The AG protocol, while gentler than AF (with ultrafiltration), is less efficient at removing some materials (Brock et al. 2007), and so may not have removed whatever

compounds appeared in the final 'yield'. Unfortunately, adding ultrafiltration did not help, as it is unlikely the samples contained collagen. Analysis with FTIR and SEM revealed the material to not reflect typical bone collagen, though the material could not be easily identified. Similar FTIR spectra have been previously observed, though not characterised, in diagenetically-altered bone (Gianfrate et al. 2007), suggesting these yields are not unique to the particular sites investigated or due to some lab-specific process. That the spectra do not reflect a single apatite form, such as fluorapatite or brushite, may be due to samples being composed of multiple materials. Biogenic apatites also tend to have different crystal structures from geological apatites, leading to differences in FTIR spectra in the literature depending on apatite source (Lloret et al. 2006; Wopenka and Pasteris 2005). As discussed above, the FTIR spectra do not reflect commonly identified contaminants or conservation materials, though there was no reason to suspect the samples had been treated.

SEM and EDX analysis have also identified elemental and morphological substitutions of bone. The presence of P and Ca is typical of hydroxyapatite (Barakat et al. 2009; Demnati et al. 2014; Joschek et al. 2000). Small amounts of Na, Al, S, and O may be incorporated in bone matrix (da Cruz et al. 2007; Joschek et al. 2000; Ooi et al. 2007), and the small amounts of Si and Br identified in the raw bone mineral could be either exogenous inclusions or substitutions in apatite (Pan and Fleet 2002). In general bone is expected to be 35% Ca and 15% P by weight, pure hydroxyapatite 40% Ca and 18% P (Joschek et al. 2000; Wopenka and Pasteris 2005), and bone collagen negligable amounts of both (though tooth dentin has 0.4% P) (Veis and Schlueter 1964). The reduction in both these elements in the AG product suggests partial, but not complete, removal of apatite.

The presence of Cl may be evidence that samples had partially recrystallized as chlorapatite during diagenesis. The proportional increase in Cl in the AG product may reflect isolation of the Cl-containing fraction of the original bone sample, or else addition of exogenous Cl during the pretreatment process. Chlorapatite has the same Ca/P ratio as pure apatite (1.67) and the Cl content depends on the rate of substitution of Cl for an OH group in apatite; pure chlorapatite has ~6.5% weight

Cl (Kannan et al. 2006), which is higher than observed for the raw bone samples but considerably lower than the AG samples. Little Na seems to be present in the AG yields, suggesting insignificant isolation/formation of NaCl, but Na measurement by EDX is not particularly accurate (Welton 1984). Brock et al. (2013a) found Cl in collagen yields after ultrafiltration and attribute the Cl to salts. The samples analysed here were AG yields (not ultrafiltered), but Brock et al.'s results imply that Cl was present in gelatin after Ezee-filtering, as ultrafiltration uses only MilliQ water and does not introduce Cl. Salts may be contributing to the Cl content here, even if some of it was orginally present as chlorapatite.

The 'sheet' morphology of some samples after pretreatment also suggests extraction of a non-collagen product. Treatment of bone with NaOH at high temperatures produces a more homogenous and non-crystalline material (Barakat et al. 2009), and hydroxyapatite will also form rectangular flakes and aggregates in higher pH conditions (Ochoa-Lugo et al. 2017; Wang et al. 2010). Both of these features can explain the flake-like and combined flake-globules in some samples after NaOH pretreatment (Fig. 10.4), suggesting the persistence of apatite-based products through AG pretreatment. However, the form is not a typical form of crystalline chlorapatite, or at least the chlorapatite is not the sole material in the samples, based on comparison of FTIR spectra.

10.5 Conclusions

Several bones produced a white substance after AG extraction that failed to contain sufficient carbon for radiocarbon dating. The composition of this material was investigated with FTIR and SEM analyses, which confirmed the non-proteinaceous nature of the material. This phenomenon has been observed in samples from multiple sites and reflects diagenetic alterations of both the organic and inorganic fractions of the bones due to the burial environment and/or post excavation treatments. The consistency in the FTIR spectra across samples from multiple burial environments, and the increase in the chlorine content of the AG yield compared to the raw bone, suggests at least some of the alterations occurred during pretreatment.

11 Dialysis collagen extraction

Using dialysis to purify the acid-soluble fraction of collagen was investigated. Both the size of collagen yields and the quality of the collagen were evaluated. With sufficient size and purity, dialysis yields might be radiocarbon dated directly; if of sufficient size but not yet of suitable quality, samples might undergo further purification with ultrafiltration or HPLC.

11.1 Collagen yields

The soluble protein fraction from bone samples was dialysed and the resulting yield compared with the nonsoluble protein fraction, which was subject to ABA pretreatment. Dialysis %yields were less than the ABA %yields of most samples (Fig. 11.1). When the overall %yield was very low, the proportional %yield from dialysis increased and exceeded the ABA %yield in two cases. The relative contribution of dialysis collagen to total yield varied by sample, and even within Latton bone trials dialysis produced variable relative yields.

Overall, dialysis yields were low, with even well-preserved standards producing collagen yields below the ~25 mg required for HPLC HYP dating (Devièse pers. comm.) (Fig. 11.1). In some archaeological samples where the preservation was expected to be low, very large starting weights (~900 mg) were used but

did not necessarily produce sufficient collagen for radiocarbon dating. At the ORAU the usual minimum required yield is 10 mg and >1% of starting sample mass, though samples of 5–10 mg may be used with a health warning. Of the non-standards samples, only Vasil C produced >5 mg and >1% yield collagen from its dialysis fraction.

The ABA results from the insoluble fraction are not identical to AG yields, as the experimental samples were decalcified in 1 M HCl for 24 hr before separating the solute for dialysis and the insoluble fraction underwent the rest of the routine ABA protocol. AG replaces HCl more frequently and uses 0.5 M HCl (Brock et al. 2010b). To more directly compare AG yields, Ash Bend (P19651), a Pleistocene bone standard, was also tested. Three aliquots of ∼300 mg each were AG extracted and a separate three aliquots underwent the dialysis protocol, leaving the nonsoluble fraction unused. AG mean yields were higher (36.17 mg or 12.01% yield) than the dialysis yields (17.07 mg or 5.73% yield). Compared to the mean dialysis yields of Latton bone (1.72%), Ash Bend mean dialysis %yields (5.73%) were greater (Fig. 11.2), keeping with the generally higher AG yields of Ash Bend. Latton dialysis yields are also lower than Latton AG yields, though the AG yields here are not from the same aliquot of bone powder and so may have different initial collagen content (chapter 12.6).

11.2 Collagen quality

11.2.1 Carbon and nitrogen content

The quality of the dialysis fraction was also poorer than the ABA fraction. The CN ratios of the dialysis fractions usually exceeded the accepted limit of 3.5 (Brock et al. 2010b) and the %C values were variable but generally below the expected ∼45% for bone collagen (Ho 1967; Nehlich and Richards 2009) (Fig. 11.3). Compared to AG and AF fractions previously obtained from the ORAU database, the Latton bone dialysis fractions had higher CN ratios and lower %C values. The variability in these values was also higher than for the routine collagen samples. Dialysis

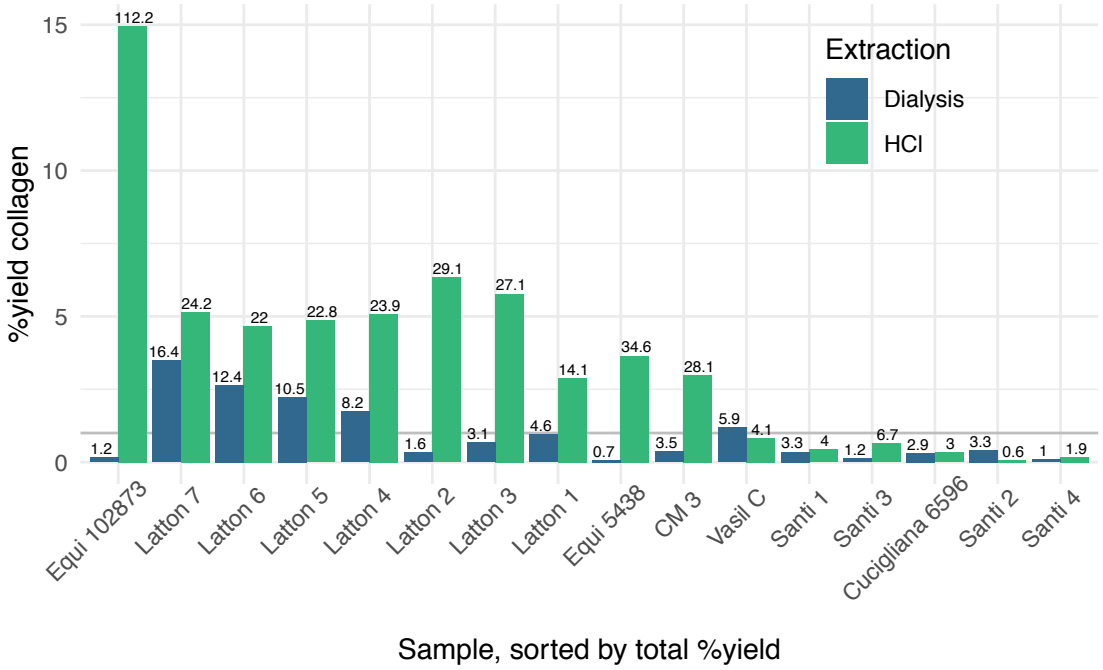


Figure 11.1: Comparison of %yield of the acid-soluble (dialysis) fraction and ABA (HCl) yield of the acid-insoluble fraction on a series of bone samples. Bars are labelled with the yield in mg. The 1% yield threshold has been marked as an additional bold line on the y-axis.

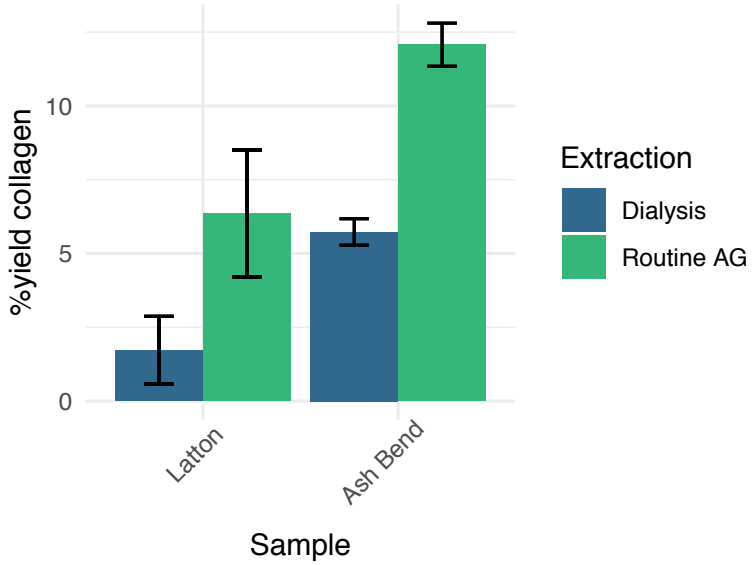


Figure 11.2: Comparing mean %yields of dialysis and routine AG products of two bone standards. Each bone had dialysis yields extracted three times; Ash bend is compared with three AG extractions, and Latton with eleven AG extractions (from chapter 12). The error bars reflect standard deviation of %yields.

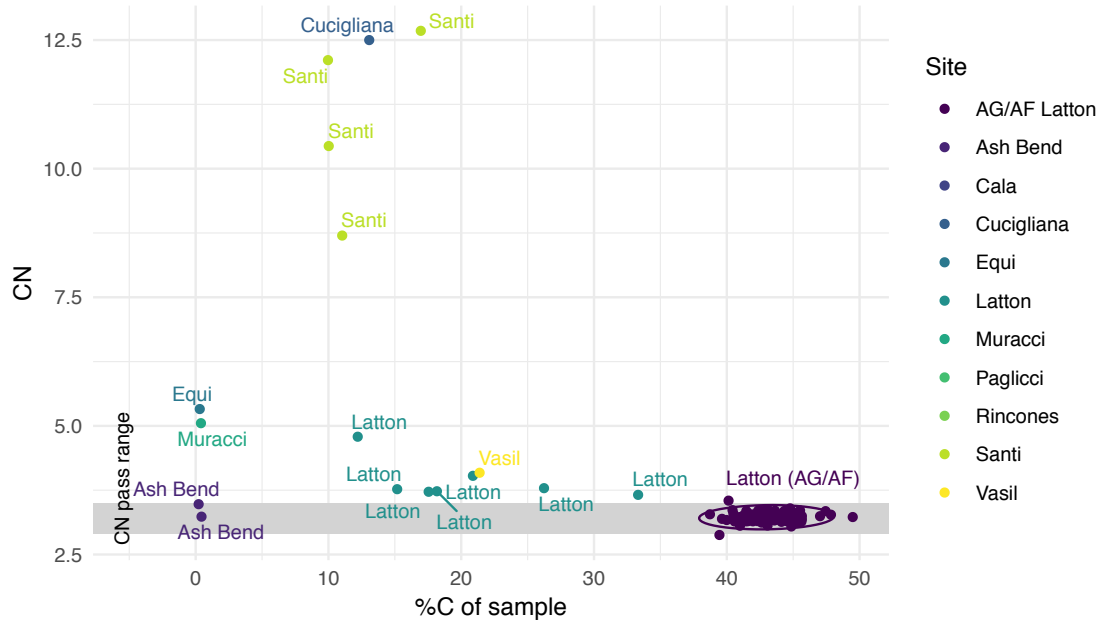


Figure 11.3: CN vs %C values of dialysis fractions compared to Latton bone standards extracted with routine AG and AF protocols (from the ORAU database). The ellipse covers 98% of the range of observed values for Latton collagen. Shaded rectangle is acceptable CN ratio of 2.9–3.5.

fractions from Ash Bend, another standard, just fell within the 3.5 CN limit, but their %C values were very low.

Both %C and %N in dialysis fractions were variable and not correlated with higher overall %yield. Two simple linear regressions predicting %C and %N to %yield did not produce significant relationships (%C $F(1, 15) = 2.78$, $p = 0.12$, $R^2 = 0.16$; %N $F(1, 15) = 0.22$, $p = 0.64$, $R^2 = 0.01$). Pleistocene mammal bone collagen is expected to have %C around 45% and %N around 16% (Ho 1967; Nehlich and Richards 2009), but the dialysis fractions were lower in both values (%C max = 33.32 and %N max = 10.62). The lower %C and %N content suggests a significant non-collagen component in the dialysis fraction.

11.2.2 FTIR

FTIR was also used to evaluate the dialysis fraction of samples. Some samples looked similar to AF-extracted Latton collagen, but others did not (Fig. 11.4 and Table 11.1). Vasil C looks most similar to AF collagen, particularly in the

reduction of the phosphate region at ~1030 cm^{-1} (Lebon et al. 2008; Lebon et al. 2016). Equi 5438 and the Latton dialysis yield also look similar to AF collagen, but have altered profiles particularly between 1200–1500 cm^{-1} and persistance of the phosphate peak at 1030 cm^{-1}. Equi 5438 also has a pronounced peak at 2930 cm^{-1} related to C-H stretching, probably from persisting carbonates (Brock et al. 2013a). None of these samples had high %yield or good CN ratios and Equi in particular had very low %C and %yield (Figs. 11.1 and 11.3).

Collagen-related peaks (Table 11.1) include a broad band between 2600–3600 cm^{-1} that corresponds to water and overwrites N-H stretching. A peak at 2920 cm^{-1} reflects C-H stretching observed in collagen. The double peaks at 2359 and 2341 cm^{-1} reflect atmospheric CO_2. Bands corresponding to amides I, II, and III are present in some of the samples, though Santi 1 is missing the amide II peak (1555 cm^{-1}) and amide III (1250 cm^{-1}) is either missing or hidden in the phosphate peak in the dialysis fractions of Latton (Table 11.2; also see Table 9.1). The dialysis fractions of Santi 1, Ash Bend, and Latton bone lack some peaks 1200–1500 cm^{-1} that reflect phosphates and amide side chains (Boskey and Camacho 2007). The double peaks at 1454 and 1413 cm^{-1} and the small peak at 873 cm^{-1} correspond to carbonates. The 'blunted' peaks in the AF collagen between 1000–1100 cm^{-1} are characteristic of vC-O and vC-O-C bands from structural carbohydrates in collagen (Belbachir et al. 2009; Boskey and Camacho 2007). In some samples this is overwritten by a stronger peak at 1030 cm^{-1}, which corresponds to phosphate and carbonate (Table 11.2); this phosphate region is distinctive of apatite and persists in some of the dialysis samples (Lebon et al. 2008; Lebon et al. 2016). All the dialysis fractions have lost the double phosphate 'mineral' peaks between 550-600 cm^{-1} (Brock et al. 2010a; Khwaileh et al. 2018; Dal Sasso et al. 2016).

The FTIR spectra suggest that, despite prior demineralization with 1 M HCl, dialysis did not always remove some of the mineral components from the samples. In particular the carbonate-phosphate peak at 1030 cm^{-1} is ideally removed in clean samples, as evidenced by the ultrafiltered sample spectra. The removal of this peak in ultrafiltered collagen has been observed in other studies, as is its persistence in

samples that were not filtered (Brock et al. 2013a; D'Elia et al. 2007; Gianfrate et al. 2007). The lack of consistency between samples in terms of removal may reflect their initial quality, both in terms of collagen content and relative content of contaminants like humics and salts. While none of the peaks in the samples suggest contaminants beyond apatite, humics can produce bands at locations that overlap with bone-related peaks, including at ~1100 cm^{-1} ~1600 cm^{-1} (Gianfrate et al. 2007; Lebon et al. 2016). That said, there are no evidence of nitrates, a humic peak at 1715 cm^{-1} (Lebon et al. 2016), or (unlikely) conservatives (Brock et al. 2018; D'Elia et al. 2007).

Dialysis spectra may also reflect initially poor-quality bone. The lack of amide double-peak around 1500 cm^{-1} in Santi 1 has been previously observed in the acid-soluble fraction (the precursor to the dialyis yield) of highly degraded bones (DeNiro and Weiner 1988). The ABA yield of Santi 1 was low (4.04 mg, 0.42 %yield) and it had a very high CN ratio (>10), fitting this interpretation.

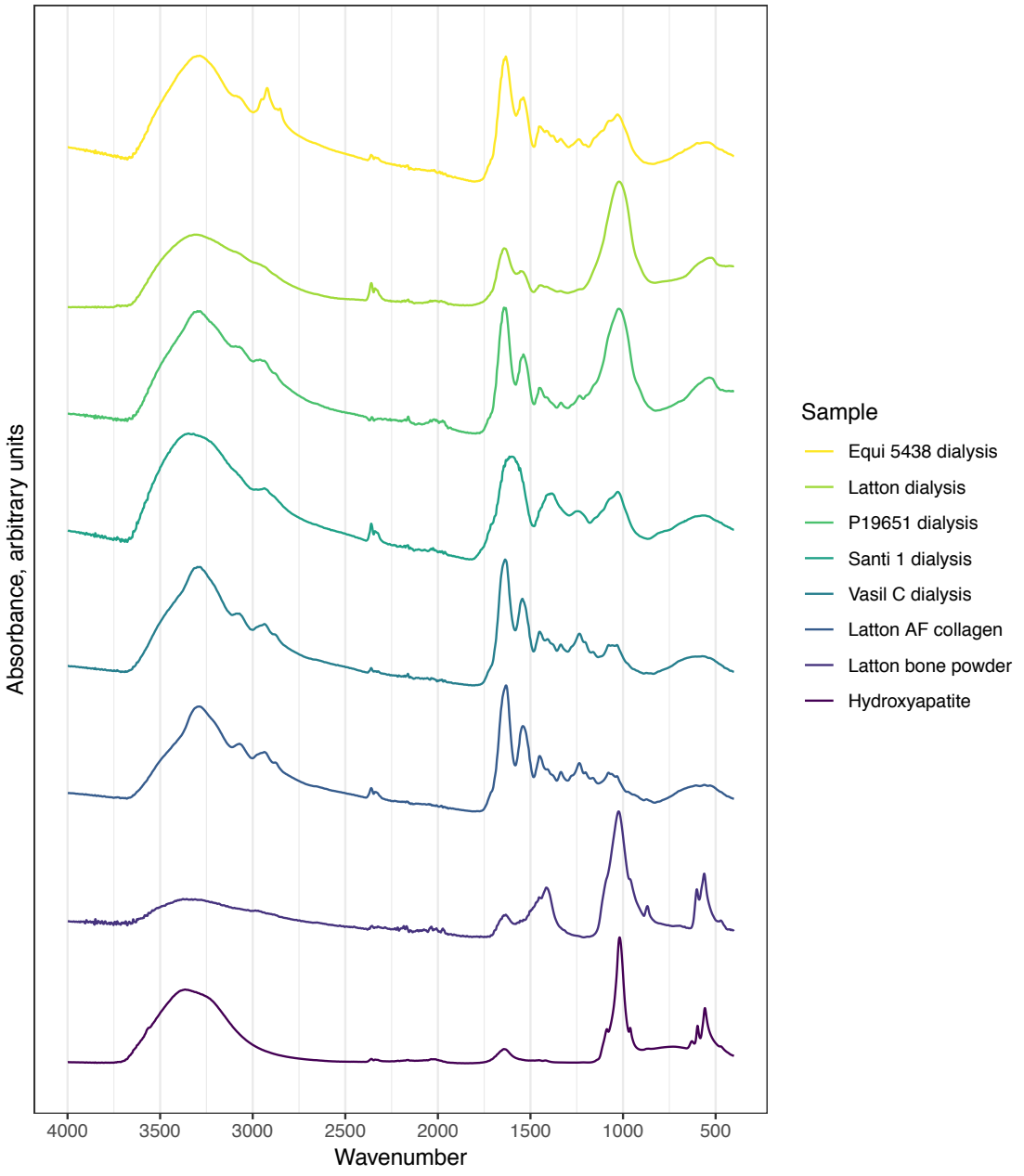


Figure 11.4: FTIR spectra of dialysis fraction samples compared to standards: hydroxyapatite, raw Latton bone powder, and AF-extracted Latton collagen. The spectra have all been normalised.

Table 11.1: FTIR bands reflecting collagen-related peaks, observed in Latton AF standard and most dialysis samples. v and v_1 = symmetric stretching, v_2 = asymmetric stretching (nonlinear) / bending (linear), v_3 = bending vibrations (nonlinear), v_4 = bending vibrations (antisymmetric).

Value cm^{-1}	Assignment	References
~3300	$v H_2O$, vN–H (Amide A)	Chang and Tanaka (2002); Devièse (2009); Gianfrate et al. (2007); Raif and Harmand (1993); Reiche et al. (2002)
3072	$v H_2O$, vN–H (Amide B)	Chang and Tanaka (2002); Devièse (2009); Gianfrate et al. (2007); Raif and Harmand (1993)
2938	vC–H	Chang and Tanaka (2002); Devièse (2009); Gianfrate et al. (2007); Raif and Harmand (1993)
1631	Amide I	Boskey and Camacho (2007); Chang and Tanaka (2002); Devièse (2009); Gianfrate et al. (2007); Raif and Harmand (1993)
1540	Amide II	Boskey and Camacho (2007); Chang and Tanaka (2002); Devièse (2009); Gianfrate et al. (2007); Raif and Harmand (1993)
1450	$v_3 CO_3^{2-}$	Chang and Tanaka (2002); Devièse (2009); Gianfrate et al. (2007); Ooi et al. (2007); Raif and Harmand (1993); Reiche et al. (2002)
1409	$v_3 CO_3^{2-}$	Gianfrate et al. (2007); Raif and Harmand (1993); Reiche et al. (2002)
1336	vC–N; C–H	Boskey and Camacho (2007); Chang and Tanaka (2002); Raif and Harmand (1993)
1236	Amide III	Boskey and Camacho (2007); Chang and Tanaka (2002); Gianfrate et al. (2007); Raif and Harmand (1993)
1077	vC–O–C	Boskey and Camacho (2007); Belbachir et al. (2009); Gianfrate et al. (2007); Raif and Harmand (1993)
1033	vC–O	Boskey and Camacho (2007); Belbachir et al. (2009); Gianfrate et al. (2007); Raif and Harmand (1993)
~600	Amides IV–VI	Chang and Tanaka (2002); Raif and Harmand (1993)

Table 11.2: FTIR bands reflecting apatite-related peaks, observed in Latton bone powder and some dialysis samples. v and v_1 = symmetric stretching, v_2 = asymmetric stretching (nonlinear) / bending (linear), v_3 = bending vibrations (nonlinear), v_4 = bending vibrations (antisymmetric).

Value cm^{-1}	Assignment	References
~3300	$v H_2O$, OH^-	Chang and Tanaka (2002); Joschek et al. (2000); Reiche et al. (2002); Wang et al. (2010)
1633	$v CO_3$ with H_2O	Lopes et al. (2018); Joschek et al. (2000); Reiche et al. (2002); Wang et al. (2010)
1454	$v_3 CO_3^{2-}$	Chang and Tanaka (2002); Devièse (2009); Ooi et al. (2007); Raif and Harmand (1993); Reiche et al. (2002)
1415	$v_3 CO_3^{2-}$	Beasley et al. (2014); Chang and Tanaka (2002); Devièse (2009); Reiche et al. (2002)
1023	$v_3 PO_4^{3-}$	Chang and Tanaka (2002); Ooi et al. (2007); Paschalis et al. (2011); Reiche et al. (2002); Dal Sasso et al. (2016); Walters et al. (1990)
960	$v_1 PO_4^{3-}$	Chang and Tanaka (2002); Devièse (2009); Ooi et al. (2007); Paschalis et al. (2011); Walters et al. (1990)
873	$v_2 CO_3^{2-}$	Chang and Tanaka (2002); Devièse (2009); Ooi et al. (2007); Paschalis et al. (2011); Reiche et al. (2002); Walters et al. (1990)
705	$v_4 CO_3^{2-}$	Chang and Tanaka (2002); Dal Sasso et al. (2016); Trueman et al. (2004)
602	$v_4 PO_4$	Leung et al. (1990); Lopes et al. (2018); Ooi et al. (2007); Reiche et al. (2002); Uysal et al. (2013)
563	$v_4 PO_4$	Leung et al. (1990); Lopes et al. (2018); Ooi et al. (2007); Reiche et al. (2002); Uysal et al. (2013)
470	$v_4 PO_4$	Lopes et al. (2018); Ooi et al. (2007)

11.3 Discussion

Dialysis produced more collagen than the ABA-extracted fraction in two cases, though overall dialysis results were low. Interestingly, the two collagen fractions were not always correlated, suggesting different diagenic processes affect their preservation. In all cases the CN ratio of dialysis collagen was outside the acceptable range, suggesting the method is not sufficiently purifying the fraction. The HCl liquid fraction in the ABA method is discarded, but in dialysis these contaminants are retained. In theory the 3.5 kD dialysis membrane would remove small contaminants much like an ultrafilter, but the slow re-forming of collagen fibres—which does not have time to occur in gelatin ultrafiltration—may include the re-binding of contaminants. The inconsistent quality of the dialysis fraction is also evident in the FTIR spectra. While most of the samples produced collagen-like spectra, some show evidence of exogenous material, and one (Santi 1) appears to not contain much protein at all. Despite the poor quality of the extracts, the FTIR spectra suggest that the dialysis fractions contained proteinaceous material in most cases.

Goldenberg et al. (2017) also found inconsistent quality in dialysis fractions, though three of their ten dialysis fraction dates agreed statistically with the respective gelatin fraction dates. All of their samples were Holocene, so the high yield and good age agreement of dialysis fractions may be a product of the comparative youth of the samples—the effect of contamination on young samples may be proportionally smaller than for near-background samples. However, this is not reflected consistently in the samples in this study, where the best CN ratios came from Ash Bend standards of background age.

When sufficient collagen is produced, it can undergo further purification steps. The ABA collagen and dialysis collagen could be recombined and then passed through HPLC. This would be particularly useful for bones from hot/arid sites, where there is often little or no insoluble collagen fraction left. Isolation of hydroxyproline with HPLC requires 20–30 mg collagen, which none of the low-collagen samples here produced. However, collecting multiple amino acids has shown potential: a

method that collected eight AAs captured 70% of total carbon from collagen and so required proportionally less collagen than HYP (Devièse pers. comm.), and subsets of amino acids have been radiocarbon dated (McCullagh et al. 2010). This method could isolate sufficient carbon from samples like Vasil C (10.06 mg combined yield), for example. This assumes that the collagen-like dialysis fraction is mostly collagen, despite CN ratios that suggest contamination. If the fraction is largely contaminants, it will contribute little protein to the HPLC product. That said, FTIR spectra of most samples largely reflected collagen, suggesting the bulk of the dialysis yield was proteinaceous. Further purification of the yield could produce a collagen to be recombined with the non-soluble fraction.

11.4 Conclusions

Analyses of dialysed collagen suggest that the acid soluble fraction of collagen retains contaminants through dialysis and tends not to produce large yields relative to the acid-insoluble fraction. Despite this, dialysis has value in that it recovers proteinaceous material otherwise lost in ABA-based protocols, including hydrolysis for HPLC extraction. In cases where less carbon is required for measurement, such as on some AMS instruments or an HPLC protocol that collected multiple amino acids (McCullagh et al. 2010), the method's ability to contribute additional collagen yield may be useful.

12 EDTA decalcification

EDTA decalcification was investigated as an alternative to acid demineralization of bone. The resulting collagen yield sizes and qualities were characterised. Because EDTA is typically slow-acting, different conditions were tried to optimise both yields and speed.

12.1 Comparison with HCl decalcification

First experiments compared decalcification by 0.5 M HCl and 0.5 M EDTA without use of microwave. Overall, the highest collagen yields came from crushed bone demineralised in regularly-replaced HCl over ~14 hours. HCl %yields were significantly greater than EDTA %yields except when samples were agitated, where EDTA %yields were comparable or larger (Table 12.1). However, HCl %yields were more variable than EDTA %yields. HCl crushed bone yields ranged from 6.36–90.00 mg, whereas EDTA crushed bones range only from 15.57–24.08 mg. All samples come from the same bone and were crushed at the same time, so all samples were approximately homogenized. The samples were also processed as a set, minimising variation in external conditions. Handling losses are expected, but as EDTA samples were processed at the same time, more variation would be expected in their results as well if this were the dominant source of variation. As a check, the overnight crushed

Table 12.1: Mean yields of collagen from ~500 mg bone starting weight. Percentage yields account for slight starting weight variations in samples. Each condition mean consists of 2–7 samples (Fig. 12.1). P value is result of Welch's two-sample, two-tailed t-test on the %yield of EDTA and HCl for each condition. * denotes significance at the 5% level, ** at 1%, and *** at 0.1%.

Conditions	Bone	EDTA (mg)	%yield	HCl (mg)	%yield	p value
Agitated	Crushed	21.62	4.33%	24.65	4.97%	0.551
Agitated	Powder	23.53	4.83%	9.67	1.92%	0.022*
Still	Crushed	17.87	3.59%	64.65	12.82%	0.0002***
Still	Powder	24.50	4.77%	47.87	9.58%	0.014*
Overnight	Crushed	19.21	3.93%	39.63	8.08%	0.047*
Overnight	Powder	14.35	3.02%	50.16	9.93%	0.017*
Overall mean		20.60	4.08%	39.36	9.14%	<0.0001***

HCl was repeated on five samples, which produced less variable but lower results: range 25.01–39.2 mg, mean 32.87 mg. While this is a less dramatic result, the overall variation in HCl suggests it may be sensitive to conditions not tested here.

Other conditions varied in their impacts. Crushed bones produced higher %yields than powdered bones in both agitated and not agitated HCl samples, but not in samples left overnight (Fig. 12.1). Overall this difference between crushed and powdered bones was not significant for either HCl %yields ($p = 0.262$, Welch's two-sample t-test) or EDTA %yields ($p = 0.401$). If anything, the effect for EDTA was reversed, as powdered non-agitated EDTA produced a slightly higher mean %yield than crushed non-agitated EDTA. Leaving HCl samples overnight (~24 hr) produced a lower mean %yield than regular solution replacement ($p < 0.0001$), but there was no significant difference for EDTA ($p = 0.132$). Agitation made no difference for EDTA %yields ($p = 0.438$) but significantly reduced the yields for HCl samples ($p < 0.0001$).

In sum, varying extraction conditions had little effect on final EDTA %yields. HCl samples were more strongly affected, with the impact perhaps more apparent due to the overall larger yields of HCl samples. HCl yields were maximised with regular solution replacement and no agitation on crushed bone, while EDTA yields were similar regardless of whether the solution was regularly replaced or samples were agitated.

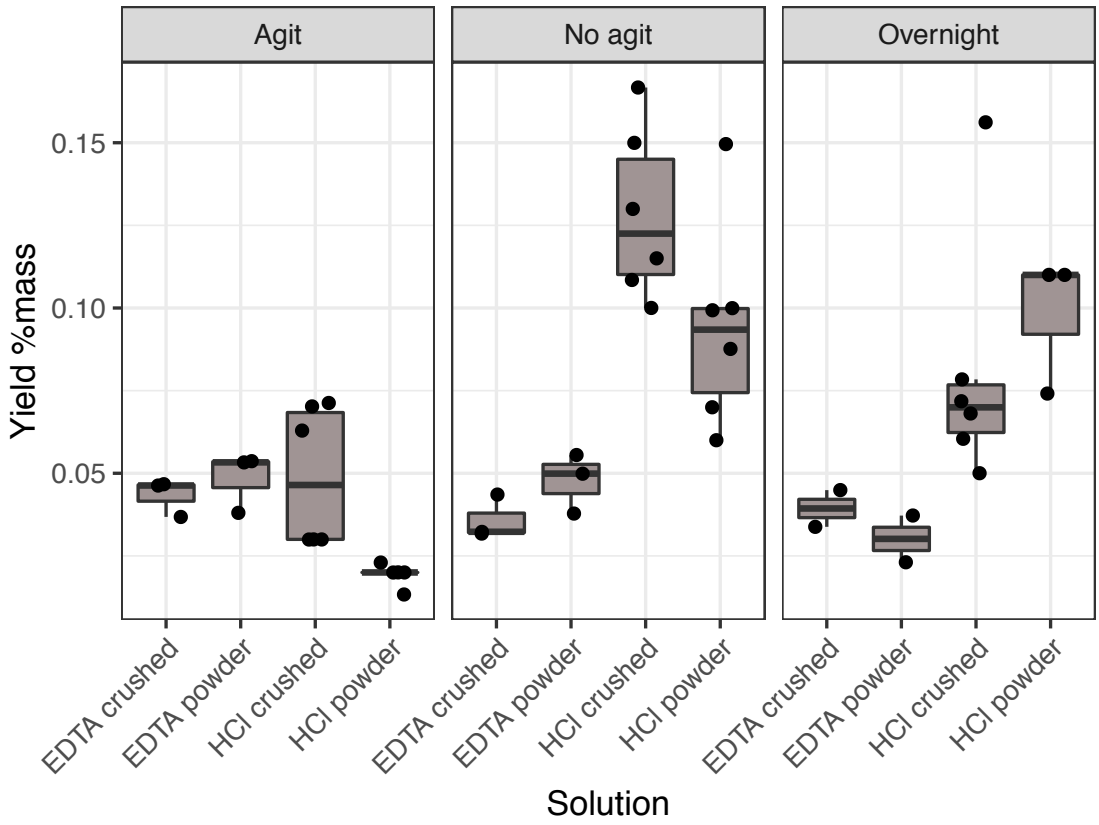


Figure 12.1: Gelatin yields of bone samples that were crushed or powdered. Samples were agitated (Agit), left on the bench between 2 hr solution changes (No agit), or left unchanged on the bench for ~24 hr (overnight).

12.2 Decalcification over days

Crushed bone samples of ~500 mg each were soaked in 20 mL of 0.5 M EDTA at room temperature. One sample was removed every 24 hr to measure the change in yield over five and ten days. Consistent with the results in Kiviranta et al. (1980), EDTA yields peaked at 4–5 days when replaced once every 24 hr. EDTA yields decreased in days 5–10 days, though the proportional difference in yield was small (1.5% difference between days 4 and 8) (Fig. 12.2). Though the drilled bone was homogenised before separating into each day's sample, the variation in %yield suggests some sample variation in collagen content. If EDTA acted extremely slowly, the between-aliquot variation may have masked any marginal daily increase in %yield. The five-day experiment yield (20.82 mg) was comparable to the more intensive 14 hr protocol where the EDTA was replaced every 2 hr (mean 20.60

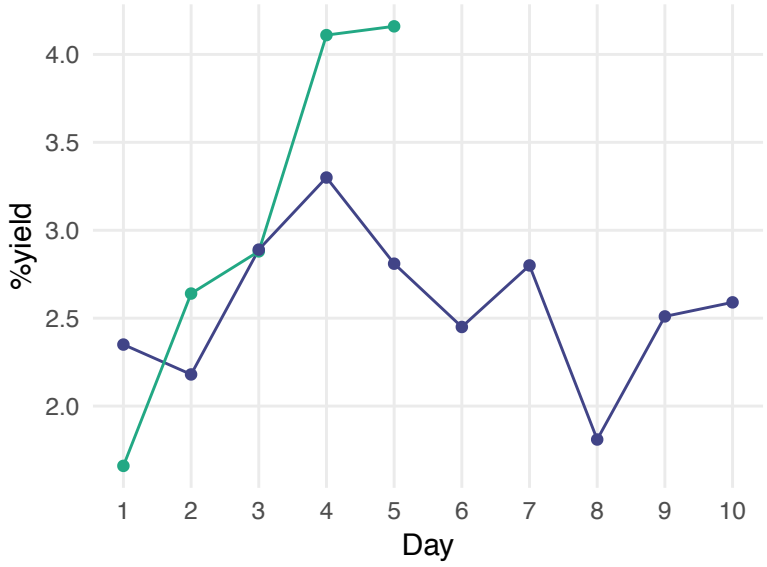


Figure 12.2: Collagen yield (mg) of samples (500 mg bone powder) decalcified in EDTA that was replaced every 24 hr for 5 days and 10 days.

mg), but the experiments used different drill batches of bone, which subsequently was shown to have an effect on overall yields (see below).

This result does not challenge protocols from Tuross (2012) and Cersoy et al. (2016), where bone was decalcified over weeks; given several weeks, %yields would be expected to increase in line with these much longer protocols. Rather, by demonstrating that increases in %yields slow by 5 days, the potential advantages of an accelerated protocol are confirmed.

12.3 EDTA and temperature

After soaking in EDTA for 72 hr, aliquots of powdered Latton bone (200 mg each) were placed in a heating block for 90 minutes to evaluate the effect of EDTA and temperature. A pair of 200 mg aliquots were also AG treated as comparison %yield values.

The %yield of samples decreased as heat block temperature increased (Fig. 12.3). Sample %yield fell from a max of 5.9% to a minimum 1.6%, though all %yields were higher than the AG comparison from the same batch of powdered Latton bone. The relatively high %yield compared to the mean AG %yield can

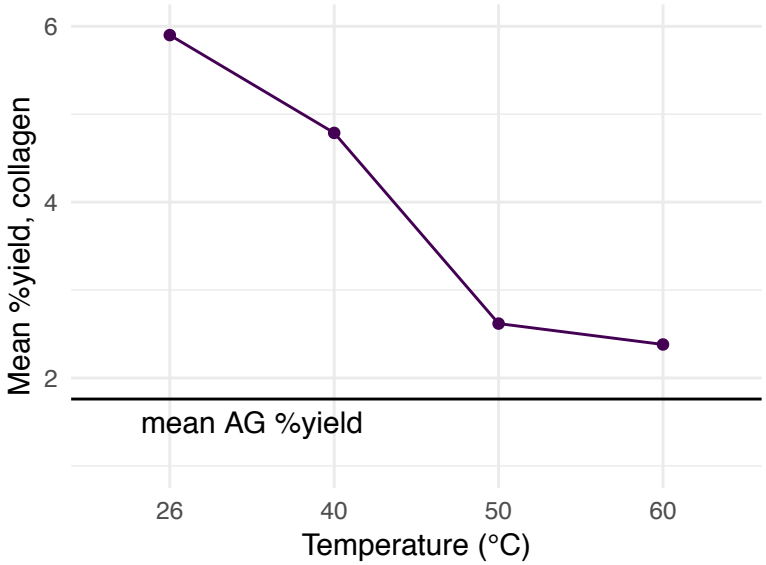


Figure 12.3: Mean %yield collagen of Latton bone decalcified in EDTA, then heated at different temperatures for 90 min. Horizontal line represents the mean AG %yield from the same batch of drilled bone powder. The first point (26° C) was not actively heated; room temperture on the day of the experiment was recorded.

probably be attributed to the 72 hr soak in EDTA prior to the heating block step of the experiment. From the ORAU database, Latton bone AG yields can vary from <1% to >9%, depending on the batch, and this fraction of bone appears to have been a relatively low-yield one.

The steep decline in %yield with temperature can be explained as gelatinisation of the collagen fibrils. Usually collagen is gelatinised in acidic (pH 3) water at 70° C (Brock et al. 2010b), but even at lower temperatures and in the EDTA solution's pH 8 environment, the collagen appears to be denaturing.

12.4 EDTA in the microwave

To test the effect of heat and agitation, samples in EDTA solution were placed in a microwave digestion system. Aliquots were extracted with the AG protocol (chapter 6) to compare relative %yields. Three Latton bone aliquots were also processed with the AG protocol, except the NaOH step was skipped to more specifically compare the effect of HCl comapared to EDTA.

12.4.1 Time and EDTA replacements

Bone samples of ~200 mg were placed in the microwave with 10 mL of 0.5 M EDTA and removed at different times to measure the extent of decalcification.

As a comparison baseline, each batch of drilled Latton bone had aliquots extrcacted with the AG protocal and a modified acid-only (skipping NaOH) protocol. The difference between the AG %yields and the modified acid-only (skipping NaOH) %yields was not significant ($p = 0.354$, t-test with equal variances (F test, $p = 0.628$)). This variation was tested to see if addition of the NaOH step made a significant difference and would be more comparable to the EDTA results, as the EDTA protocol does not require NaOH. However, given that this modification does not differ significantly from the AG %yields, AG and EDTA %yields are directly compared below.

In one set of experiments, the EDTA solution was replaced after 90 and 270 minutes in a 360 min run to test if replacement increased yields. Compared to Latton bone run for 360 min without replacement, the with-replacement %yields were significantly lower ($p = 0.032$, t-test with equal variances (F test, $p = 0.345$)). The %yield mean of the EDTA-replaced sample was 2% and non-replaced was 7.06%. Possibly the handling losses from repeated centrifugation and pouring away of the EDTA solvent meant that overall collagen yields were lower. It also suggests the 10 mL of EDTA was not rapidly exhausted as a chelator, though this did not specifically test if it became exhausted over the course of a 360 min run.

Overall, samples run in the microwave without replacement showed an upward trend in EDTA mean %yield from 10–270 min with a small divergence in %yield at 360 min (Fig. 12.4). The date on which the bone powder was drilled (drill batch) affected the overall yields, suggesting that there is within-bone variation in collagen content of Latton bone (as observed in chapter 8). Both drill batches produced %yields as high as AG and acid-only %yields, though the time at which this %yield was reached/surpassed depended on the batch. The first drill batch produced comparable %yields to the AG yield from the first 10 min but surpassed

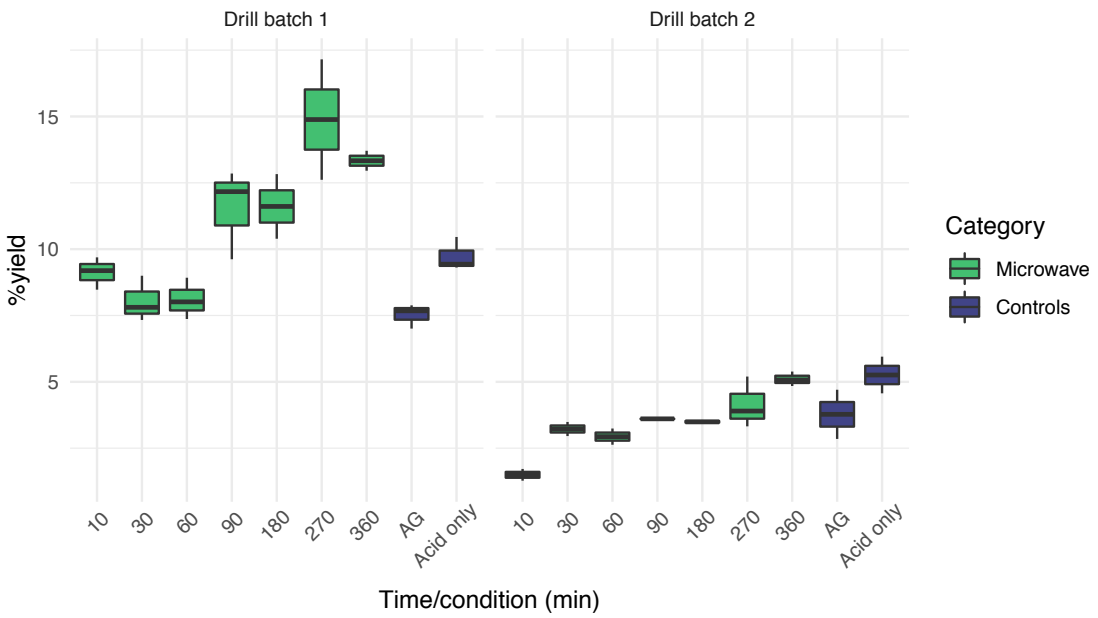


Figure 12.4: %yield collagen of powdered Latton bone microwaved 30° C in EDTA for increasing durations, compared to %yields of acid protocols used on the same batch of Latton powder. Axis labels refer to minutes samples were in run in the microwave, except for the non-EDTA protocols. 'Acid only' is a modified AG protocol where the NaOH step was skipped.

AG and acid-only %yields at 90 min. The second drill batch also produced %yields to AG yield at 90 min but only reached the acid-only %yields at 270–360 min.

To model %yields and microwave time, a mixed-effects linear model was produced. The dataset's %yield was non-normal as observed through visual inspection of Q-Q and histogram plots. Normality was also rejected at the 5% level using the Shapiro-Wilk normality test ($p = 0$) (Royston 1995). Data did not fail the Bartlett test of homogeneity of variance ($p = 0$) (Bartlett 1937). Data was normalised through log transformation. The resulting transformed data improved normality ($p = 0.026$) and satisfied homogeneity of variance ($p = 0.373$). Evaluation of a Box-Cox transformation (Venables and Ripley 2002) also supported a log transformation ($\lambda = 0$).

Using the log-transformed data, linear mixed effects analysis was performed for the relationship between EDTA %yield and time in the microwave (Bates et al. 2015). Time (min) was entered as the fixed effect and experimental batch was

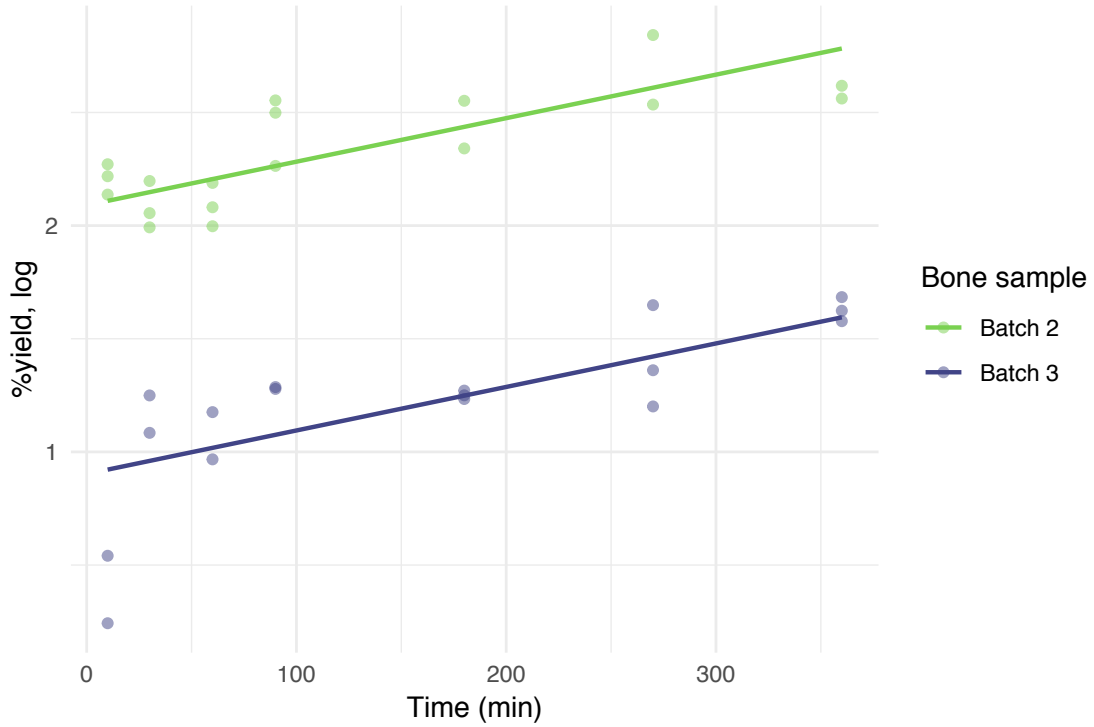


Figure 12.5: Modelled %yield collagen of Latton bone decalcified in the microwave over time. Experiment was run on two batches of drilled Latton bone, which produced different mean AG %yields and so likely contained different amounts of collagen. %yield data was log-transformed %yield to satisfy normality tests.

entered as a random intercept-slope effect. P-values were obtained by the likelihood ratio tests of the full model against a reduced model without time as a variable.

Compared to the null model, time significantly explained %yield ($\chi^2(1) = 15.281$, $p = 0.009$). Slope and standard error for the transformed response was 7×10^{-4} and 3×10^{-4}. Interpreted, the model predicts that for every 10 minutes in the microwave, %yield increased by 0.742.

12.4.2 Sample size and grain size

EDTA is slow-acting relative to HCl and it was possible that sample size and grain size would affect the rate at which EDTA decalcified samples. Most samples were ~200 mg, but samples of ~400 mg were also tested. Both crushed bone and powdered (drilled) bone were tested in the microwave setup as above, with aliquots removed after different durations in the microwave.

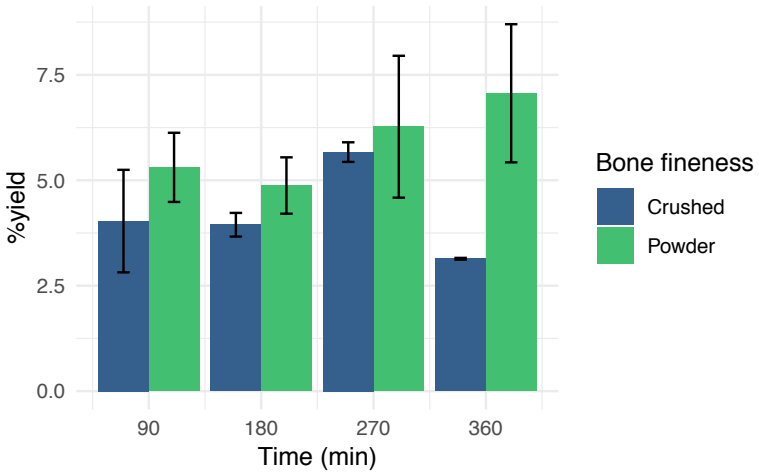


Figure 12.6: Mean %yield collagen of Latton bone decalcified in EDTA in the microwave for 90–360 min. Comparing whether the bone was crushed into chunks or drilled as a fine powder. Bars are of mean's standard error.

Bone chunks (200 mg) were tested at times of 90, 180, 270, and 360 minutes. The mean %yield for crushed bone was 4.15% and powdered bone at the same times was 5.44%. An F test found the variances of the two groups to be unequal ($p = 0.001$), so a Welch two sample t-test was used and found the crushed bone mean %yield to be significantly lower than powdered bone ($p = 0.029$).

Latton bone samples of 400 mg and 200 mg were also run at the same time for 180 min to see if %yields were different. Three aliquots of each size were run. The mean %yield of the 400 mg bone aliquots was 4.23% and 200 mg bone was 3.37%, though the difference was not significant ($p = 0.259$, variances equal (F test, $p = 0.451$)). Using larger pieces of bone did not make a large difference in proportional yields.

12.4.3 Bone preservation

In the majority of cases, lab standard bone from Latton was used. This Pleistocene bone is known to have good collagen preservation while being of background radiocarbon age. However, other bones were tested and their EDTA %yields compared to their AG %yields. Because EDTA is a chelater and HCl an acid, it was possible that the two substances would interact with poorly-preserved collagen differently. Of particular interest was whether EDTA might solubilise

fragmentary collagen chains in poorly-preserved samples less than HCl, thereby producing relatively greater yields.

Samples of Lemon Mine (P18801) and Mary Rose (P40018) were extracted with EDTA and compared to AG yields, both of the particular aliquot and of the larger ORAU database. Samples of 200 mg in 10 mL 0.5 M EDTA were run in the microwave as above (40° C with a 10 min ramp), removed at 90 or 180 minutes without replacing EDTA. Samples were rinsed, gelatinised, filtered, and freeze-dried as above. Compared to all EDTA samples regardless of time spent in the microwave, the Lemon Mine EDTA %yields were significantly different from their AG counterparts ($p = 0.001$*, t-test with equal variance (F test $p = 0.15$)). The Mary Rose sample set was too small to run a t-test on, but the AG %yield was over twice as high as the EDTA %yield. These samples are included in Fig. 12.7.

To look at a larger trend, the EDTA %yields were also comapared with yields recorded in the ORAU database for these standards (Fig. 12.7). This approach ignores likely intra-bone variability in collagen preservation, but at large sample sizes across multiple drilling batches (particularly the large dataset of Latton bone) variation may be averaged. When looking at these larger datasets, EDTA yields are not significantly different from ORAU AF yields for any of the bone standards (Table 12.2), though only three Mary Rose samples were EDTA-extracted. There is variation in %yield of samples in the database, which suggests variability in EDTA yields may not be unique to the EDTA protocol.

In addition to the bone standards, five archaeological bones known to have relatively poor preservation from Mediterranean sites were EDTA-extracted. A bone from Carigüela had %N <0.1, while the other archaeological samples had %N values between 0.3–1.1%, suggesting at least some collagen content remained to be extracted. In all cases the AG protocol produced a higher yield, except in the case of the Carigüela bone where both protocols failed to produce any yield (Fig. 12.8).

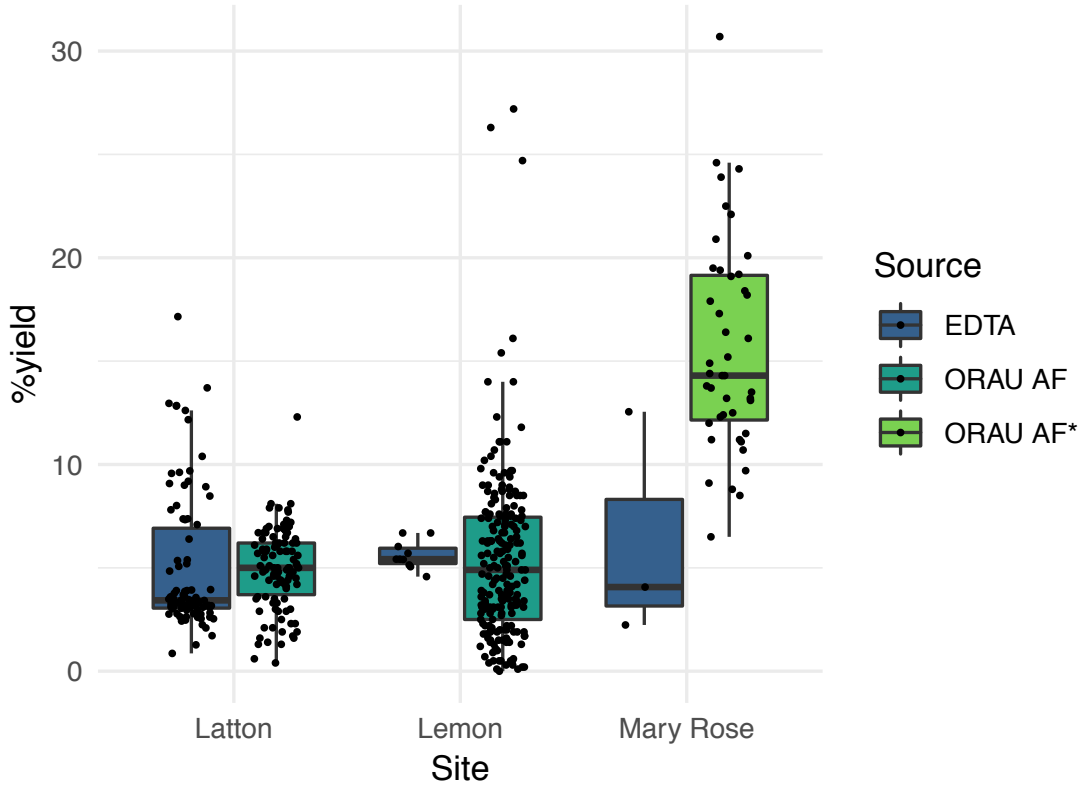


Figure 12.7: Mean %yield collagen of bone standards decalcified in EDTA compared to yields from the ORAU database. Mary Rose bone is routinely defatted and so compared with AF*, while the Latton bones are more commonly treated with AF.

Table 12.2: Comparison of EDTA and AF yields of bone standards from ORAU database. SD is standard deviation; p value is of a Welch's two-way t-test comparing the EDTA and AF means of the standard.

Site	Source	Mean	SD	Samples (n)	P value
Latton	EDTA	5.04	3.38	86	0.84
Latton	ORAU AF	4.95	1.95	106	
Lemon	EDTA	5.61	0.68	10	0.51
Lemon	ORAU AF	5.38	4.08	207	
Mary Rose	EDTA	6.29	5.50	3	0.09
Mary Rose	ORAU AF*	15.62	5.13	43	

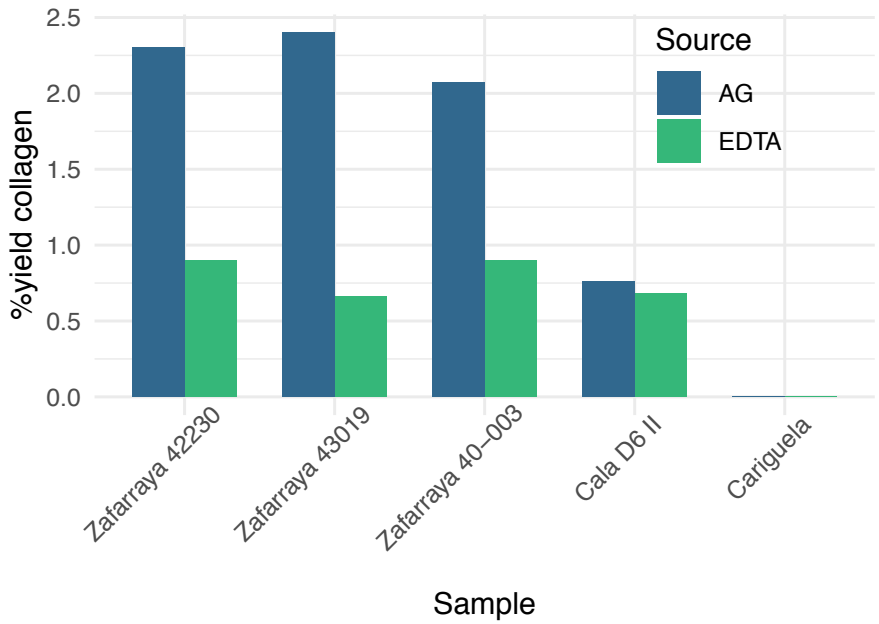


Figure 12.8: AG and EDTA %yields of archaeological samples. Samples were decalcified in EDTA in the microwave for 90 min, as described in this section. The bone from Carigüela produced no yield.

12.4.4 Microwave temperature

As samples were found to partially solubilize at 40° C, it was tested whether agitation in the microwave at a lower temperature could still accelerate decalcification. In this experiment, the microwave was set to run at 25° C (at 25 W) instead of 40° C. The glassware and EDTA solution were refrigerated at 5° C overnight beforehand. The relative %yield compared to the AG %yield from the same bone drill batch was low compared to the microwave %yields at increased temperature. At 40° C EDTA %yields reached AG %yields at 90–180 min (Fig. 12.4), while when chilled the %yields were still only about a third of the AG yield (Fig. 12.9).

12.5 Analysis of EDTA-extracted collagen

12.5.1 FTIR

FTIR was used to check for remaining EDTA contamination in the collagen by comparing EDTA powder, HCl collagen, and EDTA collagen spectra.

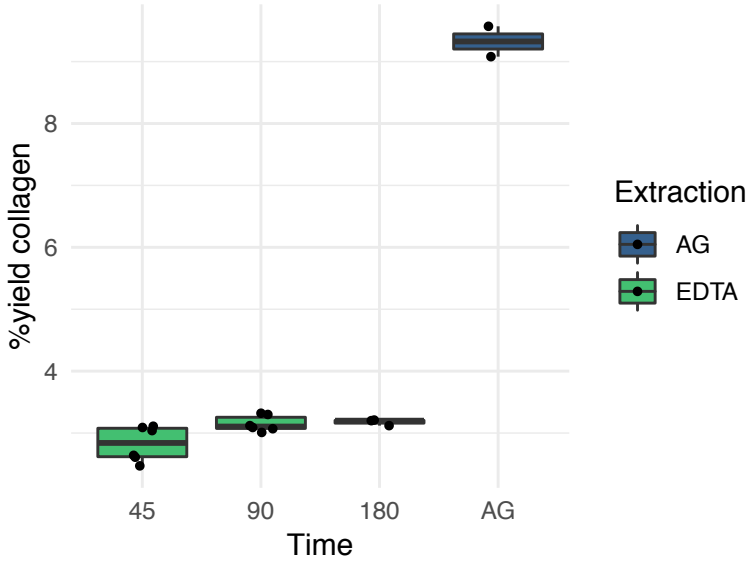


Figure 12.9: Mean %yield collagen of Latton bone decalcified in EDTA in the microwave at lower temperatures with chilled solvent and glassware. The EDTA yields are compared to the AG yields from the same drill batch.

EDTA is composed of C, O, and N, with two Na in the salt form used here (Hart 2011). The FTIR spectrum of pure EDTA has strong bands related to -COOH carboxylic group stretching in 1700–1500 cm^{-1} and a number of bands <1400 cm^{-1} related to CH-OH and C-N groups (Fig. 12.10). The broad bands >3000 cm^{-1} relates to -OH and -CH_2 stretching (Lanigan and Pidsosny 2007; Rajesh et al. 2000; Zhao et al. 2004). There is overlap between EDTA and collagen peaks in some positions, particularly at ~1600, which reflects Amide I νC=O stretching in collagen (Belbachir et al. 2009) but carboxylic stretching in EDTA (Zhao et al. 2004) (see also chapter 9.2). There are more EDTA peaks <1500 cm^{-1} that are distinct from collagen, presenting opportunities to identifying remaining EDTA in samples after decalcification.

The AG and acid-only extracted spectra are indistinguishable (Fig. 12.10) and are typical of collagen (chapter 11.2.2). EDTA-extracted gelatin showed slight differences in FTIR spectra depending on how long the sample was soaked in EDTA (Fig. 12.10 and Fig. 12.11). While even 10 minutes of EDTA extraction produced gelatin with a spectrum similar to AG- and acid-extracted gelatin spectra, EDTA-extracted spectra displayed small peaks at 1050 and 1350 cm^{-1}, suggesting

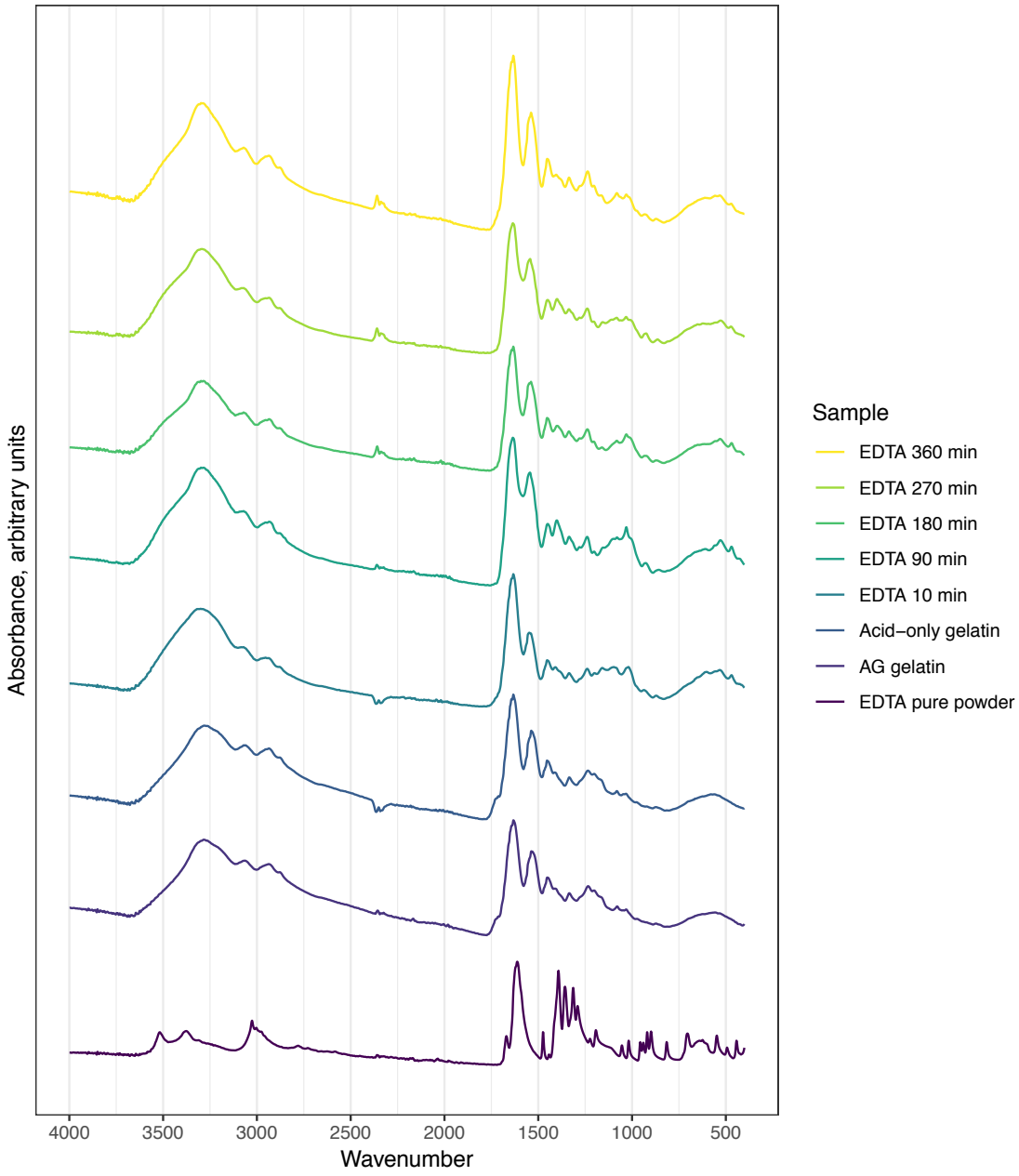


Figure 12.10: FTIR spectra of Latton bone product after soaking in 0.5 M EDTA for increasing lengths of time and gelatinised. Compared to pure EDTA powder, AG-extracted gelatin, and acid-only (no base wash) extracted gelatin.

continued inclusion of non-collagen components even after gelatinization. Samples also show minor peaks below 500 cm^{-1}, while acid-extracted gelatin does not. As the spectra are similar to collagen at 10 min, changes are subtle with increasing time in EDTA, though the samples at 270 and 360 min have weaker peaks at 1200 cm^{-1} and below 500 cm^{-1}.

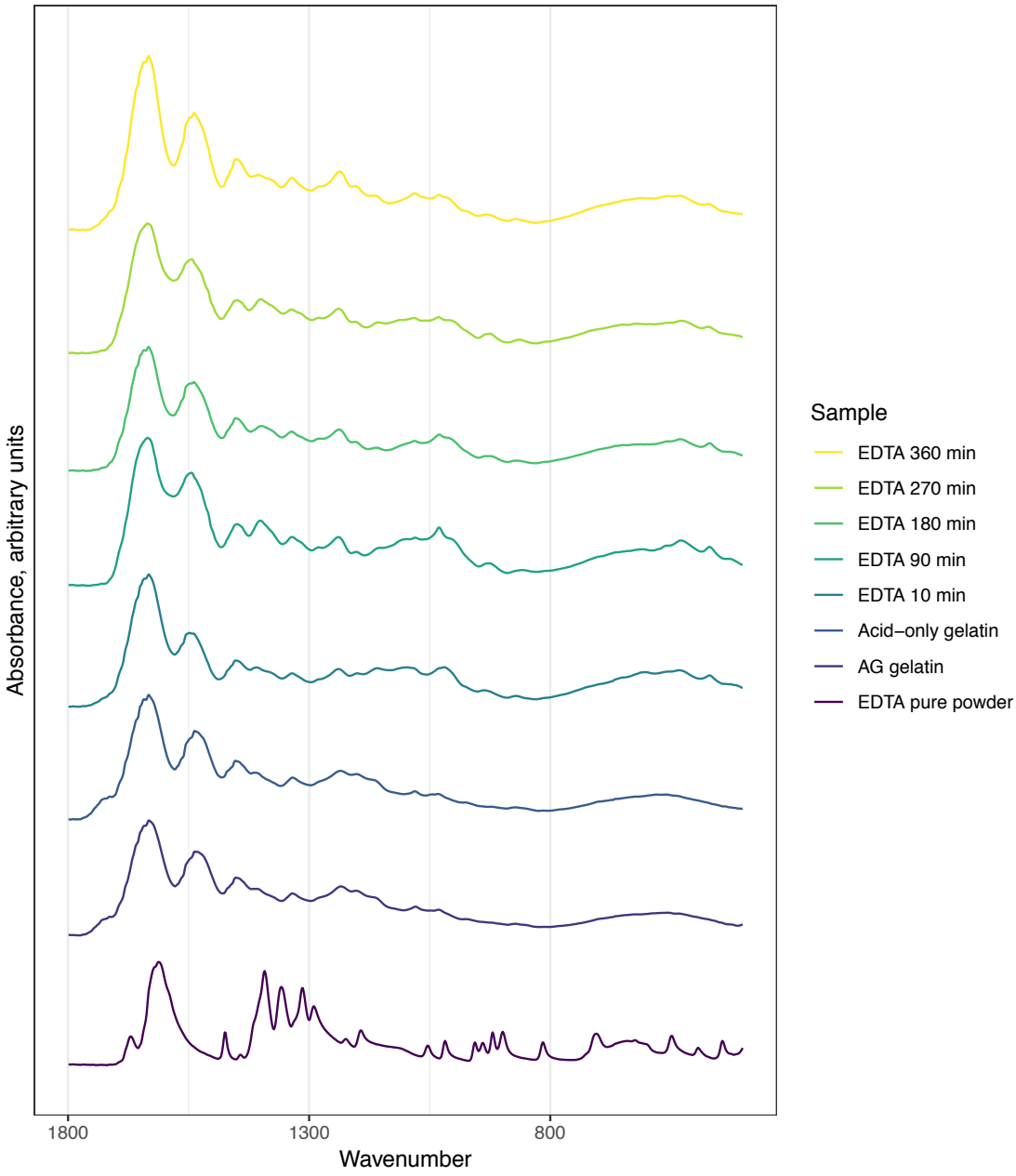


Figure 12.11: Close up of diagnostic region in Fig. 12.10.

Table 12.3: FTIR peaks from pure EDTA powder. v and v_1 = symmetric stretching, v_2 = asymmetric stretching (nonlinear) / bending (linear), δ = bending vibrations.

Value cm^{-1}	Assignment	References
3376, 3519	vNH, $-OH^-$	Lanigan and Pidsosny (2007); Rajesh et al. (2000); Zhao et al. (2004)
2780, 3025	$v CH_2$	Zhao et al. (2004)
1670	$v_2 CO_2$, possibly NH	Bargar et al. (1999); Lanigan and Pidsosny (2007)
1612	$v_2 CO_2$	Bargar et al. (1999); Lanigan and Pidsosny (2007)
1442, 1475	δCH_2	Bargar et al. (1999); Lanigan and Pidsosny (2007); Jones et al. (2007)
1392	$v COO^-$	Bargar et al. (1999); Lanigan and Pidsosny (2007); Jones et al. (2007)
1357	vCO, δNH	Lanigan and Pidsosny (2007); Zhao et al. (2004)
1290, 1313	$-COOH^-$	Lanigan and Pidsosny (2007); Zhao et al. (2004)
1195, 1224	$\delta CH_2(COO-)$	Lanigan and Pidsosny (2007); Zhao et al. (2004)
1018, 1055	δOH(COOH)	Lanigan and Pidsosny (2007); Zhao et al. (2004)
700–956 (multiple)	$vC-C(COO)$, $vC-C(COO^-)$, –COOH	Lanigan and Pidsosny (2007); Zhao et al. (2004)
440–640 (multiple)	v2C–C	Lanigan and Pidsosny (2007); Zhao et al. (2004)

12.5.2 %N and CN ratios

EDTA-extracted collagen was analysed for %C and CN ratios to evaluate whether EDTA collagen quality differs from acid-extracted collagen. Other than one outlier with a CN >3.6, all the EDTA sample CN values clustered between 3.3–3.4 without a meaningful trend with extraction time. This falls within the acceptable CN range of 2.9–3.5 and the observed CN range of Latton bones extracted with AG and AF protocols in the ORAU database. However, Latton bone from the same drill batch as the EDTA bone powder had lower CN values (3.1–3.2) when extracted with acid-only or AG protocols, suggesting EDTA extraction produced

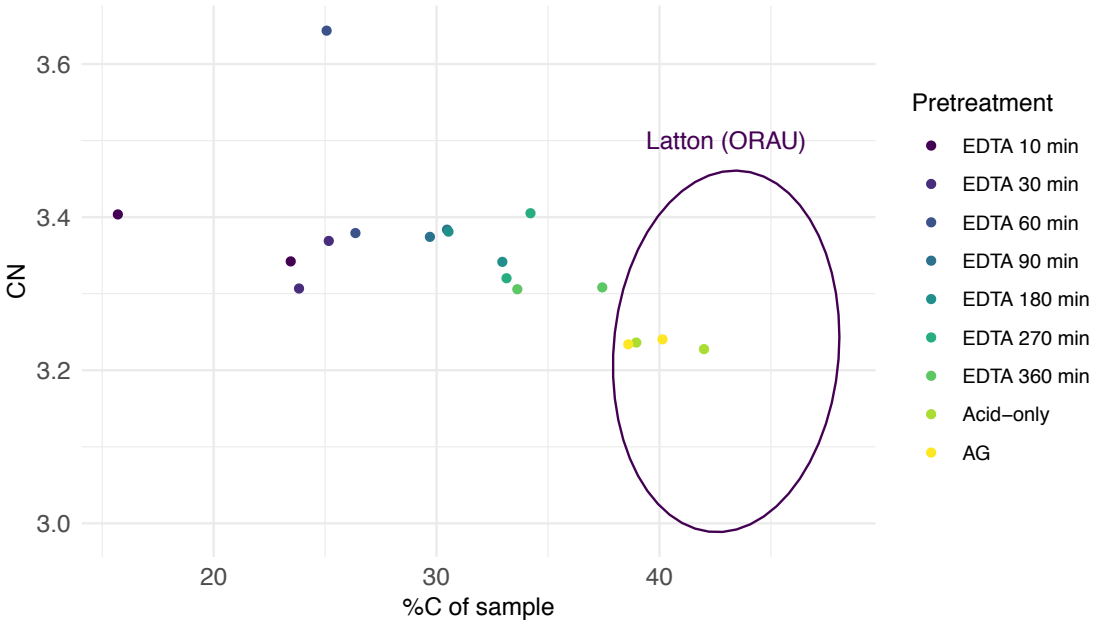


Figure 12.12: CN *vs* %C values of EDTA-extracted Latton collagen, as well as acid-only and AG-extracted collagen from the same drill batch of bone powder. The ellipse covers 98% of the range of observed values for Latton collagen extracted with routine AG and AF protocols (from the ORAU database; also described in Fig. 11.3).

relatively elevated CN values.

%C of EDTA-extracted collagen showed a positive trend with time. Samples extracted for <90 min had %C <25%, while longer extractions had %C around 30–37%. The acid/AG-extracted collagen had higher %C, around 38–42% C. Only one EDTA sample, extracted for 360 min, approached 38% C, with the extractions of 270 and 360 min mostly clustering around 33–35%. None of the EDTA collagen had %C as high as normally expected for AG/AF Latton collagen, while the acid/AG collagen from the same drill batch fell within the typical %C range.

12.5.3 Radiocarbon ages

Two Latton bone samples and one Mary Rose sample that were decalcified with EDTA were able to be dated. Both samples deviated from expected values, but in opposing directions: the Latton bone samples had more modern carbon than expected (should be background age), while the Mary Rose had more dead carbon than expected (should be ~311 BP) (Table 12.4) (Brock et al. 2010b). The fraction

Table 12.4: Radiocarbon dating results of three bones decalcified with EDTA. 'F. ^{14}C' is fraction modern carbon, C (mg) is carbon yield from combustion, %yield is the ratio of gelatin yield to original sample mass, %C is mass of sample carbon, CN is atomic mass ratio of carbon:nitrogen.

Site	Fraction	F. ^{14}C	F. ^{14}C error	Date BP	Date error	C (mg)	%yield	%C	CN
Latton	25774/118.26/121/NRC	0.00453	0.00065	43400	1200	1.7044	2.8	36.0	3.373
Latton	25774/118.26/122/NRC	0.00397	0.00068	44400	1400	1.6471	3.9	32.7	3.476
Mary Rose	40018/118.26/46/NRC	0.92047	0.00302	666	26	1.6437	2.2	32.9	3.651

modern carbon (F14C) of the Latton bones was higher than the F14C of AF- and AG-pretreated Latton bones before the lab's pretreatment background correction has been applied. Latton bones after AG/AF pretreatment produce F14C <0.004 and the F14C increases inversely with sample size, particularly for samples that produce <2 mg C from combustion (Wood 2011). The Mary Rose sample's F14C was lower than average for AF* F14C (0.961) (Bronk Ramsey et al. 2004b; McCullagh et al. 2010). The CN ratios of the Latton bones were <3.5, but the Mary Rose CN level was elevated, and all three had %C below the expected ~40%. The results show a mix of modern and dead exogenous carbon was introduced into samples during EDTA decalcification, gelatinization, and Ezee-filtering.

12.6 Discussion

Because EDTA works as a chelator that targets metal ions, it has been suggested that EDTA may not degrade protein chains as much as HCl (Tuross 2012). EDTA is regularly used in histology as it does not deform the structure of bone thin sections; it was hypothesised this preservation might extend to collagen yields. However, EDTA did not produce higher collagen yields in low-%N samples as compared to AG pretreatment. EDTA is a weaker agent than HCl, and it appears that in these samples the gentleness of EDTA does not outweigh the effectiveness of HCl. However, the bone used was a well-preserved medieval femur. It is possible that HCl is more destructive to partially degraded collagen. Poor quality collagen is likely to

be more prevalent in marginally preserved bones, such as the Zafarraya bones used in the %N experiments (chapter 8). It is possible that EDTA may produce better yields in such low-collagen bones as the HCl may destroy what little protein remains.

While HCl overall produced better yields than EDTA at room temperature, individual results were highly variable. This variability is a potential concern for the routine protocol, given that all these results came from the same bone. The bone used is well-preserved medieval bone; there is no reason to suspect that it contains intra-bone variation in the way that the marginally preserved Pleistocene bones did in the %N experiments (chapter 8). It is possible that some untested parameter affects the way HCl interacts with the bone. Yields for HCl crushed bone powder were also higher, except for those samples left overnight. The amount of sample handling may explain this. Samples left overnight did not have the HCl solution replaced, which meant there was no centrifuging and pouring off of liquid. The bench and agitated samples had their solution replaced every 2 hours. Powder was probably more likely to be accidently poured away, leading to an overall lower collagen yield.

Agitation failed to produce higher yields. It was thought agitation would prevent bone from settling to the bottom of the test tube and keep free acid and EDTA circulating through bone, increasing collagen yields. The reason for the lower results is unknown. It is possible that centrifuging was not fully effective with these more agitated samples, though this effect would not likely be significant in the crushed bone samples. Samples were agitated in a water bath, which seemed to moderately increase in temperature over time. This aspect was not considered at the time of these experiments, but later work suggests that the heat may have gelatinized some collagen, which would have been lost during the subsequent water rinses (see below).

Use of heat is another way to accelerate EDTA decalcification (Madden and Henson 1997), which could make its use more practical than current protocols that requires days to weeks of decalcification (Korlević et al. 2018; Tuross 2012). Duration spent in the microwave was correlated with %yield and produced %yields comparable to, and sometimes greater than, AG %yields from the same sample. The %yields of 90–180 min the microwave were comparable to %yields of AG

samples and samples decalcified in EDTA at room temperature for three days. That said, the gains in %yield between 10 min and 360 min were not always consistent. The experiment with the heatblock showed that temperature, even without the additional agitation of microwave action, partially solubilized collagen into the EDTA solution, so that some collagen was likely lost when the EDTA solvent was discarded after microwaving. This may also explain the reduced %yields in the experiments where the EDTA solution was replaced multiple times, as discarding the solvent also discarded solubilised collagen.

Given this evidence of solubilisation at higher temperatures, it was tested whether adjusting the microwave protocol to run at a lower temperature might reduce the amount of collagen lost to gelatinization while still subjecting samples to agitation and heat. However, decalcification with chilled EDTA and reduced temperature in the microwave did not produce higher %yields than the higher-temperature protocol. Instead, it seems decalcification at higher temperatures increases collagen yields more than the chilled protocol, even if some collagen is lost to gelatinization.

EDTA using the microwave protocol did not produce higher yields than the AG protocol on bones with low %N, though yields were sometimes comparable. The yields with well-preserved Lemon Mine, a background age standard, were similar to Latton bone in that they were comparable to AG yields. Yields from Mary Rose, a medieval and well-preserved standard (Brock et al. 2010b), were lower, though fewer samples were extracted. This does not support the hypothesis that EDTA, as a chelator, would produce higher collagen yields than HCl in degraded samples.

Another feature of these results is the variability in yields even from the same bone. Latton bone is a large mammoth bone, and so repeated drilling may have introduced heterogeneity in collagen content between batches in this series of experiments. Variation in collagen preservation is not always consistent across a bone, as found in the %N experiment (chapter 8), and while Latton bone is generally considered well-preserved, the ORAU database does show some variation in yields (*e.g.* in Fig. 12.7). Results of different drill batches were separated to control for this variation, and an aliquot from each drill batch had an AG extraction to

compare yields with. The importance of controlling for this variation is evident in the different AG yields and clear separation in yield trendlines by drill batch in the microwave experimental results. This feature ought to be considered in future experiments that rely on large amounts of bone sample to develop and test protocols.

In terms of the quality of the collagen yields, samples microwaved for longer durations showed increased %C content, with samples microwaved for 360 min approaching expected %C levels for ABA-extracted collagen. CN ratios of all bones, regardless of time in the microwave, fell within the lab's accepted range but were slightly higher than expected for ABA-extracted Latton bone. This matches results in Cersoy et al. (2016), which found EDTA-extracted samples to have either similar to slightly higher CN ratios than their HCl-extracted fractions. FTIR analysis of the samples also suggests the quality of the extracted collagen improves with duration in the microwave, with samples run for 360 min having FTIR spectra similar to AG-extracted collagen.

Nonetheless, radiocarbon results suggest that a mix of background and modern exogenous carbon is introduced to samples during the EDTA decalcification protocol. This contrasts with Korlević et al. (2018)'s suggestion that EDTA is produced with dead carbon sources. Alternatively the modern carbon fraction may not derive directly from the EDTA but from some other step in the protocol. After decalcification, samples underwent routine gelatinization and Ezee-filtering, and the microwave test tubes were cleaned and baked alongside other lab glassware (Brock et al. 2010b). However, the EDTA solution is slightly basic, which can encourage dissolution of CO_2 in the solution. In the routine ABA protocol, 0.5 HCl is added after the base-wash step to remove dissolved CO_2. The EDTA protocol is gelatinized in pH 3 water, but this is not as acidic as the ABA protocol's final acid wash, so it is possible some atmospheric CO_2 was retained.

If the modern carbon can be shown to be a consistent contribution, a background correction could be developed similar to the lab's correction for ultrafiltration (Wood 2011), but at the moment it appears to be a significant contribution that would ideally be reduced. With the exception of very young samples like the Mary Rose,

dead carbon has less impact on final date estimates and might be corrected for along the lines of the HYP correction (Devièse et al. 2017; Devièse et al. 2018), but again further work is needed to demonstrate the consistency of this dead carbon contribution and try to better remove residual EDTA.

Korlević et al. (2018) used a combined EDTA-ABA protocol to extract DNA and collagen from the same sample, and found the radiocarbon dates to agree with expectations. When two samples were dated here without the subseqent ABA step, they showed inclusion of exogenous carbon. The extra ABA pretreatment in Korlević et al. (2018) is currently necessary to ensure reliable radiocarbon dates from an accelerated EDTA protocol. The other approach involves a very slow extraction over weeks, which found the resulting collagen quality metrics and radiocarbon dates to be acceptable (Cersoy et al. 2016; Tuross 2012).

Further work might investigate ways of recovering the solubilized collagen and improving its quality. As EDTA quickly precipitates out of solutions below pH 8, the addition of small amounts of acid to the EDTA solution after microwaving would precipitate EDTA salts, and the remaining liquid could be directly gelatinized. This could be recombined with the gelatinized pellet afterwards to increase yields. EDTA extraction might also be combined with ultrafiltration. EDTA has a molecular mass of 292.2 Da and would pass through the ultrafilter's 3.5 kDA pore size, potentially improving the collagen quality. A protocol with EDTA extraction of less than 6 hr, overnight gelatinization, and ultrafiltration would take less than two days and require less manual handling (through water rinses) than current ABA-ultrafiltration protocols. The additional cost of EDTA solvent and microwave extraction would need to be weighed against the ability to extract DNA samples from the same bone and the slightly improved pretreatment time.

12.7 Conclusions

An efficient EDTA decalcification protocol would enable DNA analysis and radiocarbon dating of the same sample. Current EDTA decalcification protocols require long times for EDTA to work or combine EDTA with subsequent ABA

pretreatment of the radiocarbon aliquot. It was also hypothesised that a chelating agent might destroy less low-quality protein than acid, potentially making EDTA preferable for decalcifying poorly-preserved bones.

Use of the microwave accelerated EDTA action, with %yields reaching AG yields at around 90 min at 30° C, but %C content of the sample continuing to increase up to the maximum tested time (360 min). Though 70° C is usually used to solubilize collagen, collagen partially solubilized in EDTA solution at 30° C, so that repeatedly replacing the EDTA solution dampened the apparent effect of the microwave. EDTA did not produce increased %yields in low-%N samples, though in one case the yields were similar. Radiocarbon dating show both modern and background exogenous carbon remained in the samples after pretreatment, with the background carbon probably due to incomplete removal of EDTA solvent and modern carbon perhaps from dissolution of atmospheric CO_2 in the basic solution.

EDTA is periodically revisited in radiocarbon dating and has long been used in histology and genetics analysis. The investigations here suggest that while EDTA has potential to be optimised for efficient combined genetics-radiocarbon studies, further work is necessary to ensure collagen quality.

13
Summary of experimental results

Radiocarbon dating of bone is hampered by poor preservation of collagen in hot climates and the potential for samples to be contaminated through both diagenetic and post-excavation processes. This limitation leads to chronological datasets that are not representative across space and that depend on increasingly indirect and imprecise age estimates. While the focus of this project is on the implications of radiocarbon dating for megafauna in Europe, improving radiocarbon dating of poorly preserved bone would be useful in many other research contexts.

The experiments here characterised low-preservation and potentially contaminated bones. They also tested whether two alternatives to the standard ABA pretreatment protocol could produce better yields, particularly in degraded bone. The main results are summarised here:

- Even in the relatively stable environment of a cave (Zafarraya), samples varied in their collagen preservation. Large-scale %N screening of bone samples could quickly identify those most likely to succeed and revealed rare, well-preserved bones even when most were low-collagen.

- Hyena samples from Caldey Island, Wales, that were suspected of being treated with conservative appeared to be clean collagen when analysed. One sample,

produced through ampoule, had low %C content and should be regarded cautiously.

- Several samples produced a non-collagen white powder after AG pretreatment. Analysis suggested that the yield contained the diagenetically-altered mineral component of bone and that pretreatment itself introduced—or at least concentrated—chlorine and other apatite substituents. The similarities between samples from different sites (including in the literature) suggested that these 'false yields' arose from a common diagenetic process.

- Individual bones contained heterogenous collagen content. This was found both in Zafarraya bones and in Latton bone, a lab standard.

- ABA extraction sometimes produced variable yields from the same sample. Unexpectedly, agitating samples in HCl solution significantly reduced yields.

- Dialysis extraction of the acid-soluble fraction of bone failed to produce large collagen yields, regardless of the preservation of the bone. The collagen also failed to satisfy quality metrics such as %C and the CN ratio.

- EDTA decalcification, which normally takes weeks, was accelerated by microwaving samples in solvent. Yields approached comparable AG yields in 90–180 minutes, but the collagen quality only approached expected %C and CN ratios at 360 minutes. The EDTA-extracted collagen contained exogenous carbon, both modern and background, and EDTA yields of poorly preserved samples were generally lower than AG yields.

- In EDTA solution, collagen partially solubilised well below the 70° C usually used for gelatinisation, limiting the collagen yields from the microwave protocol.

Interesting findings include the within-sample heterogeneity of collagen, the potential for large-scale %N screening to recover samples with collagen, and the (not fully realised) potential for an accelerated EDTA decalcification protocol. The

Caldey Island results support the reliability of the dates, but rely on absence of evidence, and the samples were unfortunately too small to re-date. The Caldey dates are included in the following chapters on megafauna, though they are given reliability scores like other dates. Experimental results are discussed more in chapter 18, including limitations and suggestions for future work.

Part IV

Radiocarbon results and models

14
New samples

ZooMS, %N, pretreatment, and radiocarbon results of samples collected for this project are presented here, with more details in related appendices. Radiocarbon dates are combined with published dates for extinction models in chapters 15 and 16.

14.1 ZooMS results

The majority of faunal material available from Zafarraya, Spain was fragmentary, and so 72 samples were analysed with the ZooMS technique to identify their genus and possibly species (Appendix D). The samples were selected from the highest levels of the stratigraphy, which is most relevant to determining last appearances, and they had already had sufficient collagen extracted to be run. In some cases samples failed to produce diagnostic spectra, and the imprecise resolution of the technique meant that even successful samples could not be identified to species level. In particular, while 6 carnivores were identified, neither the genus nor species could be distinguished. The inability to distinguish large and small carnivores was particularly frustrating.

Two samples labelled by excavators as *Panthera* sp. (sample P06/112.5/115 C; note 'Tarso cuboscaphoide pantera (?)' and P06/112.5/84, 'P. pardus') turned out have peptide markers of herbivores. One of these had already been registered for

Table 14.1: Summary of ZooMS results obtained from Zafarraya. Samples were processed at the Universities of Manchester and York. Species are as reported from labs. 'No ID' includes samples that failed to produce spectra and those without reference library matches.

ZooMS ID	Count
Bovid/deer	5
Canivore	6
Deer	4
Goat	13
Goat/deer	3
Goat/Reindeer	26
No ID	14
Sheep	1
Total	**72**

dating by the time the ZooMS results were obtained (P43533). Even without specific genus identification, the results eliminate possibilities and illustrate the value of having species identifications confirmed through multiple methods when possible.

Unidentified samples ('No ID' results) either produced no spectra or produced spectra without matches in the ZooMS reference libraries. Both instances could be attributed to degraded collagen. That said, %N preservation had little correlation with whether a sample was identifiable or not. Of the 48 samples also measured for %N as part of %N experiments, 37 had %N <0.76 and 32 produced results other than 'No ID', while 11 had %N $\geqslant 0.76$ of which 9 produced a result other than 'No ID'.

Of the samples registered for radiocarbon dating, the majority were selected as part of the PalaeoChron project. Soil samples from the site were also analysed for DNA, and the results, not yet available, may better establish the presence of carnivore species in stratigraphic layers (Slon et al. 2017; Willerslev et al. 2003). The high-resolution chronology built of the site, while primarily driven by archaeological questions, may yet inform carnivore presence.

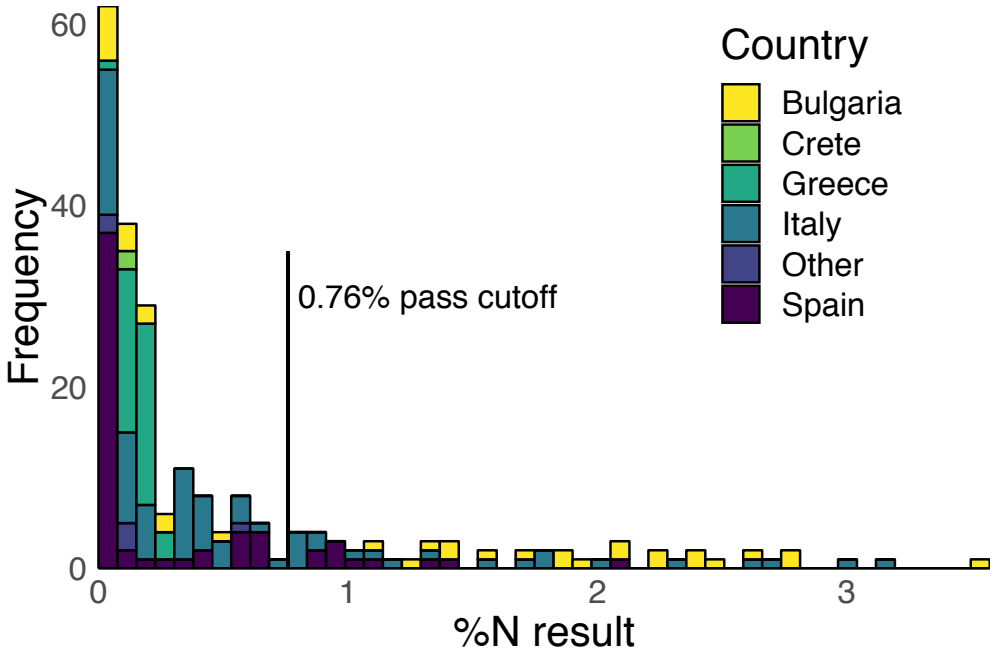


Figure 14.1: %N results for samples collected for this thesis, coloured by country of origin.

14.2 %N and pretreatment

Sample %N results by species are reported in chapter 5.3. Of the 22 sites sampled, 10 failed to produce any samples with %N ⩾0.5 (Table 14.2). Of the remaining, some turned out to be 'false positives', where the samples passed %N thresholds but failed to produce collagen or failed on combustion. Preservation varied by region, with Bulgarian sites most likely to pass %N, along with some of the Italian caves (Fig. 14.1). Bulgaria has a more temperate climate than most of the sites sampled here, and some of the better-%N sites were higher-elevation caves, such as Equi, La Sassa, and Zafarraya. Sites in low-elevation Mediterranean regions like Malta, Crete, southern Spain, and Greek islands largely failed to produce sufficient %N. The exposure to heat and aridity likely explains the greater deterioration of the bones in these settings, despite some of them coming from caves.

In total collagen extraction was attempted 121 times on 110 unique samples (Appendix E.1), with some samples being extracted multiple times with different pretreatments. Just over half of these extractions (56.2%) produced ⩾1 %yield

Table 14.2: Samples collected for this project by site and their %N results. Includes count of samples (N), minimum and maximum %N values, and counts of samples that passed the 0.5 and 0.76 %N ORAU thresholds.

Site	Country	N	Min	Max	%N ≥0.5	%N ≥0.76
Bulgaria						
Kozarnika	Bulgaria	4	1.14	2.40	4	4
Manastira	Bulgaria	16	0.03	2.12	4	4
Redaka II	Bulgaria	13	1.29	3.57	13	13
Vasil Levski	Bulgaria	2	0.10	0.53	1	0
Crete						
Crete (museum)	Crete	2	0.09	0.09	0	0
Greece						
Akrotiri	Greece	1	0.04	0.04	0	0
Tilos	Greece	41	0.08	0.26	0	0
Italy						
Cala	Italy	4	0.02	0.34	0	0
Castelcivita	Italy	6	0.03	0.39	0	0
Cucigliana	Italy	9	0.04	0.56	1	0
Equi	Italy	26	0.08	2.63	12	9
Muracci	Italy	11	0.20	3.13	7	5
Paglicci	Italy	8	0.03	0.19	0	0
Santi	Italy	4	0.02	0.06	0	0
Sassa	Italy	8	0.46	2.68	7	6
Other						
Lough Boora	Other	4	0.09	0.55	1	0
Tawain sea	Other	2	0.04	0.04	0	0
Spain						
Carigüela	Spain	35	0.03	2.07	2	1
Llera	Spain	1	0.02	0.02	0	0
Rincones	Spain	11	0.04	1.34	6	3
Silluca	Spain	3	0.02	0.22	0	0
Zafarraya	Spain	12	0.25	1.38	10	6
Total	**NA**	**223**	**NA**	**NA**	**68**	**51**

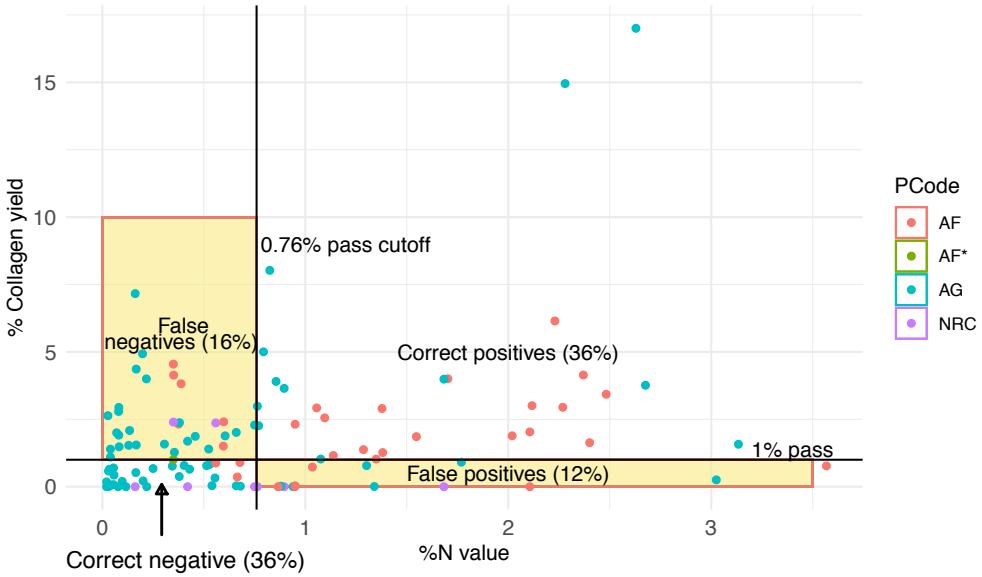


Figure 14.2: Graph showing the relationship between %N and collagen yields from 110 bones, coloured by chemistry pretreatment. The lines on the graph represent the thresholds used at the ORAU (%N >0.76 and collagen yield >1%).

Table 14.3: Pretreatments and resulting success in %yield and dating for this project. NRC (HPLC dates) are not counted for %yield in this case, as collagen had to already be hydrolysed in sufficient quantities to attempt extraction.

PCode	n	%yield pass	Dates
AF	39	27	30
AF*	4	2	3
AG	68	36	5
NRC	10	NA	7
Total	**121**	**65**	**45**

collagen (Fig. 14.2). While it appears from Table 14.3 that AG extractions were particularly unreliable in terms of %yield and combustion success, this is misleading, as AF and NRC extractions were not attempted on the most 'marginal' %N samples.

In total, dates were successfully obtained from 10 of the attempted sites and 38 of the 241 (15.8%) samples collected, though in total 45 dates were obtained as some samples were dated with different pretreatments. Of the 67 attempted combustions, 32.84% failed (Table 14.4). This is a low success rate for samples

Table 14.4: By site, samples that produced ⩾1 %yield collagen and subsequently produced a radiocarbon date. There were 121 extractions, though only 110 unique samples were extracted, as some were extracted multiple times. %yield pass is ⩾1% collagen yield relative to starting mass of the sample.

Site	N extractions	%yield pass	Combusted	Dates
Cala	4	1	2	0
Castelcivita	6	5	4	3
Cucigliana	1	0	0	0
Equi	13	10	5	3
Kozarnika	3	3	3	3
Manastira	5	4	5	5
Muracci	12	4	5	3
Paglicci	5	3	2	0
Redaka II	7	6	6	6
Rincones	12	4	4	0
Santi	4	0	2	0
Sassa	8	7	4	4
Silluca	1	1	1	0
Tilos	11	6	3	0
Vasil Levski	2	0	1	1
Zafarraya	27	14	20	17
Total	**121**	**68**	**67**	**45**

that produced a supposed yield, suggesting the 'collagen' was not truly collagen like the examples characterised in chapter 10. There were a high number of false negatives between %N and %yield in these samples, but given the subsequent failure on combustion, it appears the low %N might have been reflecting the non-collagen composition of the samples.

14.3 Radiocarbon dates

Of the 45 dates successfully obtained for this project, seven were HPLC (PCode 'NRC') dates and the remainder conventional collagen pretreatments (AF, AF*, and AG) (Table 14.5). The HPLC dates have an additional correction applied to them due to the introduction of background carbon from the HPLC instrument and preparation chemistry; the equation and data used in this correction is in Appendix I.

The sample quality metrics are evaluated by-species below, though sites are summarised in Appendix B and a couple of features are worth noting here. The samples from Manastira and Redaka II marked as 'unknown' species reflect hyena activity, as the bones had chew marks distinctive of hyena activity (Table 14.6). Most of the 'OxA-X-' dates (OxA code '-88' in the database) reflect the non-routine HPLC protocol, though four dates below were flagged due to low %C content on combustion and high CN values (>3.4) (Table 14.5). Two AG results from Cava Muracci (P45507 and P45508) were background age or near-to, and an AG date from La Sassa (P45514) had a similar age to three AF dates obtained from the site. The site has little stratigraphic structure, so while agreement may be coincidence, the other three samples suggest that the palaeontological material reflects relatively constrained period of activity. The remaining sample with a health warning is an AF date from Zafarraya (P43018) with a CN ratio of 3.49. This sample is significantly younger than the other date obtained from the same square and cultural affiliation, suggesting complexity to the site's taphonomy (Barroso Ruiz 2010; Wood et al. 2013a). As the species of this sample is unknown and not identified by ZooMS (chapter 14.1), it was not included in subsequent species-specific analysis. The other three were included below, but they were scored and down-weighted accordingly (chapter 5.1).

Table 14.5: New dates obtained for this thesis. OxA numbers with the X- prefix reflect health warnings or experimental treatments. All NRC dates here are HPLC dates.

Site	Country	Species	P	PCode	OxA	Date	±	HPLC Date	HPLC ±	%C	δ^{13}C	δ^{15}N	CN
Castelcivita Cave	Italy	Cave hyena	45630	AF	37221	34500	600	NA	NA	40.0	-18.16	11.55	3.32
Castelcivita Cave	Italy	Leopard	45631	AF	37222	43400	1800	NA	NA	38.0	-18.33	8.83	3.34
Castelcivita Cave	Italy	Leopard	45632	AF	37223	38800	1000	NA	NA	39.2	-18.11	10.06	3.35
Cava Muracci	Italy	Cave hyena	44418	NRC	X-2756-42	44400	3700	49270	10188	38.4	-27.30	11.95	4.99
Cava Muracci	Italy	Cave hyena	45506	AG	X-2772-28	41700	>	NA	NA	20.6	-20.82	6.14	3.64
Cava Muracci	Italy	Narrow-nosed rhino	45507	AG	X-2772-33	46500	3900	NA	NA	20.5	-21.92	6.10	3.63
Grotte di Equi	Italy	Cave lion	45510	AG	37177	21920	160	NA	NA	43.4	-20.02	5.62	3.50
Grotte di Equi	Italy	Leopard	44416	NRC	X-2756-41	41000	1800	43011	3513	37.0	-27.41	8.27	5.00
Grotte di Equi	Italy	Wolf	44415	NRC	X-2756-40	19360	140	19480	214	45.7	-26.02	7.56	5.00
Kozarnica	Bulgaria	Cave hyena	42395	AF	35556	34350	600	NA	NA	42.4	-19.35	14.42	3.35
Kozarnica	Bulgaria	Cave hyena	42397	AF	35557	49100	3600	NA	NA	44.8	-19.07	14.41	3.30
Kozarnica	Bulgaria	Cave lion	42398	AF	35558	16395	80	NA	NA	45.2	-19.80	9.84	3.29
La Sassa	Italy	Brown bear	45511	AF	37283	30220	360	NA	NA	41.7	-18.80	6.49	3.25
La Sassa	Italy	Cave hyena	45512	AF	37218	29190	310	NA	NA	40.1	-17.73	10.87	3.28
La Sassa	Italy	Cave hyena	45513	AF	37219	30150	350	NA	NA	40.2	-18.23	11.09	3.26
La Sassa	Italy	Cave lion	45514	AG	X-2772-34	29300	400	NA	NA	24.8	-18.61	12.14	3.54
Manastira	Bulgaria	Bovid	42409	AF	35568	49900	>	NA	NA	43.2	-19.96	9.89	3.20
Manastira	Bulgaria	Unknown	42406	AF	35565	47700	>	NA	NA	45.3	-20.44	10.85	3.35
Manastira	Bulgaria	Unknown	42407	AF	35566	50200	>	NA	NA	43.3	-19.21	8.17	3.21
Manastira	Bulgaria	Unknown	42408	AF	35567	50200	>	NA	NA	43.4	-19.19	10.76	3.22
Manastira	Bulgaria	Unknown	42408	AF	35567	50200	>	NA	NA	43.4	-19.19	10.76	3.22
Redaka II	Bulgaria	Cave hyena	42399	AF	35559	30910	380	NA	NA	46.3	-20.14	11.23	3.42
Redaka II	Bulgaria	Cave hyena	42400	AF	35560	32700	500	NA	NA	44.0	-18.70	13.94	3.29
Redaka II	Bulgaria	Cave hyena	42401	AF	35561	30920	380	NA	NA	45.3	-19.30	11.44	3.27
Redaka II	Bulgaria	Cave hyena	42402	AF	35562	33850	550	NA	NA	46.0	-18.47	12.77	3.38
Redaka II	Bulgaria	Cave hyena	42403	AF	35563	47200	>	NA	NA	43.4	-19.65	12.01	3.25

Table 14.5: New dates obtained for this thesis. OxA numbers with the X- prefix reflect health warnings or experimental treatments. All NRC dates here are HPLC dates. *(continued)*

Site	Country	Species	P	PCode	OxA	Date	±	HPLC Date	HPLC ±	%C	δ^{13}C	δ^{15}N	CN
Redaka II	Bulgaria	Unknown	42405	AF	35564	45400	>	NA	NA	43.2	-20.95	8.02	3.23
Vasil Levski	Bulgaria	Cave hyena	45645	AG	37323	38100	1100	NA	NA	40.4	-18.54	9.27	3.44
Zafarraya	Spain	Unknown	42796	AF*	35500	30360	360	NA	NA	43.3	-19.32	4.64	3.30
Zafarraya	Spain	Unknown	42796	AF*	35500	30360	360	NA	NA	43.3	-19.32	4.64	3.30
Zafarraya	Spain	Unknown	42796	NRC	X-2730-9	31000	290	31245	417	41.8	-27.81	6.17	4.94
Zafarraya	Spain	Unknown	42798	AF	35226	27460	270	NA	NA	40.0	-19.01	6.47	3.27
Zafarraya	Spain	Unknown	42798	NRC	X-2732-18	27400	310	27672	463	44.3	-23.32	8.16	5.05
Zafarraya	Spain	Unknown	42800	AF	35227	42400	1600	NA	NA	43.9	-20.06	4.98	3.27
Zafarraya	Spain	Unknown	43017	AF	35540	34100	600	NA	NA	44.2	-19.45	6.73	3.46
Zafarraya	Spain	Unknown	43017	NRC	X-2730-10	36850	550	37371	845	46.3	-22.93	8.75	4.92
Zafarraya	Spain	Unknown	43018	AF	X-2720-37	34100	650	NA	NA	43.1	-19.27	8.04	3.48
Zafarraya	Spain	Unknown	43019	AF	35541	43200	1700	NA	NA	42.9	-19.56	6.24	3.37
Zafarraya	Spain	Unknown	43022	AF	35542	31950	450	NA	NA	43.8	-19.95	6.17	3.29
Zafarraya	Spain	Unknown	43023	AF	35543	31140	400	NA	NA	44.2	-19.00	7.82	3.33
Zafarraya	Spain	Unknown	43024	AF	35544	30730	380	NA	NA	46.2	-19.32	5.92	3.30
Zafarraya	Spain	Unknown	43025	AF	35545	43500	1800	NA	NA	42.2	-19.62	5.97	3.33
Zafarraya	Spain	Unknown	43025	NRC	X-2732-28	42200	1200	43359	1999	42.9	-24.19	7.47	4.97
Zafarraya	Spain	Unknown	43025	AF*	35791	41200	1500	NA	NA	34.5	-19.98	6.23	3.41
Zafarraya	Spain	Unknown	43026	AF	35546	44600	2000	NA	NA	45.3	-19.40	7.06	3.31

Table 14.6: Further information on dated sample identification and context.

Site	P	Species	Sample	Element	Context	Z-depth
Castelcivita	45630	Cave hyena	Castel 1	Radius, right	H14 I, layer RCP, level 15	NA
Castelcivita	45631	Leopard	Castel 6	Humerus, right	G13 I-II, layer GAR, level 27	NA
Castelcivita	45632	Leopard	Castel 5	Ulna, right	G14 IV, layer RSA, level 12	NA
Equi	44415	Wolf	5438v	Humerus, right	Level V, sample 5438 (poor context records)	NA
Equi	44416	Leopard	5357v	Ulna, right	Level V, sample 5357 (poor context records)	NA
Equi	45510	Cave lion	6081	Metatarsal, left	Level V, sample 6081 (poor context records)	NA
Kozarnika	42395	Cave hyena	Koz CC1	Phalange (label illegible)	G8, level VI inf (upper VII), c. 5c	445-450
Kozarnika	42397	Cave hyena	Koz CC3	Premolar 3, broken	H7, level c. 6/7	465-470
Kozarnika	42398	Cave lion	Koz PS1	Phalange, I	D9, level II - III / 3b	318-360
Manastira	42406	Unknown	Mana 4	Chewed long bone fragment	level G, square 21-1	NA
Manastira	42407	Unknown	Mana 5	Chewed long bone fragment	level G, square 21-3	NA
Manastira	42408	Unknown	Mana 6	Chewed long bone fragment	level H, square 24-13	NA
Manastira	42408	Unknown	Mana 6	Chewed long bone fragment	level H, square 24-13	NA
Manastira	42409	Bovid	Mana 7	Tibia, proximal	level H, square 23-1	NA
Muracci	44418	Cave hyena	CM 3	Molar	sector A, area 3	NA
Muracci	45506	Cave hyena	CM 261	Ulna, proximal left	sector A, area 3	NA
Muracci	45507	Narrow-nosed rhino	CM 363	NA	NA	NA
Redaka II	42399	Cave hyena	Red CC1	Chewed (incl. puncture) long bone	Square E6, level c. 4bc b	NA

Table 14.6: Further information on dated sample identification and context. *(continued)*

Site	P	Species	Sample	Element	Context	Z-depth
Redaka II	42400	Cave hyena	Red CC2	Premolar 4/ d/c	Square D2, level c. 4BC	NA
Redaka II	42401	Cave hyena	Red CC3	Phalange I	Square D4, level c. 4bc b	NA
Redaka II	42402	Cave hyena	Red CC4	Incisor 3/	Square E4 , level c. 5?	NA
Redaka II	42403	Cave hyena	Red CC5	Metacarpal V	Suare D4, level c. 4bc b	NA
Redaka II	42405	Unknown	Red NID5	Tibia, chewed	Square E4, level c. 4bc	NA
Sassa	45511	Brown bear	Sassa 3	Radius, right distal	Sample R. 3, Room 6	NA
Sassa	45512	Cave hyena	Sassa 516B	Humerus	Sample R. 516B, Room 3	NA
Sassa	45513	Cave hyena	Sassa 516A	Tibia	Sample R. 516A, Room 3	NA
Sassa	45514	Cave lion	Sassa 23	Molar	Sample R. 23, Room 1	NA
Vasil Levski	45645	Cave hyena	Vasil C	Canine, lower left	Square BG	NA
Zafarraya	42796	Unknown	ZAF 1 EJ	Bone	Square P14, level UA	103
Zafarraya	42796	Unknown	ZAF 1 EJ	Bone	Square P14, level UA	103
Zafarraya	42796	Unknown	ZAF 1 EJ	Bone	Square P14, level UA	103
Zafarraya	42798	Unknown	ZAF 3 EJ	Bone	Square P06, level UA	115.5
Zafarraya	42798	Unknown	ZAF 3 EJ	Bone	Square P06, level UA	115.5
Zafarraya	42800	Unknown	ZAF 5 EJ	Bone	Square P14, level UB	126.3
Zafarraya	43017	Unknown	Zaf N40-009	Bone	Square P14, level UA	109
Zafarraya	43017	Unknown	Zaf N40-009	Bone	Square P14, level UA	109
Zafarraya	43018	Unknown	Zaf N40071	Tooth	Square P11, level UA	110-115
Zafarraya	43019	Unknown	Zaf P11H92	Bone	Square P11, level UA	110-115
Zafarraya	43022	Unknown	Zaf N40-010	Bone	Square P11, level UB	120
Zafarraya	43023	Unknown	Zaf N40-032	Bone	Square P06, level UB	120
Zafarraya	43024	Unknown	Zaf N40-172	Bone	Square P06, level UB	120
Zafarraya	43025	Unknown	Zaf N40-130	Bone	Square P06, level UB	121
Zafarraya	43025	Unknown	Zaf N40-130	Bone	Square P06, level UB	121
Zafarraya	43025	Unknown	Zaf N40-130	Bone	Square P06, level UB	121
Zafarraya	43026	Unknown	Zaf N18	Bone	Square P11, level UB	130

14.3.1 Other species

Two other carnivores were successfully radiocarbon dated for this project: one wolf and one brown bear. The wolf, from Equi cave, was dated to test previous suggestions that carnivores had coexisted with each other in the cave rather than the stratigraphy being mixed (Ghezzo et al. 2014; Ghezzo and Rook 2015). Similarly, the brown bear from La Sassa cave was found with cave lions and hyenas, suggesting a possibly mixed use of the cave (Gatta pers. comm.). These two species are not further modelled here as they are not extinct, but reviews of their Pleistocene demography and genetic population dynamics exist (Leonard et al. 2007; Mecozzi and Lucenti 2018; Sommer and Benecke 2005; Stiner 2004; Valdiosera et al. 2007). The four dates from La Sassa are similar, but the three dates from Equi are different, with the leopard in particular being much older. This suggests Equi is stratigraphically mixed or that the labels from the historical excavations do not reflect stratigraphy.

15
Species chronologies

Here radiocarbon dates of cave lions, cave hyenas, and leopards are evaluated and used to estimate their extinctions. The focus is on Europe, but both lions and hyenas lived across Eurasia, and these literature dates are included in regional models (Fig. 15.1).

15.1 Evaluation scores

Scores are discussed on a by-species basis in more detail below, but a summary is presented here. Of the 307 evaluated dates, about half received a high score (147), and roughly equal proportions received medium and low scores. About 30 were outright rejected, usually due to issues of species identification or specimens being Holocene re-introductions. Looking at the point scores of non-HPLC dates, which were evaluated on a slightly different scale, a bimodal distribution emerges, where dates tend to receive either low or high scores. Some of these very low scores are due to lack of published metrics, so it is unclear whether dates really do tend to fail on several metrics, or if there would be a more even distribution of scores if more data were available.

The metrics most commonly failed were the carbon and nitrogen isotopes. PCode also often failed, where the samples were not pretreated with the AF or HPLC

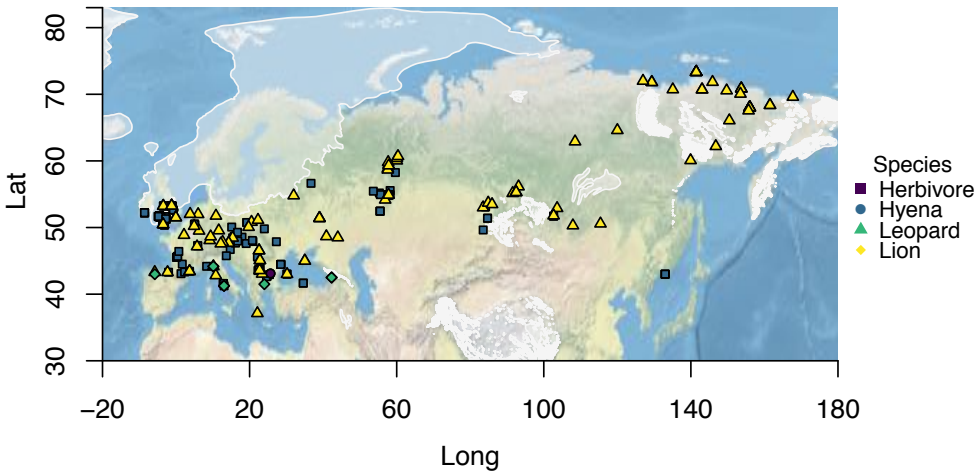


Figure 15.1: Radiocarbon dates included in the analyses below. Only successful and non-rejected dates are plotted. Herbivore refers to bones of herbivores that have chew marks or pitting/gloss from partial digestion by hyenas. Dates are both from literature and new to this project.

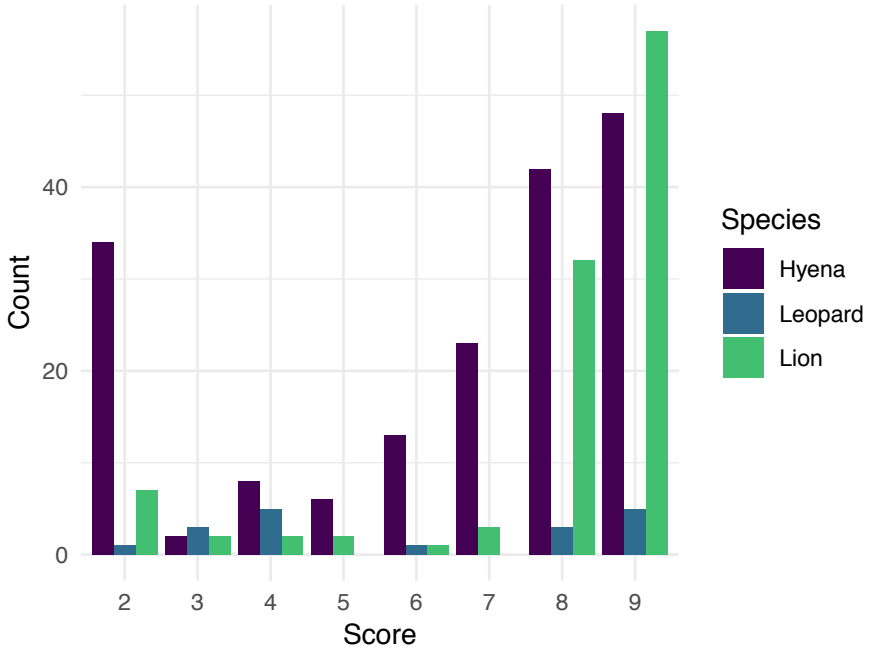


Figure 15.2: Scores received by non-HPLC pretreated radiocarbon dates (n = 300), by species. HPLC dates were scored out of a maximum 7 points, not 9, and so not included.

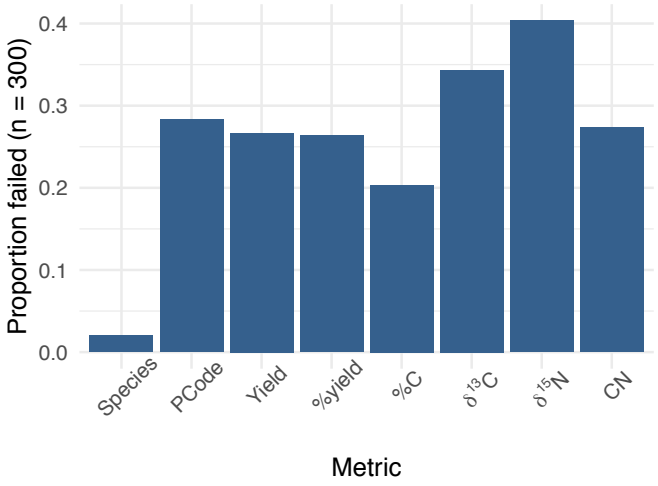


Figure 15.3: Proportion of fails, by evaluation metric. Does not include HPLC dates.

protocols. Species and material (not shown in figures) had nearly no fails, which was due to the selection of samples: because sample identification was crucial to this project, only samples with confident species attribution were included in the first place. Despite this, a handful of dates subsequently failed, usually because of a discrepency in the ORAU database record and the published species identification. These samples were rejected rather than given a lower score. 'Material' similarly had no failures in this project due to only including bone and tooth samples. In practice, this meant that the material and species criteria had little meaning and that most samples received two 'free' points. In other contexts these metrics might be more usefully employed or modified. In a project including indirect dates, for example, material might be modified to penalise indirect materials like charcoal.

15.2 Cave lions

Cave lions had a wide range across Eurasia and into Beringia/northern North America (Fig. 15.4). Whether to include Beringian lions is a somewhat arbitrary choice for this project. Genetic evidence suggests they were distinct from southern North American *P. atrox* (Barnett et al. 2016; Barnett et al. 2009) and Stuart and Lister (2011) include them as members of the same species, but they were also living far outside the European focus of this project. Here western Beringian lions

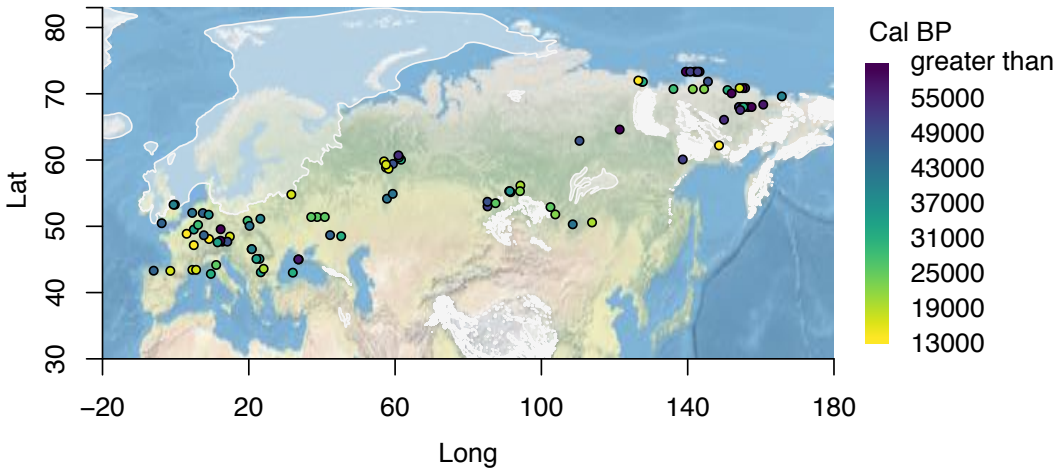


Figure 15.4: Radiocarbon dates of cave lions, shading by mean calibrated age BP. Only successful and non-rejected dates are plotted. Dates are both from literature and new to this project; sources are in Appendix F.2.

(modern Russia) are included, but not eastern Beringian (modern Alaska) and North American lions.

In total 96 dates of Eurasian cave lions were considered, with another eight rejected/failed (Appendix F.2). When compiling these dates, a couple features were noted:

- Modern *P. leo* has been found in Neolithic and Classical contexts in southern Europe, which was likely an expansion from north Africa (Sommer and Benecke 2006; Stuart and Lister 2011). These are not recognised as being *P. spelaea*.
- A couple of papers did not conclusively differentiate between *P. leo* and *P. pardus*, and were not included here (*e.g.* Pettitt et al. 2012).
- OxA-13110 appears to be incorrectly reported as 49900 ± 1500 BP in Barnett et al. (2009), where it is 49900 ± 2500 BP in the ORAU database. The ORAU database value is used here.

About half of the included dates (52) received a high score, 33 received a medium score and 11 a low score (Appendix F.2; score details in Appendix G). The most common issue to be flagged was enriched δ^{13}C, usually between -17– -18‰.

15.2.1 Extinction estimates

The youngest uncalibrated date of cave lion in Eurasia comes from western Europe at Le Closeau, France (AA-41882, 12248 ± 66 BP) (Table 15.1). There are a couple of similarly-aged lions from the terminal Pleistocene in western Europe at Zigeunerfels (OxA-17268) and Abri des Cabones (OxA-12021), and there are several lions from 13–12 ka BP in Siberia. In general the radiocarbon dataset is continuous from the terminal Pleistocene to background ages.

Table 15.1: Calibrations of all lion dates that were not rejected and were not greater-than ages. Those with finite calibrated ages were used in GRIWM estimates. References, along with all other dates, are in Appendix F.2. Date BP and Date error are uncalibrated age determinations and their measurement uncertainty; Cal BP and Cal error are the calibrated dates; and Score is the date's evaluation result.

Site	Subregion	Sample/OxA	Lab	P	Score	Date BP	Date error	Cal BP	Cal error
Le Closeau	Central Europe	41882 [2]	AA	NA	Low	12248	66	14192	144
Zigeunerfels	Central Europe	17268	OxA	18959	High	12375	50	14431	170
Lena	Asia	12901	OxA	14915	High	12450	60	14590	203
Arga Yurekh	Asia	13833	OxA	16034	High	12525	50	14787	183
Abri des Cabones	Central Europe	12021	OxA	13908	High	12565	50	14882	154
Podsemnich Ochotnikov	Asia	11349	OxA	13030	Med	13500	65	16258	117
Grotto Verhnequbahinsky	Asia	10909	OxA	12584	Med	13560	70	16345	125
Grotto Viasher 2	Asia	10908	OxA	12583	Med	13570	70	16359	126
Alazeya	Asia	13835	OxA	16036	High	13770	55	16647	133
Urtiaga	Southern Europe	10121	OxA	11430	Med	13770	120	16653	200
La Garma	Southern Europe	18698	OxA	21340	High	13830	55	16737	130
La Garma	Southern Europe	18699	OxA	21340	High	13835	60	16744	134
Smolensk region	Northern Europe	17034	OxA	19312	Med	14055	60	17085	126
Grotto Holodny	Asia	10910	OxA	12585	High	14750	70	17947	104
Schusterlucke	Central Europe	10513	OxA	12041	Med	15400	130	18659	135
Kozarnica	Southern Europe	35558	OxA	42398	High	16395	80	19788	122
Onon	Asia	16982	OxA	19316	Med	17910	75	21697	119
Kubekovo	Asia	17054	OxA	19339	Med	17915	70	21704	114
Elovka	Asia	20672	OxA	24281	Med	18350	75	22214	123

Table 15.1: Calibrations of all lion dates that were not rejected and were not greater-than ages. Those with finite calibrated ages were used in GRIWM estimates. References, along with all other dates, are in Appendix F.2. Date BP and Date error are uncalibrated age determinations and their measurement uncertainty; Cal BP and Cal error are the calibrated dates; and Score is the date's evaluation result. *(continued)*

Site	Subregion	Sample/OxA	Lab	P	Score	Date BP	Date error	Cal BP	Cal error
Khroma	Asia	17041	OxA	19323	High	19725	75	23755	126
Khroma	Asia	17040	OxA	19323	Med	19755	80	23786	128
Volchikha II	Asia	20251	OxA	23780	Med	20085	80	24151	120
Mal'ta	Asia	17033	OxA	19311	Med	21500	100	25804	96
Grotte di Equi	Southern Europe	37177	OxA	45510	Med	21920	160	26168	176
Togul River Basin	Asia	18711	OxA	21732	High	22080	80	26286	129
Kostenki IV	Northern Europe	17042	OxA	19324	Med	23080	100	27389	107
Kostenki I	Northern Europe	17032	OxA	19310	Med	23190	120	27468	111
Kostenki I	Northern Europe	17372	OxA	19872	Med	23400	100	27597	93
Raj	Northern Europe	11096	OxA	12870	Med	25190	350	29328	431
Kurtak 4	Asia	17373	OxA	19873	Med	25700	130	29894	237
Trou Magrite	Northern Europe	6593	OxA	7799	Med	25980	340	30178	390
Yana RHS Site	Asia	173066	Beta	NA	Low	26050	240	30278	315
Kerem(e)sit	Asia	16983	OxA	19317	Med	27720	140	31458	147
Beryozovka	Asia	13831	OxA	16032	High	27950	140	31698	226
Gremsdorf	Southern Europe	14862	OxA	17157	Med	28310	50	32175	221
Bykovskiy Peninsula	Asia	17038	OxA	19320	Med	28450	140	32385	299
Volga Don Canal	Asia	17031	OxA	19309	Med	28480	200	32428	364

Table 15.1: Calibrations of all lion dates that were not rejected and were not greater-than ages. Those with finite calibrated ages were used in GRIWM estimates. References, along with all other dates, are in Appendix F.2. Date BP and Date error are uncalibrated age determinations and their measurement uncertainty; Cal BP and Cal error are the calibrated dates; and Score is the date's evaluation result. *(continued)*

Site	Subregion	Sample/OxA	Lab	P	Score	Date BP	Date error	Cal BP	Cal error
Bykovskiy Peninsula	Asia	17037	OxA	19319	High	28550	140	32550	298
Duvanny Yar	Asia	12981	OxA	14709	Med	28720	160	32843	295
Grotto Cheremuhovo 1-1	Asia	10894	OxA	12580	Med	29120	230	33307	274
La Sassa	Southern Europe	X-2772-34	OxA	45514	Low	29300	400	33408	438
Grotto Cheremuhovo 1-2	Asia	10895	OxA	12581	High	30140	240	34203	218
Lakatnik	Southern Europe	11422	OxA	13175	Med	31200	330	35142	339
Altwies	Central Europe	4944	KIA	NA	Low	31690	500	35650	546
Tischofer	Central Europe	16510	KIA	NA	Low	31890	300	35782	329
Closani	Southern Europe	22125	OxA	25501	High	32500	450	36630	635
Closani	Southern Europe	22124	OxA	25501	High	33150	500	37393	656
Baumanns	Northern Europe	6209	Erl	NA	Low	34645	365	39205	403
Derbina IV	Asia	20257	OxA	23782	High	35390	280	39988	349
Pin Hole	Northern Europe	19092	OxA	21894	High	35650	450	40287	509
Derbina IV	Asia	20252	OxA	23781	High	35750	400	40394	453
Chukotka / Kyttyk Peninsula	Asia	19359	OxA	22222	High	36550	290	41172	303
Wierchowska Gorna	Northern Europe	10087	OxA	11686	High	38650	600	42713	445

Table 15.1: Calibrations of all lion dates that were not rejected and were not greater-than ages. Those with finite calibrated ages were used in GRIWM estimates. References, along with all other dates, are in Appendix F.2. Date BP and Date error are uncalibrated age determinations and their measurement uncertainty; Cal BP and Cal error are the calibrated dates; and Score is the date's evaluation result. *(continued)*

Site	Subregion	Sample/OxA	Lab	P	Score	Date BP	Date error	Cal BP	Cal error
Ursilor	Southern Europe	22123	OxA	25500	Med	38600	1000	42846	818
Zawalona	Northern Europe	11156	OxA	12872	High	38800	1100	43052	922
Ursilor	Southern Europe	22122	OxA	25499	High	39000	1000	43158	824
New Siberian Islands / no exact locality	Asia	18712	OxA	21733	High	40210	350	43826	353
Eurogeul	Northern Europe	23151	GrA	NA	Low	42230	570	45604	532
Ignatievskaya	Asia	10887	OxA	12555	Med	41900	1200	45619	1237
Teufelslucke	Asia	2545	VERA	NA	Low	42400	1800	46293	1640
Kent's Cavern	Northern Europe	14285	OxA	15999	Low	43600	3600	46705	1945
Lathum	Northern Europe	16715	OxA	18958	High	44850	650	48233	767
Jou'l Llobu	Southern Europe	10186	OxA	11760	High	46400	2100	48471	1061
Duvanny Yar	Asia	13024	OxA	14712	Med	46200	1500	48711	901
Gamssulzen	Central Europe	13110	OxA	14707	High	49900	1500	50375	1677
Nizhnyaya Tunguska	Asia	16980	OxA	19314	Med	50500	1300	50845	1410
Chumysh	Asia	17043	OxA	19325	High	51400	1200	51690	1285
Bolshoy Liakhovsky Island	Asia	18812	OxA	21436	High	52000	1500	52475	1677
Priobskoye Steppe Plateau	Asia	16981	OxA	19315	High	52800	1600	53350	1820

Table 15.1: Calibrations of all lion dates that were not rejected and were not greater-than ages. Those with finite calibrated ages were used in GRIWM estimates. References, along with all other dates, are in Appendix F.2. Date BP and Date error are uncalibrated age determinations and their measurement uncertainty; Cal BP and Cal error are the calibrated dates; and Score is the date's evaluation result. *(continued)*

Site	Subregion	Sample/OxA	Lab	P	Score	Date BP	Date error	Cal BP	Cal error
Krestovka	Asia	13830	OxA	16031	High	54100	1800	54823	2128
Chukochya	Asia	13475	OxA	14713	High	54600	1700	55232	1970
Grotto Shaitansky	Asia	10907	OxA	12582	High	54500	2600	56289	3676
Alazeya	Asia	13021	OxA	14708	High	55300	2500	56920	3455
Emine Bair Khosar	Southern Europe	17044	OxA	19331	High	56400	2100	57448	2648
Chukochya	Asia	13025	OxA	14713	High	55700	3000	58272	4620
Alazeya	Asia	13474	OxA	14708	High	58200	3500	61968	5884
Gamssulzen	Central Europe	13110	OxA	14707	High	49900	2500	NA	NA
Tyung	Asia	17010	OxA	19306	Med	46700	1300	NA	NA
Bolshoy Liakhovsky Island	Asia	17035	OxA	19313	High	47700	800	NA	NA
Zoolithen	Central Europe	14863	OxA	17158	High	47600	900	NA	NA
Siegsdorf	Central Europe	14406	KIA	NA	Low	47180	1190	NA	NA

Table 15.2: GRIWM results estimating extinction date for cave lions. Score refers to the lowest score category included in the model (Med includes high- and medium-score dates).

Dates run	2.5% min probability	median	97.5% max probability
High	12749	13691	14490
Med	13078	13766	14472
Low	12973	13546	14234

15.2.1.1 GRIWM estimates

In total 81 finite ages were calibrated, of which 76 were still finite after calibration and could be used in the GRIWM simulations (Table 15.1). The GRIWM simulation was run twice: once only with high-scoring dates and once with all dates (Table 15.2).

The two estimates were not found to be significantly different with a Welch two-sample t-test (t = -0.11, p = 0.91), though the high-score extinction estimate has a greater uncertainty due to the smaller sample size. Both estimate an extinction in the very late Pleistocene around 13.5 ka BP.

The dates were subdivided into four regions and GRIWM estimates run for each subset of the data, both for high-score and all-score dates (Table 15.3). Some of the subregions had few dates, especially when only high-scoring dates were run. Those with few dates, especially less than the recommended five (Saltré et al. 2015), risk producing divergent estimates. This is the case with the northern Europe estimates, as only four high-score dates came from the region. When their high-score and all-score results were compared, the other subregions produced similar estimates.

Comparison between regions finds different extinction estimates (Table 15.4 and Table 15.5). Regardless of dates included, southern Europe's estimate was found to be significantly older than both Asia's and central Europe's estimates. However, the discrepancy between northern Europe's two estimates means that northern and southern Europe have different relationships. In the high-score date estimates, southern Europe has a younger GRIWM estimate; but when all dates are included, northern Europe produces the younger estimate.

Table 15.3: Subregion GRIWM estimates for cave lions. All regions were run twice, once with all dates and once with only high-scoring dates included. P values are from a Welch two-sample t-test comparing equivalent subregions: for example, the GRIWM estimates for Northern Europe with all-score dates and Northern Europe with high-score dates.

Subregion	Scores run	2.5% min probability	median	98.5% max probability	Dates (n)	High/low p-value
Asia	All	12365	13409	14606	54	0.107
Central Europe	All	12214	13321	14244	8	0.765
Northern Europe	All	7704	8131	8540	14	0.000*
Southern Europe	All	14848	16090	16685	15	0.836
Asia	High	11258	13036	14616	32	0.107
Central Europe	High	11381	13002	14527	4	0.765
Northern Europe	High	34316	36802	39582	4	0.000*
Southern Europe	High	14610	16028	16743	9	0.836

Table 15.4: Comparison of the means of cave lion GRIWM estimates of subregions. Dates of all scores were included in the estimates. Welch two-sample t-tests were used to compare estimates. * denotes significance at <5% level.

	Asia	**Central Europe**	**Northern Europe**	**Southern Europe**
Asia	NA	0.5267	0.000*	0.000*
Central Europe	0.5267	NA	0.000*	0.000*
Northern Europe	0.000*	0.000*	NA	0.000*
Southern Europe	0.000*	0.000*	0.000*	NA

Table 15.5: Comparison of the means of cave lion GRIWM estimates of subregions. Only high-scoring dates were included in the estimates. Welch two-sample t-tests were used to compare estimates. * denotes significance at <5% level.

	Asia	**Central Europe**	**Northern Europe**	**Southern Europe**
Asia	NA	0.9849	0.000*	0.000*
Central Europe	0.9849	NA	0.000*	0.031*
Northern Europe	0.000*	0.000*	NA	0.000*
Southern Europe	0.000*	0.031*	0.000*	NA

Table 15.6: OxCal boundary results estimating extinction date for lions in Europe. Score refers to the lowest score category included in the model (Med was high- and medium-score dates).

Score	Mean date	Error	Median date
High	13465	1042	13787
Med	13951	524	14086
Low	13801	450	13919

15.2.1.2 OxCal estimates

OxCal boundaries were modelled to estimate the extinction date of cave lions. Regardless of how restrictive the dataset was in terms of scores, all the boundary estimates are similar, though the estimate uncertainty is wider with the smaller, high-score dates dataset (Table 15.6). The OxCal boundaries are only a couple of centuries older than the global GRIWM estimates. As the sample size increases, the GRIWM estimate assumes less distance between the last observation and the true extinction date. The relatively large cave lion dataset therefore decreases the discrepancy between the GRIWM estimates and OxCal boundaries.

OxCal models produced for subregions sometimes came with high uncertainty, particularly for the high-score models with smaller samples (Table 15.7). The high-score estimate for northern Europe, for example, has a 68.2% range that includes the future. Only central Europe's all- and high-score estimates differed significantly.

With all dates included, southern Europe's boundary is older than northern Europe's, but the high uncertainty means the two are not different in the high-score models (Tables 15.8 and 15.9). A youngest subregion is not distinguishable with the high uncertainties.

The GRIWM estimates are sometimes older than the mean OxCal boundaries and usually have smaller uncertainties (Table 15.3). The small sample sizes make some of the t-test comparisons weak, though the central Europe and Asia estimates are significantly different (Table 15.10). The GRIWM estimates are younger for central Europe but vary depending on the scores for northern Europe; the high-score

Table 15.7: Subregion OxCal boundary estimates for cave lions. All regions were run twice, once with all dates and once with only high-scoring dates included. P-values are from a Welch two-sample t-test comparing equivalent subregions: for example, the estimates for Northern Europe with all-score dates and Northern Europe with high-score dates. The number of samples run sometimes differ from the equivalent GRIWM estimates because OxCal did not model radiocarbon dates that calibrated >50 ka cal BP.

Subregion	Scores run	Date	Error	Dates (n)	High/low p-value
Southern Europe	All	14283	2594	14	0.34
Central Europe	All	14999	2425	13	0.000*
Asia	All	13737	937	44	0.081
Northern Europe	All	11313	3575	10	0.404
Southern Europe	High	12080	5413	7	0.34
Central Europe	High	37534	3292	4	0.000*
Asia	High	12489	2433	14	0.081
Northern Europe	High	7822	8157	5	0.404

Table 15.8: Comparison of the means of cave lion OxCal estimates of subregions. Dates of all scores were included in the estimates. Welch two-sample t-tests were used to compare estimates. * denotes significance at <5% level.

	Asia	**Central Europe**	**Northern Europe**	**Southern Europe**
Asia	NA	0.0891	0.0613	0.453
Central Europe	0.0891	NA	0.013*	0.4654
Northern Europe	0.0613	0.013*	NA	0.040*
Southern Europe	0.453	0.4654	0.040*	NA

Table 15.9: Comparison of the means of cave lion OxCal estimates of subregions. Only high-scoring dates were included in the estimates. Welch two-sample t-tests were used to compare estimates. * denotes significance at <5% level.

	Asia	**Central Europe**	**Northern Europe**	**Southern Europe**
Asia	NA	0.000*	0.2725	0.8541
Central Europe	0.000*	NA	0.000*	0.000*
Northern Europe	0.2725	0.000*	NA	0.3451
Southern Europe	0.8541	0.000*	0.3451	NA

Table 15.10: Comparison of OxCal and GRIWM subregion extirpation estimates for lions. Welch two-sample t-tests were used to compare the estimates. * denotes significance at 5% level.

Score	Southern Europe	Central Europe	Asia	Northern Europe
All	0.279	0.033*	0.000*	0.003*
High	0.692	0.000*	0.000*	0.097

GRIWM estimate for northern Europe is much older than the OxCal estimate (36.8 *vs* 8 ka cal BP), though the latter has high uncertainty.

15.2.2 Non-radiocarbon evidence

In contrast to the leopard results below, the radiocarbon dataset for cave lions is larger and better aligns with non-radiocarbon palaeontological and archaeological evidence for their extinction. Cave lions have been found in Middle and Upper Palaeolithic contexts, including Magdalenian contexts of ∼14 ka BP (Cueto et al. 2016; Sommer and Benecke 2006; Stuart and Lister 2011). They had a wide range across Eurasia into high latitudes, including Siberia, but that range may not have been continuous or stable throughout the Late Pleistocene (Appendix J.2).

Genetics studies suggest similarity with cave lions across Eurasia and into Beringia and north-west America (Barnett et al. 2009). This project has focused on the Eurasian story, but it is worth noting that Beringian and north-west American lions have a similar, and perhaps slightly later, LAD of ∼12 ka BP (Barnett et al. 2009; Stuart and Lister 2011).

There is no evidence for cave lion's survival beyond the initial Holocene, though as mentioned earlier, *P. leo* were found in southern Europe in the Neolithic and Iron Age (Sommer and Benecke 2006). It appears cave lions went extinct around the terminal Pleistocene in Europe.

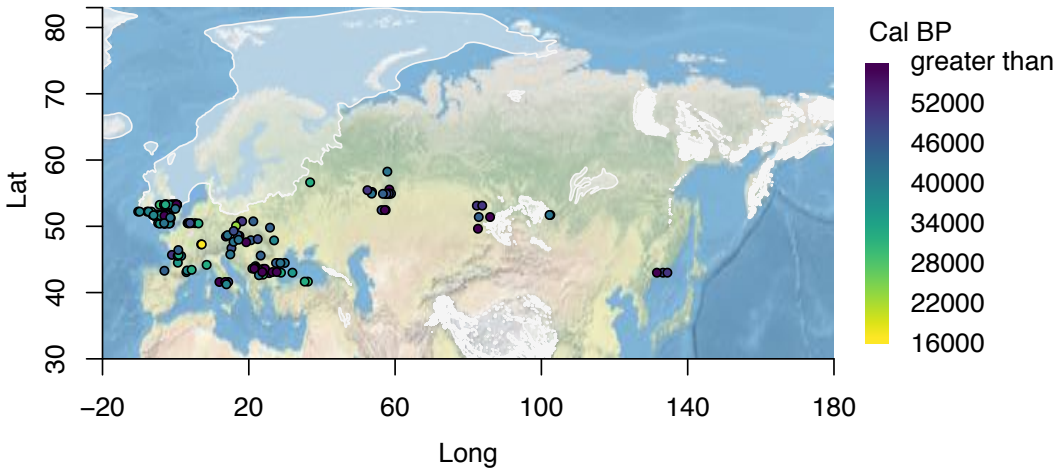


Figure 15.5: Radiocarbon dates of cave hyenas, shading by mean calibrated age BP. Only successful and non-rejected dates are plotted. Dates are both from literature and new to this project; sources are listed in Appendix F.3.

15.3 Cave hyenas

Cave hyenas lived across Eurasia, though not in the highest Siberian latitudes or Beringia (Stuart and Lister 2014). The radiocarbon dataset for hyenas is biased towards Britain, where hyenas were numerous and the subject of earlier studies (Higham et al. 2006a; Jacobi et al. 2006; Stuart and Lister 2014). There are few dates from southern Europe, despite their reported presence in sites (Carrión et al. 2001; Gatta et al. 2016; Sardella and Petrucci 2012; Stiner 2004). In total 182 radiocarbon dates were produced/compiled for analysis, of which 44 come from southern Europe (Fig. 15.5; more details in Appendix F.3).

Hyenas are known to intensively chew bones and sometimes swallow bones and spit them up (Stuart and Lister 2014). These partially-digested bones have a distinct glossy finish that, while not direct hyena remains, are evidence of hyena activity. There is the possibility of a time lag if the animal was scavenged, but the lag cannot be too large if there was flesh/marrow left for the hyenas to eat. Bones in the table below attributed to species other than hyena are chewed/digested.

Table 15.11: Count of scores from hyena radiocarbon date evaluation.

Score	Count
High	89
Med	30
Low	52
Rejected	11

About a fifth of hyena radiocarbon dates ranked low in the scoring system or were rejected outright (Table 15.11). Several of these were produced in labs other than ORAU, which does not necessarily make them unreliable but limited access to criteria for evaluation like isotopic data. Others were produced with pretreatment methods other than AF, AG, or HPLC. Pretreatment code 'AI' refers to the ion-exchange method introduced in the 1980s (Hedges et al. 1989) but is no longer used (Brock et al. 2010b). When compared to ultrafiltered dates, ion-exchange dates were often found to be younger than expected (Jacobi et al. 2006). Some of these were produced pre-2000 and have since been re-dated (Higham et al. 2006a).

15.3.1 Extinction estimates

The youngest date in the dataset comes from France (Ly 3162 (Poz)), but it has a low score because it was produced outside the ORAU with few health metrics (Table 15.12; more details in Appendix F.3). Otherwise, the youngest dates come mostly from the UK. One young date from Nizhniy Tsasuchey, Russia turned out to be misidentified (Lister pers. comm.). The latest southern European hyena comes from Italy (OxA-10523) with an age of 26120 ± 330 BP, millennia older than the youngest UK hyenas. None of the youngest dates are indirect (chewed/digested bones) and some were high-scoring.

Table 15.12: Calibrations of all hyena (or hyena-chewed bone) dates that were not rejected and were not greater-than ages. Those with finite calibrated ages were used in GRIWM simulations. Samples with asymmetric errors were calibrated with the mean of the errors. Corrected dates are reported for HPLC dates. Cal BP/error are calibrated date and measurement error.

Site	Subregion	*Species*	Sample/OxA	Lab	P	Score	Date BP	Date error	Cal BP	Cal error
Grotte Grappin	Central Europe	*C. crocuta*	3162 (Poz)	Ly	NA	Low	15335	115	18596	125
Paviland	Northern Europe	*C. crocuta*	7087	OxA	8261	High	17880	180	21644	252
Paviland	Northern Europe	*C. crocuta*	13378	OxA	8261	Low	18430	70	22304	106
Ffynnon Beuno	Northern Europe	*C. crocuta*	9696	OxA	11186	High	18520	130	22378	157
Caerwent Quarry	Northern Europe	*C. crocuta*	9027	OxA	10415	Med	20860	160	25137	246
Caerwent Quarry	Northern Europe	*C. crocuta*	9028	OxA	10416	High	22130	180	26387	234
Robin Hood	Northern Europe	*C. crocuta*	6115	OxA	7401	Med	22880	240	27162	257
Robin Hood	Northern Europe	*C. crocuta*	6114	OxA	7400	Med	22980	480	27189	462
Church Hole	Northern Europe	*C. crocuta*	5800	OxA	7042	Low	24000	260	28102	249
Castlepook	Northern Europe	*C. crocuta*	4234	OxA	5173	Med	24000	300	28115	277
Ffynnon Beuno	Northern Europe	*C. crocuta*	9090	OxA	10413	Low	24000	450	28171	408
Ash Tree	Northern Europe	*C. crocuta*	5798	OxA	7040	Low	25660	380	29869	458
Grotta Paglicci	Southern Europe	*C. crocuta*	10523	OxA	12118	High	26120	330	30307	370
Coygan	Northern Europe	*C. crocuta*	9029	OxA	10418	High	26480	280	30681	266
Balkan Range	Southern Europe	*C. crocuta*	11551	OxA	13170	Med	26600	170	30837	136
Church Hole	Northern Europe	*C. crocuta*	5799	OxA	7041	Low	26840	420	30928	342
Arene Candide	Southern Europe	*C. crocuta*	10658	OxA	12127	Med	27050	550	31178	553
Goyet	Northern Europe	*C. crocuta*	2812	GrA	NA	Low	27230	260	31186	170
Ogof-yr-Ychen	Northern Europe	*C. crocuta*	9692	OxA	11182	High	27200	360	31212	280
Potter's	Northern Europe	*C. crocuta*	19215	OxA	22190	High	27470	240	31333	192
Paviland	Northern Europe	*C. crocuta*	6980	OxA	8226	Low	27750	500	31862	561
Potter's	Northern Europe	*C. crocuta*	9693	OxA	11183	High	28000	310	31935	417
Les Garennes	Southern Europe	*C. crocuta*	216143	Beta	NA	Low	28410	230	32338	387
Kent's	Northern Europe	*C. crocuta*	11174	OxA	12760	Low	28390	330	32350	478
Grotte Grappin	Central Europe	*C. crocuta*	19633	OxA	23377	High	28570	150	32581	309

Table 15.12: Calibrations of all hyena (or hyena-chewed bone) dates that were not rejected and were not greater-than ages. Those with finite calibrated ages were used in GRIWM simulations. Samples with asymmetric errors were calibrated with the mean of the errors. Corrected dates are reported for HPLC dates. Cal BP/error are calibrated date and measurement error. *(continued)*

Site	Subregion	*Species*	Sample/OxA	Lab	P	Score	Date BP	Date error	Cal BP	Cal error
La Garma	Southern Europe	*C. crocuta*	18700	OxA	21341	High	28660	150	32743	295
La Sassa	Southern Europe	*C. crocuta*	37218	OxA	45512	Med	29190	310	33337	349
Outside West Pin Hole	Northern Europe	*C. crocuta*	5803	OxA	7045	Low	29300	420	33399	463
Agios Georgios	Northern Europe	*C. crocuta*	17009	OxA	19302	Med	29340	240	33521	253
Grotta Paglicci	Southern Europe	*C. crocuta*	10657	OxA	12119	Med	29100	1600	33710	1912
La Sassa	Southern Europe	*C. crocuta*	37219	OxA	45513	High	30150	350	34229	292
Kent's	Northern Europe	*C. crocuta*	30351	OxA	35815	High	30630	380	34611	354
Redaka II	Southern Europe	*C. crocuta*	35559	OxA	42399	High	30910	380	34878	380
Redaka II	Southern Europe	*C. crocuta*	35561	OxA	42401	High	30920	380	34888	380
Robin Hood	Northern Europe	*C. crocuta*	5802	OxA	7044	Low	31050	500	35051	494
Desnisukhi Peck	Southern Europe	*C. crocuta*	11552	OxA	13171	High	31810	370	35712	400
Ogof-yr-Ychen	Northern Europe	*C. crocuta*	X-2278-44	OxA	22189	High	31750	600	35786	700
Cefn	Northern Europe	*C. crocuta*	9698	OxA	11188	High	31900	450	35841	519
Igue du Gral	Southern Europe	*C. crocuta*	20763	OxA	24886	High	31990	240	35883	265
Coygan	Northern Europe	*C. crocuta*	14400	OxA	16380	High	32140	250	36032	277
Coygan	Northern Europe	*C. crocuta*	14473	OxA	16382	High	32400	550	36555	743
Pin Hole	Northern Europe	*C. crocuta*	1206	OxA	1840	Low	32200	1000	36575	1202
Redaka II	Southern Europe	*C. crocuta*	35560	OxA	42400	High	32700	500	36913	684
Magura	Southern Europe	*C. crocuta*	31009	OxA	37104	High	32750	500	36972	680
Bench Tunnel	Northern Europe	*C. crocuta*	5961	OxA	7199	Med	32500	1200	37000	1419
Ogof-yr-Ychen	Northern Europe	*C. crocuta*	X-2278-43	OxA	22188	High	33000	600	37263	757
Grotte de Canecaude	Southern Europe	*C. crocuta*	16691	OxA	18956	High	33130	220	37326	426
Castlepook	Northern Europe	*C. crocuta*	19531	OxA	22734	High	33240	220	37481	426
Mas d'Azil	Southern Europe	*C. crocuta*	12022	OxA	13910	High	33320	260	37581	455

Table 15.12: Calibrations of all hyena (or hyena-chewed bone) dates that were not rejected and were not greater-than ages. Those with finite calibrated ages were used in GRIWM simulations. Samples with asymmetric errors were calibrated with the mean of the errors. Corrected dates are reported for HPLC dates. Cal BP/error are calibrated date and measurement error. *(continued)*

Site	Subregion	*Species*	Sample/OxA	Lab	P	Score	Date BP	Date error	Cal BP	Cal error
Robin Hood	Northern Europe	*C. crocuta*	5801	OxA	7043	Low	33450	700	37742	872
Redaka II	Southern Europe	*C. crocuta*	35562	OxA	42402	High	33850	550	38188	741
Kozarnica	Southern Europe	*C. crocuta*	35556	OxA	42395	High	34350	600	38889	744
Castlepook	Northern Europe	*C. crocuta*	13625	I	NA	Low	34300	1800	39061	2060
Pin Hole	Northern Europe	*C. crocuta*	1207	OxA	1839	Low	34500	1200	39066	1378
Castelcivita	Southern Europe	*C. crocuta*	37221	OxA	45630	High	34500	600	39082	711
Bench Tunnel	Northern Europe	*C. crocuta*	1620	OxA	2035	Low	34500	1400	39099	1576
Little Hoyle	Northern Europe	*C. crocuta*	1491	OxA	1655	Low	34590	1500	39218	1676
Goyet	Northern Europe	*C. crocuta*	8958	UtC	NA	Low	35000	400	39563	463
Duruitoarea Veche	Central Europe	*C. crocuta*	11691	OxA	13478	High	35350	380	39949	457
Coygan	Northern Europe	*C. crocuta*	NA	OxA	16241	High	35350	450	39956	525
Zaktui	Asia	*C. crocuta*	19719	OxA	23169	High	35560	300	40184	367
Zaktui	Asia	*C. crocuta*	23169	OxA	23169	Low	35560	300	40184	367
Grange Farm, Glaston	Northern Europe	*C. crocuta*	21308	OxA	25398	Low	35610	300	40240	366
Ust-Kataavakaya	Asia	*C. crocuta*	10890	OxA	12559	High	35650	450	40287	509
Les Rois	Southern Europe	*C. crocuta*	X-2294-11	OxA	22708	Med	35750	800	40370	794
Melwurmhohle	Central Europe	*C. crocuta*	2540	VERA	NA	Low	35900	600/560	40528	598
Coygan	Northern Europe	*C. crocuta*	14402	OxA	16383	High	36000	500	40633	517
Sandford Hill	Northern Europe	*C. crocuta*	1526	BM	NA	Low	36000	1900	40823	2085
Scladina	Northern Europe	*C. crocuta*	23791	OxA	28263	High	36450	750	40999	681
Kent's	Northern Europe	*C. crocuta*	10806	OxA	12470	Low	36750	450	41313	408
La Adam	Southern Europe	*C. crocuta*	22129	OxA	25566	Med	36850	750	41344	642
Bench Tunnel	Northern Europe	*C. crocuta*	13512	OxA	7199	High	36800	450	41357	402
Pin Hole	Northern Europe	*C. crocuta*	15520	OxA	1839	High	37150	450	41648	360
Ogof-yr-Ychen	Northern Europe	*C. crocuta*	9691	OxA	11181	High	37400	700	41812	544

Table 15.12: Calibrations of all hyena (or hyena-chewed bone) dates that were not rejected and were not greater-than ages. Those with finite calibrated ages were used in GRIWM simulations. Samples with asymmetric errors were calibrated with the mean of the errors. Corrected dates are reported for HPLC dates. Cal BP/error are calibrated date and measurement error. *(continued)*

Site	Subregion	*Species*	Sample/OxA	Lab	P	Score	Date BP	Date error	Cal BP	Cal error
Bench Tunnel	Northern Europe	*C. crocuta*	13324	OxA	7199	High	37500	900	41897	732
Rhino (Nosorogov)	Asia	*C. crocuta*	17003	OxA	19295	High	37700	360	42049	258
Kent's	Northern Europe	*C. crocuta*	11152	OxA	12759	Low	37750	500	42083	350
Pin Hole	Northern Europe	*C. crocuta*	15518	OxA	1839	High	37800	500	42117	348
Grange Farm, Glaston	Northern Europe	*Coelodonta antiquitatis*	21309	OxA	25399	Low	38120	360	42317	248
Teufelslucke	Central Europe	*C. crocuta*	2536	VERA	NA	Low	38060	855	42357	664
Pin Hole	Northern Europe	*C. crocuta*	4754	OxA	5698	Low	37800	1600	42425	1574
Vasil Levski	Southern Europe	*C. crocuta*	37323	OxA	45645	Low	38100	1100	42468	930
Ghilingic	Southern Europe	*C. crocuta*	22126	OxA	25563	High	38200	900	42484	712
Grotta Pocala	Southern Europe	*C. crocuta*	2532	VERA	NA	Low	38220	920/820	42490	681
Grange Farm, Glaston	Northern Europe	*Coelodonta antiquitatis*	22149	OxA	25912	Low	38400	900	42644	714
Grange Farm, Glaston	Northern Europe	*Coelodonta antiquitatis*	21310	OxA	25400	Low	38800	390	42751	282
Windener	Central Europe	*C. crocuta*	2538	VERA	NA	Low	38680	920	42874	741
La Adam	Southern Europe	*C. crocuta*	22127	OxA	25564	Med	38700	1000	42926	819
La Adam	Southern Europe	*C. crocuta*	22128	OxA	25565	High	39100	1000	43234	826
Amalda	Southern Europe	*C. crocuta*	10398	OxA	12044	High	39900	700	43692	596
Ignatievskaya	Asia	*C. crocuta*	19660	OxA	22742	High	40240	380	43856	375
Kent's	Northern Europe	*C. crocuta*	19509	OxA	22670	Low	40200	600	43880	532
Teufelslucke	Central Europe	*C. crocuta*	1425	VERA	NA	Low	40170	875	43955	748
Ust Katak	Asia	*C. crocuta*	19675	OxA	22737	High	40480	390	44056	390
Coygan	Northern Europe	*C. crocuta*	14403	OxA	16384	High	39700	1700	44160	1636

Table 15.12: Calibrations of all hyena (or hyena-chewed bone) dates that were not rejected and were not greater-than ages. Those with finite calibrated ages were used in GRIWM simulations. Samples with asymmetric errors were calibrated with the mean of the errors. Corrected dates are reported for HPLC dates. Cal BP/error are calibrated date and measurement error. *(continued)*

Site	Subregion	*Species*	Sample/OxA	Lab	P	Score	Date BP	Date error	Cal BP	Cal error
Les Roches de Villeneuve	Southern Europe	*C. crocuta*	177765	BETA	NA	Low	40700	900	44366	805
Vinckova	Southern Europe	*C. crocuta*	12893	OxA	13037	High	40950	550	44483	514
Scladina	Northern Europe	*C. crocuta*	23790	OxA	28262	High	40800	1300	44702	1258
Bukovinka	Central Europe	*C. crocuta*	2529	VERA	NA	Low	41300	1200	45056	1195
Komarowa	Northern Europe	*C. crocuta*	11161	OxA	12884	High	41700	1100	45363	1115
Eel Point	Northern Europe	*C. crocuta*	9694	OxA	11184	High	41400	1600	45414	1578
Igric	Central Europe	*C. crocuta*	2534	VERA	NA	Low	41800	1300	45585	1332
Ust Katak	Asia	*C. crocuta*	19657	OxA	22736	High	42300	450	45628	420
Komarowa	Northern Europe	*C. crocuta*	11158	OxA	12881	High	42200	800	45679	789
Denisova	Asia	*C. crocuta*	25284	KIA	NA	Low	42300	900	45832	917
Scladina	Northern Europe	*C. crocuta*	47943	GrA	NA	Low	42560	550/440	45871	481
Pin Hole	Northern Europe	*C. crocuta*	1448	OxA	1971	Low	42200	3000	46145	2047
Geographical Society	Asia	*C. crocuta*	17005	OxA	19299	High	42950	600	46285	629
Scladina	Northern Europe	*C. crocuta*	32581	GrA	NA	Low	43150	950/700	46613	889
Coygan	Northern Europe	*C. crocuta*	14401	OxA	16381	High	43000	2100	46720	1672
Coygan	Northern Europe	*C. crocuta*	NA	OxA	16240	High	43300	1200	46924	1206
Cava Muracci	Southern Europe	*C. crocuta*	X-2756-42	OxA	44418	Med	49270	10188	47028	1825
Ust Katak	Asia	*C. crocuta*	19676	OxA	22738	Med	43950	550	47256	669
Creswell Crags	Northern Europe	*C. crocuta*	21995	OxA	25382	High	44200	2000	47480	1421
Pin Hole	Northern Europe	*Rangifer tarandus*	11796	OxA	13663	Low	44200	800	47608	900
Robin Hood	Northern Europe	*C. crocuta*	15598	OxA	17654	High	44200	900	47631	968
Griifen	Southern Europe	*C. crocuta*	1835	VERA	NA	Low	44300	1800/1500	47638	1285
Ignatievskaya	Asia	*C. crocuta*	19659	OxA	22741	High	44300	600	47646	738
Miskolc III	Central Europe	*C. crocuta*	2533	VERA	NA	Low	44400	1750	47669	1302

Table 15.12: Calibrations of all hyena (or hyena-chewed bone) dates that were not rejected and were not greater-than ages. Those with finite calibrated ages were used in GRIWM simulations. Samples with asymmetric errors were calibrated with the mean of the errors. Corrected dates are reported for HPLC dates. Cal BP/error are calibrated date and measurement error. *(continued)*

Site	Subregion	*Species*	Sample/OxA	Lab	P	Score	Date BP	Date error	Cal BP	Cal error
Daylight Rock Fissure	Northern Europe	*C. crocuta*	9695	OxA	11185	High	46400	3800	47786	1482
Creswell Crags	Northern Europe	*C. crocuta*	21996	OxA	25383	High	45400	2200	48008	1262
Scladina	Northern Europe	*C. crocuta*	23789	OxA	28261	High	46000	2400	48176	1212
Robin Hood	Northern Europe	*C. crocuta*	12771	OxA	14515	High	45300	1000	48503	881
Vypustek	Central Europe	*C. crocuta*	2531	VERA	NA	Low	46000	1610	48557	979
Smelovskay	Asia	*C. crocuta*	17004	OxA	19298	Med	46200	1500	48711	901
Hyaena Den	Northern Europe	*C. crocuta*	13917	OxA	15846	High	48600	1000	48797	1047
Castlepook	Northern Europe	*C. crocuta*	19532	OxA	22735	High	45700	700	48960	647
Komarowa	Northern Europe	*C. crocuta*	11062	OxA	12890	High	46100	900	49063	658
Geographical Society	Asia	*C. crocuta*	17046	OxA	19332	Med	46000	700	49154	575
Zarinskiy District	Asia	*C. crocuta*	17007	OxA	19300	High	50400	1300	50745	1410
Zarinskiy District	Asia	*C. crocuta*	17006	OxA	19300	High	51200	1400	51607	1541
Ustinovo	Asia	*C. crocuta*	19536	OxA	22744	High	51400	1500	51875	1677
Bacho Kiro	Southern Europe	*C. crocuta*	11421	OxA	13169	Med	51500	2400	52961	3242
Ignatievskaya	Asia	*C. crocuta*	19537	OxA	22745	High	47500	900	NA	NA
Denisova	Asia	*C. crocuta*	29855	OxA	35673	High	47900	3100	NA	NA
Kozarnica	Southern Europe	*C. crocuta*	35557	OxA	42397	High	49100	3600	NA	NA
Cava Muracci	Southern Europe	*C. crocuta*	X-2772-33	OxA	45507	Med	46500	3900	NA	NA
Robin Hood	Northern Europe	*C. crocuta*	14944	OxA	7044	Low	49800	NA	NA	NA
Certova pec	Central Europe	*C. crocuta*	2530	VERA	NA	Low	51200	2950	NA	NA
Geographical Society	Asia	*C. crocuta*	25285	KIA	NA	Low	48650	2380/1840	NA	NA

Table 15.13: GRIWM results estimating extinction date for hyenas in Europe. Score refers to the lowest score category included in the model (Med includes high- and medium-score dates).

Dates run	2.5% min probability	median	97.5% max probability
High	18653	19500	20995
Med	19178	19908	21113
Low	16504	16784	17075

15.3.1.1 GRIWM estimates

GRIWM estimates for hyena extinction either fall within or postdate the LGM, depending on how restrictive the dataset is (Table 15.13). Removing the low-scoring dates increases the estimated median extinction age by ~3000 years. The more robust dataset pushes the extinction to be about coincident with the LGM (21–19 ka cal BP). Interestingly, the majority of the young dates come from the UK, which was largely under ice at the time of the LGM. Hyenas near the LGM would have been living at the borders of the glaciers.

The two GRIWM estimates suggest different extinction narratives for hyenas, with the larger, less restrictive dataset suggesting millennia of survival beyond the LGM. The other, older GRIWM suggest extinction with the LGM—a quite traditional climatic explanation for extinction.

Subregion GRIWM estimates also differ from each other. The high-score central Europe estimate should not be considered valid, as only two dates fell in this sample. There is also more discussion about GRIWM estimates of hyenas in northwest Europe in the Caldey Island experiment results (chapter 4.2).

Northern and southern European estimates are younger in the high-score estimates relative to their respective all-date estimates. In both cases, northern Europe's estimate is significantly younger than southern Europe's. The northern European estimates both suggest a last appearance around the LGM, whereas the southern European estimates fall before the LGM around ~26–30 ka cal BP. The Asia estimates are the oldest at ~38.6 ka cal BP.

Table 15.14: Subregion GRIWM estimates for hyenas. All regions were run twice, once with all dates and once with only high-scoring dates included. P-values are from a Welch two-sample t-test comparing equivalent subregions: for example, the GRIWM estimates for Northern Europe with all-score dates and Northern Europe with high-score dates.

Subregion	Scores run	2.5% min probability	median	98.5% max probability	Dates (n)	High/low p-value
Asia	All	37394	38948	40118	16	0.64
Central Europe	All	4022	4514	5009	11	0.051
Northern Europe	All	19476	20274	21544	80	0.000*
Southern Europe	All	27753	29135	30528	33	0.000*
Asia	High	36656	38563	40248	11	0.64
Central Europe	High	19528	21548	23558	2	0.051
Northern Europe	High	18138	19148	20926	41	0.000*
Southern Europe	High	26451	27572	28721	18	0.000*

Table 15.15: Comparison of the means of cave hyena GRIWM estimates of subregions. Dates of all scores were included in the estimates. Welch two-sample t-tests were used to compare estimates. * denotes significance at <5% level.

	Asia	**Central Europe**	**Northern Europe**	**Southern Europe**
Asia	NA	0.000*	0.000*	0.000*
Central Europe	0.000*	NA	0.000*	0.000*
Northern Europe	0.000*	0.000*	NA	0.000*
Southern Europe	0.000*	0.000*	0.000*	NA

The central European estimates are in extreme disagreement with each other and the global estimates, with the all-score GRIWM estimate suggesting survival in the Holocene. No date from central Europe is so young (the youngest, 3162 (Poz), is 18596 ± 125 cal BP), but there are only 11 dates spanning 30 ky. The wide spread and small dataset 'stretch' the GRIWM estimate, as it assumes the sample is less representative of the true LAD than a larger dataset spanning less time.

Table 15.16: Comparison of the means of cave hyena GRIWM estimates of subregions. Only high-scoring dates were included in the estimates. Welch two-sample t-tests were used to compare estimates. * denotes significance at <5% level.

	Asia	**Central Europe**	**Northern Europe**	**Southern Europe**
Asia	NA	0.030*	0.000*	0.000*
Central Europe	0.030*	NA	0.3882	0.137
Northern Europe	0.000*	0.3882	NA	0.000*
Southern Europe	0.000*	0.137	0.000*	NA

Table 15.17: OxCal results estimating extinction date for hyenas in Europe. Score refers to the lowest score category included in the model (Med was high- and medium-score dates).

Score	Mean date	Error	Median date
High	21414	495	21499
Med	21508	437	21570
Low	21578	386	21628

15.3.1.2 OxCal estimates

To estimate extinction of hyenas using OxCal, a simple phase boundary model was constructed, with the last boundary representing an estimate for extinction. Only finite uncalibrated dates were used. Whether a larger, less strict dataset was used made little difference in the boundary estimate, with the median changing from 21499 cal BP (high) to 21628 cal BP (low). Unlike with the GRIWM estimates, the size of the dataset and the distribution of dates had little effect on the boundary estimate. In none of the three runs did the boundary postdate the LGM.

OxCal boundaries were also modelled for subregions (Table 15.18). Whether samples were restricted to high-score dates or not had little effect on the estimates. Similar to the GRIWM estimates, subregions showed variation, with Asia's extirpation being much older than the rest (Table 15.19). Southern Europe's estimate was significantly older than northern Europe's (∼29.5 *vs* ∼21.1 ka cal BP), and northern Europe also had the youngest boundary estimate of the four subregions. The northern Europe estimate was similar to the global extinction estimates (Table 15.17).

The OxCal and GRIWM estimates significantly differ from each other for all subregions except central Europe, where the small sample limits the t-test power (Table 15.21). In general the OxCal estimates were older than the GRIWM estimates, as would be expected. The largest difference was between the central Europe estimates, where the small sample size produced a particularly young GRIWM estimate but a more expected OxCal boundary.

Table 15.18: Subregion OxCal boundary estimates for hyenas. All regions were run twice, once with all dates and once with only high-scoring dates included. P-values are from a Welch two-sample t-test comparing equivalent subregions: for example, the estimates for Northern Europe with all-score dates and Northern Europe with high-score dates. The number of samples run sometimes differ from the equivalent GRIWM estimates because OxCal did not model radiocarbon dates that calibrated >50 ka cal BP.

Subregion	Scores run	Date	Error	Dates (n)	High/low p-value
Southern Europe	All	29736	849	19	0.379
Central Europe	All	28291	3709	2	1.000
Asia	All	39422	915	16	0.485
Northern Europe	All	21388	498	78	0.056
Southern Europe	High	29349	1320	12	0.379
Central Europe	High	28291	3709	2	1.000
Asia	High	39097	1241	10	0.485
Northern Europe	High	21144	696	39	0.056

Table 15.19: Comparison of the means of hyena OxCal estimates of subregions. Dates of all scores were included in the estimates. Welch two-sample t-tests were used to compare estimates. * denotes significance at <5% level.

	Asia	**Central Europe**	**Northern Europe**	**Southern Europe**
Asia	NA	0.145	0.000*	0.000*
Central Europe	0.145	NA	0.2306	0.6793
Northern Europe	0.000*	0.2306	NA	0.000*
Southern Europe	0.000*	0.6793	0.000*	NA

Table 15.20: Comparison of the means of hyena OxCal estimates of subregions. Only high-scoring dates were included in the estimates. Welch two-sample t-tests were used to compare estimates. * denotes significance at <5% level.

	Asia	**Central Europe**	**Northern Europe**	**Southern Europe**
Asia	NA	0.1449	0.000*	0.000*
Central Europe	0.1449	NA	0.2234	0.756
Northern Europe	0.000*	0.2234	NA	0.000*
Southern Europe	0.000*	0.756	0.000*	NA

Table 15.21: Comparison of the OxCal and GRIWM subregion extirpation estimates. Welch two-sample t-tests were used to compare estimates. * denotes significance at <5% level.

Species	Score	Southern Europe	Central Europe	Asia	Northern Europe
Hyena	All	0.000*	0.069	0.000*	0.000*
Hyena	High	0.000*	0.189	0.000*	0.000*

15.3.2 Non-radiocarbon evidence

Of the three carnivores, cave hyenas have the largest radiocarbon dataset, thanks to previous investigations (Jacobi et al. 2006; Stuart and Lister 2014) and, perhaps, their tendency to be found in caves also occupied by humans (Dusseldorp 2013; Fernandez and Guadelli 2008; Guadelli et al. 2013; Stiner 2004). While hyenas lived in southern Europe (Gatta et al. 2016; Mangano 2011; Sardella and Petrucci 2012; Stiner 2004), they were also numerous in high latitudes where collagen preservation is better (Diedrich 2011; Diedrich 2012; Stuart and Lister 2014). In general, the radiocarbon dataset agrees with the palaeontological record. There is little archaeological evidence that hyenas survived much beyond the LGM, except for a couple of potential outliers in southern Europe (Stuart and Lister 2014). It is possible the legacy of investigation in Wales and England has skewed the dataset towards the UK being home to the last hyenas, though re-dating with ultrafiltration has shown some of these UK dates to be too young (Jacobi et al. 2006).

Radiocarbon and archaeological evidence both support survival of hyenas after modern humans arrived, and cave excavations sometimes show close coexistence of hyenas and modern humans. However, the chance for stratigraphic mixing through scavenging is high. At Redaka II in Bulgaria, for example, hyenas predated expected AMH arrival, despite digestion-polished AMH teeth being recovered from the cave (Fernandez and Guadelli 2008; Guadelli et al. 2013).

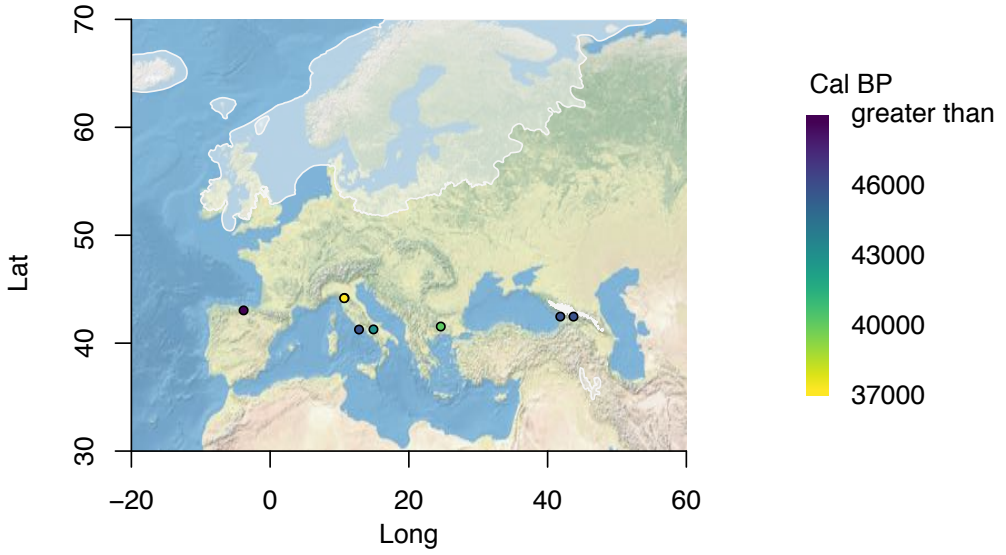


Figure 15.6: Radiocarbon dates of leopard, shading by mean calibrated age BP. Only successful and non-rejected dates are plotted. Dates are both from literature and new to this project; sources are listed in Appendix F.1.

15.4 Leopards

Combined with literature dates, there are 10 direct dates of leopards (*P. pardus*) (Fig. 15.6; more details in Appendix F.1). Of these, two are medieval introductions (P15522 and P36343) and not included in analyses. Another 10 samples of leopards failed to produce dates (Appendix E.2). Dates come from Bulgaria, Italy, Spain and the Caucasus. Leopards have been observed farther north, including France, Germany, Poland, and possibly the UK, but the remains are not directly dated (chapter 15.4.2).

Of the dates, most received high reliability scores (Appendix G). OxA-11416 received a score of 8 for having δ^{13}C slightly out of range. The date from Beta Analytic (Beta/360175) received a low score as the only health information reported with the date was its δ^{13}C.

Table 15.22: Calibrations of leopard dates. Those with finite calibrated dates were used for the GRIWM simulations. Corrected dates were calibrated for HPLC dates. Cal BP/error are calibrated date and measurement error.

Site	ID	Score	Age BP	Error BP	Cal BP	Cal error
Castelcivita Cave	OxA/37222/45631/AF	High	43400	1800	47027	1494
Castelcivita Cave	OxA/37223/45632/AF	High	38800	1000	43004	820
Grotte di Equi	OxA/-88/44416/NRC	High	43011	3513	46456	2028
Jou'l Llobu (Asturias)	OxA/10173/11757/AF*	High	46600	2300	NA	NA
Triagalnata Peshtera	OxA/11416/13176/AF	Med	37500	650	41895	490
Kudaro 3	OxA/-1/30086/AF	High	44500	2000	47645	1365
Kudaro 3	OxA/25736/30086/AF	High	43900	1900	47332	1442
Grotte di Equi	Beta/360175/NA/NA	Low	33000	260	37165	457

15.4.1 Extinction estimates

The radiocarbon LAD for leopards is Beta/360175 at Equi (33000 ± 260 BP) followed by OxA-11416 at Triagalnata Peshtera (37500 ± 650). These are the two lowest-scoring dates. The Beta date was published with little health information, and OxA-11416 just fell outside δ^{13}C range and has a borderline CN ratio of 3.496. The youngest date with a high score is OxA-45632 from Castelcivita Cave (38800 ± 1000 BP). Castelcivita's archaeological chronology has been published, which means this date can be put into a robust radiocarbon chronology (Giaccio et al. 2008; Douka et al. 2014).

There are barely enough dates to run a GRIWM estimate for extinction. One date cannot be included in the GRIWM run as it calibrates beyond 50 ka cal BP (background) (Table 15.22). Therefore no subregion models were run, and the global GRIWM simulation was only run twice: once with all dates and once without the low-scoring date. The low-score GRIWM estimate is much later due to the low-scoring date also being the youngest by several millennia (Table 15.23). A Welch two-sample t-test found the difference of the two GRIWM estimates to be significant ($t = -5.99$, $p<0.001$).

OxCal boundary models for leopards are limited by the small dataset. As for the GRIWM model, only two models were run: a high-score only model, and a

Table 15.23: GRIWM results estimating extinction date for leopards in Europe, depending on whether the low-scoring radiocarbon date was included. Because there were few calibrated dates, a high-only run was not included.

Dates run	2.5% min probability	median	97.5% max probability
Low	28909	30848	32770
Med	36618	39338	42068

Table 15.24: OxCal results estimating extinction date for pardus in Europe. Score refers to which dates were included in the model.

Score	Mean date	Error	Median date
High	42378	2276	42687
Med/Low	35662	2047	36229

model with both medium- and low-scoring dates included. The resulting estimates are different, mostly due to the young low-scoring date.

15.4.2 Non-radiocarbon evidence

The very early dates for leopards contrast with claims that leopards survived in Europe at least until the LGM and, in Spain, possibly into the early Holocene (Diedrich 2013; Sanchis et al. 2015; Sauqué and Cuenca-Bescós 2013; Sommer and Benecke 2006). Leopards have been found in association with modern human material from the Aurignacian and Gravettian in the Balkans, Greece, Spain, Italy, western France, and Germany, but the leopard remains have not been directly dated. More convincing is a painting of a spotted cat at Chauvet Cave. While the age of the painting is uncertain (it is thought to be Aurignacian, with the cave in use 37–28 ka cal BP (Quiles et al. 2016)), it does show that modern humans and leopards overlapped in Europe.

Claims for post-LGM survival of leopards in particular are not robust. In Spain, terminal Pleistocene survival is claimed for Cueva de la Riera and Holocene survival is claimed for Cueva de las Pajucas, but the chronology is based on indirect radiocarbon dates produced pre-2000 (Altuna 1972; Álvarez-Lao 2003). An earlier

claim for a late glacial presence at Triagalnata Peshtera is based on two dates of bears found in the cave, but there is little evidence to support that the leopards are of the same age (Spassov and Raychev 1997). Finally, leopards have been found in Classical Rome and Hellenistic towns, but these are probably imports (Sommer and Benecke 2006).

In total, there is little robust evidence for survival of leopards in Europe after the LGM, and even LGM presence is based on association with Gravettian material rather than direct dating. However, the radiocarbon dataset is likely missing last-surviving leopards, as none of the dates are young enough to overlap with the painting at Chauvet Cave.

16 Spatio-temporal modelling

16.1 Spatial extinction models

Spatial statistical modelling is regularly used in ecology to study species distributions, model their preferred environments, and predict their ranges under current and future conditions. These ecological tools have been combined with extinction estimators to model species' Pleistocene ranges and predict when and where they went extinct. The methods are detailed in chapter 7, but to summarise the models presented:

- A `SpatExtinct` spatio-temporal map built with the `SpatSB` function, shaded by estimated time of extinction. Ecological models do not inform this map; it is built only with radiocarbon dates. A map of estimate variance is also produced.

- A `SpatExtinct` probability of persistence map at a specific time: the median GRIWM estimate of high-score dates.

- A `MaxEnt` ecological niche model (ENM) built with radiocarbon dates as 'sightings' and LGM bioclimatic variables.

- A combined persistence-niche map, where the niche model and persistence maps are multiplied together to create a map of likely locations of extinction.

Maps reflect LGM sea levels but models were not restricted by ice sheet extents.

16.1.1 Lions

The spatial extinction model favours late (<20 ka cal BP) survival of lions in both south-west Europe and eastern Asia, though the latter has greater variance (Fig. 16.1). The ENM identifies an arc of high suitability from the British Isles down across south-central Europe, then back up into eastern Europe north of the Black Sea (Fig. 16.2). It does not particularly highlight the Italian or Iberian peninsulas as highly suitable, despite a couple of dates from northern Iberia and northern Italy. When the distribution model is multiplied by the GRIWM-estimate model, a region of high probability emerges just west of the Alps, approximately following the Rhône basin along a north-south axis. An arc of increased probability also crosses northern Italy and spreads into eastern Europe up to the Black Sea.

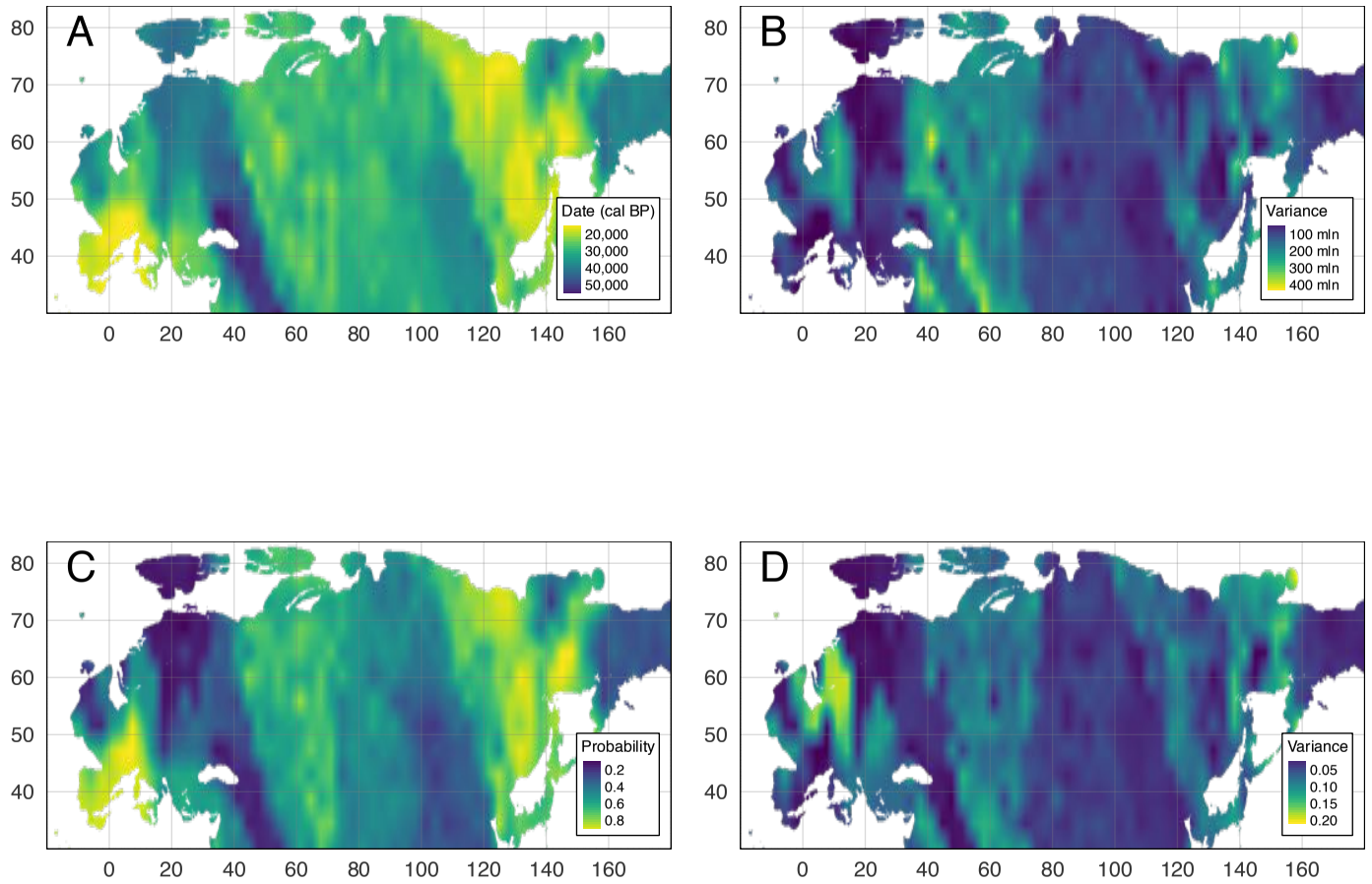


Figure 16.1: Spatio-temporal estimation of lion extinction across Eurasia. Dates are calibrated. These models are not weighted by environment suitability. A) Estimated time of extinction across space. B) Variogram of A. C) Probability of persistence for given date (the GRIWM extinction estimate). D) Variogram of C.

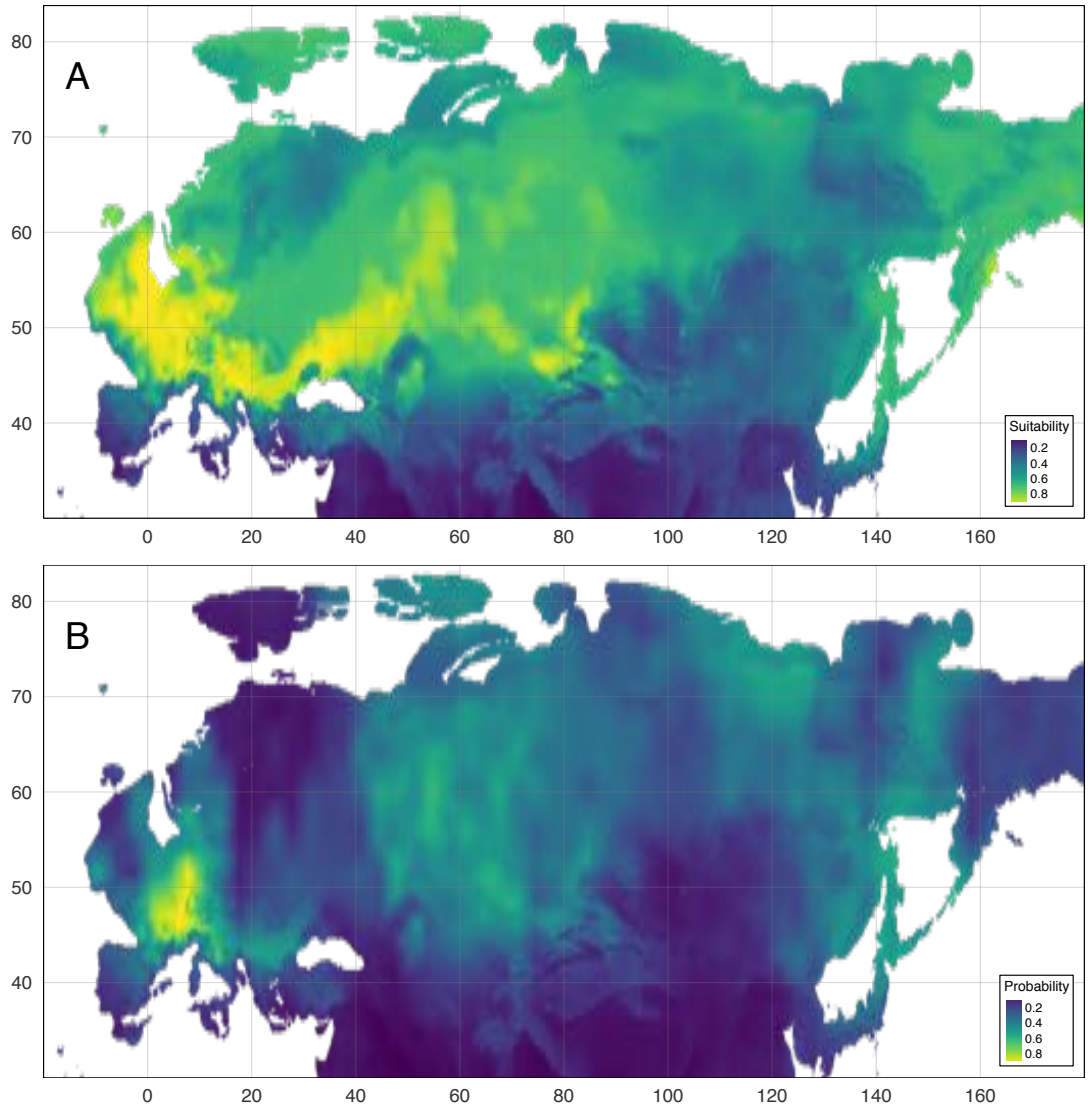


Figure 16.2: Lion ecological niche and weighted extinction models. A) Ecological niche model under LGM conditions, using WorldClim bioclimatic variables. B) The model was then multiplied by probability of extinction to create a weighted probability of persistence.

16.1.2 Hyenas

The `SpatSB` extinction model suggests hyenas went extinct in Europe later than Asia, with later persistence (~25 ka cal BP) in the British Isles and central Europe. Survival past 30 ka cal BP is estimated broadly across Europe, including Mediterranean peninsulas, though variance is high in northern Europe (Fig. 16.3). The ENM model is highly structured, with high suitability somewhat similar to that of cave lions: an arc from the British Isles south-east towards the Alps, then across towards the Black Sea (Fig. 16.4). The suitability scores are more extreme in the hyena model, with northern Europe and Asia receiving lower scores, despite a handful of observations across Asia. The overall pattern of the distribution model persists in the GRIWM-weighted model, though the region of high suitability splits into two clusters: one in the British Isles, and one immediately north of the Alps that extends west. Areas identified as relatively suitable in southern Europe, such as northern Iberia and Italy, become less likely in the weighted model.

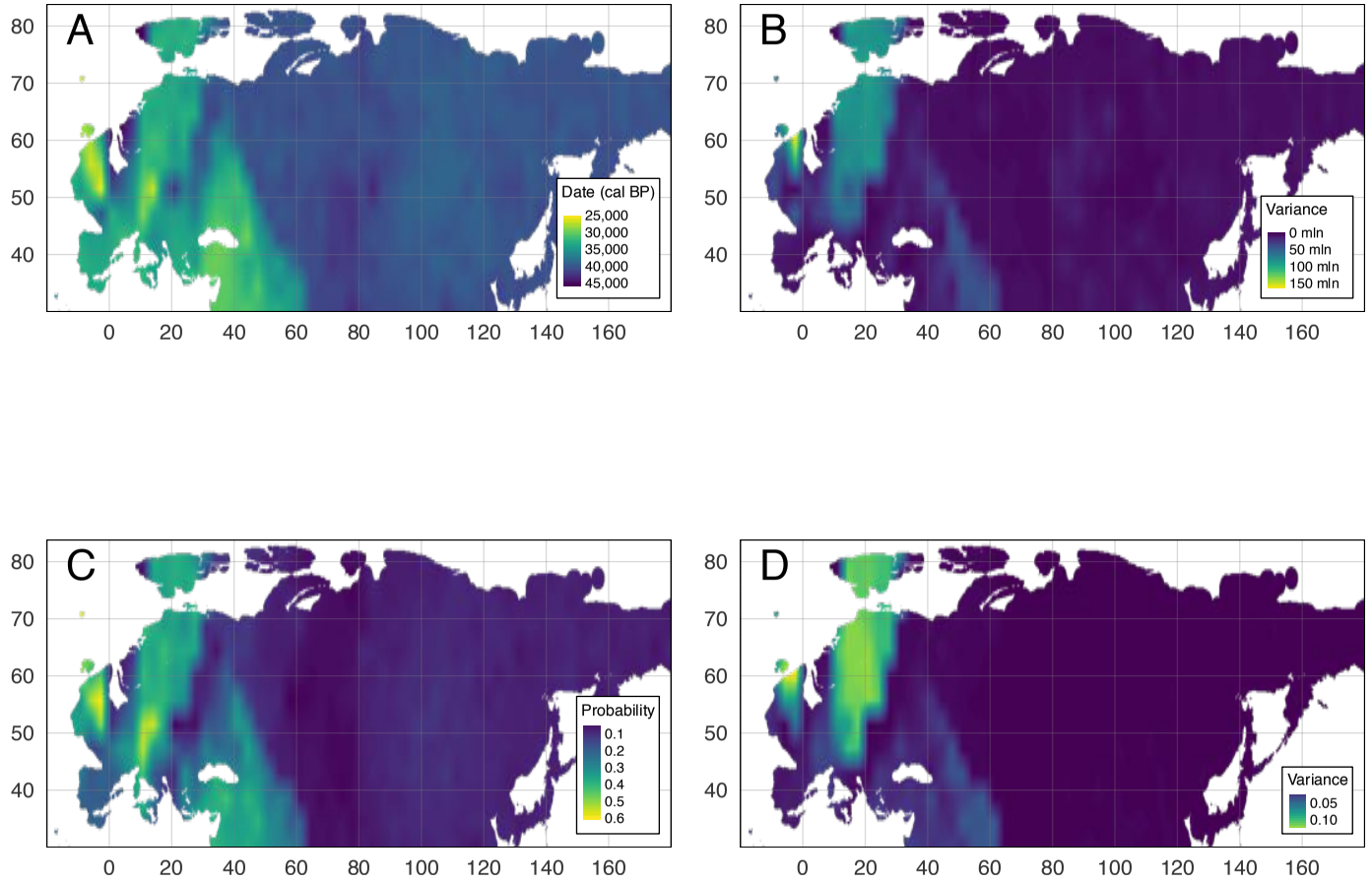


Figure 16.3: Spatio-temporal estimation of hyena extinction across Eurasia. Dates are calibrated. These models are not weighted by environment suitability. A) Estimated time of extinction across space. B) Variogram of A. C) Probability of persistence for given date (the GRIWM extinction estimate). D) Variogram of C.

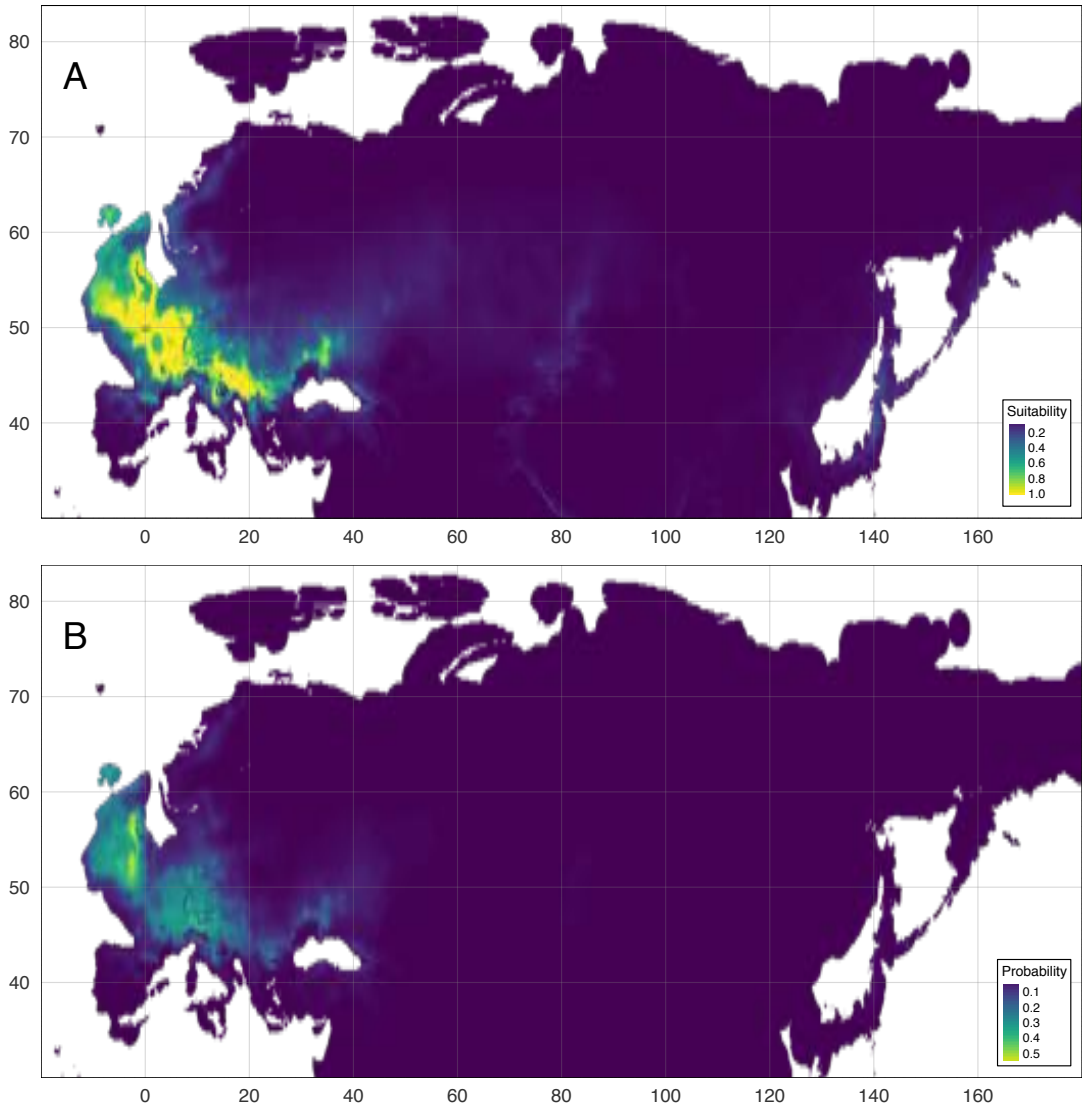


Figure 16.4: Hyena ecological niche and weighted extinction models. A) Ecological niche model under LGM conditions, using WorldClim bioclimatic variables. B) The model was then multiplied by probability of extinction to create a weighted probability of persistence.

16.1.3 Leopards

Few finite radiocarbon dates are available for Eurasian leopards and, in contrast to the other carnivores, these exclusively come from southern Europe. With so few dates, the models were restricted to a European map and the ENM model was built with jackknife validation, which is recommended for small datasets (chapter 7.4). The spatial extinction map did not identify the lack of observations in northern latitudes (Fig. 16.5) and generally was unconstrained. The probability of persistence at the GRIWM estimate was similarly 'flat'. The distribution model has more structure (Fig. 16.6). It identifies coastal areas and higher-altitude environments as particularly suitable. The preference for coasts creates an arc of high suitability through the British Isles and into Scandinavia, which would have been under ice at the LGM and was north of the known range of leopards. The lack of structure in the persistence probability model flattens the ENM when the two are multiplied, so that no high-probability region emerges outside a slight peak in the middle of the Italian peninsula. Despite considerations for small sample size in the modelling process, the models did not produce structured spatial patterns.

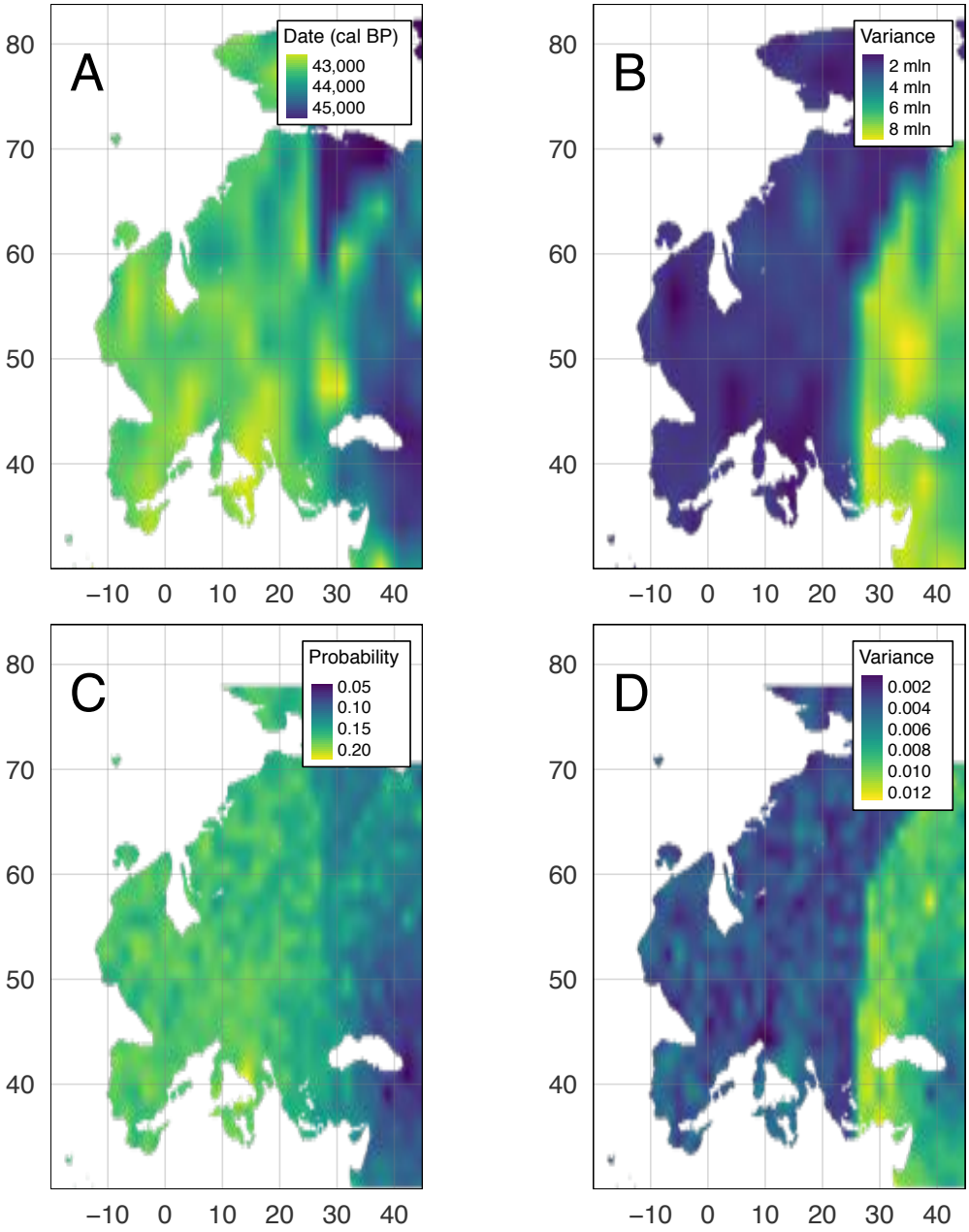


Figure 16.5: Spatio-temporal estimation of leopard extinction in Europe. Dates are calibrated. These models are not weighted by environment suitability. A) Estimated time of extinction across space. B) Variogram of A. C) Probability of persistence for given date (the GRIWM extinction estimate). D) Variogram of C.

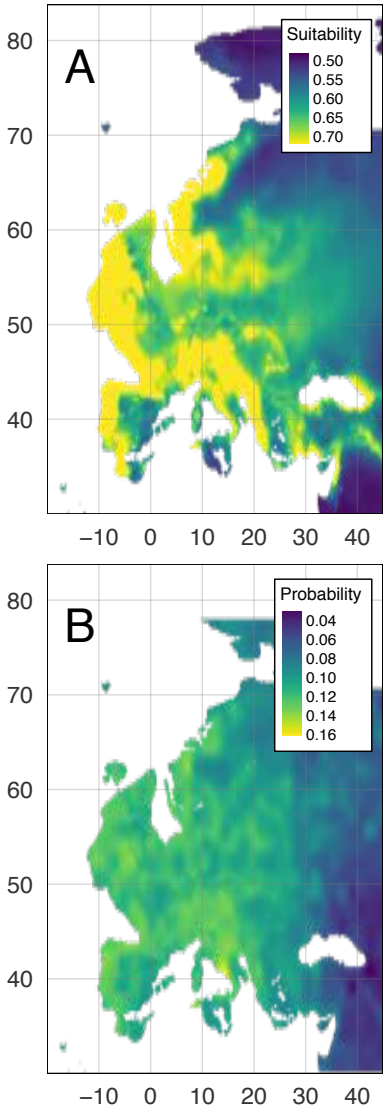


Figure 16.6: Leopard ecological niche and weighted extinction models. A) Ecological niche model under LGM conditions, using WorldClim bioclimatic variables. B) The model was then multiplied by probability of extinction to create a weighted probability of persistence.

16.2 KDE models

The kernel density models combine frequentist and Bayesian statistical approaches as an alternative to summed radiocarbon dates (Bronk Ramsey 2017). This approach minimises the noise introduced by the calibration curve and models the distribution of dates through time. Interpreting the models requires consideration of the statistics' underlying assumptions, particularly regarding the independence of events. KDE

relies on large datasets to represent meaningful patterns, and so the small (<20 dates) leopard dataset was not modelled. Similarly, to maximise sample size, the dates were only divided into all-score and high/medium score groups.

Adding low-score dates did not dramatically change the KDE models of either lions or hyenas (Figs. 16.7 and 16.8), though the high-score hyena KDE had a greater density before 40 ka cal BP. The sharp spike at 50 ka cal BP in the models is an artefact of the calibration curve, which is limited to 50 ka cal BP and so cuts off the probability density. The rise in probability density leading up to 50 ka cal BP reflects that dates are observed up to 50 ka, with no information >50 ka. This makes sense in both cases, as some finite uncalibrated dates became greater-than ages when calibrated (their calibrated distributions reached beyond 50 ka cal BP). Furthermore, while the lion and hyena KDE models are relatively distinct, the cyclicity of their peaks may reflect the influence of climatic cycles on sample preservation more than on true population levels. It is possible that climatic conditions affected sample taphonomy, such as through increased hydrological action post-cold events damaging samples and degrading collagen.

The hyena KDE model shows a downward trend towards their last appearance, with probability dropping to near-zero at ∼20 ka cal BP. Lions, in contrast, show increased density just prior to their final drop ∼16 ka cal BP. The shoulder of this final peak is narrower, but still present, in the high-score model. The hyena KDE has particularly pronounced minima at roughly 5 ky periods at approximately 39, 34, 29, and 24 ka cal BP, with a small rise in probability just before its termination at 20 ka. The lion KDE has minima at 43, 39, and 20 ka cal BP; both also have less extreme local minima within regions of elevated density. How these models relate to climate and human activity is explored more below (chapter 16.3).

16.3 Time series

In addition to the faunal KDE models, climate and AMH records were used in time series models. For climate, the GISP2 Greenland ice core δ^{18}O records were used (Rasmussen et al. 2014; Seierstad et al. 2014). For modern humans, an OxCal

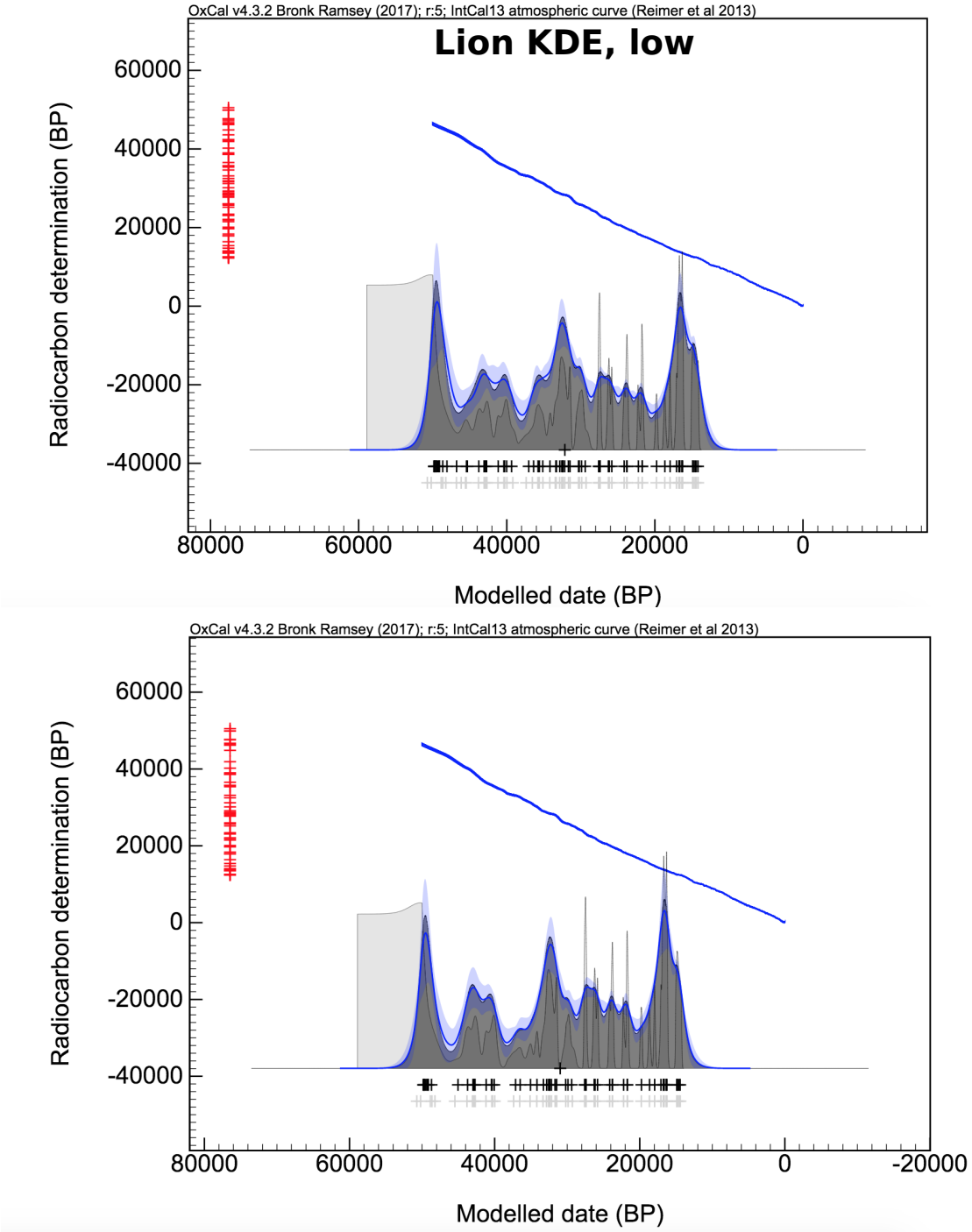


Figure 16.7: KDE model of cave lion radiocarbon dates. In the 'low' model, all finite dates were included, including low-scoring dates, and in the other only medium and high-scoring dates were included. The light grey rug plots are the median likelihoods of calibrated dates, red are the mean values of uncalibrated dates, and black are the median of the marginal posterior distributions. The KDE_Model distribution is shown in dark grey with the sum distribution a lighter-grey background. The blue distribution and bands show the mean and $\pm 1\ \sigma$ of the ensembles of snapshot KDE distributions from the MCMC analysis. The calibration curve is displayed above the distribution.

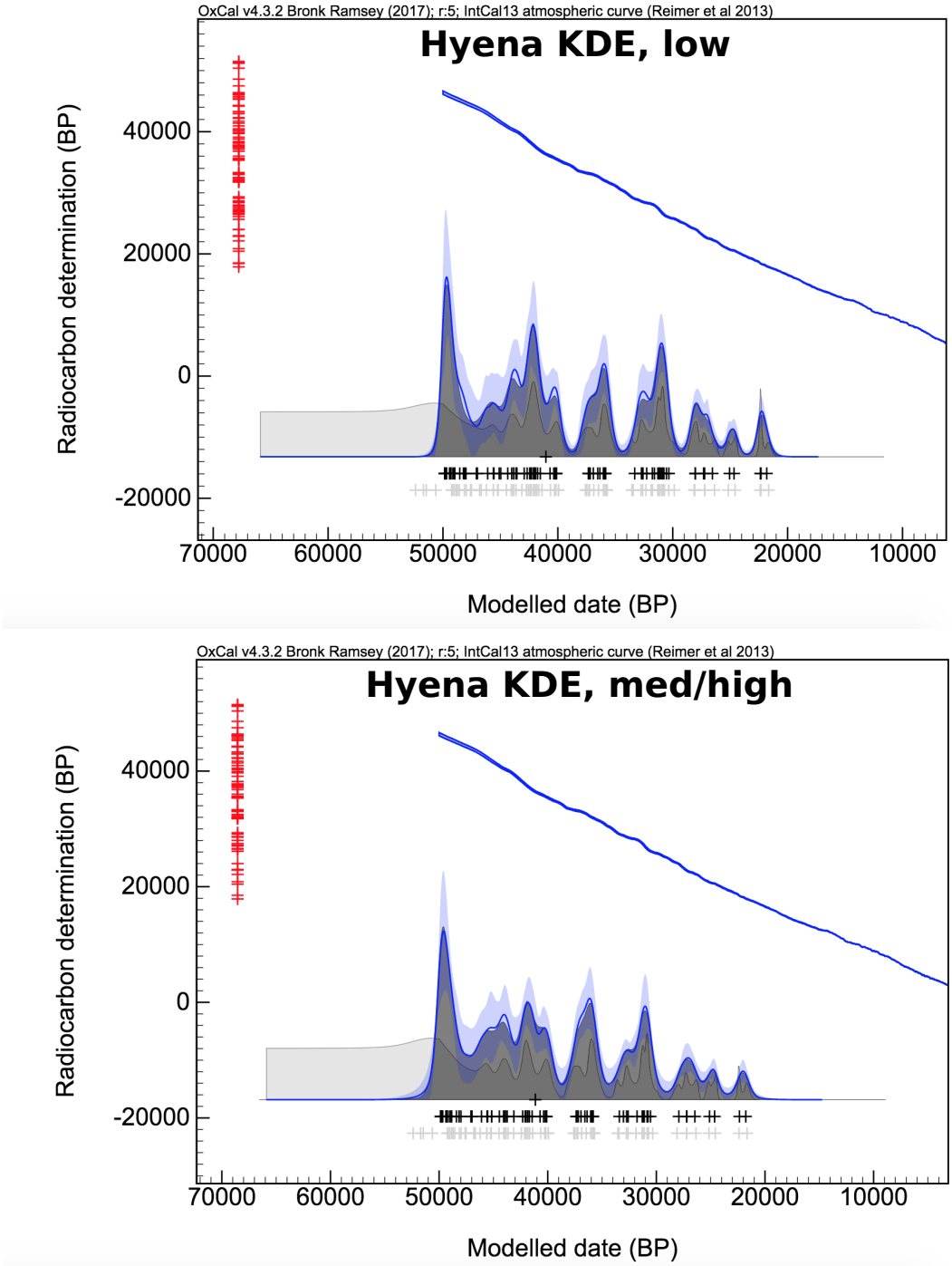


Figure 16.8: KDE model of cave hyena radiocarbon dates. In the 'low' model, all finite dates were included, including low-scoring dates, and in the other only medium and high-scoring dates were included. The light grey rug plots are the median likelihoods of calibrated dates, red are the mean values of uncalibrated dates, and black are the median of the marginal posterior distributions. The KDE_Model distribution is shown in dark grey with the sum distribution a lighter-grey background. The blue distribution and bands show the mean and ± 1 σ of the ensembles of snapshot KDE distributions from the MCMC analysis. The calibration curve is displayed above the distribution.

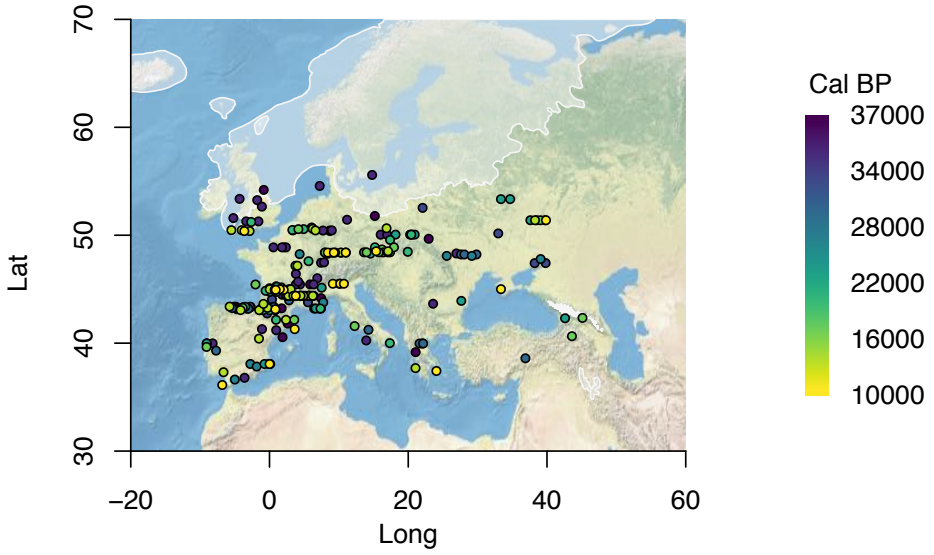


Figure 16.9: AMH radiocarbon dates used for modelling in this thesis. Randomly sampled from Carotenuto et al. (2018). White shading shows maximum extent of ice at the LGM; land topography is modern.

KDE model was produced using the radiocarbon dataset from Carotenuto et al. (2018). The dataset includes more than 2400 radiocarbon dates, which proved to be unfeasibly slow to run (unfinished after 5 days of running on a personal computer). A random 10% sample (242 dates) was run instead (Figs. 16.9 and 16.10; dates in Appendix H). The AMH KDE model is relatively smooth compared to the carnivore models, as it contains far more dates. Because the large peak in both species KDEs at 50 ka is an artefact of dates that calibrate beyond 50 ka, and as the AMH KDE only begins to have non-zero probability after 45 ka, all time series were cropped to 44.5 ka cal BP.

When the records are plotted on a common timeline, there appears to be some suggestion of synchroneity between AMH and the hyena KDE models, though not particularly lions and AMH (Fig. 16.11). The climate record is more structured than the KDE records.

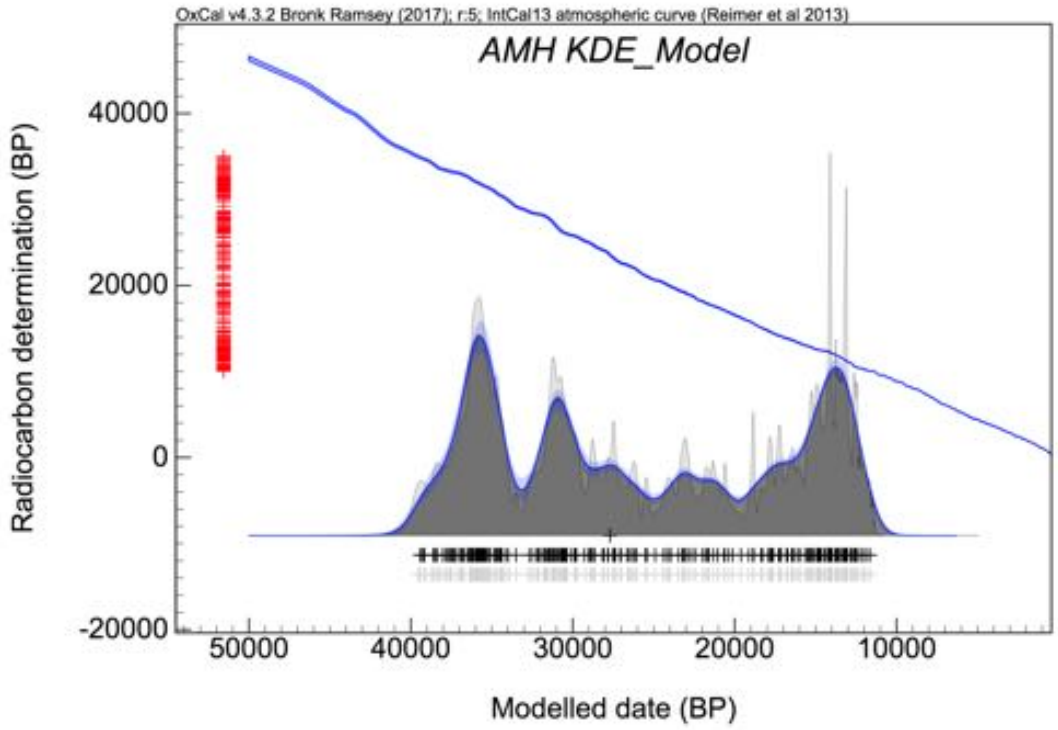


Figure 16.10: AMH KDE distribution in Eurasia after 50 ka cal BP. Subset of 242 dates randomly sampled from Carotenuto et al. (2018). The light grey rug plots are the median likelihoods of calibrated dates and black are the median of the marginal posterior distributions. The KDE_Model distribution is shown in dark grey with the Sum distribution a lighter-grey background. The blue lines and bands show the mean and ± 1 σ of the ensembles of snapshot KDE distributions from the MCMC analysis.

16.3.1 Results

The lead-lag test did not find significance when climate was the dependent variable, suggesting that offsets between climate and radiocarbon records are not systematic enough to produce spurious lags (Table 16.1).

The δ^{18}O record Granger-caused the lion KDE distribution when the more restricted radiocarbon dataset was used, but not when all dates were included (Table 16.2). In constrast, the AMH KDE Granger-caused the restricted-score hyena distribution, but not the all-score distribution. The AMH record had no causality on lions, and no causality was found between AMH and climate.

The lack of relationship between AMH and climate may be a true signal, but the later introduction of AMH ~42 ka cal BP creates a low-probability tail up to 45 ka cal BP, which artificially dampens any possible relationship between the

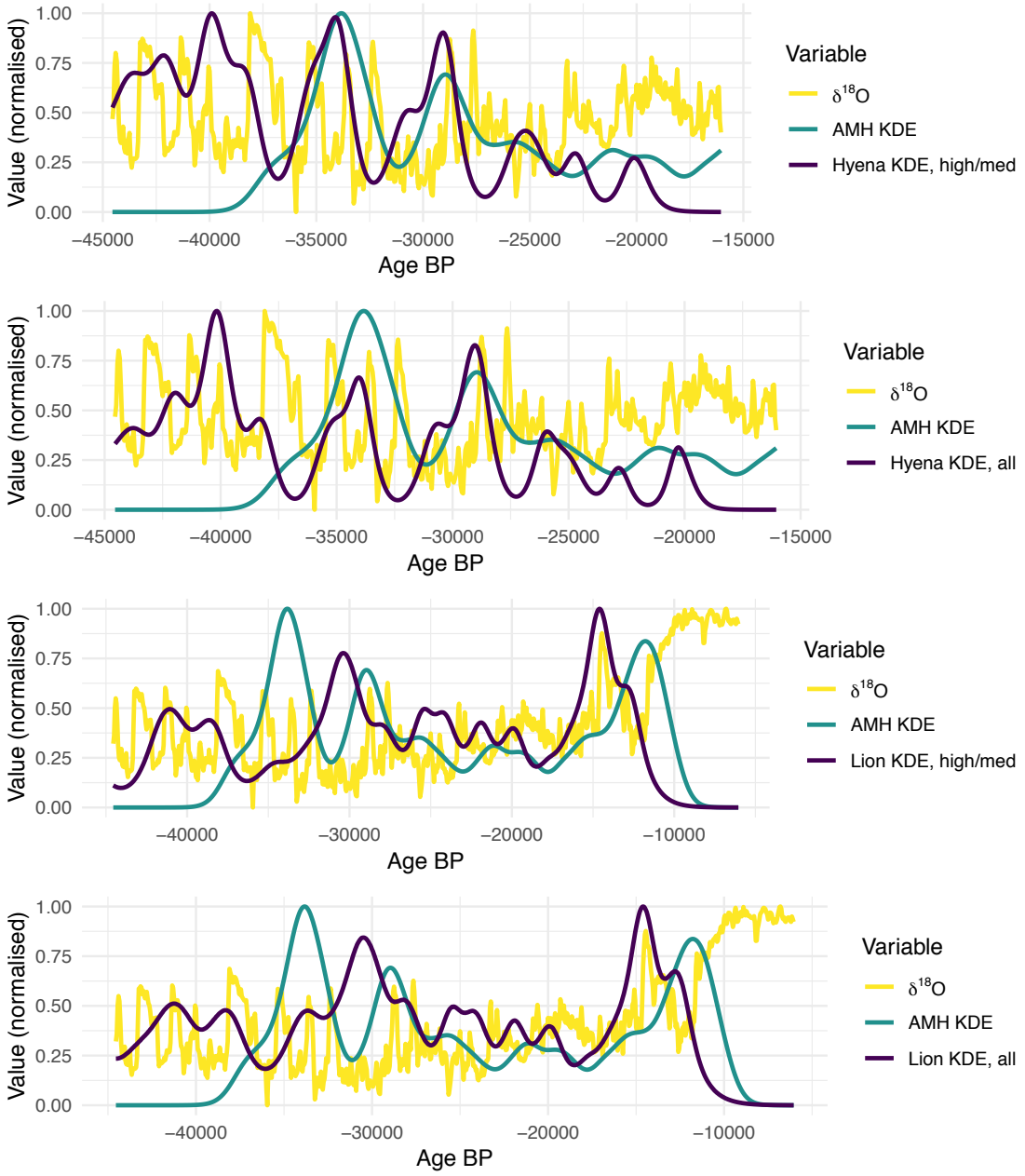


Figure 16.11: Time series tested for causality. All data have been normalised to a shared y-axis for display. Oxygen isotopes are from the GISP2 ice core records (Rasmussen et al. 2014; Seierstad et al. 2014) and AMH radiocarbon dates from Carotenuto et al. (2018). Hyena and lion KDEs were produced twice, once with all-score radiocarbon dates (all) and once with only medium- and high-scoring dates (med/high).

Table 16.1: Results of the modified Wald chi-square statistics used to test non-causality on the 'reverse' relationships as a check for spurious relationships. Direction is the lead/lag relationship tested, *e.g.* 'Variable → species' implies the variable leads the species. Sum is the sum of lagged coefficients of the variable. * denotes significance at the <5% level.

Species	Variable	p	Sum	Direction
AMH	Climate	0.671	1.00	Species → variable
Hyena, all	Climate	0.303	-11.00	Species → variable
Hyena, med/high	Climate	0.116	-9.27	Species → variable
Lion, all	Climate	0.396	-2.29	Species → variable
Lion, med/high	Climate	0.372	-4.66	Species → variable

Table 16.2: Results of the modified Wald chi-square statistics used to test non-causality. Direction is the lead/lag relationship tested, *e.g.* 'Variable → species' implies the variable leads the species. Sum is the sum of lagged coefficients of the variable. * denotes significance at the <5% level.

Species	Variable	p	Sum	Direction
AMH	Climate	0.163	-1e-07	Variable → species
Hyena, all	AMH	0.274	1e+00	Variable → species
Hyena, all	AMH	0.388	1e+00	Species → variable
Hyena, all	Climate	0.196	-4e-07	Variable → species
Hyena, med/high	AMH	0.017*	1e+00	Variable → species
Hyena, med/high	AMH	0.157	1e+00	Species → variable
Hyena, med/high	Climate	0.115	-4e-07	Variable → species
Lion, all	AMH	0.36	1e+00	Variable → species
Lion, all	AMH	0.52	1e+00	Species → variable
Lion, all	Climate	0.267	0e+00	Variable → species
Lion, med/high	AMH	0.557	1e+00	Variable → species
Lion, med/high	AMH	0.834	1e+00	Species → variable
Lion, med/high	Climate	0.038*	0e+00	Variable → species

two. The lack of relationship in the low-score carnivore KDE distributions may be due to additional dates altering the KDE models, particularly if the dates are less accurate and fall outside the expected high-score distribution. This would potentially introduce spurious structure (peaks) in the density model.

Part V

Discussion and conclusions

17 Carnivore extinctions in Pleistocene Europe

17.1 Summary of extinctions

17.1.1 When do they go extinct?

Three carnivore species were investigated in this project, with their extinctions modelled with multiple tools. Overall, the different models suggest that the three species went extinct at different times from each other, with leopards >30000 cal BP, hyenas >18000 cal BP, and lions >12000 cal BP (Fig. 17.1). The three non-spatial extinction estimates—GRIWM estimate, OxCal boundary, and the LAD—broadly agree with each other, though the hyena all-score OxCal boundary is significantly older than the other two estimates. As would be expected, the GRIWM estimates are the youngest (Saltré et al. 2015), but the OxCal models sometimes produce older estimates than the LAD. The model may be down-weighting the LAD date in the phase model, particularly in cases where the LAD is an outlier relative to the bulk of the available dates. While the GRIWM estimator produces a skewed probability distribution where the species is assumed to have survived beyond the last sighting, the OxCal boundary prioritises convergence of the overall dataset, which can mean the LAD becomes part of the boundary's tail and has

less influence over the final distribution mean.

The close agreement and high-precision estimates of the lion extinction estimates suggest extinction during, or at the end of, GI-1 (Rasmussen et al. 2014). The other two species have more uncertainty. High-score estimates for hyena suggest extinction around the LGM, and all-score estimates more towards its aftermath. The wide uncertainties with the leopard estimates and general concerns with the dataset being unrepresentative (chapter 15.4) make it impossible to pinpoint the climatic conditions under which they went extinct. Several extreme climatic oscillations occurred during the estimates' ranges 30–45 ka.

Restriction of the datasets to high-score radiocarbon dates affected some estimates. The difference in high- and all-score estimates for leopards was dramatic due to the small dataset and a low-score date also being the LAD by several thousand years. The lion estimates changed little depending on scores, though the 95% intervals were wider in the high-score estimates. The hyena dataset, despite being larger than the lion dataset, was more affected by the inclusion of low/medium score dates. High-score dates made up 53% of hyenas and 54% of lions, not including rejected dates, but low-score dates were more frequent in the hyena dataset (31%) than the lion dataset (11%). Possibly the inclusion of low-score dates specifically, and not just medium-score dates, had a more dramatic effect on extinction estimates. This is interesting, as some low-score dates are likely accurate: their low scores arise from lack of published health metrics rather than *knowing* the metrics to be outside of acceptable ranges. However, several hyenas were re-dated at ORAU in the 2000s (Higham et al. 2006a; Jacobi et al. 2006), and the earlier AG and AI dates likely contributed to the low-score dates.

17.1.2 Where do they go extinct?

Spatial estimates suggest hyenas and lions went extinct in southern Europe earlier than northern Europe, with last survivals likely in central latitudes. OxCal and GRIWM subregion extirpation estimates for hyenas suggest disappearance from southern Europe ~30–26 ka cal BP and northern Europe ~22–18 ka cal BP (Fig.

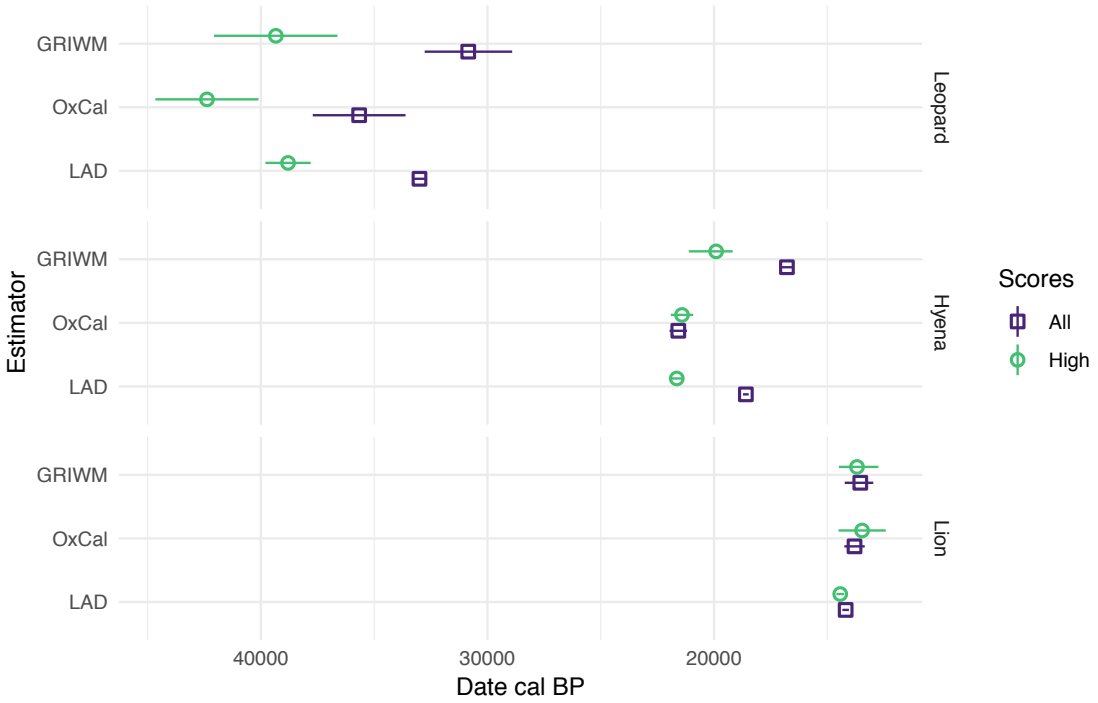


Figure 17.1: Extinction estimates for three species. GRIWM are the global GRIWM estimates, OxCal are OxCal boundary models, and LAD are the calibrated last appearance dates. Lines represent the 95% confidence interval; points are the medians of GRIWM estimates and means of the others. Scores refer to what dates were included in the estimates. For hyenas and lions, 'High' includes only high-score dates, but for leopards medium-score dates were included as well (chapter 15.4).

17.1). Hyenas disappear in Asia earlier than in any other subregion by several thousand years, around ~40–37 ka cal BP. Only two dates were available for high-score central Europe and the all-score OxCal estimate (due to exclusion of calibrated ages >50 ka cal BP), so little confidence can be given these estimates. The all-score GRIWM estimate is very late, probably due to the relatively small dataset (n=11) covering a very broad time. The wide span increases the 'tail' of the estimator, as it assumes sparser sampling through time and therefore a longer gap between the LAD and the estimated extinction. This is the only region for hyenas with such large disagreements between the GRIWM estimates and the region's LAD; in general, OxCal and GRIWM estimates fall around or somewhat later than the LADs.

The `spatExtinct` extinction model generally supports these patterns, with Asia showing the earliest disappearances and pockets of late survival ~25 ka cal BP in the British Isles and north of Italy. When the persistence model is weighted with the

ENM model, an arc of high probability emerges from the British Isles through central Europe to the Black Sea. This suggests either the UK (included in northern Europe) or central/northern continental Europe was the most likely place where hyenas disappeared. This provides an interesting insight as the OxCal/GRIWM estimates did not produce reliable estimates for central Europe, whereas the `spatExtinct`-ENM model suggest this was a region of late survival. Further work in central Europe might reveal it to coincide with the UK pattern, or the UK might become a refuge.

For lions, some 95% intervals for OxCal and GRIWM estimates overlap between north and south, particularly for the high-score estimates. The reduction in sample sizes likely increased estimates' uncertainty. In particular, the high-score dataset for northern Europe has only four dates, all much older than the all-score LAD for the region (Fig. 15.3), causing the high- and all-score GRIWM estimates to diverge. The high-score OxCal estimate for northern Europe also has large uncertainty (95% covers over 15 ky). If the outlying high-score GRIWM estimate is disregarded, then lions went extinct in southern Europe ~17–12 ka cal BP and northern Europe ~15–8 ka cal BP. A relatively large number of dates are available from Asia and Siberia, which suggest disappearance slightly after/overlapping southern Europe, and before/overlapping with northern Europe. As for hyenas, the central Europe dataset is inconclusive; the OxCal estimates suggest an earlier/overlapping disappearance than in southern Europe, but the GRIWM estimates suggest the opposite. The central Europe dataset is very small, particularly the high-score subset (n=4); conservatively, it can be said to overlap with both northern and southern Europe.

The `spatExtinct` model for lions is less clearly structured than for hyenas, with a particular north-south band of high variance around 40–60° E (the Black Sea eastwards). However, an arc of late survival is suggested from coastal Spain into northern Italy, spreading north into central France. Another region of late survival is present in eastern Siberia south into east Asia. The southern coasts/western Europe survival is also present in the persistence model, though more constrained. The `spatExtinct`-ENM model restricts this high-probability region to only its

north/central portion, with relatively high probability remaining for northern Greece and southeastern Europe.

Because the `spatExtinct` model is spatially continuous, it may be capturing a pattern masked in the GRIWM/OxCal subregion estimates. The (unweighted) extinction estimate map's band of late survival is continuous from Spain through northern France, while the subregion estimates split the dates in this region into two groups. Furthermore, the map shows relatively early disappearance of lions in northernmost Europe and northeast Europe, but later survival in northwest Europe. The subregion estimates group all these dates together. The ENM-weighted map restricts last survival to central-west Europe, but the ENM model uses LGM bioclimatic conditions, which is more valid for the hyenas than the later-surviving lions. It also assumes the lack of dates in central/southern Spain to be true 'evidence of absence' and therefore unsuitable ecologically. Overall the evidence suggests lions last survived in western Europe in central/northern latitudes, but the non-ENM spatial model suggests southern Europe may turn out to contain late survivors.

The small dataset for leopards prevents clarifying regional patterns of extirpation, though they tended not to be found as far north as the other two carnivores (chapter 15.4). The few available dates are all >37 ka cal BP. Archaeological associations suggest much later survival of the species in Spain, but the only direct date from Spain is background age. Despite attempting to account for the small dataset, spatial models were inconclusive and high variance. In particular, the lack of dates from central/northern Europe meant that the `spatExtinct` extinction estimate was unconstrained in the north-south direction, and the ENM model heavily favours coastlines, regardless of latitude. Obtaining direct dates from central Europe would enable regional comparisons. Without verification of archaeological associations, current evidence suggests leopards went extinct before the other two carnivores, with regional patterns yet to be discerned.

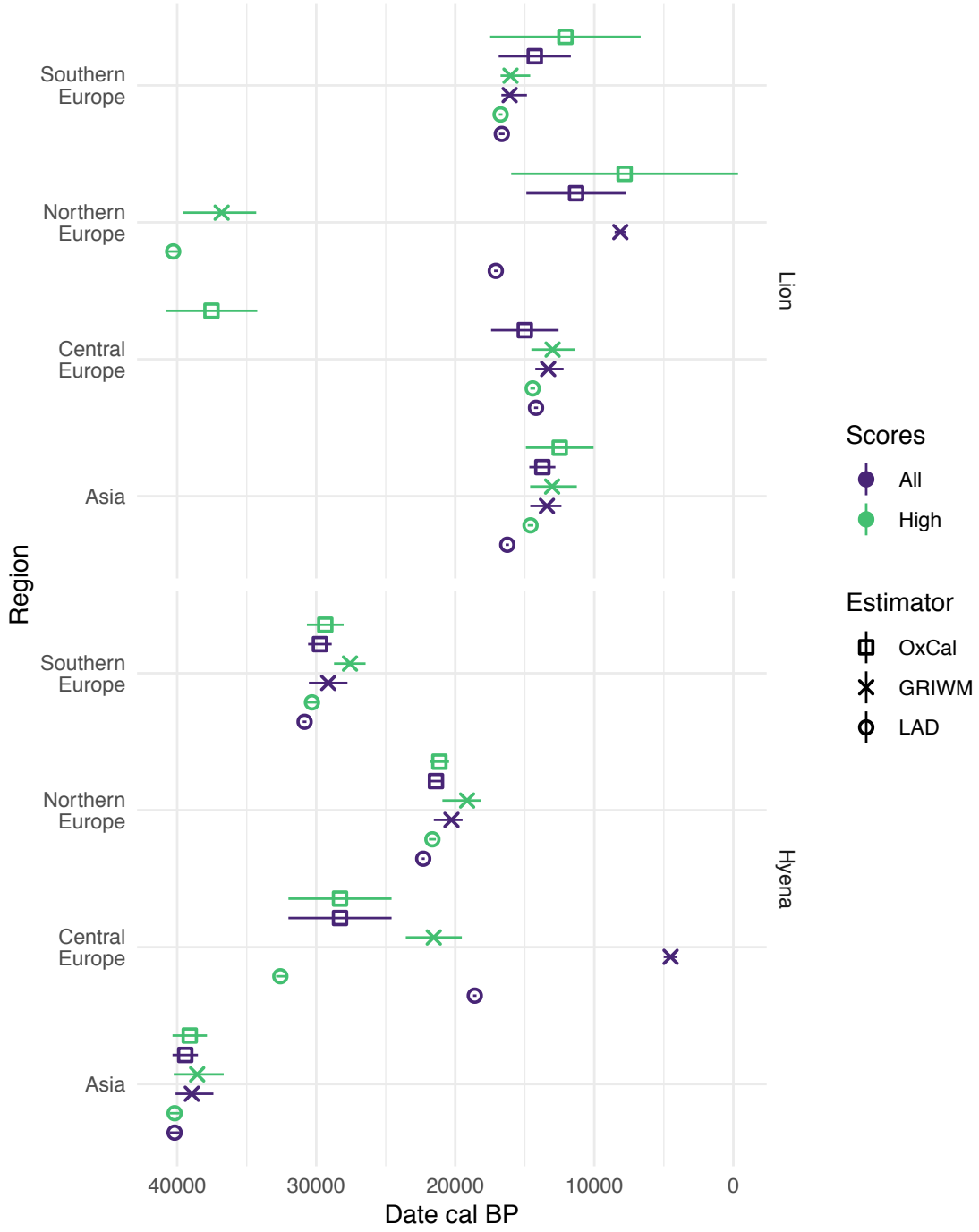


Figure 17.2: Extinction estimates for lions and hyenas by region using the GRIWM estimator, OxCal boundary models, and LADs. Lines represent the 95% confidence interval; points are the medians of GRIWM estimates and means of the LAD dates and OxCal models. Scores refer to what dates were included in the estimates: 'High' includes only high-score dates, and 'All' adds medium- and low-score dates.

17.1.3 Comparison with literature

The overall extinction chronologies for cave lions and hyenas agree with recent literature, as the additional southern dates did not produce new LADs (Barnett et al. 2016; Stuart and Lister 2011; Stuart and Lister 2014; Varela et al. 2010). More interesting are the regional patterns in their respective range contractions. The lack of radiocarbon evidence for leopards at the LGM contradicts stratigraphic and archaeological evidence, particularly in Spain (Sauqué and Cuenca-Bescós 2013; Sommer and Benecke 2006; Spassov and Raychev 1997). There are very few direct dates of leopards; the discrepancy between the radiocarbon and archaeological chronologies could be a product of limited data. That said, sometimes radiocarbon dates have significantly revised LADs and found age estimates based on stratigraphic association to be incorrect (Appendix A). As the radiocarbon dataset grows, the 'ageing' of leopard's extirpation may well be confirmed.

17.2 Extinctions in context

17.2.1 Other Eurasian extinctions

Several species went extinct in LP Eurasia, and this project's carnivores were part of this larger extinction narrative. Mainland megafauna extinctions are summarised in Appendix A and placed on the timeline with the carnivores in Fig. 17.3. Some species have uncertainties around their chronologies, highlighted in the appendix; the figure inevitably glosses over some of these.

The carnivores did not go extinct as a group, but were spread between 40–12 ka cal BP with other Eurasian extinctions. Seven species disappeared 40–30 ka cal BP, including leopards. There followed a gap in extinctions 29–20 ka cal BP, during which only cave bears and hyenas (high-score estimate) went extinct ~22–19 ka cal BP. Steppe bison may also have gone extinct around then in Europe (Appendix A). There was a wave of extinctions in the terminal Pleistocene and early Holocene (15–10 ka cal BP), of which Eurasian cave lions were a part. Small

populations sometimes survived well into the Holocene in Siberia, including giant deer, Wrangel Island mammoths, and musk ox.

The later LP/Holocene transition extinctions were generally species with the most northerly ranges, particularly the classic steppe tundra megaherbivores and cave lions. This fits with the conclusions from ecotype modelling in Varela et al. (2014), where tundra species extinctions were determined by climatic variables, and temperate species were more susceptible to AMH expansion. There were some exceptions to this generalization: a genetic clade of mammoths went extinct 40–30 ka cal BP in Europe (Palkopoulou et al. 2013). The LP/Holocene transition extinctions have also been explained as due to the expansion of forest cover, which was unable to extend so far north during brief interstadials but took long-term hold at the Holocene transition (Huntley et al. 2013; Stuart et al. 2004). The idea of a two-wave extinction in Europe, with temperate species disappearing first, was proposed by Barnosky et al. (2004), and while new data has revised the specifics of the timings, the general pattern remains.

17.2.2 Modern humans and climate

A key question for this project was whether species went extinct in southern Europe at a different time than northern Europe. Both lions and hyenas went extinct earlier in southern Europe than central and northern Europe, and ENM-weighted `spatExtinct` models suggest northwest or central Europe as a region of likely latest survival. Leopards only lived in southern and central Europe, but current data suggest they went extinct earlier than the other two carnivores.

Disappearance in northwest/central Europe suggests a 'pincer' effect for extinction of hyenas and lions. While similar to the *coup de grâce* extinction model (Elias and Schreve 2007), the pincer effect has a specific spatial element. The hyena density models (KDE) lagged the AMH KDE but not climate cycles, suggesting that they responded to AMH expansion and were relatively resilient to short-term fluctuations in climate. However, their KDE shows a general downward trend in the lead up to the LGM and after AMH arrival. Possibly AMH occupation of Europe added

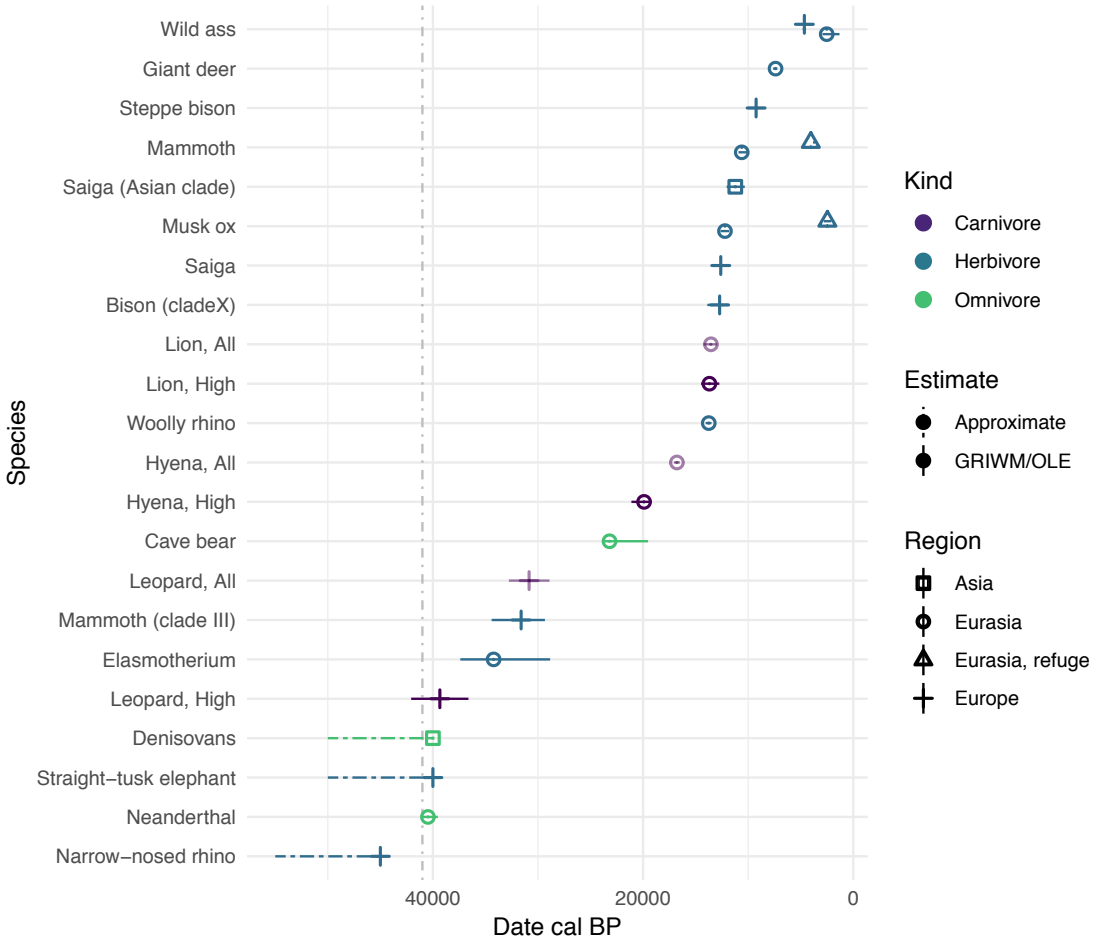


Figure 17.3: Extinction estimates from Appendix A compared to this project's estimates for leopards, hyenas, and lions. Solid lines cover 95.4% interval of the extinction estimate with symbols at the median; dashed lines are approximations with the symbol at the young end of the range. Fainter purple shapes represent GRIWM estimates including low-score dates. Symbols represent the geographic range of dates included in the estimate, as some species had sufficient dates for regional estimates. Date scores included in the carnivore GRIWM estimates are reported with the species name. Dashed vertical line represents approximate AMH arrival based on the Aurignacian technocomplex. ('Omnivore' has been applied to *U. spelaeus* though there is debate around their diet.)

pressure when stadial conditions restricted the hyena range, so that hyenas last survived in the middle. This agrees with ecological modelling for LP hyenas, which suggested their range was restricted in northern latitudes during the LGM but that southern Europe would have remained environmentally suitable (Varela et al. 2010).

Lions also had a likely last presence in central or northwest Europe, but they survived right up to the Holocene transition. They also had late surviving populations in Beringia. In constrast to hyenas, the lion KDE series was correlated

with climate but not AMH. This may reflect their more northerly range where climate had dramatic effects but AMH were slow to encroach. Possibly the forestation of the steppe tundra at the Holocene transition (Huntley et al. 2013) meant a loss of refugia and the fragmentation of the steppe community, increasing extinction risk (Tilman et al. 1994; Villard and Metzger 2014). Lions coexisted with AMH in southern Europe until 18 ka cal BP, but perhaps having a source population in the north, rather than the south, was key to sustaining this coexistence (Mann et al. 2015; Lister and Stuart 2008).

Some other species may have similarly retracted towards middle European latitudes. Neanderthals (Higham et al. 2014), steppe bison (Soubrier et al. 2016), woolly rhino (Stuart and Lister 2012), and mammoths (Stuart et al. 2002) have possible European LADs in central Europe. Cave bears may have fitted this pattern or else had a more southern contraction; they survived last in Croatia and northern Italy, with another late-surviving population in the Urals. However, mammoth and woolly rhino continued to survive much longer in Siberia, and saiga antelope and giant deer retracted northwards without later survival in central Europe (Appendix A).

Relatively early AMH arrival and a modest number of LQE extinctions in Eurasia lend support for climatic explanations of extinction. However, the tundra and Siberia represented a significant barrier to human expansion millennia after their arrival in southern Europe, central Europe, and the UK (Hoffecker 2005). This left enormous AMH-free ranges for tundra species but not Mediterranean species. This, combined with species-specific ecological tolerances, may largely explain the extinctions of Mediterranean species >30 ka and the tendency for species to disappear from southern Europe early in their retraction towards extinction.

Such a narrative generally fits with the literature for Eurasia, which tends to find climatic explanations, or combined climate-AMH explanations, most convincing (*e.g.* Bartlett et al. 2016; Di Febbraro et al. 2017; Lister and Stuart 2008; Lorenzen et al. 2011; Mann et al. 2015; Stuart and Lister 2007; Stuart et al. 2004). It fits less well with multi-continent models, which tend not to account for ecological niches of

individual species or sub-continental patterns. For example, unlike Cooper et al. (2015), where interstadials are correlated with extinctions, the KDE models for lions suggest a lagged response to stadials and, for hyenas, extinction around the LGM. Contraction to central Europe also does not fit a model of interstadial northward retreat. Araujo et al.'s (2017) global extinction study did not find correlations between most Eurasian extinctions and either climatic or AMH signals, whereas this project's KDEs found lead-lag relationships for both for hyenas and lions. The LQE was a global phenomenon, but the disagreement between Eurasian- and global-scale studies suggests the latter are losing some meaningful patterns in the Eurasian dataset.

17.2.3 Species-specific responses

Modern ecological studies suggest loss of large carnivores can precipitate trophic cascades (Daskin and Pringle 2016; Ripple et al. 2014; Ritchie and Johnson 2009; Terborgh et al. 2001), but there is little evidence Eurasian carnivores preceded megaherbivore losses. This contrasts with a study of LP extinctions in Patagonia that suggests large carnivores went extinct before herbivores (Villavicencio et al. 2016). The stepped loss of carnivores also does not accord with the LQE boom-bust model (Whitney-Smith 2001), where loss of large predators caused a boom and collapse in herbivore populations. Rather, the extinction of carnivores throughout the LP supports the idea of species-specific extinction risks (Di Febbraro et al. 2017; Lorenzen et al. 2011; Stewart 2009; Stewart 2008). This seems relevent to the three carnivores, as they were not restricted to a LP steppe-tundra megaherbivore species assemblage (Lundelius 1989; Stuart 2005). Hyenas in particular were relatively isolated in their extinction time at the LGM, with only steppe bison and cave bears possibly going extinct around the same time. Leopards disappear near the end of a set of extinctions ~45–30 ka. Lions went extinct alongside multiple herbivores, including woolly rhino, saiga antelope, a genetic clade of bison, and musk ox (Fig. 17.3). If they preceded these extinctions, it was within estimate error.

17.2.4 Refugia

The radiocarbon records of both hyenas and lions were relatively continuous up to their LADs. Possibly the Caldey Island hyenas represent a regional hang-on, but they do not postdate the global extinction estimate, and no exceptionally late 'residual' populations have been found for either species. This contrasts with some Eurasian herbivores with restricted, late-surviving populations that create a gap in the radiocarbon record between their 'functional' extinction and their true LAD. These include mammoths on Wrangel Island and the Taimyr peninsula (MacPhee et al. 2002; Stuart 2005; Vartanyan et al. 2008a), musk ox in northeast Siberia (Markova et al. 2015; MacPhee and Greenwood 2007), and giant deer in western Russia and Siberia (Stuart et al. 2004). Leopards, of course, remain extant outside Europe, and with their small radiocarbon dataset, there is no ability to discern refugial populations. Possibly Iberia harboured a later-surviving population (Sauqué and Cuenca-Bescós 2013), but this project was unable to confirm this.

17.2.5 Inter-specific interactions

Carnivore chronologies do not suggest dependence on particular extinct prey species. Dietary isotope signals in cave lions and hyenas in Europe differ, suggesting they selected different prey from each other (Bocherens et al. 2011; Bocherens 2015). Cave lions particularly seemed to prefer reindeer and caves bears, but they went extinct despite the survival of reindeer in Scandinavia and Siberia. Bocherens (2015) suggests this was due to being outcompeted by wolves after the LGM, whose isotopic signals also suggested reindeer consumption. Evidence suggests the three large carnivores practiced at least partial dietary segregation, but none seem to have been overly dependent on an extinct prey species.

At the site level, carnivores may have avoided each other, but there is little evidence of their fates being co-determined. Ecological studies suggest dietary segregation between lions and leopards and that lion population growth has detrimental effects on leopard populations, particularly survival of leopard cubs (du Preez 2014; du Preez et al. 2017; Van der Weyde et al. 2018). Modern leopards

avoid large carnivores, both in territory and prey choice, and LP leopards largely avoided hyena dens (Ghezzo and Rook 2015), suggesting they may have been particularly vulnerable to territorial encroachment by AMH or southern expansions of hyenas and lions. The relationship between lion and hyena KDEs were not tested with time series analysis, but from visual inspection alone they do not show a strong relationship. There is little evidence the success of either was determined by competitive exclusion, at least beyond the level of individual caves.

17.2.6 The global LQE

This work follows multiple studies that did not reveal either AMH or climate to be the dominant force in European extinctions (Barnosky et al. 2004; Bartlett et al. 2016; Elias and Schreve 2007; Lorenzen et al. 2011; Prescott et al. 2012). KDE models suggest that, depending on the species, either AMH or climate could best explain species patterns. The retraction of lions and hyenas towards central latitudes also complicates a simple narrative of retreat into a southern climate refuge. AMH may have been an exclusionary force in Mediterranean Europe, with their disruption of ecological ranges growing as they expanded northwards and the open steppe tundra disappeared (Araujo et al. 2017; Barnosky et al. 2004; Lister and Stuart 2008; Mann et al. 2015). A two-wave extinction, first of temperate species then steppe-tundra species, also makes more sense of Europe's protracted extinctions compared to other continents.

The indirect role of AMH in Europe contrasts with some global LQE studies which pin extinctions on AMH hunting and subsequent collapse of prey populations (Araujo et al. 2017; Wroe et al. 2013; also see citations in Monjeau et al. 2017). The most compelling argument for AMH-driven extinctions in the Americas is the compressed extinction wave in the terminal Pleistocene after the emergence of the Clovis industry in North America (Fiedel 2009). However, a similar wave of terminal Pleistocene extinctions occurred for steppe-tundra species in Holarctic Eurasia, despite much longer coexistence with AMH; it was the earlier extinctions of more temperate species that were responsible for the wider span of time in which

extinctions occurred in Europe. With 30–50% species in the Americas lacking direct radiocarbon dates (Broughton and Weitzel 2018; Burney and Flannery 2005; Price et al. 2018), the 'compressed' extinction wave could be an artefact of which species are considered, and adding species to the radiocarbon dataset may reveal more spatially and temporally diverse extinction patterns.

The Australian debate is even more burdened by limited chronological data. With AMH arrival ~65 ka (Clarkson et al. 2017), 15–20 ky of potential AMH-fauna interactions lay beyond radiocarbon's range, and some species appear to have gone extinct >50 ka (Wroe et al. 2013). Issues of collagen preservation limit datasets even within the last 50 ky. There is necessarily increased dependence on stratigraphic association through luminescence, U-series, and charcoal radiocarbon dates. Chronological information is not distributed across the continent, with almost all megafauna in Saltré et al. (2016) coming from southeast Australia and Tasmania. Species-specific and subregional analyses are not yet viable for most Australian species, and so its relationship to LQE extinctions in Europe remains unclear.

Eurasian radiocarbon datasets of AMH and megafauna are relatively large, especially for its steppe species. This has enabled higher-resolution dynamics to be discerned throughout the LP. It has also enabled formulation of an extinction narrative that is species-specific and includes both AMH and environmental factors. At the moment Eurasia's late LP/Holocene extinction wave accords with North America's, which was connected through Beringia, but the fate of temperate species is less clear outside Europe. North America, with increasing radiocarbon dates from the mainland US, may begin to reveal spatial trends in species retractions. The story is as yet unclear for South America and Australia. If these continents follow Eurasia, they will have their extinctions complicated, rather than simplified, with the addition of directly-dated species and wider spatial coverage.

17.3 Practical lessons

17.3.1 Size and quality of radiocarbon datasets

This project found that screening radiocarbon dates for reliability affected models, sometimes to the point where high- and all-score datasets produced opposite results. While issues of limited datasets and unrepeatable results were raised in chapter 2.3, the quality of the underlying datasets were not highlighted. Papers focused on the radiocarbon dates themselves evaluate dates for reliability (Dinnis et al. 2016; Lister and Sher 2015; Stuart and Lister 2014; Turvey et al. 2013), but the larger multi-species modelling papers tend to trust their sources have already screened dates for reliability (Araujo et al. 2017; Bartlett et al. 2016; Broughton and Weitzel 2018; Carotenuto et al. 2018; Cooper et al. 2015; Lima-Ribeiro and Diniz-Filho 2017; Prescott et al. 2012). It is sometimes implicitly assumed that the relative influence of inaccurate dates shrink as datasets increase, but in this work the largest dataset—hyenas—was more inconsistent between scores than lions. The importance of chronological datasets being accurate, and not just large, also affects the AMH datasets used for in these studies (Lima-Ribeiro et al. 2012).

The statistical models used in this project rely on representative radiocarbon datasets of sufficient size. The small leopard dataset was insufficient for spatial modelling, though an overall GRIWM estimate could be produced. The ~70–100 finite dates for hyenas and lions, which span the majority of their ranges, were able to produce meaningful spatial and KDE models. Testing the north/south retraction hypothesis and producing accurate niche models relies on radiocarbon dates across a species' entire range, not just where collagen preservation is best. Many species, both in Europe and other continents, lack such spatially representative datasets, and so the ability to use these statistical tools is restricted to few species.

Better understanding of spatio-temporal extinction dynamics has enabled subtler explanations of extinctions in Eurasia in which AMH and environmental factors have unequal, species-specific roles. Refugia and regional disappearances are more convincing when the gaps in the radiocarbon dataset are not due to sparse sampling.

LADs are more reliable when the specimen is directly dated with reliable radiocarbon protocols, rather than relying on stratigraphic associations or legacy dates no longer considered robust. This emphasises the need for increased chronometric datasets from other continents. This will be difficult in Australia, where persistent issues of preservation and samples >50 ka limit radiocarbon's usefulness, but the Americas would benefit from targeting undated species and filling in spatial gaps.

Unreliable chronological information affects not just extinction estimates, but also the ENMs and statistical models built on top of these estimates. Researchers may be understandably reluctant to reject dates from already small datasets, but it is clear that models are not always robust to outliers and that including inaccurate dates affects conclusions. The issue of data quality has recently been raised by Price et al. (2018), and hopefully their criticism and advice will be heeded.

17.3.2 LQE research

This work presents opportunities for further LQE research. Subdividing Europe into regions informed by climate research (temperature-dominated steppe *vs* aridity-dominated Mediterranean) revealed patterns in species' histories masked in continent-scale analyses. Studies of whole continents might benefit from dividing continents based on Pleistocene ecozones. North America, for example, could be divided into a northern region and the southern mainland that never saw glaciers. The effect of major geological features, like the Rockies, might also be used as a divider. While in theory this could be applied to Australia and South America, the limited datasets available may mean subdivided datasets are too small to work with. These imbalances between regions can determine priorities for future dating programmes.

This work also supports independent species responses to LP events. Members of classic species assemblages did not always respond in unison (Lorenzen et al. 2011; Stewart 2009; Stewart 2008). Carnivores did not necessarily follow an exemplar steppe herbivore like woolly rhino or mammoth. Many LQE papers consider multiple species, but carnivores are often under-represented due to their smaller datasets.

They are also usually not considered separately from herbivores (with exceptions like Carotenuto et al. (2018), Varela et al. (2014), and Valkenburgh et al. (2016)), despite modern ecology suggesting large carnivores face particular challenges with AMH and each other (Athreya et al. 2013; Hayward 2006; du Preez 2014; Ripple et al. 2014). This work suggests Europe's LP carnivores were resilient to some of these forces, but other carnivores may have different stories. Future LQE studies might benefit from considering carnivores explicitly.

Monjeau et al. (2017) argue that the back-and-forth in LQE research around causation is due to a 'conceptual blockage' where papers frame humans/climate as mutually exclusive drivers of extinctions. The authors argue instead for a mathematical approach that allows both to have partial, and not predetermined, explanatory power. This has been done, for example in Bartlett et al. (2016), but the coupled KDE and time-series analysis used in this project also tries to look beyond the binary human/climate LQE debate. KDE models do not just model the single point of extinction, but presence through time, allowing for testing of the influence of climate and AMH activity through more of a species' history. This enables testing of whether its KDE model is influenced by climate change and allows AMH to influence species long after initial AMH arrival. Both, or neither, can inform the lead-lag analysis, and influence each other, which contrasts with models that assume AMH and climate are independent. Time series analysis doesn't single-handedly break a 'conceptual blockage', but it does go alongside work like Lorenzen et al. (2011) that tries to include a species' dynamic history and not just the final, single event of extinction.

17.3.3 Conservation and ecology

Current conservation strategies need to know which species are most vulnerable and what factors most affect species' resilience. Ecologists are currently more likely than archaeologists and palaeontologists to accept overkill as the explanation for the LQE (Nagaoka et al. 2018), likely due to their first-hand experience of current human destruction. However, this project suggests that some European species were

able to coexist with modern humans for tens of millennia, and KDE models suggest species-specific cyclicity of population densities with climate changes and AMH. Today, large-scale habitat modification is a key feature of extinctions and naturally receives much attention in conservation research (cf. Fisher and Blomberg 2010), but Pleistocene species were susceptible to extinction even without anthropogenic habitat change. Setting aside land might not be sufficient to protect species in the face of rapid climate change; management of the land to keep it suitable to species and mitigation of anthropogenic climate change may both need to be prioritized.

The results here also reveal species-specific trends: hyenas followed a long, protracted trend towards extinction, as seen in some species' genetic histories (Lorenzen et al. 2011), while lions had an abrupt termination. The idea that protecting a 'flagship' or keystone species will ensure diversity in the rest of the ecosystem does not seem to have been the case in the past, even within the same guild. This has been noticed in some ecological case studies; for example, protection of lions on a reserve came at the expense of the leopard population (du Preez 2014).

Research tools used here can also be applied to ecology. Time series analysis might be used on a higher-resolution scale to track seasonal patterns and test if species are co-dependent (Damos 2016), and studies of carnivore interactions might be compared with past evidence (du Preez 2014; Van der Weyde et al. 2018). Finally, work like Smith et al. (2016) starts to build continuity between the Pleistocene and modern extinctions, and hopefully will lead to clearer criteria for evaluating the suitability of rewilding and reintroduction strategies (Brown et al. 2011).

18 Conclusions

18.1 Summary findings

This project aimed to improve understanding of bone diagenesis in southern sites, obtain dates of under-represented species, and model spatio-temporal dynamics of these species.

It was found that collagen preservation remains a major challenge to improving chronology in southern Europe, with multiple sites and species failing to produce dates. Investigation of these samples found that large-scale screening of bones can reveal variation in preservation at a site and within single samples. The former suggests value in intensive screening of bones at key sites, such as in Spain; the latter is most important when individual samples are valuable and may explain discrepancies between %N and collagen yields. Alternative pretreatment protocols based on dialysis and EDTA extraction failed to produce larger collagen yields than ABA, though EDTA showed potential as an accelerated protocol that could extract protein for DNA/radiocarbon analysis from the same sample.

Furthermore, radiocarbon dates should be evaluated critically. LAD dates, such as Caldey Island hyenas, were investigated for evidence of contamination, and the lack of identified contaminants increases confidence in their accuracy. Use of a simple date scoring system showed that exclusion of less-robust dates can influence

extinction estimates and models. This is particularly important when multi-species and multi-continent statistical tests are done, as authors necessarily rely on source papers for radiocarbon dates and may not evaluate the quality of individual dates.

Three species were successfully dated in this project: cave hyenas, cave lions, and leopards. Extinction (or extirpation for leopards) models suggest the three species went extinct at different times in the Late Pleistocene, all after the arrival of AMH and under different climatic conditions. Lead-lag testing of species KDE models with climatic and AMH KDE models suggested that observation densities of lions lag climate changes and hyenas AMH density, and spatial modelling predicted that both species retracted from both their northern- and southern-most ranges to go extinct in mid-latitude Europe. The leopard dataset remains too small to meaningfully model, and disagreement between the radiocarbon dataset and archaeological associations requires further investigation. Tentatively a 'pincer' effect is proposed to explain their extinctions, where AMH in southern Europe prevented carnivores from retracting into southern Europe when climatic conditions at the northern extent of their ranges became unfavourable. However, this model is based on probabilistic models and new LADs could be discovered outside their predicted range of extinction.

In the wider context of Eurasian extinctions, the large carnivores are spaced across the LP and do not precede herbivore extinctions. Eurasian extinctions support species-specific responses to LP events, with a broader trend of temperate species going extinct before the LGM and holarctic species around the LP/Holocene transition (with some residual population surviving well into the Holocene). This level of dynamic understanding is a privilege of relatively large radiocarbon datasets; the picture from other continents is generally less clear, with many species lacking chronometric dates or dates across their full geographic range.

18.2 Limitations

18.2.1 Experiments

The experimental work here is incomplete; it established promising avenues of future work and helped characterize poorly-preserved samples. Here some general limitations are highlighted beyond the specific ones discussed in the results of each experiment.

While experiments highlighted the potential for inter-bone variation in collagen preservation, the dataset was based on two sites (Zafarraya and Latton bone standard), and the general applicability of this issue is not established. It seems likely to be of greatest concern in sites with irregular collagen preservation *between* samples as well (like Zafarraya), but this has not been tested.

The Caldey Island evaluations depend on absence of evidence, and more sensitive analysis may identify contamination in the sample matrix. The small size of the samples precluded re-dating the samples with HPLC, but future reductions in the required sample size might make this possible.

The dialysis experiments established that collagen yields were poorer quality than routine protocol yields, but did not create a solution to this issue. Also, due to the focus of this project, Pleistocene samples were used; more recent samples might perform better, though then there would probably be less need for additional acid-soluble collagen in the first place. No work was done exploring optimisation of the initial HCl extraction, and it is possible that using a different acid concentration or demineralization the samples for a different duration might affect the yield and its quality.

The characterization of the failed samples failed to conclusively decide what the final yield was, only establish connections to similar samples in the literature and make some suggestions. Further tests, such as with pyrolysis GC-MS, might clarify the composition of the false yields.

Finally, EDTA experiments established some first steps but did not fully establish a protocol for preparing radiocarbon samples with EDTA. Reliance on Latton bone,

which was very large but revealed to contain heterogeneous collagen content, made some results incomparable, and the samples retained EDTA even after gelatinisation.

18.2.2 Megafauna

This project attempted to improve the chronology of European species in the Mediterranean, where direct radiocarbon dates are sparse but important to understanding species' responses to climate change and modern human expansion. Despite attempting to date both carnivores and some herbivores, only three extinct carnivores were successfully dated. Of those three, the leopard dataset remains very small, making most models inconclusive, and the lions and hyenas added to more extensive previous work. The models produced here, and the interpretations drawn from them, are subject to future expansions of the dataset. In particular, archaeological associations suggest that later-surviving leopards have yet to be radiocarbon dated in Iberia; their addition have the potential to radically change the GRIWM estimates and make spatial modelling more viable.

None of the Spanish samples collected for this project contained sufficient collagen to be radiocarbon dated. Iberia remains a gap in the datasets of these carnivores, with implications for the interpretation of the spatial model results. Extinction and niche modelling interprets absence of evidence meaningfully. This issue of 'absence as evidence' has been discussed in ecological niche modelling (Fourcade et al. 2014; Morales et al. 2017), and its influence depends on underlying biases in sampling and data success. For Spain, at least, absence of evidence reflects collagen preservation, whereas in regions with larger datasets, gaps in the timeline may be a more meaningful reflection of species presence. Continued work in Iberia is needed to resolve this issue.

The KDE and `spatExtinct` models do not fully account for statistical uncertainty. The `spatExtinct` models used means of calibrated dates, with weighting only the reliability of the date (and not its error). While the KDE models do incorporate dates' uncertainties, the KDE models themselves come with uncertainties that were ignored in the lead-lag tests.

The time-series analysis also uses a relatively conservative radiocarbon dataset for modern humans in the sense that transitional industries, like the Uluzzian in Italy and Greece, are not attributed to AMH (Carotenuto et al. 2018). The AMH KDE is built on dates after ~42 ka cal BP, but AMH may have arrived in Italy several thousand years earlier (Douka et al. 2014). Whether adding these transitional industries to the KDE model affects the lead-lag tests was not tested here. Attribution of transitional industries to AMH is not conclusive and they tended to be more regionally constrained than the (nearly) pan-European Aurignacian, but considering their impact on models would be worthwhile.

The niche models built in this thesis use only a climate snapshot for the LGM, as the WorldClim database does not have climate data for an interstadial and comparable climate variables could not be found in other sources. The weighted `spatExtinct`-niche models of extinction reflect a climatic worst-case scenario. Hyenas appear to have gone extinct around the LGM, but lions go extinct at the terminal Pleistocene, making the use of LGM climate conditions less valid.

The scoring system used in this thesis on radiocarbon dates is simplistic. It does not allow for contextual evaluation of a date's validity. For example, a date might have a slightly high CN ratio but agree with other samples from its context, but the score system cannot account for this. Criteria are also assigned a simple pass/fail status, so that samples only just outside the threshold receive the same score as extreme outliers. Many of the metrics are interrelated, so a problematic sample would be expected to violate multiple criteria and produce a lower score, but a graduated system might account for this more directly.

18.3 Future work

18.3.1 Experimental

For the method experiments, further work could improve the quality of collagen extractions. The dialysed samples could be recombined with the ABA yield and purified with HPLC. The EDTA protocol showed potential in terms of yields but

again needs further work to purify the collagen. Several ideas were suggested in chapter 12.6, including adding an ultrafiltration step or encouraging precipitation of the EDTA from solution by lowering the solution pH after microwaving. Additionally, the test tubes used in the microwave are large and incompatible with the lab centrifuges, requiring samples to be manually pipetted into new test tubes. This may introduce handling losses and could be streamlined in the future.

18.3.2 Megafauna

There is a large gap in the radiocarbon dataset of megafauna in the Iberian peninsula, particularly south of the northern coast. Iberia has been presented as a final refuge for multiple species, including Neanderthals and leopards (Jennings et al. 2011; Sauqué and Cuenca-Bescós 2013), and testing these theories requires a robust chronology for Spain's fauna. Large-scale screening of %N at Zafarraya found well-preserved bones even when most failed; however, no bones from Carigüela, further south, had even marginal preservation. Improving chronologies of fauna in Iberia will require finding more sites like Zafarraya, where degradation of bones is incomplete and successes can still be found.

In general, the leopard dataset remains too small to build regional models with. Samples from central European caves would have better preservation than the southern samples tried here, so directly dating leopards from these sites ought to be more successful and would begin to produce regional information.

Alternatively, less direct chronological information through stratigraphic association could be critically assessed and modelled. Some research in this regard has been done (Sauqué and Cuenca-Bescós 2013). Other dating methods, like U-series and OSL, could be used to establish *terminus post quem* dates, which might be sufficient to improve chronological constraints on some species. For example, straight-tusked elephant has so little chronometric information that a well-dated site sequence with stratigraphic association might be enough to establish its presence in or after MIS3. Such inference seems to be a necessity for the truly southernmost Mediterranean sites and species, like the Mediterranean island dwarf species. This

kind of 'bracketing' chronological information lends itself to tools like OxCal's phase models but not to ecology sightings-based tools. However, if sufficiently high-resolution stratigraphic models were built, the phase estimates might be built into GRIWM estimates as (imprecise) data points.

Increasing the radiocarbon dataset does not necessarily require more dates on morphologically-identifiable bones. Another approach is to take dated bones and identify the species through genetics, proteomics, and ZooMS analysis. Large-scale ZooMS screening at sites have identified species from fragmentary assemblages (Douka et al. 2019; Welker et al. 2015). Despite its limitations in this project, ZooMS could be the first step to screen likely carnivores (or whatever genus of interest), which could then be identified to species-level with DNA (as done for hominins at Denisova Cave (Douka et al. 2019)). ZooMS is far quicker and cheaper than genomic analysis, and such a two-step procedure is more viable than DNA screening large numbers of bones. Less direct genetics analyses may also be useful: Grealy et al. (2015) identified species from whole batches of bones, and Slon et al. (2017) identified species in stratigraphic layers through analysis of DNA in soil. This introduces an extra inference step between the species and the chronology, but at sites where bones are highly fragmentary, or where bones are already radiocarbon dated but their species unidentified, these approaches could add valuable information.

It would be relatively straightforward to apply this project's modelling tools to other species that already have larger radiocarbon datasets. In Europe, steppe tundra species, Neanderthals, and cave bears have relatively large datasets (Cooper et al. 2015; Higham et al. 2014). Outside Europe, direct dates can be sparse, particularly in South America and Australia, but some North American species, like lions and mastodons, have larger datasets (Broughton and Weitzel 2018). It would be interesting to test, for example, whether tundra species show a stronger lead-lag relationship to climate than more temperate species, or whether herbivores show a different relationship to modern humans than carnivores. It would also be possible to test inter-species relationships, such as whether a key prey species leads or lags a carnivore. The spatial extinction models could also be applied, for example to test

whether North American species share a spatial contraction pattern or responded differently to the terminal Pleistocene and modern human expansion.

The niche models built in this thesis use a climate snapshot for the LGM. The WorldClim database does not have data for an interstadial, and climate papers tend to focus on one point in time (making models incomparable) or one variable through time. Future palaeoclimate models might release more snapshots or produce simpler models that cover more time in the Pleistocene, which would make it possible to compare species' niches under stadial and interstadial conditions.

Finally, the statistical tools used here all come with caveats that could be improved upon. The `spatExtinct` package does not incorporate radiocarbon date uncertainties; possibly it could be adapted to resample from the whole distribution rather than the mean estimate in a manner similar to OxCal's modelling procedure. A challenge would be reducing computing time, as `spatExtinct` already takes several hours to run on a laptop, and sampling from a distribution may make convergence even slower. The lead-lag tests also use the mean of the KDE distribution without uncertainties and might be adapted to better incorporate uncertainty.

18.4 Final reflections

In this project, I tried to combine radiocarbon dating best-practices, ecological modelling, chronological modelling, and ecological theories to address the LQE. Radiocarbon-specific expertise was particularly valuable in evaluating dates. I also noticed a sometimes large divide between ecological and LQE literature. I believe LQE research could benefit from better integration with modern ecological ideas and methodological issues. It also would benefit from more critical evaluation of the underlying chronological data that, however indirectly, it depends on.

This project sampled from more than three carnivore species, but in the end preservation in southern Europe was a stubborn barrier, and these three species emerged as the most successful samples. As it is, this was fortuitous: a few dates in southern Europe helped fill in a spatial gap for species that have substantial

datasets further north, enabling meaningful modelling of spatio-temporal dynamics. Leopard radiocarbon dates are out of sync from stratigraphic evidence, but this project produced some of the only direct dates of this species in Europe, which hopefully targeted sampling can build on.

The broadest lessons from this research have been the importance of evaluating the underlying quality of radiocarbon dates and the understanding that global LQE studies rely on unequal datasets between continents. Europe has the most complete radiocarbon dataset for LP fauna, despite several species extinctions being barely constrained. With this relatively large dataset, the ecological division between southern and northern Europe seems to be a valid and significant one. Studies that treat Europe and Eurasia as a single unit risk obscuring these differences and confounding temporal signals. This suggests such regional patterns are waiting to be found in other continents, but due to a variety of methodological challenges, most species do not yet have sufficiently representive datasets to discern spatio-temporal patterns.

The biggest leaps forward in understanding Eurasia's extinctions have been chronology-focused, such as the recent addition of *Elasmotherium* to Eurasia's LP extinctions, the discovery of Holocene survival of multiple steppe species in Siberia, and revision of Neanderthal extinction. New statistical approaches are interesting but only as good as the underlying data. Targeted sampling of species without direct chronometric information and sampling from underrepresented regions will make lasting contributions to LQE studies, as will transparency in how chronological datasets are compiled.

In the midst of modern anthropogenic extinctions, the LQE is more than an academic interest. But key to the LQE is good chronometric data, and where datasets are largest and most robust, extinction stories are most interesting. More surprises are waiting to be found—and with them, a more complex LQE story.

Appendices

A

Extinctions and extirpations <100 ka

The following are short summaries of chronologies of medium- and large-bodied mammals that went extinct or were extirpated from Europe in the last 100 ky. These were evaluated largely to enable comparisons with the project's three carnivores, particularly by producing GRIWM estimates when sufficient direct dates were available. Cooper et al. (2015) produced GRIWM estimates for several Eurasian species, but they understandably excluded some species with smaller datasets, and recent work has added dates that potentially change GRIWM estimates. Therefore a reevaluation seemed warranted.

Species have been ordered alphabetically by Latin name.

Bison *(Bison priscus* and *Bison* sp. cladeX)

The majority of dated steppe bision (*Bison priscus*) come from the northern steppe and Siberia, and *B. bonasus* (Wisent) remain extant (Markova et al. 2015; Soubrier et al. 2016). While the steppe bison mostly went extinct ~32 ka cal BP, a specimen from southern France dated to 15880 ± 70 BP (~19000 cal BP) has been identified and confirmed as a steppe bison with genetic analysis (Marsolier-Kergoat et al. 2015). The genetic predecessor to Wisent (CladeX) persisted as a distinct genetic clade until ~12 ka cal BP, occupying a separate niche from steppe bison (Soubrier et al. 2016). Morphological similarities between steppe bison and the

Table A.1: GRIWM estimates for steppe bison and CladeX bison. Sources described in text.

Genotype	Dates (n)	2.5% min probability	median	97.5% max probability
CladeX	21	11968	12719	13890
Steppe bison	13	8503	9248	9982

Wisent predecessor restricts the radiocarbon dataset to samples that are confidently identified as steppe bison with genetic analysis. The late French steppe bison date is one of few direct dates of the species from central/southern Europe, and most dates come from the Urals, Caucasus, and northernmost Europe. The steppe bison's LAD in France and representation in cave art suggests survival until the LGM (Soubrier et al. 2016), possibly with central Europe being the latest region of presence.

GRIWM estimates have been produced for both CladeX and steppe bison based on the dataset in Soubrier et al. (2016). Because of the large gap between most of the steppe bison dates and its LAD, its extinction estimate is very late; the CladeX estimate better matches the data. Further dating of genetically-identified steppe bison from around the LGM will better resolve its extinction estimate.

Baikal yak *(Bos* or *Poephagus baikalensis)*

The Baikal yak has been documented in Siberia, but its relationship with extant yak is not very clear (Agadjanian and Shunkov 2018; Mead et al. 2007; Vasil'ev 2003). About its only chronological restriction is that it has been found with Mousterian artefacts (Agadjanian and Shunkov 2018; Vasil'ev 2003). Due to its geographic restriction to Siberia, unclear genetic status, and dearth of direct radiocarbon dates, this species is not considered further.

Woolly rhino *(Coelodonta antiquitatis)*

Woolly rhino chronology and spatial patterns have been discussed in Stuart and Lister (2012) and their extinction estimated in Cooper et al. (2015). Woolly rhinos have been found in northern Spain in association with Gravettian material and a direct date produced in the 1990s suggests presence as late as ~20 ka cal BP, though this date should be regarded cautiously (Álvarez-Lao and García 2010).

Table A.2: GRIWM estimate for extirpation of *Elasmotherium sibiricum*. All dates from Kosintsev et al. (2019).

Dates (n)	2.5% min probability	median	97.5% max probability
18	28849	34224	37391

Direct dates from southern Europe are otherwise >35 ka cal BP. Woolly rhino abandoned the UK ~35 ka cal BP and retracted into northwest (Belgium, France) and central Europe until 14 ka cal BP. They survived for another ~1000 years in western Russia and Siberia (Stuart and Lister 2012).

Elasmotherium *(Elasmotherium sibiricum)*

Elasmotherium sibiricum lived as far west as eastern Europe, with its range mostly in western Asia and western/central Russia. Until very recently, *Elasmotherium* was thought to have gone extinct before the last glacial cycle, but recent radiocarbon dating has confirmed its survival until ~35 ka cal BP (Kosintsev et al. 2019). The dates include HYP HPLC dates and ultrafiltered dates from multiple labs. Using the finite, calibrated dates considered most robust by Kosintsev et al. (2019), a GRIWM estimate has been produced (Table A.2). The wide 95.4% range is probably due to the large uncertainties in the individual dates.

European wild ass *(Equus hydruntinus)*

The European wild ass lived across southern Europe, central Europe, western Asia, and parts of Siberia (Crees and Turvey 2014; Mead et al. 2007). It survived well into the Holocene, disappearing from Europe ~4500 cal BP and western Asia in the early Iron Age (~3000 cal BP) (Crees and Turvey 2014). Crees and Turvey (2014) identify LADs for Europe in southern Spain, the Danube basin, and Ukraine; they suggest earlier disappearances in southern France and Italy. They also produce estimates for extinction using optimal linear estimation (Solow 2005): 2530 cal BP (95% 2930–1315) cal BP globally, and 4658 cal BP (95% 4936–3780) cal BP for central Europe. The wild ass' very recent extinction and close association with higher-resolution archaeological sequences of the Neolithic and later lend

these extinction estimates confidence, despite being based on indirect radiocarbon dates. More problematic may be differentiating wild ass from domestic ass; Crees and Turvey (2014) highlight cases where genetic identification disagreed with the initial morphological assignment. With this caveat in mind, the OLE estimates are included as approximate extinctions.

Neanderthals *(Homo neanderthalensis)*

Neanderthals lived across Eurasia as far east as the Altai Mountains (Douka et al. 2019) and as far south as Gibraltar and, intermittently, the Levant (Barton et al. 1999; Shea 2008). They interbred with AMH and it has been estimated they overlapped with early AMH in Europe for ~2600–5400 years (Higham et al. 2014). Their extinction is complicated by transitional lithic industries 50–35 ka BP that may have been produced by Neanderthals, AMH, or both. Cooper et al. (2015) use data from Higham et al. (2014) to produce a GRIWM estimate for the extinction of Neanderthals of 41013–39528 (median 40472) cal BP, which agrees with the OxCal model in Higham et al. (2014) for termination of the Mousterian at 41030–39260 cal BP. The GRIWM estimate is used here.

Denisovans *(Homo* sp. *Altai)*

Denisovans are so far only known from Denisova Cave and Baishiya Karst Cave in Asia, where they have been dated to 195–52 ka BP (Chen et al. 2019; Douka et al. 2019; Reich et al. 2010). Whether Denisovans or AMH made Upper Palaeolithic artefacts in more recent layers (49–43 ka BP) is unclear. Denisovans have contributed genetic material to some AMH populations, implying they survived beyond AMH expansion into Eurasia. For now, Denisovan extinction is estimated at 50–40 ka cal BP in Asia, pending further finds.

Scimitar-toothed cat *(Homotherium latidens)*

Generally the scimitar-toothed cat is thought to have been extirpated from Europe before the last glacial cycle, with later survival up to ~36 ka BP in Beringia (Fox-Dobbs et al. 2008). Evidence of European survival beyond ~300 ka needs corroboration. *Homotherium* teeth from LP layers at Kent's Cavern, UK, have been attributed to redeposition by humans based on their fluorine/uranium profiles

(McFarlane and Lundberg 2013). Reumer et al. (2003) produced six dates from a *Homotherium* jaw dredged from the North Sea spanning 31.3–26.9 ka BP. The dates were not ultrafiltered, and the discrepencies between dates from the same individual are attributed to incomplete removal of conservation material (polyvinylacetate). In light of these concerns, LP presence of *Homotherium* in Eurasia cannot be confirmed. However, as the *Elasmotherium* story shows, robust dating of samples may yield surprises.

Mammoth *(Mammuthus primigenius)*

Mammoths occasionally ventured as far south as northern Spain (Álvarez-Lao and García 2010) and northern Italy (Mussi and Villa 2008). Included in Fig. 17.3 is a genetic clade restricted to northern Europe (Mammoth.III) from Palkopoulou et al. (2013), mainland mammoth dates without specific genomic affiliation from Cooper et al. (2015), and the refugial Wrangel Island mammoths from Vartanyan et al. (2008b). With the exception of Wrangel Island's late survivors, mammoths appear to have gone extinct arund 11–10 ka cal BP, with its last survivors near the Baltic Sea and Siberia (Stuart et al. 2002; Stuart et al. 2004). LADs for southern Europe were much earlier, with the latest dates from northern Spain ~20 ka cal BP (Álvarez-Lao and García 2010) and Italy ~38 ka cal BP (Stuart et al. 2002). Western Europe, central Europe, and the UK all have LADs 14.5–13.5 cal ka BP. The few dates from northernmost Europe (Scandinavia) suggest slightly earlier abandonment around 15.5 cal ka BP, with Baltic Sea mammoths dated to 11.6 ka cal BP perhaps representing a re-expansion from Siberia (Stuart et al. 2002). While mammoths continued to survive into the Holocene in Siberia, in Europe they were last found in the UK and central Europe, with the caveat that the very late mammoths from the Baltic coast may represent either continuity or recolonization.

Giant deer *(Megaloceros giganteus)*

There are a few direct dates of giant deer from southern Europe, with most dates from northern Europe and Siberia. The youngest dates from southern Europe come from Spain at 25.3 ka cal BP and from Italy at 29 ka cal BP (Stuart et al. 2004). Giant deer survived into the Holocene in western Russia and Siberia. GRIWM

Table A.3: Subregion GRIWM estimates for giant deer and a global estimate using all dates. Sources described in text.

Subregion	Dates (n)	2.5% min probability	median	97.5% max probability
Asia	33	6909	7289	7750
Central Europe	11	9696	12041	14055
Northern Europe	60	7029	7420	7641
Southern Europe	18	6507	7398	8304
global	122	7228	7467	7632

estimates using dates from Lister and Stuart (2019) and included citations show extinction across Europe and Asia around 7.4–7.2 ka cal BP (Table A.3).

Musk ox *(Ovibos moschatus)*

During the LP, musk ox spanned northern Eurasia, Beringia, and North America (Markova et al. 2015). Though reintroduced to Eurasia in the twentieth century, its natural range was restricted to North America's arctic and Greenland. Musk ox survived latest in Siberia, with Holocene dates either representing a refugial population or re-expansion from North America (Markova et al. 2015; MacPhee and Greenwood 2007). It has been found in Europe in the terminal Pleistocene in central/eastern Europe, though this evidence is based more on archaeological association than direct dates, which are few and produced in the 1990s or earlier (Markova et al. 2015; Pushkina and Raia 2008). It has been rarely found in southern Europe, including northern Spain, where a direct date from the 1990s produced a date of 20.7 ka cal BP (Álvarez-Lao and García 2010). Musk ox have also been found with Mousterian artefacts in Iberia, but they have not been found in Italy (Berto and Rubinato 2013).

A literature review did not find an exhaustive published radiocarbon dataset for musk ox, and Cooper et al. (2015) only model a specific genetic clade that went extinct in Eurasia ~46–36 ka cal BP. Therefore a table of dates from multiple sources has been compiled here to produce two extinction estimates: an estimate excluding the mid/late Holocene refugial population, and one including it. Only finite ages are included in the table, and dates with no location information were

Table A.4: GRIWM estimates for extinction of musk ox, depending on whether Siberian mid/late Holocene dates are included or excluded. Dates in text.

Dates (n)	2.5% min probability	median	97.5% max probability	Dataset
131	2098	2465	2801	With refuge
121	11802	12210	12640	Without refuge

excluded. Because dates from Europe are few and often produced pre-2000, no Europe-specific GRIWM estimate is made.

Table A.5: Radiocarbon dates of musk ox used in GRIWM estimates. Only includes dates with finite estimates after calibration.

Region	Lab code	Date BP	Error	Cal BP	Cal error	Source
W. Russia	GrA-39244	13680	60	16507	131	Markova et al. (2015)
W. Russia	GrA-42204	41860	460	45259	414	Markova et al. (2015)
Taimyr	B177044	44760	1700	47889	1225	MacPhee et al. (2005)
NESiberia	B193436	40270	450	43894	426	MacPhee et al. (2005)
Taimyr	B157714	2970	40	3135	67	MacPhee et al. (2005)
Taimyr	B148652	22550	100	26870	176	MacPhee et al. (2005)
Taimyr	B156194	22360	80	26651	179	MacPhee et al. (2005)
Wrangel	B193434	22280	120	26539	208	MacPhee et al. (2005)
Taimyr	B148627	19230	80	23177	144	MacPhee et al. (2005)
Taimyr	B148628	18310	70	22174	122	MacPhee et al. (2005)
Siberia	GIN-10259	3180	100	3396	125	MacPhee and Greenwood (2007)
Siberia	GIN-3131	12150	40	14031	72	MacPhee and Greenwood (2007)
Siberia	GIN-3803	2700	70	2825	68	MacPhee and Greenwood (2007)
Siberia	GIN-8248	15250	60	18519	83	MacPhee and Greenwood (2007)
Siberia	GIN-9872	3200	80	3425	97	MacPhee and Greenwood (2007)
Siberia	LU-1666	10750	90	12668	70	MacPhee and Greenwood (2007)
Siberia	LU-52	3790	80	4181	124	MacPhee and Greenwood (2007)
Taimyr	AAR11749	5364	49	6146	82	Campos et al. (2010b)
NESiberia	OxA-17076	51500	1200	51790	1285	Campos et al. (2010b)
Taimyr	OxA-17073	48100	800	48224	823	Campos et al. (2010b)
NESiberia Kolyma Lowland	AAR12096	46400	2700	48202	1222	Campos et al. (2010b)
Taimyr	AAR11751	45900	2300	48179	1202	Campos et al. (2010b)

Table A.5: Radiocarbon dates of musk ox used in GRIWM estimates. Only includes dates with finite estimates after calibration. *(continued)*

Region	Lab code	Date BP	Error	Cal BP	Cal error	Source
NE Siberia Indigirka Lowland	OxA-18864	45250	700	48602	742	Campos et al. (2010b)
New Siberian Islands	AAR11726	43400	1700	47038	1453	Campos et al. (2010b)
Taimyr		42590	1240	46301	1274	Campos et al. (2010b)
NE Siberia		42550	450	45845	437	Campos et al. (2010b)
Taimyr	OxA-17064	4082	30	4604	95	Campos et al. (2010b)
Urals (north)	AAR11734	39900	1000	43819	850	Campos et al. (2010b)
NESiberia Yana Lowland	AAR11740	39000	700	43018	560	Campos et al. (2010b)
Taimyr	OxA-17077	35830	240	40475	305	Campos et al. (2010b)
Taimyr	AAR12076	34150	600	38611	782	Campos et al. (2010b)
Taimyr	AAR12078	33850	600	38190	796	Campos et al. (2010b)
Taimyr	AAR11744	3372	43	3616	59	Campos et al. (2010b)
Taimyr	OxA-17063	2918	28	3062	52	Campos et al. (2010b)
Taimyr	OxA-17062	2756	27	2844	38	Campos et al. (2010b)
Urals (north)	AAR11762	27500	300	31410	285	Campos et al. (2010b)
Taimyr		27370	150	31240	110	Campos et al. (2010b)
Urals (middle)	AAR11716	26700	350	30830	280	Campos et al. (2010b)
Taimyr	AAR11715	25490	230	29652	336	Campos et al. (2010b)
Taimyr	AAR11721	25310	240	29408	325	Campos et al. (2010b)
Taimyr	OxA-17150	25300	110	29353	167	Campos et al. (2010b)
Taimyr	AAR11770	24940	230	29010	258	Campos et al. (2010b)
Urals (middle)	OxA-17082	24870	110	28903	152	Campos et al. (2010b)
Taimyr		24580	110	28617	132	Campos et al. (2010b)
Urals (north)	OxA-17080	24310	110	28351	161	Campos et al. (2010b)
Taimyr	AAR11745	24270	160	28302	196	Campos et al. (2010b)
Urals (north)	AAR12059	24150	210	28203	223	Campos et al. (2010b)
NESiberia	OxA-17061	24150	110	28186	163	Campos et al. (2010b)
Taimyr	AAR12069	24000	210	28085	216	Campos et al. (2010b)
Urals (north)	AAR11768	23860	190	27960	192	Campos et al. (2010b)
Urals (middle)	OxA-17081	23430	100	27614	92	Campos et al. (2010b)
Taimyr	AAR12064	23220	180	27481	142	Campos et al. (2010b)
Taimyr	AAR12071	22630	180	26933	233	Campos et al. (2010b)
Taymir		22550	100	26870	176	Campos et al. (2010b)
Urals (north)	OxA-17084	22470	90	26792	173	Campos et al. (2010b)
Urals (north)	OxA-17083	22170	90	26380	149	Campos et al. (2010b)
Urals (north)	AAR11712	22100	160	26342	206	Campos et al. (2010b)
Taimyr	AAR11750	21840	210	26117	217	Campos et al. (2010b)
Taimyr		21420	100	25742	102	Campos et al. (2010b)
Taimyr		21270	70	25617	101	Campos et al. (2010b)
Taimyr	AAR12070	21210	150	25542	163	Campos et al. (2010b)
Taimyr	AAR12066	21140	160	25475	177	Campos et al. (2010b)
Taimyr		21110	90	25455	123	Campos et al. (2010b)
Taimyr	OxA-17086	21060	90	25410	123	Campos et al. (2010b)

Table A.5: Radiocarbon dates of musk ox used in GRIWM estimates. Only includes dates with finite estimates after calibration. *(continued)*

Region	Lab code	Date BP	Error	Cal BP	Cal error	Source
Taimyr	AAR12079	21050	160	25386	194	Campos et al. (2010b)
Taimyr	AAR12067	20850	150	25127	237	Campos et al. (2010b)
Urals (middle)	AAR12055	20350	160	24503	249	Campos et al. (2010b)
Taimyr	AAR12074	20230	160	24333	225	Campos et al. (2010b)
Taimyr	OxA-17075	19925	80	23977	126	Campos et al. (2010b)
Taimyr	AAR11767	19860	130	23899	171	Campos et al. (2010b)
Taimyr	AAR12065	19840	140	23876	180	Campos et al. (2010b)
Taimyr	AAR12068	19790	160	23822	200	Campos et al. (2010b)
Taimyr	OxA-17148	19780	75	23812	125	Campos et al. (2010b)
Taimyr		19640	70	23664	127	Campos et al. (2010b)
Taimyr	AAR11759	19570	130	23575	190	Campos et al. (2010b)
Taimyr	AAR12073	19310	140	23260	192	Campos et al. (2010b)
Taimyr		19230	80	23177	144	Campos et al. (2010b)
Urals (north)	OxA-17078	19140	70	23070	140	Campos et al. (2010b)
Urals (north)	AAR12060	18960	130	22834	180	Campos et al. (2010b)
Taimyr	AAR11753	18830	170	22724	194	Campos et al. (2010b)
Taimyr	AAR12080	18750	120	22634	142	Campos et al. (2010b)
Urals (north)	AAR11766	18630	130	22517	150	Campos et al. (2010b)
Taimyr	AAR12086	18600	140	22481	165	Campos et al. (2010b)
Taimyr		18310	70	22174	122	Campos et al. (2010b)
Taimyr	AAR11717	18100	110	21949	165	Campos et al. (2010b)
Urals (middle)	AAR12054	17930	120	21713	171	Campos et al. (2010b)
Taimyr	OxA-17074	17900	65	21689	112	Campos et al. (2010b)
Taimyr	AAR11748	17690	120	21402	192	Campos et al. (2010b)
Urals (middle)	AAR12056	17660	120	21361	192	Campos et al. (2010b)
Urals (north)	AAR11713	17520	110	21174	175	Campos et al. (2010b)
Taimyr	AAR12052	16810	150	20283	190	Campos et al. (2010b)
Urals (north)	AAR11747	16310	110	19703	150	Campos et al. (2010b)
Taimyr	OxA-17072	16295	60	19683	106	Campos et al. (2010b)
Taimyr	AAR12077	16010	100	19317	143	Campos et al. (2010b)
Taimyr	OxA-17068	15875	60	19140	103	Campos et al. (2010b)
Taimyr	OxA-17065	15770	55	19020	81	Campos et al. (2010b)
Urals (north)	AAR11728	15750	100	19017	124	Campos et al. (2010b)
Urals (north)	AAR12061	15720	100	18983	121	Campos et al. (2010b)
Taimyr		15710	50	18952	69	Campos et al. (2010b)
Urals (north)	AAR11711	15680	90	18934	105	Campos et al. (2010b)
Taimyr	AAR12084	15380	100	18645	107	Campos et al. (2010b)
Taimyr	AAR12081	15300	90	18566	105	Campos et al. (2010b)
Taimyr	AAR12085	15100	100	18344	137	Campos et al. (2010b)
Taimyr	AAR12082	15020	90	18247	128	Campos et al. (2010b)
Urals (north)	AAR11746	14730	90	17923	125	Campos et al. (2010b)
Urals (north)	OxA-17085	14585	60	17766	97	Campos et al. (2010b)
Taimyr	AAR12083	14270	90	17372	140	Campos et al. (2010b)
Urals (north)	OxA-17079	14055	50	17085	114	Campos et al. (2010b)
Urals (north)	AAR11754	14000	80	16993	155	Campos et al. (2010b)

Table A.5: Radiocarbon dates of musk ox used in GRIWM estimates. Only includes dates with finite estimates after calibration. *(continued)*

Region	Lab code	Date BP	Error	Cal BP	Cal error	Source
NESiberia Yana Lowland	AAR11723	13270	80	15955	127	Campos et al. (2010b)
Taimyr	AAR11773	13125	80	15745	150	Campos et al. (2010b)
Taimyr	AAR12075	12965	80	15505	144	Campos et al. (2010b)
Taimyr	AAR12090	12830	80	15323	141	Campos et al. (2010b)
Urals (north)	AAR12058	10755	65	12679	44	Campos et al. (2010b)
Europe	AAR-4188	28490	350	32469	504	Bennike and Liljegren (2014)
Europe	LuS-9260	44000	1500	47476	1277	Bennike and Liljegren (2014)
Europe	Ua-2866	32000	1042	36395	1243	Bennike and Liljegren (2014)

Straight-tusked elephant *(Palaeoloxodon antiquus)*

After the Eemian, straight-tusk elephant appears to have retracted to southern Europe, but attempts to constrain its extinction have struggled with poor collagen preservation. The only direct radiocarbon dates considered reliable come from Cueva del Castillo in Spain, with one date background age (>47 ka BP) and the other 46600 ± 1400 cal BP (Stuart 2005). The samples were associated with Mousterian material and generally agree with the site chronology (Wood et al. 2018). *P. antiquus* has not been confidently associated with post-LGM archaeological material, and they may have gone extinct 50–40 ka cal BP (Stuart 2005).

Saiga antelope *(Saiga tartarica)*

Saiga antelope is today restricted to the central Asia, but at its maximum extent after the LGM it spanned England to the Yukon (Campos et al. 2010a; Nadachowski et al. 2016; Ratajczak et al. 2016). It did not inhabit very southern Europe, including the Iberian and Italian peninsulas. A distinct genetic subpopulation restricted to the Urals went extinct around 10 ka BP (Campos et al. 2010a); the extinction of this clade is modelled in Cooper et al. (2015). In Europe, *Saiga* LADs come from southern Poland 14–13.5 ka cal BP, the UK 14 ka cal BP, and central Germany 15.5 ka cal BP. Further south, three dates from France span 19.3–17.8 ka cal BP, and a number of indirect dates based on stratigraphic layers suggest the species

Table A.6: GRIWM estimate for extirpation of saiga antelope from Europe, not including Urals or Siberian dates. All dates from Nadachowski et al. (2016).

Dates (n)	2.5% min probability	median	97.5% max probability
17	12272	12611	13136

reached its southernmost extent at the northern Pyrenees around then (Nadachowski et al. 2016). It has a very late presence in Crimea, where it has been dated to the Holocene transition (Péan et al. 2013). It has been suggested that *Saiga* repeatedly expanded into Europe from Siberia throughout the LP (Nadachowski et al. 2016); alternatively continuity may be lost in the patchy chronological record or a European refuge existed alongside the Siberian one.

For this project, a Europe-only GRIWM estimate has been produced akin to the leopard extirpation. Subregions have not been modelled due to the small dataset, but the dates suggest a retraction northwards after ~16 ka cal BP, with extirpation from Europe (excluding Crimea) 13.1–12.2 ka cal BP (Table A.6).

Screw-horn antelope *(Spirocerus kiakhtensis)*

Spirocerus lived as far west as Kazakhstan, but most finds are from Lake Baikal and the Transbaikal region (Kalmykov et al. 2014). While found in LP layers in association with human artefacts, the antelope's extinction within the last 100 ky is unclear (Erbajeva and Alexeeva 2000). Recently T. Higham and the PalaeoChron team produced two direct dates of *Spirocerus* of ~42–41 ka BP from an archaeological site in the Transbaikal region (Higham pers. comm.), but further work is needed to establish this species' LAD. As there are insufficient dates for modelling and the species never reached Europe, *Spirocerus* is not further discussed.

Narrow-nosed rhinoceros *(Stephanorhinus hemitoechus)* and Merck's rhinoceros *(Stephanorhinus kirchbergensis)*

Stephanorhinus occupied northern Europe, including the UK, in the Middle Pleistocene, but during the last glaciation <100 ka retracted to southern Europe, including southern France, Iberia, Italy, Bulgaria, and the Balkans (van Asperen

Table A.7: Direct dates of *S. hemitoechus* from El Castillo, Spain. Dates are from de Quirós et al. (2006) and Wood (2011).

Archaeology	OxA	Date BP	Error	Cal BP	Cal error	Code	%C	CN
Magdalenian?	OxA-10296	31800	700	35900	840	AF*	7.7	3.6
Mousterian	OxA-10233	42100	1500	46000	1500	AF*	42.6	3.3
Mousterian	OxA-10328	45700	1700	>45700		AF*	43.2	3.4
Mousterian	OxA-10327	>45700				AF*	39.9	3.7

and Kahlke 2015; Cerdeño 1990; Pushkina and Raia 2008). *S. kirchbergensis* may have gone extinct earlier than *S. hemitoechus*, with the former last documented in Italy in MIS4 (71–57 ka) (or, less likely, MIS3) (van Asperen and Kahlke 2015; Berto and Rubinato 2013; Pandolfi and Tagliacozzo 2015). *S. hemitoechus* has been found in Italy through MIS4 and at a site in Monaco attributed to MIS3 (57–29 ka) (van Asperen and Kahlke 2015; Pandolfi and Tagliacozzo 2015). Though found with Mousterian artefacts across Spain, *S. hemitoechus* has not been confidently associated with UP material (Cerdeño 1990; Stuart and Lister 2007).

The only direct dates found for this project are four ultrafiltered dates Spain (de Quirós et al. 2006; Wood 2011) (Table A.7). Of these, two have high CN ratios, and one of them also has a very low %C. Through stratigraphic association, Stuart and Lister (2007) suggest a possible LAD at Bacho Kiro, Bulgaria of 37.6 ka BP, but the associated charcoal date was produced in the 1980s.

With no direct dates and a likely extinction beyond radiocarbon's limit, *S. kirchbergensis* is not considered further here. There are insufficient dates for modelling the extinction of *S. hemitoechus*. If the indirect charcoal date and the poor-quality El Castillo dates are rejected, then two dates remain. Of these, one calibrates >50 ka cal BP; the only finite date is 46000 ± 1500 cal BP. Extinction at ~55–45 ka cal BP agrees with its stratigraphic disappearance across southern Europe in MIS3 and is here tentatively suggested as its extinction.

Cave bear *(Ursus spelaeus)*

Cave bears lived across most of Europe, excluding northernmost Europe, the UK, and southern Iberia. They have been found in northern Iberia, Italy, and

Table A.8: Subregion GRIWM estimates for cave bear and a global estimate using all dates. Dates are from Baca et al. (2016) and Pacher and Stuart (2009).

Subregion	Dates (n)	2.5% min probability	median	97.5% max probability
Asia	47	21873	23084	24078
Central Europe	41	17286	25516	26312
Northern Europe	4	22361	23388	24581
Southern Europe	47	21543	21881	22219
global	139	19528	23194	23698

Greece; they also lived north of the Black Sea and throughout the Urals (Mackiewicz et al. 2017; Pacher and Stuart 2009). They appear to have gone extinct relatively abruptly across Europe. When radiocarbon datasets published in Baca et al. (2016) and Pacher and Stuart (2009) are combined, the resulting GRIWM estimates for subregions overlap and the global estimate for extinction is around the LGM at 23.7–19.5 ka cal BP (Fig. 17.3).

Cave bear's GRIWM estimate for southern Europe is younger than for northern Europe (Table A.8), but the northern Europe estimate is based on just four dates from southern Poland, and the species is generally rare so far north (Pacher and Stuart 2009). The central Europe estimate has a long tail that does not agree with the dataset (LAD ~26 ka cal BP); the median is more reflective. Looking at LADs as well as the GRIWM estimates, cave bears appear to have last survived in northern Italy, Croatia, and the Urals, with LADs of these regions ~3000 years younger than the LADs for central Europe. They abandon northern Spain and peninsular Italy earlier (Mackiewicz et al. 2017), hinting at contraction towards south-central Europe.

B
Sites sampled for this project

B.1 Successfully dated

Castelcivita

Castelcivita in Salerno, Italy, contains a long archaeological sequence from the MP to UP, including the Uluzzian (Douka et al. 2014; Gambassini 1997; Higham et al. 2014). It contains carnivores including stratigraphically late appearances of leopards. Four cave hyenas and two leopards were sampled.

Equi

Grotte di Equi, located north of the Apuane Alps in Italy, has an exceptional number and proportion of carnivores (90% of fauna), including over 200 leopards (Ghezzo and Rook 2015). The site has been periodically excavated since 1909, including ongoing excavations since 2009 (Ghezzo et al. 2014). Five dates were previously obtained (Bigagli et al. 2013; Ghezzo and Rook 2015). One leopard date showed a seeming layer inversion (33 ka above the 27 ka layer). The authors suggested it may be due to mislabelling of the specimen (Bigagli et al. 2013). Some samples from the early excavations are well labelled but a significant number lack contextual information, so direct dating of specimens is essential. Twenty-six samples were screened for %N and the highest-%N samples drilled for radiocarbon dating.

Kozarnica

Kozarnica Cave, Bulgaria contains a sequence from the Lower Pleistocene through human occupation (Guadelli 2011; Sirakov et al. 2010). The Upper Pleistocene sequence is unusual for its latitude as it contains many temperate species and few cold-type species, suggesting the region may have had an unusually mild microclimate. The site has undergone extensive archaeological excavation and further radiocarbon dating has been completed (Hopkins pers. comm.). Cave hyenas and a lion were sampled.

Muracci

Area 3 (Cisterna di latina, Latium, Italy), is one of multiple caves in the Cava Muracci quarry that has been periodically excavated since the 1950s (Gatta and Rolfo 2017). Middle and Upper Palaeolithic artefacts have been found, and while some of the excavation areas may have been mixed during flooding events, Area 3 is stratigraphically intact (Gatta and Rolfo 2017, pg. 112). This cave contains hyena coprolites, skeletal remains, and chewed bones, suggesting it was a hyena den, but carnivores were found in other excavation areas too. Before this project, Cava Muracci already had radiocarbon dates from coprolites and faunal bones. However, the coprolites dates are exceptionally young, the bones were not ultrafiltered, and dates came from only two of seven excavation areas. Eleven samples were taken.

La Sassa

La Sassa in Sonnio, central Italy is a karstic cave discovered in 2015 (Gatta pers. comm.). A radiocarbon date (30210 ± 180 BP, GrA-64830) from a bear femur was previously obtained. This bone was found in a thick layer containing multiple carnivore species, including bear, hyena, wolf, and cave lion. Multiple carnivores in the same layer is otherwise unknown in central Italy (Gatta pers. comm.), and so direct dating of the fauna was important in understanding whether they were coeval and in what climate they might have coexisted. Though one date had already been obtained for a bear, the sample here came from a different individual. Skeletal analysis of the bears from Room 6 shows two individuals represented. Stratigraphic associations between rooms have not been established

and mixing has not been precluded, and so direct dates from the carnivores were crucial. Eight samples were taken.

Manastira

Manastira, Bulgaria is a hyena den that also contained chewed herbivore bones and teeth attributed to modern humans (Guadelli pers. comm.). The teeth were polished, suggesting hyenas may have digested them. Radiocarbon dating was important to establish whether the site formed rapidly or represented a longer span where hyenas and humans alternated use. The potentially human teeth were too small to date, but 16 samples of hyenas and chewed herbivores were taken.

Redaka II

Redaka II, Bulgaria was excavated as a rescue operation and contained hyena remains, chewed bones, and possibly human remains (Fernandez and Guadelli 2008; Guadelli et al. 2013). The cave stratigraphy is complex and there is possible mixing of material. Twelve samples were taken.

Vasil Levski

Vasil Levski, Bulgaria contained an Upper Palaeolithic archaeological sequence and was sampled as part of the Palaeochron project (Hopkins pers. comm.). Two hyena teeth recovered during the excavation were kindly provided for radiocarbon dating.

Zafarraya

Zafarraya is a cave from Malaga, Spain that contains a Middle Palaeolithic archaeological sequence with Neanderthal remains. The precise chronology remains contested, and previous work showed significant variation in bone preservation (Wood 2011; Wood et al. 2013a). Palaeochron obtained a large number of fragmented bones from the entire Pleistocene sequence (layers UA to UE), enabling this project's %N investigation. These samples were mostly unidentifiable fragments, but previous analyses found several mammal species, including carnivores and herbivores (Barroso Ruiz 2010; Barroso Ruiz 2003; Geraads 1995; Geraads et al. 2013). Previous work struggled to find bones with sufficient collagen preservation, and the hope was

that large scale screening and identification of species with ZooMS could overcome the site's poor preservation.

B.2 Failed to be dated

Cala

Grotta della Cala, Salerno, Italy contains a MP and UP sequence and, by stratigraphic association, late-surviving leopards (Benini et al. 1997; Borgia 2008). Leopards were sampled for this project.

Carigüela

Carigüela (or Carihuela) is a cave in the very south of Spain with a pollen record, Neanderthal remains, and an abundance of fauna (Carrión 1992; Carrión et al. 1998; Fernández et al. 2007; de la Peña 2013). Excavations have been conducted since the 1960s, but the death of an excavator (Fryxell et al. 1970) left questions about how the stratigraphies of different excavation seasons relate. A large corpus of radiocarbon, ESR, and U-series dates have been produced (Carrión 1992; Carrión et al. 1998; Carrión et al. 2019; de la Peña 2013; Volterra 2000), but the radiocarbon dates were produced from bulk soil or combined batches of bones, both of which are problematic (Wood et al. 2013b).

The only samples in this project with sufficient %N, taken from human remains, had been treated with conservation material and failed to produce collagen (Comeskey pers. comm.). All the faunal bones had extremely low %N and the few extracted produced no collagen.

Cucigliana

Grotta Cucigliana, located near Monte Pisano, Italy was discovered in the nineteenth century. Hyenas dominate the carnivore assemblage, but wolves, cave and brown bears, and leopards were also present (Farina 2011). No lions were recorded. Only hyenas were sampled for this project.

Greece and Crete: Akrotiri, Tilos

Dwarf elephants and mammoths from Mediterranean islands have little chronological constraint on their extinctions, with dates from the apatite fraction of dwarf elephant bones suggesting survival up to human arrival (Herridge and Lister 2012; Poulakakis et al. 2002; Stathopoulou and Theodorou 2001; Theodorou and Symeonides 2001). Many samples, including non-elephant fauna in association, were sampled here. Unfortunately, despite some evidence of slight protein preservation and obtaining AG yields >5 mg, combustion found the samples did not contain sufficient carbon.

Paglicci

Grotta Paglicci, Apulia, Italy contains an Upper Palaeolithic archaeological sequence and evidence of use as a hyena den (Crezzini et al. 2016). Hyenas were sampled for this project.

Rincones

Los Rincones, Zaragoza, Spain is a mountain cave with many leopards and the bones of prey (Sauqué et al. 2014; Sauqué et al. 2016b; Sauqué et al. 2016a). It also contained brown bears, and it was wondered if the two coexisted or if the bears represent a later accumulation phase. Both leopards and bears were sampled.

Santi

Grotta dei Santi, Tuscany, Italy, contained both hyenas and leopards (but not lions), which were sampled for this project. A more recent attempt to date bone at the site also failed to produce sufficient collagen, though the site has OSL and charcoal dates (Moroni et al. 2018).

C Experimental results data

C.1 %N Zafarraya

Table C.1: Results of %N and %yield of bone samples from Zafarraya (chapter 8). Information is included on whether the sample was registered for radiocarbon dating (P code). Does not include previously reported %N results in Wood et al. (2013a). Samples with %yield have their result categorised depending on whether the %N threshold (positive $\geqslant$0.76, negative <0.76) correctly predicted whether the %yield would be >1.

Sample	P code	%N	%yield	Result
1	P43021	0.866	0.001	False positive
2		0.116	0.002	True negative
3		0.503	0.014	True negative
4	P43020	0.950	0.030	False positive
5		0.048	0.045	True negative
6		0.057	0.052	True negative
7		0.168	0.111	True negative
8		0.055	0.113	True negative
9		0.371	0.310	True negative
10	P43016	0.665	0.400	True negative
11		0.552	0.431	True negative
12		0.108	0.487	True negative
13	P42237	0.870	0.600	False positive
14		0.438	0.614	True negative
15		0.465	0.694	True negative
16	P42232	1.060	0.700	False positive

Table C.1: Results of %N and %yield of bone samples from Zafarraya (chapter 8). Information is included on whether the sample was registered for radiocarbon dating (P code). Does not include previously reported %N results in Wood et al. (2013a). Samples with %yield have their result categorised depending on whether the %N threshold (positive ⩾0.76, negative <0.76) correctly predicted whether the %yield would be >1. *(continued)*

Sample	P code	%N	%yield	Result
17		0.525	0.755	True negative
18		0.268	0.764	True negative
19	P42231	0.990	0.800	False positive
20	P42235	1.110	0.900	False positive
21	P43018	0.678	0.900	True negative
22	P43017	0.559	0.900	True negative
23		0.615	0.962	True negative
24		0.217	0.970	True negative
25	P42801	0.810	1.100	True positive
26	P42798	0.280	1.100	False negative
27		0.207	1.134	False negative
28		1.169	1.261	True positive
29	P42234	1.620	1.300	True positive
30	P42227	0.995	1.300	True positive
31	P42800	0.960	1.300	True positive
32	P42796	0.460	1.300	False negative
33		0.485	1.755	False negative
34	P42233	1.220	1.900	True positive
35		0.575	2.075	False negative
36		0.340	2.077	False negative
37	P42230	1.100	2.300	True positive
38	P43024	0.995	2.300	True positive
39	P43019	0.598	2.400	False negative
40	P42228	1.470	2.500	True positive
41	P43022	1.096	2.600	True positive
42	P42225	1.950	2.900	True positive
43	P43026	1.378	2.900	True positive
44	P43023	1.056	2.900	True positive
45	P42226	0.930	2.900	True positive
46		0.952	2.992	True positive
47	P42229	0.990	3.400	True positive
48	P43025	0.735	4.500	False negative
49	P42236	1.410	7.400	True positive
50		3.197	9.395	True positive
51		1.240		

Table C.1: Results of %N and %yield of bone samples from Zafarraya (chapter 8). Information is included on whether the sample was registered for radiocarbon dating (P code). Does not include previously reported %N results in Wood et al. (2013a). Samples with %yield have their result categorised depending on whether the %N threshold (positive $\geqslant$0.76, negative <0.76) correctly predicted whether the %yield would be >1. *(continued)*

Sample	P code	%N	%yield	Result
52		0.990		
53		0.960		
54		0.954		
55		0.820		
56		0.756		
57		0.710		
58		0.700		
59		0.696		
60		0.680		
61		0.664		
62		0.640		
63		0.630		
64		0.610		
65		0.600		
66		0.600		
67		0.563		
68		0.550		
69		0.542		
70		0.540		
71		0.537		
72		0.525		
73		0.520		
74		0.520		
75		0.516		
76		0.508		
77		0.507		
78		0.500		
79		0.500		
80		0.500		
81		0.490		
82		0.454		
83		0.454		
84		0.440		
85		0.432		
86		0.426		

Table C.1: Results of %N and %yield of bone samples from Zafarraya (chapter 8). Information is included on whether the sample was registered for radiocarbon dating (P code). Does not include previously reported %N results in Wood et al. (2013a). Samples with %yield have their result categorised depending on whether the %N threshold (positive ⩾0.76, negative <0.76) correctly predicted whether the %yield would be >1. *(continued)*

Sample	P code	%N	%yield	Result
87		0.422		
88		0.420		
89		0.420		
90		0.410		
91		0.410		
92		0.400		
93		0.400		
94		0.400		
95		0.399		
96		0.395		
97		0.394		
98		0.393		
99		0.390		
100		0.387		
101		0.385		
102		0.380		
103		0.369		
104		0.360		
105		0.360		
106		0.355		
107		0.343		
108		0.342		
109		0.339		
110		0.337		
111		0.337		
112		0.333		
113		0.325		
114		0.320		
115		0.320		
116		0.315		
117		0.315		
118		0.314		
119		0.310		
120		0.300		
121		0.296		

Table C.1: Results of %N and %yield of bone samples from Zafarraya (chapter 8). Information is included on whether the sample was registered for radiocarbon dating (P code). Does not include previously reported %N results in Wood et al. (2013a). Samples with %yield have their result categorised depending on whether the %N threshold (positive $\geqslant$0.76, negative <0.76) correctly predicted whether the %yield would be >1. *(continued)*

Sample	P code	%N	%yield	Result
122		0.293		
123		0.291		
124		0.282		
125		0.280		
126		0.280		
127		0.275		
128		0.270		
129		0.268		
130		0.263		
131		0.260		
132		0.260		
133		0.260		
134		0.254		
135		0.250		
136		0.246		
137		0.242		
138		0.240		
139		0.240		
140		0.240		
141		0.240		
142		0.236		
143		0.235		
144		0.233		
145		0.230		
146		0.230		
147		0.221		
148		0.220		
149		0.215		
150		0.210		
151		0.205		
152		0.200		
153		0.200		
154		0.200		
155		0.200		
156		0.198		

Table C.1: Results of %N and %yield of bone samples from Zafarraya (chapter 8). Information is included on whether the sample was registered for radiocarbon dating (P code). Does not include previously reported %N results in Wood et al. (2013a). Samples with %yield have their result categorised depending on whether the %N threshold (positive ⩾0.76, negative <0.76) correctly predicted whether the %yield would be >1. *(continued)*

Sample	P code	%N	%yield	Result
157		0.195		
158		0.191		
159		0.190		
160		0.190		
161		0.190		
162		0.190		
163		0.190		
164		0.180		
165		0.180		
166		0.180		
167		0.180		
168		0.170		
169		0.169		
170		0.162		
171		0.162		
172		0.160		
173		0.160		
174		0.154		
175		0.153		
176		0.150		
177		0.147		
178		0.143		
179		0.140		
180		0.138		
181		0.130		
182		0.130		
183		0.130		
184		0.120		
185		0.120		
186		0.118		
187		0.114		
188		0.113		
189		0.113		
190		0.110		
191		0.106		

Table C.1: Results of %N and %yield of bone samples from Zafarraya (chapter 8). Information is included on whether the sample was registered for radiocarbon dating (P code). Does not include previously reported %N results in Wood et al. (2013a). Samples with %yield have their result categorised depending on whether the %N threshold (positive $\geqslant$0.76, negative <0.76) correctly predicted whether the %yield would be >1. *(continued)*

Sample	P code	%N	%yield	Result
192		0.103		
193		0.100		
194		0.100		
195		0.100		
196		0.097		
197		0.095		
198		0.090		
199		0.090		
200		0.086		
201		0.085		
202		0.084		
203		0.081		
204		0.080		
205		0.080		
206		0.077		
207		0.073		
208		0.072		
209		0.070		
210		0.070		
211		0.068		
212		0.063		
213		0.060		
214		0.060		
215		0.058		
216		0.058		
217		0.055		
218		0.051		
219		0.050		
220		0.044		
221		0.044		
222		0.044		
223		0.040		
224		0.040		
225		0.040		
226		0.032		

Table C.1: Results of %N and %yield of bone samples from Zafarraya (chapter 8). Information is included on whether the sample was registered for radiocarbon dating (P code). Does not include previously reported %N results in Wood et al. (2013a). Samples with %yield have their result categorised depending on whether the %N threshold (positive ⩾0.76, negative <0.76) correctly predicted whether the %yield would be >1. *(continued)*

Sample	P code	%N	%yield	Result
227		0.030		
228		0.029		
229		0.026		

C.2 Dialysis

Table C.2: Results of dialysis extractions of bone samples (chapter 11). Details of extraction methods, including the modified ABA protocol (here "HCl"), are in chapter 4.4. Starting sample weight and resulting yields are in mg. The Ash Bend samples were extracted as separate aliquots to compare yields of larger samples. The dialysis yield of Equi 5438 was too small to analyse for %N and CN.

Sample	Weight	HCl yield	Dialysis yield	HCl %yield	Dialysis %yield	%N	CN
Ash Bend 19651	311.98	37.37		11.98			
Ash Bend 19651	292.66	37.60		12.85		0.16	3.24
Ash Bend 19651	294.17	33.53		11.40			
Ash Bend 19651	302.12		15.75				
Ash Bend 19651	300.55		18.02			0.08	3.48
Ash Bend 19651	291.56		17.43				
CM 3	940.00	28.07	3.48	2.99	0.37	0.09	5.05
Cucigliana 6596	910.00	2.95	2.90	0.32	0.32	1.22	12.50
Equi 102873	750.00	112.17	1.17	14.96	0.16	0.07	5.33
Equi 5438	950.00	34.65	0.68	3.65	0.07		
Latton 1	490.00	14.13	4.61	2.88	0.94	2.97	4.79
Latton 2	460.00	29.10	1.55	6.33	0.34	8.08	3.79
Latton 3	470.00	27.14	3.13	5.77	0.67	6.04	4.03
Latton 4	470.00	23.89	8.22	5.08	1.75	4.70	3.77
Latton 5	470.00	22.79	10.52	4.85	2.24	5.68	3.73
Latton 6	470.00	21.97	12.44	4.67	2.65	5.50	3.72
Latton 7	470.00	24.19	16.40	5.15	3.49	10.62	3.66
Santi 1	940.00	4.04	3.34	0.43	0.36	1.12	10.44
Santi 2	800.00	0.60	3.32	0.08	0.42	1.56	12.68
Santi 3	1030.00	6.68	1.21	0.65	0.12	0.96	12.11
Santi 4	1070.00	1.91	1.02	0.18	0.10	1.48	8.70
Vasil C	500.00	4.13	5.93	0.83	1.19	6.10	4.09

C.3 EDTA

C.3.1 Agitation and bone grain size

Table C.3: Comparison of EDTA- and HCl-extracted collagen from Latton bone under different conditions (chapter 12). Conditions (agitated, not agitated, overnight) are detailed in chapter 4.5. Sample start weight and yield in mg. Two samples have no yields due to laboratory mistakes (test tubes broken).

Agitation	Grain size	Solution	Start weight	Yield	%yield
Agitated	crushed	EDTA	520	24.08	4.63
Agitated	crushed	EDTA	480	22.41	4.67
Agitated	crushed	EDTA	500	18.38	3.68
Agitated	powder	EDTA	450	17.10	3.80
Agitated	powder	EDTA	500	26.65	5.33
Agitated	powder	EDTA	500	26.84	5.37
Not agitated	crushed	EDTA	510	22.22	4.36
Not agitated	crushed	EDTA	490	15.57	3.18
Not agitated	crushed	EDTA	490	15.83	3.23
Not agitated	powder	EDTA	520	19.68	3.78
Not agitated	powder	EDTA	500	24.93	4.99
Not agitated	powder	EDTA	520	28.88	5.55
Overnight	crushed	EDTA	480	21.53	4.49
Overnight	crushed	EDTA	500	16.88	3.38
Overnight	powder	EDTA	460	17.13	3.72
Overnight	powder	EDTA	500	11.56	2.31
Agitated	crushed	HCl	480	33.69	7.02
Agitated	crushed	HCl	490	30.82	6.29
Agitated	crushed	HCl	510	36.35	7.13
Agitated	crushed	HCl	500	14.41	3.00
Agitated	crushed	HCl	500	17.09	3.00
Agitated	crushed	HCl	500	15.54	3.00
Agitated	powder	HCl	480	6.36	1.33
Agitated	powder	HCl	530	12.17	2.30
Agitated	powder	HCl			
Agitated	powder	HCl	500	11.36	2.00
Agitated	powder	HCl	500	9.24	2.00
Agitated	powder	HCl	500	9.24	2.00
Not agitated	crushed	HCl	540	90.00	16.67
Not agitated	crushed	HCl	470	51.01	10.85
Not agitated	crushed	HCl	500	57.52	11.50
Not agitated	crushed	HCl	500	73.50	15.00

Table C.3: Comparison of EDTA- and HCl-extracted collagen from Latton bone under different conditions (chapter 12). Conditions (agitated, not agitated, overnight) are detailed in chapter 4.5. Sample start weight and yield in mg. Two samples have no yields due to laboratory mistakes (test tubes broken). *(continued)*

Agitation	Grain size	Solution	Start weight	Yield	%yield
Not agitated	crushed	HCl	500	66.00	13.00
Not agitated	crushed	HCl	500	49.86	10.00
Not agitated	powder	HCl	480	42.04	8.76
Not agitated	powder	HCl	500	49.64	9.93
Not agitated	powder	HCl	510	76.28	14.96
Not agitated	powder	HCl	500	37.26	7.00
Not agitated	powder	HCl	500	31.77	6.00
Not agitated	powder	HCl	500	50.21	10.00
Overnight	crushed	HCl	470	73.41	15.62
Overnight	crushed	HCl	500	30.19	6.04
Overnight	crushed	HCl			
Overnight	crushed	HCl	500	34.05	6.81
Overnight	crushed	HCl	500	35.90	7.18
Overnight	crushed	HCl	500	25.01	5.00
Overnight	crushed	HCl	500	39.20	7.84
Overnight	powder	HCl	520	38.54	7.41
Overnight	powder	HCl	500	55.38	11.00
Overnight	powder	HCl	500	56.57	11.00

C.3.2 Carbon and %N content

Table C.4: Percentages nitrogen and carbon (%N and %C) and the atomic carbon:nitrogen (CN) ratio of EDTA-extracted collagen from Latton bone (chapter 12.5). Pretreatment refers to minutes extracted in microwave, or else the AG / acid-only extraction used as comparison.

Pretreatment	Sample	%N	%C	CN
10	10-1	8.19	23.46	3.34
10	10-2	5.38	15.70	3.40
180	180-1	11.50	32.95	3.34
180	180-2	10.54	30.53	3.38
270	270-1	11.72	34.22	3.41
270	270-2	11.64	33.14	3.32
30	30-1	8.71	25.16	3.37
30	30-2	8.41	23.83	3.31
360	360-1	11.87	33.62	3.31
360	360-2	13.20	37.43	3.31
60	60-1	8.03	25.07	3.64
60	60-2	9.10	26.36	3.38
90	90-1	10.51	30.47	3.38
90	90-2	10.27	29.70	3.37
Acid-only	Acid1	15.18	42.00	3.23
Acid-only	Acid2	14.05	38.96	3.24
AG	AG1	14.45	40.14	3.24
AG	AG2	13.93	38.60	3.23

C.3.3 Microwave yields

Table C.5: Yields of Latton bone decalcified in 0.5 M EDTA in the microwave for different durations. Also includes yields from AG and acid-only extractions from the same aliquot of bone. Weight and yield in mg; time in minutes. Grain size denotes whether bone was crushed or drilled into a homogenized powder. Drill batch refers to the sample of bone, as the Latton bone was sampled multiple times over the course of experiments.

Sample	Grain size	Time	Batch	Weight	Yield	%yield
Latton	Powder	10	1	197.21	19.11	9.69
Latton	Powder	10	1	197.61	18.16	9.19
Latton	Powder	10	1	196.61	16.66	8.47
Latton	Bone	180	1	207.75	8.77	4.22
Latton	Bone	180	1	202.3	8.93	4.41
Latton	Bone	180	1	210.02	6.6	3.14
Latton	Bone	180	1	202.01	8.09	4.00
Latton	Powder	180	1	203.7	26.13	12.83
Latton	Powder	180	1	206.69	21.48	10.39
Latton	Bone	270	1	202.52	11.95	5.90
Latton	Bone	270	1	194.45	10.57	5.44
Latton	Powder	270	1	202.07	25.49	12.61
Latton	Powder	270	1	203.05	34.83	17.15
Latton	Powder	30	1	204.04	18.36	9.00
Latton	Powder	30	1	206.83	16.15	7.81
Latton	Powder	30	1	202.95	14.88	7.33
Latton	Bone	360	1	204.38	6.37	3.12
Latton	Bone	360	1	236.76	7.48	3.16
Latton	Powder	360	1	194.73	25.23	12.96
Latton	Powder	360	1	193.25	26.49	13.71
Latton	Powder	60	1	199.59	17.81	8.92
Latton	Powder	60	1	200.91	16.1	8.01
Latton	Powder	60	1	199.1	14.67	7.37
Latton	Bone	90	1	194.58	5.48	2.82
Latton	Bone	90	1	211.72	11.11	5.25
Latton	Powder	90	1	203.9	26.2	12.85
Latton	Powder	90	1	199.3	24.25	12.17
Latton	Powder	90	1	197.1	18.96	9.62
Latton	Powder	Acid only	1	213.97	22.38	10.46
Latton	Powder	Acid only	1	195.16	18.41	9.43
Latton	Powder	Acid only	1	208.1	19.37	9.31
Latton	Bone	AG	1	179.16	17.98	10.04
Latton	Bone	AG	1	192.05	13.12	6.83
Latton	Bone	AG	1	289.41	28.93	10.00
Latton	Powder	AG	1	207.08	14.51	7.01
Latton	Powder	AG	1	203.61	16.05	7.88
Latton	Powder	AG	1	197.5	15.16	7.68
Latton	Powder	Bench 90 min	1	208.29	13.75	6.60
Latton	Powder	Bench 90 min	1	201.04	14.11	7.02
Latton	Powder	Bench 90 min	1	199.56	15.14	7.59

Table C.5: Yields of Latton bone decalcified in 0.5 M EDTA in the microwave for different durations. Also includes yields from AG and acid-only extractions from the same aliquot of bone. Weight and yield in mg; time in minutes. Grain size denotes whether bone was crushed or drilled into a homogenized powder. Drill batch refers to the sample of bone, as the Latton bone was sampled multiple times over the course of experiments. *(continued)*

Sample	Grain size	Time	Batch	Weight	Yield	%yield
Latton	Powder	Bench overnight	1	199.28	12.92	6.48
Latton	Powder	Bench overnight	1	197.8	25.6	12.94
Latton	Bone	Bench overnight	1	205.57	11.22	5.46
Latton	Bone	Bench overnight	1	211	11.06	5.24
Latton	Powder	Bench overnight	1	197.82	25.79	13.04
Latton	Powder	Bench overnight	1	197.23	16.92	8.58
Latton	Bone	Bench overnight	1	252.45	12.51	4.96
Latton	Bone	Bench overnight	1	238.42	14.27	5.99
Latton	Bone	Bench overnight	1	192.04	12.89	6.71
Latton	Powder	Bench overnight	1	199.81	15.89	7.95
Latton	Powder	Bench overnight	1	207.51	13.91	6.70
Latton	Powder	Bench overnight	1	Lost in centrifuge	Lost in centrifuge	
Latton	Powder	10	2	203.75	3.5	1.72
Latton	Powder	10	2	200.81	2.56	1.27
Latton	Powder	180	2	199.2	6.84	3.43
Latton	Powder	180	2	201.43	7.03	3.49
Latton	Powder	180	2	202.32	7.21	3.56
Latton	Powder	180	2	204.37	6.08	2.97
Latton	Powder	180	2	200.63	6.35	3.17
Latton	Powder	180	2	194.68	5.41	2.78
Latton	Powder	180	2	196.73	6.73	3.42
Latton	Powder	180	2	204.93	6.73	3.28
Latton	Powder	270	2	201.82	7.87	3.90
Latton	Powder	270	2	198.62	6.6	3.32
Latton	Powder	270	2	203.88	10.6	5.20
Latton	Powder	270	2	198.6	6.69	3.37
Latton	Powder	270	2	206.23	6.84	3.32
Latton	Powder	270	2	205.83	7.47	3.63
Latton	Powder	270	2	197.4	7.75	3.93
Latton	Powder	30	2	198.52	5.87	2.96
Latton	Powder	30	2	206.96	7.22	3.49
Latton	Powder	30	2	204	4.27	2.09
Latton	Powder	30	2	200.82	5.67	2.82
Latton	Powder	30	2	198.33	4.81	2.43
Latton	Powder	360	2	201.4	10.85	5.39
Latton	Powder	360	2	199.85	9.68	4.84
Latton	Powder	360	2	200.1	10.15	5.07
Latton	Powder	360	2	204.05	7.55	3.70
Latton	Powder	360	2	204.77	7.72	3.77
Latton	Powder	45	2	201.48	5.56	2.76

Table C.5: Yields of Latton bone decalcified in 0.5 M EDTA in the microwave for different durations. Also includes yields from AG and acid-only extractions from the same aliquot of bone. Weight and yield in mg; time in minutes. Grain size denotes whether bone was crushed or drilled into a homogenized powder. Drill batch refers to the sample of bone, as the Latton bone was sampled multiple times over the course of experiments. *(continued)*

Sample	Grain size	Time	Batch	Weight	Yield	%yield
Latton	Powder	45	2	204.93	5.21	2.54
Latton	Powder	60	2	197.49	6.4	3.24
Latton	Powder	60	2	199.99	5.26	2.63
Latton	Powder	60	2	196.18	4.41	2.25
Latton	Powder	60	2	194.04	6.18	3.18
Latton	Powder	60	2	203.96	5.17	2.53
Latton	Powder	720	2	201.32	7.85	3.90
Latton	Powder	720	2	194.97	6.65	3.41
Latton	Powder	720	2	202.21	1.74	0.86
Latton	Powder	720	2	201.22	5.56	2.76
Latton	Powder	90	2	201.39	7.29	3.62
Latton	Powder	90	2	200.81	7.21	3.59
Latton	Powder	90	2	204.33	14.49	7.09
Latton	Powder	90	2	210.67	15.53	7.37
Latton	Powder	90	2	209.35	13.38	6.39
Latton	Powder	90	2	194.92	6.2	3.18
Latton	Powder	90	2	198	5.18	2.62
Latton	Powder	Acid only	2	205.93	12.25	5.95
Latton	Powder	Acid only	2	199.04	9.09	4.57
Latton	Powder	AG	2	204.37	9.61	4.70
Latton	Powder	AG	2	203.6	5.8	2.85
Latton	Powder	AG	2	198.76	15.93	8.01
Latton	Powder	AG	2	190.3	16	8.41

Table C.6: Yields of non-Latton bones decalcified in 0.5 M EDTA in the microwave. Also includes yields from AG extractions from the same aliquot of bone. Weight and yield in mg; time in minutes.

Sample	Grain size	Time	Weight	Yield	%yield
Bordersley	Powder	90	239	1.45	0.61
Cala D6 II	Powder	90	236	1.61	0.68
Cariguela	Powder	360	202.45	0	0.00
Cariguela	Powder	360	195.19	0	0.00
Cariguela	Powder	AG	137.73	0	0.00
Cariguela	Powder	AG	198.11	0	0.00
Cariguela	Powder	AG	201.23	0	0.00
Lemon	Powder	180	193.38	11.03	5.70
Lemon	Powder	180	191.49	8.76	4.57
Lemon	Powder	270	194.2	9.98	5.14
Lemon	Powder	270	194.28	9.82	5.05
Lemon	Powder	360	203.78	10.61	5.21
Lemon	Powder	360	204.39	11.98	5.86
Lemon	Powder	360	193.02	11.64	6.03
Lemon	Powder	360	194.25	10.5	5.41
Lemon	Powder	90	192.47	12.87	6.69
Lemon	Powder	90	190.28	10.31	5.42
Lemon	Powder	90	192.47	12.87	6.69
Lemon	Powder	90	190.28	10.31	5.42
Lemon	Powder	AG	206.7	0.3	0.15
Lemon	Powder	AG	200.67	0.13	0.06
Lemon	Powder	AG	189.73	17.77	9.37
Lemon	Powder	AG	196.93	14.61	7.42
Mary Rose	Powder	180	229	5.12	2.24
Mary Rose	Powder	180	215	8.75	4.07
Mary Rose	Powder	180	61.91	7.77	12.55
Zafarraya	Powder	360	204.06	0	0.00
Zafarraya	Powder	360	194.75	1.76	0.90
Zafarraya	Powder	AG	205.35	0	0.00
Zafarraya	Powder	AG	193.49	0	0.00
Zafarraya 40-003	Powder	90	222	1.99	0.90
Zafarraya 42230	Powder	90	223	2	0.90
Zafarraya 43019	Powder	90	203	1.34	0.66

Table C.7: Yields of Latton bones decalcified in 0.5 M EDTA in the microwave under modified conditions. Experiments either modified the starting bone sample size (sample start size) or chilled solvents/glassware and ran the microwave at a reduced 25 W (low temperature). Also includes yields from AG extractions from the same aliquot of bone. Weight and yield in mg; time in minutes.

Experiment	Sample	Grain size	Time	Batch	Weight	Yield	%yield
Sample start size	Latton	Powder	180	3	400.36	21.43	5.35
Sample start size	Latton	Powder	180	3	397.77	13.53	3.40
Sample start size	Latton	Powder	180	3	398.28	15.72	3.95
Sample start size	Latton	Powder	90	3	203.03	5.65	2.78
Sample start size	Latton	Powder	180	3	204.24	7.88	3.86
Sample start size	Latton	Powder	180	3	199.22	6.89	3.46
Sample start size	Latton	Powder	AG	3	402.81	36.57	9.08
Sample start size	Latton	Powder	AG	3	396.06	37.9	9.57
Low temperature	Latton	Powder	45	3	192.5	5.99	3.11
Low temperature	Latton	Powder	45	3	194.62	4.81	2.47
Low temperature	Latton	Powder	45	3	194.61	6.01	3.09
Low temperature	Latton	Powder	90	3	195.71	6.11	3.12
Low temperature	Latton	Powder	90	3	202.49	6.69	3.30
Low temperature	Latton	Powder	90	3	198.96	6.11	3.07
Low temperature	Latton	Powder	45	3	192.68	5.08	2.64
Low temperature	Latton	Powder	45	3	192.23	5.85	3.04
Low temperature	Latton	Powder	45	3	197.28	5.14	2.61
Low temperature	Latton	Powder	90	3	205.25	6.35	3.09
Low temperature	Latton	Powder	90	3	201.91	6.7	3.32
Low temperature	Latton	Powder	90	3	193.85	5.84	3.01
Low temperature	Latton	Powder	180	3	195	6.25	3.21
Low temperature	Latton	Powder	180	3	198.61	6.35	3.20
Low temperature	Latton	Powder	180	3	193.45	6.03	3.12

D
ZooMS results

Table D.1: ZooMS results from Zafarraya. Samples registered for radiocarbon dating were given an internal lab number (P) and some were measured for %N as part of the %N experiments. Species IDs are as reported by the respective labs.

Sample	Zone	Depth (cm)	P	Lab	ZooMS result	%N
P06/115/40189	P06	115-120		York	Bovidae, Cervidae	0.508
P06/112.5/115 C	P06	112.5		York	Bovidae, Cervidae	0.118
P06/125/40-025	P06	125		York	Bovidae, Cervidae	0.563
P6/125/40-042	P6	125		York	Bovidae, Cervidae	
P6/125/40-045	P6	125		York	Bovidae, Cervidae	
Q11/188/122	Q11	188		Manchester	Capra	0.340
P06/125/40-028	P06	125		Manchester	Capra	0.438
P06/118/50011	P06	118-123		Manchester	Capra	0.268
P06/125/40-039	P06	125		Manchester	Capra	1.169
P06/125/40-033	P06	125		Manchester	Capra	0.525
P06/128.5/584	P06	128.5		Manchester	Capra	0.108
P14/103/20	P14	103	42796	Manchester	Capra	0.460
P14/126.3/59	P14	126.3	42800	Manchester	Capra	0.960
P14/103.5/4	P14	103.5	43016	Manchester	Capra	0.665
P11/110/	P11	110-115	43019	Manchester	Capra	0.598
P06/120/40-172	P06	120	43024	Manchester	Capra	0.995
P06/121/40-130	P06	121	43025	Manchester	Capra	0.735
P06/112.5/84	P06	112.5	43533	Manchester	Capra	0.236
P07/147.5/125	P07	147.5		Manchester	Capra, Cervine	0.055
P06/119/442	P06	119		Manchester	Capra, Cervine	0.952
P11/130/18	P11	130	43026	Manchester	Capra, Cervine	1.378
Q6/127/40-078	Q6	127		York	Carnivora (possible cat, tiger, lynx, bear, polecat)	

Table D.1: ZooMS results from Zafarraya. Samples registered for radiocarbon dating were given an internal lab number (P) and some were measured for %N as part of the %N experiments. Species IDs are as reported by the respective labs. *(continued)*

Sample	Zone	Depth (cm)	P	Lab	ZooMS result	%N
P06/115.5/286	P06	115.5		York	Carnivora (possible spotted hyena, tiger, marten, wolverine, European polecat, sea otter, lion)	0.081
P06/113.5/290	P06	113.5		York	Carnivora (possible spotted hyena, tiger, marten, wolverine, European polecat, sea otter, lion)	0.315
P6/118/R50012	P6	118-123		York	Carnivora (possible spotted hyena, tiger, marten, wolverine, European polecat, sea otter, lion)	
P06/112.5/122	P06	112.5		York	Carnivora (possible tiger, dog, wolf, European polecat)	0.954
Q8/118.5/NA	Q8	118.5-123.5		York	Carnivora, possible	
P06/118.5/305b	P06	118.5		Manchester	Cervine	0.615
Q6/135/40-003	Q6	135		Manchester	Cervine	0.575
P14/109/40-009	P14	109	43017	Manchester	Cervine	0.559
P11/120/40-010	P11	120	43022	Manchester	Cervine	1.096
P11/126/8	P11	126	42226	York	Goat, Reindeer	0.930
P06/115.5/185	P06	115.5	42798	York	Goat, Reindeer	0.280
P9/102.5/NA	P9	102.5-115		York	Goat, Reindeer	
P06/112.5/241b	P06	112.5		York	Goat, Reindeer	0.291
P6/113.1/R50010	P6	113.1-118		York	Goat, Reindeer	
P6/115/5697	P6	115-120		York	Goat, Reindeer	
P11/115/NA	P11	115		York	Goat, Reindeer	
P06/117/366	P06	117		York	Goat, Reindeer	0.246
P6/117/340B	P6	117		York	Goat, Reindeer	
Q6/118/NA	Q6	118-123		York	Goat, Reindeer	
P6/118/R25012	P6	118-123		York	Goat, Reindeer	
P6/123/R50030B	P6	123-128		York	Goat, Reindeer	
P06/125/40-027	P06	125		York	Goat, Reindeer	0.233
Q6/125/40-031	Q6	125		York	Goat, Reindeer	
P06/125/40-034	P06	125		York	Goat, Reindeer	0.369
P06/125/40-035	P06	125		York	Goat, Reindeer	0.296
Q6/125/40-040	Q6	125		York	Goat, Reindeer	
P6/125/40-046	P6	125		York	Goat, Reindeer	

Table D.1: ZooMS results from Zafarraya. Samples registered for radiocarbon dating were given an internal lab number (P) and some were measured for %N as part of the %N experiments. Species IDs are as reported by the respective labs. *(continued)*

Sample	Zone	Depth (cm)	P	Lab	ZooMS result	%N
Q6/125.5/238	Q6	125.5		York	Goat, Reindeer	0.103
P07/126/30	P07	126		York	Goat, Reindeer	0.106
Q6/126.5/284	Q6	126.5		York	Goat, Reindeer	0.293
P06/128/610	P06	128		York	Goat, Reindeer	0.242
P8/128/40-023	P8	128		York	Goat, Reindeer	
Q6/129.5/274	Q6	129.5		York	Goat, Reindeer	0.169
Q6/130/40-023	Q6	130		York	Goat, Reindeer	0.210
Q6/130/40-030	Q6	130		York	Goat, Reindeer	0.162
P06/115.5/301	P06	115.5		Manchester	No ID	0.217
P07/110/40390	P07	110-115		Manchester	No ID	0.485
P07/110/3753	P07	110-113	43020	York	No ID	0.950
P06/120/40-032	P06	120	43023	Manchester	No ID	1.056
Q8/113.5/	Q8	113.5-118.5		York	No ID	0.454
Q6/115.7/104	Q6	115.7		York	No ID	
P06/118.7/330b	P06	118.7		York	No ID	0.542
P6/120/40-138	P6	120		York	No ID	
P6/120/40-170	P6	120		York	No ID	
P06/125/40-037	P06	125		York	No ID	0.756
P6/125/40-044B	P6	125		York	No ID	
P6/125/40-047	P6	125		York	No ID	
P6/125/40-051	P6	125		York	No ID	
P6/125/40-052	P6	125		York	No ID	
Q6/123/5397	Q6	123-125		Manchester	Ovis?	3.197

E
Samples collected for radiocarbon dating

E.1 Collected samples and %N values

Table E.1: All samples collected for this thesis. Samples without %N values were skipped due to limited material.

Site	Country	Species	Sample	%N	Extracted	P
Akrotiri Aetokremnos	Greece	Straight-tusked elephant	Akrotiri1	0.039	No	41287
Akrotiri Aetokremnos	Greece	Straight-tusked elephant	Akrotiri2		No	41288
Cariguela	Spain	Cave hyena	Cariguela_6602	0.045	No	
Cariguela	Spain	Human (H. sapiens)	Cariguela_2360	0.543	No	
Cariguela	Spain	Human (H. sapiens)	Cariguela_5.874	2.071	No	
Cariguela	Spain	Leopard	Cariguela_6600	0.048	No	
Cariguela	Spain	Neanderthal	Cariguela_5.875	0.047	No	
Cariguela	Spain	Neanderthal	Cariguela_5.876	0.070	No	
Cariguela	Spain	Unknown	Cariguela_6	0.029	No	
Cariguela	Spain	Unknown	Cariguela_1	0.031	No	
Cariguela	Spain	Unknown	Cariguela_2	0.039	No	
Cariguela	Spain	Unknown	Cariguela_3	0.039	No	
Cariguela	Spain	Unknown	Cariguela_4	0.040	No	
Cariguela	Spain	Unknown	Cariguela_5	0.041	No	
Cariguela	Spain	Unknown	Cariguela_6	0.042	No	
Cariguela	Spain	Unknown	Cariguela_7	0.045	No	
Cariguela	Spain	Unknown	Cariguela_8	0.045	No	
Cariguela	Spain	Unknown	Cariguela_9	0.047	No	
Cariguela	Spain	Unknown	Cariguela_10	0.049	No	
Cariguela	Spain	Unknown	Cariguela_11	0.049	No	
Cariguela	Spain	Unknown	Cariguela_12	0.049	No	
Cariguela	Spain	Unknown	Cariguela_13	0.049	No	
Cariguela	Spain	Unknown	Cariguela_14	0.056	No	
Cariguela	Spain	Unknown	Cariguela_15	0.058	No	

Table E.1: All samples collected for this thesis. Samples without %N values were skipped due to limited material. *(continued)*

Site	Country	Species	Sample	%N	Extracted	P
Cariguela	Spain	Unknown	Cariguela_16	0.059	No	
Cariguela	Spain	Unknown	Cariguela_2	0.060	No	
Cariguela	Spain	Unknown	Cariguela_5	0.061	No	
Cariguela	Spain	Unknown	Cariguela_4	0.065	No	
Cariguela	Spain	Unknown	Cariguela_5	0.075	No	
Cariguela	Spain	Unknown	Cariguela_3	0.078	No	
Cariguela	Spain	Unknown	Cariguela_4		No	
Cariguela	Spain	Unknown	Cariguela_6569	0.037	No	
Cariguela	Spain	Unknown	Cariguela_6565	0.037	No	
Cariguela	Spain	Unknown	Cariguela_6535	0.051	No	
Cariguela	Spain	Unknown	Cariguela_6540	0.040	No	
Cariguela	Spain	Unknown	Cariguela_6559	0.050	No	
Cariguela	Spain	Unknown	Cariguela_6562	0.058	No	
Cariguela	Spain	Unknown	Cariguela_7	0.065	No	
Castelcivita Cave	Italy	Cave hyena	Castel 4	0.071	Yes	45633
Castelcivita Cave	Italy	Cave hyena	Castel 3	0.030	Yes	
Castelcivita Cave	Italy	Cave hyena	Castel 1	0.376	Yes	45630
Castelcivita Cave	Italy	Cave hyena	Castel 2	0.167	Yes	
Castelcivita Cave	Italy	Leopard	Castel 6	0.351	Yes	45631
Castelcivita Cave	Italy	Leopard	Castel 5	0.388	Yes	45632
Cava Muracci	Italy	Cave hyena	CM 261	0.355	Yes	45506
Cava Muracci	Italy	Cave hyena	CM 3	0.764	Yes	44418
Cava Muracci	Italy	Cave hyena	CM 355	3.134	Yes	45505
Cava Muracci	Italy	Cave hyena	CM 641	1.769	Yes	45508
Cava Muracci	Italy	Cave hyena	CM 1101	0.403	Yes	
Cava Muracci	Italy	Cave hyena	CM 1186	0.514	Yes	
Cava Muracci	Italy	Cave hyena	CM 632	1.302	Yes	
Cava Muracci	Italy	Cave hyena	CM 290	3.025	Yes	

Table E.1: All samples collected for this thesis. Samples without %N values were skipped due to limited material. *(continued)*

Site	Country	Species	Sample	%N	Extracted	P
Cava Muracci	Italy	Deer	CM 313	0.201	Yes	
Cava Muracci	Italy	Narrow-nosed rhino	CM 363	0.605	Yes	45507
Cava Muracci	Italy	Narrow-nosed rhino	CM 365	0.379	Yes	
Crete (museum)	Crete	Human (H. sapiens)	Crete human bone	0.088	No	
Crete (museum)	Crete	Human (H. sapiens)	Crete milatos 1985	0.093	No	
Cucigliana	Italy	Cave hyena	6596	0.555	Yes	45636
Cucigliana	Italy	Cave hyena	Cucigliana_6601	0.039	No	
Cucigliana	Italy	Cave hyena	Cucigliana_6597	0.045	No	
Cucigliana	Italy	Cave hyena	Cucigliana_6569	0.065	No	
Cucigliana	Italy	Cave hyena	Cucigliana_6565	0.068	No	
Cucigliana	Italy	Cave hyena	Cucigliana_6596	0.111	No	
Cucigliana	Italy	Cave hyena	Cucigliana_6568	0.116	No	
Cucigliana	Italy	Cave hyena	Cucigliana_6561	0.148	No	
Cucigliana	Italy	Cave hyena	Cucigliana_6560	0.202	No	
Grotta dei Santi	Italy	Cave hyena	Santi 3	0.035	Yes	45637
Grotta dei Santi	Italy	Cave hyena	Santi 4	0.021	Yes	
Grotta dei Santi	Italy	Leopard	Santi 1	0.058	Yes	45638
Grotta dei Santi	Italy	Leopard	Santi 2	0.055	Yes	
Grotta della Cala	Italy	Leopard	Cala 2	0.306	Yes	45634
Grotta della Cala	Italy	Leopard	Cala 3	0.345	Yes	45635
Grotta della Cala	Italy	Leopard	Cala 1	0.031	Yes	
Grotta della Cala	Italy	Leopard	Cala 4	0.021	Yes	
Grotta Paglicci	Italy	Cave hyena	Paglicci 5	0.134	Yes	45640
Grotta Paglicci	Italy	Cave hyena	Paglicci_39 I parete	0.189	No	
Grotta Paglicci	Italy	Cave hyena	Paglicci 3	0.046	Yes	
Grotta Paglicci	Italy	Cave hyena	Grotta Paglicci_26 H	0.074	No	
Grotta Paglicci	Italy	Cave hyena	Paglicci 2	0.027	Yes	45639
Grotta Paglicci	Italy	Cave hyena	Paglicci 4	0.055	Yes	

Table E.1: All samples collected for this thesis. Samples without %N values were skipped due to limited material. *(continued)*

Site	Country	Species	Sample	%N	Extracted	P
Grotta Paglicci	Italy	Cave hyena	Paglicci 1	0.081	Yes	
Grotta Paglicci	Italy	Cave hyena	Paglicci_IT9	0.159	No	
Grotte di Equi	Italy	Cave lion	6081	1.076	Yes	45510
Grotte di Equi	Italy	Cave lion	6092v	0.750	Yes	44414
Grotte di Equi	Italy	Cave lion	Equi_6089	0.083	No	
Grotte di Equi	Italy	Cave lion	Equi_6085	0.086	No	
Grotte di Equi	Italy	Cave lion	Equi_6079	0.127	No	
Grotte di Equi	Italy	Cave lion	Equi_6087	0.130	No	
Grotte di Equi	Italy	Cave lion	Equi_6084	0.202	No	
Grotte di Equi	Italy	Cave lion	Equi_6041	0.308	No	
Grotte di Equi	Italy	Cave lion	Equi_6080	0.358	No	
Grotte di Equi	Italy	Cave lion	Equi_6082	0.440	No	
Grotte di Equi	Italy	Deer	102840	0.825	Yes	
Grotte di Equi	Italy	Deer	102873	2.280	Yes	
Grotte di Equi	Italy	Deer	102820	2.629	Yes	
Grotte di Equi	Italy	Leopard	5357v	1.683	Yes	44416
Grotte di Equi	Italy	Leopard	5351	0.524	Yes	45509
Grotte di Equi	Italy	Leopard	Equi_5337	0.130	No	
Grotte di Equi	Italy	Leopard	Equi_5352	0.386	No	
Grotte di Equi	Italy	Leopard	5350	0.452	No	
Grotte di Equi	Italy	Leopard	Equi_5339	1.163	No	
Grotte di Equi	Italy	Leopard	Equi_5353	1.551	No	
Grotte di Equi	Italy	Wolf	Equi_100452	1.763	No	
Grotte di Equi	Italy	Wolf	5438v	0.896	Yes	44415
Grotte di Equi	Italy	Wolf	Equi_6246	0.358	No	
Grotte di Equi	Italy	Wolf	Equi_6379	0.365	No	
Grotte di Equi	Italy	Wolf	6380	0.380	Yes	
Grotte di Equi	Italy	Wolf	5435	0.660	Yes	

Table E.1: All samples collected for this thesis. Samples without %N values were skipped due to limited material. *(continued)*

Site	Country	Species	Sample	%N	Extracted	P
Kozarnica	Bulgaria	Cave hyena	Koz CC2	1.892	No	42396
Kozarnica	Bulgaria	Cave hyena	Koz CC1	1.138	Yes	42395
Kozarnica	Bulgaria	Cave hyena	Koz CC3	2.401	Yes	42397
Kozarnica	Bulgaria	Cave lion	Koz PS1	2.370	Yes	42398
La Llera	Spain	Woolly rhino	Llera I	0.021	No	41280
La Sassa	Italy	Brown bear	Sassa 3	1.035	Yes	45511
La Sassa	Italy	Brown bear	Sassa 29	0.770	Yes	
La Sassa	Italy	Brown bear	Sassa 329	0.794	Yes	
La Sassa	Italy	Brown bear	Sassa 24	0.856	Yes	
La Sassa	Italy	Cave hyena	Sassa 516B	2.019	Yes	45512
La Sassa	Italy	Cave hyena	Sassa 516A	0.596	Yes	45513
La Sassa	Italy	Cave hyena	Sassa 401	2.676	Yes	
La Sassa	Italy	Cave lion	Sassa 23	0.458	Yes	45514
La Silluca Cave	Spain	Straight-tusked elephant	Silluca 1	0.019	No	41279
La Silluca Cave	Spain	Straight-tusked elephant	11419	0.217	Yes	45646
La Silluca Cave	Spain	Straight-tusked elephant	Silluca 2	0.029	No	
Los Rincones	Spain	Brown bear	MPZ 2015/720	0.420	Yes	44417
Los Rincones	Spain	Brown bear	MPZ 2015/790	0.540	Yes	
Los Rincones	Spain	Brown bear	MPZ 2015/781	0.660	Yes	
Los Rincones	Spain	Brown bear	MPZ 2015/824	0.880	Yes	
Los Rincones	Spain	Brown bear	MPZ 2015/844	1.340	Yes	
Los Rincones	Spain	Leopard	MPZ 2015/600	0.040	Yes	45641
Los Rincones	Spain	Leopard	MPZ 2015/665	0.130	Yes	45642
Los Rincones	Spain	Leopard	MPZ 2015/613	0.040	Yes	45643
Los Rincones	Spain	Leopard	MPZ 2015/616	0.430	Yes	45644
Los Rincones	Spain	Leopard	MPZ 2015/617	0.680	Yes	
Los Rincones	Spain	Leopard	MPZ 2015/629	0.940	Yes	
Lough Boora	Other	Boar	LB_boar	0.547	No	

Table E.1: All samples collected for this thesis. Samples without %N values were skipped due to limited material. *(continued)*

Site	Country	Species	Sample	%N	Extracted	P
Lough Boora	Other	Giant elk	LB 1		No	41283
Lough Boora	Other	Giant elk	LB2	0.089	No	41284
Lough Boora	Other	Giant elk	LB3	0.113	No	41285
Lough Boora	Other	Giant elk	LB4	0.140	No	41286
Manastira	Bulgaria	Bovid	Mana 7	1.349	Yes	42409
Manastira	Bulgaria	Cave hyena	Mana 12	0.038	No	
Manastira	Bulgaria	Cave hyena	Mana 11	0.030	No	
Manastira	Bulgaria	Cave hyena	Mana 10	0.081	No	
Manastira	Bulgaria	Cave hyena	Mana 8	0.060	No	
Manastira	Bulgaria	Cave hyena	Mana 9	0.081	No	
Manastira	Bulgaria	Cave hyena	Mana 14	0.057	No	
Manastira	Bulgaria	Cave hyena	Mana 15	0.070	No	
Manastira	Bulgaria	Cave hyena	Mana 16	0.053	No	
Manastira	Bulgaria	Cave hyena	Mana 13	0.206	No	
Manastira	Bulgaria	Horse	Mana 2	0.186	No	
Manastira	Bulgaria	Horse	Mana 3	0.230	No	
Manastira	Bulgaria	Horse	Mana 1	0.303	No	
Manastira	Bulgaria	Human (H. sapiens)	Mana 17		No	
Manastira	Bulgaria	Human (H. sapiens)	Mana 18		No	
Manastira	Bulgaria	Human (H. sapiens)	Mana 19		No	
Manastira	Bulgaria	Unknown	Mana 4	1.381	Yes	42406
Manastira	Bulgaria	Unknown	Mana 5	2.117	Yes	42407
Manastira	Bulgaria	Unknown	Mana 6	2.106	Yes	42408
Redaka II	Bulgaria	Cave hyena	Red CC2	1.287	Yes	42400
Redaka II	Bulgaria	Cave hyena	Red CC6	3.567	Yes	42404
Redaka II	Bulgaria	Cave hyena	Red CC3	2.230	Yes	42401
Redaka II	Bulgaria	Cave hyena	Red CC5	2.483	Yes	42403
Redaka II	Bulgaria	Cave hyena	Red CC4	2.269	Yes	42402

Table E.1: All samples collected for this thesis. Samples without %N values were skipped due to limited material. *(continued)*

Site	Country	Species	Sample	%N	Extracted	P
Redaka II	Bulgaria	Cave hyena	Red CC1	1.702	Yes	42399
Redaka II	Bulgaria	Human (H. sapiens)	Red_E3 - 753	1.946	No	
Redaka II	Bulgaria	Human (H. sapiens)	Red_E5-E6 - 233		No	
Redaka II	Bulgaria	Unknown	Red_D5 - 155	1.882	No	
Redaka II	Bulgaria	Unknown	Red_E3 - 132	2.606	No	
Redaka II	Bulgaria	Unknown	Red NID5	1.547	Yes	42405
Redaka II	Bulgaria	Unknown	Red_E4 - 363	1.442	No	
Redaka II	Bulgaria	Unknown	Red_E4 - 240	2.795	No	
Redaka II	Bulgaria	Unknown	Red_E5 - 395	2.795	No	
Taiwanese Palaeoloxodon	Other	Straight-tusked elephant	Tawain 1	0.043	No	41281
Taiwanese Palaeoloxodon	Other	Straight-tusked elephant	Tawain 2	0.038	No	41282
Tilos	Greece	Deer	Tilos deer open site	0.167	No	
Tilos	Greece	Pygmy elephant	T.1172	0.083	Yes	44408
Tilos	Greece	Pygmy elephant	T.10376	0.081	Yes	44409
Tilos	Greece	Pygmy elephant	T.1052	0.080	Yes	44410
Tilos	Greece	Pygmy elephant	T.8074	0.198	Yes	44411
Tilos	Greece	Pygmy elephant	T.8072	0.167	Yes	44412
Tilos	Greece	Pygmy elephant	AMPG 1900	0.162	Yes	44413
Tilos	Greece	Pygmy elephant	T.1057	0.078	Yes	
Tilos	Greece	Pygmy elephant	T.2151	0.082	No	
Tilos	Greece	Pygmy elephant	T.1242	0.083	No	
Tilos	Greece	Pygmy elephant	T.1060	0.084	No	
Tilos	Greece	Pygmy elephant	T.1223	0.086	No	
Tilos	Greece	Pygmy elephant	T.10399	0.088	No	
Tilos	Greece	Pygmy elephant	T.1337	0.089	No	
Tilos	Greece	Pygmy elephant	T.3211	0.099	No	

Table E.1: All samples collected for this thesis. Samples without %N values were skipped due to limited material. *(continued)*

Site	Country	Species	Sample	%N	Extracted	P
Tilos	Greece	Pygmy elephant	T.5944	0.100	No	
Tilos	Greece	Pygmy elephant	T.6482	0.101	No	
Tilos	Greece	Pygmy elephant	T.1188	0.104	No	
Tilos	Greece	Pygmy elephant	T.5680	0.113	No	
Tilos	Greece	Pygmy elephant	T.1176	0.116	Yes	
Tilos	Greece	Pygmy elephant	T.2264	0.127	No	
Tilos	Greece	Pygmy elephant	T.618/96	0.154	No	
Tilos	Greece	Pygmy elephant	T.8070	0.160	No	
Tilos	Greece	Pygmy elephant	T.370	0.165	Yes	
Tilos	Greece	Pygmy elephant	T.13140	0.169	No	
Tilos	Greece	Pygmy elephant	T.10233	0.172	No	
Tilos	Greece	Pygmy elephant	T.1654	0.172	No	
Tilos	Greece	Pygmy elephant	T.1241	0.177	No	
Tilos	Greece	Pygmy elephant	T.01.47a	0.182	No	
Tilos	Greece	Pygmy elephant	T.01215	0.186	No	
Tilos	Greece	Pygmy elephant	T.5822	0.186	No	
Tilos	Greece	Pygmy elephant	T.1815	0.196	No	
Tilos	Greece	Pygmy elephant	T.1401	0.200	No	
Tilos	Greece	Pygmy elephant	T.5803	0.214	No	
Tilos	Greece	Pygmy elephant	T.10403	0.216	No	
Tilos	Greece	Pygmy elephant	T.7800	0.219	Yes	
Tilos	Greece	Pygmy elephant	T.1174	0.226	No	
Tilos	Greece	Pygmy elephant	T.6309	0.234	No	
Tilos	Greece	Pygmy elephant	T.19.174.1	0.260	No	
Tilos	Greece	Pygmy elephant	T.2557	0.265	No	
Tilos	Greece	Tortoise	T.12738	0.113	No	
Vasil Levski	Bulgaria	Cave hyena	Vasil C	0.529	Yes	45645
Vasil Levski	Bulgaria	Cave hyena	Vasil M	0.098	Yes	

Table E.1: All samples collected for this thesis. Samples without %N values were skipped due to limited material. *(continued)*

Site	Country	Species	Sample	%N	Extracted	P
Zafarraya	Spain	Leopard	Zaf N84	0.250	Yes	43533
Zafarraya	Spain	Unknown	Zaf N40-172	0.950	Yes	43024
Zafarraya	Spain	Unknown	Zaf N40-032	1.056	Yes	43023
Zafarraya	Spain	Unknown	Zaf N40-010	1.096	Yes	43022
Zafarraya	Spain	Unknown	Zaf N40071	0.678	Yes	43018
Zafarraya	Spain	Unknown	ZAF 5 EJ		Yes	42800
Zafarraya	Spain	Unknown	Zaf P11H92	0.598	Yes	43019
Zafarraya	Spain	Unknown	Zaf N18	1.378	Yes	43026
Zafarraya	Spain	Unknown	Zaf N40-130	0.350	Yes	43025
Zafarraya	Spain	Unknown	ZAF 3 EJ		Yes	42798
Zafarraya	Spain	Unknown	Zaf N40-009	0.559	Yes	43017
Zafarraya	Spain	Unknown	ZAF 1 EJ		Yes	42796
Zafarraya	Spain	Unknown	ZAF 2 EJ		Yes	42797
Zafarraya	Spain	Unknown	ZAF 4 EJ		Yes	42799
Zafarraya	Spain	Unknown	ZAF 6 EJ		Yes	42801
Zafarraya	Spain	Unknown	Zaf N4	0.665	Yes	43016
Zafarraya	Spain	Unknown	Zaf N3753	0.950	Yes	43020
Zafarraya	Spain	Unknown	Zaf N5172	0.866	Yes	43021

E.2 Pretreatment results of new samples

Table E.2: All pretreatment extractions attempted for this thesis.

Site	Species	Sample	P	PCode	Used	Yield	%yield	Combusted
Castelcivita Cave	Cave hyena	Castel 1	45630	AF	800.00	18.57	2.32	Yes
Castelcivita Cave	Leopard	Castel 6	45631	AF	810.00	33.52	4.14	Yes
Castelcivita Cave	Leopard	Castel 5	45632	AF	850.00	32.46	3.82	Yes
Castelcivita Cave	Cave hyena	Castel 4	45633	AG	820.00	16.41	2.00	Yes
Castelcivita Cave	Cave hyena	Castel 3		AG	1310.00	7.60	0.58	No
Castelcivita Cave	Cave hyena	Castel 2		AG	940.00	14.54	1.55	No
Cava Muracci	Cave hyena	CM 3	44418	NRC	26.39	0.00	0.00	Yes
Cava Muracci	Cave hyena	CM 3	44418	AG	940.00	28.07	2.99	No
Cava Muracci	Cave hyena	CM 355	45505	AG	980.00	15.42	1.57	Yes
Cava Muracci	Cave hyena	CM 261	45506	AG	1090.00	13.91	1.28	Yes
Cava Muracci	Narrow-nosed rhino	CM 363	45507	AG	1130.00	21.31	1.89	Yes
Cava Muracci	Cave hyena	CM 641	45508	AG	1060.00	9.65	0.91	Yes
Cava Muracci	Deer	CM 313		AG	600.00	1.29	0.22	No
Cava Muracci	Narrow-nosed rhino	CM 365		AG	1090.00	4.12	0.38	No
Cava Muracci	Cave hyena	CM 1101		AG	1010.00	7.95	0.79	No
Cava Muracci	Cave hyena	CM 1186		AG	940.00	7.33	0.78	No
Cava Muracci	Cave hyena	CM 632		AG	1020.00	7.98	0.78	No
Cava Muracci	Cave hyena	CM 290		AG	540.00	1.37	0.25	No
Cucigliana	Cave hyena	6596	45636	AG	910.00	2.95	0.32	No
Grotta dei Santi	Cave hyena	Santi 3	45637	AG	1030.00	6.68	0.65	Yes
Grotta dei Santi	Leopard	Santi 1	45638	AG	940.00	4.04	0.43	Yes
Grotta dei Santi	Cave hyena	Santi 4		AG	1070.00	1.91	0.18	No
Grotta dei Santi	Leopard	Santi 2		AG	800.00	0.60	0.08	No
Grotta della Cala	Leopard	Cala 2	45634	AG	1160.00	18.33	1.58	Yes
Grotta della Cala	Leopard	Cala 3	45635	AG	1310.00	9.99	0.76	Yes

Table E.2: All pretreatment extractions attempted for this thesis. *(continued)*

Site	Species	Sample	P	PCode	Used	Yield	%yield	Combusted
Grotta della Cala	Leopard	Cala 1		AG	640.00	0.00	0.00	No
Grotta della Cala	Leopard	Cala 4		AG	640.00	0.00	0.00	No
Grotta Paglicci	Cave hyena	Paglicci 2	45639	AG	1080.00	28.46	2.64	Yes
Grotta Paglicci	Cave hyena	Paglicci 5	45640	AG	1200.00	25.02	2.08	Yes
Grotta Paglicci	Cave hyena	Paglicci 3		AG	650.00	0.41	0.06	No
Grotta Paglicci	Cave hyena	Paglicci 4		AG	1130.00	7.87	0.70	No
Grotta Paglicci	Cave hyena	Paglicci 1		AG	970.00	28.52	2.94	No
Grotte di Equi	Cave lion	6092v	44414	AG	1050.00	24.00	2.29	No
Grotte di Equi	Cave lion	6092v	44414	NRC	22.40	0.00	0.00	Yes
Grotte di Equi	Wolf	5438v	44415	NRC	23.38	0.00	0.00	Yes
Grotte di Equi	Wolf	5438v	44415	AG	950.00	34.65	3.65	No
Grotte di Equi	Leopard	5357v	44416	NRC	23.26	0.00	0.00	Yes
Grotte di Equi	Leopard	5357v	44416	AG	610.00	24.34	3.99	Yes
Grotte di Equi	Leopard	5351	45509	AG	1140.00	15.91	1.40	Yes
Grotte di Equi	Cave lion	6081	45510	AG	690.00	7.07	1.02	Yes
Grotte di Equi	Wolf	6380		AG	950.00	22.57	2.38	No
Grotte di Equi	Wolf	5435		AG	950.00	19.14	2.01	No
Grotte di Equi	Deer	102840		AG	570.00	45.74	8.02	No
Grotte di Equi	Deer	102873		AG	750.00	112.17	14.96	No
Grotte di Equi	Deer	102820		AG	580.00	98.63	17.01	No
Kozarnica	Cave hyena	Koz CC1	42395	AF	557.00	6.45	1.16	Yes
Kozarnica	Cave hyena	Koz CC3	42397	AF	410.00	6.69	1.63	Yes
Kozarnica	Cave lion	Koz PS1	42398	AF	402.00	16.65	4.14	Yes
La Sassa	Brown bear	Sassa 3	45511	AF	1070.00	7.78	0.73	Yes
La Sassa	Cave hyena	Sassa 516B	45512	AF	780.00	14.73	1.89	Yes
La Sassa	Cave hyena	Sassa 516A	45513	AF	870.00	13.10	1.51	Yes
La Sassa	Cave lion	Sassa 23	45514	AG	950.00	17.74	1.87	Yes
La Sassa	Brown bear	Sassa 29		AG	810.00	18.33	2.26	No

Table E.2: All pretreatment extractions attempted for this thesis. *(continued)*

Site	Species	Sample	P	PCode	Used	Yield	%yield	Combusted
La Sassa	Brown bear	Sassa 329		AG	1170.00	58.54	5.00	No
La Sassa	Brown bear	Sassa 24		AG	1040.00	40.62	3.91	No
La Sassa	Cave hyena	Sassa 401		AG	910.00	34.24	3.76	No
La Silluca Cave	Straight-tusked elephant	11419	45646	AG	1030.00	41.19	4.00	Yes
Los Rincones	Brown bear	MPZ 2015/720	44417	AG	1200.00	20.25	1.69	No
Los Rincones	Brown bear	MPZ 2015/720	44417	NRC	20.00	0.00	0.00	No
Los Rincones	Leopard	MPZ 2015/600	45641	AG	1070.00	14.91	1.39	Yes
Los Rincones	Leopard	MPZ 2015/665	45642	AG	870.00	13.35	1.53	Yes
Los Rincones	Leopard	MPZ 2015/613	45643	AG	980.00	10.77	1.10	Yes
Los Rincones	Leopard	MPZ 2015/616	45644	AG	920.00	5.95	0.65	Yes
Los Rincones	Brown bear	MPZ 2015/790		AG	1290.00	0.50	0.04	No
Los Rincones	Brown bear	MPZ 2015/781		AG	980.00	0.31	0.03	No
Los Rincones	Leopard	MPZ 2015/617		AG	1050.00	0.19	0.02	No
Los Rincones	Brown bear	MPZ 2015/824		AG	1130.00	0.22	0.02	No
Los Rincones	Leopard	MPZ 2015/629		AG	980.00	0.00	0.00	No
Los Rincones	Brown bear	MPZ 2015/844		AG	1060.00	0.08	0.01	No
Manastira	Unknown	Mana 4	42406	AF	406.00	5.14	1.27	Yes
Manastira	Unknown	Mana 5	42407	AF	434.00	13.05	3.01	Yes
Manastira	Unknown	Mana 6	42408	AF	516.00	0.00	0.00	Yes
Manastira	Unknown	Mana 6	42408	AF	521.00	10.59	2.03	Yes
Manastira	Bovid	Mana 7	42409	AF	544.00	5.57	1.02	Yes
Redaka II	Cave hyena	Red CC1	42399	AF	480.00	19.22	4.00	Yes
Redaka II	Cave hyena	Red CC2	42400	AF	437.00	6.01	1.38	Yes
Redaka II	Cave hyena	Red CC3	42401	AF	506.00	31.11	6.15	Yes
Redaka II	Cave hyena	Red CC4	42402	AF	406.00	11.96	2.95	Yes
Redaka II	Cave hyena	Red CC5	42403	AF	401.00	13.75	3.43	Yes
Redaka II	Cave hyena	Red CC6	42404	AF	320.00	2.47	0.77	No
Redaka II	Unknown	Red NID5	42405	AF	509.00	9.45	1.86	Yes

Table E.2: All pretreatment extractions attempted for this thesis. *(continued)*

Site	Species	Sample	P	PCode	Used	Yield	%yield	Combusted
Tilos	Pygmy elephant	T.1172	44408	AG	753.00	11.16	1.48	No
Tilos	Pygmy elephant	T.10376	44409	AG	725.00	13.86	1.91	No
Tilos	Pygmy elephant	T.1052	44410	AG	748.00	20.87	2.79	Yes
Tilos	Pygmy elephant	T.8074	44411	AG	722.00	35.60	4.93	Yes
Tilos	Pygmy elephant	T.8072	44412	AG	670.00	29.23	4.36	Yes
Tilos	Pygmy elephant	AMPG 1900	44413	AG	942.00	67.48	7.16	No
Tilos	Pygmy elephant	AMPG 1900	44413	NRC	50.42	0.00	0.00	No
Tilos	Pygmy elephant	T.1057		AG	760.00	0.00	0.00	No
Tilos	Pygmy elephant	T.1176		AG	683.00	0.00	0.00	No
Tilos	Pygmy elephant	T.370		AG	776.00	4.07	0.52	No
Tilos	Pygmy elephant	T.7800		AG	686.00	0.00	0.00	No
Vasil Levski	Cave hyena	Vasil C	45645	AG	500.00	4.13	0.83	Yes
Vasil Levski	Cave hyena	Vasil M		AG	600.00	1.19	0.20	No
Zafarraya	Unknown	ZAF 1 EJ	42796	AF*	930.00	5.30	0.57	Yes
Zafarraya	Unknown	ZAF 1 EJ	42796	AF*	810.00	10.53	1.30	Yes
Zafarraya	Unknown	ZAF 1 EJ	42796	NRC	1990.00	47.86	2.41	Yes
Zafarraya	Unknown	ZAF 2 EJ	42797	AF*	1960.00	0.53	0.03	No
Zafarraya	Unknown	ZAF 3 EJ	42798	AF	1520.00	16.51	1.09	Yes
Zafarraya	Unknown	ZAF 3 EJ	42798	NRC	1950.00	14.23	0.73	Yes
Zafarraya	Unknown	ZAF 4 EJ	42799	AF	1540.00	0.54	0.04	No
Zafarraya	Unknown	ZAF 4 EJ	42799	AF	1280.00	0.19	0.01	No
Zafarraya	Unknown	ZAF 5 EJ	42800	AF	1040.00	13.46	1.29	Yes
Zafarraya	Unknown	ZAF 6 EJ	42801	AF	1000.00	6.84	0.68	Yes
Zafarraya	Unknown	ZAF 6 EJ	42801	AF	720.00	8.25	1.15	Yes
Zafarraya	Unknown	Zaf N4	43016	AF	720.00	2.60	0.36	No
Zafarraya	Unknown	Zaf N40-009	43017	AF	690.00	6.05	0.88	Yes
Zafarraya	Unknown	Zaf N40-009	43017	NRC	1690.00	40.01	2.37	Yes
Zafarraya	Unknown	Zaf N40071	43018	AF	380.00	3.41	0.90	Yes

Table E.2: All pretreatment extractions attempted for this thesis. *(continued)*

Site	Species	Sample	P	PCode	Used	Yield	%yield	Combusted
Zafarraya	Unknown	Zaf P11H92	43019	AF	930.00	22.38	2.41	Yes
Zafarraya	Unknown	Zaf N3753	43020	AF	610.00	0.01	0.00	No
Zafarraya	Unknown	Zaf N3753	43020	AF	640.00	0.21	0.03	No
Zafarraya	Unknown	Zaf N5172	43021	AF	680.00	0.00	0.00	No
Zafarraya	Unknown	Zaf N40-010	43022	AF	630.00	16.09	2.55	Yes
Zafarraya	Unknown	Zaf N40-032	43023	AF	1040.00	30.39	2.92	Yes
Zafarraya	Unknown	Zaf N40-172	43024	AF	620.00	14.36	2.32	Yes
Zafarraya	Unknown	Zaf N40-130	43025	AF	780.00	35.46	4.55	Yes
Zafarraya	Unknown	Zaf N40-130	43025	NRC	1000.00	23.97	2.40	Yes
Zafarraya	Unknown	Zaf N40-130	43025	AF*	930.00	9.34	1.00	Yes
Zafarraya	Unknown	Zaf N18	43026	AF	660.00	19.14	2.90	Yes
Zafarraya	Leopard	Zaf N84	43533	AG	970.00	6.54	0.67	Yes

E.3 Combustion and AMS results of new samples

Table E.3: All combustions attempted for this thesis and radiocarbon results. Some samples were failed at combustion due to low carbon yield or poor health metrics.

Site	Species	Sample	P	PCode	C (mg)	%C	δ^{13}C	δ^{15}N	CN	OxA	Date	±
Castelcivita Cave	Cave hyena	Castel 1	45630	AF	2.02	40.0	-18.16	11.55	3.32	37221	34500	600
Castelcivita Cave	Leopard	Castel 6	45631	AF	1.90	38.0	-18.33	8.83	3.34	37222	43400	1800
Castelcivita Cave	Leopard	Castel 5	45632	AF	1.97	39.2	-18.11	10.06	3.35	37223	38800	1000
Castelcivita Cave	Cave hyena	Castel 4	45633	AG	0.86	18.3	-19.67	8.96	3.76			
Cava Muracci	Cave hyena	CM 3	44418	NRC	0.57	38.4	-27.30	11.95	4.99	X-2756-42	44400	3700
Cava Muracci	Cave hyena	CM 355	45505	AG	0.60	11.9	-22.80	12.55	4.38			
Cava Muracci	Cave hyena	CM 261	45506	AG	1.03	20.6	-20.82	6.14	3.64	X-2772-28	41700	0
Cava Muracci	Narrow-nosed rhino	CM 363	45507	AG	1.00	20.5	-21.92	6.10	3.63	X-2772-33	46500	3900
Cava Muracci	Cave hyena	CM 641	45508	AG	0.78	16.6	-18.44	12.92	3.77			
Grotta dei Santi	Cave hyena	Santi 3	45637	AG	0.02	0.4	-25.43	0.00	0.00			
Grotta dei Santi	Leopard	Santi 1	45638	AG	0.14	3.7	-18.97	0.00	0.00			
Grotta della Cala	Leopard	Cala 2	45634	AG	0.97	19.8	-21.75	5.56	4.01			
Grotta della Cala	Leopard	Cala 3	45635	AG	0.12	2.5	-21.90	0.00	0.00			
Grotta Paglicci	Cave hyena	Paglicci 2	45639	AG	0.01	0.2	-24.88	0.00	0.00			
Grotta Paglicci	Cave hyena	Paglicci 5	45640	AG	0.33	6.5	-19.16	9.45	4.09			
Grotte di Equi	Cave lion	6092v	44414	NRC	0.00		0.00	0.00	0.00			
Grotte di Equi	Wolf	5438v	44415	NRC	0.68	45.7	-26.02	7.56	5.00	X-2756-40	19360	140
Grotte di Equi	Leopard	5357v	44416	NRC	0.76	37.0	-27.41	8.27	5.00	X-2756-41	41000	1800
Grotte di Equi	Leopard	5357v	44416	AG	0.00	0.0	0.00	0.00	0.00			
Grotte di Equi	Leopard	5351	45509	AG	0.06	1.2	-21.56	0.00	0.00			
Grotte di Equi	Cave lion	6081	45510	AG	2.15	43.4	-20.02	5.62	3.50	37177	21920	160
Kozarnica	Cave hyena	Koz CC1	42395	AF	2.04	42.4	-19.35	14.42	3.35	35556	34350	600
Kozarnica	Cave hyena	Koz CC3	42397	AF	2.13	44.8	-19.07	14.41	3.30	35557	49100	3600

Table E.3: All combustions attempted for this thesis and radiocarbon results. Some samples were failed at combustion due to low carbon yield or poor health metrics. *(continued)*

Site	Species	Sample	P	PCode	C (mg)	%C	δ^{13}C	δ^{15}N	CN	OxA	Date	±
Kozarnica	Cave lion	Koz PS1	42398	AF	2.18	45.2	-19.80	9.84	3.29	35558	16395	80
La Sassa	Brown bear	Sassa 3	45511	AF	2.00	41.7	-18.80	6.49	3.25	37283	30220	360
La Sassa	Cave hyena	Sassa 516B	45512	AF	2.02	40.1	-17.73	10.87	3.28	37218	29190	310
La Sassa	Cave hyena	Sassa 516A	45513	AF	2.01	40.2	-18.23	11.09	3.26	37219	30150	350
La Sassa	Cave lion	Sassa 23	45514	AG	1.26	24.8	-18.61	12.14	3.54	X-2772-34	29300	400
La Silluca Cave	Straight-tusked elephant	11419	45646	AG	0.01	0.1	-24.87	0.00	0.00			
Los Rincones	Leopard	MPZ 2015/600	45641	AG	0.01	0.2	-21.77	0.00	0.00			
Los Rincones	Leopard	MPZ 2015/665	45642	AG	0.02	0.4	-29.80	0.00	0.00			
Los Rincones	Leopard	MPZ 2015/613	45643	AG	0.03	0.6	-27.34	0.00	0.00			
Los Rincones	Leopard	MPZ 2015/616	45644	AG	0.03	0.7	-20.90	0.00	0.00			
Manastira	Unknown	Mana 4	42406	AF	2.26	45.3	-20.44	10.85	3.35	35565	47700	0
Manastira	Unknown	Mana 5	42407	AF	2.17	43.3	-19.21	8.17	3.21	35566	50200	0
Manastira	Unknown	Mana 6	42408	AF	2.13	43.4	-19.19	10.76	3.22	35567	50200	0
Manastira	Unknown	Mana 6	42408	AF	2.13	43.4	-19.19	10.76	3.22	35567	50200	0
Manastira	Bovid	Mana 7	42409	AF	2.14	43.2	-19.96	9.89	3.20	35568	49900	0
Redaka II	Cave hyena	Red CC1	42399	AF	2.31	46.3	-20.14	11.23	3.42	35559	30910	380
Redaka II	Cave hyena	Red CC2	42400	AF	2.13	44.0	-18.70	13.94	3.29	35560	32700	500
Redaka II	Cave hyena	Red CC3	42401	AF	2.23	45.3	-19.30	11.44	3.27	35561	30920	380
Redaka II	Cave hyena	Red CC4	42402	AF	2.26	46.0	-18.47	12.77	3.38	35562	33850	550
Redaka II	Cave hyena	Red CC5	42403	AF	2.05	43.4	-19.65	12.01	3.25	35563	47200	0
Redaka II	Unknown	Red NID5	42405	AF	2.06	43.2	-20.95	8.02	3.23	35564	45400	0
Tilos	Pygmy elephant	T.1052	44410	AG	0.00	0.0	0.00	0.00	0.00			
Tilos	Pygmy elephant	T.8074	44411	AG	0.00	0.0	0.00	0.00	0.00			
Tilos	Pygmy elephant	T.8072	44412	AG	0.00	0.0	0.00	0.00	0.00			
Vasil Levski	Cave hyena	Vasil C	45645	AG	1.69	40.4	-18.54	9.27	3.44	37323	38100	1100
Zafarraya	Unknown	ZAF 1 EJ	42796	AF*	2.12	43.3	-19.32	4.64	3.30	35500	30360	360

Table E.3: All combustions attempted for this thesis and radiocarbon results. Some samples were failed at combustion due to low carbon yield or poor health metrics. *(continued)*

Site	Species	Sample	P	PCode	C (mg)	%C	δ^{13}C	δ^{15}N	CN	OxA	Date	±
Zafarraya	Unknown	ZAF 1 EJ	42796	AF*	2.12	43.3	-19.32	4.64	3.30	35500	30360	360
Zafarraya	Unknown	ZAF 1 EJ	42796	NRC	1.59	41.8	-27.81	6.17	4.94	X-2730-9	31000	290
Zafarraya	Unknown	ZAF 3 EJ	42798	AF	1.92	40.0	-19.01	6.47	3.27	35226	27460	270
Zafarraya	Unknown	ZAF 3 EJ	42798	NRC	0.89	44.3	-23.32	8.16	5.05	X-2732-18	27400	310
Zafarraya	Unknown	ZAF 5 EJ	42800	AF	2.09	43.9	-20.06	4.98	3.27	35227	42400	1600
Zafarraya	Unknown	ZAF 6 EJ	42801	AF	0.07	1.5	-21.10	0.00	0.00			
Zafarraya	Unknown	ZAF 6 EJ	42801	AF	0.07	1.5	-21.10	0.00	0.00			
Zafarraya	Unknown	Zaf N40-009	43017	AF	2.12	44.2	-19.45	6.73	3.46	35540	34100	600
Zafarraya	Unknown	Zaf N40-009	43017	NRC	1.62	46.3	-22.93	8.75	4.92	X-2730-10	36850	550
Zafarraya	Unknown	Zaf N40071	43018	AF	1.49	43.1	-19.27	8.04	3.48	X-2720-37	34100	650
Zafarraya	Unknown	Zaf P11H92	43019	AF	2.06	42.9	-19.56	6.24	3.37	35541	43200	1700
Zafarraya	Unknown	Zaf N40-010	43022	AF	2.10	43.8	-19.95	6.17	3.29	35542	31950	450
Zafarraya	Unknown	Zaf N40-032	43023	AF	2.11	44.2	-19.00	7.82	3.33	35543	31140	400
Zafarraya	Unknown	Zaf N40-172	43024	AF	2.13	46.2	-19.32	5.92	3.30	35544	30730	380
Zafarraya	Unknown	Zaf N40-130	43025	AF	2.05	42.2	-19.62	5.97	3.33	35545	43500	1800
Zafarraya	Unknown	Zaf N40-130	43025	NRC	1.42	42.9	-24.19	7.47	4.97	X-2732-28	42200	1200
Zafarraya	Unknown	Zaf N40-130	43025	AF*	1.64	34.5	-19.98	6.23	3.41	35791	41200	1500
Zafarraya	Unknown	Zaf N18	43026	AF	2.14	45.3	-19.40	7.06	3.31	35546	44600	2000
Zafarraya	Leopard	Zaf N84	43533	AG	0.58	11.8	-19.59	6.92	4.03			

F
Species radiocarbon dates

F.1 Leopards

Table F.1: Direct radiocarbon dates of leopards in Europe. The HPLC-corrected date for P44416 (NRC) is 43011 ± 3513 BP.

Site	ID	PCode	Material	>	Date BP	Error	Score	Source
Castelcivita Cave	OxA/37222/45631/AF	AF	Bone		43400	1800	High	Thesis
Castelcivita Cave	OxA/37223/45632/AF	AF	Bone		38800	1000	High	Thesis
Grotte di Equi	OxA/-88/44416/NRC	NRC	Bone		41000	1800	High	Thesis
Grotte di Equi	Beta/360175/NA/NA		Bone		33000	260	Low	Ghezzo and Rook 2015
Jou'l Llobu (Asturias)	OxA/10173/11757/AF*	AF*	Bone		46600	2300	High	Pinto Llona 2007
Kudaro 3	OxA/-1/30086/AF	AF	Bone		44500	2000	High	Baryshnikov 2011
Kudaro 3	OxA/25736/30086/AF	AF	Bone		43900	1900	High	Baryshnikov 2011
Lion Tower and Moat	OxA/13495/15522/AF*	AF*	Bone		386	25	Rejected	O'Regan et al. 2005
Plymouth Museum	OxA/30390/36343/AF	AF	Tooth		187	24	Rejected	Freedman and Evans 2015
Triagalnata Peshtera	OxA/11416/13176/AF	AF	Tooth		37500	650	Med	ORAU database

F.2 Lions

Table F.2: Direct radiocarbon dates of cave lions in Europe and Asia.

Site	Subregion	OxA	Lab	P	PCode	Material	>	Date BP	Error	Score	Source
Abri des Cabones	Central Europe	12021	OxA	13908	AF*	Bone/tooth		12565	50	High	Stuart and Lister, 2011
Alazeya	Asia	13021	OxA	14708	AF	Bone/tooth		55300	2500	High	Barnett et al., 2009
Alazeya	Asia	13474	OxA	14708	AF	Bone/tooth		58200	3500	High	Barnett et al., 2009
Alazeya	Asia	13835	OxA	16036	AF	Bone/tooth		13770	55	High	Barnett et al., 2009
Altwies	Central Europe	4944	KIA			Bone/tooth		31690	500	Low	Baales and Le Brun-Ricalens, 1996
Arga Yurekh	Asia	13833	OxA	16034	AF	Bone/tooth		12525	50	High	Barnett et al., 2009
Baumanns	Northern Europe	6209	Erl			Bone/tooth		34645	365	Low	Rosendahl et al., 2005
Beryozovka	Asia	13831	OxA	16032	AF	Bone/tooth		27950	140	High	Barnett et al., 2009
Bolshoy Liakhovsky Island	Asia	13836	OxA	16037	AF	Bone/tooth	>	60700		High	Barnett et al., 2009
Bolshoy Liakhovsky Island	Asia	13837	OxA	16038	AF	Bone/tooth	>	62100		High	Barnett et al., 2009
Bolshoy Liakhovsky Island	Asia	17035	OxA	19313	AF*	Bone/tooth		47700	800	High	Stuart and Lister, 2011

Table F.2: Direct radiocarbon dates of cave lions in Europe and Asia. *(continued)*

Site	Subregion	OxA	Lab	P	PCode	Material	>	Date BP	Error	Score	Source
Bolshoy Liakhovsky Island	Asia	17039	OxA	19321	AF	Bone/tooth	>	62100		High	Stuart and Lister, 2011
Bolshoy Liakhovsky Island	Asia	18812	OxA	21436	AF*	Bone/tooth		52000	1500	High	Stuart and Lister, 2011
Bolshoy Liakhovsky Island	Asia	18813	OxA	21437	AF	Bone/tooth	>	52600		High	Stuart and Lister, 2011
Bykovskiy Peninsula	Asia	17037	OxA	19319	AF*	Bone/tooth		28550	140	High	Stuart and Lister, 2011
Bykovskiy Peninsula	Asia	17038	OxA	19320	AF	Bone/tooth		28450	140	Med	Stuart and Lister, 2011
Chukochya	Asia	13025	OxA	14713	AF	Bone/tooth		55700	3000	High	Barnett et al., 2009
Chukochya	Asia	13475	OxA	14713	AF	Bone/tooth		54600	1700	High	Barnett et al., 2009
Chukotka / Kyttyk Peninsula	Asia	19359	OxA	22222	AF	Bone/tooth		36550	290	High	Stuart and Lister, 2011
Chumysh	Asia	17043	OxA	19325	AF	Bone/tooth		51400	1200	High	Stuart and Lister, 2011
Closani	Southern Europe	22124	OxA	25501	AF*	Bone/tooth		33150	500	High	Stuart and Lister, 2011
Closani	Southern Europe	22125	OxA	25501	AF*	Bone/tooth		32500	450	High	Stuart and Lister, 2011
Derbina IV	Asia	20252	OxA	23781	AF*	Bone/tooth		35750	400	High	Stuart and Lister, 2011
Derbina IV	Asia	20257	OxA	23782	AF	Bone/tooth		35390	280	High	Stuart and Lister, 2011

Table F.2: Direct radiocarbon dates of cave lions in Europe and Asia. *(continued)*

Site	Subregion	OxA	Lab	P	PCode	Material	>	Date BP	Error	Score	Source
Duvanny Yar	Asia	12981	OxA	14709	AF	Bone/tooth		28720	160	Med	Barnett et al., 2009
Duvanny Yar	Asia	13022	OxA	14710	AF	Bone/tooth	>	53200		High	Barnett et al., 2009
Duvanny Yar	Asia	13024	OxA	14712	AF	Bone/tooth		46200	1500	Med	Barnett et al., 2009
Duvanny Yar	Asia	13829	OxA	16030	AF	Bone/tooth	>	61500		High	Barnett et al., 2009
Elovka	Asia	20672	OxA	24281	AF	Bone/tooth		18350	75	Med	Stuart and Lister, 2011
Emine Bair Khosar	Southern Europe	17044	OxA	19331	AF	Bone/tooth		56400	2100	High	Stuart and Lister, 2011
Emine Bair Khosar	Southern Europe	17045	OxA	19331	AF	Bone/tooth	>	60200		High	Stuart and Lister, 2011
Eurogeul	Northern Europe	23151	GrA			Bone/tooth		42230	570	Low	Mol et al., 2006
Gamssulzen	Central Europe	13110	OxA	14707	AF	Bone/tooth		49900	2500	High	Barnett et al., 2009
Gremsdorf	Southern Europe	14862	OxA	17157	AF	Bone/tooth		28310	50	Med	Barnett et al., 2009
Grotte di Equi	Southern Europe	37177	OxA	45510	AG	Bone/tooth		21920	160	Med	Thesis
Grotto Cheremuhovo 1-1	Asia	10894	OxA	12580	AF	Bone/tooth		29120	230	Med	Stuart and Lister, 2011
Grotto Cheremuhovo 1-2	Asia	10895	OxA	12581	AF	Bone/tooth		30140	240	High	Stuart and Lister, 2011

Table F.2: Direct radiocarbon dates of cave lions in Europe and Asia. *(continued)*

Site	Subregion	OxA	Lab	P	PCode	Material	>	Date BP	Error	Score	Source
Grotto Holodny	Asia	10910	OxA	12585	AF	Bone/tooth		14750	70	High	Stuart and Lister, 2011
Grotto Shaitansky	Asia	10907	OxA	12582	AF	Bone/tooth		54500	2600	High	Stuart and Lister, 2011
Grotto Verhnequbahinsky	Asia	10909	OxA	12584	AF	Bone/tooth		13560	70	Med	Stuart and Lister, 2011
Grotto Viasher 2	Asia	10908	OxA	12583	AF	Bone/tooth		13570	70	Med	Stuart and Lister, 2011
Ignatievskaya	Asia	10887	OxA	12555	AF*	Bone/tooth		41900	1200	Med	Stuart and Lister, 2011
Jou'l Llobu	Southern Europe	10186	OxA	11760	AF	Bone/tooth		46400	2100	High	Stuart and Lister, 2011
Kent's Cavern	Northern Europe	14285	OxA	15999	AF*	Bone/tooth		43600	3600	Low	Higham et al., 2006
Kerem(e)sit	Asia	16983	OxA	19317	AF*	Bone/tooth		27720	140	Med	Stuart and Lister, 2011
Khomus Yuryakh Bol.	Asia	17036	OxA	19318	AF*	Bone/tooth	>	62400		Med	Stuart and Lister, 2011
Khroma	Asia	17040	OxA	19323	AF*	Bone/tooth		19755	80	Med	Stuart and Lister, 2011
Khroma	Asia	17041	OxA	19323	AF*	Bone/tooth		19725	75	High	Stuart and Lister, 2011
Khromskaya Guba	Asia	13023	OxA	14711	AF	Bone/tooth	>	50600		High	Barnett et al., 2009
Kostenki I	Northern Europe	17032	OxA	19310	AF*	Bone/tooth		23190	120	Med	Stuart and Lister, 2011
Kostenki I	Northern Europe	17372	OxA	19872	AF*	Bone/tooth		23400	100	Med	Stuart and Lister, 2011

Table F.2: Direct radiocarbon dates of cave lions in Europe and Asia. *(continued)*

Site	Subregion	OxA	Lab	P	PCode	Material	>	Date BP	Error	Score	Source
Kostenki IV	Northern Europe	17042	OxA	19324	AF	Bone/tooth		23080	100	Med	Stuart and Lister, 2011
Kozarnica	Southern Europe	35558	OxA	42398	AF	Bone/tooth		16395	80	High	Thesis
Krestovka	Asia	13830	OxA	16031	AF	Bone/tooth		54100	1800	High	Barnett et al., 2009
Kubekovo	Asia	17054	OxA	19339	AF*	Bone/tooth		17915	70	Med	Stuart and Lister, 2011
Kurtak 4	Asia	17373	OxA	19873	AF*	Bone/tooth		25700	130	Med	Stuart and Lister, 2011
La Garma	Southern Europe	18698	OxA	21340	AF	Bone/tooth		13830	55	High	Cueto et al., 2016
La Garma	Southern Europe	18699	OxA	21340	AF	Bone/tooth		13835	60	High	Cueto et al., 2016
La Sassa	Southern Europe	X-2772-34	OxA	45514	AG	Bone/tooth		29300	400	Low	Thesis
Lakatnik	Southern Europe	11422	OxA	13175	AF	Bone/tooth		31200	330	Med	Stuart and Lister, 2011
Lathum	Northern Europe	16715	OxA	18958	AF*	Bone/tooth		44850	650	High	Stuart and Lister, 2011
Le Closeau	Central Europe	41882 [2]	AA			Bone/tooth		12248	66	Low	Bodu and Mevel, 2008
Lena	Asia	12901	OxA	14915	AF	Bone/tooth		12450	60	High	Barnett et al., 2009
Mal'ta	Asia	17033	OxA	19311	AF*	Bone/tooth		21500	100	Med	Stuart and Lister, 2011
New Siberian Islands / no exact locality	Asia	18712	OxA	21733	AF	Bone/tooth		40210	350	High	Stuart and Lister, 2011

Table F.2: Direct radiocarbon dates of cave lions in Europe and Asia. *(continued)*

Site	Subregion	OxA	Lab	P	PCode	Material	>	Date BP	Error	Score	Source
Nizhnyaya Tunguska	Asia	16980	OxA	19314	AF*	Bone/tooth		50500	1300	Med	Stuart and Lister, 2011
Onon	Asia	16982	OxA	19316	AF*	Bone/tooth		17910	75	Med	Stuart and Lister, 2011
Pin Hole	Northern Europe	19092	OxA	21894	AF*	Bone/tooth		35650	450	High	Stuart and Lister, 2011
Pobeda	Asia	10845	OxA	12554	AF*	Bone/tooth	>	39800		Med	Stuart and Lister, 2011
Podsemnich Ochotnikov	Asia	11349	OxA	13030	AF*	Bone/tooth		13500	65	Med	Stuart and Lister, 2011
Priobskoye Steppe Plateau	Asia	16981	OxA	19315	AF*	Bone/tooth		52800	1600	High	Stuart and Lister, 2011
Raj	Northern Europe	11096	OxA	12870	AF	Bone/tooth		25190	350	Med	Stuart and Lister, 2011
Robin Hood	Northern Europe	12799	OxA	14513	AF	Bone/tooth	>	38500		Low	Jacobi et al., 2006
Schusterlucke	Central Europe	10513	OxA	12041	AF	Bone/tooth		15400	130	Med	Stuart and Lister, 2011
Sededema	Asia	17057	OxA	19322	AF*	Bone/tooth	>	56800		High	Stuart and Lister, 2011
Sibyllenhoehle	Central Europe	15354	OxA	17446	AF	Bone/tooth	>	48100		High	Barnett et al., 2009
Siegsdorf	Central Europe	14406	KIA			Bone/tooth		47180	1190	Low	Burger et al., 2004
Smolensk region	Northern Europe	17034	OxA	19312	AF*	Bone/tooth		14055	60	Med	Stuart and Lister, 2011
Stanchikovskiy Yar	Asia	17030	OxA	19308	AF*	Bone/tooth	>	58100		High	Stuart and Lister, 2011

Table F.2: Direct radiocarbon dates of cave lions in Europe and Asia. *(continued)*

Site	Subregion	OxA	Lab	P	PCode	Material	>	Date BP	Error	Score	Source
Tain	Asia	10888	OxA	12556	AF*	Bone/tooth	>	49600		High	Stuart and Lister, 2011
Teufelslucke	Asia	2545	VERA			Bone/tooth		42400	1800	Low	M. Pacher, pers. comm.
Tischofer	Central Europe	16510	KIA			Bone/tooth		31890	300	Low	Burger et al., 2004
Togul River Basin	Asia	18711	OxA	21732	AF	Bone/tooth		22080	80	High	Stuart and Lister, 2011
Trou Magrite	Northern Europe	6593	OxA	7799	AI	Bone/tooth		25980	340	Med	Charles et al., 2003
Tyung	Asia	17010	OxA	19306	AF*	Bone/tooth		46700	1300	Med	Stuart and Lister, 2011
Ursilor	Southern Europe	22122	OxA	25499	AF*	Bone/tooth		39000	1000	High	Stuart and Lister, 2011
Ursilor	Southern Europe	22123	OxA	25500	AF*	Bone/tooth		38600	1000	Med	Stuart and Lister, 2011
Urtiaga	Southern Europe	10121	OxA	11430	AF	Bone/tooth		13770	120	Med	Stuart and Lister, 2011
Vetrenny	Asia	17029	OxA	19307	AF*	Bone/tooth	>	55400		High	Stuart and Lister, 2011
Volchikha II	Asia	20251	OxA	23780	AF	Bone/tooth		20085	80	Med	Stuart and Lister, 2011
Volga Don Canal	Asia	17031	OxA	19309	AF*	Bone/tooth		28480	200	Med	Stuart and Lister, 2011
Wierchowska Gorna	Northern Europe	10087	OxA	11686	AF	Bone/tooth		38650	600	High	Barnett et al., 2009
Yana RHS Site	Asia	173066	Beta			Bone/tooth		26050	240	Low	Pitulko et al., 2004

Table F.2: Direct radiocarbon dates of cave lions in Europe and Asia. *(continued)*

Site	Subregion	OxA	Lab	P	PCode	Material	>	Date BP	Error	Score	Source
Zawalona	Northern Europe	11156	OxA	12872	AF	Bone/tooth		38800	1100	High	Stuart and Lister, 2011
Zigeunerfels	Central Europe	17268	OxA	18959	AF*	Bone/tooth		12375	50	High	Stuart and Lister, 2011
Zoolithen	Central Europe	14863	OxA	17158	AF	Bone/tooth		47600	900	High	Barnett et al., 2009

F.3 Hyenas

Table F.3: Direct radiocarbon dates of cave hyenas and bones chewed/digested by hyenas in Europe and Asia.

Site	Subregion	OxA	Lab	P	PCode	Material	>	Date BP	Error	Score	Source
Agios Georgios	Northern Europe	17009	OxA	19302	AF	Tooth		29340	240	Med	Stuart and Lister (2014)
Allander Tropfsteinhohle	Central Europe	10299	OxA	11796	AF	Bone	>	36200		Rejected	Stuart and Lister (2014)
Amalda	Southern Europe	10398	OxA	12044	AF	Bone		39900	700	High	Stuart and Lister (2014)
Arene Candide	Southern Europe	10658	OxA	12127	AF	Bone		27050	550	Med	Stuart and Lister (2014)
Ash Tree	Northern Europe	5798	OxA	7040	AI	Tooth		25660	380	Low	Hedges et al. (1996)
Bacho Kiro	Southern Europe	11421	OxA	13169	AF	Tooth		51500	2400	Med	Stuart and Lister (2014)
Balkan Range	Southern Europe	11551	OxA	13170	AF	Tooth		26600	170	Med	Stuart and Lister (2014)
Baranica	Southern Europe	13946	OxA	15903	AF	Tooth	>	53100		High	Stuart and Lister (2014)
Bench Tunnel	Northern Europe	13512	OxA	7199	AF	Bone		36800	450	High	Jacobi et al. (2006)
Bench Tunnel	Northern Europe	13324	OxA	7199	AG*	Bone		37500	900	High	Currant (2004)
Bench Tunnel	Northern Europe	5961	OxA	7199	AI	Bone		32500	1200	Med	Jacobi et al. (2006)
Bench Tunnel	Northern Europe	1620	OxA	2035	AC	Bone		34500	1400	Low	Jacobi et al. (2006)
Bukhtarma	Asia	17028	OxA	19297	AF	Tooth	>	45200		High	Stuart and Lister (2014)

Table F.3: Direct radiocarbon dates of cave hyenas and bones chewed/digested by hyenas in Europe and Asia. *(continued)*

Site	Subregion	OxA	Lab	P	PCode	Material	>	Date BP	Error	Score	Source
Bukovinka	Central Europe	2529	VERA			Tooth		41300	1200	Low	Rohland et al. (2005)
Castelcivita	Southern Europe	37221	OxA	45630	AF	Bone		34500	600	High	Thesis
Castlepook	Northern Europe	4234	OxA	5173	AI	Bone		24000	300	Med	Woodman et al. (1997)
Castlepook	Northern Europe	4237	OxA	5176	AI	Bone	>	45200	1	Med	Woodman et al. (1997)
Castlepook	Northern Europe	19531	OxA	22734	AF	Bone		33240	220	High	Stuart and Lister (2014)
Castlepook	Northern Europe	19532	OxA	22735	AF	Tooth		45700	700	High	Stuart and Lister (2014)
Castlepook	Northern Europe	13625	I			Bone		34300	1800	Low	Stuart and van Wijngaarden-Bakker (1985)
Cathole	Northern Europe	29411	OxA	35510	AF	Tooth	>	45800		High	Walker et al. (2014)
Cava Muracci	Southern Europe	X-2756-42	OxA	44418	NRC	Bone		44400	3700	Med	Thesis
Cava Muracci	Southern Europe	X-2756-42	OxA	44418	NRC	Bone		44400	3700	Rejected	Thesis
Cava Muracci	Southern Europe	X-2772-28	OxA	45506	AG	Bone	>	41700		Med	Thesis
Cava Muracci	Southern Europe	X-2772-33	OxA	45507	AG	Bone		46500	3900	Med	Thesis
Cefn	Northern Europe	9698	OxA	11188	AF	Bone		31900	450	High	Currant (2004)

Table F.3: Direct radiocarbon dates of cave hyenas and bones chewed/digested by hyenas in Europe and Asia. *(continued)*

Site	Subregion	OxA	Lab	P	PCode	Material	>	Date BP	Error	Score	Source
Certova pec	Central Europe	2530	VERA			Tooth		51200	2950	Low	Rohland et al. (2005)
Church Hole	Northern Europe	21995	OxA	25382	AF	Tooth		44200	2000	High	Dodge et al. (2012)
Church Hole	Northern Europe	14926	OxA	7041	AF	Tooth	>	40000		High	Higham et al. (2006a)
Church Hole	Northern Europe	5799	OxA	7041	AI	Tooth		26840	420	Low	Jacobi et al. (2006)
Church Hole	Northern Europe	5800	OxA	7042	AI	Tooth		24000	260	Low	Hedges et al. (1996)
Coygan	Northern Europe	14400	OxA	16380	AF	Tooth		32140	250	High	Higham et al. (2006a)
Coygan	Northern Europe	14401	OxA	16381	AF	Tooth		43000	2100	High	Higham et al. (2006a)
Coygan	Northern Europe	14402	OxA	16383	AF	Tooth		36000	500	High	Higham et al. (2006a)
Coygan	Northern Europe	14403	OxA	16384	AF	Tooth		39700	1700	High	Higham et al. (2006a)
Coygan	Northern Europe	14473	OxA	16382	AF	Tooth		32400	550	High	Higham et al. (2006a)
Coygan	Northern Europe	16766	OxA	16240	AF	Tooth	>	41300		High	Currant (2004)
Coygan	Northern Europe	16767	OxA	16241	AF	Bone	>	37700		Med	Currant (2004)
Creswell Crags	Northern Europe	21997	OxA	25384	AF	Tooth	>	45500		High	Dodge et al. (2012)
Creswell Crags	Northern Europe	21996	OxA	25383	AF	Tooth		45400	2200	High	Dodge et al. (2012)

Table F.3: Direct radiocarbon dates of cave hyenas and bones chewed/digested by hyenas in Europe and Asia. *(continued)*

Site	Subregion	OxA	Lab	P	PCode	Material	>	Date BP	Error	Score	Source
Creswell Crags	Northern Europe	X-2352-10	OxA	25381		Tooth	>	44500		Low	Dodge et al. (2012)
Daylight Rock Fissure	Northern Europe	9695	OxA	11185	AF	Tooth		46400	3800	High	Currant (2004)
Denisova	Asia	29855	OxA	35673	AF	Bone		47900	3100	High	Douka et al. (2019)
Denisova	Asia	25284	KIA			Tooth		42300	900	Low	Rohland et al. (2005)
Desnisukhi Peck	Southern Europe	11552	OxA	13171	AF	Tooth		31810	370	High	Stuart and Lister (2014)
Duruitoarea Veche	Central Europe	11691	OxA	13478	AF	Bone		35350	380	High	Stuart and Lister (2014)
Eel Point	Northern Europe	9694	OxA	11184	AF	Tooth		41400	1600	High	Currant (2004)
Ffynnon Beuno	Northern Europe	9696	OxA	11186	AF	Bone		18520	130	High	Aldhouse-Green et al. (2015)
Ffynnon Beuno	Northern Europe	X-2198-8	OxA	11186	AF	Bone		18850	650	Rejected	Aldhouse-Green et al. (2015)
Geographical Society	Asia	17005	OxA	19299	AF	Bone		42950	600	High	Stuart and Lister (2014)
Geographical Society	Asia	17046	OxA	19332	AF	Bone		46000	700	Med	Stuart and Lister (2014)
Geographical Society	Asia	25285	KIA			aDNA		48650	2380/1840	Low	Rohland et al. (2005)
Goyet	Northern Europe	2812	GrA			Bone		27230	260	Low	Peigné et al. (2009)
Goyet	Northern Europe	8958	UtC			Tooth		35000	400	Low	Peigné et al. (2009)

Table F.3: Direct radiocarbon dates of cave hyenas and bones chewed/digested by hyenas in Europe and Asia. *(continued)*

Site	Subregion	OxA	Lab	P	PCode	Material	>	Date BP	Error	Score	Source
Grange Farm, Glaston	Northern Europe	21309	OxA	25399		Chewed bone		38120	360	Low	Cooper et al. (2012)
Grange Farm, Glaston	Northern Europe	21310	OxA	25400		Chewed bone		38800	390	Low	Cooper et al. (2012)
Grange Farm, Glaston	Northern Europe	22149	OxA	25912		Chewed bone		38400	900	Low	Cooper et al. (2012)
Grange Farm, Glaston	Northern Europe	21308	OxA	25398		Bone		35610	300	Low	Cooper et al. (2012)
Griifen	Southern Europe	1835	VERA			aDNA		44300	1800/1500	Low	Rohland et al. (2005)
Grotta Paglicci	Southern Europe	10523	OxA	12118	AF	Tooth		26120	330	High	Stuart and Lister (2014)
Grotta Paglicci	Southern Europe	10657	OxA	12119	AF	Bone		29100	1600	Med	Stuart and Lister (2014)
Grotta Pocala	Southern Europe	2532	VERA			aDNA		38220	920/820	Low	Rohland et al. (2005)
Grotte de Canecaude	Southern Europe	16691	OxA	18956	AF	Tooth		33130	220	High	Stuart and Lister (2014)
Grotte Grappin	Central Europe	19633	OxA	23377	AF	Bone		28570	150	High	Stuart and Lister (2014)
Grotte Grappin	Central Europe	3162 (Poz)	Ly			Bone		15335	115	Low	Cupillard and Welte (2006)
Grotto Sikiyaz Tamak 7	Asia	10889	OxA	12558	AF	Bone	>	47600		Med	Stuart and Lister (2014)
Hyaena Den	Northern Europe	13917	OxA	15846	AF	Tooth		48600	1000	High	Currant (2004)
Ignatievskaya	Asia	10846	OxA	12557	AF	Tooth	>	40100		Med	Stuart and Lister (2014)

Table F.3: Direct radiocarbon dates of cave hyenas and bones chewed/digested by hyenas in Europe and Asia. *(continued)*

Site	Subregion	OxA	Lab	P	PCode	Material	>	Date BP	Error	Score	Source
Ignatievskaya	Asia	19537	OxA	22745	AF	Tooth		47500	900	High	Stuart and Lister (2014)
Ignatievskaya	Asia	19658	OxA	22739	AF	Bone	>	62300		High	Kosintsev et al. (2016)
Ignatievskaya	Asia	19659	OxA	22741	AF	Tooth		44300	600	High	Kosintsev et al. (2016)
Ignatievskaya	Asia	19660	OxA	22742	AF	Bone		40240	380	High	Kosintsev et al. (2016)
Igric	Central Europe	2534	VERA			Tooth		41800	1300	Low	Rohland et al. (2005)
Igue du Gral	Southern Europe	20763	OxA	24886	AF	Bone		31990	240	High	Stuart and Lister (2014)
Kent's	Northern Europe	11152	OxA	12759	NRC	Bone		37750	500	Low	Stuart and Lister (2014)
Kent's	Northern Europe	19509	OxA	22670		Tooth		40200	600	Low	Currant (2004)
Kent's	Northern Europe	30351	OxA	35815	AF	Bone		30630	380	High	Proctor et al. (2017)
Kent's	Northern Europe	10806	OxA	12470		Bone		36750	450	Low	Jacobi (2007)
Kiskevelyi	Central Europe	2535	VERA			Tooth	>	48500		Low	Rohland et al. (2005)
Komarowa	Northern Europe	11158	OxA	12881	AF	Bone		42200	800	High	Stuart and Lister (2014)
Komarowa	Northern Europe	11161	OxA	12884	AF	Bone		41700	1100	High	Stuart and Lister (2014)
Komarowa	Northern Europe	11062	OxA	12890	AF	Tooth		46100	900	High	Stuart and Lister (2014)

Table F.3: Direct radiocarbon dates of cave hyenas and bones chewed/digested by hyenas in Europe and Asia. *(continued)*

Site	Subregion	OxA	Lab	P	PCode	Material	>	Date BP	Error	Score	Source
Kozarnica	Southern Europe	35556	OxA	42395	AF	Bone		34350	600	High	Thesis
Kozarnica	Southern Europe	35557	OxA	42397	AF	Tooth		49100	3600	High	Thesis
La Adam	Southern Europe	22127	OxA	25564	AF	Tooth		38700	1000	Med	Stuart and Lister (2014)
La Adam	Southern Europe	22128	OxA	25565	AF	Bone		39100	1000	High	Stuart and Lister (2014)
La Adam	Southern Europe	22129	OxA	25566	AF	Tooth		36850	750	Med	Stuart and Lister (2014)
La Sassa	Southern Europe	37218	OxA	45512	AF	Bone		29190	310	Med	Thesis
La Sassa	Southern Europe	37219	OxA	45513	AF	Bone		30150	350	High	Thesis
Les Garennes	Southern Europe	216143	Beta			Bone		28410	230	Low	Henry-Gambier et al. (2007)
Les Roches de Villeneuve	Southern Europe	177765	BETA			Bone		40700	900	Low	Rohland et al. (2005)
Les Rois	Southern Europe	X-2294-11	OxA	22708		Bone		35750	800	Low	Higham pers. comm.
Little Hoyle	Northern Europe	1491	OxA	1655	AC	Tooth		34590	1500	Low	Currant (2004)
Magura	Southern Europe	31009	OxA	37104	AF	Bone		32750	500	High	Ivanova et al. (2016)
Manastira	Southern Europe	35565	OxA	42406	AF	Bone	>	47700		High	Thesis
Manastira	Southern Europe	35566	OxA	42407	AF	Bone	>	50200		High	Thesis

Table F.3: Direct radiocarbon dates of cave hyenas and bones chewed/digested by hyenas in Europe and Asia. *(continued)*

Site	Subregion	OxA	Lab	P	PCode	Material	>	Date BP	Error	Score	Source
Manastira	Southern Europe	35567	OxA	42408	AF	Bone	>	50200		High	Thesis
Melwurmhohle	Central Europe	2540	VERA			aDNA		35900	600/560	Low	Rohland et al. (2005)
Miskolc III	Central Europe	2533	VERA			Tooth		44400	1750	Low	Rohland et al. (2005)
Nanna's	Northern Europe	9673	OxA	11180	AF	Tooth		27100	750	Rejected	Currant (2004)
Nizhniy Tsasuchey	Northern Europe	16329	OxA	18548	AF	Bone		20440	90	Rejected	Stuart and Lister (2014)
Ogof-yr-Ychen	Northern Europe	9691	OxA	11181	AF	Tooth		37400	700	High	Currant (2004)
Ogof-yr-Ychen	Northern Europe	9692	OxA	11182	AF	Tooth		27200	360	High	Currant (2004)
Ogof-yr-Ychen	Northern Europe	X-2278-43	OxA	22188	AF	Tooth		33000	600	High	Lister pers. comm.
Ogof-yr-Ychen	Northern Europe	X-2278-44	OxA	22189	AF	Tooth		31750	600	High	Lister pers. comm.
Outside West Pin Hole	Northern Europe	5803	OxA	7045		Bone		29300	420	Low	Hedges et al. (1996)
Paviland	Northern Europe	13659	OxA	8261	AF	Bone		23120	130	Rejected	Jacobi and Higham (2008)
Paviland	Northern Europe	6980	OxA	8226	AG	Tooth		27750	500	Low	Currant (2004)
Paviland	Northern Europe	7087	OxA	8261	AG	Bone		17880	180	High	Aldhouse-Green and Pettitt (1998)
Paviland	Northern Europe	13378	OxA	8261	NRC	Bone		18430	70	Low	Jacobi and Higham (2008)

Table F.3: Direct radiocarbon dates of cave hyenas and bones chewed/digested by hyenas in Europe and Asia. *(continued)*

Site	Subregion	OxA	Lab	P	PCode	Material	>	Date BP	Error	Score	Source
Pin Hole	Northern Europe	15518	OxA	1839	AF	Bone		37800	500	High	Currant (2004)
Pin Hole	Northern Europe	15520	OxA	1839	AF	Bone		37150	450	High	Currant (2004)
Pin Hole	Northern Europe	11796	OxA	13663		Chewed bone		44200	800	Low	Stuart and Lister (2014)
Pin Hole	Northern Europe	15548	OxA	1840	AF	Bone	>	35500		Med	Jacobi and Higham (2011)
Pin Hole	Northern Europe	1448	OxA	1971	AC	Bone		42200	3000	Low	Currant (2004)
Pin Hole	Northern Europe	4754	OxA	5698	AI	Tooth		37800	1600	Low	Currant (2004)
Pin Hole	Northern Europe	1207	OxA	1839		Bone		34500	1200	Low	Hedges et al. (1988)
Pin Hole	Northern Europe	1206	OxA	1840		Bone		32200	1000	Low	Hedges et al. (1988)
Potter's	Northern Europe	9693	OxA	11183	AF	Bone		28000	310	High	Currant (2004)
Potter's	Northern Europe	19215	OxA	22190	AF	Bone		27470	240	High	Currant (2004)
Priory Farm	Northern Europe	9674	OxA	11190	AF	Tooth	>	40800		Med	Currant (2004)
Redaka II	Southern Europe	35559	OxA	42399	AF	Bone		30910	380	High	Thesis
Redaka II	Southern Europe	35560	OxA	42400	AF	Tooth		32700	500	High	Thesis
Redaka II	Southern Europe	35561	OxA	42401	AF	Bone		30920	380	High	Thesis

Table F.3: Direct radiocarbon dates of cave hyenas and bones chewed/digested by hyenas in Europe and Asia. *(continued)*

Site	Subregion	OxA	Lab	P	PCode	Material	>	Date BP	Error	Score	Source
Redaka II	Southern Europe	35562	OxA	42402	AF	Tooth		33850	550	High	Thesis
Redaka II	Southern Europe	35563	OxA	42403	AF	Bone	>	47200		High	Thesis
Rhino (Nosorogov)	Asia	17003	OxA	19295	AF	Tooth		37700	360	High	Stuart and Lister (2014)
Robin Hood	Northern Europe	12800	OxA	14514	AF	Tooth	>	42000		High	Jacobi et al. (2006)
Robin Hood	Northern Europe	12771	OxA	14515	AF	Bone		45300	1000	High	Currant (2004)
Robin Hood	Northern Europe	12736	OxA	14518	AF	Bone	>	52800		High	Currant (2004)
Robin Hood	Northern Europe	6114	OxA	7400	AI	Tooth		22980	480	Med	Hedges et al. (1996)
Robin Hood	Northern Europe	6115	OxA	7401	AI	Tooth		22880	240	Med	Jacobi et al. (2006)
Robin Hood	Northern Europe	5801	OxA	7043		Bone		33450	700	Low	Hedges et al. (1996)
Robin Hood	Northern Europe	5802	OxA	7044		Bone		31050	500	Low	Jacobi et al. (2006)
Robin Hood	Northern Europe	14944	OxA	7044		Bone		49800		Low	Currant (2004)
Sandford Hill	Northern Europe	1526	BM			Bone		36000	1900	Low	Stuart (1991)
Schusterlucke	Central Europe	10396	OxA	12040	AF	Bone	>	46400		High	Stuart and Lister (2014)
Scladina	Northern Europe	23789	OxA	28261	AF	Tooth		46000	2400	High	Stuart and Lister (2014)

Table F.3: Direct radiocarbon dates of cave hyenas and bones chewed/digested by hyenas in Europe and Asia. *(continued)*

Site	Subregion	OxA	Lab	P	PCode	Material	>	Date BP	Error	Score	Source
Scladina	Northern Europe	23790	OxA	28262	AF	Tooth		40800	1300	High	Stuart and Lister (2014)
Scladina	Northern Europe	23791	OxA	28263	AF	Tooth		36450	750	High	Stuart and Lister (2014)
Scladina	Northern Europe	47943	GrA			Tooth		42560	550/440	Low	Bonjean et al. (2013)
Scladina	Northern Europe	32581	GrA			Tooth		43150	950/700	Low	Pirson et al. (2012)
Smelovskay	Asia	17004	OxA	19298	AF	Tooth		46200	1500	Med	Stuart and Lister (2014)
Smelovskaya II	Asia	19534	OxA	22743	AF	Tooth	>	60800		Med	Stuart and Lister (2014)
Smelovskaya II	Asia	19535	OxA	22743	AF	Tooth	>	59800		Med	Stuart and Lister (2014)
Soldier's Hole	Northern Europe	10899	OxA	12477	AF	Bone	>	36800		Med	Jacobi (2007)
Teufelslucke	Central Europe	2536	VERA			Tooth		38060	855	Low	Rohland et al. (2005)
Teufelslucke	Central Europe	1425	VERA			Tooth		40170	875	Low	Rohland et al. (2005)
Ust-Kataavakaya	Asia	10890	OxA	12559	AF	Bone		35650	450	High	Stuart and Lister (2014)
Ust-Katavskaya	Asia	19533	OxA	22740	AF	Tooth	>	59200		High	Stuart and Lister (2014)
Ustinovo	Asia	19536	OxA	22744	AF	Tooth		51400	1500	High	Stuart and Lister (2014)
Vasil Levski	Southern Europe	37323	OxA	45645	AG	Bone		38100	1100	Low	Thesis

Table F.3: Direct radiocarbon dates of cave hyenas and bones chewed/digested by hyenas in Europe and Asia. *(continued)*

Site	Subregion	OxA	Lab	P	PCode	Material	>	Date BP	Error	Score	Source
Vypustek	Central Europe	2531	VERA			Tooth		46000	1610	Low	Rohland et al. (2005)
Windener	Central Europe	2538	VERA			Bone		38680	920	Low	Rohland et al. (2005)
Zaktui	Asia	19719	OxA	23169	AF	Bone		35560	300	High	Shchetnikov et al. (2012)
Zaktui	Asia	23169	OxA	23169		Bone		35560	300	Low	Stuart and Lister (2014)
Zarinskiy District	Asia	17006	OxA	19300	AF	Bone		51200	1400	High	Stuart and Lister (2014)
Zarinskiy District	Asia	17007	OxA	19300	AF	Bone		50400	1300	High	Stuart and Lister (2014)

G
Radiocarbon date evaluation scores

G.1 Leopards

Table G.1: Matrix of date scores for leopards. Failed metrics have a note with the outlying value; missing metrics (could not be found) are marked NA. 'Mat.' is material dated. Details of criteria are in chapter 5.1.

ID	Species	Mat.	PCode	Yield	%yield	%C	δ^{13}C	δ^{15}N	CN	NRC	Total	Score	Comment
OxA/37222/45631/AF	PASS	PASS	PASS	PASS	PASS	PASS	PASS	PASS	PASS		9	High	NA
OxA/37223/45632/AF	PASS	PASS	PASS	PASS	PASS	PASS	PASS	PASS	PASS		9	High	NA
OxA/-88/44416/NRC	PASS	PASS	PASS	FAIL	FAIL	PASS	PASS	PASS	PASS	Evaluated as HPLC date	7	High	NA
OxA/10173/11757/AF*	PASS	PASS	PASS	PASS	PASS	PASS	PASS	PASS	PASS		9	High	NA
OxA/-1/30086/AF	PASS	PASS	PASS	PASS	PASS	PASS	PASS	PASS	PASS		9	High	NA
OxA/25736/30086/AF	PASS	PASS	PASS	PASS	PASS	PASS	PASS	PASS	PASS		9	High	NA
Beta/360175/NA/NA	PASS	PASS	FAIL	FAIL	FAIL	FAIL	PASS	FAIL	FAIL	NA	3	Low	NA
OxA/11416/13176/AF	PASS	PASS	PASS	PASS	PASS	PASS	FAIL	PASS	PASS		8	Med	NA
OxA/13495/15522/AF*	PASS	PASS	PASS	PASS	PASS	PASS	PASS	FAIL	PASS		8	Rejected	Date probably correct, but not natural range
OxA/30390/36343/AF	PASS	PASS	PASS	PASS	PASS	PASS	FAIL	PASS	PASS		8	Rejected	Date probably correct, but not natural range

G.2 Lions

Table G.2: Matrix of date scores for lions. Failed metrics have a note with the outlying value; missing metrics (could not be found) are marked NA. 'Mat.' is material dated. Details of criteria are in chapter 5.1

P	OxA	Species	Mat.	PCode	Yield	%yield	%C	δ^{13}C	δ^{15}N	CN	NRC	Total	Score	Comment
21894	19092	PASS	PASS	PASS	PASS	PASS	PASS	PASS	PASS	PASS		9	High	NA
11760	10186	PASS	PASS	PASS	PASS	PASS	PASS	PASS	PASS	PASS		9	High	NA
12556	10888	PASS	PASS	PASS	PASS	PASS	PASS	PASS	PASS	PASS		9	High	NA
12581	10895	PASS	PASS	PASS	PASS	PASS	PASS	PASS	PASS	PASS		9	High	NA
12582	10907	PASS	PASS	PASS	PASS	PASS	PASS	PASS	PASS	PASS		9	High	NA
12585	10910	PASS	PASS	PASS	PASS	PASS	PASS	PASS	PASS	PASS		9	High	NA
12872	11156	PASS	PASS	PASS	PASS	PASS	PASS	PASS	PASS	PASS		9	High	NA
13908	12021	PASS	PASS	PASS	PASS	PASS	PASS	PASS	PASS	PASS		9	High	NA
14707	13110	PASS	PASS	PASS	PASS	PASS	PASS	PASS	PASS	PASS		9	High	NA
14707	13110	PASS	PASS	PASS	PASS	PASS	PASS	PASS	PASS	PASS		9	High	NA
14708	13021	PASS	PASS	PASS	PASS	PASS	PASS	PASS	PASS	PASS		9	High	NA
14708	13474	PASS	PASS	PASS	PASS	PASS	PASS	PASS	PASS	PASS		9	High	NA
14710	13022	PASS	PASS	PASS	PASS	PASS	PASS	PASS	PASS	PASS		9	High	NA
14711	13023	PASS	PASS	PASS	PASS	PASS	PASS	PASS	PASS	PASS		9	High	NA
14713	13025	PASS	PASS	PASS	PASS	PASS	PASS	PASS	PASS	PASS		9	High	NA
14713	13475	PASS	PASS	PASS	PASS	PASS	PASS	PASS	PASS	PASS		9	High	NA
16030	13829	PASS	PASS	PASS	PASS	PASS	PASS	PASS	PASS	PASS		9	High	NA
16031	13830	PASS	PASS	PASS	PASS	PASS	PASS	PASS	PASS	PASS		9	High	NA
16032	13831	PASS	PASS	PASS	PASS	PASS	PASS	PASS	PASS	PASS		9	High	NA
16034	13833	PASS	PASS	PASS	PASS	PASS	PASS	PASS	PASS	PASS		9	High	NA
16036	13835	PASS	PASS	PASS	PASS	PASS	PASS	PASS	PASS	PASS		9	High	NA
16037	13836	PASS	PASS	PASS	PASS	PASS	PASS	PASS	PASS	PASS		9	High	NA
16038	13837	PASS	PASS	PASS	PASS	PASS	PASS	PASS	PASS	PASS		9	High	NA
18958	16715	PASS	PASS	PASS	PASS	PASS	PASS	PASS	PASS	PASS		9	High	NA
19315	16981	PASS	PASS	PASS	PASS	PASS	PASS	PASS	PASS	PASS		9	High	NA

Table G.2: Matrix of date scores for lions. Failed metrics have a note with the outlying value; missing metrics (could not be found) are marked NA. 'Mat.' is material dated. Details of criteria are in chapter 5.1. *(continued)*

P	OxA	Species	Mat.	PCode	Yield	%yield	%C	δ^{13}C	δ^{15}N	CN	NRC	Total	Score	Comment
19307	17029	PASS	PASS	PASS	PASS	PASS	PASS	PASS	PASS	PASS		9	High	NA
19308	17030	PASS	PASS	PASS	PASS	PASS	PASS	PASS	PASS	PASS		9	High	NA
19313	17035	PASS	PASS	PASS	PASS	PASS	PASS	PASS	PASS	PASS		9	High	NA
19319	17037	PASS	PASS	PASS	PASS	PASS	PASS	PASS	PASS	PASS		9	High	NA
19321	17039	PASS	PASS	PASS	PASS	PASS	PASS	PASS	PASS	PASS		9	High	NA
19323	17041	PASS	PASS	PASS	PASS	PASS	PASS	PASS	PASS	PASS		9	High	NA
19325	17043	PASS	PASS	PASS	PASS	PASS	PASS	PASS	PASS	PASS		9	High	NA
19331	17044	PASS	PASS	PASS	PASS	PASS	PASS	PASS	PASS	PASS		9	High	NA
19331	17045	PASS	PASS	PASS	PASS	PASS	PASS	PASS	PASS	PASS		9	High	NA
19322	17057	PASS	PASS	PASS	PASS	PASS	PASS	PASS	PASS	PASS		9	High	NA
18959	17268	PASS	PASS	PASS	PASS	PASS	PASS	PASS	PASS	PASS		9	High	NA
21732	18711	PASS	PASS	PASS	PASS	PASS	PASS	PASS	PASS	PASS		9	High	NA
21733	18712	PASS	PASS	PASS	PASS	PASS	PASS	PASS	PASS	PASS		9	High	NA
21436	18812	PASS	PASS	PASS	PASS	PASS	PASS	PASS	PASS	PASS		9	High	NA
21437	18813	PASS	PASS	PASS	PASS	PASS	PASS	PASS	PASS	PASS		9	High	NA
25499	22122	PASS	PASS	PASS	PASS	PASS	PASS	PASS	PASS	PASS		9	High	NA
25501	22124	PASS	PASS	PASS	PASS	PASS	PASS	PASS	PASS	PASS		9	High	NA
25501	22125	PASS	PASS	PASS	PASS	PASS	PASS	PASS	PASS	PASS		9	High	NA
17446	15354	PASS	PASS	PASS	PASS	PASS	PASS	PASS	PASS	PASS		9	High	NA
17158	14863	PASS	PASS	PASS	PASS	PASS	PASS	PASS	PASS	PASS		9	High	NA
11686	10087	PASS	PASS	PASS	PASS	PASS	PASS	PASS	PASS	PASS		9	High	NA
23781	20252	PASS	PASS	PASS	PASS	PASS	PASS	PASS	PASS	PASS		9	High	NA
23782	20257	PASS	PASS	PASS	PASS	PASS	PASS	PASS	PASS	PASS		9	High	NA
22222	19359	PASS	PASS	PASS	PASS	PASS	PASS	PASS	FAIL	PASS		8	High	NA
14915	12901	PASS	PASS	PASS	PASS	PASS	PASS	PASS	PASS	PASS		9	High	NA
42398	35558	PASS	PASS	PASS	PASS	PASS	PASS	PASS	FAIL	PASS		8	High	NA

Table G.2: Matrix of date scores for lions. Failed metrics have a note with the outlying value; missing metrics (could not be found) are marked NA. 'Mat.' is material dated. Details of criteria are in chapter 5.1. *(continued)*

P	OxA	Species	Mat.	PCode	Yield	%yield	%C	δ^{13}C	δ^{15}N	CN	NRC	Total	Score	Comment
21340	18698	PASS	PASS	PASS	PASS	PASS	PASS	PASS	PASS	PASS		9	High	NA
21340	18699	PASS	PASS	PASS	PASS	PASS	PASS	PASS	PASS	PASS		9	High	NA
15999	14285	PASS	PASS	PASS	FAIL	FAIL	FAIL	FAIL	FAIL	PASS		4	Low	NA
14513	12799	PASS	PASS	PASS	FAIL	FAIL	PASS	FAIL	PASS	PASS		6	Low	NA
45514	X-2772-34	PASS	PASS	FAIL	PASS	PASS	FAIL	PASS	FAIL	FAIL		5	Low	NA
NA	23151	PASS	PASS	FAIL	FAIL	FAIL	FAIL	FAIL	FAIL	FAIL	NA	2	Low	NA
NA	4944	PASS	PASS	FAIL	FAIL	FAIL	FAIL	FAIL	FAIL	FAIL	NA	2	Low	NA
NA	41882 [2]	PASS	PASS	FAIL	FAIL	FAIL	FAIL	FAIL	FAIL	FAIL	NA	2	Low	NA
NA	14406	PASS	PASS	FAIL	FAIL	FAIL	FAIL	PASS	FAIL	FAIL	NA	3	Low	NA
NA	2545	PASS	PASS	FAIL	FAIL	FAIL	FAIL	FAIL	FAIL	FAIL	NA	2	Low	NA
NA	6209	PASS	PASS	FAIL	FAIL	FAIL	FAIL	FAIL	FAIL	FAIL	NA	2	Low	NA
NA	16510	PASS	PASS	FAIL	FAIL	FAIL	FAIL	FAIL	FAIL	FAIL	NA	2	Low	NA
NA	173066	PASS	PASS	FAIL	FAIL	FAIL	FAIL	FAIL	FAIL	FAIL	NA	2	Low	NA
11430	10121	PASS	PASS	PASS	FAIL	PASS	PASS	PASS	PASS	PASS		8	Med	NA
12041	10513	PASS	PASS	PASS	PASS	PASS	PASS	PASS	PASS	FAIL		8	Med	NA
12554	10845	PASS	PASS	PASS	FAIL	FAIL	PASS	PASS	PASS	PASS		7	Med	NA
12555	10887	PASS	PASS	PASS	PASS	PASS	PASS	FAIL	PASS	PASS		8	Med	NA
12580	10894	PASS	PASS	PASS	PASS	PASS	PASS	FAIL	PASS	PASS		8	Med	NA
12583	10908	PASS	PASS	PASS	PASS	PASS	PASS	FAIL	PASS	PASS		8	Med	NA
12584	10909	PASS	PASS	PASS	PASS	PASS	PASS	FAIL	PASS	PASS		8	Med	NA
12870	11096	PASS	PASS	PASS	FAIL	FAIL	PASS	PASS	PASS	PASS		7	Med	NA
13030	11349	PASS	PASS	PASS	PASS	PASS	PASS	FAIL	PASS	PASS		8	Med	NA
13175	11422	PASS	PASS	PASS	PASS	PASS	PASS	FAIL	PASS	PASS		8	Med	NA
14709	12981	PASS	PASS	PASS	PASS	PASS	PASS	PASS	FAIL	PASS		8	Med	NA
14712	13024	PASS	PASS	PASS	PASS	PASS	PASS	FAIL	PASS	PASS		8	Med	NA
19314	16980	PASS	PASS	PASS	PASS	PASS	PASS	FAIL	PASS	PASS		8	Med	NA

Table G.2: Matrix of date scores for lions. Failed metrics have a note with the outlying value; missing metrics (could not be found) are marked NA. 'Mat.' is material dated. Details of criteria are in chapter 5.1. *(continued)*

P	OxA	Species	Mat.	PCode	Yield	%yield	%C	δ^{13}C	δ^{15}N	CN	NRC	Total	Score	Comment
19316	16982	PASS	PASS	PASS	PASS	PASS	PASS	FAIL	PASS	PASS		8	Med	NA
19317	16983	PASS	PASS	PASS	PASS	PASS	PASS	PASS	FAIL	PASS		8	Med	NA
19306	17010	PASS	PASS	PASS	PASS	PASS	PASS	FAIL	PASS	PASS		8	Med	NA
19311	17033	PASS	PASS	PASS	PASS	PASS	PASS	FAIL	PASS	PASS		8	Med	NA
19312	17034	PASS	PASS	PASS	PASS	PASS	PASS	FAIL	PASS	PASS		8	Med	NA
19339	17054	PASS	PASS	PASS	PASS	PASS	PASS	FAIL	PASS	PASS		8	Med	NA
19318	17036	PASS	PASS	PASS	PASS	PASS	PASS	PASS	FAIL	PASS		8	Med	NA
19320	17038	PASS	PASS	PASS	PASS	PASS	PASS	PASS	FAIL	PASS		8	Med	NA
19323	17040	PASS	PASS	PASS	PASS	PASS	PASS	PASS	FAIL	PASS		8	Med	NA
19324	17042	PASS	PASS	PASS	PASS	PASS	PASS	PASS	FAIL	PASS		8	Med	NA
19309	17031	PASS	PASS	PASS	PASS	PASS	PASS	FAIL	PASS	PASS		8	Med	NA
19310	17032	PASS	PASS	PASS	PASS	PASS	PASS	FAIL	PASS	PASS		8	Med	NA
19872	17372	PASS	PASS	PASS	PASS	PASS	PASS	FAIL	PASS	PASS		8	Med	NA
19873	17373	PASS	PASS	PASS	PASS	PASS	PASS	FAIL	PASS	PASS		8	Med	NA
45510	37177	PASS	PASS	FAIL	PASS	PASS	PASS	PASS	PASS	FAIL		7	Med	NA
25500	22123	PASS	PASS	PASS	PASS	PASS	PASS	FAIL	PASS	PASS		8	Med	NA
7799	6593	PASS	PASS	FAIL	PASS	PASS	PASS	PASS	PASS	PASS		8	Med	NA
17157	14862	PASS	PASS	PASS	PASS	PASS	PASS	FAIL	PASS	PASS		8	Med	NA
23780	20251	PASS	PASS	PASS	PASS	PASS	PASS	FAIL	PASS	PASS		8	Med	NA
24281	20672	PASS	PASS	PASS	PASS	PASS	PASS	FAIL	PASS	PASS		8	Med	NA
15919	13988	PASS	PASS	PASS	PASS	PASS	PASS	PASS	PASS	PASS		9	Reject	Pettitt et al. (2012) question species ID; Ursus in db
15921	13991	PASS	PASS	PASS	PASS	PASS	PASS	PASS	PASS	PASS		9	Reject	Pettitt et al. (2012) question species ID; P. leo in db
15340	13456	PASS	PASS	PASS	PASS	PASS	PASS	PASS	PASS	PASS		9	Reject	Higham et al. (2011) uncertain species ID ('cf. Panthera leo')
15523	13496	PASS	PASS	PASS	PASS	PASS	PASS	PASS	PASS	PASS		9	Reject	Modern P. leo

Table G.2: Matrix of date scores for lions. Failed metrics have a note with the outlying value; missing metrics (could not be found) are marked NA. 'Mat.' is material dated. Details of criteria are in chapter 5.1. *(continued)*

P	OxA	Species	Mat.	PCode	Yield	%yield	%C	δ^{13}C	δ^{15}N	CN	NRC	Total	Score	Comment
15525	13498	PASS	PASS	PASS	PASS	PASS	PASS	PASS	PASS	PASS		9	Reject	Modern P. leo
2352	1806	PASS	PASS	FAIL	PASS	PASS	FAIL	PASS	FAIL	FAIL		5	Reject	P. spelaea (Stuart 1991). Redated in Stuart and Lister (2011); varnish/glue
19308	-1	PASS	PASS	PASS	PASS	PASS	PASS	PASS	PASS	PASS		9	Reject	Duplicated; dates disagree
19394	17155	PASS	PASS	PASS	PASS	PASS	PASS	PASS	PASS	PASS		9	Reject	Modern P. leo (Stuart and Lister, 2011)

G.3 Hyenas

Table G.3: Matrix of date scores for hyenas. Failed metrics have a note with the outlying value; missing metrics (could not be found) are marked NA. 'Mat.' is material dated. Details of criteria are in chapter 5.1.

P	OxA	Species	Mat.	PCode	Yield	%yield	%C	δ^{13}C	δ^{15}N	CN	NRC	Total	Score	Comment
11188	9698	PASS	PASS	PASS	PASS	PASS	PASS	PASS	PASS	PASS		9	High	NA
7199	13512	PASS	PASS	PASS	PASS	PASS	PASS	PASS	PASS	PASS		9	High	NA
16380	14400	PASS	PASS	PASS	PASS	PASS	PASS	PASS	PASS	PASS		9	High	NA
16381	14401	PASS	PASS	PASS	PASS	PASS	PASS	PASS	PASS	PASS		9	High	NA
16383	14402	PASS	PASS	PASS	PASS	PASS	FAIL	PASS	PASS	PASS		8	High	NA
16384	14403	PASS	PASS	PASS	PASS	PASS	PASS	FAIL	PASS	PASS		8	High	NA
16382	14473	PASS	PASS	PASS	PASS	PASS	PASS	PASS	PASS	PASS		9	High	NA
1839	15518	PASS	PASS	PASS	PASS	PASS	PASS	PASS	FAIL	PASS		8	High	NA
1839	15520	PASS	PASS	PASS	PASS	PASS	PASS	PASS	FAIL	PASS		8	High	NA
25382	21995	PASS	PASS	PASS	PASS	PASS	PASS	PASS	PASS	PASS		9	High	NA
14514	12800	PASS	PASS	PASS	FAIL	PASS	PASS	PASS	PASS	PASS		8	High	NA
7041	14926	PASS	PASS	PASS	FAIL	PASS	PASS	PASS	PASS	PASS		8	High	NA
11181	9691	PASS	PASS	PASS	PASS	PASS	PASS	PASS	PASS	PASS		9	High	NA
11182	9692	PASS	PASS	PASS	PASS	PASS	PASS	PASS	PASS	PASS		9	High	NA
11183	9693	PASS	PASS	PASS	PASS	PASS	PASS	PASS	PASS	PASS		9	High	NA
11184	9694	PASS	PASS	PASS	PASS	PASS	PASS	PASS	PASS	PASS		9	High	NA
22190	19215	PASS	PASS	PASS	PASS	PASS	PASS	PASS	FAIL	PASS		8	High	NA
10416	9028	PASS	PASS	FAIL	PASS	PASS	PASS	PASS	PASS	PASS		8	High	NA
10418	9029	PASS	PASS	FAIL	PASS	PASS	PASS	PASS	PASS	PASS		8	High	NA
11185	9695	PASS	PASS	PASS	PASS	PASS	PASS	PASS	FAIL	PASS		8	High	NA
11186	9696	PASS	PASS	PASS	PASS	PASS	PASS	PASS	PASS	PASS		9	High	NA
11893	10336	PASS	PASS	PASS	PASS	PASS	PASS	PASS	PASS	PASS		9	High	NA
12040	10396	PASS	PASS	PASS	PASS	PASS	PASS	PASS	PASS	PASS		9	High	NA
12044	10398	PASS	PASS	PASS	PASS	PASS	PASS	PASS	PASS	PASS		9	High	NA

Table G.3: Matrix of date scores for hyenas. Failed metrics have a note with the outlying value; missing metrics (could not be found) are marked NA. 'Mat.' is material dated. Details of criteria are in chapter 5.1. *(continued)*

P	OxA	Species	Mat.	PCode	Yield	%yield	%C	δ^{13}C	δ^{15}N	CN	NRC	Total	Score	Comment
12118	10523	PASS	PASS	PASS	PASS	PASS	PASS	PASS	PASS	PASS		9	High	NA
12559	10890	PASS	PASS	PASS	PASS	PASS	PASS	PASS	PASS	PASS		9	High	NA
12881	11158	PASS	PASS	PASS	PASS	PASS	PASS	PASS	PASS	PASS		9	High	NA
12884	11161	PASS	PASS	PASS	PASS	PASS	PASS	PASS	PASS	PASS		9	High	NA
12890	11062	PASS	PASS	PASS	PASS	PASS	PASS	PASS	PASS	PASS		9	High	NA
13037	12893	PASS	PASS	PASS	PASS	PASS	PASS	PASS	PASS	PASS		9	High	NA
13171	11552	PASS	PASS	PASS	PASS	PASS	PASS	PASS	FAIL	PASS		8	High	NA
13478	11691	PASS	PASS	PASS	PASS	PASS	PASS	PASS	PASS	PASS		9	High	NA
13910	12022	PASS	PASS	PASS	PASS	PASS	PASS	PASS	FAIL	PASS		8	High	NA
14515	12771	PASS	PASS	PASS	PASS	PASS	PASS	PASS	PASS	PASS		9	High	NA
14518	12736	PASS	PASS	PASS	PASS	PASS	PASS	PASS	PASS	PASS		9	High	NA
15846	13917	PASS	PASS	PASS	PASS	PASS	PASS	PASS	PASS	PASS		9	High	NA
15903	13946	PASS	PASS	PASS	PASS	PASS	PASS	PASS	FAIL	PASS		8	High	NA
16240	-1	PASS	PASS	PASS	PASS	PASS	PASS	PASS	PASS	PASS		9	High	NA
16240	16766	PASS	PASS	PASS	FAIL	PASS	PASS	PASS	PASS	PASS		8	High	NA
16241	-1	PASS	PASS	PASS	PASS	PASS	PASS	PASS	PASS	PASS		9	High	NA
17654	15598	PASS	PASS	PASS	PASS	PASS	PASS	PASS	PASS	PASS		9	High	NA
18548	16329	PASS	PASS	PASS	PASS	PASS	PASS	FAIL	PASS	PASS		8	High	NA
18956	16691	PASS	PASS	PASS	PASS	PASS	PASS	PASS	FAIL	PASS		8	High	NA
7199	13324	PASS	PASS	FAIL	PASS	PASS	PASS	PASS	PASS	PASS		8	High	NA
8261	7087	PASS	PASS	FAIL	PASS	PASS	PASS	PASS	PASS	PASS		8	High	NA
19295	17003	PASS	PASS	PASS	PASS	PASS	PASS	PASS	FAIL	PASS		8	High	NA
19299	17005	PASS	PASS	PASS	PASS	PASS	PASS	PASS	PASS	PASS		9	High	NA
19300	17006	PASS	PASS	PASS	PASS	PASS	PASS	PASS	PASS	PASS		9	High	NA
19300	17007	PASS	PASS	PASS	PASS	PASS	PASS	PASS	PASS	PASS		9	High	NA
19297	17028	PASS	PASS	PASS	PASS	PASS	PASS	FAIL	PASS	PASS		8	High	NA

Table G.3: Matrix of date scores for hyenas. Failed metrics have a note with the outlying value; missing metrics (could not be found) are marked NA. 'Mat.' is material dated. Details of criteria are in chapter 5.1. *(continued)*

P	OxA	Species	Mat.	PCode	Yield	%yield	%C	δ^{13}C	δ^{15}N	CN	NRC	Total	Score	Comment
21341	18700	PASS	PASS	PASS	PASS	PASS	PASS	PASS	PASS	PASS		9	High	NA
22188	X-2278-43	PASS	PASS	PASS	PASS	PASS	PASS	PASS	FAIL	PASS		8	High	NA
22189	X-2278-44	PASS	PASS	PASS	PASS	PASS	PASS	PASS	FAIL	PASS		8	High	NA
22734	19531	PASS	PASS	PASS	PASS	PASS	PASS	PASS	PASS	PASS		9	High	NA
22735	19532	PASS	PASS	PASS	PASS	PASS	PASS	PASS	PASS	PASS		9	High	NA
22740	19533	PASS	PASS	PASS	PASS	PASS	PASS	PASS	FAIL	PASS		8	High	NA
22744	19536	PASS	PASS	PASS	PASS	PASS	PASS	FAIL	PASS	PASS		8	High	NA
22745	19537	PASS	PASS	PASS	PASS	PASS	PASS	PASS	PASS	PASS		9	High	NA
22736	19657	PASS	PASS	PASS	PASS	PASS	PASS	PASS	FAIL	PASS		8	High	NA
22737	19675	PASS	PASS	PASS	PASS	PASS	PASS	PASS	PASS	PASS		9	High	NA
22739	19658	PASS	PASS	PASS	PASS	PASS	PASS	FAIL	PASS	PASS		8	High	NA
22741	19659	PASS	PASS	PASS	PASS	PASS	PASS	FAIL	PASS	PASS		8	High	NA
22742	19660	PASS	PASS	PASS	PASS	PASS	PASS	PASS	PASS	PASS		9	High	NA
23377	19633	PASS	PASS	PASS	PASS	PASS	PASS	PASS	PASS	PASS		9	High	NA
23169	19719	PASS	PASS	PASS	PASS	PASS	PASS	PASS	PASS	PASS		9	High	NA
24886	20763	PASS	PASS	PASS	PASS	PASS	PASS	PASS	PASS	PASS		9	High	NA
25384	21997	PASS	PASS	PASS	PASS	PASS	PASS	PASS	PASS	PASS		9	High	NA
25383	21996	PASS	PASS	PASS	PASS	PASS	PASS	PASS	PASS	PASS		9	High	NA
25563	22126	PASS	PASS	PASS	PASS	PASS	PASS	FAIL	PASS	PASS		8	High	NA
25565	22128	PASS	PASS	PASS	PASS	PASS	PASS	PASS	FAIL	PASS		8	High	NA
28261	23789	PASS	PASS	PASS	PASS	PASS	PASS	PASS	PASS	PASS		9	High	NA
28262	23790	PASS	PASS	PASS	PASS	PASS	PASS	PASS	PASS	PASS		9	High	NA
28263	23791	PASS	PASS	PASS	PASS	PASS	PASS	PASS	PASS	PASS		9	High	NA
35510	29411	PASS	PASS	PASS	PASS	PASS	PASS	PASS	PASS	PASS		9	High	NA
35673	29855	PASS	PASS	PASS	PASS	PASS	PASS	FAIL	PASS	PASS		8	High	NA

Table G.3: Matrix of date scores for hyenas. Failed metrics have a note with the outlying value; missing metrics (could not be found) are marked NA. 'Mat.' is material dated. Details of criteria are in chapter 5.1. *(continued)*

P	OxA	Species	Mat.	PCode	Yield	%yield	%C	δ^{13}C	δ^{15}N	CN	NRC	Total	Score	Comment
35815	30351	PASS	PASS	PASS	PASS	PASS	PASS	PASS	PASS	PASS		9	High	NA
37104	31009	PASS	PASS	PASS	PASS	PASS	PASS	PASS	PASS	PASS		9	High	NA
42395	35556	PASS	PASS	PASS	PASS	PASS	PASS	PASS	FAIL	PASS		8	High	NA
42397	35557	PASS	PASS	PASS	PASS	PASS	PASS	PASS	FAIL	PASS		8	High	NA
42399	35559	PASS	PASS	PASS	PASS	PASS	PASS	PASS	FAIL	PASS		8	High	NA
42400	35560	PASS	PASS	PASS	PASS	PASS	PASS	PASS	FAIL	PASS		8	High	NA
42401	35561	PASS	PASS	PASS	PASS	PASS	PASS	PASS	FAIL	PASS		8	High	NA
42402	35562	PASS	PASS	PASS	PASS	PASS	PASS	PASS	FAIL	PASS		8	High	NA
42403	35563	PASS	PASS	PASS	PASS	PASS	PASS	PASS	FAIL	PASS		8	High	NA
45513	37219	PASS	PASS	PASS	PASS	PASS	PASS	PASS	FAIL	PASS		8	High	NA
45630	37221	PASS	PASS	PASS	PASS	PASS	PASS	PASS	FAIL	PASS		8	High	NA
42406	35565	PASS	PASS	PASS	PASS	PASS	PASS	PASS	FAIL	PASS		8	High	NA
42407	35566	PASS	PASS	PASS	PASS	PASS	PASS	PASS	FAIL	PASS		8	High	NA
42408	35567	PASS	PASS	PASS	PASS	PASS	PASS	PASS	FAIL	PASS		8	High	NA
12759	11152	PASS	PASS	PASS	FAIL	FAIL	PASS	FAIL	FAIL	FAIL	Evaluated as HPLC date	4	Low	NA
22670	19509	PASS	PASS	FAIL	FAIL	FAIL	PASS	FAIL	FAIL	FAIL	NA	3	Low	NA
13663	11796	PASS	PASS	FAIL	FAIL	FAIL	PASS	FAIL	FAIL	FAIL	NA	3	Low	NA
25399	21309	PASS	PASS	FAIL	FAIL	FAIL	PASS	PASS	FAIL	FAIL	NA	4	Low	NA
25400	21310	PASS	PASS	FAIL	FAIL	FAIL	PASS	PASS	FAIL	FAIL	NA	4	Low	NA
25912	22149	PASS	PASS	FAIL	FAIL	FAIL	PASS	PASS	FAIL	FAIL	NA	4	Low	NA
10413	9090	PASS	PASS	FAIL	FAIL	FAIL	FAIL	PASS	PASS	FAIL		4	Low	NA
12760	11174	PASS	PASS	PASS	FAIL	FAIL	PASS	FAIL	PASS	FAIL	Evaluated as HPLC date	5	Low	NA
7040	5798	PASS	PASS	FAIL	FAIL	FAIL	PASS	PASS	FAIL	FAIL		4	Low	NA

Table G.3: Matrix of date scores for hyenas. Failed metrics have a note with the outlying value; missing metrics (could not be found) are marked NA. 'Mat.' is material dated. Details of criteria are in chapter 5.1. *(continued)*

P	OxA	Species	Mat.	PCode	Yield	%yield	%C	δ^{13}C	δ^{15}N	CN	NRC	Total	Score	Comment
7041	5799	PASS	PASS	FAIL	FAIL	FAIL	PASS	PASS	FAIL	FAIL		4	Low	NA
7042	5800	PASS	PASS	FAIL	FAIL	FAIL	PASS	PASS	FAIL	FAIL		4	Low	NA
8226	6980	PASS	PASS	FAIL	FAIL	FAIL	PASS	FAIL	PASS	PASS		5	Low	NA
8261	13378	PASS	PASS	PASS	FAIL	FAIL	PASS	FAIL	PASS	FAIL	Evaluated as HPLC date	5	Low	NA
45645	37323	PASS	PASS	FAIL	FAIL	FAIL	PASS	PASS	FAIL	PASS		5	Low	NA
1655	1491	PASS	PASS	FAIL	FAIL	PASS	FAIL	PASS	FAIL	FAIL		4	Low	NA
1971	1448	PASS	PASS	FAIL	PASS	PASS	FAIL	PASS	FAIL	FAIL		5	Low	NA
2035	1620	PASS	PASS	FAIL	PASS	PASS	FAIL	PASS	FAIL	FAIL		5	Low	NA
5698	4754	PASS	PASS	FAIL	PASS	PASS	PASS	FAIL	FAIL	FAIL		5	Low	NA
1839	1207	PASS	PASS	FAIL	FAIL	FAIL	FAIL	FAIL	FAIL	FAIL	NA	2	Low	NA
1840	1206	PASS	PASS	FAIL	FAIL	FAIL	FAIL	FAIL	FAIL	FAIL	NA	2	Low	NA
25381	X-2352-10	PASS	PASS	FAIL	FAIL	FAIL	FAIL	FAIL	FAIL	FAIL	NA	2	Low	NA
22708	X-2294-11	PASS	PASS	FAIL	FAIL	FAIL	FAIL	FAIL	FAIL	FAIL	NA	2	Low	NA
23169	23169	PASS	PASS	FAIL	FAIL	FAIL	FAIL	FAIL	FAIL	FAIL	NA	2	Low	NA
7043	5801	FAIL	PASS	FAIL	FAIL	FAIL	PASS	FAIL	FAIL	FAIL	NA	2	Low	NA
7044	5802	FAIL	PASS	FAIL	FAIL	FAIL	PASS	FAIL	FAIL	FAIL	NA	2	Low	NA
7045	5803	FAIL	PASS	FAIL	FAIL	FAIL	PASS	FAIL	FAIL	FAIL	NA	2	Low	NA
12470	10806	FAIL	PASS	FAIL	FAIL	FAIL	PASS	FAIL	FAIL	FAIL	NA	2	Low	NA
7044	14944	FAIL	PASS	FAIL	FAIL	FAIL	PASS	FAIL	FAIL	FAIL	NA	2	Low	NA
25398	21308	FAIL	PASS	FAIL	FAIL	FAIL	PASS	FAIL	FAIL	FAIL	NA	2	Low	NA
NA	2529	PASS	PASS	FAIL	FAIL	FAIL	FAIL	FAIL	FAIL	FAIL	NA	2	Low	NA
NA	2530	PASS	PASS	FAIL	FAIL	FAIL	FAIL	FAIL	FAIL	FAIL	NA	2	Low	NA
NA	25284	PASS	PASS	FAIL	FAIL	FAIL	FAIL	FAIL	FAIL	FAIL	NA	2	Low	NA

Table G.3: Matrix of date scores for hyenas. Failed metrics have a note with the outlying value; missing metrics (could not be found) are marked NA. 'Mat.' is material dated. Details of criteria are in chapter 5.1. *(continued)*

P	OxA	Species	Mat.	PCode	Yield	%yield	%C	δ^{13}C	δ^{15}N	CN	NRC	Total	Score	Comment
NA	25285	PASS	PASS	FAIL	FAIL	FAIL	FAIL	FAIL	FAIL	FAIL	NA	2	Low	NA
NA	2812	PASS	PASS	FAIL	FAIL	FAIL	FAIL	FAIL	FAIL	FAIL	NA	2	Low	NA
NA	8958	PASS	PASS	FAIL	FAIL	FAIL	FAIL	FAIL	FAIL	FAIL	NA	2	Low	NA
NA	1835	PASS	PASS	FAIL	FAIL	FAIL	FAIL	FAIL	FAIL	FAIL	NA	2	Low	NA
NA	2532	PASS	PASS	FAIL	FAIL	FAIL	FAIL	FAIL	FAIL	FAIL	NA	2	Low	NA
NA	2534	PASS	PASS	FAIL	FAIL	FAIL	FAIL	FAIL	FAIL	FAIL	NA	2	Low	NA
NA	2535	PASS	PASS	FAIL	FAIL	FAIL	FAIL	FAIL	FAIL	FAIL	NA	2	Low	NA
NA	216143	PASS	PASS	FAIL	FAIL	FAIL	FAIL	FAIL	FAIL	FAIL	NA	2	Low	NA
NA	177765	PASS	PASS	FAIL	FAIL	FAIL	FAIL	FAIL	FAIL	FAIL	NA	2	Low	NA
NA	2540	PASS	PASS	FAIL	FAIL	FAIL	FAIL	FAIL	FAIL	FAIL	NA	2	Low	NA
NA	2533	PASS	PASS	FAIL	FAIL	FAIL	FAIL	FAIL	FAIL	FAIL	NA	2	Low	NA
NA	47943	PASS	PASS	FAIL	FAIL	FAIL	FAIL	FAIL	FAIL	FAIL	NA	2	Low	NA
NA	32581	PASS	PASS	FAIL	FAIL	FAIL	FAIL	FAIL	FAIL	FAIL	NA	2	Low	NA
NA	2536	PASS	PASS	FAIL	FAIL	FAIL	FAIL	FAIL	FAIL	FAIL	NA	2	Low	NA
NA	1425	PASS	PASS	FAIL	FAIL	FAIL	FAIL	FAIL	FAIL	FAIL	NA	2	Low	NA
NA	2531	PASS	PASS	FAIL	FAIL	FAIL	FAIL	FAIL	FAIL	FAIL	NA	2	Low	NA
NA	2538	PASS	PASS	FAIL	FAIL	FAIL	FAIL	FAIL	FAIL	FAIL	NA	2	Low	NA
NA	1526	PASS	PASS	FAIL	FAIL	FAIL	FAIL	FAIL	FAIL	FAIL	NA	2	Low	NA
NA	3162 (Poz)	PASS	PASS	FAIL	FAIL	FAIL	FAIL	FAIL	FAIL	FAIL	NA	2	Low	NA
NA	13625	PASS	PASS	FAIL	FAIL	FAIL	FAIL	FAIL	FAIL	FAIL	NA	2	Low	NA
12477	10899	PASS	PASS	PASS	FAIL	FAIL	PASS	PASS	PASS	PASS		7	Med	NA
1840	15548	PASS	PASS	PASS	FAIL	FAIL	PASS	PASS	PASS	PASS		7	Med	NA
10415	9027	PASS	PASS	FAIL	PASS	PASS	FAIL	PASS	PASS	PASS		7	Med	NA
11190	9674	PASS	PASS	PASS	FAIL	FAIL	PASS	PASS	PASS	PASS		7	Med	NA
12119	10657	PASS	PASS	PASS	FAIL	FAIL	PASS	PASS	PASS	PASS		7	Med	NA
12127	10658	PASS	PASS	PASS	FAIL	FAIL	FAIL	PASS	PASS	PASS		6	Med	NA

Table G.3: Matrix of date scores for hyenas. Failed metrics have a note with the outlying value; missing metrics (could not be found) are marked NA. 'Mat.' is material dated. Details of criteria are in chapter 5.1. *(continued)*

P	OxA	Species	Mat.	PCode	Yield	%yield	%C	δ^{13}C	δ^{15}N	CN	NRC	Total	Score	Comment
12557	10846	PASS	PASS	PASS	FAIL	FAIL	PASS	FAIL	PASS	PASS		6	Med	NA
12558	10889	PASS	PASS	PASS	PASS	FAIL	PASS	FAIL	FAIL	PASS		6	Med	NA
13169	11421	PASS	PASS	PASS	PASS	PASS	PASS	FAIL	FAIL	PASS		7	Med	NA
13170	11551	PASS	PASS	PASS	PASS	PASS	PASS	PASS	FAIL	FAIL		7	Med	NA
16241	16767	PASS	PASS	PASS	FAIL	FAIL	PASS	PASS	PASS	PASS		7	Med	NA
5173	4234	PASS	PASS	FAIL	PASS	PASS	PASS	PASS	FAIL	FAIL		6	Med	NA
5176	4237	PASS	PASS	FAIL	PASS	PASS	PASS	PASS	FAIL	FAIL		6	Med	NA
7199	5961	PASS	PASS	FAIL	PASS	PASS	PASS	PASS	FAIL	FAIL		6	Med	NA
7400	6114	PASS	PASS	FAIL	PASS	PASS	PASS	PASS	FAIL	FAIL		6	Med	NA
7401	6115	PASS	PASS	FAIL	PASS	PASS	PASS	PASS	FAIL	FAIL		6	Med	NA
19298	17004	PASS	PASS	PASS	PASS	PASS	PASS	FAIL	FAIL	PASS		7	Med	NA
19302	17009	PASS	PASS	PASS	PASS	PASS	PASS	FAIL	FAIL	PASS		7	Med	NA
19332	17046	PASS	PASS	PASS	PASS	PASS	PASS	FAIL	FAIL	PASS		7	Med	NA
22743	19534	PASS	PASS	PASS	PASS	PASS	PASS	FAIL	FAIL	PASS		7	Med	NA
22743	19535	PASS	PASS	PASS	PASS	PASS	PASS	FAIL	FAIL	PASS		7	Med	NA
22738	19676	PASS	PASS	PASS	PASS	PASS	PASS	FAIL	FAIL	PASS		7	Med	NA
22708	X-2294-11	PASS	PASS	PASS	FAIL	FAIL	PASS	FAIL	PASS	PASS		6	Med	NA
25381	X-2352-10	PASS	PASS	PASS	FAIL	FAIL	PASS	PASS	PASS	PASS		7	Med	NA
25564	22127	PASS	PASS	PASS	PASS	PASS	PASS	FAIL	FAIL	PASS		7	Med	NA
25566	22129	PASS	PASS	PASS	PASS	PASS	PASS	FAIL	FAIL	PASS		7	Med	NA
44418	X-2756-42	PASS	PASS	PASS	FAIL	FAIL	PASS	PASS	PASS	PASS	Evaluated as HPLC date	7	Med	NA
45506	X-2772-28	PASS	PASS	FAIL	PASS	PASS	FAIL	PASS	PASS	FAIL		6	Med	NA

Table G.3: Matrix of date scores for hyenas. Failed metrics have a note with the outlying value; missing metrics (could not be found) are marked NA. 'Mat.' is material dated. Details of criteria are in chapter 5.1. *(continued)*

P	OxA	Species	Mat.	PCode	Yield	%yield	%C	δ^{13}C	δ^{15}N	CN	NRC	Total	Score	Comment
45507	X-2772-33	PASS	PASS	FAIL	PASS	PASS	FAIL	PASS	PASS	FAIL		6	Med	NA
45512	37218	PASS	PASS	PASS	PASS	PASS	PASS	FAIL	FAIL	PASS		7	Med	NA
11180	9673	PASS	PASS	PASS	PASS	PASS	FAIL	FAIL	PASS	PASS		7	Rejected	Very low %C
8261	13659	PASS	PASS	PASS	PASS	PASS	PASS	PASS	PASS	PASS		9	Rejected	Redated (OxA-13378), underestimate (Jacobi and Higham 2008)
11186	X-2198-8	PASS	PASS	PASS	FAIL	FAIL	PASS	PASS	PASS	PASS		7	Rejected	NA
11189	-1	PASS	PASS	PASS	FAIL	FAIL	PASS	PASS	PASS	PASS		7	Rejected	NA
11796	10299	PASS	PASS	PASS	FAIL	FAIL	PASS	PASS	PASS	FAIL		6	Rejected	CN; low yields
13037	0	PASS	PASS	PASS	FAIL	FAIL	PASS	FAIL	PASS	FAIL		5	Rejected	Failed; no date recorded
44418	X-2756-42	PASS	PASS	PASS	FAIL	FAIL	PASS	PASS	PASS	PASS	Evaluated as HPLC date	7	Rejected	NRC

H
Modern human dates

Table H.1: Random sample of 242 radiocarbon dates of AMH from Carotenuto et al. (2018) used in KDE, environmental niche, and OxCal boundary models.

Site	Latitude	Longitude	Lab code	Date BP	Error BP
Grotta Arene Candide	44.17	8.33	OxA-10998	10065	55
Flixton II	54.20	-0.38	OxA-6319	10150	80
Closeau	48.88	2.16	LYON-1555	10240	150
Balma del Gai	41.82	2.14	GifA-95617	10260	90
Khummi	50.21	137.08	AA-13391	10345	100
Kopytowa	49.67	21.62	Poz-28515	10480	60
Gross Lieskow	51.78	14.45	LZ-1351	10520	100
Can Manel	40.55	0.52	Beta-179899	10540	60
Abeilles 4	43.23	0.63	LYON-949	10580	115
Cheimadio SS94-2	39.17	20.61	OxA-17828	10655	45
Ekain	43.24	-2.26	GifA-95376	10830	150
La Fru	45.44	5.80	LYON-925	10950	110
Hassleberga	55.58	13.32	Ua-3293	11180	95
Conduche	44.48	1.63	OxA-2847	11210	90
Cathole	51.59	-4.11	AA-23371	11230	100
Closeau	48.88	2.16	LYON-566 (OxA)	11240	90
Closeau	48.88	2.16	AA-21677 (LYON-358)	11240	80
Blenien	47.45	7.39	Ua-44710	11279	77
Balma de la Griera	41.20	1.56	Beta-244009	11350	70

Table H.1: Random sample of 242 radiocarbon dates of AMH from Carotenuto et al. (2018) used in KDE, environmental niche, and OxCal boundary models. *(continued)*

Site	Latitude	Longitude	Lab code	Date BP	Error BP
Andernach-Martinsberg 2	50.43	7.40	OxA-998	11370	160
La Fru	45.44	5.80	GrA-25062	11420	60
Kozarnika	43.65	22.70	GifA-98345	11550	100
Giganti Cave	40.25	15.19	LYON-4715(OxA)	11560	55
Gough's Cave	51.28	-2.77	OxA-2236	11700	100
Kettig	50.40	7.47	GrA-14171	11720	60
Andernach-Martinsberg 2	50.43	7.40	OxA-997	11800	160
Baume Flandin	44.30	4.43	LYON-672	11865	70
Kendrick's Cave, Great Orme's Head	53.37	-3.92	OxA-17089	11905	50
Douattes	46.02	5.95	LYON-1417	11945	85
La Fru	45.44	5.80	OxA-5264 (LYON-134)	12110	110
Dzierzyslaw 1	50.05	17.99	Poz-7318	12150	70
Buttenloch	47.48	7.55	UtC-12577	12180	90
Ahrenshoft LA 73	54.57	9.07	KIA-3605	12200	60
Berelekh	70.50	144.03	Beta-216796	12200	40
Church Hole	53.25	-1.22	OxA-735	12240	150
La Chora	43.33	-3.51	LYON-2738	12240	55
Isturitz	43.37	-1.20	OxA-19837	12245	60
Hort de la Boquera	41.30	0.76	OxA-13595	12250	60
Cueva del Hoyo de la Mina, Hoyo Mina	36.79	-4.34	Ua-19443	12255	100
Dzierzyslaw 35	50.05	17.99	Ki-8851	12300	400
Condover	52.65	-2.75	OxA-1456	12330	120
Gough's New Cave	51.28	-2.77	OxA-465	12360	170
Fees	46.41	3.64	OxA-6426	12475	80
Felsstalle	48.28	9.65	OxA-6428	12505	80
Closeau	48.88	2.16	LYON-1550 (GrA-18860)	12510	80

Table H.1: Random sample of 242 radiocarbon dates of AMH from Carotenuto et al. (2018) used in KDE, environmental niche, and OxCal boundary models. *(continued)*

Site	Latitude	Longitude	Lab code	Date BP	Error BP
Afontova Gora 2, Old Excavation CL C3	56.00	92.85	AA-59609	12560	70
Bonn-Oberkassel	50.71	7.17	OxA-28150	12560	55
La Peyzie	45.27	0.53	GifA-90033	12580	190
Climautsi II, Klimautsy II, Klimauts II, Climautsy II, Climauti	48.31	27.61	OxA-24990	12590	50
Gonnersdorf	50.45	7.42	OxA-5728	12730	130
La Fru	45.44	5.80	LYON-132/OxA-5262	12770	110
Goyet 3	50.45	5.01	OxA-V-2223-48	12775	55
Abri Stendel	51.43	9.92	OxA-10471	12860	75
Bange	45.70	5.80	GrA-13441	12900	60
Faurelie	45.09	0.92	Lyon-5369(SacA-12062)	12980	80
Buraca Grande - 9A	39.98	-8.55	OxA-5522	13050	100
Coimbre	43.33	-4.69	Beta-297105	13230	60
Etxauri	42.75	0.83	Beta-284730	13370	60
Courbet	44.05	1.67	GifA-90169	13410	240
El Castillo	43.29	-3.96	GifA-95226	13570	130
La Garma	43.15	-3.90	OxA-8722	13610	100
El Miron, Burial area	43.25	-3.45	GX-22703	13660	70
Carriot	44.48	1.65	GifA-93081	13820	120
Afontova Gora 2	56.00	92.85	AA-68664	13870	80
Isturitz, Saint-Martin	43.37	-1.20	OxA-19832	14075	60
Arlanpe	43.20	-2.77	Beta-287336	14150	60
Klithi	39.97	20.66	OxA-749	14200	200
Granne	52.53	22.52	Ly-4866	14200	50
Altamira	43.38	-4.12	GifA-90057	14480	250
Altamira	43.38	-4.12	GifA-90047	14520	260
Gontsy, Gintsy	50.17	32.82	OxA-5932	14550	150
Bignalats	43.12	-0.44	OxA-28121	14635	70

Table H.1: Random sample of 242 radiocarbon dates of AMH from Carotenuto et al. (2018) used in KDE, environmental niche, and OxCal boundary models. *(continued)*

Site	Latitude	Longitude	Lab code	Date BP	Error BP
El Castillo	43.29	-3.96	GifA-98156	14740	140
Altamira inner vestibule	43.38	-4.12	GifA-96062	15050	180
Kamennaya Balka II	47.42	38.67	GrA-21619	15120	110
Cosquer	43.21	5.45	GifA-92446	15570	150
Kamennaya Balka II	47.42	38.67	GrA-17349	15610	80
Fanciulli	43.78	7.53	LTL-13785A	15615	100
Karain B	38.60	35.00	OxA-8407	15860	100
Klithi	39.97	20.66	OxA-2327	16250	170
Klithi	39.97	20.66	OxA-2971	16650	190
El Castillo	43.29	-3.96	OxA-971	16850	220
Arlanpe	43.20	-2.77	Beta-238178	17070	80
Fontgrasse	43.97	4.53	Erl-8927	17100	144
Dzerava skala	48.52	17.30	Poz-7064	17400	180
La Boja	38.07	-1.49	VERA-5364b	17430	70
El Miron, Burial area	43.25	-3.45	UG-15181	17620	40
Kosautsy - Cosautsi - Cosaoutsy	48.22	28.28	OxA-5257	17840	180
Kosautsy - Cosautsi - Cosaoutsy	48.22	28.28	OxA-5236	17840	180
Kosautsy - Cosautsi - Cosaoutsy	48.22	28.28	OxA-5233	17900	200
Gruta Nova da Columbeira	39.31	-9.20	KN-5596	18000	185
Fossellone	41.24	13.10	UtC-11551	18160	240
Cosquer	43.21	5.45	GifA-92492	18530	190
Amvrosievka	47.79	38.48	OxA-4890	18700	240
Krakow Spadzista	50.06	19.91	Poz-51375	18950	90
Bossats	48.25	2.66	Erl-17854	19096	121
Cosquer	43.21	5.45	GifA-92418	19200	240
Brinzeni I, Brynzeny 1	48.08	27.25	OxA-4118	19220	180

Table H.1: Random sample of 242 radiocarbon dates of AMH from Carotenuto et al. (2018) used in KDE, environmental niche, and OxCal boundary models. *(continued)*

Site	Latitude	Longitude	Lab code	Date BP	Error BP
La Boja	38.07	-1.49	VERA-5365_2	19240	90
Balma Grande	43.78	7.53	GifA-95073	19280	220
Cougnac	44.75	1.35	GifA-91234	19500	270
La Vina	43.31	-5.83	OxA-4092	19930	220
Cueva Ambrosio	37.83	-2.10	GifA-95577	19950	210
Bajondillo	36.63	-4.50	MAD-2405	19990	480
Brinzeni I, Brynzeny 1	48.08	27.25	OxA-4898	20140	260
Aitzbitarte III Ext	43.27	-1.89	Ua-11149	20290	260
Kurtak-4	55.17	91.58	AA-72146	20690	240
La Boja	38.07	-1.49	VERA-5213HS	21060	110
Giurgiu - Malu Rosu	43.92	25.99	GrA-5094	21140	120
Buraca Escura	39.98	-8.55	OxA-5524	21820	200
Blot	45.17	3.48	LYON-1648	21870	230
Krakow Spadzista trench	50.06	19.91	Poz-51373	22090	110
Combe SauniíÂre	45.23	0.88	OxA-486	22100	440
La Passagere	45.13	5.53	OxA-179	22200	600
Krakow Spadzista, site D	50.06	19.91	Poz-26226	22330	160
Buraca Escura	39.98	-8.55	OxA-5523	22700	240
Khotylevo 2	53.34	34.11	OxA-27225	22720	150
Cosquer	43.21	5.45	GifA-95308	23080	640
Aggsbach	48.29	15.39	KIA-43238	23140	130
Dzudzuana Cave	42.30	43.32	RTA-3823 (RTT?)	23240	200
Khotylevo 2	53.34	34.11	OxA-27001	23240	160
Kostenki (Kostienki) 14 (Markina Gora)	51.39	39.03	GrA-5244	23600	440
Krakow Spadzista, site C	50.06	19.91	LuS-7418	23750	150
Krakow Spadzista, site B "Workshops”	50.06	19.91	Poz-225	23980	280
Kostenki (Kostienki) 14 (Markina Gora)	51.39	39.03	GrA-5143	24030	440

Table H.1: Random sample of 242 radiocarbon dates of AMH from Carotenuto et al. (2018) used in KDE, environmental niche, and OxCal boundary models. *(continued)*

Site	Latitude	Longitude	Lab code	Date BP	Error BP
Krems-Hundssteig	48.41	15.60	VERA-670	24400	1000
Grande Grotte	47.59	3.77	OxA-4999	24600	400
Hyaena Den	51.23	-2.68	OxA-3451	24600	300
La Vina	43.31	-5.83	OxA-21688	24640	190
Facteur	44.96	1.03	OxA-586	24690	600
Cejkov I	48.47	21.77	Beta-159851	24800	110
Flageolet I	44.85	1.08	OxA-597	24800	600
Cougnac	44.75	1.35	GifA-92425	25120	390
Grotte de la Princesse Pauline	50.48	4.95	GrA-28204	25580	170
Chauvet	44.39	4.42	GifA-11114/SacA-24654	25610	280
Kranawetberg	48.42	16.83	GrA-28184	25640	160
Chauvet	44.39	4.42	GifA-95158	25700	850
Gargas	43.05	-0.54	LYON-3405 GrA	25700	120
Krems-Wachtberg	48.41	15.60	VERA-4538	26050	200
Antolinako Koba	43.37	-2.65	Beta-215542	26080	200
Arbreda	42.16	2.75	OxA-21668	26100	210
Dolni Vestonice IIa	48.88	16.64	GrA-15132	26190	390
Hranice	49.57	17.34	OxA-3889	26300	460
Huccorgne - Hermitage	50.56	5.18	OxA-3886	26300	350
Cosquer	43.21	5.45	GifA-92349	26360	440
Gargas	43.05	-0.54	LYON-3410 GrA	26380	120
Hohle Fels, Hohler Fels	48.38	9.75	OxA-4976	26450	550
Capo Grosso	40.00	15.35	GifA-100404	26490	390
Chauvet	44.39	4.42	GifA-11113/SacA-24653	26650	460
La Boja	38.07	-1.49	VERA-5789HS	26760	230
Gargas	43.05	-0.54	GifA-92369	26860	460
Labeko Koba	43.06	-2.48	Ua-3320	26910	500
Bondi Cave	42.34	43.25	OxA-23902	27120	240
Alberndorf I	48.68	16.11	GrA-5223	27140	650
Krems-Hundssteig	48.41	15.60	VERA-2291	27200	240
Krems-Wachtberg	48.41	15.60	VERA-3933	27420	240

Table H.1: Random sample of 242 radiocarbon dates of AMH from Carotenuto et al. (2018) used in KDE, environmental niche, and OxCal boundary models. *(continued)*

Site	Latitude	Longitude	Lab code	Date BP	Error BP
Kostenki (Kostienki) 17 (Spitsynskaya site)	51.39	39.05	GrA-20141	27490	165
Geissenklosterle	48.39	9.78	OxA-4857	27500	550
Ferrassie	44.95	0.94	OxA-403	27530	720
Caldeirao	39.65	-8.42	OxA-1941	27600	600
Kostenki (Kostienki) 14 (Markina Gora)	51.39	39.03	OxA-4117	27710	410
Chez-Pinaud I	45.44	-0.42	GrA-20853 (LYON-1776)	27780	200
Isoletta	41.58	13.57	ISGS-A-0186	27933	224
Krems-Hundssteig	48.41	15.60	VERA-3281	27970	270
Geissenklosterle	48.39	9.78	OxA-5227	28050	550
Arbreda	42.16	2.75	OxA-21782	28280	290
Huccorgne - Hermitage	50.56	5.18	CAMS-5891	28390	430
Aitzbitarte III Ext	43.27	-1.89	Ua-37962	28530	645
Dolni Vestonice IIa	48.88	16.64	OxA-17812	28550	150
Grotte des Gorges	47.17	5.56	Beta-55063	28650	160
Kalavan 2	40.64	45.11	UGAMS-2295A	29230	110
Chauvet	44.39	4.42	GifA-99239	29740	390
Hohle Fels, Hohler Fels	48.38	9.75	KIA-8965	30010	220
Kent's Cavern	50.47	-3.53	OxA-6108	30220	460
Biryuchya Balka 2	55.55	89.04	Beta-183591	30240	360
Covalejos, Cobalejos	43.39	-3.96	GrA-22443	30380	250
Geissenklosterle	48.39	9.78	OxA-6628	30450	550
Engis	50.59	5.59	GrA-21545	30460	210
Chauvet	44.39	4.42	GrA-46922	30530	240
Krems-Hundssteig	48.41	15.60	VERA-1616	30750	290
Chauvet-Pont d'Arc	44.39	4.42	GrA-28195	30760	80
Chauvet	44.39	4.42	GrA-28202	30900	270
Arbreda	42.16	2.75	OxA-19935	30950	220
Dzerava skala	48.52	17.30	OxA-15335	31000	1100

Table H.1: Random sample of 242 radiocarbon dates of AMH from Carotenuto et al. (2018) used in KDE, environmental niche, and OxCal boundary models. *(continued)*

Site	Latitude	Longitude	Lab code	Date BP	Error BP
La Dehesa	37.30	-6.73	OxA-4603	31100	500
Kent's Cavern	50.47	-3.53	OxA-14715	31150	330
Aitzbitarte III Ext	43.27	-1.89	Ua-18467	31210	860
Chauvet	44.39	4.42	ETH-46133 b	31297	227
Chauvet	44.39	4.42	GifA-99238	31430	420
Chauvet	44.39	4.42	GrA-47166	31430	260
Labeko Koba	43.06	-2.48	Ua-3321	31455	915
Henrykow 15	50.64	17.00	Poz-60000	31550	350
Chauvet	44.39	4.42	GifA-90219/SacA-14204	31570	360
Chauvet	44.39	4.42	GifA-80107/SacA-11409	31580	280
Klisoura Cave 1, Klissoura Cave 1	37.69	22.81	AA-73817	31630	250
Goyet 3	50.45	5.01	OxA-V-2223-44	31750	200
Chauvet	44.39	4.42	GifA-13095/SacA-33473	31830	450
Chauvet	44.39	4.42	ETH-46134 b	31864	245
Geissenklosterle	48.39	9.78	KIA-8958	31870	260
Chauvet	44.39	4.42	ETH-46134 a	31875	265
Chauvet	44.39	4.42	ETH-46134 d	31886	247
Chauvet	44.39	4.42	OxA-26473	31900	280
Fumane	45.51	10.97	UtC-2049	31900	500
Chauvet	44.39	4.42	GifA-8007 (SacA-9880)	31970	350
Castanet North	44.99	1.10	OxA-21645	32000	450
Castanet	44.99	1.10	OxA-21561	32050	450
Chauvet	44.39	4.42	GifA-99775	32080	430
Labeko Koba	43.06	-2.48	OxA-21841	32150	450
Abrigo de Buendia	40.42	-2.50	OxA-28336	32270	170
Kostenki (Kostienki) 14 (Markina Gora)	51.39	39.03	CURL-17832	32280	530
Castanet	44.99	1.10	GifA-99179	32310	520
Chauvet	44.39	4.42	OxA-X-2131-14	32350	210
Chauvet	44.39	4.42	KiA-28573 GifA-50128	32357	350

Table H.1: Random sample of 242 radiocarbon dates of AMH from Carotenuto et al. (2018) used in KDE, environmental niche, and OxCal boundary models. *(continued)*

Site	Latitude	Longitude	Lab code	Date BP	Error BP
Chauvet	44.39	4.42	GifA-70148 (SacA-9871)	32370	360
Chauvet	44.39	4.42	SacA-29314	32380	410
Hyenes	43.64	-0.69	GifA-98105	32410	370
Chauvet	44.39	4.42	GifA-80010 (SacA-9883)	32410	350
Bench Quarry, Bench Tunnel Cavern	50.38	-3.50	OxA-5961	32500	1200
Grotte des Gorges	47.17	5.56	GifA-12197/SacA-29929	32600	1000
Castanet	44.99	1.10	OxA-21563	32600	450
Buran Kaya III	45.00	34.40	OxA-13302	32790	280
Cueva Anton	38.06	1.50	OxA-21244	32890	200
Chauvet	44.39	4.42	GifA-13133/SacA-33761	33000	0
Geissenklosterle	48.39	9.78	OxA-21656	33000	500
Kostenki (Kostienki) 14 (Markina Gora)	51.39	39.03	OxA-X-2395-15	33250	500
Fumane	45.51	10.97	OxA-8021	33300	400
Geissenklosterle	48.39	9.78	OxA-18718	33380	390
Abri Pataud	44.94	1.01	OxA-21580	33550	550
Labattut, Labatut	45.00	1.11	OxA-21768	33600	500
Chauvet-Pont d'Arc	44.39	4.42	GifA-13109/SacA-33487	33600	3900
Geissenklosterle	48.39	9.78	OxA-6076	33600	1900
Gatzarria	43.14	-0.89	OxA-22553	33800	550
Fumane	45.51	10.97	OxA-17981	33890	220
Geissenklosterle	48.39	9.78	OxA-21727	34100	550
Fumane	45.51	10.97	UtC-2690	34200	900
Abri Pataud	44.94	1.01	OxA-21600	34200	550
Bench Quarry, Bench Tunnel Cavern	50.38	-3.50	OxA-1620	34500	1400
Gorham's Cave	36.12	-5.34	OxA-10295	34600	900
Abri Pataud	44.94	1.01	OxA-21599	34850	600
Dzerava skala	48.52	17.30	Poz-8793	34900	600

Table H.1: Random sample of 242 radiocarbon dates of AMH from Carotenuto et al. (2018) used in KDE, environmental niche, and OxCal boundary models. *(continued)*

Site	Latitude	Longitude	Lab code	Date BP	Error BP
Canyars	41.30	1.98	OxA-24057	34900	340
Franchthi	37.42	23.13	OxA-20253	34980	220

I HPLC background correction notes

HPLC dates need an additional background correction to account for carbon introduced in the chemistry stages. The equation used for the correction is published in Devièse et al. (2017). The additional data required for the correction is included here, alongside the corrections for the HPLC dates produced for this thesis (Table I.1).

For the background correction in this thesis, 0.018 was used as the measurement error for the mass spectrometers used in combustion (D. Comeskey and P. Ditchfield pers. comm.). Background values were selected on two background standards that were extracted and combusted alongside the thesis' unknown-age samples (Table I.2). The R function used to calculate the correction is included below. It takes two dataframes, one with the unknown sample to be corrected and the other with the standards to use in evaluation. The columns are specified by name rather than index here for clarity (Table I.3).

Table I.1: HPLC dates obtained for this thesis and their corrected results. F14C is fraction modern carbon, Date/error BP are uncorrected, and HPLC date/error are the background-corrected dates.

P	Site	OxA	F14C	Error F14C	Date BP	Error BP	HPLC date	HPLC error
42796	Zafarraya	X-2730-9	0.02108	0.00077	31000	290	31245	417
42798	Zafarraya	X-2732-18	0.03302	0.00128	27400	310	27672	463
43017	Zafarraya	X-2730-10	0.01016	7e-04	36850	550	37371	845
43025	Zafarraya	X-2732-28	0.00524	0.00077	42200	1200	43359	1999
44415	Grotte di Equi	X-2756-40	0.08985	0.00159	19360	140	19480	214
44416	Grotte di Equi	X-2756-41	0.00606	0.00138	41000	1800	43011	3513
44418	Cava Muracci	X-2756-42	0.00395	0.00183	44400	3700	49270	10188

Table I.2: Standards (Ash Bend) used for the HPLC background corrections of dates obtained for this thesis. F14C is fraction modern carbon.

P	Target	F14C	Error F14C
19651	19651/117.18/170/NRC3/01	0.00257	0.00132
19651	19651/117.40/180/NRC2/01	0.00000	0.00104

I.1 R code for HPLC correction

Table I.3: Description of input variables required for the HPLC background correction. The function requires two data frames: uncorrected samples (`hplc.samples`) and background measurements (`stds`).

Variable	Description
`mg.C`	Milligrams carbon measured from combustion
`F14C`	Fraction modern carbon, from the AMS
`ErrorF14`	Error measurement fraction modern carbon, from the AMS
`mass.spec.error`	Estimated measurement error for combustion instrument

```
hplc.correct <- function(hplc.samples, stds, mass.spec.error) {
# Uncorrected sample information
mgC_sample <- hplc.samples$mg.C
f14C_sample <- hplc.samples$F14C
f14C_sample_error <- hplc.samples$ErrorF14
# Standards
mgC_std_list <- stds$mg.C
f14C_std_list <- stds$F14C
f14C_std_error_list <- stds$ErrorF14
mass.spec.error <- 0.018
# Weighted means
mgC_std <- mean(mgC_std_list)
f14C_std <- weighted.mean(f14C_std_list, mgC_std_list)
f14C_std_error <- weighted.mean(f14C_std_error_list, mgC_std_list)
# Date correction #
# Mass fraction modern C, estimated from modern C in stds
mass.mod.c <- (f14C_std * mgC_std) / mgC_sample
# Background correction
background.cor <- (f14C_sample - mass.mod.c) / (1 - mass.mod.c)
# Age BP
age.BP <- round((log(background.cor) * (-8033)), 0)
# Error correction #
error.weighted <- (mass.spec.error * ((f14C_std_error_list[1] *
          mgC_std_list[1]) + (f14C_std_error_list[2] *
          mgC_std_list[2]))) / sum(mgC_std_list)
# Error - fraction modern C
error.mass.mod.c <- error.weighted / (mass.spec.error * mgC_sample)
# Elements of error correction #
sq1 <- (f14C_sample_error / (1-mass.mod.c))^2
sq2 <- (error.mass.mod.c / (1-mass.mod.c))^2
```

```
sq3 <- (((f14C_sample - mass.mod.c) /
          ((1-mass.mod.c)^2)) * error.mass.mod.c)^2
# Error corrected
error.cor <- sqrt(sq1 + sq2 + sq3)
# Error BP
error.BP <- round((8033 * error.cor / background.cor), 0)
new.date <- c(hplc.samples$Target, age.BP, error.BP)
return(new.date)
}
```

J
Models and code

OxCal was used to calibrate dates, estimate species extinctions, and produce KDE models. Generalised code is presented below to show how models were produced.

J.1 OxCal extinction estimates

```
Plot()
{
 Sequence("species")
 {
  Boundary("fad_species");
  Phase("species")
  {
   R_Date();
  };
  Boundary("lad_species");
 };
};
```

J.2 KDE models

```
Plot()
{
  KDE_Model("species")
  {
   R_Date();
  };
};
```

J.3 MaxEnt features

Feature types and interpretation are described in `MaxEnt` helpfiles and publications (Merow et al. 2013; Muscarella et al. 2018; Muscarella et al. 2014; Phillips et al. 2017). Variables are WorldClim bioclimatic variable names (Hijmans et al. 2005) (Table J.1) and 'layer' reflects topography/elevation (NASA 2009).

Table J.1: Bio-climatic variables used in niche models. Descriptions from http://worldclim.org/bioclim.

Prefix	Number	Description
cclgmbi	1	Annual Mean Temperature
cclgmbi	4	Temperature Seasonality (standard deviation *100)
cclgmbi	7	Temperature Annual Range (BIO5-BIO6)
cclgmbi	12	Annual Precipitation
cclgmbi	15	Precipitation Seasonality (Coefficient of Variation)

J.3.1 Leopards

Table J.2: Features of MaxEnt model with LGM climate predictors for leopards.

Feature	Lambda	Min/Hinge	Max	Type
cclgmbi1	0.00	-333.49	247.66	Raw
cclgmbi12	0.00	2.00	3762.62	Raw
cclgmbi15	0.00	9.00	153.27	Raw
cclgmbi4	0.00	2270.69	23655.70	Raw
cclgmbi7	0.00	126.29	763.14	Raw
layer	0.00	-39.61	218.91	Raw
‘cclgmbi12	-0.66	2.00	840.44	Reverse hinge

Table J.3: Feature metrics of the above MaxEnt model for leopards.

	Feature metric	Value
11	entropy	6.88
10	numBackgroundPoints	1000.00
9	densityNormalizer	716.19
8	linearPredictorNormalizer	0.00

J.3.2 Lions

Table J.4: Features of MaxEnt model with LGM climate predictors for lions.

Feature	Lambda	Min/Hinge	Max	Type
‘cclgmbi15	0.61	9.00	32.99	Reverse hinge
‘cclgmbi15	0.31	9.00	96.59	Reverse hinge
‘cclgmbi15	0.22	9.00	31.26	Reverse hinge
‘cclgmbi15	0.20	9.00	31.43	Reverse hinge
‘cclgmbi15	0.11	9.00	96.55	Reverse hinge
‘cclgmbi15	0.10	9.00	32.93	Reverse hinge
‘cclgmbi15	0.07	9.00	31.22	Reverse hinge
‘cclgmbi15	0.06	9.00	31.34	Reverse hinge
‘cclgmbi15	0.05	9.00	32.97	Reverse hinge
‘cclgmbi15	0.04	9.00	31.59	Reverse hinge
‘cclgmbi15	0.02	9.00	31.19	Reverse hinge
cclgmbi1	0.00	-333.49	247.66	Raw
cclgmbi12	0.00	2.00	3762.62	Raw
cclgmbi15	0.00	9.00	153.27	Raw
cclgmbi4	0.00	2270.69	23655.70	Raw
cclgmbi7	0.00	126.29	763.14	Raw
layer	0.00	-39.61	218.91	Raw
’cclgmbi15	-0.30	50.60	153.27	Forward hinge
’cclgmbi7	-0.45	591.95	763.14	Forward hinge
’cclgmbi15	-0.89	50.65	153.27	Forward hinge
’cclgmbi1	-0.92	9.58	247.66	Forward hinge
’layer	-1.71	18.72	218.91	Forward hinge
’cclgmbi1	-2.08	10.02	247.66	Forward hinge

Table J.5: Feature metrics of the above MaxEnt model for lions.

	Feature metric	Value
27	entropy	6.54
26	numBackgroundPoints	1000.00
25	densityNormalizer	141.55
24	linearPredictorNormalizer	1.68

J.3.3 Hyenas

Table J.6: Features of MaxEnt model with LGM climate predictors for hyenas.

Feature	Lambda	Min/Hinge	Max	Type
‘cclgmbi15	1.35	9.00	18.98	Reverse hinge
‘cclgmbi7	1.33	126.29	340.00	Reverse hinge
‘cclgmbi7	0.52	126.29	340.14	Reverse hinge
‘cclgmbi15	0.48	9.00	18.78	Reverse hinge
‘cclgmbi15	0.39	9.00	19.52	Reverse hinge
‘cclgmbi7	0.38	126.29	341.76	Reverse hinge
‘cclgmbi15	0.32	9.00	53.09	Reverse hinge
‘cclgmbi15	0.28	9.00	54.49	Reverse hinge
‘cclgmbi15	0.24	9.00	21.01	Reverse hinge
‘cclgmbi15	0.22	9.00	58.97	Reverse hinge
‘cclgmbi15	0.22	9.00	58.69	Reverse hinge
‘cclgmbi15	0.15	9.00	63.01	Reverse hinge
‘cclgmbi15	0.12	9.00	19.45	Reverse hinge
‘cclgmbi15	0.11	9.00	20.85	Reverse hinge
‘cclgmbi7	0.09	126.29	342.05	Reverse hinge
‘cclgmbi15	0.04	9.00	58.63	Reverse hinge
cclgmbi1	0.00	-333.49	247.66	Raw
cclgmbi12	0.00	2.00	3762.62	Raw
cclgmbi15	0.00	9.00	153.27	Raw
cclgmbi4	0.00	2270.69	23655.70	Raw
cclgmbi7	0.00	126.29	763.14	Raw
layer	0.00	-39.61	218.91	Raw
’cclgmbi7	-0.10	277.67	763.14	Forward hinge
’layer	-0.21	8.69	218.91	Forward hinge
’cclgmbi15	-0.25	10.59	153.27	Forward hinge
’layer	-0.43	10.55	218.91	Forward hinge
‘cclgmbi7	-0.45	126.29	262.39	Reverse hinge
’layer	-0.48	10.56	218.91	Forward hinge
’cclgmbi7	-0.67	278.40	763.14	Forward hinge
‘cclgmbi7	-0.80	126.29	258.25	Reverse hinge
‘cclgmbi15	-0.83	9.00	9.12	Reverse hinge
‘cclgmbi12	-0.96	2.00	311.98	Reverse hinge
’layer	-0.97	8.64	218.91	Forward hinge
‘cclgmbi1	-1.52	-333.49	-11.34	Reverse hinge
‘cclgmbi15	-1.62	9.00	10.39	Reverse hinge
’cclgmbi15	-1.73	11.07	153.27	Forward hinge
‘cclgmbi12	-1.77	2.00	810.73	Reverse hinge
‘cclgmbi1	-1.85	-333.49	-11.86	Reverse hinge
‘layer	-3.20	-39.61	8.64	Reverse hinge
’cclgmbi1	-6.95	14.69	247.66	Forward hinge

Table J.7: Feature metrics of the above MaxEnt model for hyenas.

	Feature metric	Value
44	entropy	4.48
43	numBackgroundPoints	1000.00
42	densityNormalizer	9.09
41	linearPredictorNormalizer	3.13

J.3.4 AMH

Table J.8: Features of MaxEnt model with LGM climate predictors for modern humans.

Feature	Lambda	Min/Hinge	Max	Type
‘cclgmbi4	3.00	2270.69	4210.07	Reverse hinge
‘cclgmbi4	2.94	2270.69	3934.83	Reverse hinge
‘layer	1.51	-39.61	75.89	Reverse hinge
‘cclgmbi15	1.38	9.00	13.80	Reverse hinge
‘cclgmbi7	0.96	126.29	326.47	Reverse hinge
‘cclgmbi4	0.83	2270.69	8151.52	Reverse hinge
‘cclgmbi4	0.83	2270.69	8679.34	Reverse hinge
‘layer	0.55	-39.61	76.24	Reverse hinge
‘layer	0.53	-39.61	29.87	Reverse hinge
‘layer	0.30	-39.61	76.68	Reverse hinge
‘layer	0.25	-39.61	77.01	Reverse hinge
‘cclgmbi15	0.16	9.00	21.62	Reverse hinge
cclgmbi1	0.00	-333.49	247.66	Raw
cclgmbi12	0.00	2.00	3762.62	Raw
cclgmbi15	0.00	9.00	153.27	Raw
cclgmbi4	0.00	2270.69	23655.70	Raw
cclgmbi7	0.00	126.29	763.14	Raw
layer	0.00	-39.61	218.91	Raw
’cclgmbi7	-0.10	264.69	763.14	Forward hinge
‘cclgmbi1	-0.13	-333.49	5.65	Reverse hinge
‘layer	-0.19	-39.61	12.16	Reverse hinge
’cclgmbi1	-0.20	119.84	247.66	Forward hinge
’cclgmbi1	-0.23	8.33	247.66	Forward hinge
’cclgmbi1	-0.26	8.02	247.66	Forward hinge
‘cclgmbi15	-0.35	9.00	10.04	Reverse hinge
‘layer	-0.47	-39.61	12.15	Reverse hinge
’cclgmbi1	-0.47	94.84	247.66	Forward hinge
’cclgmbi7	-0.49	266.24	763.14	Forward hinge
’layer	-0.53	12.52	218.91	Forward hinge
‘cclgmbi15	-0.53	9.00	10.21	Reverse hinge
’cclgmbi1	-0.72	120.13	247.66	Forward hinge
’cclgmbi1	-0.87	96.54	247.66	Forward hinge
‘cclgmbi12	-0.88	2.00	423.14	Reverse hinge
’cclgmbi7	-0.91	265.97	763.14	Forward hinge
‘cclgmbi15	-0.99	9.00	9.89	Reverse hinge
‘cclgmbi1	-1.06	-333.49	2.40	Reverse hinge
’cclgmbi7	-1.06	264.37	763.14	Forward hinge
‘cclgmbi7	-1.28	126.29	175.43	Reverse hinge
‘layer	-1.29	-39.61	11.91	Reverse hinge
‘layer	-1.42	-39.61	12.08	Reverse hinge
’cclgmbi1	-1.60	9.82	247.66	Forward hinge
‘cclgmbi1	-1.66	-333.49	2.61	Reverse hinge
’cclgmbi12	-1.71	825.82	3762.62	Forward hinge
‘cclgmbi12	-1.74	2.00	825.53	Reverse hinge

Table J.8: Features of MaxEnt model with LGM climate predictors for modern humans. *(continued)*

Feature	Lambda	Min/Hinge	Max	Type
‘cclgmbi7	-1.81	126.29	177.16	Reverse hinge
’cclgmbi12	-2.12	825.53	3762.62	Forward hinge
’layer	-2.47	13.65	218.91	Forward hinge
‘cclgmbi4	-2.92	2270.69	3280.77	Reverse hinge
‘layer	-3.53	-39.61	12.45	Reverse hinge
’cclgmbi15	-4.39	29.05	153.27	Forward hinge
‘layer	-6.36	-39.61	12.21	Reverse hinge

Table J.9: Feature metrics of the above MaxEnt model for modern humans.

	Feature metric	Value
55	entropy	4.78
54	numBackgroundPoints	1000.00
53	densityNormalizer	16.73
52	linearPredictorNormalizer	2.43

Works Cited

Agadjanian, A. K. and M. V. Shunkov (2018). Paleolithic man of Denisova Cave and zoogeography of Pleistocene mammals of Northwestern Altai. *Paleontological Journal* 52(1), 66–89.

Ajie, H. O., P. V. Hauschka, I. R. Kaplan, and H. Sobel (1991). Comparison of bone collagen and osteocalcin for determination of radiocarbon ages and paleodietary reconstruction. *Earth and Planetary Science Letters* 107(2), 380–388.

Aldhouse-Green, S., R. Dinnis, K. Scott, and E. A. Walker (2015). The nature of human activity at Cae Gwyn and Ffynnon Beuno caves and the dating of prey and predator presences. N. Ashton and C. Harris (Eds.), *No Stone Unturned: papers in honour of Roger Jacobi*. London: Lithic Studies Society, p. 77–92.

Aldhouse-Green, S. and P. Pettitt (1998). Paviland Cave: Contextualizing the 'Red Lady'. *Antiquity* 72(278), 756–772.

Alroy, J. (1999). Putting North America's end-Pleistocene megafaunal extinction in context. R. D. E. MacPhee (Ed.), *Extinctions in Near Time*. Advances in Vertebrate Paleobiology 2. Springer US, p. 105–143.

Altuna, J. (1972). *Fauna de mamíferos de los yacimientos prehistóricos de Guipúzcoa. Con catálogo de los Mamíferos Cuaternarios del Cantábrico y del Pirineo Occidental*. San Sebastian: Sociedad de Ciencias Naturales Aranzadi.

Álvarez-Lao, D. J. and N. García (2010). Chronological distribution of Pleistocene cold-adapted large mammal faunas in the Iberian Peninsula. *Quaternary International* 212(2): *Quaternary Changes of Mammalian Communities Across and Between Continents*, 120–128.

Álvarez-Lao, D. (2003). Macromamíferos fósiles del Pleistoceno de Asturias: Revisión bibliográfica y datos actuales. *Naturalia Cantabricae* 2, 11–23.

Ambrose, S. (1990). Preparation and characterization of bone and tooth collagen for isotopic analysis. *Journal of Archaeological Science* 17(4), 431–451.

Amiri, A. and B. Ventelou (2012). Granger causality between total expenditure on health and GDP in OECD: Evidence from the Toda–Yamamoto approach. *Economics Letters* 116(3), 541–544.

Anderson, E. (1984). Who's who in the Pleistocene: a mammalian bestiary. P. S. Martin and R. G. Klein (Eds.), *Quaternary Extinctions: A Prehistoric Revolution*. Tuscon: University of Arizona Press.

Anikovich, M. V., A. A. Sinitsyn, J. F. Hoffecker, V. T. Holliday, V. V. Popov, S. N. Lisitsyn, S. L. Forman, et al. (2007). Early Upper Paleolithic in Eastern Europe and implications for the dispersal of modern humans. *Science* 315(5809), 223–6.

Antonakos, A., E. Liarokapis, and T. Leventouri (2007). Micro-Raman and FTIR studies of synthetic and natural apatites. *Biomaterials* 28(19), 3043–3054.

Araujo, B. B. A., L. G. R. Oliveira-Santos, M. S. Lima-Ribeiro, J. A. F. Diniz-Filho, and F. A. S. Fernandez (2017). Bigger kill than chill: The uneven roles of humans and

climate on late Quaternary megafaunal extinctions. *Quaternary International* 431: *Pleistocene Human Dispersals: Climate, Ecology and Social Behavior*, 216–222.

Arslanov, K. A. and Y. S. Svezhentsev (1993). An improved method for radiocarbon dating fossil bones. *Radiocarbon* 35(3), 387–391.

Asner, G. P. and S. R. Levick (2012). Landscape-scale effects of herbivores on treefall in African savannas. *Ecology Letters* 15(11), 1211–1217.

Athreya, V., M. Odden, J. D. C. Linnell, J. Krishnaswamy, and U. Karanth (2013). Big cats in our backyards: persistence of large carnivores in a human dominated landscape in India. *PLOS ONE* 8(3), e57872.

Baca, M., D. Popović, K. Stefaniak, A. Marciszak, M. Urbanowski, A. Nadachowski, and P. Mackiewicz (2016). Retreat and extinction of the Late Pleistocene cave bear (*Ursus spelaeus* sensu lato). *The Science of Nature* 103(11), 92.

Bailey, S. E., T. D. Weaver, and J.-J. Hublin (2009). who made the Aurignacian and other early Upper Paleolithic industries? *Journal of Human Evolution* 57(1), 11–26.

Bakker, E. S., J. L. Gill, C. N. Johnson, F. W. Vera, C. J. Sandom, G. P. Asner, and J.-C. Svenning (2016). Combining paleo-data and modern exclosure experiments to assess the impact of megafauna extinctions on woody vegetation. *Proceedings of the National Academy of Sciences* 113(4), 847–855.

Balmford, A. (1996). Extinction filters and current resilience: the significance of past selection pressures for conservation biology. *Trends in Ecology & Evolution* 11(5), 193–196.

Barakat, N. A. M., M. S. Khil, A. M. Omran, F. A. Sheikh, and H. Y. Kim (2009). Extraction of pure natural hydroxyapatite from the bovine bones bio waste by three different methods. *Journal of Materials Processing Technology* 209(7), 3408–3415.

Bargar, J. R., P. Persson, and G. E. Brown (1999). Outer-Sphere adsorption of Pb(II)EDTA on goethite. *Geochimica et Cosmochimica Acta* 63(19), 2957–2969.

Barnett, R., M. Z. Mendoza, A. R. Soares, S. Ho, G. Zazula, N. Yamaguchi, B. Shapiro, et al. (2016). Mitogenomics of the extinct cave lion, *Panthera spelaea* (Goldfuss, 1810), resolve its position within the panthera cats. *Open Quaternary* 2(4), 1–11.

Barnett, R., B. Shapiro, I. Barnes, S. Y. W. Ho, J. Burger, N. Yamaguchi, T. F. G. Higham, et al. (2009). Phylogeography of lions (*Panthera leo* ssp.) reveals three distinct taxa and a late Pleistocene reduction in genetic diversity. *Molecular Ecology* 18(8), 1668–1677.

Barnosky, A. D., P. L. Koch, R. S. Feranec, S. L. Wing, and A. B. Shabel (2004). Assessing the causes of late Pleistocene extinctions on the continents. *Science* 306(5693), 70–75.

Barnosky, A. D. and E. L. Lindsey (2010). Timing of Quaternary megafaunal extinction in South America in relation to human arrival and climate change. *Quaternary International* 217(1), 10–29.

Barnosky, A. D., N. Matzke, S. Tomiya, G. O. U. Wogan, B. Swartz, T. B. Quental, C. Marshall, et al. (2011). Has the Earth's sixth mass extinction already arrived? *Nature* 471(7336), 51–57.

Barroso Ruiz, C., ed. (2003). *El Pleistoceno Superior de la Cueva del Boquete de Zafarraya*. Arqueologia Monografias. Junta de Andalucía: Consejería de Cultura.

Barroso Ruiz, C. and S. Bailon (2003). Los anfibios y los reptiles del Pleistoceno Superior de la Cueva del Boquete de Zafarraya. C. Barroso Ruiz (Ed.), *El Pleistoceno Superior de la Cueva del Boquete de Zafarraya*. Arqueologia Monografias. Junta de Andalucía: Consejería de Cultura, p. 267–278.

Barroso Ruiz, C. (2010). La Cueva del Boquete de Zafarraya, un lugar visitado por los neandertales hace 40.000 años. *PH: Boletín del Instituto Andaluz del Patrimonio Histórico* 18(74), 27.

Bartlett, L. J., D. R. Williams, G. W. Prescott, A. Balmford, R. E. Green, A. Eriksson, P. J. Valdes, et al. (2016). Robustness despite uncertainty: regional climate data reveal the dominant role of humans in explaining global extinctions of late Quaternary megafauna. *Ecography* 39(2), 152–161.

Bartlett, M. S. (1937). Properties of sufficiency and statistical tests. *Proceedings of the Royal Society A* 160(901), 268–282.

Barton, R. N. E., A. P. Currant, Y. Fernandez-Jalvo, J. C. Finlayson, P. Goldberg, R. MacPhail, P. B. Pettitt, et al. (1999). Gibraltar Neanderthals and results of recent excavations in Gorham's, Vanguard and Ibex Caves. *Antiquity* 73(279), 13–23.

Bates, D., M. Mächler, B. Bolker, and S. Walker (2015). Fitting linear mixed-effects models using Lme4. *Journal of Statistical Software* 67(1), 1–48.

Bauer, D. and A. Maynard (2012). Persistence-robust surplus-lag Granger causality testing. *Journal of Econometrics* 169(2), 293–300.

Bayliss, A. (2009). Rolling out revolution: using radiocarbon dating in archaeology. *Radiocarbon* 51(01), 123–147.

Bayliss, A., C. B. Ramsey, J. Van der Plicht, and A. Whittle (2007). Bradshaw and Bayes: towards a timetable for the Neolithic. *Cambridge Archaeological Journal* 17(S1), 1–28.

Beasley, M. M., E. J. Bartelink, L. Taylor, and R. M. Miller (2014). Comparison of transmission FTIR, ATR, and DRIFT spectra: implications for assessment of bone bioapatite diagenesis. *Journal of Archaeological Science* 46, 16–22.

Belbachir, K., R. Noreen, G. Gouspillou, and C. Petibois (2009). Collagen types analysis and differentiation by FTIR spectroscopy. *Analytical and Bioanalytical Chemistry* 395(3), 829–837.

Benazzi, S., V. Slon, S. Talamo, F. Negrino, M. Peresani, S. E. Bailey, S. Sawyer, et al. (2015). The makers of the Protoaurignacian and implications for Neandertal extinction. *Science* 348(6236), 793–796.

Benazzi, S., K. Douka, C. Fornai, C. C. Bauer, O. Kullmer, J. Svoboda, I. Pap, et al. (2011). Early dispersal of modern humans in Europe and implications for Neanderthal behaviour. *Nature* 479(7374), 525.

Benini, A., P. Boscato, and P. Gambassini (1997). Grotta della Cala (Salerno): industrie litiche e faune uluzziane ed aurignaziane. *Rivista di Scienze Preistoriche* 48, 37–95.

Bennett, K. D. and J. Provan (2008). What do we mean by 'refugia'? *Quaternary Science Reviews* 27(27–28): *Ice Age Refugia and Quaternary Extinctions: An Issue of Quaternary Evolutionary Palaeoecology*, 2449–2455.

Bennike, O. and R. Liljegren (2014). Dating of a muskox (*Ovibos moschatus*) skull fragment from Jamtland, Sweden: Middle Weichselian age. *Geologiska Foreningens i Stockholm Forhandlingar* 136(2), 406–409.

Bereuter, T. L., W. Mikenda, and C. Reiter (1997). Iceman's mummification—implications from infrared spectroscopical and histological studies. *Chemistry—A European Journal* 3(7), 1032–1038.

Berger, R., A. G. Horney, and W. F. Libby (1964). Radiocarbon dating of bone and shell from their organic components. *Science* 144(3621), 999–1001.

Berger, R. and W. F. Libby (1966). UCLA radiocarbon dates V. *Radiocarbon* 8(1), 467–497.

Berto, C. and G. Rubinato (2013). The Upper Pleistocene mammal record from Caverna Degli Orsi (San Dorligo Della Valle – Dolina, Trieste, Italy): a faunal complex between eastern and western Europe. *Quaternary International* 284, 7–14.

Bigagli, C., R. Iardella, A. Palchetti, and E. Paribeni (2013). Equi Terme: saggio nella Grotta della Tecchia. *Notiziario della Soprintendenza per i Beni Archeologici della Toscana* 8, 187–189.

Bocherens, H. (2015). Isotopic tracking of large carnivore palaeoecology in the mammoth steppe. *Quaternary Science Reviews* 117, 42–71.

Bocherens, H., D. G. Drucker, D. Bonjean, A. Bridault, N. J. Conard, C. Cupillard, M. Germonpré, et al. (2011). Isotopic evidence for dietary ecology of cave lion (*Panthera spelaea*) in North-Western Europe: prey choice, competition and implications for extinction. *Quaternary International* 245(2): *Late Quaternary Mammal Ecology: Insight from New Approaches*, 249–261.

Bohm, T. and O. Höner (2015). *Crocuta crocuta. The IUCN Red List of Threatened Species 2015*, e.T5674A45194782, http://www.iucnredlist.org/details/5674/0.

Bolker, B. M., M. E. Brooks, C. J. Clark, S. W. Geange, J. R. Poulsen, M. H. H. Stevens, and J.-S. S. White (2009). Generalized linear mixed models: a practical guide for ecology and evolution. *Trends in Ecology & Evolution* 24(3), 127–135.

Bond, A. L., C. J. Carlson, and K. R. Burgio (2019). Local extinctions of insular avifauna on the most remote inhabited island in the world. *Journal of Ornithology* 160(1), 49–60.

Bond, G., H. Heinrich, W. Broecker, L. Labeyrie, J. Mcmanus, J. Andrews, S. Huon, et al. (1992). Evidence for massive discharges of icebergs into the North Atlantic ocean during the last glacial period. *Nature* 360(6401), 245–249.

Bonjean, D., G. Abrams, K. Di Modica, and S. Pirson (2013). Andenne/Sclayn: La Grotte Scladina, nouvelles datations au radiocarbone. *Chronique de l'Archéologie Wallonne* 20, 241–244.

Borgia, V. (2008). Ancient Gravettian in the south of Italy: functional analysis of backed points from Grotta Paglicci (Foggia) and Grotta Della Cala (Salerno). *Palethnology* 1: *Projectile Weapon Elements from the Upper Palaeolithic to the Neolithic*, 45–65.

Boskey, A. and N. P. Camacho (2007). FT-IR imaging of native and tissue-engineered bone and cartilage. *Biomaterials* 28(15), 2465–2478.

Bowler, D. E. and T. G. Benton (2005). Causes and consequences of animal dispersal strategies: relating individual behaviour to spatial dynamics. *Biological Reviews* 80(2), 205–225.

Bowman, D. M. J. S. (1998). The impact of Aboriginal landscape burning on the Australian biota. *New Phytologist* 140(3), 385–410.

Bradshaw, C. J. A., A. Cooper, C. S. M. Turney, and B. W. Brook (2012). Robust estimates of extinction time in the geological record. *Quaternary Science Reviews* 33, 14–19.

Brauer, A., I. Hajdas, S. P. E. Blockley, C. Bronk Ramsey, M. Christl, S. Ivy-Ochs, G. E. Moseley, et al. (2014). The importance of independent chronology in integrating records of past climate change for the 60–8 Ka INTIMATE time interval. *Quaternary Science Reviews* 106, 47–66.

Brock, F., M. Dee, A. Hughes, C. Snoeck, R. Staff, and C. B. Ramsey (2018). Testing the effectiveness of protocols for removal of common conservation treatments for radiocarbon dating. *Radiocarbon* 60(1), 35–50.

Brock, F., V. Geoghegan, B. Thomas, K. Jurkschat, and T. F. G. Higham (2013a). Analysis of bone collagen extraction products for radiocarbon dating. *Radiocarbon* 55(2–3), 445–463.

Brock, F., T. Higham, and C. Bronk Ramsey (2010a). Pre-screening techniques for identification of samples suitable for radiocarbon dating of poorly preserved bones. *Journal of Archaeological Science* 37(4), 855–865.

Brock, F., T. Higham, P. Ditchfield, and C. Bronk Ramsey (2010b). Current pretreatment methods for AMS radiocarbon dating at the Oxford Radiocarbon Accelerator Unit (ORAU). *Radiocarbon* 52(1), 103–112.

Brock, F., T. Higham, and C. Bronk Ramsey (2013b). Comments on the use of Ezee-Filters™ and Ultrafilters at ORAU. *Radiocarbon* 55(1), 211–212.

Brock, F., C. B. Ramsey, and T. Higham (2007). Quality assurance of ultrafiltered bone dating. *Radiocarbon* 49(2), 187–192.

Brock, F., R. Wood, T. F. Higham, P. Ditchfield, A. Bayliss, and C. Bronk Ramsey (2012). Reliability of nitrogen content (%N) and carbon:nitrogen atomic ratios (C:N) as indicators of collagen preservation suitable for radiocarbon dating. *Radiocarbon* 54(3-4), 879–886.

Bronk Ramsey, C. (2008). Radiocarbon dating: revolutions in understanding*. *Archaeometry* 50(2), 249–275.

— (2009). Bayesian analysis of radiocarbon dates. *Radiocarbon* 51, 337–360.

Bronk Ramsey, C., T. Gigham, and P. Leach (2004a). Towards high-precision AMS: progress and limitations. *Radiocarbon* 46(1), 17–24.

Bronk Ramsey, C. and R. E. M. Hedges (1997). Hybrid ion sources: radiocarbon measurements from microgram to milligram. *Nuclear Instruments and Methods in Physics Research Section B: Beam Interactions with Materials and Atoms* 123(1-4), 539–545.

Bronk Ramsey, C., T. Higham, A. Bowles, and R. Hedges (2004b). Improvements to the pretreatment of bone at Oxford. *Radiocarbon* 46(1), 155–164.

Bronk Ramsey, C., P. B. Pettitt, R. E. M. Hedges, G. W. L. Hodgins, and D. C. Owen (2000). Radiocarbon dates from the Oxford AMS system: *Archaeometry* datelist 30. *Archaeometry* 42(2), 459–479.

Bronk Ramsey, C. (2017). Methods for summarizing radiocarbon datasets. *Radiocarbon* 59(6), 1809–1833.

Brook, B. W. and D. M. J. S. Bowman (2004). The uncertain blitzkrieg of Pleistocene megafauna. *Journal of Biogeography* 31(4), 517–523.

Brooks, T. M., S. L. Pimm, and J. O. Oyugi (1999). Time lag between deforestation and bird extinction in tropical forest fragments. *Conservation Biology* 13(5), 1140–1150.

Broughton, J. M. and E. M. Weitzel (2018). Population reconstructions for humans and megafauna suggest mixed causes for North American Pleistocene extinctions. *Nature Communications* 9(1), 5441.

Brown, C., R. McMorran, and M. F. Price (2011). Rewilding – A new paradigm for nature conservation in Scotland? *Scottish Geographical Journal* 127(4), 288–314.

Brown, J. H. and A. Kodric-Brown (1977). Turnover rates in insular biogeography: effect of immigration on extinction. *Ecology* 58(2), 445–449.

Brown, T. A., D. E. Nelson, J. S. Vogel, and J. R. Southon (1988). Improved collagen extraction by modified Longin method. *Radiocarbon* 30(2), 171–177.

Brugal, J.-P. and R. Croitor (2007). Evolution, ecology and biochronology of herbivore associations in Europe during the last 3 million years. *Quaternaire: Revue de l'Association Française pour l'Étude du Quaternaire* 18(2), 129–152.

Buckley, M., M. Collins, J. Thomas-Oates, and J. C. Wilson (2009). Species identification by analysis of bone collagen using matrix-assisted laser desorption/ionisation time-of-flight mass spectrometry. *Rapid Communications in Mass Spectrometry* 23(23), 3843–3854.

Burjanadze, T. V. and M. O. Bezhitadze (1992). Presence of a thermostable domain in the helical part of the type I collagen molecule and its role in the mechanism of triple helix folding. *Biopolymers* 32(8), 951–956.

Burney, D. A. (1999). Rates, patterns, and processes of landscape transformation and extinction in Madagascar. R. MacPhee (Ed.), *Extinctions in Near Time*. Vol. 2. Advances in Vertebrate Paleobiology. Boston: Springer, p. 145–164.

Burney, D. A. and T. F. Flannery (2005). Fifty millennia of catastrophic extinctions after human contact. *Trends in Ecology & Evolution* 20(7), 395–401.

Cahill, A. E., M. E. Aiello-Lammens, M. C. Fisher-Reid, X. Hua, C. J. Karanewsky, H. Y. Ryu, G. C. Sbeglia, et al. (2013). How does climate change cause extinction? *Proceedings of the Royal Society B: Biological Sciences* 280(1750), 20121890.

Callis, G. and D. Sterchi (1998). Decalcification of bone: literature review and practical study of various decalcifying agents, methods, and their effects on bone histology. *Journal of Histotechnology* 21(1), 49–58.

Campos, P. F., T. Kristensen, L. Orlando, A. Sher, M. V. Kholodova, A. Götherström, M. Hofreiter, et al. (2010a). Ancient DNA sequences point to a large loss of mitochondrial genetic diversity in the saiga antelope (*Saiga tatarica*) since the Pleistocene. *Molecular Ecology* 19(22), 4863–4875.

Campos, P. F., E. Willerslev, A. Sher, L. Orlando, E. Axelsson, A. Tikhonov, K. Aaris-Sørensen, et al. (2010b). Ancient DNA analyses exclude humans as the driving force behind Late Pleistocene musk ox (*Ovibos moschatus*) population dynamics. *Proceedings of the National Academy of Sciences* 107(12), 5675–5680.

Cardillo, M., G. M. Mace, K. E. Jones, J. Bielby, O. R. Bininda-Emonds, W. Sechrest, C. D. L. Orme, et al. (2005). Multiple causes of high extinction risk in large mammal species. *Science* 309(5738), 1239–1241.

Carlson, C. J., A. L. Bond, and K. R. Burgio (2018a). Reevaluating sighting models and moving beyond them to test and contextualize the extinction of the thylacine. *Conservation Biology* 32(5), 1198–1199.

Carlson, C. J., K. R. Burgio, T. A. Dallas, and A. L. Bond (2018b). Spatial extinction date estimation: a novel method for reconstructing spatiotemporal patterns of extinction and identifying potential zones of rediscovery. *bioRxiv*, 279679.

Carlson, C. J., K. R. Burgio, E. R. Dougherty, A. J. Phillips, V. M. Bueno, C. F. Clements, G. Castaldo, et al. (2017). Parasite biodiversity faces extinction and redistribution in a changing climate. *Science Advances* 3(9), e1602422.

Carotenuto, F., M. Di Febbraro, M. Melchionna, A. Mondanaro, S. Castiglione, C. Serio, L. Rook, et al. (2018). The well-behaved killer: Late Pleistocene humans in Eurasia were significantly associated with living megafauna only. *Palaeogeography, Palaeoclimatology, Palaeoecology* 500, 24–32.

Carrión, J. S. (1992). Late Quaternary pollen sequence from Carihuela Cave, southern Spain. *Review of Palaeobotany and Palynology* 71(1), 37–77.

Carrión, J. S., S. Fernández, J. M. Jiménez-Arenas, M. Munuera, J. Ochando, G. Amorós, M. Ponce de León, et al. (2019). The sequence at Carihuela Cave and its potential for research into Neanderthal ecology and the Mousterian in southern Spain. *Quaternary Science Reviews* 217, 194–216.

Carrión, J. S., J. A. Riquelme, C. Navarro, and M. Munuera (2001). Pollen in hyaena coprolites reflects late glacial landscape in southern Spain. *Palaeogeography, Palaeoclimatology, Palaeoecology* 176(1–4), 193–205.

Carrión, J., M. Munuera, and C. Navarro (1998). The palaeoenvironment of Carihuela Cave (Granada, Spain): a reconstruction on the basis of palynological investigations of cave sediments. *Review of Palaeobotany and Palynology* 99(3–4), 317–340.

Castania, V. A., J. W. d. S. da Silveira, A. C. Issy, D. L. Pitol, M. L. Castania, A. D. Neto, E. A. Del Bel, et al. (2015). Advantages of a combined method of decalcification compared to EDTA. *Microscopy Research and Technique* 78(2), 111–118.

Castaños, P. (1983). Estudio de los macromamíferos del yacimiento prehistórico de Bolinkoba. *Kobie* 13, 261–298.

Cerdeño, E. (1990). *Stephanorhinus hemitoechus* (falc.) (Rhinocerolidae, Mammalia) del Pleistoceno medio y superior de España. *Estudios Geológicos* 46(5-6), 465–479.

Cersoy, S., A. Zazzo, M. Lebon, J. Rofes, and S. Zirah (2016). Collagen extraction and stable isotope analysis of small vertebrate bones: a comparative approach. *Radiocarbon*, 1–16.

Chang, M. C. and J. Tanaka (2002). FT-IR study for hydroxyapatite/collagen nanocomposite cross-linked by glutaraldehyde. *Biomaterials* 23(24), 4811–4818.

Chappell, J., J. Head, and J. Magee (1996). Beyond the radiocarbon limit in Australian archaeology and Quaternary research. *Antiquity* 70(269), 543–552.

Chatfield, C. (2003). *The Analysis of Time Series : An Introduction, Sixth Edition*. Boca Rotan: Chapman and Hall/CRC.

Chen, F., F. Welker, C.-C. Shen, S. E. Bailey, I. Bergmann, S. Davis, H. Xia, et al. (2019). A Late Middle Pleistocene Denisovan mandible from the Tibetan plateau. *Nature* 569(7756), 409.

Child, A. M. (1995). Towards an understanding of the microbial decomposition of archaeological bone in the burial environment. *Journal of Archaeological Science* 22(2), 165–174.

Clarkson, C., Z. Jacobs, B. Marwick, R. Fullagar, L. Wallis, M. Smith, R. G. Roberts, et al. (2017). Human occupation of northern Australia by 65,000 years ago. *Nature* 547(7663), 306.

Cleland, T. P., E. R. Schroeter, and M. H. Schweitzer (2015). Biologically and diagenetically derived peptide modifications in moa collagens. *Proceedings of the Royal Society B: Biological Sciences* 282(1808), 20150015.

Coleman, M. M., D. J. Skrovanek, J. Hu, and P. C. Painter (1988). Hydrogen bonding in polymer blends. 1. FTIR studies of urethane-ether blends. *Macromolecules* 21(1), 59–65.

Collins, M. J., C. M. Nielsen–Marsh, J. Hiller, C. I. Smith, J. P. Roberts, R. V. Prigodich, T. J. Wess, et al. (2002). The survival of organic matter in bone: a review. *Archaeometry* 44(3), 383–394.

Cooper, A., C. Turney, K. A. Hughen, B. W. Brook, H. G. McDonald, and C. J. A. Bradshaw (2015). Abrupt warming events drove Late Pleistocene Holarctic megafaunal turnover. *Science* 349(6248), 602–606.

Cooper, L., J. Thomas, M. Beamish, A. Gouldwell, S. Collcutt, J. Williams, R. Jacobi, et al. (2012). An early Upper Palaeolithic open-air station and mid-Devensian hyaena den at Grange Farm, Glaston, Rutland, UK. *Proceedings of the Prehistoric Society* 78, 73–93.

Coplen, T. B. (1994). Reporting of stable hydrogen, carbon, and oxygen isotopic abundances (technical report). *Pure and Applied Chemistry* 66(2), 273–276.

Crees, J. J. and S. T. Turvey (2014). Holocene extinction dynamics of *Equus hydruntinus*, a late-surviving European megafaunal mammal. *Quaternary Science Reviews* 91, 16–29.

Crema, E. R., J. Habu, K. Kobayashi, and M. Madella (2016). Summed probability distribution of 14C dates suggests regional divergences in the population dynamics of the Jomon Period in eastern Japan. *PLOS ONE* 11(4), e0154809.

Crezzini, J., P. Boscato, S. Ricci, A. Ronchitelli, V. Spagnolo, and F. Boschin (2016). A spotted hyaena den in the Middle Palaeolithic of Grotta Paglicci (Gargano Promontory, Apulia, southern Italy). *Archaeological and Anthropological Sciences* 8(2), 227–240.

Cueto, M., E. Camarós, P. Castaños, R. Ontañón, and P. Arias (2016). Under the skin of a lion: unique evidence of Upper Paleolithic exploitation and use of cave lion (*Panthera spelaea*) from the Lower Gallery of La Garma (Spain). *PLOS ONE* 11(10), e0163591.

Cupillard, C. and A.-C. Welte (2006). Le Magdalénien de La Grotte «Grappin» à Arlay (Jura, France): nouveaux regards. *L'anthropologie* 110(4), 624–683.

Currant, A. (2004). The Quaternary mammal collections at the Somerset County Museum, Taunton. D. Schreve (Ed.), *The Quaternary Mammals of Southern and Eastern England Field Guide*. London: Quaternary Research Association, p. 101–109.

D'Errico, F. and M. F. Sánchez Goñi (2003). Neandertal extinction and the millennial scale climatic variability of OIS 3. *Quaternary Science Reviews* 22(8–9), 769–788.

D'Elia, M., G. Gianfrate, G. Quarta, L. Giotta, G. Giancane, and L. Calcagnile (2007). Evaluation of possible contamination sources in the 14C analysis of bone samples by FTIR spectroscopy. *Radiocarbon* 49(2), 201–210.

Da Cruz, G. A., S. de Toledo, E. A. Sallum, and A. F. M. de Lima (2007). Morphological and chemical analysis of bone substitutes by scanning electron microscopy and microanalysis by spectroscopy of dispersion energy. *Brazilian Dental Journal* 18(2), 129–133.

Dakos, V. and A. Hastings (2013). Editorial: Special issue on regime shifts and tipping points in ecology. *Theoretical Ecology* 6(3), 253–254.

Dal Sasso, G., M. Lebon, I. Angelini, L. Maritan, D. Usai, and G. Artioli (2016). Bone diagenesis variability among multiple burial phases at Al Khiday (Sudan) investigated by ATR-FTIR spectroscopy. *Palaeogeography, Palaeoclimatology, Palaeoecology* 463, 168–179.

Damos, P. (2016). Using multivariate cross correlations, Granger causality and graphical models to quantify spatiotemporal synchronization and causality between pest populations. *BMC Ecology* 16(33).

Dansgaard, W., S. J. Johnsen, H. B. Clausen, D. Dahl-Jensen, N. S. Gundestrup, C. U. Hammer, C. S. Hvidberg, et al. (1993). Evidence for general instability of past climate from a 250-kyr ice-core record. *Nature* 364(6434), 218.

El-Daoushy, M. F. A. F., I. U. Olsson, and F. H. Oro (1978). The EDTA and HCl methods of pre-treating bones. *Geologiska Föreningen i Stockholm Förhandlingar* 100(2), 213–219.

Daskin, J. H. and R. M. Pringle (2016). Does primary productivity modulate the indirect effects of large herbivores? A global meta-analysis. *Journal of Animal Ecology* 85(4), 857–868.

Davidson, A. D., M. J. Hamilton, A. G. Boyer, J. H. Brown, and G. Ceballos (2009). Multiple ecological pathways to extinction in mammals. *Proceedings of the National Academy of Sciences* 106(26), 10702–10705.

Davies, K. F., C. R. Margules, and J. F. Lawrence (2004). A synergistic effect puts rare, specialized species at greater risk of extinction. *Ecology* 85(1), 265–271.

De la Peña, P. (2013). The transition in southern Iberia: insights from paleoclimatology and the early Upper Palaeolithic. *Proceedings of the National Academy of Sciences* 110(23), E2086–E2086.

De Lafontaine, G., C. A. Amasifuen Guerra, A. Ducousso, M.-F. Sánchez-Goñi, and R. J. Petit (2014). Beyond skepticism: uncovering cryptic refugia using multiple lines of evidence. *New Phytologist* 204(3), 450–454.

De Quirós, F. B., V. C. Valdés, and A. J. Stuart (2006). Nuevas dataciones para el Musteriense y el Magdaleniense de la cueva de El Castillo. V. C. Valdés, F. B. de Quirós, and J. Fernández (Eds.), *En el centenario de la cueva de El Castillo: el ocaso de los neandertales*. España: Universidad Nacional de Educación a Distancia, p. 453–458.

Dee, M. and C. Bronk Ramsey (2000). Refinement of graphite target production at ORAU. *Nuclear Instruments and Methods in Physics Research Section B: Beam Interactions with Materials and Atoms* 172(1), 449–453.

Demnati, I., D. Grossin, O. Marsan, G. Bertrand, G. Collonges, C. Combes, M. Parco, et al. (2014). Comparison of physical-chemical and mechanical properties of chlorapatite and hydroxyapatite plasma sprayed coatings. *Open Biomedical Engineering Journal* 9(1-M3), 42–55.

DeNiro, M. J. and S. Weiner (1988). Chemical, enzymatic and spectroscopic characterization of "collagen" and other organic fractions from prehistoric bones. *Geochimica et Cosmochimica Acta* 52(9), 2197–2206.

Devictor, V., R. Julliard, and F. Jiguet (2008). Distribution of specialist and generalist species along spatial gradients of habitat disturbance and fragmentation. *Oikos* 117(4), 507–514.

Devièse, T. (2009). Elucidating funeral rituals in burials from the end of the Roman Empire: development of a multi-analytical approach. PhD thesis. Paris 6.

Devièse, T., D. Comeskey, J. McCullagh, C. Bronk Ramsey, and T. Higham (2018). New protocol for compound-specific radiocarbon analysis of archaeological bones. *Rapid Communications in Mass Spectrometry* 32(5), 373–379.

Devièse, T., I. Karavanić, D. Comeskey, C. Kubiak, P. Korlević, M. Hajdinjak, S. Radović, et al. (2017). Direct dating of Neanderthal remains from the site of Vindija Cave and implications for the Middle to Upper Paleolithic transition. *Proceedings of the National Academy of Sciences* 114(40), 10606–10611.

Di Febbraro, M., F. Carotenuto, S. Castiglione, D. Russo, A. Loy, L. Maiorano, and P. Raia (2017). Does the jack of all trades fare best? Survival and niche width in Late Pleistocene megafauna. *Journal of Biogeography* 44(12), 2828–2838.

Dickey, D. A. and W. A. Fuller (366a 1979). Distribution of the estimators for autoregressive time series with a unit root. *Journal of the American Statistical Association* 74, 427–431.

Diedrich, C. and K. Zák (2006). Prey deposits and den sites of the Upper Pleistocene hyena *Crocuta crocuta spelaea* (Goldfuss, 1823) in horizontal and vertical caves of the Bohemian Karst (Czech Republic). *Bulletin of Geosciences* 81(4), 237–276.

Diedrich, C. G. (2011). The *Crocuta crocuta spelaea* (Goldfuss, 1823) population and its prey from the Late Pleistocene Teufelskammer Cave hyena den besides the famous Paleolithic Neandertal cave (NRW, NW Germany). *Historical Biology* 23(2-3), 237–270.

— (2012). Typology of Ice Age spotted hyena *Crocuta crocuta spelaea* (Goldfuss, 1823) coprolite aggregate pellets from the European Late Pleistocene and their significance at dens and scavenging sites. *New Mexico Museum of Natural History and Science* 57, 369–377.

— (2013). Late Pleistocene leopards across Europe – Northernmost European German population, highest elevated records in the Swiss Alps, complete skeletons in the Bosnia Herzegowina Dinarids and comparison to the Ice Age cave art. *Quaternary Science Reviews* 76, 167–193.

Dinnis, R., A. Pate, and N. Reynolds (2016). Mid-to-Late Marine Isotope Stage 3 mammal faunas of Britain: a new look. *Proceedings of the Geologists' Association* 127(4), 435–444.

Dobberstein, R. C., M. J. Collins, O. E. Craig, G. Taylor, K. E. H. Penkman, and S. Ritz-Timme (2009). Archaeological collagen: why worry about collagen diagenesis? *Archaeological and Anthropological Sciences* 1(1), 31–42.

Dodge, D. R., A. S. Bouwman, P. B. Pettitt, and T. A. Brown (2012). Mitochondrial DNA haplotypes of Devensian hyaenas from Creswell Crags, England. *Archaeological and Anthropological Sciences* 4(2), 161–166.

Dogandžić, T. and S. P. McPherron (2013). Demography and the demise of Neandertals: a comment on 'Tenfold population increase in Western Europe at the Neandertal-to-modern human transition'. *Journal of Human Evolution* 64(4), 311–313.

Donlan, J. (2005). Re-Wilding North America. *Nature* 436(7053), 913–914.

Doughty, C. E., A. Wolf, and C. B. Field (2010). Biophysical feedbacks between the Pleistocene megafauna extinction and climate: the first human-induced global warming? *Geophysical Research Letters* 37(15), L15703.

Douka, K., S. Grimaldi, G. Boschian, A. del Lucchese, and T. F. G. Higham (2012). A new chronostratigraphic framework for the Upper Palaeolithic of Riparo Mochi (Italy). *Journal of Human Evolution* 62(2), 286–299.

Douka, K., T. F. G. Higham, R. Wood, P. Boscato, P. Gambassini, P. Karkanas, M. Peresani, et al. (2014). On the chronology of the Uluzzian. *Journal of Human Evolution* 68, 1–13.

Douka, K., V. Slon, Z. Jacobs, C. B. Ramsey, M. V. Shunkov, A. P. Derevianko, F. Mafessoni, et al. (2019). Age estimates for hominin fossils and the onset of the Upper Palaeolithic at Denisova Cave. *Nature* 565(7741), 640–644.

Du Preez, B., J. Purdon, P. Trethowan, D. W. Macdonald, and A. J. Loveridge (2017). Dietary niche differentiation facilitates coexistence of two large carnivores. *Journal of Zoology* 302(3), 149–156.

Du Preez, B. D. (2014). The impact of intraguild competition with lion *Panthera leo* on leopard *Panthera pardus* behavioural ecology. PhD thesis. University of Oxford.

Dusseldorp, G. L. (2013). Neanderthals and cave hyenas: co-existence, competition or conflict? J. L. Clark and J. D. Speth (Eds.), *Zooarchaeology and Modern Human Origins*. Vertebrate Paleobiology and Paleoanthropology. Dordrecht: Springer, p. 191–208.

Elias, S. and D. Schreve (2007). Vertebrate Records | Late Pleistocene Megafaunal Extinctions. S. Elias (Ed.), *Encyclopedia of Quaternary Science*. Amsterdam: Elsevier, p. 700–712.

Elith, J., M. Kearney, and S. Phillips (2010). The art of modelling range-shifting species. *Methods in Ecology and Evolution* 1(4), 330–342.

Elster, H., E. Gil-Av, and S. Weiner (1991). Amino acid racemization of fossil bone. *Journal of Archaeological Science* 18(5), 605–617.

Erbajeva, M. A. and N. V. Alexeeva (2000). Pliocene and Pleistocene biostratigraphic succession of Transbaikalia with emphasis on small mammals. *Quaternary International* 68-71, 67–75.

Evin, J., G. Marien, and C. Pachiaud (1971). Lyon Natural Radiocarbon Measurements II. *Radiocarbon* 13(1), 52–73.

Farina, S. (2011). Late Pleistocene mammals from Grotta Cucigliana (Monte Pisano, Italy). *Atti della Società Toscana di Scienze Naturali: Memorie, Serie B* 118, 67–74.

Farre, B., P. Massard, J. Nouet, and Y. Dauphin (2014). Preservation of rodent bones from El Harhoura 2 Cave (Morocco, Neolithic–Middle Palaeolithic): microstructure, mineralogy, crystallinity and composition. *Journal of African Earth Sciences* 92, 1–13.

Fernandes, R. (2013). Challenges, approaches, and opportunities in radiocarbon reservoir effects. PhD thesis. University of Kiel.

Fernandez, P. and J.-L. Guadelli (2008). Étude préliminaire des grands mammifères du repaire d'hyènes de Redaka II (Bulgarie du nord-ouest). *Quaternaire: Revue de l'Association Française pour l'Étude du Quaternaire* 19(1), 43–68.

Fernández, S., N. Fuentes, J. S. Carrión, P. González-Sampériz, E. Montoya, G. Gil, G. Vega-Toscano, et al. (2007). The Holocene and Upper Pleistocene pollen sequence of Carihuela Cave, southern Spain. *Géobios* 40(1), 75–90.

Fiedel, S. (2009). Sudden deaths: the chronology of terminal Pleistocene megafaunal extinction. G. Haynes (Ed.), *American Megafaunal Extinctions at the End of the Pleistocene*. Vertebrate Paleobiology and Paleoanthropology. Dordrecht: Springer, p. 21–37.

Firestone, R. B., A. West, J. P. Kennett, L. Becker, T. E. Bunch, Z. S. Revay, P. H. Schultz, et al. (2007). Evidence for an extraterrestrial impact 12,900 years ago that contributed to the megafaunal extinctions and the Younger Dryas cooling. *Proceedings of the National Academy of Sciences* 104(41), 16016–16021.

Fisher, D. O. and S. P. Blomberg (2010). Correlates of rediscovery and the detectability of extinction in mammals. *Proceedings of the Royal Society B: Biological Sciences* 278(1708), 1090–1097.

Forster, M. A. (2003). Self-organised instability and megafaunal extinctions in Australia. *Oikos* 103(1), 235–239.

Fourcade, Y., J. O. Engler, D. Rödder, and J. Secondi (2014). Mapping species distributions with MAXENT using a geographically biased sample of presence data: a performance assessment of methods for correcting sampling bias. *PLOS ONE* 9(5), e97122.

Fourvel, J.-B., P. Fosse, J.-P. Brugal, E. Cregut-Bonnoure, L. Slimak, and J.-F. Tournepiche (2014). Characterization of bear remains consumption by Pleistocene large carnivores (Felidae, Hyaenidae, Canidae). *Quaternary International* 339–340: *Fossil Remains in Karst and Their Role in Reconstructing Quaternary Paleoclimate and Paleoenvironments*, 232–244.

Fox-Dobbs, K., J. A. Leonard, and P. L. Koch (2008). Pleistocene megafauna from eastern Beringia: paleoecological and paleoenvironmental interpretations of stable carbon and nitrogen isotope and radiocarbon records. *Palaeogeography, Palaeoclimatology, Palaeoecology* 261(1–2), 30–46.

Freedman, J. and J. Evans (2015). Working with the public: how an unusual museum enquiry turned into travels through time and space. *Open Quaternary* 1(1), Art. 8.

French, J. C. (2015). Demography and the Palaeolithic archaeological record. *Journal of Archaeological Method and Theory* 23(1), 150–199.

Fryxell, R., H. T. Irwin, M. Serna, and M. A. Gorbea (1970). Avance a la investigación arqueológica, geocronológica y ecológica de La Cueva de La Carigüela (Piñar, Granada). *Trabajos de Prehistoria* 27(1), 45–60.

Fu, Q., M. Hajdinjak, O. A. Moldovan, S. Constantin, S. Mallick, P. Skoglund, N. Patterson, et al. (2015). An early modern human from Romania with a recent Neanderthal ancestor. *Nature* 524(7564), 216.

Gadaleta, S., E. Paschalis, F. Betts, R. Mendelsohn, and A. Boskey (1996). Fourier transform infrared spectroscopy of the solution-mediated conversion of amorphous calcium phosphate to hydroxyapatite: new correlations between X-ray diffraction and infrared data. *Calcified Tissue International* 58(1), 9–16.

Gambassini, P., ed. (1997). *Il Paleolitico Di Castelcivita: Culture e Ambiente*. Napoli: Electa Napoli.

Gatta, M. and M. Rolfo (2017). Cava Muracci: a new Middle-Upper Palaeolithic site in west-central Italy. *Mediterranean Archaeology & Archaeometry* 17(2), 105–116.

Gatta, M., G. Sinopoli, M. Giardini, B. Giaccio, I. Hajdas, L. Pandolfi, G. Bailey, et al. (2016). Pollen from Late Pleistocene hyena (*Crocuta crocuta spelaea*) coprolites: an interdisciplinary approach from two Italian sites. *Review of Palaeobotany and Palynology: Supplement C* 233, 56–66.

Geraads, D. (1995). Carnívoros Musterienses de La Cueva de Zafarraya (Málaga). *Cuaternario y Geomorfología* 9(3-4), 51–57.

Geraads, D., F. Amani, A. Ben-Ncer, S. P. McPherron, J.-P. Raynal, and J.-J. Hublin (2013). The rodents from the Late Middle Pleistocene hominid-bearing site of J'bel Irhoud, Morocco, and their chronological and paleoenvironmental implications. *Quaternary Research* 80(3), 552–561.

Ghezzo, E., A. Palchetti, and L. Rook (2014). Recovering data from historical collections: stratigraphic and spatial reconstruction of the outstanding carnivoran record from the Late Pleistocene Equi Cave (Apuane Alps, Italy). *Quaternary Science Reviews* 96: *Predators, Prey and Hominins - Celebrating the Scientific Career of Alan Turner (1947-2012)*, 168–179.

Ghezzo, E. and L. Rook (2015). The remarkable *Panthera pardus* (Felidae, Mammalia) record from Equi (Massa, Italy): taphonomy, morphology, and paleoecology. *Quaternary Science Reviews* 110, 131–151.

Giaccio, B., R. Isaia, F. G. Fedele, E. Di Canzio, J. Hoffecker, A. Ronchitelli, A. A. Sinitsyn, et al. (2008). The Campanian Ignimbrite and Codola tephra layers: two temporal/stratigraphic markers for the Early Upper Palaeolithic in southern

Italy and eastern Europe. *Journal of Volcanology and Geothermal Research* 177(1): *Explosive Volcanism in the Central Mediterranean Area during the Late Quaternary - Linking Sources and Distal Archives*, 208–226.

Gianfrate, G., M. D'Elia, G. Quarta, L. Giotta, L. Valli, and L. Calcagnile (2007). Qualitative application based on IR spectroscopy for bone sample quality control in radiocarbon dating. *Nuclear Instruments and Methods in Physics Research Section B: Beam Interactions with Materials and Atoms* 259(1), 316–319.

Gill, J. L. (2014). Ecological impacts of the Late Quaternary megaherbivore extinctions. *New Phytologist* 201(4), 1163–1169.

Gill, J. L., J. W. Williams, S. T. Jackson, K. B. Lininger, and G. S. Robinson (2009). Pleistocene megafaunal collapse, novel plant communities, and enhanced fire regimes in North America. *Science* 326(5956), 1100–1103.

Gillespie, R., R. E. M. Hedges, and J. O. Wand (1984). Radiocarbon dating of bone by accelerator mass spectrometry. *Journal of Archaeological Science* 11(2), 165–170.

Gillespie, R., R. M. Hedges, and M. J. Humm (2A 1986). Routine AMS dating of bone and shell proteins. *Radiocarbon* 28, 451–456.

Goldenberg, L., L. Regev, E. Mintz, and E. Boaretto (2017). Dating reassembled collagen from fossil bones. *Radiocarbon*, 1–10.

Graham, R. W. and E. C. Grimm (1990). Effects of global climate change on the patterns of terrestrial biological communities. *Trends in Ecology & Evolution* 5(9), 289–292.

Graham, R. W. and E. L. Lundelius (1984). Coevolutionary disequilibrium and Pleistocene extinctions. P. S. Martin and R. G. Klein (Eds.), *Quaternary Extinctions: A Prehistoric Revolution*. Tuscson: University of Arizona Press.

Grayson, D. K. (2001). The archaeological record of human impacts on animal populations. *Journal of World Prehistory* 15(1), 1–68.

Grayson, D. K. and F. Delpech (2003). Ungulates and the Middle-to-Upper Paleolithic transition at Grotte XVI (Dordogne, France). *Journal of Archaeological Science* 30(12), 1633–1648.

Grealy, A. C., M. C. McDowell, P. Scofield, D. C. Murray, D. A. Fusco, J. Haile, G. J. Prideaux, et al. (2015). A critical evaluation of how ancient DNA bulk bone metabarcoding complements traditional morphological analysis of fossil assemblages. *Quaternary Science Reviews* 128, 37–47.

Green, R. E., J. Krause, A. W. Briggs, T. Maricic, U. Stenzel, M. Kircher, N. Patterson, et al. (2010). A draft sequence of the Neandertal genome. *Science* 328(5979), 710–722.

GRIP members (1993). Climate Instability during the Last Interglacial Period Recorded in the GRIP Ice Core. *Nature* 364, 203–207.

Guadelli, A., J.-L. Guadelli, P. Fernandez, and N. Sirakov (2013). Preliminary GIS and intra-site spatial analysis of the faunal remains from Redaka II Cave. V. Stamenova and S. Stamenov (Eds.), *Second European SCGIS Conference: Conservation of Natural and Cultural Heritage for Sustainable Development: GIS-Based Approach*. Sofia: Bulgarian Academy of Sciences, p. 54–61.

Guadelli, J.-L. (2011). Project de Recherche Conjoint: Les plus Anciennes Manifestations de La Présence Humaine Dans Les Balkans (MAEE). Rapport de La Mission Préhistorique Française En Bulgarie Du Nord. l'Académie Bulgare des Sciences et Université de Bordeaux.

Guillevic, M., L. Bazin, A. Landais, P. Kindler, A. Orsi, V. Masson-Delmotte, T. Blunier, et al. (2013). Spatial gradients of temperature, accumulation and δ18O-ice in

Greenland over a series of Dansgaard–Oeschger events. *Climate of the Past* 9(3), 1029–1051.

Gurfinkel, D. (1987). Comparative study of the radiocarbon dating of different bone collagen preparations. *Radiocarbon* 29(1), 45–52.

Guthrie, R. (1984). Mosaics, allelochemicals and nutrients: an ecological theory of Late Pleistocene megafaunal extinctions. P. S. Martin and R. G. Klein (Eds.), *Quaternary Extinctions: A Prehistoric Revolution*. Tuscson: University of Arizona Press, p. 259–298.

Hall, Q. and M. C. Cannon (2002). The cell wall hydroxyproline-rich glycoprotein RSH is essential for normal embryo development in arabidopsis. *The Plant Cell* 14(5), 1161–1172.

Han, Y., L. Han, Y. Yao, Y. Li, and X. Liu (2018). Key factors in FTIR spectroscopic analysis of DNA: the sampling technique, pretreatment temperature and sample concentration. *Analytical Methods* 10(21), 2436–2443.

Hanski, I. (1994). A practical model of metapopulation dynamics. *Journal of Animal Ecology* 63(1), 151–162.

— (1998). Metapopulation dynamics. *Nature* 396(6706), 41–49.

— (2015). Habitat fragmentation and species richness. *Journal of Biogeography* 42(5), 989–993.

Hart, J. R. (2011). Ethylenediaminetetraacetic acid and related chelating agents. F. Ullmann and M. Bohnet (Eds.), *Ullmann's Encyclopedia of Industrial Chemistry*. 7th ed. Weinheim: Wiley-VCH.

Hassan, A. A. and P. E. Hare (1978). Amino acid analysis in radiocarbon dating of bone collagen. G. F. Carter (Ed.), *Archaeological Chemistry—II*. Vol. 171. Advances in Chemistry. Washington: American Chemical Society, p. 109–116.

Hawks, J. (2008). From genes to numbers: effective population sizes in human evolution. J.-P. Bocquet-Appel (Ed.), *Recent Advances in Palaeodemography*. Dordrecht: Springer, p. 9–30.

Hayward, M. W. (2006). Prey preferences of the spotted hyaena (*Crocuta crocuta*) and degree of dietary overlap with the lion (*Panthera leo*). *Journal of Zoology* 270(4), 606–614.

Hayward, M. W. and G. I. H. Kerley (2008). Prey preferences and dietary overlap amongst Africa's large predators. *South African Journal of Wildlife Research* 38(2), 93–108.

Head, M., W. Ambrose, and J. Mummery (1987). Categorisation of organic sediments from archaeological sites. *Archaeometry: Further Australian Studies*. 2nd Australian Archaeometry Conference. Canberra: Australian National University, p. 143–159.

Hedges, R. E. M. (2002). Bone diagenesis: an overview of processes. *Archaeometry* 44(3), 319–328.

Hedges, R. E. M., R. A. Housley, I. A. Law, and C. Perry (1988). Radiocarbon dates from the Oxford AMS system: archaeometry datelist 7. *Archaeometry* 30(1), 155–164.

Hedges, R. E. M., I. A. Law, C. R. Bronk, and R. A. Housley (1989). The Oxford accelerator mass spectrometry facility: technical developments in routine dating. *Archaeometry* 31(2), 99–113.

Hedges, R. E. M., P. B. Pettitt, C. B. Ramsey, and G. J. V. Klinken (1996). Radiocarbon dates from the Oxford AMS system: archaeometry datelist 22. *Archaeometry* 38(2), 391–415.

Hedges, R. M. and G. Van Klinken (1992). A review of current approaches in the pretreatment of bone for radiocarbon dating by AMS. *Radiocarbon* 34(3), 279–291.

Heinrich, H. (1988). Origin and consequences of cyclic ice rafting in the northeast Atlantic Ocean during the past 130,000 years. *Quaternary Research* 29(2), 142–152.

Hemming, S. R. (2004). Heinrich events: massive Late Pleistocene detritus layers of the North Atlantic and their global climate imprint. *Reviews of Geophysics* 42(1), RG1005.

Henry-Gambier, D., C. dric Beauval, J. Airvaux, N. Aujoulat, J. Baratin, and J. Buisson-Catil (2007). New hominid remains associated with Gravettian parietal art (Les Garennes, Vilhonneur, France). *Journal of Human Evolution* 53(6), 747–750.

Herridge, V. and A. Lister (2012). Extreme insular dwarfism evolved in a mammoth. *Proceedings of the Royal Society B: Biological Sciences* 279(1741), 3193–3200.

Higham, T. (2011). European Middle and Upper Palaeolithic radiocarbon dates are often older than they look: problems with previous dates and some remedies. *Antiquity* 85(327), 235–249.

Higham, T. F., R. M. Jacobi, and C. B. Ramsey (2006a). AMS radiocarbon dating of ancient bone using ultrafiltration. *Radiocarbon* 48(2), 179–195.

Higham, T., F. Brock, M. Peresani, A. Broglio, R. Wood, and K. Douka (2009). Problems with radiocarbon dating the Middle to Upper Palaeolithic transition in Italy. *Quaternary Science Reviews* 28(13–14), 1257–1267.

Higham, T., R. Jacobi, M. Julien, F. David, L. Basell, R. Wood, W. Davies, et al. (2010). Chronology of the Grotte Du Renne (France) and implications for the context of ornaments and human remains within the Châtelperronian. *Proceedings of the National Academy of Sciences* 107(47), 20234–20239.

Higham, T., T. Compton, C. Stringer, R. Jacobi, B. Shapiro, E. Trinkaus, B. Chandler, et al. (2011). The earliest evidence for anatomically modern humans in northwestern Europe. *Nature* 479(7374), 521.

Higham, T., K. Douka, R. Wood, C. B. Ramsey, F. Brock, L. Basell, M. Camps, et al. (2014). The timing and spatiotemporal patterning of Neanderthal disappearance. *Nature* 512(7514), 306–309.

Higham, T., C. B. Ramsey, I. Karavanić, F. H. Smith, and E. Trinkaus (2006b). Revised direct radiocarbon dating of the Vindija G_1 Upper Paleolithic Neandertals. *Proceedings of the National Academy of Sciences* 103(3), 553–557.

Hijmans, R. J., S. E. Cameron, J. L. Parra, P. G. Jones, and A. Jarvis (2005). Very high resolution interpolated climate surfaces for global land areas. *International Journal of Climatology* 25(15), 1965–1978.

Hijmans, R. J., S. Phillips, J. Leathwick, and J. Elith (2013). *Dismo: Species distribution modeling*. Version 0.9.3. URL: `http://CRAN.R-project.org/package=dismo`.

Ho, T. Y., L. F. Marcus, and R. Berger (1969). Radiocarbon dating of petroleum-impregnated bone from tar pits at Rancho La Brea, California. *Science* 164(3883), 1051–1052.

Ho, T.-Y. (1967). The amino acids of bone and dentine collagens in Pleistocene mammals. *Biochimica et Biophysica Acta* 133(3), 568–573.

Hobbs, N. T. (1996). Modification of ecosystems by ungulates. *Journal of Wildlife Management* 60(4), 695–713.

Hoffecker, J. F. (2005). Innovation and technological knowledge in the Upper Paleolithic of northern Eurasia. *Evolutionary Anthropology: Issues, News, and Reviews* 14(5), 186–198.

Hofreiter, M., S. Münzel, N. J. Conard, J. Pollack, M. Slatkin, G. Weiss, and S. Pääbo (2007). Sudden replacement of cave bear mitochondrial DNA in the Late Pleistocene. *Current Biology* 17(4), R122–R123.

Hofreiter, M. and J. Stewart (2009). Ecological change, range fluctuations and population dynamics during the Pleistocene. *Current Biology* 19(14), R584–R594.

Holt, B. M. and V. Formicola (2008). Hunters of the Ice Age: the biology of Upper Paleolithic people. *AmeriCan Journal of Physical Anthropology* 137(S47), 70–99.

Höner, O. P., B. Wachter, M. L. East, and H. Hofer (2002). The response of spotted hyaenas to long-term changes in prey populations: functional response and interspecific kleptoparasitism. *Journal of Animal Ecology* 71(2), 236–246.

Hu, J., X. Li, J. Gao, and Q. Zhao (2009). Ageing behavior of acrylic polyurethane varnish coating in artificial weathering environments. *Progress in Organic Coatings* 65(4), 504–509.

Hublin, J. J. (2009). The origin of Neandertals. *National Academy of Sciences* 106(38), 16022–16027.

Huntley, B., M. J. Alfano, J. R. M. Allen, D. Pollard, P. C. Tzedakis, J.-L. de Beaulieu, E. Grüger, et al. (2003). European vegetation during Marine Oxygen Isotope Stage 3. *Quaternary Research* 59(2), 195–212.

Huntley, B., J. R. M. Allen, Y. C. Collingham, T. Hickler, A. M. Lister, J. Singarayer, A. J. Stuart, et al. (2013). Millennial climatic fluctuations are key to the structure of last glacial ecosystems. *PLOS ONE* 8(4), e61963.

Imaizumi, K., K. Taniguchi, and Y. Ogawa (2013). An evaluation of the effect of microwave irradiation on bone decalcification aimed to DNA extraction. *Legal Medicine* 15(5), 272–277.

Ivanova, S., M. Gurova, N. Spassov, L. Hristova, N. Tzankov, V. Popov, E. Marinova, et al. (2016). Magura Cave, Bulgaria: a multidisciplinary study of Late Pleistocene human palaeoenvironment in the Balkans. *Quaternary International* 415: *Climate Change in the Balkan-Carpathian Region during Late Pleistocene and Holocene*, 86–108.

Jacobi, R. M., T. F. G. Higham, and C. B. Ramsey (2006). AMS radiocarbon dating of Middle and Upper Palaeolithic bone in the British Isles: improved reliability using ultrafiltration. *Journal of Quaternary Science* 21(5), 557–573.

Jacobi, R. (2007). The Stone Age Archaeology of Church Hole, Creswell Crags, Nottinghamshire. P. Pettitt, P. Bahn, and S. Ripoll (Eds.), *Palaeolithic Cave Art at Creswell Crags in European Context*. Oxford: Oxford University Press, p. 75–111.

Jacobi, R. and T. Higham (2008). The "Red Lady" ages gracefully: new ultrafiltration AMS determinations from Paviland. *Journal of Human Evolution* 55(5), 898–907.

Jacobi, R. and T. Higham (2011). The British earlier Upper Palaeolithic: settlement and chronology. N. Ashton, S. G. Lewis, and C. Stringer (Eds.), *The Ancient Human Occupation of Britain*. Vol. 14. Developments in Quaternary Sciences. Amsterdam: Elsevier, p. 181–222.

Jdeidi, T., M. Masseti, I. Nader, K. de Smet, and F. Cuzin (2010). *Canis lupus. The IUCN Red List of Threatened Species 2010*, e.T3746A119623865, http://www.iucnredlist.org/details/3746/3.

Jennings, R., C. Finlayson, D. Fa, and G. Finlayson (2011). Southern Iberia as a refuge for the last Neanderthal populations. *Journal of Biogeography* 38(10), 1873–1885.

Jones, F., P. Jones, M. I. Ogden, W. R. Richmond, A. L. Rohl, and M. Saunders (2007). The interaction of EDTA with barium sulfate. *Journal of Colloid and Interface Science* 316(2), 553–561.

Joschek, S., B. Nies, R. Krotz, and A. Göpferich (2000). Chemical and physicochemical characterization of porous hydroxyapatite ceramics made of natural bone. *Biomaterials* 21(16), 1645–1658.

Kahlke, R.-D. (2014). The origin of Eurasian mammoth faunas (*Mammuthus-Coelodonta* faunal complex). *Quaternary Science Reviews* 96: *Predators, Prey and Hominins - Celebrating the Scientific Career of Alan Turner (1947-2012)*, 32–49.

Kalmykov, N. P., D. V. Kobylkin, M. A. Grigoryeva, and V. N. Chernykh (2014). Validity of the spiral-horned antelope species of the genus *Spirocerus* (Mammalia, Artiodactyla) in Central Asia. *Doklady Biological Sciences* 457(1), 233–235.

Kamińska, A. and A. Sionkowska (1996). Effect of UV radiation on the infrared spectra of collagen. *Polymer Degradation and Stability* 51(1), 19–26.

Kaminská, L., J. Kozłowski, and P. Škrdla (2011). New approach to the Szeletian - chronology and cultural variability. *Eurasian Prehistory* 8(1-2), 29–49.

Kannan, S., J. H. G. Rocha, and J. M. F. Ferreira (2006). Synthesis of hydroxy-chlorapatites solid solutions. *Materials Letters* 60(7), 864–868.

Karanth, K. U. and R. Chellam (2009). Carnivore conservation at the crossroads. *Oryx* 43(1), 1–2.

Kemp, B. M., C. Monroe, K. G. Judd, E. Reams, and C. Grier (2014). Evaluation of methods that subdue the effects of polymerase chain reaction inhibitors in the study of ancient and degraded DNA. *Journal of Archaeological Science* 42, 373–380.

Khwaileh, A., A. Al-Shorman, W. Al Sekhaneh, and J. Rose (2018). FTIR analysis of human bone biostructure from Middle Bronze Age and the Byzantine period in northern Jordan. *Revista Romana de Materiale* 48(3), 377–380.

Kiviranta, I., M. Tammi, R. Lappalainen, T. Kuusela, and H. J. Helminen (1980). The rate of calcium extraction during EDTA decalcification from thin bone slices as assessed with atomic absorption spectrophotometry. *Histochemistry* 68(2), 119–127.

Klinken, G. J. V. and W. G. Mook (1990). Preparative high-performance liquid chromatographic separation of individual amino acids derived from fossil bone collagen. *Radiocarbon* 32(2), 155–164.

Koch, P. L. and A. D. Barnosky (2006). Late Quaternary extinctions: state of the debate. *Annual Review of Ecology, Evolution, and Systematics* 37, 215–250.

Korlević, P., S. Talamo, and M. Meyer (2018). A combined method for DNA analysis and radiocarbon dating from a single sample. *Scientific Reports* 8(1), 4127.

Kosintsev, P. A., V. V. Gasilin, D. O. Gimranov, and O. P. Bachura (2016). Carnivores (Mammalia, Carnivora) of the Urals in the Late Pleistocene and Holocene. *Quaternary International* 420: *The Quaternary of the Urals: Global Trends and Pan-European Quaternary Records*, 145–155.

Kosintsev, P., K. J. Mitchell, T. Devièse, J. van der Plicht, M. Kuitems, E. Petrova, A. Tikhonov, et al. (2019). Evolution and extinction of the giant rhinoceros *Elasmotherium sibiricum* sheds light on Late Quaternary megafaunal extinctions. *Nature Ecology & Evolution* 3(1), 31–38.

Krajcarz, M., M. Pacher, M. Krajcarz, L. Laughlan, G. Rabeder, M. Sabol, P. Wojtal, et al. (2016). Isotopic variability of cave bears (δ15N, δ13C) across Europe during MIS 3. *Quaternary Science Reviews* 131, 51–72.

Krasinski, K. E. and G. Haynes (2010). The eastern Beringian chronology of Quaternary extinctions: a methodological approach to radiocarbon evaluation. *Alaska Journal of Anthropology* 8(1), 39–60.

Kwiatkowski, D., P. C. Phillips, P. Schmidt, and Y. Shin (1992). Testing the null hypothesis of stationarity against the alternative of a unit root: how sure are we that economic time series have a unit root? *Journal of Econometrics* 54(1-3), 159–178.

Labs-Hochstein, J. and B. J. MacFadden (2006). Quantification of diagenesis in Cenozoic sharks: elemental and mineralogical changes. *Geochimica et Cosmochimica Acta* 70(19), 4921–4932.

Lanigan, K. C. and K. Pidsosny (2007). Reflectance FTIR spectroscopic analysis of metal complexation to EDTA and EDDS. *Vibrational Spectroscopy* 45(1), 2–9.

Larkin, P. (2011). IR and Raman spectra—structure correlations: characteristic group frequencies. *Infrared and Raman Spectroscopy*. Oxford: Elsevier, p. 73–115.

Law, I. A. and R. M. Hedges (1989). A semi-automated bone pretreatment system and the pretreatment of older and contaminated samples. *Radiocarbon* 31(3), 247–253.

Lawton, J. H., P. N. M. Brotherton, V. K. Brown, C. Elphick, A. H. Fitter, J. Forshaw, R. W. Haddow, et al. (2010). *Making Space for Nature: A Review of England's Wildlife Sites and Ecological Network*. Report to UK government (Department for Environment, Food and Rural Affairs).

Lebon, M., I. Reiche, J. J. Bahain, C. Chadefaux, A. M. Moigne, F. Fröhlich, F. Sémah, et al. (2010). New parameters for the characterization of diagenetic alterations and heat-induced changes of fossil bone mineral using Fourier transform infrared spectrometry. *Journal of Archaeological Science* 37(9), 2265–2276.

Lebon, M., I. Reiche, F. Fröhlich, J.-J. Bahain, and C. Falguères (2008). Characterization of archaeological burnt bones: contribution of a new analytical protocol based on derivative FTIR spectroscopy and curve fitting of the N1ν3 PO_4 Domain. *Analytical and Bioanalytical Chemistry* 392(7), 1479–1488.

Lebon, M., I. Reiche, X. Gallet, L. Bellot-Gurlet, and A. Zazzo (2016). Rapid quantification of bone collagen content by ATR-FTIR spectroscopy. *Radiocarbon* 58(1), 131–145.

Leonard, J. A., C. Vilà, K. Fox-Dobbs, P. L. Koch, R. K. Wayne, and B. Van Valkenburgh (2007). Megafaunal extinctions and the disappearance of a specialized wolf ecomorph. *Current Biology* 17(13), 1146–1150.

Leung, Y., M. A. Walters, and R. Z. LeGeros (1990). Second derivative infrared spectra of hydroxyapatite. *Spectrochimica Acta Part A: Molecular Spectroscopy* 46(10), 1453–1459.

Lichtenfeld, L. L., C. Trout, and E. L. Kisimir (2015). Evidence-based conservation: predator-proof bomas protect livestock and lions. *Biodiversity and Conservation* 24(3), 483–491.

Lima-Ribeiro, M. S. and J. A. F. Diniz-Filho (2017). Climate change, human overkill, and the extinction of megafauna: a macroecological approach based on pattern-oriented modelling. *Evolutionary Ecology Research* 18(1), 97–121.

Lima-Ribeiro, M. S., D. Nogués-Bravo, K. A. Marske, F. A. S. Fernandez, B. Araujo, and J. A. F. Diniz-Filho (2012). Human arrival scenarios have a strong influence on interpretations of the Late Quaternary extinctions. *Proceedings of the National Academy of Sciences* 109(37), E2409–E2410.

Lister, A. M. and A. V. Sher (2015). Evolution and dispersal of mammoths across the Northern Hemisphere. *Science* 350(6262), 805–809.

Lister, A. M. and A. J. Stuart (2008). The impact of climate change on large mammal distribution and extinction: evidence from the last glacial/interglacial transition. *Comptes Rendus Geoscience* 340(9–10): *Ecosystèmes et Événements Climatiques extrêmes (Ecosystems and Extreme Climatic Events)*, 615–620.

— (2013). Extinction chronology of the woolly rhinoceros *Coelodonta antiquitatis*: reply to Kuzmin. *Quaternary Science Reviews* 62, 144–146.

— (2019). The extinction of the giant deer *Megaloceros giganteus* (Blumenbach): New radiocarbon evidence. *Quaternary International* 500, 185–203.

Litton, C. D. and C. E. Buck (1995). The Bayesian approach to the interpretation of archaeological data. *Archaeometry* 37(1), 1–24.

Lloret, P. Á., A. B. R. Navarro, and C. Romanek (2006). Quantitative analysis of bone mineral using FTIR. *Macla: Revista de la Sociedad Española de Mineralogía* (6), 45–47.

Löe, J. and E. Röskaft (2004). Large carnivores and human safety: a review. *AMBIO: A Journal of the Human Environment* 33(6), 283–288.

Longin, R. (1971). New method of collagen extraction for radiocarbon dating. *Nature* 230(5291), 241–242.

Lopes, C. d. C. A., P. H. J. O. Limirio, V. R. Novais, and P. Dechichi (2018). Fourier transform infrared spectroscopy (FTIR) application chemical characterization of enamel, dentin and bone. *Applied Spectroscopy Reviews* 53(9), 747–769.

Lorenzen, E. D., D. Nogués-Bravo, L. Orlando, J. Weinstock, J. Binladen, K. A. Marske, A. Ugan, et al. (2011). Species-specific responses of late Quaternary megafauna to climate and humans. *Nature* 479(7373), 359–364.

Lovis, W. A., R. Whallon, and R. E. Donahue (2006). Social and spatial dimensions of Mesolithic mobility. *Journal of Anthropological Archaeology* 25(2), 271–274.

Lundelius, E. L. (1989). The implications of disharmonious assemblages for Pleistocene extinctions. *Journal of Archaeological Science* 16(4), 407–417.

Lütkepohl, H. (2007). *New Introduction to Multiple Time Series Analysis*. 2nd edition. Berlin: Springer.

Mackiewicz, P., M. Baca, D. Popović, P. Socha, K. Stefaniak, A. Marciszak, and A. Nadachowski (2017). Estimating the extinction time of two cave bears, *Ursus spelaeus* and *U. ingressus*. *Acta Zoologica Cracoviensia* 60(2), 1–14.

Maclean, I. M. D. and R. J. Wilson (2011). Recent ecological responses to climate change support predictions of high extinction risk. *Proceedings of the National Academy of Sciences* 108(30), 12337–12342.

MacPhee, R. D. E. and A. D. Greenwood (2007). Continuity and change in the extinction dynamics of late Quaternary muskox (*Ovibos*): genetic and radiometric evidence. *Bulletin of Carnegie Museum of Natural History* 39, 203–212.

MacPhee, R. D., A. N. Tikhonov, D. Mol, C. De Marliave, H. Van Der Plicht, A. D. Greenwood, C. Flemming, et al. (2002). Radiocarbon chronologies and extinction dynamics of the late Quaternary mammalian megafauna of the Taimyr Peninsula, Russian Federation. *Journal of Archaeological Science* 29(9), 1017–1042.

MacPhee, R. D., A. N. Tikhonov, D. Mol, and A. D. Greenwood (2005). Late Quaternary loss of genetic diversity in muskox (*Ovibos*). *BMC Evolutionary Biology* 5(1), 49.

Madden, V. J. and M. M. Henson (1997). Rapid decalcification of temporal bones with preservation of ultrastructure. *Hearing Research* 111(1–2), 76–84.

Malhi, Y., C. E. Doughty, M. Galetti, F. A. Smith, J.-C. Svenning, and J. W. Terborgh (2016). Megafauna and ecosystem function from the Pleistocene to the Anthropocene. *Proceedings of the National Academy of Sciences* 113(4), 838–846.

Mangano, G. (2011). An exclusively hyena-collected bone assemblage in the Late Pleistocene of Sicily: taphonomy and stratigraphic context of the large mammal remains from San Teodoro Cave (North-Eastern Sicily, Italy). *Journal of Archaeological Science* 38(12), 3584–3595.

Mann, D. H., P. Groves, R. E. Reanier, B. V. Gaglioti, M. L. Kunz, and B. Shapiro (2015). Life and extinction of megafauna in the Ice-Age Arctic. *Proceedings of the National Academy of Sciences* 112(46), 14301–14306.

Markova, A., A. Puzachenko, T. van Kolfschoten, P. Kosintsev, T. Kuznetsova, A. Tikhonov, O. Bachura, et al. (2015). Changes in the Eurasian distribution of the musk ox (*Ovibos moschatus*) and the extinct bison (*Bison priscus*) during the Last 50 Ka BP. *Quaternary International* 378, 99–110.

Marlowe, F. W. (2004). Dictators and ultimatums in an egalitarian society of hunter-gatherers: The Hadza of Tanzania. J. P. Henrich, R. Boyd, S. Bowles, E. Fehr, C. Camerer, and H. Gintis (Eds.), *Foundations of Human Sociality: Economic Experiments and Ethnographic Evidence From Fifteen Small-Scale Societies*. New York: Oxford University Press, p. 168–193.

Marom-Rotem, A., R. E. M. Hedges, and J. S. O. McCullagh (2012). Development and application of an analytical method for radiocarbon dating bones using the amino acid hydroxyproline. PhD thesis. Oxford.

Marom, A., J. S. McCullagh, T. F. Higham, and R. E. Hedges (2013). Hydroxyproline dating: experiments on the 14C analysis of contaminated and low-collagen bones. *Radiocarbon* 55(2–3), 698–708.

Marom, A., J. S. McCullagh, T. F. Higham, A. A. Sinitsyn, and R. E. Hedges (2012). Single amino acid radiocarbon dating of Upper Paleolithic modern humans. *Proceedings of the National Academy of Sciences* 109(18), 6878–6881.

Marsolier-Kergoat, M.-C., P. Palacio, V. Berthonaud, F. Maksud, T. Stafford, R. Bégouën, and J.-M. Elalouf (2015). Hunting the extinct steppe bison *(Bison priscus*) mitochondrial genome in the Trois-Frères Paleolithic painted cave. *PLOS ONE* 10(6), e0128267.

Martin, P. S. (1984). Prehistoric overkill: the global model. P. S. Martin and R. G. Klein (Eds.), *Quaternary Extinctions: A Prehistoric Revolution*. Tuscson: University of Arizona Press, p. 354–403.

Martínez-Meyer, E., A. Townsend Peterson, and W. W. Hargrove (2004). Ecological niches as stable distributional constraints on mammal species, with implications for Pleistocene extinctions and climate change projections for biodiversity. *Global Ecology and Biogeography* 13(4), 305–314.

Mason, H. E., F. M. McCubbin, A. Smirnov, and B. L. Phillips (2009). Solid-State NMR and IR Spectroscopic Investigation of the Role of Structural Water and F in Carbonate-Rich Fluorapatite. *American Mineralogist* 94(4), 507–516.

Masseti, M. (2001). Did endemic dwarf elephants survive on Mediterranean islands up to protohistorical times? G. Cavarretta, P. Gioia, M. Mussi, and M. Palombo (Eds.), *The World of Elephants: Proceedings of the 1st International Congress*. Rome: Consiglio Nazionale delle Ricerche, p. 16–20.

Masters, P. M. (1987). Preferential preservation of noncollagenous protein during bone diagenesis: implications for chronometric and stable isotopic measurements. *Geochimica et Cosmochimica Acta* 51(12), 3209–3214.

May, R. M., J. H. Lawton, and N. E. Stork (1995). Assessing extinction rates. J. H. Lawton and R. M. May (Eds.), *Extinction Rates*. New York: Oxford University Press, p. 1–24.

McCullagh, J. O., A. Marom, and R. M. Hedges (2010). Radiocarbon dating of individual amino acids from archaeological bone collagen. *Radiocarbon* 52(2), 620–634.

McCullagh, P. (1983). *Generalized Linear Models*. In collab. with J. A. Nelder. Monographs on Statistics and Applied Probability. London: Chapman and Hall.

McFarlane, D. A. and J. Lundberg (2013). On the occurrence of the scimitar-toothed cat, *Homotherium latidens* (Carnivora; Felidae), at Kents Cavern, England. *Journal of Archaeological Science* 40(4), 1629–1635.

McInnes, L. (2006). *Heinrich events against temperature proxy data*. Figure, GNU license. Viewed Sept 2015. https://commons.wikimedia.org/wiki/File:Heinrich-events.png.

McLellan, B. N., C. Servheen, D. Huber, and S. Michael (2017). *Ursus arctos. The IUCN Red List of Threatened Species 2017*, e.T41688A121229971, https://www.iucnredlist.org/species/41688/121229971.

McLeod, A. I. and Y. Zhang (2006). Partial autocorrelation parameterization for subset autoregression. *Journal of Time Series Analysis* 27(4), 599–612.

McLeod, A., Y. Zhang, and C. Xu (2013). *Package 'FitAR'*. Version 1.94. URL: https://CRAN.R-project.org/package=FitAR.

Mead, J. I., L. D. Agenbroad, N. J. Czaplewski, and L. D. Agenbroad (2007). Late Pleistocene of Northern Asia. *Radiocarbon* 34, 1–19.

Mecozzi, B. and S. B. Lucenti (2018). The Late Pleistocene *Canis lupus* (Canidae, Mammalia) from Avetrana (Apulia, Italy): reappraisal and new insights on the European glacial wolves. *Italian Journal of Geosciences* 137(1), 138–150.

Mellars, P. and J. C. French (2011). Tenfold population increase in western Europe at the Neandertal–to–modern human transition. *Science* 333(6042), 623–627.

Merow, C., M. J. Smith, and J. A. Silander (2013). A practical guide to MaxEnt for modeling species' distributions: what it does, and why inputs and settings matter. *Ecography* 36(10), 1058–1069.

Mitchell, F. J. (2005). How open were European primeval forests? Hypothesis testing using palaeoecological data. *Journal of Ecology* 93(1), 168–177.

Monjeau, J., B. Araujo, G. Abramson, M. Kuperman, M. Laguna, and J. Lanata (2017). The controversy space on Quaternary megafaunal extinctions. *Quaternary International* 431: *Pleistocene human dispersals: Climate, ecology and social behavior*, 194–204.

Morales, N. S., I. C. Fernández, and V. Baca-González (2017). MaxEnt's parameter configuration and small samples: are we paying attention to recommendations? A systematic review. *PeerJ* 5, e3093.

Moreno-Amat, E., R. G. Mateo, D. Nieto-Lugilde, N. Morueta-Holme, J.-C. Svenning, and I. García-Amorena (2015). Impact of model complexity on cross-temporal transferability in Maxent species distribution models: an assessment using paleobotanical data. *Ecological Modelling* 312, 308–317.

Moroni, A., G. Boschian, J. Crezzini, G. Montanari-Canini, G. Marciani, G. Capecchi, S. Arrighi, et al. (2018). Late Neandertals in central Italy. High-resolution chronicles

from Grotta Dei Santi (Monte Argentario - Tuscany). *Quaternary Science Reviews* 217, 130–151.

Mudelsee, M. (2013). *Climate Time Series Analysis*. Vol. 51. Atmospheric and Oceanographic Sciences Library. Cham: Springer.

Müller, U. C., J. Pross, P. C. Tzedakis, C. Gamble, U. Kotthoff, G. Schmiedl, S. Wulf, et al. (2011). The role of climate in the spread of modern humans into Europe. *Quaternary Science Reviews* 30(3), 273–279.

Muscarella, R., P. J. Galante, M. Soley-Guardia, R. A. Boria, J. M. Kass, and M. U. a. R. P. Anderson (2018). *ENMeval: Automated runs and evaluations of ecological niche models*. Version 0.3.0. URL: https://CRAN.R-project.org/package=ENMeval (visited on 01/28/2019).

Muscarella, R., P. J. Galante, M. Soley-Guardia, R. A. Boria, J. M. Kass, M. Uriarte, and R. P. Anderson (2014). ENMeval: An R package for conducting spatially independent evaluations and estimating optimal model complexity for Maxent ecological niche models. *Methods in Ecology and Evolution* 5(11), 1198–1205.

Mussi, M. and P. Villa (2008). Single carcass of *Mammuthus primigenius* with lithic artifacts in the Upper Pleistocene of northern Italy. *Journal of Archaeological Science* 35(9), 2606–2613.

Nadachowski, A., G. Lipecki, U. Ratajczak, K. Stefaniak, and P. Wojtal (2016). Dispersal events of the saiga antelope (*Saiga tatarica*) in central Europe in response to the climatic fluctuations in MIS 2 and the early part of MIS 1. *Quaternary International* 420: *The Quaternary of the Urals: Global Trends and Pan-European Quaternary Records*, 357–362.

Nagaoka, L., T. Rick, and S. Wolverton (2018). the overkill model and its impact on environmental research. *Ecology and Evolution* 8(19), 9683–9696.

Nalawade-Chavan, S., J. McCullagh, and R. Hedges (2014a). New hydroxyproline radiocarbon dates from Sungir, Russia, confirm early Mid Upper Palaeolithic burials in Eurasia. *PLOS ONE* 9(1), e76896.

Nalawade-Chavan, S., G. Zazula, F. Brock, J. Southon, R. MacPhee, and P. Druckenmiller (2014b). New single amino acid hydroxyproline radiocarbon dates for two problematic American mastodon fossils from Alaska. *Quaternary Geochronology* 20, 23–28.

Narola, B., A. Singh, M. Mitra, P. Santhakumar, and T. Chandrashekhar (2011). A validated reverse phase HPLC method for the determination of disodium EDTA in Meropenem drug substance with UV-detection using precolumn derivatization technique. *Analytical Chemistry Insights* 6, 7–14.

NASA (2009). *Topography (Visible Earth Project)*. URL: https://visibleearth.nasa.gov/view.php?id=73934 (visited on 02/19/2019).

Nebout, N. C., J. L. Turon, R. Zahn, L. Capotondi, L. Londeix, and K. Pahnke (2002). Enhanced aridity and atmospheric high-pressure stability over the western Mediterranean during the North Atlantic cold events of the past 50 k.y. *Geology* 30(10), 863–866.

Nehlich, O. and M. P. Richards (2009). Establishing collagen quality criteria for sulphur isotope analysis of archaeological bone collagen. *Archaeological and Anthropological Sciences* 1(1), 59–75.

Nelson, D. E. (1991). A new method for carbon isotopic analysis of protein. *Science* 251(4993), 552–4.

NGRIP members (2004). Heinrich events: massive Late Pleistocene detritus layers of the North Atlantic and their global climate imprint. *Nature* 431, 147–151.

Nigst, P. R., P. Haesaerts, F. Damblon, C. Frank-Fellner, C. Mallol, B. Viola, M. Götzinger, et al. (2014). Early modern human settlement of Europe north of the Alps occurred 43,500 years ago in a cold steppe-type environment. *Proceedings of the National Academy of Sciences* 111(40), 14394–14399.

Nogués-Bravo, D., R. Ohlemüller, P. Batra, and M. B. Araújo (2010). Climate predictors of late Quaternary extinctions. *Evolution* 64(8), 2442–2449.

O'Connell, T. C. and R. E. M. Hedges (2001). Isolation and isotopic analysis of individual amino acids from archaeological bone collagen: a new method using RP-HPLC. *Archaeometry* 43(3), 421–438.

Ochoa-Lugo, M., J. Cervini-Silva, M. de Lourdes Muñoz, E. Palacios, G. Pérez-Ramirez, E. Ramos-Cruz, A. Montoya, et al. (2017). The effect of depositional conditions on mineral transformation, chemical composition, and preservation of organic material in archaeological Hg-enriched bone remains. *Journal of Archaeological Science: Reports* 15, 213–218.

Olsson, I. U. (2000). Further tests of the EDTA treatment of bones. *Radiocarbon* 42(1), 49–52.

Olsson, I. U., M. F. A. F. El-Daoushy, A. I. Abdel-Mageed, and M. Klasson (1974). A comparison of different methods for pretreatment of bones. *Geologiska Föreningen i Stockholm Förhandlingar* 96(2), 171–181.

Ooi, C. Y., M. Hamdi, and S. Ramesh (2007). Properties of hydroxyapatite produced by annealing of bovine bone. *Ceramics International* 33(7), 1171–1177.

Owen-Smith, N. (1987). Pleistocene extinctions: the pivotal role of megaherbivores. *Paleobiology* 13(3), 351–362.

Pacher, M. and A. J. Stuart (2009). Extinction chronology and palaeobiology of the cave bear (*Ursus spelaeus*). *Boreas* 38(2), 189–206.

Palkopoulou, E., L. Dalén, A. M. Lister, S. Vartanyan, M. Sablin, A. Sher, V. N. Edmark, et al. (2013). Holarctic genetic structure and range dynamics in the woolly mammoth. *Proceedings of the Royal Society B: Biological Sciences* 280(1770), 20131910.

Pan, Y. and M. E. Fleet (2002). Compositions of the apatite-group minerals: substitution mechanisms and controlling factors. *Reviews in Mineralogy and Geochemistry* 48(1), 13–49.

Pandolfi, L. and A. Tagliacozzo (2015). *Stephanorhinus hemitoechus* (Mammalia, Rhinocerotidae) from the Late Pleistocene of Valle Radice (Sora, Central Italy) and re-evaluation of the morphometric variability of the species in Europe. *Geobios* 48(2), 169–191.

Pardini, O. R. and J. I. Amalvy (2008). FTIR, 1H-NMR spectra, and thermal characterization of water-based polyurethane/acrylic hybrids. *Journal of Applied Polymer Science* 107(2), 1207–1214.

Paschalis, E. P., F. Betts, E. DiCarlo, R. Mendelsohn, and A. L. Boskey (1997). FTIR microspectroscopic analysis of normal human cortical and trabecular bone. *Calcified Tissue International* 61(6), 480–486.

Paschalis, E. P., R. Mendelsohn, and A. L. Boskey (2011). Infrared assessment of bone quality: a review. *Clinical Orthopaedics and Related Research* 469(8), 2170–2178.

Péan, S., S. Puaud, L. Crépin, S. Prat, A. Quiles, J. van der Plicht, H. Valladas, et al. (2013). The Middle to Upper Paleolithic sequence of Buran-Kaya III (Crimea,

Ukraine): New stratigraphic, paleoenvironmental, and chronological results. *Radiocarbon* 55(3), 1454–1469.

Pearson, R. G., C. J. Raxworthy, M. Nakamura, and A. T. Peterson (2007). Predicting species distributions from small numbers of occurrence records: a test case using cryptic geckos in Madagascar. *Journal of Biogeography* 34(1), 102–117.

Peigné, S., C. Goillot, M. Germonpré, C. Blondel, O. Bignon, and G. Merceron (2009). Predormancy omnivory in European cave bears evidenced by a dental microwear analysis of *Ursus spelaeus* from Goyet, Belgium. *Proceedings of the National Academy of Sciences* 106(36), 15390–15393.

Pérez-Heredia, M., C. M. Ferrer-Luque, M. P. González-Rodríguez, F. J. Martín-Peinado, and S. González-López (2008). Decalcifying effect of 15% EDTA, 15% citric acid, 5% phosphoric acid and 2.5% sodium hypochlorite on root canal dentine. *International Endodontic Journal* 41(5), 418–423.

Perrin, F. X., M. Irigoyen, E. Aragon, and J. L. Vernet (2000). Artificial aging of acrylurethane and alkyd paints: a micro-ATR spectroscopic study. *Polymer Degradation and Stability* 70, 469–475.

Pestle, W. J. (2010). Chemical, elemental, and isotopic effects of acid concentration and treatment duration on ancient bone collagen: an exploratory study. *Journal of Archaeological Science* 37(12), 3124–3128.

Pestle, W. J. and M. Colvard (2012). Bone collagen preservation in the tropics: a case study from ancient Puerto Rico. *Journal of Archaeological Science* 39(7), 2079–2090.

Pettitt, P., R. Housley, and T. Higham (2012). Last glaciation faunas: the radiocarbon determinations. S. Aldhouse-Green, R. Peterson, and K. Walker (Eds.), *Neanderthals in Wales: Pontnewydd and the Elwy Valley Caves*. Cardiff: Oxbow, p. 301–319.

Pettitt, P. and J. Zilhão (2015). Problematizing Bayesian approaches to prehistoric chronologies. *World Archaeology* 47(4), 525–542.

Phillips, S. (2017). *Maxnet: Fitting 'Maxent' species distribution models with 'Glmnet'*. Version 0.1.2. URL: `https://CRAN.R-project.org/package=maxnet` (visited on 01/28/2019).

Phillips, S. J., R. P. Anderson, M. Dudík, R. E. Schapire, and M. E. Blair (2017). Opening the black box: an open-source release of Maxent. *Ecography* 40(7), 887–893.

Phillips, S. J. and M. Dudík (2008). Modeling of species distributions with Maxent: new extensions and a comprehensive evaluation. *Ecography* 31(2), 161–175.

Pimm, S. L., C. N. Jenkins, R. Abell, T. M. Brooks, J. L. Gittleman, L. N. Joppa, P. H. Raven, et al. (2014). The biodiversity of species and their rates of extinction, distribution, and protection. *Science* 344(6187), 1246752.

Pinhasi, R., D. Fernandes, K. Sirak, M. Novak, S. Connell, S. Alpaslan-Roodenberg, F. Gerritsen, et al. (2015). Optimal ancient DNA yields from the inner ear part of the human petrous bone. *PLOS ONE* 10(6), e0129102.

Pinto Llona, A. (2007). El yacimiento arqueopaleontológico de Jou'l Llobu (Onís, Asturias). *Excavaciones Arqueológicas En Asturias 1999-02*. Consejería de Cultura, Comunicación Social y Turismo, p. 87–90.

Pirson, S., D. Flas, G. Abrams, D. Bonjean, M. Court-Picon, K. Di Modica, C. Draily, et al. (2012). Chronostratigraphic context of the Middle to Upper Palaeolithic transition: recent data from Belgium. *Quaternary International* 259, 78–94.

Polishchuk, L. V. (2010). The three-quarter power scaling of extinction risk in late Pleistocene mammals, and a new theory of the size selectivity of extinction. *Evolutionary Ecology Research* 12(1), 1–22.

Poulakakis, N., G. E. Theodorou, E. Zouros, and M. Mylonas (2002). Molecular phylogeny of the extinct Pleistocene dwarf elephant *Palaeoloxodon antiquus falconeri* from Tilos Island, Dodekanisa, Greece. *Journal of Molecular Evolution* 55(3), 364–374.

Prescott, G. W., D. R. Williams, A. Balmford, R. E. Green, and A. Manica (2012). Quantitative global analysis of the role of climate and people in explaining late Quaternary megafaunal extinctions. *Proceedings of the National Academy of Sciences of the United States of America* 109(12), 4527–31.

Pretsch, E., P. Buehlmann, C. Affolter, E. Pretsch, P. Bhuhlmann, and C. Affolter (2000). *Structure Determination of Organic Compounds*. Berlin: Springer.

Price, G. J., J. Louys, J. T. Faith, E. Lorenzen, and M. C. Westaway (2018). Big data little help in megafauna mysteries. *Nature* 558(7708), 23–25.

Proctor, C., K. Douka, J. W. Proctor, and T. Higham (2017). The age and context of the KC4 maxilla, Kent's Cavern, UK. *European Journal of Archaeology* 20(01), 74–97.

Purvis, A., K. E. Jones, and G. M. Mace (2000). Extinction. *BioEssays* 22(12), 1123–1133.

Pushkina, D. and P. Raia (2008). Human influence on distribution and extinctions of the late Pleistocene Eurasian megafauna. *Journal of Human Evolution* 54(6), 769–782.

Quarta, G., I. Tiberi, M. Rossi, G. Aprile, E. Braione, M. D'Elia, E. Ingravallo, et al. (2014). The Copper Age mound necropolis in Salve, Lecce, Italy: radiocarbon dating results on charcoals, bones, cremated bones, and pottery. *Radiocarbon* 56(3), 949–957.

Queiroz, D. P., M. N. de Pinho, and C. Dias (2003). ATR-FTIR studies of poly(propylene oxide)/polybutadiene bi-soft segment urethane/urea membranes. *Macromolecules* 36(11), 4195–4200.

Quiles, A., H. Valladas, H. Bocherens, E. Delqué-Količ, E. Kaltnecker, J. van der Plicht, J.-J. Delannoy, et al. (2016). A high-precision chronological model for the decorated Upper Paleolithic cave of Chauvet-Pont d'Arc, Ardèche, France. *Proceedings of the National Academy of Sciences* 113(17), 4670–4675.

R Core Team (2018). *R: A Language and Environment for Statistical Computing*. R Foundation for Statistical Computing. URL: http://www.R-project.org/.

Raif, E. M. and M.-F. Harmand (1993). Molecular interface characterization in human bone matrix: biochemical and IR spectroscopic studies. *Biomaterials* 14(13), 978–984.

Rajesh, N. P., K. Meera, K. Srinivasan, P. Santhana Raghavan, and P. Ramasamy (2000). Effect of EDTA on the metastable zone width of ADP. *Journal of Crystal Growth* 213(3), 389–394.

Ramesh, T., R. Kalle, and C. T. Downs (2016). Predictors of mammal species richness in KwaZulu-Natal, South Africa. *Ecological Indicators* 60, 385–393.

Rasmussen, S. O. and A. M. Svensson (2016). Comment on 'Abrupt Warming Events Drove Late Pleistocene Holarctic Megafaunal Turnover'. *Science* 351(6276), 927.

Rasmussen, S. O., M. Bigler, S. P. Blockley, T. Blunier, S. L. Buchardt, H. B. Clausen, I. Cvijanovic, et al. (2014). A stratigraphic framework for abrupt climatic changes during the last glacial period based on three synchronized Greenland ice-core records: refining and extending the INTIMATE event stratigraphy. *Quaternary Science Reviews* 106, 14–28.

Ratajczak, U., A. V. Shpansky, D. G. Malikov, K. Stefaniak, A. Nadachowski, P. Wojtal, B. Ridush, et al. (2016). Quaternary skulls of the saiga antelope from eastern Europe and Siberia: *Saiga borealis* versus *Saiga tatarica* – one species or two? *Quaternary*

International 420: *The Quaternary of the Urals: Global Trends and Pan-European Quaternary Records*, 329–347.

Reed, D. H. (2004). Extinction risk in fragmented habitats. *Animal Conservation Forum* 7(2), 181–191.

Reich, D., R. E. Green, M. Kircher, J. Krause, N. Patterson, E. Y. Durand, B. Viola, et al. (2010). Genetic history of an archaic hominin group from Denisova Cave in Siberia. *Nature* 468(7327), 1053–1060.

Reiche, I., C. Vignaud, and M. Menu (2002). The crystallinity of ancient bone and dentine: new insights by transmission electron microscopy. *Archaeometry* 44(3), 447–459.

Reimer, P. J., E. Bard, A. Bayliss, J. W. Beck, P. G. Blackwell, C. Bronk Ramsey, C. E. Buck, et al. (2013). IntCal13 and Marine13 Radiocarbon Age Calibration Curves 0-50,000 Years Cal BP. *Radiocarbon* 55(4), 1869–1887.

Ren, F., Y. Ding, and Y. Leng (2014). Infrared spectroscopic characterization of carbonated apatite: a combined experimental and computational study. *Journal of Biomedical Materials Research Part A* 102(2), 496–505.

Reumer, J. W. F., L. Rook, K. V. D. Borg, K. Post, D. Mol, and J. De Vos (2003). Late Pleistocene survival of the saber-toothed cat *Homotherium* in northwestern Europe. *Journal of Vertebrate Paleontology* 23(1), 260–262.

Ripple, W. J., J. A. Estes, R. L. Beschta, C. C. Wilmers, E. G. Ritchie, M. Hebblewhite, J. Berger, et al. (2014). Status and ecological effects of the world's largest carnivores. *Science* 343(6167), 1241484.

Ritchie, E. G. and C. N. Johnson (2009). Predator interactions, mesopredator release and biodiversity conservation. *Ecology Letters* 12(9), 982–998.

Rohland, N., J. L. Pollack, D. Nagel, C. Beauval, J. Airvaux, S. Pääbo, and M. Hofreiter (2005). The population history of extant and extinct hyenas. *Molecular Biology and Evolution* 22(12), 2435–2443.

Ronseal Quick Drying Varnish (2009). Product Data Sheet No. 11001. Ronseal Ltd.

Royston, P. (1995). Remark AS R94: A remark on algorithm AS 181: The W-test for normality. *Journal of the Royal Statistical Society: Series C (Applied Statistics)* 44(4), 547–551.

Salnicki, J., M. Teichmann, V. J. Wilson, and F. Murindagomo (2001). Spotted hyaenas *Crocuta crocuta* prey on new-born elephant calves in Hwange National Park, Zimbabwe. *Koedoe* 44(2), 79–83.

Saltré, F., B. W. Brook, M. Rodríguez-Rey, A. Cooper, C. N. Johnson, C. S. M. Turney, and C. J. A. Bradshaw (2015). Uncertainties in dating constrain model choice for inferring extinction time from fossil records. *Quaternary Science Reviews* 112, 128–137.

Saltré, F., M. Rodríguez-Rey, B. W. Brook, C. N. Johnson, C. S. M. Turney, J. Alroy, A. Cooper, et al. (2016). Climate change not to blame for late Quaternary megafauna extinctions in Australia. *Nature Communications* 7, 10511.

Sánchez Goñi, M. F., E. Bard, A. Landais, L. Rossignol, and F. d'Errico (2013). Air–sea temperature decoupling in western Europe during the last interglacial–glacial transition. *Nature Geoscience* 6, 837–841.

Sánchez Goñi, M. F. and S. P. Harrison (2010). Millennial-scale climate variability and vegetation changes during the last glacial: concepts and terminology. *Quaternary Science Reviews* (29), 2823–2827.

Sánchez Goñi, M. F., A. Landais, W. J. Fletcher, F. Naughton, S. Desprat, and J. Duprat (2008). Contrasting impacts of Dansgaard–Oeschger events over a western European latitudinal transect modulated by orbital parameters. *Quaternary Science Reviews* 27(11), 1136–1151.

Sanchis, A., C. Tormo, V. Sauqué, V. Sanchis, R. Díaz, A. Ribera, and V. Villaverde (2015). Pleistocene leopards in the Iberian Peninsula: new evidence from palaeontological and archaeological contexts in the Mediterranean region. *Quaternary Science Reviews* 124, 175–208.

Sanderson, C., K. Radley, and L. Mayton (1995). Ethylenediaminetetraacetic acid in ammonium hydroxide for reducing decalcification time. *Biotechnic & Histochemistry* 70(1), 12–18.

Sandom, C., S. Faurby, B. Sandel, and J.-C. Svenning (2014). Global late Quaternary megafauna extinctions linked to humans, not climate change. *Proceedings of the Royal Society of London B: Biological Sciences* 281(1787), 20133254.

Sangeetha, R., K. Uma, and V. Chandavarkar (2013). Comparison of routine decalcification methods with microwave decalcification of bone and teeth. *Journal of Oral and Maxillofacial Pathology* 17(3), 386.

Sardella, R. and M. Petrucci (2012). The earliest Middle Pleistocene *Crocuta crocuta* (Erxleben, 1777) at Casal Selce (Rome, Italy). *Quaternary International* 267: *The Genus Homo from Africa to Europe: Evolution of Terrestrial Ecosystems and Dispersal Routes*, 103–110.

Sauqué, V. and G. Cuenca-Bescós (24 2013). The Iberian Peninsula, the last European refugium of *Panthera pardus* (Linnaeus 1758) during the Upper Pleistocene. *Quaternaire* (1), 35–48.

Sauqué, V., R. García-González, and G. Cuenca-Bescós (2016a). A late Pleistocene (MIS3) ungulate mammal assemblage (Los Rincones, Zaragoza, Spain) in the Eurosiberian–Mediterranean boundary. *Historical Biology* 28(3), 358–389.

Sauqué, V., R. Rabal-Garcés, and G. Cuenca-Bescós (2016b). Carnivores from Los Rincones, a leopard den in the highest mountain of the Iberian range (Moncayo, Zaragoza, Spain). *Historical Biology* 28(4), 479–506.

Sauqué, V., R. Rabal-Garcés, C. Sola-Almagro, and G. Cuenca-Bescós (2014). Bone accumulation by leopards in the late Pleistocene in the Moncayo Massif (Zaragoza, NE Spain). *PLOS ONE* 9(3), e92144.

Scheffer, M., S. Carpenter, J. A. Foley, C. Folke, and B. Walker (2001). Catastrophic shifts in ecosystems. *Nature* 413(6856), 591–596.

Schmitt, T. and Z. Varga (2012). Extra-Mediterranean refugia: the rule and not the exception? *Frontiers in Zoology* 9, 22.

Seierstad, I. K., P. M. Abbott, M. Bigler, T. Blunier, A. J. Bourne, E. Brook, S. L. Buchardt, et al. (2014). Consistently dated records from the Greenland GRIP, GISP2 and NGRIP ice cores for the past 104 ka reveal regional millennial-scale δ18O gradients with possible Heinrich event imprint. *Quaternary Science Reviews* 106, 29–46.

Sen, S., E. Barrier, and X. Crété (2014). Late Pleistocene dwarf elephants from the Aegean islands of Kassos and Dilos, Greece. *Annales Zoologici Fennici* 51(1-2), 27–42.

Sergio, F., I. Newton, L. Marchesi, and P. Pedrini (2006). Ecologically justified charisma: preservation of top predators delivers biodiversity conservation. *Journal of Applied Ecology* 43(6), 1049–1055.

Shah, K. M., J. C. H. Goh, R. Karunanithy, S. L. Low, S. D. Das, and K. Bose (1995). Effect of decalcification on bone mineral content and bending strength of feline femur. *Calcified Tissue International* 56(1), 78–82.

Shchetnikov, A. A., D. White, I. A. Filinov, and N. Rutter (2012). Late Quaternary geology of the Tunka Rift Basin (Lake Baikal region), Russia. *Journal of Asian Earth Sciences* 46, 195–208.

Shea, J. (2008). Transitions or turnovers? Climatically-forced extinctions of *Homo sapiens* and Neanderthals in the east Mediterranean Levant. *Quaternary Science Reviews* 27(23-24), 2253–2270.

Sirakov, N., J.-L. Guadelli, S. Ivanova, S. Sirakova, M. Boudadi-Maligne, I. Dimitrova, F. Ph, et al. (2010). An ancient continuous human presence in the Balkans and the beginnings of human settlement in western Eurasia: A Lower Pleistocene example of the Lower Palaeolithic levels in Kozarnika Cave (North-western Bulgaria). *Quaternary International* 223-224, 94–106.

Slon, V., C. Hopfe, C. L. Weiß, F. Mafessoni, M. De la Rasilla, C. Lalueza-Fox, A. Rosas, et al. (2017). Neandertal and Denisovan DNA from Pleistocene sediments. *Science* 356(6338), 605–608.

Smith, F., C. Doughty, Y. Malhi, J.-C. Svenning, and J. Terborgh (2016). Megafauna in the Earth system. *Ecography* 39(2), 99–108.

Smith, F. A., S. K. Lyons, S. K. M. Ernest, K. E. Jones, D. M. Kaufman, T. Dayan, P. A. Marquet, et al. (2003). Body mass of late Quaternary mammals. *Ecology* 84(12), 3403.

Solow, A. R. (2005). Inferring extinction from a sighting record. *Mathematical Biosciences* 195(1), 47–55.

Solow, A. R. and A. R. Beet (2014). On uncertain sightings and inference about extinction. *Conservation Biology* 28(4), 1119–1123.

Sołtysiak, A., E. A. Miśta-Jakubowska, M. Dorosz, T. Kosiński, and I. Fijał-Kirejczyk (2018). Estimation of collagen presence in dry bone using combined X-ray and neutron radiography. *Applied Radiation and Isotopes* 139, 141–145.

Sommer, R. and N. Benecke (2005). Late-Pleistocene and early Holocene history of the canid fauna of Europe (Canidae). *Mammalian Biology* 70(4), 227–241.

— (2006). Late Pleistocene and Holocene development of the felid fauna (Felidae) of Europe: a review. *Journal of Zoology* 269(1), 7–19.

Soubrier, J., G. Gower, K. Chen, S. M. Richards, B. Llamas, K. J. Mitchell, S. Y. W. Ho, et al. (2016). Early cave art and ancient DNA record the origin of European bison. *Nature Communications* 7, 13158.

Spassov, N. and D. Raychev (1997). Late Würm *Panthera pardus* remains from Bulgaria: The European fossil leopards and the question of the probable species survival until the Holocene on the Balkans. *Historia Naturalis Bulgarica* 7, 71–96.

Stafford, T. W., R. C. Duhamel, C. V. Haynes, and K. Brendel (1982). Isolation of proline and hydroxyproline from fossil bone. *Life sciences* 31(9), 931–938.

Stafford, T. W., P. E. Hare, L. Currie, A. T. Jull, and D. J. Donahue (1991). Accelerator radiocarbon dating at the molecular level. *Journal of Archaeological Science* 18(1), 35–72.

Stafford, T. W., K. Brendel, and R. C. Duhamel (1988). Radiocarbon, 13C and 15N analysis of fossil bone: removal of humates with XAD-2 resin. *Geochimica et Cosmochimica Acta* 52(9), 2257–2267.

Stahler, D. R., D. W. Smith, and D. S. Guernsey (2006). Foraging and feeding ecology of the gray wolf (*Canis lupus*): lessons from Yellowstone National Park, Wyoming, USA. *The Journal of Nutrition* 136(7), 1923S–1926S.

Stathopoulou, E. and G. Theodorou (2001). Observations on the diagenesis of dwarf elephant skeletal remains from the island of Tilos (Dodekanese, Greece). G. Cavarretta, P. Gioia, M. Mussi, and M. Palombo (Eds.), *The World of Elephants: Proceedings of the 1st International Congress*. Rome: Consiglio Nazionale delle Ricerche, p. 557–562.

Steffensen, J. P., K. K. Andersen, M. Bigler, H. B. Clausen, D. Dahl-Jensen, H. Fischer, K. Goto-Azuma, et al. (2008). High-resolution Greenland ice core data show abrupt climate change happens in few years. *Science* 321(5889), 680–684.

Stein, A. B., V. Athreya, P. Gerngross, G. Balme, P. Henschel, U. Karanth, D. Miquelle, et al. (2016). *Panthera pardus. The IUCN Red List of Threatened Species 2016*, e. T15954A50659089, https://www.iucnredlist.org/species/15954/102421779.

Stewart, J. R. (3-4 2004). Neanderthal–modern human competition? A comparison between the mammals associated with Middle and Upper Palaeolithic industries in Europe during OIS 3. *International Journal of Osteoarchaeology* 14, 178–189.

— (2009). The evolutionary consequence of the individualistic response to climate change. *Journal of Evolutionary Biology* 22(12), 2363–2375.

Stewart, J. R., M. Van Kolfschoten, A. Markova, and R. Musil (2003). The mammalian faunas of Europe during Oxygen Isotope Stage Three. T. van Andel and W. Davies (Eds.), *Neanderthals and Modern Humans in the European Landscape during the Last Glaciation, 60,000 to 20,000 Years Ago: Archaeological Results of the Stage 3 Project*. McDonald Institute Monograph Series. Cambridge: McDonald Institute for Archaeological Research, p. 103–129.

Stewart, J. R. (2008). The progressive effect of the individualistic response of species to Quaternary climate change: an analysis of British mammalian faunas. *Quaternary Science Reviews* 27(27), 2499–2508.

Stewart, J. R. and A. Cooper (2008). Ice Age refugia and Quaternary extinctions: an issue of Quaternary evolutionary palaeoecology. *Quaternary Science Reviews* 27(27-28), 2443–2448.

Stewart, J. R. and A. M. Lister (2001). Cryptic northern refugia and the origins of the modern biota. *Trends in Ecology & Evolution* 16(11), 608–613.

Stiner, M. C. (2004). Comparative ecology and taphonomy of spotted hyenas, humans, and wolves in Pleistocene Italy. *Revue de Paléobiologie* 23(2), 771–785.

Stiner, M. C. and S. L. Kuhn (2006). Changes in the 'connectedness' and resilience of Paleolithic societies in Mediterranean ecosystems. *Human Ecology* 34(5), 693–712.

Stuart, A. J. (1991). Mammalian extinctions in the late Pleistocene of northern Eurasia and North America. *Biological Reviews of the Cambridge Philosophical Society* 66(4), 453–562.

Stuart, A. J., P. A. Kosintsev, T. F. G. Higham, and A. M. Lister (2004). Pleistocene to Holocene extinction dynamics in giant deer and woolly mammoth. *Nature* 431(7009), 684–689.

Stuart, A. and A. Lister (2007). Patterns of late Quaternary megafaunal extinctions in Europe and northern Asia. *Courier-Forschungsinstitut Senckenberg* 259, 287–297.

Stuart, A. J. (2005). The extinction of woolly mammoth (*Mammuthus primigenius*) and straight-tusked elephant (*Palaeoloxodon antiquus*) in Europe. *Quaternary International* 126–128: *Studying Proboscideans: Knowledge, Problems and*

Perspectives. Selected Papers from "The World of Elephants" Congress, Rome, 171–177.

Stuart, A. J. and A. M. Lister (2011). Extinction chronology of the cave lion *Panthera* spelaea. *Quaternary Science Reviews* 30(17–18): *Beringia and Beyond: Papers Celebrating the Scientific Career of Andrei Vladimirovich Sher, 1939–2008*, 2329–2340.

— (2012). Extinction chronology of the woolly rhinoceros *Coelodonta antiquitatis* in the context of late Quaternary megafaunal extinctions in northern Eurasia. *Quaternary Science Reviews* 51, 1–17.

— (2014). New radiocarbon evidence on the extirpation of the spotted hyaena (*Crocuta crocuta* (Erxl.)) in northern Eurasia. *Quaternary Science Reviews* 96: *Predators, Prey and Hominins - Celebrating the Scientific Career of Alan Turner (1947-2012)*, 108–116.

Stuart, A. J., L. D. Sulerzhitsky, L. A. Orlova, Y. V. Kuzmin, and A. M. Lister (2002). The latest woolly mammoths (*Mammuthus primigenius* Blumenbach) in Europe and Asia: a review of the current evidence. *Quaternary Science Reviews* 21(14), 1559–1569.

Stuart, A. J. (1999). Late Pleistocene megafaunal extinctions. R. MacPhee (Ed.), *Extinctions in Near Time*. Vol. 2. Advances in Vertebrate Paleobiology. Boston: Springer, p. 257–269.

Stuart, A. and L. van Wijngaarden-Bakker (1985). Quaternary Vertebrates. K. J. Edwards and W. P. Warren (Eds.), *The Quaternary History of Ireland*. Orlando and London: Academic Press, p. 221–249.

Tallavaara, M., M. Luoto, N. Korhonen, H. Järvinen, and H. Seppä (2015). Human population dynamics in Europe over the Last Glacial Maximum. *Proceedings of the National Academy of Sciences* 112(27), 8232–8237.

Taylor, R. E. (1987). *Radiocarbon Dating: An Archaeological Perspective*. Orlando: Academic Press.

Terborgh, J., L. Lopez, P. Nuñez, M. Rao, G. Shahabuddin, G. Orihuela, M. Riveros, et al. (2001). Ecological meltdown in predator-free forest fragments. *Science* 294(5548), 1923–1926.

Theodorou, G. E. and N. K. Symeonides (2001). The excavations of the last ten years at Charkadio Cave on Tilos Island, Dodekanese, Greece. G. Cavarretta, P. Gioia, M. Mussi, and M. Palombo (Eds.), *The World of Elephants: Proceedings of the 1st International Congress*. Rome: Consiglio Nazionale delle Ricerche, p. 514–518.

Thomas, C. D., A. Cameron, R. E. Green, M. Bakkenes, L. J. Beaumont, Y. C. Collingham, B. F. N. Erasmus, et al. (2004). Extinction risk from climate change. *Nature* 427(6970), 145–148.

Thuiller, W., D. Georges, and R. Engler (2014). *Biomod2: Ensemble platform for species distribution modeling*. Version 3.1.64. URL: http://CRAN.R-project.org/package=biomod2.

Tilman, D., R. M. May, C. L. Lehman, and M. A. Nowak (1994). Habitat destruction and the extinction debt. *Nature* 371(6492), 65–66.

Toda, H. Y. and T. Yamamoto (1995). Statistical inference in vector autoregressions with possibly integrated processes. *Journal of Econometrics* 66(1), 225–250.

Tripp, J. A., M. E. Squire, R. E. M. Hedges, and R. E. Stevens (2018). Use of micro-computed tomography imaging and porosity measurements as indicators of

collagen preservation in archaeological bone. *Palaeogeography, Palaeoclimatology, Palaeoecology* 511, 462–471.

Trovati, G., E. A. Sanches, S. C. Neto, Y. P. Mascarenhas, and G. O. Chierice (2009). Characterization of polyurethane resins by FTIR, TGA, and XRD. *Journal of Applied Polymer Science* 115(1), 263–268.

Trueman, C. N. G., A. K. Behrensmeyer, N. Tuross, and S. Weiner (2004). Mineralogical and compositional changes in bones exposed on soil surfaces in Amboseli National Park, Kenya: diagenetic mechanisms and the role of sediment pore fluids. *Journal of Archaeological Science* 31(6), 721–739.

Trueman, C. N., K. Privat, and J. Field (2008). Why do crystallinity values fail to predict the extent of diagenetic alteration of bone mineral? *Palaeogeography, Palaeoclimatology, Palaeoecology* 266(3): *Beyond Documenting Diagenesis: The Fifth International Bone Diagenesis Workshop*, 160–167.

Tuross, N. (2012). Comparative decalcification methods, radiocarbon dates, and stable isotopes of the VIRI bones. *Radiocarbon* 54(3–4), 837–844.

Turvey, S. T., H. Tong, A. J. Stuart, and A. M. Lister (2013). Holocene survival of late Pleistocene megafauna in China: a critical review of the evidence. *Quaternary Science Reviews* 76, 156–166.

Uysal, I., F. Severcan, and Z. Evis (2013). Characterization by Fourier transform infrared spectroscopy of hydroxyapatite co-doped with zinc and fluoride. *Ceramics International* 39(7), 7727–7733.

Valdiosera, C. E., N. García, C. Anderung, L. Dalén, E. Crégut-Bonnoure, R.-D. Kahlke, M. Stiller, et al. (2007). Staying out in the cold: glacial refugia and mitochondrial DNA phylogeography in ancient European brown bears. *Molecular Ecology* 16(24), 5140–5148.

Valkenburgh, B. V., M. W. Hayward, W. J. Ripple, C. Meloro, and V. L. Roth (2016). The impact of large terrestrial carnivores on Pleistocene ecosystems. *Proceedings of the National Academy of Sciences* 113(4), 862–867.

Van der Weyde, L. K., C. Mbisana, and R. Klein (2018). Multi-species occupancy modelling of a carnivore guild in wildlife management areas in the Kalahari. *Biological Conservation* 220, 21–28.

Van Klinken, G. J., A. D. Bowles, and R. E. M. Hedges (1994). Radiocarbon dating of peptides isolated from contaminated fossil bone collagen by collagenase digestion and reversed-phase chromatography. *Geochimica et Cosmochimica Acta* 58(11), 2543–2551.

Van Klinken, G. J. (1999). Bone collagen quality indicators for palaeodietary and radiocarbon measurements. *Journal of Archaeological Science* 26(6), 687–695.

Van Meerbeeck, C. J., H. Renssen, D. M. Roche, B. Wohlfarth, S. J. P. Bohncke, J. A. A. Bos, S. Engels, et al. (2011). The nature of MIS 3 stadial–interstadial transitions in Europe: new insights from model–data comparisons. *Quaternary Science Reviews* 30(25), 3618–3637.

Van Nédervelde, B. J. and M. Davies (1975). *Caldey Island Cave Excavations 1975.* Report on file with the National Museum of Wales, Cardiff.

Van Asperen, E. N. and R.-D. Kahlke (2015). Dietary variation and overlap in central and northwest European *Stephanorhinus* kirchbergensis and *S. hemitoechus* (Rhinocerotidae, Mammalia) influenced by habitat diversity: "You'll have to take pot luck!" (proverb). *Quaternary Science Reviews* 107, 47–61.

Van Doorn, N. L., J. Wilson, H. Hollund, M. Soressi, and M. J. Collins (2012). Site-specific deamidation of glutamine: a new marker of bone collagen deterioration. *Rapid Communications in Mass Spectrometry* 26(19), 2319–2327.

Van Klinken, G. J. and R. E. M. Hedges (1995). Experiments on collagen-humic interactions: speed of humic uptake, and effects of diverse chemical treatments. *Journal of Archaeological Science* 22(2), 263–270.

Varela, S., M. S. Lima-Ribeiro, J. A. F. Diniz-Filho, and D. Storch (2014). Differential effects of temperature change and human impact on European Late Quaternary mammalian extinctions. *Global Change Biology* 21(4), 1475–1481.

Varela, S., J. M. Lobo, J. Rodríguez, and P. Batra (2010). Were the late Pleistocene climatic changes responsible for the disappearance of the European spotted hyena populations? Hindcasting a species geographic distribution across time. *Quaternary Science Reviews* 29(17–18), 2027–2035.

Vartanyan, S. L., K. A. Arslanov, J. A. Karhu, G. Possnert, and L. D. Sulerzhitsky (2008a). Collection of radiocarbon dates on the mammoths (*Mammuthus primigenius*) and other genera of Wrangel Island, Northeast Siberia, Russia. *Quaternary Research* 70(1), 51–59.

— (2008b). Collection of radiocarbon dates on the mammoths (*Mammuthus primigenius*) and other genera of Wrangel Island, northeast Siberia, Russia. *Quaternary Research* 70(1), 51–59.

Vasil'ev, S. A. (2003). Faunal exploitation, subsistence practices and Pleistocene extinctions in Paleolithic Siberia. *Deinsea* 9(1), 513–556.

Veis, A. and R. J. Schlueter (1964). The macromolecular organization of dentine matrix collagen: characterization of dentine collagen. *Biochemistry* 3(11), 1650–1657.

Venables, W. N. and B. D. Ripley (2002). *Modern Applied Statistics with S*. 4th edition. New York: Springer.

Vera, F. W. M. (2000). *Grazing Ecology and Forest History*. Wallingford: CABI.

Villa, P. and W. Roebroeks (2014). Neandertal demise: an archaeological analysis of the modern human superiority complex. *PLOS ONE* 9(4), e96424.

Villard, M.-A. and J. P. Metzger (2014). Review: Beyond the fragmentation debate: a conceptual model to predict when habitat configuration really matters. *Journal of Applied Ecology* 51(2), 309–318.

Villavicencio, N. A., E. L. Lindsey, F. M. Martin, L. A. Borrero, P. I. Moreno, C. R. Marshall, and A. D. Barnosky (2016). Combination of humans, climate, and vegetation change triggered late Quaternary megafauna extinction in the Última Esperanza region, southern Patagonia, Chile. *Ecography* 39(2), 125–140.

Volterra, V. (2000). A Tale of Four Caves: ESR Dating of Mousterian Layers at Iberian Archaeological Sites. PhD thesis. McMaster University.

Walker, E. A., D. Case, C. Ingrem, J. Jones, and R. Mourne (2014). Excavations at Cathole Cave, Gower, Swansea. *Proceedings of the University of Bristol Spelaeological Society* 26(2), 131–169.

Walters, M., Y. Leung, N. Blumenthal, K. Konsker, and R. LeGeros (1990). A Raman and infrared spectroscopic investigation of biological hydroxyapatite. *Journal of Inorganic Biochemistry* 39(3), 193–200.

Wang, P., C. Li, H. Gong, X. Jiang, H. Wang, and K. Li (2010). Effects of synthesis conditions on the morphology of hydroxyapatite nanoparticles produced by wet chemical process. *Powder Technology* 203(2), 315–321.

Warren, D. L. and S. N. Seifert (2011). Ecological niche modeling in Maxent: the importance of model complexity and the performance of model selection criteria. *Ecological Applications* 21(2), 335–342.

Warren, M. S., J. K. Hill, J. A. Thomas, J. Asher, R. Fox, B. Huntley, D. B. Roy, et al. (2001). Rapid responses of British butterflies to opposing forces of climate and habitat change. *Nature* 414(6859), 65–69.

Waterbolk, H. T. (1971). Working with radiocarbon dates. *Proceedings of the Prehistoric Society* 37(2), 15–33.

Webb, T. and P. J. Bartlein (1992). Global changes during the last 3 million years: climatic controls and biotic responses. *Annual Review of Ecology and Systematics* 23(1), 141–173.

Welker, F., M. Soressi, W. Rendu, J.-J. Hublin, and M. Collins (2015). Using ZooMS to identify fragmentary bone from the Late Middle/Early Upper Palaeolithic sequence of Les Cottés, France. *Journal of Archaeological Science* 54, 279–286.

Welton, J. E. (1984). *SEM Petrology Atlas*. Methods in Exploration Series 4. Tulsa: American Association of Petroleum Geologists.

Whitney-Smith, E. (2001). Second-Order predation and pleistocene extinctions: a system dynamics model. PhD thesis. George Washington University.

Willerslev, E., A. J. Hansen, J. Binladen, T. B. Brand, M. T. P. Gilbert, B. Shapiro, M. Bunce, et al. (2003). Diverse plant and animal genetic records from Holocene and Pleistocene sediments. *Science* 300(5620), 791–795.

Wilson, J., N. L. van Doorn, and M. J. Collins (2012). Assessing the extent of bone degradation using glutamine deamidation in collagen. *Analytical Chemistry* 84(21), 9041–9048.

Wolde-Rufael, Y. (2005). Energy demand and economic growth: the African experience. *Journal of Policy Modeling* 27(8), 891–903.

Wood, R. E., K. Douka, P. Boscato, P. Haesaerts, A. Sinitsyn, and T. F. G. Higham (2012). Testing the ABOx-SC method: dating known-age charcoals associated with the Campanian Ignimbrite. *Quaternary Geochronology* 9, 16–26.

Wood, R. (2011). The contribution of new radiocarbon dating pre-treatment techniques to understanding the Middle to Upper Palaeolithic transition in Iberia. PhD thesis. University of Oxford.

— (2015). From revolution to convention: the past, present and future of radiocarbon dating. *Journal of Archaeological Science* 56, 61–72.

Wood, R. E., C. Barroso-Ruíz, M. Caparrós, J. F. Jordá Pardo, B. Galván Santos, and T. F. G. Higham (2013a). Radiocarbon dating casts doubt on the late chronology of the Middle to Upper Palaeolithic transition in southern Iberia. *Proceedings of the National Academy of Sciences* 110(8), 2781–6.

Wood, R. E., C. Barroso-Ruíz, M. Caparrós, J. F. J. Pardo, B. G. Santos, and T. F. G. Higham (2013b). Reply to De La Peña: radiocarbon dating and the paleoenvironmental record of Carihuela. *Proceedings of the National Academy of Sciences* 110(23). Carihuela, e2087.

Wood, R., F. Bernaldo de Quirós, J.-M. Maíllo-Fernández, J.-M. Tejero, A. Neira, and T. Higham (2018). El Castillo (Cantabria, northern Iberia) and the Transitional Aurignacian: using radiocarbon dating to assess site taphonomy. *Quaternary International* 474(Part A), 56–70.

Wood, R., Z. Jacobs, D. Vannieuwenhuyse, J. Balme, S. O'Connor, and R. Whitau (2016). Towards an accurate and precise chronology for the colonization of Australia: the example of Riwi, Kimberley, Western Australia. *PLOS ONE* 11(9), e0160123.

Woodman, P., M. McCarthy, and N. Monaghan (1997). The Irish Quaternary Fauna Project. *Quaternary Science Reviews* 16(2), 129–159.

Wopenka, B. and J. D. Pasteris (2005). A mineralogical perspective on the apatite in bone. *Materials Science and Engineering: C* 25(2), 131–143.

Wright, L. E. and H. P. Schwarcz (1996). Infrared and isotopic evidence for diagenesis of bone apatite at Dos Pilas, Guatemala: palaeodietary implications. *Journal of Archaeological Science* 23(6), 933–944.

Wroe, S., J. H. Field, M. Archer, D. K. Grayson, G. J. Price, J. Louys, J. T. Faith, et al. (2013). Climate change frames debate over the extinction of megafauna in Sahul (Pleistocene Australia-New Guinea). *Proceedings of the National Academy of Sciences* 110(22), 8777–8781.

Wroe, S., J. Field, R. Fullagar, and L. S. Jermin (2004). Megafaunal extinction in the late Quaternary and the global overkill hypothesis. *Alcheringa* 28(1), 291–331.

Yang, X. F., C. Vang, D. E. Tallman, G. P. Bierwagen, S. G. Croll, and S. Rohlik (2001). Weathering degradation of a polyurethane coating. *Polymer Degradation and Stability* 74(2), 341–351.

Yi, H., E. Balan, C. Gervais, L. Segalen, F. Fayon, D. Roche, A. Person, et al. (2013). A carbonate-fluoride defect model for carbonate-rich fluorapatite. *American Mineralogist* 98(5-6), 1066–1069.

Yule, J. V., R. J. Fournier, C. X. J. Jensen, J. Yang, H. E. J. J. Wiens, and A. E. K. Roy (2014). A review and synthesis of late Pleistocene extinction modeling: progress delayed by mismatches between ecological realism, interpretation, and methodological transparency. *The Quarterly Review of Biology* 89(2), 91–106.

Zapata, H. O. and A. N. Rambaldi (1997). Monte Carlo evidence on cointegration and causation. *Oxford Bulletin of Economics and Statistics* 59(2), 285–298.

Zazzo, A. and J.-F. Saliège (2011). Radiocarbon dating of biological apatites: a review. *Palaeogeography, Palaeoclimatology, Palaeoecology* 310(1), 52–61.

Zeileis, A., F. Leisch, K. Hornik, and C. Kleiber (2002). Strucchange: An R package for testing for structural change in linear regression models. *Journal of Statistical Software* 7(1), 1–38.

Zeileis, A., A. Shah, and I. Patnaik (2010). Testing, monitoring, and dating structural changes in exchange rate regimes. *Computational Statistics & Data Analysis* 54(6), 1696–1706.

Zhang, Y., R. Li, and C.-L. Tsai (2010). Regularization parameter selections via generalized information criterion. *Journal of the American Statistical Association* 105(489), 312–323.

Zhang, Z., G. Li, and B. I. Shi (2006). Physicochemical properties of collagen, gelatin and collagen hydrolysate derived from bovine limed split wastes. *Society of Leather Technologists and Chemists* 90(1), 23–28.

Zhao, Y. E., C. Y. Cai, Y. Y. Luo, and Z. H. He (2004). FTIR spectra of the $M(EDTA)^{n-}$ complexes in the process of Sol-Gel technique. *Journal of Superconductivity* 17(3), 383–387.

Zilhao, J. (2006). Chronostratigraphy of the Middle-to-Upper Paleolithic transition in the Iberian Peninsula. *Pyrenae* (37), 7–84.

Zimov, S. A., N. S. Zimov, A. N. Tikhonov, and F. S. Chapin (2012). Mammoth steppe: a high-productivity phenomenon. *Quaternary Science Reviews* 57, 26–45.

Zuo, W., F. A. Smith, and E. L. Charnov (2013). A life-history approach to the late Pleistocene megafaunal extinction. *The American Naturalist* 182(4), 524–531.